COMMUNICATIONS
FROM THE
KONKOLY OBSERVATORY
OF THE
HUNGARIAN ACADEMY OF SCIENCES

MITTEILUNGEN
DER
STERNWARTE
DER UNGARISCHEN AKADEMIE
DER WISSENSCHAFTEN

BUDAPEST–SVÁBHEGY

No. 101.
(Vol. 13, Part 1)

XZ Dra: observations spanning 70 years*

Szeidl B., Jurcsik J., Benkő J. M. and Bakos G. Á.

Konkoly Observatory of the Hungarian Academy of Sciences,
P.O. Box 67, H-1525 Budapest, Hungary

BUDAPEST, 2001

*The data are available in electronic form at
http://www.konkoly.hu/Mitteilungen/Mitteilungen.html

ISBN 963 8361 395
HU ISSN 0238-2091
Felelős kiadó: Balázs Lajos

TABLE OF CONTENTS

XZ DRA: OBSERVATIONS SPANNING 70 YEARS

Abstract

During the past seventy years a great number of observations of XZ Dra have been collected at Konkoly Observatory. Here we publish 344 visual observations made by L. Detre in the years 1932 and 1934, 4440 photographic magnitudes obtained in the years 1935–1957, 40 white light photoelectric data from 1957, and 6066 $UBV(RI)_{\rm C}$ observations made between 1958–1988, and further CCD observations from 2001. All published observations are reviewed and the times of light maximum of XZ Dra are collected as well. New normal maxima have been determined in order to follow the star's long-term period changes.

Key words: Stars – variable: RR Lyrae; stars – individual: XZ Dra – Techniques: photometric – Techniques: radial velocities

INTRODUCTION

The variability of XZ Dra (AN 433.1928, BD+64°1332, GSC 04225–00305, HIP 94134, $\alpha_{2000} = 19^{\rm h}9^{\rm m}42\overset{\rm s}{.}6$, $\delta_{2000} = 64°51'32''$) was discovered by Schneller (1929) on Babelsberg plates. Soon after its discovery, Beyer (1934) made the first thorough investigation of the star's light variation. He confirmed the RR Lyrae type variability suspected by the discoverer (Schneller, 1931) and already took notice of the large scatter of observations around light maximum. Balázs & Detre (1941) based on their preliminary study demonstrated that the star had, indeed, strong light curve variation with a period of 76 days.

Since the early studies a great number of observations have been made on XZ Dra by different observers. In this paper we publish the visual, photographic, photoelectric and CCD observations obtained at Konkoly Observatory during the past 70 years and carry out a rigorous treatment and elaboration of all published observations.

Here we also publish radial velocity measurements taken at the Dominion Astrophysical Observatory (DAO, Canada) in 1971.

OBSERVATIONS

Visual Data

During the years 1931–1937 visual observations of a number of RR Lyrae stars were carried out by L. Detre at Konkoly Observatory. The 20cm Heyde-Refractor equipped with a Graff-type wedge photometer was used. A detailed description of the instrument and the observational procedure adopted is given in the paper of Detre & Lassovszky (1939).

One of Detre's program stars was XZ Dra, which was extensively observed in the years 1932–1934: 344 visual estimates were obtained during 20 nights. Detre's original visual observations are listed in Table 1. The comparison stars he used were BD+64°1331

(=TYC 4225_0931_1), TYC 4225_1323_1 and BD+64°1335 (=TYC 4225_0331_1) with visual magnitudes $V_{\rm vis}$=8.61, 10.27 and 10.61, respectively.

Table 1. Visual observations of XZ Dra

2426825 +
0.4014 10.02
0.4278 10.06
0.4306 10.05
0.4333 10.27
0.4354 10.27
0.4375 10.12
0.4396 10.22
0.4722 10.31
0.4743 10.33
0.4764 10.37
0.4785 10.36
0.4806 10.35
0.4819 10.50
0.5104 10.66
0.5128 10.56
0.5160 10.54
0.5174 10.57
0.5194 10.42
0.6215 10.47
0.5396 10.45
0.5417 10.36
0.5438 10.31
0.5458 10.22
0.5479 10.40
0.5500 10.33

2426826 +
0.3160 10.07
0.3181 9.92
0.3201 9.91
0.3215 9.95
0.3639 9.85
0.3660 9.78
0.3681 9.93
0.3701 9.90
0.3715 10.03
0.3757 10.02
0.3785 10.19
0.3806 10.09
0.4035 9.95
0.4063 10.11
0.4076 10.27
0.4097 10.32
0.4125 10.22
0.4146 10.20

2426827 +
0.3292 10.10
0.3319 10.08
0.3340 10.16
0.3361 10.14
0.3597 10.14
0.3625 10.09
0.3646 10.31
0.3674 10.32
0.3694 10.11
0.3708 10.06
0.4042 10.31
0.4063 10.28
0.4090 10.35
0.4118 10.45
0.4132 10.42
0.4153 10.48
0.4451 10.55
0.4472 10.56
0.4493 10.51
0.4514 10.46
0.4549 10.55
0.4563 10.43
0.4875 10.72
0.4896 10.65
0.4917 10.60
0.4958 10.60
0.4979 10.81
0.5000 10.76

2426828 +
0.3354 10.12
0.3375 10.16
0.3403 10.25
0.3424 10.20
0.3444 10.28
0.3465 10.35
0.3486 10.24
0.3972 10.62
0.3986 10.61
0.4007 10.61
0.4028 10.59
0.4049 10.47
0.4076 10.49
0.4222 10.57
0.4243 10.50
0.4264 10.56
0.4285 10.61
0.4299 10.66
0.4451 10.71
0.4465 10.60
0.4486 10.58
0.4500 10.72
0.4639 10.59
0.4667 10.53
0.4681 10.42
0.4701 10.62

2426831 +
0.3243 10.42
0.3264 10.55
0.3285 10.48
0.3313 10.30
0.3326 10.52
0.3347 10.54

2426832 +
0.3264 10.61
0.3285 10.48
0.3306 10.69
0.3326 10.62
0.3340 10.63

2426835 +
0.3208 10.59
0.3229 10.56
0.3257 10.77
0.3278 10.53
0.3299 10.52
0.3319 10.55
0.3347 10.49
0.3368 10.47
0.3389 10.53
0.3410 10.39
0.3431 10.42
0.3647 9.93
0.3694 9.90
0.3785 9.77
0.3806 9.64
0.3826 9.71
0.3854 9.79
0.3875 9.82
0.3896 9.74
0.3824 9.86
0.3938 9.92
0.3951 9.87

2426889 +
0.3722 10.52

2426945 +
0.3931 10.42
0.3951 10.53
0.3979 10.57
0.4000 10.42
0.4028 10.51
0.4049 10.43
0.4083 10.44
0.4104 10.28
0.4125 10.17
0.4146 10.18
0.4167 10.13
0.4188 10.03
0.4208 10.03
0.4229 9.88
0.4250 10.01
0.4271 9.86
0.4292 9.84
0.4333 9.84
0.4375 9.78
0.4403 9.73
0.4444 9.65
0.4479 9.72
0.4514 9.64
0.4528 9.63
0.4549 9.70
0.4570 9.66
0.4583 9.86
0.4611 9.88
0.4632 9.80

2426957 +
0.3743 9.81
0.3785 9.83
0.3813 9.84
0.3833 9.99
0.3854 9.98
0.3875 9.95
0.3993 9.93
0.4007 9.98
0.4021 10.02

2426960 +
0.4854 10.75
0.4889 10.57
0.4903 10.32
0.4924 10.54
0.4944 10.36
0.4958 10.45
0.4986 10.33
0.5000 10.50
0.5028 10.38
0.5063 10.43
0.5083 10.38
0.5104 10.42
0.5118 10.70
0.5139 10.64
0.5160 10.71
0.5174 10.59

2427161 +
0.2993 10.20

0.3014 9.99
0.3035 9.85
0.3063 9.83
0.3083 9.80
0.3104 9.68

2427206 +
0.3306 10.76
0.3326 10.52
0.3347 10.72
0.3368 10.60
0.3389 10.62
0.3417 10.63
0.3438 10.77
0.3458 10.68
0.3734 10.53
0.3764 10.58
0.3785 10.77
0.3806 10.75
0.3826 10.63
0.3847 10.70
0.3868 10.78
0.3889 10.71
0.3910 10.80
0.3924 10.70
0.3944 10.59
0.3965 10.75
0.3986 10.77

2427209 +
0.3292 10.86
0.3306 10.73
0.3326 10.77
0.3340 10.86
0.3368 10.87

0.3389 10.81
0.3403 10.89
0.3424 10.92
0.3438 10.92
0.3465 10.90
0.3479 10.68
0.3500 10.76
0.3528 10.82
0.3542 10.83
0.3556 10.81
0.3576 10.84
0.3590 10.79
0.3611 10.84
0.3632 10.92
0.3653 10.64
0.3681 10.82
0.3736 10.39
0.3764 10.48
0.3778 10.55
0.3792 10.56
0.3806 10.43
0.3833 10.39
0.3854 10.37
0.3868 10.32
0.3889 10.28
0.3910 10.22
0.3931 10.23
0.3944 10.29
0.3958 10.25
0.3979 10.04
0.3993 10.15

2427216 +
0.3493 10.62
0.3514 10.62

0.3535 10.60
0.3563 10.65
0.3583 10.70
0.3604 10.74
0.3625 10.68
0.3653 10.60
0.3667 10.60
0.3694 10.74
0.3715 10.70
0.3736 10.65
0.3757 10.68
0.3778 10.70
0.3799 10.66
0.3819 10.70
0.3847 10.71
0.3868 10.67
0.3889 10.65
0.3910 10.58
0.3931 10.74
0.3951 10.70
0.3979 10.66
0.4000 10.53
0.4021 10.70
0.4042 10.71
0.4069 10.69
0.4090 10.82
0.4111 10.67
0.4139 10.72
0.4160 10.67
0.4215 10.70
0.4236 10.56
0.4257 10.67
0.4278 10.77
0.4306 10.73

0.4326 10.70

2427225 +
0.3618 10.68
0.3639 10.51
0.3660 10.56
0.3681 10.53
0.3701 10.61
0.3729 10.61
0.3750 10.47
0.3771 10.51
0.3792 10.61
0.3819 10.65
0.3840 10.56
0.3868 10.72
0.3896 10.69
0.3917 10.58

2427230 +
0.3694 10.45
0.3715 10.35
0.3736 10.27
0.3764 10.27
0.3799 9.95
0.3833 10.03
0.3868 9.75
0.3896 9.86
0.3931 9.72
0.3965 9.67
0.3995 9.56
0.4021 9.53
0.4049 9.60
0.4111 9.48
0.4132 9.63
0.4153 9.66

0.4174 9.61
0.4201 9.51
0.4243 9.66
0.4271 9.61
0.4306 9.71

2427232 +
0.3542 9.89
0.3563 9.83
0.3590 9.92
0.3611 10.01
0.3639 10.04
0.3660 9.96
0.3681 10.20
0.3694 10.13
0.3715 10.02
0.3736 10.08
0.3764 10.07
0.3778 10.07
0.3806 10.14
0.3826 10.17
0.3854 10.29

2427244 +
0.3806 10.18
0.3833 10.35

2427556 +
0.3229 9.52
0.3250 9.51
0.3271 9.43
0.3292 9.57
0.3313 9.49
0.3333 9.41
0.3361 9.76

Photographic Material

A new 16cm astrograph was installed and extensive photographic observational program was started at Konkoly Observatory in 1934 in order to study the period changes and the light curve variations of RR Lyrae stars. The large focal ratio (f/14) made the telescope very suitable to series of exposures, usually several dozens of exposures were taken on each plate (for detailed description of the instrument and the observational method see Balázs & Detre, 1938).

The photographic observations of XZ Dra was commenced by Júlia Balázs in 1936 and carried out by the staff of the observatory. Until 1945 (between JD 2428356 and 2431708) Eastman 40 photographic plates were used. Later, between 1951 and 1957 (JD 2433896

and 2436142), aged Agfa Astro and Guilleminot Superfulgur plates were only available, therefore these photographic observations had inferior quality.

Throughout the photographic observations of XZ Dra three minutes exposure time was applied. Altogether 4440 utilizable exposures were taken on 188 plates during 100 nights.

Table 2. Comparison stars for photographic measurements

Tycho number	α_{2000} h m s	δ_{2000} ° ′ ″	$B_{\rm T}$ [mag]	$B_{\rm pg}$ [mag]
4224_0047_1	19 04 14.729	+65 12 19.26	9.271	
4224_0467_1	19 06 02.748	+65 26 30.43	11.073	
4224_0561_1	19 04 42.387	+64 53 17.32	10.404	
4224_0631_1	19 04 19.948	+65 25 45.13	11.455	
4224_0695_1	19 05 50.344	+65 36 10.57	10.322	
4224_0849_1	19 04 07.779	+65 02 50.19	9.948	
4224_1255_1	19 04 44.353	+65 01 45.92	9.335	
4224_1781_1	19 05 38.254	+64 27 13.48	9.887	
4224_2009_1	19 08 08.749	+64 22 56.27	9.564	
4225_0056_1	19 12 34.496	+65 22 03.77	10.181	9.80
4225_0117_1	19 11 16.524	+65 19 48.15	11.062	
4225_0141_1	19 16 57.381	+65 10 27.28	10.448	
4225_0197_1	19 16 42.116	+65 33 09.75	10.190	
4225_0404_1	19 16 22.759	+65 07 11.05	11.037	
4225_0419_1	19 09 56.270	+65 23 06.02	10.132	9.63
4225_0622_1	19 10 53.788	+65 31 27.22	10.692	10.39
4225_0742_1	19 11 40.660	+64 52 33.00	11.125	
4225_0931_1	19 09 14.637	+65 11 45.50	9.153	8.74
4225_1010_1	19 15 42.572	+65 07 49.02	9.895	
4225_1029_1	19 09 33.376	+65 19 59.44	10.879	10.51
4225_1096_1	19 11 10.372	+65 14 44.35	11.361	
4225_1323_1	19 10 50.282	+64 51 15.61	11.157	10.85
4229_0479_1	19 13 27.931	+65 41 40.94	10.421	

The plates were digitized by an Umax PowerLook 3000 commercial scanner in 2001, making 1200 dpi 8 bits FITS format output images. This resolution yielded stellar images with 3-5 pixels full width at half maximum (FWHM).

Aperture photometry (IRAF*/DAOPHOT/PHOT) of 23 or less comparison stars and the variable were derived. The comparison stars, covering about 1.5 magnitude range, were chosen among the stars given in Table 2. All those were used which could be measured reliable. Typically at least 15 comparison stars determined the magnitudes of the variable during each observational run.

Tycho $B_{\rm T}$ magnitudes of the comparison stars were adopted (ESA, 1997, Høg *et al.*,

*IRAF is distributed by the NOAO, operated by the Association of Universities for Research in Astronomy Inc., under contract with the NSF.

2000) for transforming the intensities (the plate densities) to magnitudes by fitting third or fourth order polynomials. Six of these comparison stars were originally used to define a photographic sequence. Their photographic $B_{\rm pg}$ magnitudes were determined from two plates of the North Polar Sequence taken in 1936 and 1939. These $B_{\rm pg}$ values (also given in Table 2) define a $0.^{\rm m}35$ brighter magnitude scale than the $B_{\rm T}$ magnitudes (if TYC 4225_0419_1 with its discrepant $0.^{\rm m}5$ magnitude difference is omitted). Thus the final magnitudes were shifted by $0.^{\rm m}35$ in order to match the photographic B scale of the early photographic studies. The errors of the photographic measurements range between $0.^{\rm m}05$ and $0.^{\rm m}20$ depending mostly on the quality of the plate material and its development.

The photographic observations are given in Table 3.

Table 3. Photographic observations of XZ Dra

2428356 +
0.489 10.372
0.491 10.351
0.492 10.403

2428365 +
0.436 9.528
0.439 9.699
0.441 9.669
0.443 9.698
0.445 9.678
0.447 9.753
0.449 9.794
0.451 9.766
0.453 9.842
0.455 9.748
0.457 9.729
0.459 9.746
0.461 9.855
0.464 9.906
0.466 9.971
0.468 9.860
0.470 9.943

2428392 +
0.369 10.712
0.371 10.785
0.373 10.802
0.375 10.712
0.378 10.790
0.382 10.718
0.384 10.777
0.386 10.695
0.388 10.694

2428397 +
0.332 9.726
0.334 9.611
0.336 9.826
0.338 9.840
0.340 9.671
0.342 9.783
0.344 9.791
0.346 9.915
0.348 9.830
0.350 9.760
0.353 9.798
0.355 9.789
0.357 9.788
0.359 9.844
0.362 9.793
0.364 9.850
0.366 10.058
0.368 10.038
0.370 9.935
0.372 9.970
0.374 9.888
0.376 10.003
0.378 10.104
0.380 9.987
0.382 9.928
0.384 9.962

2428402 +
0.451 10.731
0.454 10.786
0.456 10.737
0.469 10.700
0.476 10.760
0.479 10.629
0.481 10.654
0.483 10.607
0.490 10.521
0.492 10.463
0.494 10.474
0.496 10.448
0.498 10.441
0.500 10.406
0.502 10.418
0.504 10.299
0.506 10.350
0.508 10.361
0.510 10.208
0.513 10.247
0.515 10.233
0.517 10.169
0.519 10.183
0.521 10.185

2428404 +
0.445 10.020
0.448 10.025
0.450 9.997
0.452 9.843
0.454 9.930
0.456 9.920
0.458 9.976
0.460 9.878
0.463 9.856
0.465 9.879
0.467 9.846
0.469 9.912
0.471 9.832
0.473 9.868
0.475 9.745
0.477 9.872
0.479 9.895
0.481 9.786
0.483 9.914
0.485 9.887
0.488 9.865
0.490 9.808
0.492 9.896
0.494 9.953
0.496 9.960

2428427 +
0.271 10.999
0.273 10.823
0.275 10.781
0.277 10.564
0.279 10.653
0.281 10.670
0.283 10.665
0.286 10.699
0.288 10.530
0.290 10.626
0.292 10.596
0.294 10.646
0.296 10.586
0.298 10.574
0.300 10.446
0.302 10.368
0.304 10.281
0.306 10.315
0.308 10.225
0.311 10.252
0.313 10.250
0.315 10.049
0.317 10.035
0.319 10.033
0.321 10.009
0.323 9.891

2428431 +
0.368 10.628
0.370 10.579
0.372 10.688
0.374 10.685
0.376 10.640
0.379 10.708
0.381 10.579
0.383 10.691
0.385 10.664
0.387 10.725
0.389 10.721
0.391 10.721
0.393 10.675
0.395 10.700
0.397 10.664
0.399 10.675
0.401 10.718
0.404 10.629
0.406 10.635
0.408 10.681
0.410 10.632
0.412 10.625
0.414 10.620
0.416 10.758
0.418 10.700
0.420 10.797

0.422 10.824
0.424 10.730
0.426 10.621
0.429 10.694
0.431 10.800
0.433 10.712
0.435 10.773
0.437 10.789
0.439 10.633
0.441 10.772
0.443 10.729
0.445 10.783
0.447 10.742
0.449 10.706
0.451 10.749
0.454 10.693
0.456 10.761
0.458 10.810
0.460 10.740
0.462 10.663
0.464 10.714
0.467 10.703
0.470 10.730
0.472 10.739
0.474 10.760
0.476 10.785
0.479 10.785
0.481 10.795
0.483 10.769
0.486 10.758
0.489 10.770
0.491 10.781
0.493 10.764
0.495 10.868
0.499 10.746
0.501 10.850
0.504 10.703
0.506 10.885
0.508 10.737
0.510 10.922
0.512 10.713
0.515 10.738
0.517 10.831

2428784 +
0.335 10.297
0.337 10.257
0.339 10.128
0.341 10.298
0.343 10.271
0.345 10.431
0.347 10.309
0.349 10.316
0.351 10.297
0.353 10.380
0.355 10.351
0.357 10.337
0.360 10.348
0.362 10.330
0.364 10.333
0.366 10.303
0.368 10.292
0.370 10.473
0.372 10.245
0.374 10.418
0.376 10.445
0.378 10.328
0.380 10.480
0.382 10.348
0.385 10.502
0.387 10.390
0.389 10.434
0.391 10.524
0.393 10.374
0.395 10.412
0.397 10.496
0.399 10.557
0.401 10.392
0.403 10.457
0.405 10.664
0.407 10.556
0.410 10.574
0.412 10.493
0.414 10.537
0.416 10.465
0.418 10.530
0.420 10.586
0.422 10.542
0.424 10.691
0.426 10.513
0.428 10.588
0.430 10.628
0.432 10.668
0.435 10.530
0.437 10.507
0.439 10.619
0.441 10.498
0.443 10.720
0.445 10.609
0.447 10.505
0.449 10.577
0.451 10.671
0.453 10.789
0.455 10.615
0.458 10.604
0.460 10.688
0.462 10.669
0.464 10.685
0.466 10.517

2429084 +
0.366 10.505
0.369 10.361
0.371 10.311
0.373 10.202
0.375 10.315
0.377 10.220
0.379 10.159
0.381 10.183
0.383 10.238
0.385 10.086
0.387 10.072
0.389 10.111
0.391 10.073
0.394 10.027
0.396 9.934
0.398 9.988
0.400 9.983
0.402 9.869
0.404 9.858
0.406 9.838
0.408 9.718
0.410 9.681
0.412 9.862
0.414 9.713
0.416 9.770
0.419 9.853
0.421 9.752
0.423 9.652
0.425 9.748
0.428 9.665
0.431 9.801
0.433 9.755
0.435 9.717
0.438 9.823
0.440 9.868
0.442 9.865
0.444 9.854
0.446 9.869
0.448 9.857
0.450 9.814
0.453 9.863
0.455 9.911
0.457 9.970
0.468 9.835
0.470 9.898
0.472 9.803
0.474 9.960
0.476 9.918
0.478 9.941
0.480 9.981
0.482 9.976
0.484 10.078
0.487 10.029
0.489 9.999
0.491 10.039
0.493 10.066
0.512 10.178
0.514 10.231
0.516 10.112
0.518 10.286
0.520 10.202
0.522 10.236
0.524 10.200
0.526 10.331
0.528 10.192
0.530 10.302
0.532 10.226

2429102 +
0.394 10.691
0.396 10.774
0.398 10.692
0.400 10.596
0.402 10.528
0.405 10.808
0.407 10.891
0.421 10.803
0.423 10.711
0.425 10.680
0.427 10.838
0.429 10.711
0.431 10.752
0.433 10.620
0.436 10.922
0.440 10.674
0.442 10.709
0.444 10.719
0.446 10.714
0.449 10.654
0.451 10.644
0.453 10.760
0.455 10.695
0.457 10.766
0.461 10.656
0.463 10.796
0.465 10.543
0.468 10.778
0.470 10.587
0.472 10.629
0.480 10.388
0.483 10.380
0.485 10.236

2429113 +
0.360 10.923
0.362 10.840
0.364 10.755
0.366 10.810
0.368 10.834
0.370 10.822
0.372 10.820
0.374 10.747
0.376 10.884
0.379 10.854
0.381 10.814
0.383 10.901
0.385 10.886
0.387 10.810
0.389 10.919
0.391 10.805
0.393 10.869
0.397 10.774
0.399 10.868
0.401 10.860

0.404 10.919
0.406 10.918
0.408 10.844
0.410 10.795
0.412 10.833
0.414 10.830
0.416 10.669
0.418 10.767
0.422 10.737
0.424 10.823
0.426 10.760
0.429 10.788
0.431 10.690
0.433 10.683
0.435 10.747
0.437 10.643
0.439 10.682
0.441 10.581
0.443 10.455
0.445 10.512
0.447 10.418
0.449 10.449
0.454 10.287
0.456 10.180
0.458 10.060
0.460 10.055
0.462 10.056
0.468 10.008
0.470 9.949
0.472 9.856
0.474 9.842
0.476 9.760
0.479 9.675
0.481 9.744
0.483 9.639
0.485 9.766
0.487 9.702
0.489 9.688
0.491 9.683
0.493 9.799
0.495 9.668
0.497 9.650
0.499 9.663

2429141 +
0.512 10.727
0.514 10.798
0.516 10.838
0.519 10.817
0.521 10.751
0.523 10.772
0.525 10.912
0.527 10.748
0.529 10.816
0.531 10.722
0.533 10.742
0.535 10.825
0.537 10.707
0.539 10.794
0.541 10.594
0.544 10.604
0.546 10.615
0.548 10.466
0.550 10.546
0.552 10.492
0.554 10.439
0.556 10.390
0.558 10.447
0.560 10.357
0.562 10.287
0.564 10.233
0.566 10.221
0.569 10.125
0.571 10.224
0.573 10.135
0.575 10.095
0.577 9.956
0.579 10.014
0.583 9.826
0.585 9.832

2429284 +
0.465 10.935
0.467 10.705
0.469 10.819
0.472 10.779
0.474 10.773
0.476 10.881
0.478 10.856
0.480 10.617
0.482 10.791
0.484 10.707
0.486 10.776
0.488 10.498
0.490 10.733
0.492 10.637
0.494 10.480
0.496 10.768
0.499 10.719
0.501 10.471
0.503 10.574
0.505 10.637
0.507 10.561
0.509 10.473
0.511 10.303
0.513 10.419
0.515 10.467
0.517 10.430
0.520 10.291
0.522 10.303
0.526 10.010
0.532 10.052
0.534 9.979
0.536 9.849
0.538 9.810
0.540 9.857
0.542 9.774
0.546 9.706
0.555 9.407
0.557 9.308
0.559 9.712
0.561 9.367
0.563 9.799
0.565 9.419
0.567 9.731
0.569 9.659
0.571 9.620
0.574 9.733
0.576 9.785
0.578 9.730
0.580 9.854
0.582 9.875
0.584 9.835
0.586 10.058
0.590 9.979
0.593 9.890

2429292 +
0.537 10.856
0.539 10.856
0.541 10.869
0.543 10.658
0.545 10.916
0.547 10.853
0.549 10.947
0.551 10.877
0.553 10.978

2429295 +
0.414 10.812
0.416 10.796
0.418 10.562
0.420 10.792
0.422 10.753
0.424 10.671
0.426 10.737
0.428 10.805
0.430 10.708
0.432 11.002
0.439 10.859
0.441 10.686
0.444 10.968
0.446 10.736
0.448 10.691
0.452 10.722
0.454 10.780
0.456 10.541
0.458 10.644
0.464 10.383
0.466 10.354
0.468 10.439
0.470 10.185
0.472 10.355
0.474 10.046
0.476 10.118
0.478 10.104
0.480 10.160
0.482 9.937
0.489 9.715
0.491 9.828
0.494 9.654
0.496 9.494
0.498 9.690
0.500 9.497
0.502 9.694
0.504 9.731
0.506 9.514
0.508 9.562
0.514 9.489
0.516 9.529
0.519 9.444
0.522 9.535
0.524 9.680
0.526 9.647
0.528 9.443
0.530 9.500
0.532 9.632
0.534 9.722
0.541 9.807
0.543 9.762
0.545 9.864
0.547 9.884
0.549 9.790
0.551 9.953
0.553 9.776
0.555 10.006
0.557 9.862
0.559 9.877
0.565 9.986
0.567 9.891
0.569 9.970
0.571 10.005
0.573 9.921
0.576 9.960
0.578 9.912
0.580 10.011
0.582 9.956
0.584 9.955
0.589 10.025
0.592 10.089
0.594 10.037
0.598 10.136
0.600 10.133
0.602 10.098
0.604 10.108
0.606 10.134
0.608 10.128
0.613 10.146
0.615 10.217
0.617 10.307
0.619 10.125
0.627 10.225
0.629 10.206
0.631 10.166
0.633 10.329

0.635 10.366
0.637 10.164
0.639 10.327
0.642 10.210
0.644 10.351
0.646 10.460
0.648 10.316
0.650 10.273
0.652 10.247
0.654 10.277
0.656 10.357
0.658 10.284
0.660 10.408
0.663 10.394
0.665 10.448
0.667 10.380

2429304 +
0.476 10.810
0.478 10.795
0.480 10.827
0.482 10.674
0.484 10.669
0.486 10.571
0.488 10.783
0.490 10.712
0.492 10.597
0.494 10.602
0.503 10.465
0.505 10.465
0.509 10.400
0.511 10.360
0.513 10.344
0.515 10.229
0.517 10.333
0.519 10.186
0.521 10.062
0.523 10.037

2429365 +
0.483 10.754
0.485 10.849
0.487 10.727
0.489 10.843
0.491 10.793
0.494 10.449
0.496 10.520
0.498 10.502
0.500 10.611
0.502 10.479
0.504 10.388
0.506 10.400
0.509 10.348
0.511 10.293
0.513 10.351
0.515 10.256
0.517 10.316
0.519 10.252
0.521 10.147
0.523 10.099
0.525 10.004
0.528 9.978
0.530 9.878
0.532 9.795
0.534 9.689
0.536 9.783
0.538 9.783
0.540 9.669
0.542 9.617
0.544 9.644
0.546 9.466
0.548 9.627
0.550 9.469
0.553 9.541
0.555 9.516
0.557 9.535
0.559 9.387
0.561 9.471
0.563 9.461
0.565 9.416
0.570 9.486
0.572 9.512
0.574 9.464
0.576 9.482
0.578 9.623
0.580 9.487
0.582 9.586
0.584 9.661
0.587 9.558
0.589 9.629
0.591 9.632
0.593 9.657
0.595 9.756
0.597 9.676
0.600 9.679
0.602 9.785
0.604 9.726
0.606 9.708

2429366 +
0.441 10.728
0.444 10.652
0.446 10.538
0.448 10.700
0.450 10.631
0.453 10.556
0.455 10.514
0.457 10.566
0.459 10.419
0.461 10.485
0.463 10.461
0.465 10.401
0.467 10.351
0.469 10.324
0.471 10.266
0.473 10.189
0.475 10.010
0.478 9.846
0.480 9.917
0.482 9.869
0.484 9.901
0.486 9.740
0.488 9.638
0.490 9.679
0.492 9.620
0.494 9.538
0.496 9.531
0.498 9.507
0.500 9.421
0.505 9.514
0.508 9.516
0.510 9.461
0.512 9.503
0.514 9.468
0.516 9.597
0.519 9.521
0.521 9.526
0.523 9.563
0.525 9.491
0.527 9.698
0.529 9.459
0.531 9.559
0.533 9.548
0.535 9.661
0.537 9.671
0.539 9.658
0.541 9.583
0.544 9.646

2429376 +
0.389 10.891
0.391 10.742
0.393 10.872
0.395 10.877
0.397 10.902
0.399 10.733
0.401 10.728
0.403 10.758
0.405 10.703
0.407 10.853
0.409 10.862
0.412 10.825
0.414 10.822
0.416 10.895
0.418 10.800
0.420 10.788
0.422 10.879
0.424 10.805
0.426 10.855
0.428 10.792
0.430 10.790
0.433 10.798
0.435 10.647
0.437 10.736
0.439 10.629
0.441 10.621
0.444 10.526
0.446 10.536
0.448 10.549
0.450 10.604
0.452 10.434
0.454 10.530
0.456 10.406
0.458 10.401
0.460 10.376
0.462 10.356
0.464 10.341
0.466 10.190
0.469 10.251
0.471 10.077
0.473 10.161
0.475 10.071
0.477 10.079
0.479 9.978
0.481 10.125
0.487 9.776
0.489 9.712
0.491 9.654
0.494 9.742
0.496 9.609
0.498 9.591
0.500 9.662
0.502 9.559
0.504 9.560
0.506 9.628
0.508 9.488
0.510 9.575
0.512 9.576
0.514 9.500
0.516 9.481
0.519 9.705
0.521 9.741
0.523 9.652
0.525 9.626
0.527 9.597
0.529 9.647
0.531 9.547
0.533 9.683
0.535 9.632
0.537 9.578
0.539 9.734
0.541 9.757
0.544 9.746
0.546 9.785
0.548 9.803
0.550 9.882
0.552 9.810
0.554 9.894
0.556 9.762
0.558 9.861
0.560 9.777
0.564 9.800
0.566 9.857
0.569 9.883
0.571 9.919

0.573 9.951
0.575 9.864
0.577 9.910
0.579 10.108
0.581 9.989
0.583 9.981
0.585 9.950

2429377 +
0.333 10.595
0.335 10.740
0.337 10.906
0.339 10.792
0.341 10.748
0.344 10.672
0.346 10.792
0.348 11.098
0.350 10.809
0.352 10.811
0.354 10.833
0.356 10.856
0.358 10.769
0.360 10.987
0.362 10.938
0.364 10.690
0.366 10.640
0.396 10.485
0.398 10.564
0.400 10.508
0.403 10.590
0.405 10.497
0.407 10.497
0.409 10.493
0.411 10.439
0.413 10.159
0.415 10.232
0.417 10.078
0.419 10.209
0.421 10.169
0.423 10.094
0.425 10.078
0.428 10.103
0.430 10.092
0.432 10.081
0.434 9.968
0.436 9.868
0.438 9.881
0.440 9.887
0.442 9.745
0.444 9.635
0.446 9.704
0.448 9.711
0.450 9.671
0.453 9.600
0.455 9.685
0.457 9.586
0.459 9.486
0.464 9.588
0.466 9.681
0.469 9.681
0.471 9.532
0.479 9.629
0.481 9.658
0.483 9.618
0.485 9.732
0.487 9.666
0.489 9.764
0.491 9.772
0.494 9.602
0.496 9.694
0.498 9.681
0.500 9.826
0.502 9.810
0.504 9.873
0.506 9.861
0.508 9.820
0.510 9.789
0.512 9.816
0.514 9.883
0.516 9.881
0.519 9.964
0.521 9.911
0.523 9.995
0.525 9.900
0.527 9.936
0.529 9.930
0.531 9.952
0.533 9.957
0.535 10.083
0.537 10.016
0.539 10.105
0.541 10.134
0.544 10.194
0.546 10.099
0.548 10.007
0.550 9.988
0.552 10.087
0.554 10.099
0.556 10.142
0.558 10.126
0.560 10.156
0.562 10.204
0.564 10.178
0.570 10.285
0.572 10.288
0.574 10.315

2429378 +
0.333 10.720
0.335 10.760
0.338 10.720
0.340 10.780
0.342 10.793
0.344 10.637
0.346 10.539
0.348 10.380
0.350 10.548
0.352 10.500
0.354 10.329
0.356 10.539
0.358 10.651
0.360 10.419
0.363 10.413
0.365 10.310
0.367 10.279
0.369 10.333
0.372 10.314
0.374 10.271
0.376 9.969
0.378 10.068
0.380 10.053
0.382 10.063
0.384 9.926
0.386 10.046
0.388 9.864
0.390 9.824
0.392 9.921
0.394 9.805
0.397 9.776
0.399 9.703
0.401 9.665
0.403 9.850
0.405 9.647
0.407 9.584
0.409 9.710
0.411 9.627
0.413 9.582
0.415 9.695
0.417 9.712
0.419 9.540
0.422 9.657
0.424 9.677
0.426 9.692
0.428 9.789
0.430 9.757
0.432 9.780
0.434 9.571
0.436 9.786
0.438 9.759
0.440 9.675
0.442 9.767
0.444 9.741
0.447 9.856
0.449 9.803
0.454 9.879
0.465 9.852
0.467 9.921
0.469 9.986
0.472 9.767
0.474 9.945
0.476 9.959
0.478 10.043
0.480 9.825
0.482 10.105
0.484 9.850
0.486 10.125
0.488 10.152
0.490 9.991
0.492 10.117
0.494 10.114
0.497 9.926
0.499 9.990
0.501 10.038
0.503 10.149
0.505 10.029
0.507 10.255
0.509 10.164
0.511 10.195
0.513 10.142
0.515 10.144
0.517 10.214
0.519 10.240
0.522 10.214
0.524 10.302
0.526 10.283
0.528 10.305
0.530 10.220
0.532 10.251
0.534 10.302
0.536 10.287
0.538 10.262
0.540 10.388
0.542 10.307
0.544 10.296
0.547 10.220
0.549 10.422
0.551 10.550
0.553 10.384
0.555 10.462
0.557 10.238
0.559 10.385
0.561 10.353
0.563 10.387
0.565 10.505
0.567 10.494
0.569 10.448
0.572 10.434
0.574 10.504
0.576 10.418

2429449 +
0.364 10.466
0.366 10.419
0.368 10.407
0.370 10.397
0.372 10.282
0.374 10.190
0.376 10.091
0.378 10.109
0.380 10.105
0.382 9.902
0.387 9.846
0.389 9.788
0.391 9.791
0.394 9.736

0.396 9.769
0.398 9.635
0.400 9.617
0.402 9.565
0.404 9.639
0.406 9.646
0.412 9.564
0.414 9.532
0.416 9.654
0.418 9.631
0.420 9.647
0.422 9.552
0.424 9.583
0.426 9.680
0.428 9.689
0.430 9.672
0.435 9.709
0.437 9.651
0.439 9.658
0.441 9.705
0.443 9.699
0.445 9.800
0.447 9.800
0.449 9.811
0.451 9.822
0.453 9.778

2429458 +
0.370 10.772
0.372 10.753
0.374 10.779
0.376 10.788
0.378 10.746
0.381 10.906
0.383 10.715
0.385 10.767
0.387 10.667
0.389 10.540
0.391 10.545
0.393 10.581
0.395 10.639
0.397 10.438
0.399 10.595
0.401 10.482
0.403 10.418
0.406 10.359
0.408 10.369
0.410 10.398
0.412 10.506
0.414 10.402
0.416 10.213
0.418 10.332
0.420 10.404
0.422 10.164
0.424 10.221
0.426 10.251
0.428 10.198
0.431 10.236
0.433 10.091
0.435 10.097
0.437 10.017
0.440 9.894
0.446 9.756
0.448 9.877
0.450 9.902
0.452 9.702
0.454 9.827
0.456 9.748
0.458 9.740
0.460 9.700
0.462 9.767
0.465 9.742
0.467 9.671
0.469 9.727
0.471 9.868
0.473 9.849
0.475 9.794
0.477 9.773
0.479 9.741
0.481 9.803
0.483 9.871
0.489 9.765
0.491 9.926
0.493 9.772
0.495 9.734
0.498 9.999
0.500 9.933
0.502 9.782
0.504 9.964
0.506 9.944
0.508 9.761
0.510 9.914
0.512 10.049
0.514 10.057
0.517 10.054
0.519 9.993
0.521 9.978
0.523 9.993
0.525 9.991
0.527 9.985

2429465 +
0.425 10.836
0.427 10.711
0.429 10.864
0.431 10.893
0.433 10.886
0.435 10.766
0.438 10.865

2429467 +
0.431 10.556
0.433 10.650
0.435 10.625
0.438 10.529
0.440 10.582
0.442 10.645
0.444 10.675
0.446 10.441
0.448 10.579
0.450 10.375
0.452 10.397
0.454 10.444
0.456 10.343
0.458 10.402

2429468 +
0.420 10.171
0.422 10.394
0.424 10.294
0.426 10.261
0.429 10.077
0.431 10.177
0.433 10.011
0.435 10.022
0.437 10.012
0.439 10.003
0.441 9.922
0.443 10.053
0.447 10.019
0.449 9.899
0.451 9.743
0.454 9.810
0.456 9.903
0.458 9.788
0.460 9.784
0.462 9.924
0.464 9.909
0.472 9.882
0.474 9.913
0.476 9.898
0.479 9.801
0.481 9.868
0.483 9.885
0.485 9.802
0.489 9.794
0.491 9.951
0.493 9.925
0.495 9.918
0.497 9.919
0.499 9.957
0.501 9.855
0.504 9.884
0.506 10.018
0.508 9.991
0.510 10.024
0.512 10.041
0.514 9.975
0.516 10.000
0.518 10.023
0.520 10.047
0.522 10.087
0.524 9.932
0.526 10.043
0.529 10.053
0.533 10.000
0.535 10.253
0.537 10.150
0.539 10.258

2429518 +
0.305 10.747
0.307 10.656
0.309 10.656
0.312 10.657
0.314 10.747
0.316 10.649
0.318 10.692
0.320 10.584
0.322 10.724
0.324 10.568
0.326 10.819
0.328 10.833
0.330 10.887
0.332 10.732
0.334 10.784
0.337 10.784
0.339 10.828
0.341 10.686
0.343 10.763
0.345 10.661
0.347 10.725
0.349 10.658
0.351 10.850
0.353 10.723
0.355 10.856
0.357 10.846
0.359 10.855
0.362 10.912
0.364 10.660
0.366 10.656
0.368 10.926
0.370 10.860
0.372 10.658
0.374 10.654
0.376 10.757
0.378 10.783
0.380 10.930
0.382 10.759
0.384 10.852
0.387 10.663
0.389 10.751
0.391 10.896
0.393 10.684
0.395 10.855
0.397 10.734
0.399 10.800
0.401 10.896
0.403 10.829
0.405 10.898
0.407 10.868
0.409 10.859
0.412 10.959
0.414 10.776
0.416 10.837
0.418 10.791

0.420 10.881
0.422 10.763
0.428 10.726
0.430 10.879
0.432 10.832
0.434 10.889
0.437 10.884
0.439 10.775
0.441 10.802
0.443 10.772
0.446 10.832
0.448 10.726
0.450 10.634
0.452 10.652
0.454 10.632
0.456 10.596
0.458 10.541
0.460 10.345
0.462 10.267
0.464 10.387
0.466 10.219
0.469 10.109
0.471 10.200
0.473 10.189
0.475 10.227
0.477 9.994
0.479 10.050
0.481 9.939
0.483 10.036
0.485 9.844
0.487 9.858
0.489 9.738
0.491 9.665
0.494 9.663
0.496 9.644
0.498 9.528
0.500 9.773
0.503 9.630
0.505 9.757
0.507 9.711
0.509 9.675
0.511 9.667

2429519 +
0.366 11.025
0.369 10.972
0.371 10.833
0.373 10.758
0.375 10.842
0.377 10.964
0.379 10.864
0.381 10.999
0.383 10.916
0.385 10.688
0.387 10.715
0.389 10.674
0.390 10.812
0.391 10.675
0.394 10.762
0.396 10.540
0.398 10.504
0.400 10.702
0.402 10.576
0.404 10.646
0.406 10.416
0.408 10.597
0.410 10.404
0.412 10.626
0.414 10.441
0.416 10.309
0.419 10.305
0.421 10.195
0.423 10.330
0.425 10.128
0.427 10.125
0.429 10.014
0.431 9.970
0.433 9.955
0.435 9.931
0.437 9.958
0.439 9.881
0.441 9.747
0.444 9.789
0.446 9.681
0.448 9.756
0.450 9.751
0.452 9.677
0.454 9.570
0.456 9.577
0.458 9.524
0.460 9.569
0.462 9.498
0.464 9.498
0.466 9.579
0.468 9.559
0.471 9.626
0.473 9.803
0.475 9.590
0.477 9.631
0.479 9.610
0.481 9.594
0.483 9.663
0.485 9.720
0.487 9.786
0.489 9.683
0.491 9.878
0.494 9.731
0.496 9.704
0.498 9.819
0.500 9.776

2429520 +
0.285 10.907
0.287 10.865
0.289 10.840
0.291 10.821
0.294 10.812
0.296 10.968
0.298 10.820
0.300 10.757
0.302 10.927
0.304 10.830
0.306 10.799
0.308 10.947
0.310 10.853
0.312 10.724
0.314 10.838
0.316 10.781
0.319 10.807
0.321 10.740
0.323 10.830
0.325 10.848
0.327 10.740
0.329 10.904
0.331 10.893
0.333 10.756
0.335 10.689
0.337 10.598
0.339 10.791
0.341 10.775
0.344 10.735
0.346 10.582
0.348 10.588
0.350 10.637
0.352 10.551
0.354 10.577
0.356 10.539
0.358 10.361
0.360 10.486
0.362 10.333
0.364 10.338
0.366 10.317
0.369 10.404
0.371 10.203
0.373 10.205
0.375 10.243
0.380 10.073
0.382 10.122
0.389 9.984
0.391 9.867
0.394 9.792
0.396 9.737
0.398 9.928
0.400 9.627
0.402 9.711
0.404 9.687
0.406 9.770
0.408 9.736
0.410 9.731
0.412 9.704
0.414 9.811
0.439 9.798
0.441 9.775
0.444 9.760
0.446 9.848
0.448 9.803
0.450 9.832
0.452 9.924
0.454 9.926
0.456 9.941
0.458 10.077
0.460 9.998
0.462 9.931
0.464 9.989
0.466 9.984

2429527 +
0.369 10.795
0.371 10.811
0.373 10.770
0.375 10.712
0.377 10.914
0.379 10.815
0.381 10.837
0.383 10.805
0.385 10.791
0.387 10.655
0.389 10.730
0.391 10.673
0.393 10.892
0.396 10.615
0.398 10.616
0.400 10.668
0.402 10.775
0.404 10.604
0.406 10.690
0.408 10.774
0.410 10.666
0.412 10.440
0.414 10.561
0.416 10.729
0.422 10.771
0.425 10.808
0.427 10.868
0.429 10.689
0.431 10.713
0.433 10.733
0.435 10.788
0.437 10.766
0.439 10.771
0.441 10.797
0.444 10.789
0.446 10.732
0.448 10.784
0.450 10.909
0.452 10.850
0.454 10.857
0.456 10.780
0.458 10.854
0.460 10.864
0.462 10.835
0.464 10.935
0.466 10.746
0.469 10.611
0.471 10.584

0.473 10.731
0.475 10.770
0.477 10.823
0.479 10.828
0.481 10.813
0.483 10.853
0.485 10.574
0.487 10.638
0.489 10.735
0.491 10.559
0.494 10.763
0.496 10.537
0.498 10.311
0.500 10.581
0.502 10.440
0.504 10.319
0.510 10.223
0.512 10.304
0.514 10.160
0.516 10.352
0.518 10.047
0.521 10.002
0.523 10.219
0.525 9.896
0.527 10.095
0.529 10.007
0.531 9.867
0.533 9.858
0.535 9.870
0.537 9.967
0.539 9.896
0.541 9.728
0.544 9.696
0.546 9.731
0.548 9.747
0.550 9.820
0.552 9.843
0.554 9.732
0.556 9.855
0.558 9.741
0.560 9.821
0.562 9.857
0.564 9.875
0.566 9.856
0.569 9.774
0.571 9.875
0.573 9.834
0.575 9.837
0.577 9.992
0.579 10.085
0.581 9.842
0.583 9.717
0.585 10.141
0.587 9.921
0.589 9.799
0.591 9.685
0.594 9.908
0.596 9.976
0.598 9.913
0.600 10.009
0.602 10.033
0.604 10.008
0.606 10.067
0.608 10.169
0.610 10.061

2429546 +
0.323 10.610
0.325 10.537
0.327 10.622
0.329 10.609
0.331 10.698
0.333 10.653
0.335 10.567
0.337 10.559
0.339 10.614
0.341 10.637
0.344 10.586
0.346 10.479
0.348 10.625
0.350 10.582
0.352 10.513
0.354 10.606
0.356 10.686
0.358 10.741
0.360 10.560
0.362 10.648
0.364 10.704
0.366 10.587
0.369 10.675
0.371 10.664
0.373 10.771
0.375 10.623
0.377 10.855
0.379 10.788
0.381 10.905
0.385 10.711
0.387 10.773
0.389 10.835
0.391 10.708
0.394 10.643
0.396 10.668
0.398 10.882
0.400 10.534
0.402 10.630
0.404 10.756
0.406 10.514
0.408 10.587
0.410 10.635
0.412 10.604
0.414 10.723
0.416 10.867
0.419 10.711
0.421 10.827
0.423 10.561
0.425 10.802
0.427 10.459
0.429 10.503
0.431 10.682
0.433 10.628
0.435 10.490
0.437 10.758
0.439 10.560
0.441 10.453
0.443 10.622

2429551 +
0.388 9.825
0.390 9.757
0.392 9.759
0.394 9.833
0.396 9.855
0.398 9.719
0.400 9.849
0.402 9.877
0.405 9.891
0.407 9.853
0.409 9.893
0.411 10.001
0.413 9.940
0.415 9.980
0.417 9.983
0.419 9.966
0.421 9.939
0.423 10.131
0.425 10.114
0.427 10.064
0.429 10.032
0.432 10.020
0.434 10.051
0.436 10.064
0.438 10.042
0.440 10.006
0.442 10.050
0.444 10.072
0.446 10.201
0.448 10.157

2429607 +
0.244 10.635
0.246 10.769
0.248 10.601
0.251 10.625
0.253 10.715
0.255 10.551
0.257 10.817
0.259 10.553
0.261 10.787
0.263 10.464
0.265 10.590
0.267 10.592
0.269 10.795
0.271 10.757
0.273 10.729
0.276 10.794
0.278 10.691
0.280 10.761
0.282 10.690
0.284 10.863
0.286 10.759
0.288 10.761
0.290 10.525
0.292 10.927
0.294 10.747
0.296 10.775
0.298 10.705
0.301 10.887
0.305 10.662
0.307 10.795
0.309 10.688
0.311 10.839
0.313 10.797
0.337 10.326
0.339 10.244
0.341 10.545
0.343 10.297
0.345 10.301
0.347 10.446
0.349 10.212
0.351 10.513
0.354 10.414
0.356 10.457
0.358 10.489
0.360 10.447
0.362 10.438
0.364 10.446
0.367 10.453
0.369 10.472
0.371 10.469
0.373 10.519
0.375 10.523
0.377 10.539
0.379 10.697
0.381 10.587
0.383 10.498
0.385 10.649
0.387 10.637
0.389 10.539
0.392 10.685
0.394 10.622
0.396 10.565
0.398 10.656
0.400 10.872
0.402 10.479
0.404 10.779
0.406 10.421

2429690 +
0.532 9.892
0.534 9.697
0.537 9.765
0.539 9.749
0.541 9.718
0.543 9.804
0.546 9.784

0.548 9.910
0.550 9.842
0.552 9.936
0.555 9.930
0.557 9.930
0.559 9.949
0.561 9.775
0.563 10.019
0.565 10.082
0.567 9.927
0.569 9.955
0.571 10.137
0.573 9.920
0.575 9.995
0.578 10.023
0.580 10.058
0.582 9.991
0.584 9.957
0.586 9.969
0.588 10.024
0.590 10.150
0.592 10.044
0.594 10.123
0.596 10.108
0.598 10.131
0.600 10.093
0.603 10.128
0.605 10.125
0.607 10.148
0.609 10.165
0.611 10.203
0.613 10.203
0.615 10.215
0.617 10.218
0.619 10.243
0.621 10.257
0.623 10.353
0.625 10.426
0.628 10.344
0.630 10.245
0.632 10.326

2429691 +
0.447 9.892
0.449 9.977
0.451 9.930
0.453 9.922
0.455 9.810
0.457 9.781
0.459 9.828
0.462 9.921
0.464 9.850
0.466 9.843
0.468 9.751
0.470 9.831
0.472 9.760
0.474 9.838
0.476 9.956
0.478 9.872
0.480 9.851
0.482 9.803
0.484 9.897
0.487 9.837
0.489 9.840
0.491 9.953
0.493 9.967
0.495 9.878
0.498 9.901
0.500 9.958
0.502 9.887
0.504 9.933
0.506 10.010
0.508 10.007
0.510 9.980
0.512 9.926
0.514 10.033
0.516 10.024
0.519 10.030
0.521 10.066
0.523 10.060
0.525 10.077
0.527 10.081
0.529 10.089
0.531 10.024
0.533 10.063
0.535 10.095
0.537 10.104
0.539 10.149
0.541 10.179
0.544 10.166
0.546 10.147
0.550 10.088
0.552 10.138
0.554 10.249
0.556 10.227
0.558 10.148
0.560 10.242
0.562 10.210
0.564 10.237
0.567 10.227
0.569 10.231
0.571 10.262

2429699 +
0.514 10.407
0.516 10.300
0.518 10.246
0.520 10.233
0.522 10.141
0.525 10.088
0.527 10.100
0.529 10.061
0.531 9.935
0.533 10.035
0.535 10.022
0.537 10.006
0.539 9.906
0.541 9.951
0.543 9.880
0.545 9.960
0.547 9.819
0.550 9.815
0.552 9.829
0.554 9.724
0.556 9.737
0.558 9.750
0.560 9.631
0.562 9.691
0.564 9.697
0.566 9.526
0.568 9.664
0.570 9.648
0.572 9.576
0.575 9.658
0.577 9.652
0.579 9.780
0.581 9.694
0.583 9.674
0.585 9.647
0.587 9.609
0.589 9.727
0.591 9.832
0.593 9.729
0.595 9.722
0.597 9.711
0.600 9.861
0.602 9.877
0.604 9.900
0.606 9.910
0.608 10.011
0.610 9.920
0.612 9.930
0.614 9.940
0.616 9.904
0.618 9.894
0.620 9.942
0.622 9.955
0.625 10.054
0.627 10.129
0.629 10.115
0.631 10.075
0.633 10.089

2429701 +
0.396 10.655
0.398 10.737
0.400 10.625
0.402 10.593
0.404 10.494
0.406 10.690
0.408 10.553
0.410 10.535
0.412 10.505
0.414 10.623
0.416 10.481
0.418 10.551
0.421 10.473
0.423 10.455
0.425 10.387
0.427 10.285
0.429 10.392
0.431 10.287
0.433 10.260
0.435 10.128
0.437 10.171
0.439 10.128
0.441 10.083
0.444 10.138
0.446 10.107
0.448 9.952
0.450 10.001
0.452 9.977
0.458 9.911
0.460 9.840
0.462 9.849
0.464 9.868
0.466 9.735
0.469 9.726
0.471 9.763
0.473 9.787
0.475 9.730
0.477 9.723
0.479 9.753
0.481 9.736
0.483 9.775
0.485 9.783
0.487 9.760
0.489 9.745
0.491 9.758
0.494 9.766
0.496 9.782
0.498 9.881
0.500 9.941
0.502 9.901
0.504 9.868
0.506 9.826
0.508 9.854
0.510 9.939
0.512 9.935
0.514 9.923
0.516 9.984
0.519 9.927
0.521 9.957
0.523 9.974
0.525 9.957
0.527 9.970
0.529 10.014
0.531 10.013
0.533 10.077
0.535 10.030
0.537 10.083
0.539 9.986
0.541 10.149
0.544 10.009
0.546 10.039

0.548 10.056

2429720 +
0.486 10.413
0.488 10.440
0.490 10.355
0.492 10.418
0.494 10.344
0.496 10.105
0.498 10.152
0.500 10.100
0.503 10.110
0.505 10.011
0.507 9.847
0.509 9.855
0.511 9.586
0.513 9.696
0.515 9.557
0.517 9.506
0.519 9.547
0.521 9.500
0.523 9.411
0.525 9.553
0.528 9.437
0.530 9.430
0.532 9.413
0.534 9.437
0.536 9.474
0.538 9.420
0.540 9.497
0.542 9.484
0.544 9.471
0.546 9.516
0.548 9.611
0.550 9.622
0.553 9.658
0.555 9.619
0.557 9.676
0.559 9.682
0.561 9.531
0.563 9.738
0.565 9.685
0.567 9.702
0.569 9.838
0.571 9.825
0.573 9.767
0.575 9.720

2429721 +
0.432 10.549
0.434 10.595
0.438 10.450
0.440 10.372
0.442 10.384
0.444 10.442
0.446 10.407
0.448 10.451
0.450 10.373
0.453 10.220
0.455 10.163
0.457 9.858
0.459 9.789
0.461 9.839
0.463 9.714
0.465 9.703
0.467 9.627
0.469 9.645
0.471 9.551
0.473 9.661
0.475 9.667
0.478 9.505
0.480 9.458
0.482 9.462
0.484 9.489
0.486 9.387
0.488 9.603
0.490 9.562
0.492 9.603
0.494 9.625
0.496 9.569
0.498 9.593
0.500 9.550
0.503 9.542
0.505 9.681
0.507 9.634
0.509 9.551
0.511 9.588
0.513 9.545
0.515 9.569
0.517 9.606
0.519 9.815
0.521 9.749
0.523 9.792
0.525 9.750
0.528 9.723

0.530 9.737

2429730 +
0.532 9.592
0.534 9.489
0.536 9.500
0.538 9.393
0.540 9.392
0.543 9.286
0.545 9.338
0.547 9.378
0.549 9.376
0.551 9.393
0.553 9.457
0.555 9.474
0.557 9.507
0.559 9.576
0.561 9.507
0.563 9.456
0.566 9.526
0.568 9.404
0.570 9.485
0.572 9.519
0.574 9.532
0.576 9.572
0.578 9.752
0.580 9.614
0.582 9.617
0.590 9.765
0.592 9.900
0.594 10.128
0.596 9.628
0.598 9.918
0.600 9.903
0.602 9.893
0.605 10.174
0.607 10.004

2429732 +
0.389 10.735
0.392 10.736
0.394 10.696
0.396 10.548
0.398 10.576
0.400 10.377
0.402 10.673
0.404 10.585

0.406 10.444
0.408 10.490
0.410 10.423
0.412 10.203
0.414 10.259
0.417 10.233
0.419 10.204
0.421 10.201
0.423 10.055
0.425 9.864
0.428 9.837
0.430 9.759
0.432 9.594
0.434 9.707
0.436 9.553
0.438 9.690
0.440 9.659
0.442 9.652
0.444 9.634
0.446 9.581
0.448 9.610
0.451 9.438
0.453 9.506
0.455 9.557
0.457 9.532
0.459 9.575
0.461 9.532
0.463 9.564
0.465 9.596
0.467 9.603
0.469 9.690
0.471 9.613
0.473 9.684
0.476 9.640
0.478 9.678
0.480 9.650
0.482 9.734
0.484 9.765
0.486 9.682
0.488 9.743
0.490 9.746
0.500 9.771
0.503 9.849
0.505 9.778
0.507 9.860
0.509 9.908
0.511 10.086

0.513 9.915
0.515 9.857
0.517 9.966
0.519 9.921
0.521 9.955
0.523 9.994
0.525 9.955
0.528 10.045
0.530 9.943
0.532 10.032
0.534 9.946
0.536 10.078
0.538 10.026
0.540 10.046
0.542 10.289
0.544 10.434
0.546 10.348
0.548 10.347
0.550 10.614
0.552 10.372
0.554 10.393
0.556 10.550
0.558 10.555
0.560 10.390

2429734 +
0.323 10.411
0.325 10.135
0.327 10.137
0.329 10.113
0.331 9.894
0.333 9.785
0.335 9.719
0.337 9.688
0.339 9.529
0.342 9.609
0.344 9.443
0.346 9.449
0.348 9.462
0.351 9.464
0.353 9.450
0.356 9.464
0.358 9.473
0.360 9.565
0.362 9.525
0.365 9.527
0.367 9.589

0.369 9.519
0.371 9.555
0.373 9.646
0.375 9.621
0.377 9.663
0.379 9.631
0.381 9.650
0.383 9.660
0.385 9.628
0.387 9.628
0.390 9.672

2430433 +
0.426 10.036
0.428 9.992

2430443 +
0.509 10.314
0.511 10.416
0.513 10.284
0.515 10.293
0.517 10.359
0.519 10.306
0.521 10.400
0.523 10.449
0.525 10.206
0.527 10.369
0.529 10.496
0.531 10.308
0.533 10.468
0.535 10.356
0.538 10.456
0.540 10.429
0.542 10.462
0.544 10.411

2430444 +
0.447 10.253
0.449 10.295
0.451 10.197
0.453 10.315
0.455 10.313
0.457 10.248
0.459 10.363
0.461 10.405
0.463 10.436
0.465 10.356
0.467 10.335
0.469 10.496
0.472 10.392
0.474 10.367
0.476 10.457
0.478 10.417
0.480 10.401
0.482 10.434
0.484 10.401
0.488 10.493
0.490 10.354
0.492 10.432
0.494 10.441
0.496 10.445
0.498 10.409
0.500 10.410
0.502 10.430
0.504 10.472
0.506 10.476
0.508 10.461
0.510 10.444
0.513 10.518
0.515 10.393
0.517 10.616
0.519 10.516
0.521 10.510
0.525 10.468
0.527 10.376
0.531 10.509
0.533 10.600
0.535 10.487
0.537 10.511
0.540 10.510
0.542 10.555
0.544 10.505
0.546 10.600
0.548 10.666
0.550 10.699
0.552 10.684
0.554 10.618
0.556 10.550
0.558 10.725
0.560 10.802
0.562 10.723
0.564 10.658
0.567 10.684
0.569 10.616
0.573 10.589
0.575 10.650
0.577 10.662
0.579 10.611
0.581 10.691
0.583 10.824
0.585 10.659
0.587 10.792
0.590 10.604
0.592 10.701
0.596 10.658
0.598 10.627
0.600 10.654
0.602 10.716
0.604 10.717
0.606 10.670
0.608 10.706
0.610 10.767
0.612 10.712
0.615 10.667
0.617 10.742
0.619 10.720
0.621 10.731
0.623 10.700
0.625 10.733
0.627 10.713
0.629 10.750
0.631 10.642
0.633 10.678
0.635 10.706

2430467 +
0.311 10.214
0.313 10.231
0.315 10.210
0.317 10.134
0.319 10.267
0.322 10.155
0.324 10.198
0.326 10.228
0.328 10.185
0.330 10.304
0.332 10.225
0.334 10.283
0.336 10.365
0.338 10.352
0.340 10.401
0.343 10.412
0.345 10.386
0.347 10.472
0.349 10.453
0.394 10.551
0.396 10.610
0.398 10.582
0.400 10.568
0.402 10.666
0.404 10.642
0.406 10.589
0.408 10.703
0.410 10.623
0.413 10.620
0.415 10.668
0.417 10.671
0.419 10.674
0.421 10.616
0.423 10.683
0.425 10.670
0.427 10.669
0.429 10.631
0.431 10.605
0.433 10.705

2430514 +
0.371 9.786
0.373 9.756
0.375 9.762
0.377 9.661
0.379 9.629
0.381 9.708
0.383 9.604
0.385 9.710
0.387 9.710
0.389 9.665
0.391 9.693
0.393 9.600
0.395 9.671
0.398 9.602
0.400 9.738
0.402 9.626
0.404 9.752
0.406 9.724
0.408 9.783
0.410 9.680
0.412 9.716
0.414 9.838
0.416 9.659
0.418 9.787
0.420 9.740
0.423 9.757
0.425 9.813
0.427 9.752
0.429 9.868
0.431 9.872
0.433 9.856
0.435 9.906

2431330 +
0.334 10.549
0.336 10.624
0.338 10.616
0.340 10.599
0.342 10.494
0.344 10.533
0.346 10.570
0.348 10.495
0.350 10.501
0.352 10.553
0.354 10.662
0.357 10.580
0.359 10.566
0.361 10.594
0.363 10.715
0.368 10.706
0.370 10.642
0.372 10.616
0.375 10.625
0.377 10.621
0.379 10.667
0.381 10.699
0.383 10.777
0.385 10.721
0.387 10.676
0.390 10.869
0.392 10.572
0.394 10.700
0.396 10.707
0.398 10.713
0.400 10.555
0.402 10.632
0.404 10.729
0.407 10.764
0.409 10.572

0.414 10.681
0.416 10.703
0.418 10.662
0.420 10.578
0.422 10.594
0.425 10.797
0.427 10.791
0.431 10.799
0.433 10.679
0.435 10.706
0.437 10.638
0.439 10.753
0.441 10.698
0.443 10.761
0.445 10.776
0.447 10.578
0.450 10.630
0.452 10.788
0.454 10.761
0.456 10.797
0.458 10.744
0.460 10.652
0.462 10.744
0.464 10.822
0.466 10.653
0.468 10.718
0.470 10.759
0.472 10.689
0.475 10.698
0.482 10.726
0.484 10.771
0.486 10.644
0.488 10.637
0.490 10.847
0.492 10.789
0.494 10.695
0.496 10.734
0.498 10.898
0.500 10.851
0.502 10.616
0.504 10.608
0.507 10.738
0.509 10.922
0.511 10.867
0.513 10.699
0.515 10.737
0.517 10.865

0.519 10.751
0.521 10.739
0.523 10.759
0.525 10.812
0.527 10.780
0.529 10.849
0.532 10.929
0.534 10.811
0.536 10.873
0.538 10.845
0.540 10.773
0.542 10.876
0.544 10.772
0.546 10.793
0.548 10.732
0.550 10.668
0.552 10.898
0.554 10.842
0.557 10.754
0.559 10.657
0.561 10.760
0.563 10.723
0.565 10.609
0.567 10.579
0.569 10.729
0.571 10.655
0.573 10.550
0.575 10.542
0.577 10.488
0.579 10.371
0.582 10.461
0.584 10.373

2431331 +
0.344 10.668
0.346 10.627
0.348 10.713
0.350 10.725
0.352 10.727
0.354 10.761
0.357 10.674
0.359 10.658
0.361 10.690
0.363 10.675
0.368 10.683
0.370 10.690
0.372 10.747

0.374 10.686
0.376 10.653
0.378 10.682
0.380 10.651
0.382 10.655
0.384 10.655
0.386 10.761
0.392 10.751
0.394 10.572
0.396 10.662
0.398 10.765
0.400 10.633
0.402 10.741
0.405 10.708
0.407 10.663
0.409 10.737
0.411 10.716
0.413 10.712
0.415 10.751
0.417 10.752
0.419 10.696
0.421 10.677
0.426 10.648
0.428 10.692
0.430 10.641
0.432 10.668
0.434 10.754
0.436 10.737
0.438 10.707
0.440 10.719
0.443 10.766
0.445 10.639
0.447 10.779
0.449 10.760
0.451 10.811
0.453 10.722
0.455 10.809
0.457 10.737
0.459 10.725
0.461 10.779
0.463 10.821
0.466 10.773
0.471 10.775
0.473 10.737
0.475 10.807
0.477 10.830
0.480 10.840

0.482 10.734
0.484 10.749
0.486 10.857
0.488 10.811
0.490 10.856
0.492 10.651
0.494 10.848
0.496 10.914
0.498 10.774
0.500 10.817
0.502 10.735
0.504 10.731
0.507 10.879
0.509 10.779
0.511 10.711
0.513 10.694
0.515 10.770
0.517 10.724
0.519 10.729
0.521 10.617
0.523 10.538
0.525 10.558
0.527 10.561
0.530 10.571
0.532 10.508
0.534 10.466
0.536 10.478
0.538 10.479
0.540 10.441
0.544 10.268
0.546 10.230
0.548 10.003
0.550 10.138
0.552 10.123
0.555 10.117
0.557 9.992
0.559 10.007
0.561 10.005
0.563 9.900
0.565 9.830
0.567 9.785
0.569 9.812
0.571 9.727
0.573 9.805

2431347 +
0.274 10.113

0.276 10.046
0.278 9.989
0.280 9.946
0.282 9.944
0.284 9.925
0.286 9.883
0.288 9.900
0.290 9.855
0.292 9.739
0.294 9.799
0.419 10.411
0.421 10.399
0.423 10.370
0.425 10.332
0.427 10.411
0.429 10.353
0.431 10.468
0.433 10.306
0.435 10.457
0.437 10.402
0.439 10.404
0.442 10.447
0.444 10.456
0.446 10.482
0.448 10.524
0.450 10.477
0.452 10.374
0.454 10.485
0.456 10.571
0.461 10.519
0.463 10.608
0.465 10.363
0.467 10.547
0.469 10.624
0.471 10.480
0.474 10.649
0.476 10.610
0.478 10.633
0.480 10.475
0.482 10.516
0.484 10.571
0.486 10.456
0.488 10.532
0.490 10.602
0.492 10.607
0.494 10.558
0.496 10.546

0.498 10.711
0.501 10.568
0.503 10.706
0.505 10.574
0.507 10.664
0.509 10.620
0.511 10.589
0.513 10.660
0.515 10.628
0.517 10.601
0.519 10.560
0.521 10.673
0.523 10.660
0.526 10.525
0.528 10.645
0.530 10.786
0.532 10.759
0.534 10.702
0.536 10.619
0.538 10.608
0.540 10.763
0.542 10.763
0.544 10.734
0.546 10.660
0.548 10.675
0.551 10.678
0.553 10.816
0.555 10.513
0.557 10.542
0.559 10.682
0.561 10.817
0.563 10.662
0.565 10.626
0.567 10.727
0.569 10.849
0.571 10.744
0.573 10.684
0.576 10.514
0.578 10.643
0.580 10.646
0.582 10.735
0.584 10.643

2431349 +
0.271 10.094
0.273 10.192
0.275 10.087
0.277 10.104
0.279 10.129
0.281 10.188
0.283 10.146
0.285 10.138
0.287 10.143
0.289 10.205
0.292 10.149
0.294 10.119
0.296 10.238
0.298 10.333
0.336 10.290
0.338 10.402
0.340 10.434
0.342 10.397
0.344 10.321
0.346 10.389
0.348 10.336
0.351 10.443
0.353 10.384
0.355 10.461
0.357 10.524
0.359 10.487
0.361 10.439
0.363 10.537
0.365 10.494
0.367 10.499
0.369 10.509
0.371 10.416
0.373 10.547
0.376 10.612
0.384 10.463
0.386 10.564
0.388 10.557
0.390 10.637
0.392 10.515
0.394 10.549
0.396 10.496
0.398 10.497
0.401 10.505
0.403 10.473
0.405 10.631
0.407 10.642
0.409 10.563
0.411 10.666
0.413 10.517
0.415 10.644
0.417 10.653
0.419 10.829
0.421 10.716
0.423 10.487
0.426 10.664
0.428 10.604
0.430 10.749
0.438 10.691
0.440 10.609
0.442 10.632
0.444 10.604
0.446 10.756
0.448 10.709
0.451 10.872
0.453 10.692
0.455 10.829
0.457 10.827
0.459 10.687
0.461 10.603
0.463 10.824
0.465 10.591
0.467 10.782
0.469 10.776
0.471 10.623
0.473 10.695
0.476 10.670
0.478 10.845
0.480 10.721
0.482 10.668
0.485 10.687

2431350 +
0.474 10.879
0.476 10.796
0.478 10.742
0.480 10.779
0.482 10.844
0.485 10.815
0.487 10.796
0.489 10.805
0.491 10.821
0.493 10.817
0.495 10.804
0.497 10.822
0.499 10.812
0.501 10.740
0.503 10.853
0.505 10.887
0.507 10.739
0.510 10.872
0.514 10.876
0.516 10.851
0.518 10.740
0.520 10.810
0.522 10.728
0.524 10.721
0.526 10.827
0.528 10.866
0.530 10.751
0.532 10.788
0.535 10.628
0.537 10.742
0.539 10.656
0.541 10.761
0.543 10.632
0.545 10.743
0.547 10.710
0.549 10.716
0.551 10.664
0.553 10.691
0.555 10.663
0.557 10.522
0.560 10.610
0.562 10.518
0.564 10.521
0.566 10.429
0.568 10.504
0.570 10.424
0.572 10.487
0.574 10.429
0.576 10.523
0.578 10.278
0.580 10.397
0.582 10.320
0.585 10.292
0.587 10.292
0.589 10.403
0.591 10.274
0.593 10.293
0.595 10.347

2431352 +
0.435 10.819
0.437 10.821
0.439 10.823
0.441 10.791
0.443 10.746
0.445 10.788
0.447 10.772
0.449 10.806
0.451 10.689
0.453 10.716
0.455 10.759
0.458 10.704
0.460 10.709
0.462 10.711
0.464 10.697
0.466 10.643
0.468 10.600
0.470 10.608
0.472 10.653
0.474 10.571
0.476 10.623
0.478 10.557
0.480 10.535
0.482 10.514
0.485 10.446
0.487 10.384
0.489 10.346
0.491 10.324
0.493 10.374
0.495 10.400
0.497 10.303
0.499 10.355
0.501 10.319
0.503 10.287
0.505 10.205
0.507 10.249
0.510 10.257
0.512 10.214
0.514 10.217
0.516 10.137
0.518 10.097
0.520 10.093
0.522 10.033
0.524 10.076
0.526 10.077
0.532 9.911
0.534 9.903
0.536 9.872
0.538 9.758

0.540 9.799
0.542 9.747
0.544 9.787
0.547 9.660
0.549 9.728
0.551 9.822
0.553 9.869
0.555 9.705
0.557 9.835
0.560 9.859
0.562 9.841
0.564 9.899
0.566 9.891
0.568 9.843
0.570 9.773
0.572 9.831
0.574 9.878
0.576 9.779
0.578 9.863
0.580 10.037
0.582 9.961
0.585 9.935
0.587 10.027
0.589 9.963
0.591 10.024
0.593 10.165
0.595 10.131
0.597 10.002
0.599 9.958
0.601 9.998
0.603 9.961
0.605 10.035
0.607 10.021
0.610 9.999
0.612 10.208
0.614 10.198
0.616 10.137
0.618 10.231
0.620 10.163
0.622 10.144
0.624 10.124

2431353 +
0.404 10.642
0.406 10.635
0.408 10.616
0.410 10.669
0.412 10.667
0.415 10.610
0.417 10.491
0.419 10.554
0.421 10.474
0.423 10.375
0.425 10.464
0.427 10.526
0.429 10.447
0.431 10.449
0.433 10.395
0.435 10.512
0.437 10.338
0.440 10.234
0.442 10.248
0.444 10.161
0.446 10.209
0.448 10.282
0.450 10.184
0.452 10.189
0.454 10.131
0.456 10.161
0.458 10.085
0.460 10.108
0.462 10.094
0.464 10.071
0.467 10.041
0.469 9.917
0.471 9.861
0.473 10.002
0.475 9.902
0.480 9.911
0.482 9.760
0.484 9.829
0.486 9.774
0.490 9.827
0.492 9.840
0.494 9.795
0.496 9.812
0.499 9.733
0.501 9.750
0.503 9.682
0.505 9.830
0.507 9.758
0.509 9.758
0.511 9.934
0.513 9.841
0.515 9.914
0.517 9.874
0.519 9.880
0.522 9.932
0.524 9.895
0.526 9.863
0.528 10.039
0.531 9.960
0.533 10.022
0.535 9.974
0.537 10.009
0.539 10.029
0.541 9.987
0.543 9.892
0.545 10.071
0.547 10.087
0.549 10.120
0.551 10.063
0.553 10.093
0.556 10.034
0.558 10.242
0.560 10.082
0.562 10.166

2431354 +
0.450 9.708
0.452 9.729
0.454 9.770
0.456 9.774
0.458 9.864
0.460 9.730
0.462 9.874
0.465 9.887
0.467 9.990
0.469 9.833
0.471 9.775
0.473 9.760
0.475 9.803
0.477 9.877
0.479 9.962
0.481 9.917
0.483 10.105
0.485 9.936
0.487 9.881
0.490 10.036
0.492 9.941
0.494 9.824
0.496 10.010
0.498 10.089
0.500 10.038
0.502 9.973
0.504 9.966
0.506 9.972
0.508 10.027
0.510 10.046
0.513 10.127
0.515 10.190
0.517 10.112
0.519 10.189
0.521 10.242
0.523 10.096
0.525 10.121
0.527 10.167
0.529 10.194
0.531 10.080
0.533 10.383
0.535 10.244
0.537 10.211
0.540 10.283
0.542 10.358
0.544 10.308
0.546 10.320
0.548 10.348
0.550 10.321
0.552 10.314
0.554 10.441
0.556 10.328
0.558 10.288
0.562 10.470
0.565 10.371
0.567 10.409
0.569 10.374
0.571 10.460
0.573 10.405

2431355 +
0.364 10.160
0.366 10.209
0.369 10.117
0.371 10.004
0.373 10.042
0.375 10.014
0.377 9.987
0.379 10.032
0.381 9.959
0.383 9.894
0.385 9.914
0.387 9.970
0.389 9.837
0.391 10.011

2431376 +
0.259 10.764
0.261 10.701
0.264 10.944
0.266 10.817
0.268 10.814
0.270 10.816
0.272 10.876
0.274 10.916
0.276 10.799
0.278 10.760
0.280 10.903
0.282 10.934
0.284 10.636
0.286 10.842
0.289 10.745
0.291 10.883
0.293 10.648
0.295 10.957
0.297 10.750

2431700 +
0.331 10.770
0.333 10.755
0.335 10.688
0.340 10.753
0.342 10.758
0.344 10.659
0.346 10.731
0.348 10.557
0.350 10.449
0.352 10.536
0.354 10.313
0.356 10.506
0.358 10.283
0.360 10.214
0.362 10.050
0.365 10.230
0.367 10.101
0.369 9.962

0.371 9.871
0.373 9.775
0.375 9.705
0.377 9.546
0.379 9.556
0.381 9.326
0.383 9.319
0.385 9.271
0.387 9.350
0.402 9.388
0.404 9.506
0.406 9.531
0.408 9.442
0.410 9.518
0.412 9.460
0.415 9.563
0.417 9.680
0.419 9.565
0.421 9.686
0.423 9.574
0.425 9.626
0.427 9.689
0.429 9.639
0.431 9.584
0.433 9.680
0.443 9.870
0.445 9.892
0.447 9.839
0.449 9.976
0.451 9.754
0.453 9.818
0.456 9.851
0.458 10.006
0.460 10.045
0.462 9.978
0.464 9.902
0.466 10.031
0.468 10.028
0.470 10.091
0.472 10.065
0.474 9.970
0.476 9.998
0.478 10.113
0.480 10.173
0.483 10.273
0.485 10.184
0.487 10.127

0.489 10.102
0.491 10.147
0.493 10.138
0.495 10.332
0.497 10.318
0.499 10.252
0.501 10.308
0.503 10.309
0.506 10.268
0.508 10.495
0.510 10.481
0.512 10.344
0.514 10.267
0.516 10.378
0.518 10.434
0.520 10.535
0.522 10.413
0.524 10.427

2431708 +
0.348 10.812
0.350 10.806
0.352 10.815
0.354 10.749
0.356 10.665
0.358 10.732
0.360 10.673
0.362 10.755
0.365 10.867
0.367 10.771
0.369 10.742
0.371 10.861
0.373 10.964
0.375 10.929
0.377 10.823
0.379 10.596
0.381 10.781
0.383 10.812
0.385 10.889
0.387 10.798
0.389 10.766
0.392 10.904
0.394 10.778
0.396 10.795
0.398 10.832
0.400 10.629
0.402 10.726

0.404 10.993
0.406 10.844
0.408 10.615
0.410 10.756
0.412 10.863
0.415 10.858
0.417 10.715
0.419 10.814
0.421 10.783
0.423 10.637
0.425 10.656
0.427 10.713
0.429 10.681
0.431 10.711
0.433 10.483
0.435 10.659
0.437 10.504
0.440 10.442
0.442 10.436
0.444 10.286
0.446 10.335
0.448 10.264
0.450 10.244
0.460 10.074
0.462 9.957
0.464 9.911
0.466 9.843
0.468 9.774
0.470 9.798
0.472 9.780
0.474 9.750
0.476 9.714
0.478 9.608
0.480 9.668
0.482 9.701
0.485 9.670
0.487 9.570
0.489 9.628

2433896 +
0.467 10.657
0.469 10.751
0.471 10.659
0.473 10.757
0.475 10.734
0.477 10.779
0.479 10.861

0.481 10.758
0.483 10.825
0.485 10.788
0.488 10.782
0.490 10.846
0.492 10.783
0.494 10.883
0.496 11.050
0.498 11.015
0.500 10.937
0.502 10.685
0.504 10.782
0.506 10.791
0.508 10.967
0.510 10.819
0.513 10.877
0.515 10.804
0.517 10.873
0.519 10.640
0.521 10.717
0.523 10.724
0.525 10.756

2434197 +
0.456 10.679
0.458 10.638
0.460 10.681
0.462 10.624
0.464 10.440
0.466 10.540
0.469 10.566
0.471 10.476
0.473 10.518
0.475 10.576
0.477 10.519
0.479 10.726
0.481 10.860
0.483 10.518
0.485 10.723
0.487 10.598
0.489 10.552
0.491 10.750
0.494 10.682
0.496 10.686
0.498 10.729
0.500 10.690
0.502 10.723

0.504 10.568
0.506 10.695
0.508 10.653
0.510 10.689
0.512 10.712
0.514 10.714
0.516 10.707
0.519 10.722
0.521 10.609
0.523 10.681
0.525 10.807
0.527 10.669
0.529 10.734
0.531 10.860

2434199 +
0.370 10.524
0.404 10.552
0.451 10.571

2434230 +
0.428 10.873
0.469 10.796
0.507 10.817
0.561 10.190

2434234 +
0.347 10.614
0.349 10.455
0.351 10.469
0.353 10.436
0.355 10.493
0.357 10.401
0.359 10.260
0.361 10.135
0.363 10.299
0.365 10.298
0.367 10.331
0.369 10.298
0.371 10.084
0.373 10.255
0.375 10.103
0.378 10.060
0.380 10.178
0.382 10.192
0.387 10.001
0.389 10.105
0.391 9.985

0.393 10.028
0.395 10.011
0.397 9.982
0.399 10.032
0.401 10.034
0.403 9.995
0.405 9.997
0.407 9.892
0.409 9.885
0.412 9.843
0.414 9.904
0.416 9.902

2434241 +
0.438 10.672
0.440 10.711
0.441 10.714
0.443 10.745
0.445 10.879
0.447 10.777
0.449 10.620
0.452 10.642
0.454 10.648
0.456 10.879
0.458 10.732
0.460 10.712
0.462 10.912
0.464 10.660
0.466 10.874
0.468 11.037
0.470 10.736
0.472 10.897
0.474 10.984
0.477 10.990
0.479 10.953
0.481 10.662
0.483 10.494
0.485 10.537
0.487 10.504
0.489 10.539
0.491 10.715
0.493 10.632
0.495 10.520
0.497 10.466
0.499 10.737
0.502 10.572
0.504 10.569
0.506 10.625
0.507 10.522
0.510 10.489
0.512 10.359
0.514 10.418
0.516 10.318
0.518 10.388
0.520 10.244
0.522 10.191
0.524 10.154
0.527 10.181
0.529 10.097
0.531 10.167
0.533 10.213
0.535 10.220
0.537 10.142
0.539 10.017
0.541 9.999
0.543 9.969
0.545 9.790
0.555 9.826
0.557 9.680
0.559 9.746
0.561 9.807
0.563 9.929
0.565 9.856
0.568 9.945
0.570 9.998
0.572 9.778
0.574 9.795
0.576 9.627
0.578 9.892
0.580 10.011
0.582 9.804

2434253 +
0.389 10.813
0.391 10.887
0.393 10.901
0.396 10.825
0.398 10.987
0.400 10.901
0.402 10.761
0.404 10.803
0.406 10.915
0.408 10.815
0.410 10.840
0.412 10.681
0.414 10.817
0.416 10.635
0.418 10.764
0.420 10.674
0.423 10.714
0.425 10.614
0.427 10.648
0.429 10.698
0.431 10.605
0.433 10.456
0.435 10.474
0.437 10.438
0.439 10.389
0.441 10.145
0.443 10.317
0.445 10.215
0.448 10.180
0.450 10.041
0.452 9.909
0.454 9.823
0.456 9.690
0.458 9.629
0.460 9.587
0.462 9.514
0.464 9.397
0.466 9.634
0.468 9.523
0.470 9.635
0.473 9.648
0.475 9.664
0.477 9.704
0.479 9.704
0.481 9.688
0.483 9.620
0.485 9.676
0.487 9.628
0.489 9.742
0.491 9.731
0.495 9.673
0.497 9.719
0.499 9.831
0.501 9.808
0.503 9.702

2434264 +
0.385 10.526
0.387 10.403
0.390 10.365
0.392 10.486
0.394 10.444
0.396 10.457
0.398 10.339
0.400 10.296
0.402 10.273
0.404 10.461
0.406 10.189
0.408 10.218
0.410 10.188
0.412 10.115
0.415 10.234
0.417 9.947
0.419 9.906
0.421 9.924
0.423 9.996
0.425 9.659
0.427 9.700
0.429 9.424
0.431 9.437
0.433 9.433
0.435 9.420
0.437 9.499
0.440 9.498
0.442 9.533

2434294 +
0.366 10.591
0.369 10.483
0.371 10.507
0.373 10.486
0.375 10.429
0.377 10.517
0.379 10.499
0.381 10.473
0.383 10.505
0.385 10.574
0.387 10.481
0.389 10.470
0.391 10.401
0.394 10.307
0.396 10.633
0.398 10.281
0.400 10.301
0.402 10.110
0.404 10.200
0.406 10.176

2434455 +
0.416 10.546
0.418 10.442
0.421 10.504
0.424 10.426
0.427 10.510
0.430 10.319
0.432 10.312
0.435 10.299
0.438 10.246
0.441 10.122
0.443 10.232
0.446 10.043
0.449 10.050
0.452 9.965
0.455 10.018
0.458 9.820
0.460 9.926
0.463 9.890
0.466 9.885
0.468 9.759
0.471 9.663
0.474 9.640
0.477 9.646
0.480 9.581
0.483 9.482
0.486 9.555
0.489 9.540
0.491 9.462
0.494 9.522
0.497 9.596
0.500 9.562
0.502 9.577
0.505 9.550
0.508 9.527
0.511 9.589
0.514 9.527
0.516 9.529
0.519 9.639
0.522 9.646
0.525 9.653
0.527 9.719
0.530 9.599

2434476 +
0.434 9.946
0.437 9.839
0.440 9.887
0.442 9.700
0.445 9.757
0.448 9.631
0.451 9.472
0.453 9.515
0.456 9.435
0.459 9.419
0.462 9.326
0.465 9.414
0.467 9.349
0.470 9.410
0.473 9.572
0.476 9.674
0.479 9.683
0.481 9.456
0.484 9.645
0.487 9.687

2434486 +
0.426 10.705
0.429 10.566
0.432 10.449
0.434 10.410
0.437 10.344
0.440 10.282
0.443 10.395
0.445 10.061
0.448 9.907
0.451 9.855
0.454 9.968
0.457 9.673
0.459 9.474
0.462 9.271
0.465 9.244
0.468 9.409
0.470 9.240
0.473 9.236
0.476 9.242
0.479 9.186
0.482 9.385
0.484 9.359
0.487 9.411
0.490 9.432

2434488 +
0.324 10.564
0.327 10.607
0.330 10.530
0.332 10.340
0.335 10.280
0.338 10.312
0.341 10.242
0.344 10.395
0.346 10.193
0.349 10.099
0.352 9.972
0.355 9.960
0.357 9.851
0.360 9.682
0.363 9.544
0.366 9.336
0.369 9.331
0.371 9.135
0.374 9.078
0.377 9.110
0.380 9.059
0.382 9.130

2434504 +
0.501 10.791
0.503 10.793
0.506 10.734
0.509 10.620
0.512 10.762
0.515 10.575
0.517 10.566
0.520 10.504
0.523 10.498
0.526 10.381
0.528 10.257
0.531 10.050
0.533 10.013
0.537 10.087
0.540 9.926
0.542 9.836

2434515 +
0.451 10.793
0.454 10.790
0.457 10.662
0.459 10.820
0.462 10.484
0.465 10.434
0.468 10.501
0.470 10.480
0.473 10.539
0.476 10.175
0.479 10.316
0.482 10.242
0.484 10.186
0.487 9.990
0.490 9.996
0.493 9.927
0.495 9.738
0.498 9.798
0.501 9.839
0.504 9.834
0.507 9.651
0.509 9.494
0.512 9.571
0.515 9.468
0.517 9.338
0.520 9.415
0.523 9.291
0.526 9.274
0.529 9.335
0.532 9.223
0.534 9.282
0.537 9.311
0.540 9.343

2434546 +
0.487 9.711
0.489 9.583
0.492 9.530
0.495 9.349
0.498 9.459
0.501 9.324
0.503 9.480
0.506 9.353
0.509 9.512
0.512 9.502
0.514 9.438
0.517 9.466
0.520 9.455
0.523 9.378
0.526 9.416
0.528 9.524

2434575 +
0.469 10.676
0.472 10.774
0.475 10.806
0.477 10.836
0.480 10.779
0.483 10.878
0.486 11.051
0.489 10.864
0.491 10.924
0.494 10.840
0.497 10.774
0.500 10.701
0.502 10.783
0.505 10.859
0.508 10.772
0.511 10.737
0.514 10.839
0.516 10.654
0.519 10.644
0.522 10.647
0.525 10.644
0.527 10.572
0.530 10.594
0.533 10.460
0.536 10.394
0.539 10.266
0.541 10.501
0.544 9.967
0.547 9.995
0.550 9.670
0.552 9.713

2434589 +
0.325 10.326
0.328 10.472
0.331 10.214
0.334 9.880
0.336 10.185
0.339 10.051
0.342 9.782
0.345 9.998
0.347 9.945
0.350 9.988
0.353 9.652
0.356 9.639
0.359 9.567
0.361 9.641
0.364 9.551
0.369 9.573
0.370 9.626
0.372 9.453
0.375 9.631
0.382 9.298
0.384 9.555
0.399 9.496
0.402 9.377
0.404 9.400

2434599 +
0.346 9.988
0.349 10.003
0.352 10.110
0.355 9.752
0.358 9.859
0.360 9.744
0.363 9.717
0.366 9.560
0.369 9.776
0.371 9.839
0.374 9.564
0.377 9.650
0.380 9.569
0.383 9.714
0.385 9.643
0.388 9.510
0.391 9.467
0.394 9.395
0.396 9.388
0.399 9.527
0.402 9.545
0.405 9.580
0.408 9.617
0.410 9.584
0.413 9.476
0.416 9.483

2434605 +
0.533 10.280
0.536 10.152
0.539 10.186
0.542 10.047
0.544 10.068
0.547 9.952

0.550 9.885
0.553 9.870
0.556 9.915
0.558 9.920
0.561 9.835
0.564 9.861
0.567 9.841
0.569 9.766
0.572 9.758
0.575 9.673
0.578 9.747
0.581 9.703
0.583 9.723
0.586 9.691

2434626 +
0.468 10.496
0.471 10.766
0.473 10.845
0.476 10.851
0.479 10.925
0.482 11.088
0.484 10.898
0.487 10.481
0.490 10.880
0.493 10.398
0.496 10.893
0.498 10.671
0.501 10.352
0.503 10.223

2434627 +
0.472 10.275
0.475 10.179
0.478 10.092
0.481 10.029
0.483 9.823
0.486 9.732
0.489 9.570
0.492 9.507
0.494 9.546
0.497 9.393
0.500 9.337
0.503 9.362
0.506 9.337
0.508 9.259
0.511 9.270
0.514 9.268
0.517 9.337
0.519 9.319

2435377 +
0.428 10.812
0.431 10.769
0.434 10.781
0.437 10.716
0.439 10.737
0.442 10.655
0.445 10.633
0.448 10.678
0.450 10.464
0.453 10.602
0.456 10.502
0.459 10.372
0.462 10.254
0.464 10.279
0.470 9.932
0.473 10.171
0.475 9.972
0.478 9.975
0.481 9.950
0.484 9.892
0.487 9.874
0.489 9.757
0.492 9.711
0.495 9.775
0.498 9.845
0.500 9.618
0.503 9.909
0.506 9.567
0.509 9.509
0.512 9.765
0.514 9.597
0.517 9.587
0.520 9.620
0.523 9.594
0.525 9.493
0.528 9.628
0.531 9.561
0.534 9.602
0.537 9.612
0.539 9.752
0.542 9.741

2435421 +
0.232 10.825
0.235 10.942
0.238 10.774
0.241 10.754
0.263 10.656
0.266 10.592
0.268 10.581
0.271 10.615
0.274 10.504
0.277 10.524
0.279 10.518
0.282 10.263
0.285 10.330
0.288 10.318
0.291 10.333
0.293 10.170
0.296 10.128
0.299 10.132
0.302 10.150
0.304 10.045
0.307 9.996
0.310 9.833
0.313 9.935
0.316 9.842
0.318 9.867
0.321 9.635
0.324 9.608
0.327 9.597
0.330 9.813
0.332 9.607
0.335 9.664
0.338 9.471
0.341 9.565
0.343 9.663
0.346 9.598
0.349 9.583
0.352 9.688
0.354 9.700
0.357 9.711
0.360 9.688

2435622 +
0.375 10.569
0.378 10.511
0.381 10.381
0.383 10.433
0.386 10.210
0.389 10.038
0.392 9.952
0.394 10.012
0.397 9.891
0.400 9.687
0.403 9.635
0.406 9.581
0.408 9.457
0.411 9.361
0.414 9.470
0.417 9.236
0.419 9.283
0.422 9.202
0.425 9.253
0.428 9.265
0.431 9.252
0.433 9.292
0.437 9.182
0.440 9.231
0.442 9.398
0.445 9.344
0.451 9.257
0.453 9.495
0.456 9.290
0.460 9.273
0.463 9.416
0.466 9.488
0.469 9.631
0.471 9.464
0.474 9.696
0.477 9.735
0.480 9.585
0.485 9.599
0.487 9.600
0.491 9.618
0.494 9.601
0.496 9.684
0.499 9.737

2435682 +
0.377 10.858
0.380 10.765
0.383 10.846
0.385 10.739
0.388 10.726
0.391 11.072
0.394 10.538
0.403 10.914
0.406 10.596
0.408 10.347
0.411 10.431
0.414 10.454
0.417 10.115
0.419 10.207
0.424 10.138
0.426 9.991
0.429 9.788
0.432 9.669
0.435 9.517
0.437 9.536
0.440 9.414
0.444 9.410
0.447 9.176
0.451 9.354
0.454 9.339
0.457 9.303
0.460 9.249
0.462 9.424
0.467 9.409
0.480 9.391
0.483 9.192
0.485 9.417
0.488 9.517
0.491 9.557
0.495 9.462
0.498 9.673
0.501 9.889
0.504 9.644
0.506 9.955
0.509 9.707
0.513 9.662
0.516 10.180
0.519 9.832
0.522 10.173

2435732 +
0.470 9.948
0.473 10.009
0.476 9.893
0.479 9.952
0.481 9.995
0.484 9.876
0.487 9.972

0.490 9.851
0.493 9.926
0.495 10.082
0.498 9.964
0.501 9.956
0.504 10.017
0.507 10.015
0.509 10.127
0.512 10.002
0.515 10.028
0.518 10.027
0.520 9.962
0.523 10.086
0.526 10.150
0.529 10.096
0.531 10.115
0.534 10.139
0.537 10.187
0.540 10.055
0.543 10.025

2435756 +
0.283 10.090
0.286 9.873
0.288 9.915
0.291 9.822
0.294 9.703
0.297 9.690
0.299 9.648
0.302 9.680
0.305 9.528
0.308 9.511
0.311 9.522
0.313 9.410
0.316 9.538
0.318 9.487
0.322 9.642
0.324 9.531
0.327 9.516
0.329 9.513
0.332 9.692
0.335 9.679
0.338 9.681
0.340 9.619
0.343 9.672
0.347 9.862
0.352 9.829

0.355 9.848
0.358 9.947
0.361 9.820
0.363 9.975
0.366 9.839
0.369 9.741
0.372 9.996
0.374 9.920

2435933 +
0.487 10.782
0.490 10.882
0.492 10.715
0.495 10.759
0.498 10.786
0.501 10.795
0.503 10.783
0.506 10.668
0.509 10.593
0.512 10.543
0.515 10.452
0.517 10.570
0.520 10.489
0.523 10.520
0.526 10.576
0.531 10.297
0.534 10.267
0.537 10.134
0.540 10.088
0.545 10.107
0.548 10.016
0.551 9.792
0.553 9.816
0.556 9.642
0.559 9.593
0.562 9.563
0.565 9.408
0.567 9.494
0.570 9.381
0.573 9.340
0.576 9.434
0.578 9.304
0.581 9.305

2436005 +
0.439 10.871
0.441 10.678

0.443 10.871
0.446 10.885
0.448 10.917
0.450 10.818
0.453 10.830
0.455 10.799
0.457 10.715
0.459 10.605
0.461 10.851
0.464 10.762
0.466 10.760
0.468 10.620
0.470 10.725
0.472 10.775
0.475 10.521
0.477 10.540
0.479 10.669
0.481 10.594
0.483 10.480
0.485 10.371
0.489 10.680
0.491 10.506
0.493 10.533
0.495 10.515
0.498 10.408
0.501 10.427
0.503 10.341
0.505 10.354
0.507 10.308
0.509 10.230
0.512 10.048
0.514 9.939
0.516 9.865
0.519 9.833
0.521 9.817
0.525 9.744
0.527 9.619
0.529 9.556
0.531 9.409
0.533 9.397
0.536 9.543
0.538 9.599

2436007 +
0.435 9.162
0.438 9.090
0.441 9.202

0.444 9.460
0.447 9.339
0.449 9.397
0.452 9.572
0.455 9.524
0.458 9.492
0.461 9.585
0.464 9.490
0.467 9.473
0.469 9.640
0.472 9.650
0.475 9.498
0.478 9.544
0.481 9.538
0.483 9.653
0.486 9.530

2436038 +
0.380 9.973
0.382 9.852
0.385 9.757
0.388 9.709
0.392 9.492
0.395 9.430
0.398 9.564
0.420 9.643
0.423 9.816
0.426 9.832
0.430 9.773
0.432 9.834
0.435 9.788
0.438 9.913
0.441 9.795
0.443 9.840
0.446 9.964
0.449 10.087
0.452 10.001

2436069 +
0.317 10.475
0.320 10.603
0.322 10.495
0.347 10.270
0.352 10.123
0.355 9.973
0.358 9.923
0.361 9.905

0.363 9.634
0.366 9.695
0.369 9.740
0.386 9.665
0.388 9.769
0.391 10.031

2436077 +
0.398 11.087
0.401 10.870
0.404 10.819
0.407 10.824
0.410 10.817
0.413 10.758
0.416 10.782
0.418 10.751
0.425 10.641
0.427 10.718
0.430 10.640
0.433 10.596
0.436 10.412
0.439 10.490
0.441 10.253
0.444 10.310
0.447 10.349
0.452 10.071
0.455 10.030
0.458 10.009
0.461 9.981
0.464 9.666
0.469 9.679
0.475 9.305
0.477 9.339
0.480 9.288
0.483 9.280
0.486 9.270
0.489 9.391
0.491 9.425
0.494 9.246
0.500 9.350
0.502 9.270
0.508 9.441
0.511 9.422
0.514 9.401
0.517 9.550
0.520 9.370
0.523 9.616

0.525 9.933
0.528 9.848
0.532 10.107
0.534 9.890
0.537 9.807
0.540 9.811

2436087 +
0.424 10.424
0.427 10.482
0.430 10.361
0.433 10.483
0.435 10.463
0.440 10.290
0.443 10.286
0.446 10.164
0.449 10.233
0.451 10.078
0.456 10.258
0.458 10.032
0.461 10.157
0.464 9.762
0.467 9.863
0.470 9.574
0.470 9.689
0.473 9.594
0.476 9.620
0.478 9.536
0.481 9.584
0.485 9.600
0.488 9.730
0.491 9.619
0.494 9.530
0.496 9.600
0.501 9.385
0.504 9.336
0.507 9.210
0.510 9.448
0.512 9.469
0.517 9.487
0.519 9.630
0.522 9.358
0.525 9.590
0.528 9.565
0.532 9.594
0.535 9.650
0.537 9.704
0.540 9.782
0.543 9.813

2436100 +
0.270 10.813
0.273 10.939
0.275 10.869
0.278 10.631
0.281 10.745
0.284 10.617
0.286 10.571
0.289 10.631
0.292 10.524
0.295 10.408
0.298 10.328
0.301 10.406
0.304 10.392
0.307 10.051
0.309 10.274
0.312 10.369
0.315 10.237
0.318 10.299
0.320 10.043
0.323 9.913
0.326 10.006
0.329 9.843
0.332 10.070
0.334 9.745
0.337 9.960
0.340 9.786
0.343 10.033
0.345 10.075
0.357 9.444
0.365 9.433

2436109 +
0.332 10.513
0.335 10.337
0.338 10.492
0.340 10.400
0.343 10.479
0.346 10.326
0.349 10.473
0.351 10.264

2436128 +
0.336 10.895
0.338 10.822
0.341 10.763
0.344 10.663
0.347 10.856
0.349 10.940
0.352 10.834
0.355 10.868
0.358 10.694
0.361 10.574
0.363 10.487
0.366 10.717
0.369 10.712
0.372 10.594
0.375 10.663
0.379 10.456
0.381 10.709
0.384 10.588
0.388 10.608
0.393 10.530
0.395 10.708
0.398 10.628
0.401 10.408
0.404 10.415
0.406 10.440
0.409 10.353
0.412 10.311
0.415 10.175
0.418 10.209
0.421 10.205
0.424 10.074
0.427 9.933
0.429 9.962
0.433 10.050
0.438 9.813
0.440 9.934
0.443 9.742
0.446 9.685
0.449 9.857
0.452 9.764
0.454 9.812
0.457 9.705
0.460 9.653
0.463 9.833
0.466 9.833
0.469 9.836
0.472 9.829
0.474 9.927
0.478 9.751
0.481 9.887
0.483 9.771
0.486 9.786
0.489 9.716
0.492 9.840
0.495 9.857
0.497 9.907
0.500 9.966

2436131 +
0.231 10.695
0.234 10.635
0.236 10.738
0.239 10.874
0.242 10.674
0.245 10.650
0.247 10.516
0.250 10.466
0.253 10.275
0.256 10.240
0.259 10.295
0.261 10.143
0.267 10.018
0.270 10.103
0.272 10.118
0.275 10.104
0.278 9.968
0.281 9.983
0.284 9.907
0.286 9.702
0.289 9.896
0.292 9.830
0.295 9.753
0.297 9.539
0.300 9.543
0.303 9.401
0.306 9.531
0.309 9.500
0.311 9.488
0.314 9.416
0.318 9.426
0.320 9.434
0.323 9.467
0.326 9.351
0.329 9.444
0.332 9.368
0.334 9.635
0.337 9.560
0.340 9.575
0.343 9.560
0.345 9.696
0.348 9.741
0.351 9.620
0.354 9.706

2436142 +
0.228 10.568
0.232 10.303
0.235 10.350
0.238 10.290
0.240 10.264
0.243 10.317
0.246 10.345
0.249 10.113
0.252 9.940
0.255 9.817
0.258 9.962
0.261 9.820
0.264 9.871
0.268 9.784
0.271 9.548
0.274 9.548
0.277 9.580
0.279 9.630
0.283 9.682
0.286 9.599
0.288 9.531
0.291 9.588
0.294 9.753
0.297 9.641
0.300 9.690
0.303 9.711
0.306 9.891
0.308 9.762
0.312 9.798
0.315 9.779
0.318 9.838
0.320 9.733
0.323 9.795
0.326 9.830

Photoelectric Data

The first photoelectric measurements of XZ Dra were made at Konkoly Observatory during the night April 27/28 1957 (JD=2435956). At the Newtonian focus of the 60cm Newton-Cassegrain telescope an RCA 1P21 photomultiplier was employed without any filter. During this night BD+64°1327 (=TYC 4224_0707_1) was used as a comparison star.

From 1958 the star was observed through the conventional filters of the UBV system. After the aluminization of the mirror of the 60cm telescope in 1963 an EMI 9052 B tube was used. Since 1972 photoelectric observations were also made close to the UBV system with the 50cm Cassegrain telescope at Konkoly Observatory's mountain station at Piszkéstető. At this location we used an integrating photometer equipped with an unrefrigerated EMI 9058 QB photomultiplier.

In 1988 on three nights XZ Dra was also measured by the Konkoly Observatory's 1m RCC telescope equipped with a thermoelectrically cooled $UBV(RI)_{\rm C}$ photon counting photometer furnished with an EMI 9659 QB tube.

Throughout our photoelectric photometry GSC 04225-01323 (=TYC 4225_1323_1) was chosen as a comparison star (except the first night, see above). The brightness and colours of this star were given by Sturch (1966) as:

$$V = 10.493 \quad B - V = 0.572 \quad U - B = 0.041.$$

Table 4. Telescope constants for photoelectric data.

Year	ε	μ	ψ	r	i	Telescope*
1958	−0.12	0.91				NC
1961	−0.15	1.10				NC
1966	−0.13	1.17				NC
1969	−0.065	1.10	1.14			NC
1970	−0.10	1.11	1.03			NC
1971	−0.12	1.13				NC
1972	−0.105	1.115	1.065			NC
1973	−0.11	1.11	1.065			NC
1974	−0.16	1.07	1.07			NC
1974	0.08	0.93	1.21			C**
1975	−0.16	1.07	1.07			NC
1976	−0.17	1.08				NC
1978	−0.165	1.075				NC
1983	−0.06	1.20	0.86			C
1984	−0.06	1.20	0.86			C
1985	−0.128	1.187	1.106			C
1988	−0.029	0.973	1.109	1.112	1.094	RCC

*NC = 60cm Newton–Cassegrain telescope, Budapest,
C = 50cm Cassegrain telescope, Piszkéstető Mountain Station,
RCC = 1m Ritchey–Chrétien–Coudé telescope, Piszkéstető Mountain Station.

**On JD = 2442279.

The photoelectric observations have been transformed into the UBV system in the traditional way (see e.g. Hardie, 1962). The actual transformation coefficients for different epochs and telescopes are shown in Table 4. The accuracy of the photoelectric observations depending on the sky conditions ranged typically between $0.^{m}002$–$0.^{m}010$ in B, V, R_C and $0.^{m}01$–$0.^{m}02$ in U and I_C. As the mirror has been aluminized only since 1963 the transformation of the early observations (before 1963) into the UBV system is rather uncertain.

Altogether 6106 photoelectric data were obtained. In Tables 5.a–f all these measurements are listed in the sense variable−comparison for unfiltered, U, B, V, R_C and I_C measurements, respectively.

Table 5.a Photoelectric differential observations of XZ Dra without filter

2435956 +		0.4055	0.492	0.4243	0.151	0.4432	0.084	0.4620	0.188
0.3905	0.580	0.4068	0.460	0.4257	0.140	0.4449	0.096	0.4638	0.176
0.3916	0.557	0.4115	0.315	0.4270	0.121	0.4468	0.095	0.4652	0.195
0.3929	0.558	0.4126	0.293	0.4309	0.104	0.4481	0.104	0.4668	0.203
0.3941	0.539	0.4154	0.274	0.4324	0.111	0.4524	0.123	0.4682	0.218
0.3952	0.536	0.4171	0.271	0.4338	0.100	0.4537	0.128		
0.4004	0.530	0.4181	0.253	0.4352	0.093	0.4551	0.127		
0.4024	0.525	0.4218	0.183	0.4367	0.101	0.4564	0.142		
0.4043	0.496	0.4230	0.183	0.4416	0.084	0.4576	0.156		

Table 5.b Photoelectric differential U observations of XZ Dra

2440541 +		2440676 +		0.5934	−0.911	0.5383	−0.202	0.4586	−0.671
0.2319	−0.203	0.5184	−0.080	0.5955	−0.932	0.5408	−0.229	0.4628	−0.774
0.2340	−0.245	0.5246	−0.118	0.5996	−0.943	0.5438	−0.355	0.4649	−0.895
0.2382	−0.366	0.5309	−0.164	0.6017	−0.949	0.5459	−0.376	0.4690	−0.947
0.2403	−0.399	0.5371	−0.182	0.6059	−0.972	0.5501	−0.534	0.4711	−1.074
0.2444	−0.501	0.5392	−0.192	0.6080	−0.988	0.5522	−0.579	0.4753	−1.164
0.2465	−0.643	0.5434	−0.236	0.6121	−0.980	0.5563	−0.803	0.4774	−1.307
0.2507	−0.725	0.5455	−0.281	0.6142	−0.975	0.5584	−0.818	0.4815	−1.469
0.2528	−0.776	0.5496	−0.327	0.6184	−0.973	0.5626	−0.950	0.4836	−1.458
0.2569	−0.853	0.5517	−0.355	0.6219	−0.972	0.5647	−1.083	0.4878	−1.461
0.2590	−0.904	0.5559	−0.385	0.6240	−0.963	0.5688	−1.302	0.4912	−1.436
0.2632	−0.996	0.5580	−0.413			0.5709	−1.346	0.4954	−1.355
0.2653	−1.019	0.5621	−0.481	2440707 +		0.5744	−1.487	0.4975	−1.333
0.2694	−1.079	0.5642	−0.499	0.5091	0.033	0.5765	−1.491		
0.2715	−1.095	0.5684	−0.563	0.5133	0.062	0.5807	−1.483	2442279 +	
0.2757	−1.127	0.5705	−0.611	0.5154	0.057	0.5828	−1.459	0.4882	0.009
0.2778	−1.171	0.5746	−0.693	0.5195	0.054			0.4993	−0.037
0.2819	−1.177	0.5767	−0.726	0.5216	0.036	2440780 +		0.5094	−0.296
0.2840	−1.190	0.5809	−0.746	0.5258	−0.023	0.4440	−0.317	0.5199	−0.648
0.2882	−1.154	0.5830	−0.795	0.5279	−0.044	0.4461	−0.371	0.5285	−0.962
0.2903	−1.166	0.5871	−0.853	0.5320	−0.062	0.4503	−0.434	0.5379	−1.003
		0.5892	−0.897	0.5341	−0.107	0.4524	−0.509	0.5469	−0.975

0.5567 −0.877

2445609 +
0.2844 −0.900
0.2857 −0.916
0.2870 −0.922
0.2884 −0.976
0.2897 −0.983
0.2955 −1.020
0.2969 −1.027
0.2982 −1.017
0.2996 −1.041
0.3009 −1.019
0.3062 −1.007
0.3075 −0.991
0.3089 −0.996
0.3102 −0.981
0.3115 −0.954

2445791 +
0.3604 −0.872
0.3617 −0.865
0.3631 −0.854
0.3644 −0.865
0.3658 −0.825
0.3784 −0.805
0.3797 −0.804
0.3810 −0.762
0.3824 −0.742
0.4110 −0.410
0.4124 −0.387
0.4137 −0.390
0.4150 −0.380
0.4163 −0.421
0.4177 −0.381
0.4191 −0.359
0.4204 −0.362
0.4218 −0.375
0.4231 −0.338
0.4369 −0.355
0.4382 −0.365
0.4396 −0.365
0.4409 −0.333
0.4423 −0.321
0.4436 −0.336
0.4449 −0.336
0.4464 −0.346

0.4476 −0.326
0.4490 −0.339
0.4563 −0.284
0.4577 −0.301
0.4590 −0.309
0.4604 −0.289
0.4617 −0.292
0.4631 −0.292
0.4644 −0.280
0.4658 −0.296
0.4671 −0.283
0.4684 −0.294
0.4742 −0.322
0.4755 −0.293
0.4768 −0.325
0.4781 −0.337
0.4795 −0.321
0.4809 −0.345
0.4822 −0.321
0.4836 −0.313
0.4849 −0.359
0.4862 −0.356
0.5216 −0.156
0.5230 −0.167
0.5243 −0.163
0.5257 −0.172
0.5270 −0.141
0.5283 −0.138
0.5297 −0.134
0.5310 −0.137
0.5324 −0.123
0.5337 −0.097
0.5402 −0.116
0.5416 −0.115
0.5429 −0.081
0.5442 −0.090
0.5456 −0.091
0.5469 −0.092
0.5483 −0.115
0.5496 −0.102
0.5510 −0.088
0.5523 −0.067
0.5598 −0.076
0.5611 −0.078
0.5624 −0.022
0.5638 −0.017
0.5651 −0.029

0.5665 −0.027
0.5678 0.011
0.5691 0.006
0.5705 −0.017
0.5718 −0.040
0.5782 −0.065
0.5796 −0.057
0.5809 −0.040
0.5822 0.006
0.5849 0.008

2445806 +
0.5200 −0.362
0.5213 −0.402
0.5226 −0.394
0.5240 −0.403
0.5253 −0.442
0.5309 −0.522
0.5323 −0.559
0.5337 −0.542
0.5350 −0.580
0.5364 −0.608
0.5418 −0.756
0.5431 −0.767
0.5444 −0.794
0.5458 −0.833
0.5471 −0.862
0.5522 −0.878
0.5536 −0.877
0.5549 −0.873
0.5563 −0.899
0.5576 −0.897
0.5633 −0.876
0.5646 −0.890
0.5660 −0.883
0.5673 −0.898
0.5687 −0.887
0.5739 −0.879
0.5753 −0.884
0.5766 −0.867
0.5779 −0.872
0.5793 −0.852
0.5844 −0.833
0.5858 −0.837
0.5941 −0.737
0.5954 −0.705
0.5967 −0.720

0.5981 −0.708

2446193 +
0.4381 −0.340
0.4394 −0.340
0.4408 −0.393
0.4421 −0.385
0.4434 −0.400
0.4489 −0.470
0.4502 −0.486
0.4516 −0.527
0.4529 −0.556
0.4543 −0.555
0.4595 −0.655
0.4608 −0.668
0.4621 −0.693
0.4635 −0.713
0.4648 −0.708
0.4700 −0.770
0.4714 −0.798
0.4727 −0.802
0.4740 −0.810
0.4754 −0.808
0.4812 −0.839
0.4825 −0.855
0.4839 −0.855
0.4852 −0.869
0.4866 −0.876
0.4923 −0.888
0.4936 −0.892
0.4950 −0.899
0.4963 −0.885
0.4977 −0.883
0.5037 −0.896
0.5050 −0.893
0.5063 −0.883
0.5077 −0.884
0.5090 −0.880
0.5145 −0.840
0.5158 −0.818
0.5172 −0.824
0.5185 −0.807

2447306 +
0.4916 0.053
0.4929 −0.011
0.5054 0.033

0.5067 0.007
0.5118 −0.060
0.5131 0.020
0.5187 −0.235
0.5253 −0.256
0.5266 −0.131
0.5317 −0.258
0.5330 −0.275
0.5382 −0.467
0.5395 −0.504
0.5448 −0.510
0.5460 −0.561
0.5509 −0.719
0.5522 −0.780

2447360 +
0.3671 −0.057
0.3684 −0.094
0.3740 −0.097
0.3753 −0.130
0.3804 −0.186
0.3816 −0.194
0.3865 −0.229
0.3930 −0.326
0.3943 −0.330
0.3956 −0.350
0.4028 −0.479
0.4042 −0.509
0.4055 −0.548
0.4113 −0.688
0.4126 −0.733
0.4181 −1.017
0.4194 −1.095
0.4247 −1.465
0.4260 −1.510
0.4316 −1.537
0.4329 −1.537
0.4386 −1.507
0.4483 −1.386
0.4510 −1.359
0.4585 −1.244
0.4640 −1.266
0.4653 −1.250

2447462 +
0.3529 −0.577
0.3539 −0.606

0.3587 −0.620
0.3598 −0.617
0.3661 −0.754
0.3672 −0.776
0.3785 −0.999
0.3796 −1.003
0.3844 −1.128
0.3855 −1.115
0.3931 −1.155
0.3942 −1.153
0.3989 −1.126
0.4000 −1.123
0.4051 −1.135
0.4062 −1.145
0.4126 −1.125
0.4137 −1.119
0.4186 −1.090
0.4197 −1.069
0.4241 −1.061
0.4251 −1.036

Table 5.c Photoelectric differential B observations of XZ Dra

2436410 +
0.4215 −0.036
0.4246 −0.036
0.4278 −0.039
0.4341 −0.045
0.4397 −0.024
0.4429 −0.024
0.4457 −0.053
0.4531 −0.080
0.4575 −0.125
0.4611 −0.162
0.4681 −0.232
0.4721 −0.274
0.4753 −0.349
0.4816 −0.433
0.4846 −0.462
0.4878 −0.504
0.4941 −0.601
0.4966 −0.632
0.4989 −0.685
0.5050 −0.800
0.5073 −0.818
0.5098 −0.871
0.5151 −0.985
0.5181 −1.042
0.5209 −1.088
0.5269 −1.113
0.5293 −1.093
0.5320 −1.079
0.5376 −1.058
0.5404 −1.040
0.5494 −1.025
0.5522 −1.018
0.5550 −0.997

2436413 +
0.3709 −0.956
0.3730 −0.953
0.3751 −0.968
0.3796 −1.012
0.3817 −1.055
0.3838 −1.065
0.3859 −1.097
0.3879 −1.110
0.3931 −1.120
0.3956 −1.120
0.3984 −1.109
0.4015 −1.099
0.4043 −1.054

2436420 +
0.4812 −0.439
0.4837 −0.474
0.4870 −0.508
0.4937 −0.572
0.4962 −0.657
0.4991 −0.681
0.5015 −0.689
0.5063 −0.750
0.5093 −0.760
0.5126 −0.808
0.5150 −0.827
0.5249 −0.965
0.5278 −1.018
0.5303 −1.032

2436421 +
0.3959 −0.139
0.3989 −0.153
0.4017 −0.195
0.4047 −0.221
0.4072 −0.228
0.4126 −0.247
0.4152 −0.281
0.4175 −0.301
0.4225 −0.312
0.4250 −0.325
0.4274 −0.376
0.4341 −0.433
0.4379 −0.444
0.4408 −0.515
0.4464 −0.624
0.4532 −0.695
0.4626 −0.805
0.4663 −0.850
0.4730 −0.899
0.4758 −0.919
0.4781 −0.957
0.4842 −1.014
0.4868 −1.020
0.4900 −1.033
0.4935 −1.046
0.4958 −1.072
0.4989 −1.072
0.5020 −1.058
0.5076 −1.029
0.5107 −0.997
0.5133 −0.965
0.5197 −0.941
0.5242 −0.935
0.5277 −0.912
0.5334 −0.875
0.5370 −0.854

2436443 +
0.3648 −0.289
0.3683 −0.325
0.3711 −0.366
0.3780 −0.526
0.3803 −0.573
0.3836 −0.652
0.3912 −0.796
0.3940 −0.862
0.3968 −0.944
0.4030 −1.023
0.4058 −1.046
0.4086 −1.060
0.4155 −1.066
0.4190 −1.046

2436450 +
0.4459 0.071
0.4477 0.070
0.4517 0.030
0.4538 0.006
0.4558 −0.008
0.4598 −0.031
0.4616 −0.032
0.4635 −0.048
0.4672 −0.024
0.4690 −0.029
0.4709 −0.039
0.4732 −0.038
0.4751 −0.035
0.4831 −0.008
0.4850 −0.008
0.4892 −0.029
0.4910 −0.028
0.4947 −0.087
0.4963 −0.110
0.4982 −0.126
0.5000 −0.131
0.5038 −0.152
0.5056 −0.179
0.5074 −0.205
0.5093 −0.211
0.5111 −0.221
0.5130 −0.225
0.5149 −0.229
0.5190 −0.265
0.5209 −0.286
0.5227 −0.316
0.5246 −0.353
0.5264 −0.365
0.5283 −0.375
0.5301 −0.417
0.5343 −0.471
0.5364 −0.540
0.5382 −0.622
0.5401 −0.687
0.5419 −0.750
0.5438 −0.844
0.5456 −0.916
0.5510 −1.148
0.5528 −1.183
0.5547 −1.200
0.5586 −1.249
0.5605 −1.272
0.5623 −1.270
0.5642 −1.252
0.5677 −1.221
0.5691 −1.189
0.5705 −1.156
0.5724 −1.148
0.5740 −1.130
0.5782 −1.109
0.5836 −1.067

2436451 +
0.4490 −0.053
0.4511 −0.072
0.4530 −0.073
0.4540 −0.085
0.4567 −0.094
0.4604 −0.115
0.4623 −0.139
0.4639 −0.159
0.4674 −0.203
0.4690 −0.220
0.4704 −0.250
0.4740 −0.285
0.4756 −0.309
0.4772 −0.333
0.4819 −0.485
0.4840 −0.514
0.4862 −0.546
0.4904 −0.636
0.4929 −0.691
0.4958 −0.759
0.5001 −0.883
0.5030 −0.974
0.5052 −1.005
0.5092 −1.121
0.5112 −1.197

0.5137 −1.235
0.5226 −1.184
0.5249 −1.172
0.5277 −1.156

2436454 +
0.2906 −0.009
0.2932 −0.024
0.2950 −0.030
0.2987 −0.047
0.3006 −0.054
0.3022 −0.073
0.3064 −0.082
0.3084 −0.096
0.3106 −0.100
0.3158 −0.127
0.3182 −0.134
0.3204 −0.158
0.3248 −0.235
0.3271 −0.262
0.3291 −0.292
0.3338 −0.353
0.3361 −0.397
0.3384 −0.426
0.3431 −0.488
0.3454 −0.555
0.3477 −0.601
0.3522 −0.716
0.3551 −0.773
0.3576 −0.819
0.3620 −0.921
0.3639 −0.981
0.3661 −1.023
0.3704 −1.149
0.3727 −1.214
0.3750 −1.259
0.3791 −1.268
0.3810 −1.262
0.3831 −1.227
0.3868 −1.204

2436463 +
0.3598 −0.062
0.3656 −0.096
0.3704 −0.101
0.3718 −0.108
0.3732 −0.120
0.3770 −0.171
0.3788 −0.199
0.3807 −0.251
0.3844 −0.314
0.3862 −0.350
0.3881 −0.369
0.3920 −0.437
0.3939 −0.483
0.3957 −0.518
0.3996 −0.600
0.4015 −0.652
0.4033 −0.694
0.4070 −0.791
0.4089 −0.814
0.4108 −0.850
0.4145 −0.929
0.4163 −1.004
0.4182 −1.060
0.4219 −1.171
0.4237 −1.244
0.4256 −1.296
0.4292 −1.309
0.4309 −1.302
0.4327 −1.293
0.4369 −1.262
0.4388 −1.257
0.4406 −1.232
0.4443 −1.200
0.4462 −1.171

2436474 +
0.3675 −0.978
0.3699 −1.010
0.3752 −1.051
0.3772 −1.073
0.3795 −1.080
0.3840 −1.120
0.3865 −1.151
0.3893 −1.141
0.3948 −1.140
0.3976 −1.130
0.4004 −1.105
0.4066 −1.087
0.4094 −1.047
0.4122 −1.042

2436475 +
0.2820 −0.197
0.2872 −0.300
0.2893 −0.366
0.2916 −0.419
0.2957 −0.503
0.2977 −0.535
0.3018 −0.616
0.3056 −0.689
0.3076 −0.745
0.3132 −0.879
0.3159 −0.983
0.3187 −1.015
0.3239 −1.111
0.3267 −1.152
0.3295 −1.141
0.3364 −1.176
0.3392 −1.184
0.3413 −1.175
0.3461 −1.182

2436486 +
0.2454 −0.521
0.2470 −0.537
0.2489 −0.597
0.2530 −0.637
0.2551 −0.689
0.2573 −0.703
0.2622 −0.759
0.2644 −0.782
0.2668 −0.791
0.2723 −0.847
0.2748 −0.886
0.2770 −0.901
0.2818 −0.974
0.2844 −0.974
0.2866 −0.982
0.2918 −1.030
0.2941 −1.033
0.2963 −1.039

2436503 +
0.4080 −0.648
0.4122 −0.686
0.4142 −0.713
0.4184 −0.750
0.4204 −0.790
0.4224 −0.816
0.4263 −0.830
0.4284 −0.861
0.4302 −0.914
0.4344 −0.911
0.4390 −0.907
0.4432 −0.977
0.4456 −1.003
0.4479 −1.012
0.4528 −1.039
0.4554 −1.045
0.4576 −1.050
0.4623 −1.023
0.4644 −1.019

2436506 +
0.2137 −0.076
0.2173 −0.099
0.2190 −0.099
0.2224 −0.088
0.2239 −0.102
0.2255 −0.104
0.2291 −0.116
0.2308 −0.144
0.2326 −0.169
0.2381 −0.204
0.2397 −0.223
0.2433 −0.260
0.2452 −0.276
0.2471 −0.300
0.2509 −0.361
0.2527 −0.395
0.2544 −0.440
0.2580 −0.512
0.2621 −0.596
0.2682 −0.677
0.2698 −0.693
0.2733 −0.703
0.2758 −0.722
0.2774 −0.742
0.2811 −0.793
0.2830 −0.799
0.2848 −0.839
0.2889 −0.876
0.2905 −0.926
0.2923 −0.942
0.2960 −0.977
0.2978 −0.978
0.2997 −1.000
0.3052 −1.041
0.3070 −1.046
0.3104 −1.053
0.3126 −1.049
0.3148 −1.073
0.3225 −1.017
0.3245 −1.022
0.3288 −0.982
0.3310 −0.953

2436514 +
0.3666 −0.465
0.3684 −0.498
0.3703 −0.550
0.3740 −0.635
0.3758 −0.654
0.3777 −0.696
0.3814 −0.781
0.3832 −0.829
0.3851 −0.878
0.3888 −0.997
0.3906 −1.060
0.3925 −1.090
0.3962 −1.105
0.3980 −1.116
0.3999 −1.120
0.4117 −1.094
0.4135 −1.081

2437348 +
0.5400 −0.192
0.5462 −0.183
0.5527 −0.142
0.5596 −0.128
0.5664 −0.124
0.5812 −0.109
0.5879 −0.112
0.5935 −0.062
0.6004 −0.069
0.6131 −0.016
0.6276 −0.006
0.6347 0.017
0.6415 0.048
0.6495 0.049
0.6572 0.045

2437465 +
0.4639 −0.701

0.4665 −0.796
0.4678 −0.812
0.4707 −0.887
0.4724 −0.935
0.4740 −0.981
0.4774 −1.041
0.4789 −1.059
0.4802 −1.064
0.4835 −1.119
0.4851 −1.110
0.4870 −1.128
0.4900 −1.157
0.4916 −1.157
0.4932 −1.171
0.4965 −1.158
0.4981 −1.158
0.5001 −1.158
0.5035 −1.158
0.5055 −1.147
0.5076 −1.139
0.5121 −1.133
0.5137 −1.110
0.5150 −1.111
0.5183 −1.102
0.5200 −1.106
0.5219 −1.081
0.5255 −1.067
0.5270 −1.060
0.5290 −1.060
0.5358 −1.019
0.5379 −0.980

2437467 +
0.4047 −1.196
0.4096 −1.167
0.4116 −1.145
0.4162 −1.118
0.4182 −1.091
0.4203 −1.085
0.4259 −1.076
0.4280 −1.064
0.4300 −1.061
0.4342 −1.041
0.4363 −1.012
0.4384 −0.999
0.4436 −0.998
0.4457 −0.989
0.4491 −0.973

2437475 +
0.4074 −0.133
0.4091 −0.158
0.4111 −0.165
0.4147 −0.176
0.4176 −0.198
0.4195 −0.201
0.4266 −0.275
0.4284 −0.288
0.4303 −0.330
0.4353 −0.373
0.4386 −0.421
0.4407 −0.449
0.4460 −0.527
0.4478 −0.575
0.4497 −0.588
0.4548 −0.658
0.4570 −0.717
0.4589 −0.737
0.4622 −0.777
0.4640 −0.823
0.4661 −0.839
0.4712 −0.932
0.4730 −0.941
0.4748 −0.961
0.4780 −1.010
0.4797 −1.035
0.4804 −1.028
0.4833 −1.055
0.4869 −1.088
0.4888 −1.106
0.4902 −1.103
0.4945 −1.116
0.4973 −1.101
0.5000 −1.093
0.5049 −1.099
0.5077 −1.078
0.5132 −1.069
0.5181 −1.055

2437486 +
0.3818 −0.267
0.3841 −0.284
0.3860 −0.313
0.3899 −0.364
0.3913 −0.372
0.3932 −0.394
0.3975 −0.458
0.3991 −0.455
0.4008 −0.492
0.4048 −0.525
0.4065 −0.551
0.4088 −0.608
0.4125 −0.660
0.4144 −0.659
0.4162 −0.689
0.4204 −0.762
0.4221 −0.791
0.4237 −0.823
0.4272 −0.854
0.4305 −0.889
0.4319 −0.896
0.4367 −0.953
0.4388 −0.980
0.4404 −0.987
0.4446 −0.995
0.4462 −1.014
0.4476 −1.031
0.4510 −1.047
0.4531 −1.052
0.4548 −1.053
0.4592 −1.077
0.4626 −1.069
0.4640 −1.087
0.4679 −1.091
0.4700 −1.080
0.4719 −1.088
0.4763 −1.060
0.4777 −1.057
0.4807 −1.035
0.4851 −0.996
0.4869 −1.006
0.4897 −0.979
0.4978 −0.905
0.4992 −0.905
0.5006 −0.884
0.5061 −0.863
0.5131 −0.848
0.5196 −0.785
0.5305 −0.714
0.5331 −0.696
0.5353 −0.686
0.5405 −0.677
0.5426 −0.676
0.5456 −0.656

2439391 +
0.4062 −0.195
0.4081 −0.224
0.4144 −0.288
0.4170 −0.312
0.4223 −0.345
0.4248 −0.377
0.4328 −0.525
0.4349 −0.554
0.4396 −0.614
0.4416 −0.659
0.4434 −0.674
0.4486 −0.740
0.4504 −0.779
0.4528 −0.799
0.4570 −0.882
0.4587 −0.924
0.4602 −0.947
0.4635 −0.973
0.4650 −0.989
0.4671 −1.004
0.4706 −1.006
0.4739 −1.014
0.4776 −1.016
0.4810 −1.012
0.4848 −1.016
0.4865 −1.014
0.4882 −1.014
0.4916 −0.986
0.4931 −0.976
0.4949 −0.978
0.4991 −0.967
0.5009 −0.949
0.5025 −0.943
0.5064 −0.932
0.5082 −0.919
0.5097 −0.903

2439402 +
0.4050 −0.622
0.4077 −0.681
0.4133 −0.811
0.4154 −0.873
0.4209 −0.991
0.4237 −1.064
0.4300 −1.182
0.4321 −1.202
0.4383 −1.227
0.4411 −1.228
0.4473 −1.209
0.4543 −1.175
0.4564 −1.174
0.4619 −1.143
0.4647 −1.099
0.4695 −1.066
0.4716 −1.061
0.4765 −1.032
0.4800 −1.008

2439403 +
0.3112 0.062
0.3126 0.058
0.3140 0.055
0.3182 0.018
0.3202 0.011
0.3223 −0.001
0.3258 −0.012
0.3272 −0.018
0.3293 −0.065
0.3341 −0.120
0.3362 −0.136
0.3376 −0.154
0.3411 −0.209
0.3432 −0.216
0.3453 −0.241
0.3487 −0.303
0.3508 −0.320
0.3529 −0.368
0.3564 −0.442
0.3591 −0.516
0.3612 −0.602
0.3647 −0.749
0.3668 −0.835
0.3682 −0.871
0.3716 −0.907
0.3730 −0.920
0.3744 −0.961
0.3772 −1.040
0.3786 −1.082
0.3800 −1.122

0.3834 −1.169
0.3848 −1.181
0.3869 −1.197
0.3897 −1.213
0.3911 −1.214
0.3932 −1.224
0.3959 −1.221
0.3980 −1.215
0.3994 −1.213
0.4029 −1.199
0.4050 −1.200
0.4064 −1.189
0.4098 −1.152
0.4112 −1.135
0.4126 −1.134
0.4161 −1.106
0.4175 −1.097
0.4196 −1.092
0.4223 −1.066
0.4244 −1.055
0.4258 −1.047

2440494 +
0.5097 0.007
0.5111 −0.014
0.5153 −0.018
0.5174 −0.046
0.5313 −0.218
0.5340 −0.229
0.5354 −0.260
0.5382 −0.327
0.5424 −0.445
0.5438 −0.457
0.5479 −0.498
0.5493 −0.529
0.5612 −0.791
0.5626 −0.820
0.5667 −0.941
0.5681 −0.985
0.5723 −1.028
0.5737 −1.034

2440500 +
0.2600 −0.567
0.2614 −0.586
0.2628 −0.640
0.2656 −0.681
0.2670 −0.716
0.2684 −0.729
0.2711 −0.777
0.2725 −0.807
0.2739 −0.871
0.2767 −0.979
0.2781 −1.016
0.2795 −1.073
0.2822 −1.108
0.2836 −1.109
0.2850 −1.103
0.2878 −1.119
0.2892 −1.143
0.2906 −1.155
0.2933 −1.149
0.2947 −1.160

2440504 +
0.5416 −0.424
0.5430 −0.438
0.5444 −0.471
0.5471 −0.524
0.5485 −0.560
0.5499 −0.565
0.5527 −0.628
0.5541 −0.660
0.5555 −0.705
0.5583 −0.786
0.5597 −0.814
0.5611 −0.860
0.5638 −0.937
0.5652 −0.948
0.5666 −0.974
0.5694 −1.027
0.5708 −1.020
0.5722 −1.033
0.5749 −1.061
0.5763 −1.067
0.5777 −1.077
0.5805 −1.101
0.5819 −1.112
0.5833 −1.106
0.5860 −1.113
0.5874 −1.117
0.5888 −1.106

2440516 +
0.4028 −0.144
0.4056 −0.159
0.4070 −0.166
0.4084 −0.178
0.4111 −0.186
0.4125 −0.202
0.4139 −0.212
0.4167 −0.216
0.4181 −0.216
0.4195 −0.216
0.4222 −0.227
0.4236 −0.231
0.4250 −0.245
0.4278 −0.256
0.4292 −0.256
0.4306 −0.268
0.4333 −0.286
0.4347 −0.294
0.4361 −0.314
0.4389 −0.346
0.4403 −0.356
0.4417 −0.373
0.4444 −0.375
0.4458 −0.397
0.4472 −0.413
0.4500 −0.492
0.4514 −0.503
0.4528 −0.531
0.4569 −0.592
0.4583 −0.619
0.4597 −0.641
0.4625 −0.697
0.4639 −0.722
0.4653 −0.734
0.4681 −0.773
0.4695 −0.776
0.4709 −0.777
0.4736 −0.800
0.4750 −0.810
0.4764 −0.827
0.4792 −0.868
0.4806 −0.876
0.4820 −0.910
0.4847 −0.951
0.4861 −0.972
0.4875 −0.977
0.4903 −0.977
0.4917 −0.985
0.4931 −0.989
0.4958 −0.986
0.4972 −1.001
0.4986 −0.999
0.5014 −0.987
0.5028 −0.988
0.5042 −0.982
0.5069 −0.981
0.5083 −0.981
0.5097 −0.976
0.5125 −0.973
0.5139 −0.973
0.5153 −0.958

2440528 +
0.3181 −0.027
0.3195 −0.020
0.3209 −0.021
0.3237 −0.051
0.3251 −0.060
0.3265 −0.067
0.3293 −0.079
0.3307 −0.089
0.3321 −0.083
0.3348 −0.089
0.3362 −0.098
0.3376 −0.105
0.3404 −0.143
0.3418 −0.156
0.3432 −0.171
0.3459 −0.189
0.3473 −0.197
0.3487 −0.206
0.3515 −0.236
0.3529 −0.247
0.3543 −0.270
0.3570 −0.310
0.3584 −0.334
0.3598 −0.350
0.3626 −0.407
0.3640 −0.432
0.3654 −0.458
0.3681 −0.533
0.3695 −0.549
0.3709 −0.571
0.3737 −0.599
0.3751 −0.612
0.3765 −0.619
0.3793 −0.686
0.3807 −0.712
0.3821 −0.749
0.3848 −0.805
0.3862 −0.825
0.3876 −0.838
0.3904 −0.884
0.3918 −0.917
0.3932 −0.939
0.3959 −0.974
0.3973 −0.991
0.3987 −1.008
0.4015 −1.038
0.4029 −1.052
0.4043 −1.058
0.4070 −1.085
0.4084 −1.088
0.4098 −1.090
0.4126 −1.092
0.4140 −1.097
0.4154 −1.102
0.4182 −1.104
0.4196 −1.099
0.4210 −1.093

2440530 +
0.2626 −0.286
0.2640 −0.318
0.2654 −0.349
0.2682 −0.381
0.2696 −0.389
0.2710 −0.401
0.2738 −0.442
0.2752 −0.456
0.2766 −0.473
0.2793 −0.554
0.2807 −0.599
0.2821 −0.613
0.2849 −0.672
0.2863 −0.706
0.2877 −0.732
0.2904 −0.807
0.2918 −0.825
0.2932 −0.854
0.2960 −0.890
0.2974 −0.930

0.2988 −0.955
0.3015 −0.983
0.3029 −1.001
0.3043 −1.012
0.3071 −1.059
0.3085 −1.076
0.3099 −1.109
0.3140 −1.108
0.3154 −1.100
0.3168 −1.094
0.3196 −1.085
0.3210 −1.086
0.3224 −1.089
0.3251 −1.084
0.3265 −1.083
0.3279 −1.081

2440541 +
0.2326 −0.270
0.2347 −0.299
0.2389 −0.388
0.2410 −0.429
0.2451 −0.527
0.2472 −0.580
0.2514 −0.690
0.2535 −0.746
0.2576 −0.832
0.2597 −0.882
0.2639 −1.020
0.2660 −1.070
0.2701 −1.142
0.2722 −1.173
0.2764 −1.242
0.2785 −1.261
0.2826 −1.238
0.2847 −1.245
0.2889 −1.200
0.2910 −1.181

2440676 +
0.5177 −0.072
0.5239 −0.097
0.5302 −0.124
0.5364 −0.170
0.5385 −0.192
0.5427 −0.244
0.5448 −0.269
0.5489 −0.322
0.5510 −0.340
0.5552 −0.387
0.5573 −0.414
0.5614 −0.443
0.5635 −0.477
0.5677 −0.565
0.5698 −0.603
0.5739 −0.664
0.5760 −0.705
0.5802 −0.750
0.5823 −0.791
0.5864 −0.832
0.5885 −0.866
0.5927 −0.927
0.5948 −0.943
0.5989 −0.980
0.6010 −0.995
0.6052 −1.029
0.6073 −1.031
0.6114 −1.035
0.6135 −1.020
0.6177 −1.005
0.6212 −0.986
0.6233 −0.965

2440707 +
0.5077 0.033
0.5098 0.035
0.5140 0.028
0.5161 0.036
0.5202 0.037
0.5223 0.030
0.5265 −0.032
0.5286 −0.052
0.5327 −0.102
0.5348 −0.122
0.5394 −0.185
0.5415 −0.224
0.5445 −0.284
0.5466 −0.344
0.5508 −0.454
0.5529 −0.508
0.5570 −0.689
0.5591 −0.774
0.5633 −0.930
0.5654 −1.044
0.5695 −1.191
0.5716 −1.254
0.5751 −1.376
0.5772 −1.408
0.5814 −1.419
0.5835 −1.413

2440709 +
0.4150 0.012
0.4164 0.012
0.4191 0.002
0.4205 0.006
0.4233 0.000
0.4247 0.011
0.4275 0.005
0.4289 0.001
0.4316 −0.015
0.4330 −0.019
0.4358 −0.043
0.4372 −0.070
0.4400 −0.104
0.4414 −0.123
0.4441 −0.160
0.4455 −0.185
0.4483 −0.256
0.4497 −0.282
0.4525 −0.360
0.4539 −0.391
0.4566 −0.452
0.4580 −0.476
0.4608 −0.571
0.4622 −0.629
0.4650 −0.747
0.4664 −0.803
0.4691 −0.902
0.4705 −0.951
0.4733 −1.055
0.4747 −1.096
0.4775 −1.165
0.4789 −1.222
0.4816 −1.290
0.4830 −1.330
0.4858 −1.372
0.4872 −1.390
0.4900 −1.390
0.4914 −1.397
0.4941 −1.381
0.4955 −1.367
0.4983 −1.353
0.4997 −1.344
0.5025 −1.309
0.5039 −1.292
0.5066 −1.282
0.5080 −1.273
0.5108 −1.260
0.5122 −1.249

2440731 +
0.3400 −0.151
0.3414 −0.176
0.3442 −0.220
0.3456 −0.250
0.3484 −0.273
0.3498 −0.296
0.3524 −0.340
0.3538 −0.364
0.3566 −0.400
0.3580 −0.439
0.3608 −0.484
0.3622 −0.520
0.3649 −0.576
0.3663 −0.609
0.3691 −0.664
0.3705 −0.690
0.3733 −0.728
0.3747 −0.762
0.3774 −0.810
0.3788 −0.838
0.3816 −0.900
0.3830 −0.933
0.3858 −0.980
0.3872 −1.005
0.3899 −1.048
0.3913 −1.058
0.3941 −1.097
0.3955 −1.104
0.3983 −1.138
0.3997 −1.147
0.4024 −1.173
0.4038 −1.175
0.4066 −1.174
0.4080 −1.178

2440751 +
0.3579 −0.339
0.3593 −0.342
0.3635 −0.375
0.3648 −0.384
0.3683 −0.410
0.3697 −0.420
0.3732 −0.468
0.3746 −0.486
0.3781 −0.530
0.3795 −0.561
0.3822 −0.587
0.3836 −0.617
0.3864 −0.662
0.3884 −0.696
0.3912 −0.740
0.3926 −0.771
0.3961 −0.813
0.3975 −0.844
0.4010 −0.913
0.4031 −0.950
0.4065 −0.992
0.4079 −1.000
0.4107 −1.013
0.4121 −1.025
0.4149 −1.035
0.4163 −1.040
0.4190 −1.048
0.4204 −1.041
0.4232 −1.044
0.4246 −1.044
0.4280 −1.045
0.4294 −1.038
0.4322 −1.022
0.4336 −1.013
0.4364 −1.008
0.4378 −1.002
0.4405 −0.991
0.4419 −0.981
0.4447 −0.962
0.4461 −0.950
0.4489 −0.930
0.4503 −0.918

2440780 +
0.4447 −0.308
0.4469 −0.355
0.4510 −0.440
0.4531 −0.491

0.4572 −0.602
0.4593 −0.646
0.4635 −0.758
0.4656 −0.821
0.4697 −0.952
0.4718 −1.028
0.4760 −1.147
0.4781 −1.225
0.4822 −1.313
0.4843 −1.344
0.4885 −1.360
0.4919 −1.341
0.4961 −1.307
0.4982 −1.287

2440821 +
0.4096 −0.415
0.4117 −0.437
0.4166 −0.511
0.4186 −0.551
0.4228 −0.667
0.4249 −0.690
0.4305 −0.782
0.4326 −0.806
0.4423 −0.941
0.4444 −0.963
0.4492 −1.010
0.4513 −1.020
0.4583 −1.057
0.4631 −1.094
0.4652 −1.097
0.4749 −1.089
0.4770 −1.075
0.4839 −1.019
0.4860 −1.008
0.4916 −0.932
0.4937 −0.888
0.5062 −0.756
0.5083 −0.724

2440840 +
0.4590 −0.018
0.4617 −0.030
0.4631 −0.041
0.4645 −0.073
0.4673 −0.088
0.4687 −0.097
0.4701 −0.124
0.4728 −0.174
0.4742 −0.196
0.4756 −0.201
0.4784 −0.240
0.4798 −0.252
0.4839 −0.359
0.4853 −0.392
0.4867 −0.424
0.4895 −0.477
0.4909 −0.505
0.4950 −0.586
0.4964 −0.630
0.4978 −0.651
0.5006 −0.719
0.5020 −0.749
0.5034 −0.786
0.5062 −0.833
0.5076 −0.860
0.5090 −0.895
0.5117 −0.957
0.5131 −0.982
0.5145 −1.012
0.5173 −1.047
0.5187 −1.068
0.5201 −1.088
0.5228 −1.121
0.5242 −1.129
0.5256 −1.125
0.5284 −1.107
0.5298 −1.105
0.5312 −1.100
0.5353 −1.052
0.5367 −1.044
0.5388 −1.018
0.5402 −1.014
0.5416 −1.005

2440863 +
0.3757 −0.587
0.3771 −0.618
0.3785 −0.694
0.3826 −0.855
0.3840 −0.917
0.3854 −0.978
0.3903 −1.097
0.3924 −1.141
0.3938 −1.180
0.3979 −1.269
0.3993 −1.323
0.4007 −1.344
0.4049 −1.371
0.4063 −1.374
0.4077 −1.386
0.4139 −1.377
0.4153 −1.364
0.4167 −1.357
0.4201 −1.338
0.4215 −1.311
0.4229 −1.300
0.4292 −1.218
0.4306 −1.211
0.4320 −1.202

2440925 +
0.2656 0.054
0.2670 0.055
0.2684 0.048
0.2711 0.061
0.2725 0.067
0.2739 0.050
0.2788 0.037
0.2802 0.031
0.2816 0.041
0.2843 0.022
0.2857 0.018
0.2871 0.015
0.3107 −0.352
0.3121 −0.409
0.3135 −0.448
0.3163 −0.517
0.3177 −0.572
0.3191 −0.646
0.3218 −0.775
0.3232 −0.840
0.3246 −0.917
0.3274 −1.036
0.3288 −1.078
0.3302 −1.134
0.3329 −1.185
0.3343 −1.218
0.3357 −1.236
0.3385 −1.266
0.3399 −1.271
0.3413 −1.271
0.3441 −1.257
0.3455 −1.247
0.3469 −1.242
0.3496 −1.224
0.3510 −1.220
0.3524 −1.208
0.3552 −1.174
0.3566 −1.162
0.3580 −1.134

2440937 +
0.2209 −0.292
0.2223 −0.320
0.2237 −0.332
0.2265 −0.361
0.2279 −0.383
0.2293 −0.424
0.2320 −0.484
0.2334 −0.509
0.2348 −0.538
0.2369 −0.581
0.2383 −0.605
0.2397 −0.653
0.2425 −0.720
0.2439 −0.786
0.2453 −0.838
0.2467 −0.919
0.2481 −0.960
0.2495 −1.003
0.2529 −1.093
0.2543 −1.151
0.2557 −1.169
0.2584 −1.242
0.2640 −1.293
0.2668 −1.292
0.2682 −1.292
0.2696 −1.283
0.2723 −1.272
0.2737 −1.265
0.2751 −1.245
0.2779 −1.207
0.2793 −1.199
0.2807 −1.187

2441249 +
0.2503 −0.006
0.2517 −0.016
0.2531 −0.014
0.2559 0.011
0.2573 0.026
0.2587 0.021
0.2614 0.034
0.2628 0.029
0.2649 0.030
0.2684 0.029
0.2698 0.026
0.2712 0.043
0.2740 0.032
0.2754 0.036
0.2768 0.038
0.2795 0.038
0.2809 0.034
0.2823 0.037
0.2858 0.036
0.2878 0.037
0.2899 0.030
0.2934 0.038
0.2948 0.030
0.3198 −0.047
0.3212 −0.049
0.3222 −0.058
0.3249 −0.088
0.3263 −0.117
0.3277 −0.137
0.3305 −0.184
0.3320 −0.219
0.3336 −0.248
0.3360 −0.306
0.3371 −0.328
0.3383 −0.358
0.3408 −0.406
0.3419 −0.424
0.3431 −0.443
0.3455 −0.493
0.3469 −0.515
0.3488 −0.563
0.3507 −0.607
0.3520 −0.631
0.3534 −0.655
0.3557 −0.732
0.3569 −0.748
0.3580 −0.772
0.3605 −0.865

0.3618 −0.904
0.3628 −0.939
0.3652 −0.997
0.3666 −1.017
0.3679 −1.051
0.3705 −1.087
0.3721 −1.103
0.3734 −1.114
0.3764 −1.134
0.3777 −1.142
0.3791 −1.154
0.3823 −1.167
0.3839 −1.169
0.3854 −1.169
0.3886 −1.173
0.3902 −1.172
0.3914 −1.161
0.3941 −1.158
0.3955 −1.146
0.3972 −1.136
0.4007 −1.095
0.4028 −1.075
0.4044 −1.070

2441250 +
0.2285 0.056
0.2299 0.050
0.2370 0.057
0.2384 0.065
0.2397 0.073
0.2601 0.025
0.2615 0.017
0.2628 0.006
0.2679 −0.021
0.2691 −0.027
0.2705 −0.028
0.2750 −0.080
0.2763 −0.104
0.2775 −0.113
0.2833 −0.205
0.2858 −0.252
0.2896 −0.324
0.2907 −0.343
0.2961 −0.460
0.2973 −0.488
0.2985 −0.508
0.3024 −0.571

0.3036 −0.599
0.3048 −0.639
0.3088 −0.733
0.3100 −0.752
0.3110 −0.771
0.3165 −0.922
0.3178 −0.985
0.3190 −1.014
0.3219 −1.093
0.3233 −1.104
0.3281 −1.153
0.3294 −1.161
0.3306 −1.170
0.3338 −1.176
0.3352 −1.180
0.3366 −1.178
0.3399 −1.174
0.3411 −1.167
0.3426 −1.159
0.3455 −1.144
0.3470 −1.127
0.3480 −1.123

2441539 +
0.5016 −0.053
0.5030 −0.042
0.5058 −0.057
0.5072 −0.051
0.5099 −0.046
0.5113 −0.058
0.5141 −0.045
0.5155 −0.055
0.5183 −0.080
0.5197 −0.094
0.5224 −0.131
0.5238 −0.154
0.5266 −0.170
0.5280 −0.195
0.5307 −0.259
0.5321 −0.273
0.5349 −0.334
0.5363 −0.363
0.5391 −0.420
0.5405 −0.450
0.5433 −0.490
0.5447 −0.528
0.5474 −0.645

0.5488 −0.710
0.5516 −0.874
0.5530 −0.945
0.5558 −1.083
0.5571 −1.174
0.5599 −1.220
0.5613 −1.267
0.5641 −1.305
0.5655 −1.329
0.5683 −1.361
0.5697 −1.359
0.5724 −1.356
0.5738 −1.351
0.5766 −1.334
0.5780 −1.322
0.5808 −1.305
0.5822 −1.287

2441589 +
0.5597 −0.595
0.5611 −0.620
0.5639 −0.665
0.5653 −0.683
0.5681 −0.730
0.5695 −0.758
0.5722 −0.814
0.5736 −0.823
0.5764 −0.888
0.5778 −0.917
0.5806 −0.944
0.5820 −0.965
0.5847 −1.006
0.5861 −1.021
0.5889 −1.038
0.5903 −1.041
0.5931 −1.064
0.5945 −1.085
0.5972 −1.082
0.5986 −1.076
0.6014 −1.078
0.6028 −1.078
0.6056 −1.074
0.6070 −1.065
0.6111 −1.038
0.6139 −1.034
0.6153 −1.013

2441591 +
0.4550 −0.462
0.4564 −0.486
0.4591 −0.510
0.4605 −0.520
0.4633 −0.553
0.4647 −0.578
0.4675 −0.630
0.4689 −0.647
0.4716 −0.687
0.4730 −0.722
0.4758 −0.758
0.4772 −0.783
0.4800 −0.842
0.4814 −0.881
0.4841 −0.932
0.4855 −0.952
0.4883 −0.989
0.4897 −1.015
0.4925 −1.023
0.4939 −1.031
0.4966 −1.046
0.4980 −1.050
0.5008 −1.049
0.5022 −1.055
0.5050 −1.054
0.5064 −1.052
0.5091 −1.046
0.5105 −1.039
0.5133 −1.029
0.5147 −1.013
0.5175 −1.011
0.5189 −1.002
0.5216 −0.985
0.5230 −0.976

2441606 +
0.2400 −0.413
0.2407 −0.450
0.2417 −0.471
0.2441 −0.540
0.2455 −0.567
0.2462 −0.602
0.2490 −0.671
0.2504 −0.721
0.2511 −0.761
0.2539 −0.893

0.2549 −0.925
0.2556 −0.953
0.2580 −1.026
0.2587 −1.063
0.2594 −1.081
0.2622 −1.138
0.2629 −1.154
0.2639 −1.205
0.2664 −1.244
0.2678 −1.273
0.2685 −1.289
0.2712 −1.323
0.2722 −1.340
0.2733 −1.344
0.2761 −1.346
0.2775 −1.343
0.2789 −1.343
0.2816 −1.329
0.2826 −1.323
0.2837 −1.314
0.2865 −1.277
0.2872 −1.263
0.2882 −1.241

2441622 +
0.4313 −0.221
0.4327 −0.252
0.4354 −0.284
0.4368 −0.320
0.4396 −0.384
0.4410 −0.408
0.4438 −0.453
0.4452 −0.473
0.4479 −0.527
0.4493 −0.565
0.4521 −0.639
0.4535 −0.661
0.4563 −0.742
0.4577 −0.772
0.4604 −0.858
0.4618 −0.876
0.4646 −0.943
0.4660 −0.972
0.4688 −1.009
0.4702 −1.038
0.4729 −1.071
0.4743 −1.101

0.4771 −1.139
0.4785 −1.145
0.4813 −1.182
0.4827 −1.193
0.4854 −1.206
0.4868 −1.209
0.4896 −1.206
0.4910 −1.209
0.4938 −1.208
0.4952 −1.196
0.4979 −1.186
0.4993 −1.184
0.5021 −1.169
0.5035 −1.151

2441772 +
0.5138 −0.134
0.5152 −0.170
0.5180 −0.189
0.5194 −0.205
0.5221 −0.257
0.5235 −0.297
0.5263 −0.343
0.5277 −0.385
0.5305 −0.417
0.5319 −0.459
0.5346 −0.502
0.5360 −0.521
0.5388 −0.561
0.5402 −0.584
0.5430 −0.649
0.5444 −0.686
0.5471 −0.736
0.5485 −0.760
0.5513 −0.814
0.5527 −0.852
0.5555 −0.953
0.5569 −1.011
0.5596 −1.085
0.5610 −1.123
0.5638 −1.188
0.5652 −1.219
0.5680 −1.264
0.5694 −1.277
0.5721 −1.284
0.5735 −1.298
0.5763 −1.297

0.5777 −1.286
0.5805 −1.272
0.5819 −1.257
0.5846 −1.242
0.5860 −1.232

2441803 +
0.4687 −0.337
0.4704 −0.359
0.4731 −0.405
0.4741 −0.418
0.4757 −0.434
0.4767 −0.445
0.4785 −0.465
0.4799 −0.475
0.4812 −0.493
0.4826 −0.501
0.4840 −0.523
0.4854 −0.549
0.4874 −0.558
0.4888 −0.589
0.4907 −0.615
0.4921 −0.630
0.4943 −0.654
0.4957 −0.670
0.4978 −0.695
0.4992 −0.711
0.5013 −0.742
0.5023 −0.761
0.5041 −0.788
0.5048 −0.794
0.5068 −0.809
0.5078 −0.819
0.5096 −0.820
0.5103 −0.826
0.5124 −0.857
0.5138 −0.871
0.5152 −0.885
0.5166 −0.907
0.5187 −0.931
0.5201 −0.958
0.5215 −0.972
0.5229 −0.988
0.5242 −0.995
0.5256 −1.012
0.5270 −1.024
0.5280 −1.033

0.5298 −1.050
0.5312 −1.053
0.5333 −1.065
0.5347 −1.065
0.5360 −1.061
0.5374 −1.053
0.5388 −1.051
0.5402 −1.047
0.5423 −1.031
0.5433 −1.026
0.5451 −1.020
0.5465 −1.009
0.5485 −1.003
0.5499 −1.006
0.5520 −1.001
0.5534 −0.995
0.5554 −0.989
0.5568 −0.980
0.5582 −0.975
0.5596 −0.970
0.5617 −0.958
0.5631 −0.949
0.5652 −0.945
0.5666 −0.943
0.5680 −0.931
0.5694 −0.930
0.5715 −0.908
0.5729 −0.904

2441815 +
0.4052 −0.525
0.4059 −0.542
0.4080 −0.581
0.4094 −0.613
0.4114 −0.641
0.4128 −0.655
0.4148 −0.687
0.4155 −0.716
0.4184 −0.761
0.4198 −0.782
0.4219 −0.832
0.4229 −0.860
0.4253 −0.893
0.4263 −0.903
0.4298 −0.947
0.4305 −0.967
0.4322 −0.984

0.4336 −1.002
0.4357 −1.024
0.4371 −1.033
0.4392 −1.061
0.4406 −1.071
0.4427 −1.084
0.4441 −1.084
0.4468 −1.090
0.4478 −1.104
0.4503 −1.102
0.4510 −1.094
0.4537 −1.092
0.4544 −1.093
0.4572 −1.069
0.4586 −1.068
0.4607 −1.066
0.4616 −1.060
0.4641 −1.042
0.4648 −1.032
0.4670 −1.031
0.4684 −1.024
0.4712 −1.010
0.4719 −1.004
0.4739 −0.998
0.4753 −0.985
0.4774 −0.964
0.4788 −0.950

2441833 +
0.5006 −0.115
0.5020 −0.134
0.5041 −0.164
0.5055 −0.183
0.5075 −0.208
0.5089 −0.221
0.5110 −0.252
0.5124 −0.292
0.5145 −0.322
0.5159 −0.350
0.5180 −0.373
0.5194 −0.405
0.5214 −0.434
0.5228 −0.462
0.5249 −0.518
0.5263 −0.550
0.5284 −0.606
0.5298 −0.655

0.5319 −0.739
0.5333 −0.778
0.5353 −0.870
0.5367 −0.922
0.5388 −1.001
0.5402 −1.070
0.5423 −1.145
0.5437 −1.172
0.5458 −1.219
0.5472 −1.243
0.5492 −1.266

2441835 +
0.4201 −0.235
0.4215 −0.260
0.4239 −0.296
0.4250 −0.305
0.4278 −0.349
0.4292 −0.397
0.4319 −0.459
0.4333 −0.505
0.4361 −0.591
0.4375 −0.616
0.4403 −0.719
0.4413 −0.771
0.4441 −0.939
0.4451 −0.992
0.4489 −1.173
0.4503 −1.207
0.4531 −1.264
0.4545 −1.296
0.4573 −1.330
0.4587 −1.352
0.4601 −1.358
0.4632 −1.365
0.4646 −1.367
0.4674 −1.370
0.4688 −1.362
0.4711 −1.338
0.4722 −1.330
0.4749 −1.320
0.4763 −1.309
0.4795 −1.294
0.4809 −1.281
0.4840 −1.264
0.4854 −1.246
0.4881 −1.226

0.4895 −1.211
0.4917 −1.187
0.4931 −1.177

2441905 +
0.4628 −0.391
0.4642 −0.414
0.4669 −0.484
0.4679 −0.505
0.4701 −0.545
0.4711 −0.581
0.4738 −0.633
0.4750 −0.679
0.4776 −0.734
0.4784 −0.784
0.4809 −0.882
0.4818 −0.907
0.4840 −1.020
0.4850 −1.050
0.4870 −1.106
0.4880 −1.129
0.4910 −1.169
0.4920 −1.191
0.4944 −1.228
0.4954 −1.240
0.4977 −1.246
0.4986 −1.253
0.5010 −1.250
0.5021 −1.254
0.5044 −1.254
0.5054 −1.257
0.5074 −1.253
0.5086 −1.243
0.5107 −1.228
0.5118 −1.226
0.5142 −1.223
0.5153 −1.213
0.5176 −1.195
0.5186 −1.194

2441915 +
0.4494 −0.094
0.4501 −0.102
0.4522 −0.114
0.4536 −0.121
0.4557 −0.145
0.4571 −0.154
0.4591 −0.170
0.4605 −0.185
0.4633 −0.209
0.4647 −0.250
0.4671 −0.277
0.4685 −0.290
0.4709 −0.323
0.4723 −0.337
0.4747 −0.386
0.4757 −0.400
0.4876 −0.637
0.4886 −0.663
0.4913 −0.745
0.4923 −0.786
0.4945 −0.837
0.4955 −0.872
0.4980 −0.929
0.4987 −0.953
0.5008 −1.015
0.5018 −1.048
0.5043 −1.091
0.5064 −1.140
0.5087 −1.192
0.5112 −1.230
0.5133 −1.265

2441918 +
0.3216 −0.187
0.3228 −0.208
0.3256 −0.243
0.3270 −0.259
0.3291 −0.290
0.3303 −0.305
0.3334 −0.347
0.3348 −0.369
0.3376 −0.430
0.3390 −0.466
0.3418 −0.537
0.3447 −0.602
0.3480 −0.685
0.3508 −0.725
0.3522 −0.762
0.3546 −0.790
0.3556 −0.800

2441933 +
0.5641 −0.157
0.5650 −0.175
0.5669 −0.197
0.5678 −0.213
0.5696 −0.248
0.5705 −0.260
0.5724 −0.286
0.5733 −0.308
0.5752 −0.359
0.5761 −0.364
0.5780 −0.426
0.5789 −0.455
0.5808 −0.515
0.5817 −0.540
0.5863 −0.780
0.5872 −0.845

2441934 +
0.5145 −0.138
0.5173 −0.199
0.5200 −0.262
0.5252 −0.359
0.5259 −0.384
0.5280 −0.430
0.5287 −0.455
0.5302 −0.489
0.5339 −0.553
0.5367 −0.601
0.5395 −0.647
0.5423 −0.704
0.5450 −0.750
0.5478 −0.811
0.5506 −0.900
0.5534 −0.960
0.5562 −1.027
0.5589 −1.075
0.5617 −1.101
0.5645 −1.115
0.5673 −1.132
0.5700 −1.140
0.5727 −1.148
0.5759 −1.141
0.5777 −1.123
0.5812 −1.117

2441938 +
0.3676 −1.040
0.3690 −1.058
0.3724 −1.104
0.3738 −1.115
0.3769 −1.131
0.3783 −1.135
0.3822 −1.156
0.3839 −1.152
0.3870 −1.140
0.3884 −1.138
0.3926 −1.126
0.3940 −1.118
0.3981 −1.091
0.3998 −1.089

2441939 +
0.2849 −0.434
0.2863 −0.454
0.2884 −0.476
0.2898 −0.496
0.2919 −0.532
0.2933 −0.553
0.2953 −0.593
0.2967 −0.620
0.2988 −0.656
0.3002 −0.677
0.3023 −0.701
0.3037 −0.725
0.3058 −0.765
0.3072 −0.790
0.3092 −0.828
0.3106 −0.846
0.3127 −0.889
0.3141 −0.915
0.3162 −0.973
0.3176 −1.003
0.3197 −1.037
0.3211 −1.060
0.3231 −1.095
0.3245 −1.111
0.3266 −1.120
0.3280 −1.134
0.3301 −1.148
0.3315 −1.157
0.3335 −1.159
0.3349 −1.155
0.3370 −1.161
0.3384 −1.159
0.3405 −1.156
0.3419 −1.148
0.3440 −1.143
0.3454 −1.120
0.3474 −1.112
0.3488 −1.098
0.3509 −1.088
0.3523 −1.087
0.3544 −1.080
0.3558 −1.070

2441949 +
0.2846 −0.502
0.2857 −0.515
0.2877 −0.550
0.2891 −0.570
0.2916 −0.623
0.3030 −0.760
0.3058 −0.789
0.3085 −0.815
0.3113 −0.833
0.3141 −0.865
0.3169 −0.901
0.3195 −0.924
0.3224 −0.950
0.3252 −0.991
0.3280 −1.010
0.3308 −1.020
0.3335 −1.035
0.3363 −1.036
0.3445 −1.027
0.3474 −1.017
0.3502 −0.989
0.3530 −0.980
0.3558 −0.975
0.3585 −0.947
0.3641 −0.891

2441990 +
0.2642 −0.130
0.2659 −0.133
0.2691 −0.134
0.2705 −0.150
0.2735 −0.164
0.2752 −0.188
0.2781 −0.232
0.2795 −0.248
0.2822 −0.298

0.2839 −0.330
0.2867 −0.372
0.2877 −0.385
0.2920 −0.466
0.2947 −0.521
0.2954 −0.560
0.2975 −0.624
0.2989 −0.684
0.3017 −0.780
0.3024 −0.830
0.3045 −0.965
0.3052 −0.987
0.3072 −1.126
0.3079 −1.149
0.3100 −1.215
0.3107 −1.222
0.3128 −1.230
0.3135 −1.228
0.3156 −1.263
0.3163 −1.269
0.3184 −1.308
0.3191 −1.314
0.3211 −1.325
0.3218 −1.329
0.3239 −1.351
0.3246 −1.359
0.3267 −1.364
0.3274 −1.358
0.3295 −1.349
0.3309 −1.323
0.3336 −1.308
0.3350 −1.301
0.3378 −1.273
0.3392 −1.262
0.3420 −1.241
0.3434 −1.218
0.3461 −1.201
0.3475 −1.184

2442147 +
0.4804 −0.002
0.4818 0.010
0.4846 −0.003
0.4860 0.010
0.4971 −0.024
0.4985 −0.031
0.5026 −0.049
0.5040 −0.063
0.5082 −0.110
0.5096 −0.127
0.5123 −0.166
0.5137 −0.172
0.5186 −0.242
0.5200 −0.260
0.5214 −0.298
0.5228 −0.325
0.5262 −0.385
0.5276 −0.405
0.5318 −0.466
0.5332 −0.502
0.5373 −0.566
0.5387 −0.598
0.5415 −0.656
0.5429 −0.723
0.5464 −0.809
0.5478 −0.864
0.5512 −0.957
0.5526 −1.014
0.5561 −1.126
0.5575 −1.157
0.5610 −1.217
0.5624 −1.251
0.5658 −1.276
0.5672 −1.287
0.5714 −1.290
0.5728 −1.284
0.5762 −1.285
0.5776 −1.285
0.5811 −1.273
0.5825 −1.267
0.5853 −1.237
0.5867 −1.226
0.5901 −1.204
0.5915 −1.176
0.5936 −1.149
0.5950 −1.142

2442201 +
0.3722 −0.718
0.3736 −0.725
0.3770 −0.809
0.3784 −0.827
0.3812 −0.903
0.3826 −0.941
0.3854 −1.014
0.3868 −1.041
0.3895 −1.086
0.3909 −1.109
0.3937 −1.133
0.3951 −1.151
0.3986 −1.159
0.4000 −1.163
0.4027 −1.163
0.4076 −1.152
0.4090 −1.150
0.4118 −1.136
0.4132 −1.128
0.4167 −1.124
0.4180 −1.118
0.4208 −1.098
0.4222 −1.093
0.4257 −1.081
0.4271 −1.073
0.4312 −1.053
0.4354 −1.011
0.4368 −1.005
0.4403 −0.954
0.4417 −0.950

2442220 +
0.4278 −0.223
0.4306 −0.279
0.4334 −0.369
0.4348 −0.394
0.4362 −0.436
0.4389 −0.501
0.4403 −0.548
0.4417 −0.576
0.4445 −0.665
0.4459 −0.712
0.4473 −0.743
0.4501 −0.853
0.4515 −0.906
0.4529 −0.931
0.4556 −1.005
0.4570 −1.044
0.4584 −1.107
0.4612 −1.174
0.4626 −1.206
0.4640 −1.223
0.4667 −1.270
0.4681 −1.290
0.4695 −1.299
0.4723 −1.294
0.4737 −1.293
0.4751 −1.293
0.4778 −1.281
0.4792 −1.271
0.4806 −1.271
0.4834 −1.260
0.4848 −1.245
0.4862 −1.232
0.4889 −1.205
0.4903 −1.191
0.4917 −1.188

2442242 +
0.3521 −0.579
0.3531 −0.622
0.3576 −0.725
0.3586 −0.755
0.3604 −0.799
0.3614 −0.823
0.3632 −0.865
0.3642 −0.895
0.3660 −0.926
0.3670 −0.940
0.3688 −0.972
0.3708 −1.016
0.3757 −1.098
0.3776 −1.115
0.3813 −1.129
0.3850 −1.125
0.3868 −1.122
0.3887 −1.116
0.3906 −1.098
0.3924 −1.098

2442260 +
0.4185 −0.337
0.4199 −0.345
0.4227 −0.354
0.4241 −0.358
0.4268 −0.372
0.4282 −0.401
0.4310 −0.440
0.4324 −0.463
0.4352 −0.488
0.4366 −0.500
0.4393 −0.544
0.4407 −0.562
0.4435 −0.592
0.4449 −0.610
0.4477 −0.631
0.4491 −0.637
0.4518 −0.647
0.4532 −0.670
0.4560 −0.698
0.4574 −0.714
0.4602 −0.743
0.4609 −0.750
0.4630 −0.771
0.4640 −0.788
0.4660 −0.801
0.4674 −0.818
0.4699 −0.849
0.4713 −0.878
0.4741 −0.906
0.4751 −0.919
0.4778 −0.940
0.4792 −0.945
0.4817 −0.948
0.4831 −0.957
0.4866 −0.967
0.5056 −0.998
0.5084 −0.983
0.5098 −0.973
0.5123 −0.965

2442269 +
0.4872 −0.353
0.4900 −0.390
0.4914 −0.415
0.4942 −0.443
0.4956 −0.461
0.4980 −0.505
0.4994 −0.535
0.5018 −0.566
0.5032 −0.590
0.5074 −0.649
0.5098 −0.684
0.5108 −0.693
0.5133 −0.720
0.5144 −0.739
0.5168 −0.770

0.5179 −0.792
0.5202 −0.831
0.5213 −0.861
0.5237 −0.903
0.5244 −0.913
0.5272 −0.952
0.5283 −0.970
0.5307 −0.994
0.5314 −0.996
0.5341 −1.010
0.5352 −1.022
0.5376 −1.025
0.5387 −1.028
0.5411 −1.035
0.5418 −1.032
0.5445 −1.033
0.5459 −1.036
0.5487 −1.033
0.5494 −1.029
0.5518 −1.021
0.5529 −1.025
0.5557 −1.012
0.5591 −1.000
0.5598 −1.001

2442279 +
0.4852 −0.059
0.4865 −0.074
0.4877 −0.076
0.4891 −0.094
0.4905 −0.088
0.4964 −0.147
0.4977 −0.163
0.4989 −0.173
0.5003 −0.216
0.5014 −0.224
0.5067 −0.351
0.5078 −0.380
0.5090 −0.400
0.5103 −0.443
0.5113 −0.457
0.5184 −0.644
0.5196 −0.658
0.5207 −0.688
0.5260 −0.882
0.5271 −0.908
0.5281 −0.926
0.5294 −0.974
0.5304 −0.990
0.5354 −1.090
0.5365 −1.099
0.5376 −1.129
0.5386 −1.146
0.5397 −1.177
0.5444 −1.233
0.5455 −1.235
0.5465 −1.235
0.5476 −1.235
0.5487 −1.221
0.5538 −1.183
0.5548 −1.180
0.5558 −1.172
0.5568 −1.173
0.5578 −1.170
0.5589 −1.166

2442303 +
0.3439 −0.429
0.3453 −0.440
0.3480 −0.465
0.3490 −0.473
0.3512 −0.500
0.3518 −0.508
0.3539 −0.538
0.3545 −0.550
0.3566 −0.571
0.3573 −0.586
0.3594 −0.636
0.3604 −0.664
0.3629 −0.727
0.3639 −0.756
0.3668 −0.805
0.3679 −0.840
0.3709 −0.970
0.3733 −1.022
0.3743 −1.045
0.3765 −1.077
0.3776 −1.109
0.3800 −1.150
0.3807 −1.160
0.3827 −1.165
0.3837 −1.159
0.3855 −1.155
0.3866 −1.154
0.3887 −1.152
0.3897 −1.151
0.3918 −1.151
0.3928 −1.159
0.3950 −1.152

2442636 +
0.3601 −0.231
0.3610 −0.266
0.3655 −0.289
0.3665 −0.293
0.3711 −0.327
0.3719 −0.330
0.3748 −0.343
0.3756 −0.346
0.3782 −0.351
0.3808 −0.369
0.3835 −0.420
0.3842 −0.427
0.3860 −0.486
0.3868 −0.504
0.3889 −0.531
0.3922 −0.541
0.3929 −0.534
0.3948 −0.542
0.3958 −0.546
0.3980 −0.576
0.4020 −0.618
0.4046 −0.642
0.4085 −0.688
0.4138 −0.751
0.4147 −0.763
0.4168 −0.778
0.4175 −0.793
0.4199 −0.808
0.4234 −0.843
0.4252 −0.853
0.4259 −0.869
0.4286 −0.918
0.4306 −0.928
0.4314 −0.941
0.4334 −0.939
0.4342 −0.939
0.4399 −0.985
0.4425 −0.975
0.4460 −0.982
0.4486 −0.970
0.4510 −0.946
0.4518 −0.962
0.4541 −0.945
0.4567 −0.932
0.4576 −0.920

2442948 +
0.4865 −0.271
0.4879 −0.290
0.4907 −0.327
0.4948 −0.362
0.4962 −0.382
0.4997 −0.408
0.5025 −0.439
0.5039 −0.472
0.5072 −0.524
0.5086 −0.562
0.5115 −0.633
0.5129 −0.648
0.5163 −0.659
0.5205 −0.703
0.5219 −0.724
0.5253 −0.771
0.5293 −0.805
0.5306 −0.812

2443660 +
0.3494 −0.001
0.3534 0.012
0.3584 −0.002
0.3626 0.005
0.3665 −0.007
0.3747 −0.001
0.3790 −0.005
0.3838 −0.029
0.3889 −0.017
0.3945 −0.057
0.4042 −0.097
0.4084 −0.163
0.4168 −0.297
0.4205 −0.428
0.4218 −0.457
0.4247 −0.503
0.4260 −0.548
0.4287 −0.579
0.4301 −0.630
0.4330 −0.736
0.4342 −0.759
0.4369 −0.862
0.4385 −0.933
0.4411 −1.054
0.4431 −1.136

2443700 +
0.3937 −0.091
0.3951 −0.110
0.3978 −0.118
0.3992 −0.116
0.4020 −0.136
0.4034 −0.134
0.4062 −0.165
0.4076 −0.188
0.4145 −0.250
0.4187 −0.293
0.4201 −0.307
0.4228 −0.328
0.4242 −0.345
0.4270 −0.376
0.4284 −0.399
0.4312 −0.427
0.4326 −0.440
0.4353 −0.465
0.4367 −0.482
0.4395 −0.524
0.4409 −0.552
0.4437 −0.580
0.4451 −0.602
0.4478 −0.628
0.4520 −0.689
0.4534 −0.720
0.4576 −0.783
0.4603 −0.854
0.4617 −0.868
0.4645 −0.926
0.4659 −0.954
0.4687 −0.999
0.4701 −1.011
0.4728 −1.039
0.4742 −1.040
0.4770 −1.067
0.4784 −1.061
0.4812 −1.074
0.4853 −1.059
0.4867 −1.053

0.4895 −1.032
0.4909 −1.030
0.4951 −1.018
0.4978 −1.012
0.4992 −0.998
0.5020 −0.985
0.5062 −0.971
0.5076 −0.957
0.5103 −0.941
0.5117 −0.932

2443720 +
0.4571 −0.587
0.4598 −0.640
0.4620 −0.698
0.4638 −0.731
0.4648 −0.755
0.4666 −0.815
0.4675 −0.840
0.4694 −0.895
0.4703 −0.915
0.4722 −0.991
0.4731 −1.020
0.4749 −1.070
0.4759 −1.109
0.4780 −1.149
0.4793 −1.180
0.4821 −1.217
0.4835 −1.247
0.4863 −1.268
0.4877 −1.271
0.4905 −1.275
0.4918 −1.274
0.4953 −1.262
0.4988 −1.238
0.5002 −1.229
0.5030 −1.220
0.5043 −1.208
0.5071 −1.188
0.5085 −1.172

2443730 +
0.4575 −0.241
0.4603 −0.288
0.4617 −0.306
0.4644 −0.354
0.4658 −0.375
0.4686 −0.437
0.4699 −0.481
0.4724 −0.531
0.4735 −0.563
0.4761 −0.654
0.4773 −0.690

2443732 +
0.3614 −0.109
0.3631 −0.143
0.3692 −0.272
0.3713 −0.346
0.3747 −0.411
0.3761 −0.431
0.3817 −0.584
0.3831 −0.618
0.3931 −1.083
0.3990 −1.234
0.4005 −1.306
0.4046 −1.392

2443743 +
0.3261 −0.249
0.3273 −0.262
0.3295 −0.302
0.3306 −0.327
0.3329 −0.373
0.3340 −0.403
0.3389 −0.469
0.3399 −0.516
0.3419 −0.575
0.3429 −0.628
0.3452 −0.688
0.3462 −0.715
0.3486 −0.719
0.3496 −0.749
0.3518 −0.855
0.3529 −0.903
0.3552 −0.985
0.3562 −1.008
0.3592 −1.067
0.3603 −1.087
0.3630 −1.128
0.3658 −1.163
0.3668 −1.180
0.3694 −1.198
0.3729 −1.206
0.3740 −1.197
0.3765 −1.193
0.3789 −1.189
0.3815 −1.185

2443763 +
0.3355 −0.431
0.3405 −0.537
0.3458 −0.616
0.3493 −0.678
0.3516 −0.718
0.3546 −0.773
0.3563 −0.794
0.3596 −0.850
0.3619 −0.895
0.3653 −0.939
0.3671 −0.968
0.3701 −1.001
0.3719 −1.020
0.3750 −1.036
0.3820 −1.045
0.3853 −1.041
0.3872 −1.030
0.3909 −1.021
0.3928 −1.004
0.3961 −0.990
0.3977 −0.979
0.4033 −0.928

2445609 +
0.2839 −1.098
0.2852 −1.122
0.2866 −1.152
0.2879 −1.173
0.2893 −1.188
0.2951 −1.239
0.2965 −1.252
0.2978 −1.256
0.2991 −1.256
0.3005 −1.256
0.3057 −1.251
0.3071 −1.247
0.3084 −1.239
0.3098 −1.229
0.3111 −1.210

2445791 +
0.3600 −1.075
0.3612 −1.070
0.3626 −1.068
0.3640 −1.069
0.3653 −1.061
0.3779 −0.985
0.3793 −0.976
0.3806 −0.967
0.3820 −0.951
0.4106 −0.645
0.4119 −0.645
0.4132 −0.631
0.4146 −0.619
0.4159 −0.618
0.4173 −0.607
0.4186 −0.602
0.4199 −0.589
0.4213 −0.588
0.4227 −0.581
0.4365 −0.563
0.4378 −0.559
0.4392 −0.553
0.4405 −0.542
0.4418 −0.524
0.4432 −0.518
0.4445 −0.517
0.4460 −0.518
0.4472 −0.516
0.4485 −0.508
0.4559 −0.459
0.4572 −0.458
0.4586 −0.458
0.4599 −0.448
0.4612 −0.442
0.4626 −0.434
0.4640 −0.431
0.4653 −0.431
0.4667 −0.436
0.4680 −0.431
0.4737 −0.413
0.4750 −0.414
0.4764 −0.413
0.4777 −0.422
0.4791 −0.421
0.4804 −0.420
0.4817 −0.415
0.4831 −0.412
0.4845 −0.414
0.4858 −0.415
0.5212 −0.247
0.5225 −0.247
0.5239 −0.251
0.5252 −0.246
0.5266 −0.247
0.5279 −0.243
0.5292 −0.242
0.5306 −0.233
0.5319 −0.224
0.5332 −0.223
0.5398 −0.222
0.5411 −0.217
0.5425 −0.214
0.5438 −0.205
0.5451 −0.197
0.5465 −0.192
0.5478 −0.193
0.5492 −0.190
0.5505 −0.189
0.5519 −0.189
0.5593 −0.186
0.5607 −0.186
0.5620 −0.173
0.5634 −0.168
0.5647 −0.149
0.5660 −0.137
0.5674 −0.138
0.5687 −0.139
0.5701 −0.136
0.5714 −0.155
0.5778 −0.156
0.5791 −0.156
0.5805 −0.156
0.5818 −0.139
0.5845 −0.129

2445806 +
0.4754 −0.039
0.4767 −0.049
0.4780 −0.048
0.4794 −0.062
0.4807 −0.066
0.4865 −0.107
0.4878 −0.119
0.4892 −0.130
0.4905 −0.137

0.4918 −0.147
0.4976 −0.189
0.4989 −0.202
0.5003 −0.211
0.5016 −0.215
0.5084 −0.300
0.5097 −0.324
0.5111 −0.342
0.5124 −0.351
0.5195 −0.457
0.5209 −0.485
0.5222 −0.517
0.5235 −0.543
0.5249 −0.565
0.5305 −0.684
0.5319 −0.718
0.5332 −0.733
0.5345 −0.761
0.5359 −0.784
0.5413 −0.884
0.5427 −0.907
0.5440 −0.921
0.5453 −0.942
0.5467 −0.964
0.5518 −1.027
0.5531 −1.038
0.5545 −1.051
0.5558 −1.067
0.5572 −1.082
0.5628 −1.112
0.5642 −1.123
0.5655 −1.133

0.5669 −1.147
0.5682 −1.138
0.5735 −1.135
0.5748 −1.130
0.5762 −1.122
0.5775 −1.117
0.5788 −1.111
0.5840 −1.077
0.5853 −1.064
0.5867 −1.058
0.5936 −1.006
0.5950 −0.999
0.5963 −0.998
0.5976 −0.984

2446193 +
0.4376 −0.435
0.4390 −0.451
0.4403 −0.462
0.4417 −0.488
0.4430 −0.499
0.4484 −0.581
0.4498 −0.609
0.4511 −0.632
0.4525 −0.661
0.4538 −0.695
0.4590 −0.779
0.4603 −0.807
0.4617 −0.826
0.4630 −0.851
0.4643 −0.865
0.4696 −0.933
0.4709 −0.952

0.4722 −0.973
0.4736 −0.984
0.4749 −0.993
0.4808 −1.035
0.4821 −1.048
0.4834 −1.049
0.4847 −1.057
0.4861 −1.061
0.4919 −1.070
0.4932 −1.062
0.4945 −1.065
0.4959 −1.060
0.4972 −1.051
0.5032 −1.042
0.5046 −1.037
0.5059 −1.038
0.5072 −1.032
0.5086 −1.022
0.5141 −1.001
0.5154 −0.991
0.5167 −0.977
0.5181 −0.968

2447306 +
0.4919 0.044
0.4932 0.055
0.4984 0.048
0.4996 0.049
0.5057 0.025
0.5070 0.027
0.5121 0.015
0.5134 0.010
0.5190 −0.081

0.5203 −0.105
0.5256 −0.172
0.5269 −0.179
0.5320 −0.262
0.5333 −0.282
0.5385 −0.431
0.5398 −0.446
0.5451 −0.480
0.5463 −0.546
0.5512 −0.675
0.5525 −0.735

2447360 +
0.3674 −0.027
0.3687 −0.064
0.3743 −0.063
0.3756 −0.063
0.3807 −0.122
0.3819 −0.139
0.3868 −0.172
0.3881 −0.176
0.3933 −0.269
0.3946 −0.286
0.3959 −0.305
0.4031 −0.422
0.4045 −0.429
0.4058 −0.492
0.4116 −0.646
0.4129 −0.687
0.4184 −0.950
0.4197 −1.032
0.4250 −1.307
0.4263 −1.340

0.4319 −1.381
0.4332 −1.380
0.4389 −1.375
0.4486 −1.323
0.4499 −1.284
0.4513 −1.283
0.4588 −1.200
0.4643 −1.182
0.4656 −1.174

2447462 +
0.3532 −0.502
0.3542 −0.519
0.3590 −0.565
0.3601 −0.592
0.3664 −0.710
0.3675 −0.740
0.3788 −0.945
0.3799 −0.956
0.3847 −1.032
0.3858 −1.049
0.3934 −1.079
0.3945 −1.081
0.3992 −1.087
0.4003 −1.087
0.4054 −1.079
0.4065 −1.080
0.4129 −1.044
0.4140 −1.041
0.4189 −1.010
0.4200 −1.017
0.4244 −0.975
0.4254 −0.976

Table 5.d Photoelectric differential V observations of XZ Dra

2436410 +
0.4230 0.064
0.4263 0.076
0.4322 0.057
0.4386 0.083
0.4414 0.065
0.4443 0.062
0.4515 0.058
0.4560 0.016
0.4591 −0.005
0.4665 −0.068
0.4701 −0.104

0.4730 −0.139
0.4795 −0.211
0.4832 −0.245
0.4860 −0.303
0.4927 −0.357
0.4952 −0.379
0.4978 −0.396
0.5036 −0.454
0.5061 −0.514
0.5084 −0.549
0.5138 −0.650
0.5168 −0.686

0.5195 −0.741
0.5258 −0.781
0.5281 −0.768
0.5306 −0.758
0.5390 −0.721
0.5420 −0.716
0.5480 −0.698
0.5508 −0.692
0.5536 −0.681
0.5563 −0.671

2436413 +
0.3699 −0.622

0.3720 −0.641
0.3741 −0.664
0.3786 −0.673
0.3806 −0.681
0.3827 −0.682
0.3848 −0.690
0.3869 −0.725
0.3921 −0.733
0.3942 −0.736
0.3970 −0.736
0.3998 −0.727
0.4029 −0.717

2436420 +
0.4824 −0.220
0.4851 −0.255
0.4882 −0.275
0.4948 −0.323
0.4975 −0.375
0.5025 −0.434
0.5078 −0.479
0.5111 −0.533
0.5138 −0.562
0.5162 −0.579
0.5235 −0.664

0.5261 −0.674
0.5289 −0.699
0.5318 −0.720

2436421 +
0.3973 −0.070
0.4004 −0.089
0.4033 −0.092
0.4060 −0.113
0.4085 −0.104
0.4188 −0.130
0.4236 −0.154
0.4261 −0.185
0.4287 −0.211
0.4393 −0.313
0.4424 −0.340
0.4480 −0.398
0.4516 −0.444
0.4547 −0.483
0.4612 −0.523
0.4643 −0.554
0.4677 −0.581
0.4744 −0.611
0.4768 −0.614
0.4793 −0.632
0.4854 −0.639
0.4885 −0.661
0.4913 −0.682
0.4945 −0.699
0.4974 −0.721
0.5001 −0.705
0.5032 −0.696
0.5093 −0.667
0.5121 −0.651
0.5147 −0.646
0.5220 −0.620
0.5260 −0.583
0.5291 −0.564
0.5353 −0.548
0.5388 −0.517
0.5419 −0.500

2436443 +
0.3634 −0.110
0.3669 −0.135
0.3697 −0.172
0.3766 −0.289
0.3794 −0.357
0.3822 −0.375
0.3898 −0.505
0.3926 −0.563
0.3954 −0.619
0.4016 −0.712
0.4044 −0.728
0.4072 −0.762
0.4134 −0.782
0.4169 −0.770

2436450 +
0.4468 0.151
0.4487 0.153
0.4526 0.144
0.4549 0.142
0.4568 0.119
0.4607 0.105
0.4626 0.098
0.4644 0.092
0.4681 0.086
0.4699 0.097
0.4718 0.093
0.4741 0.098
0.4822 0.136
0.4841 0.103
0.4859 0.105
0.4901 0.085
0.4920 0.050
0.4938 0.036
0.4956 0.035
0.4973 0.022
0.4991 0.019
0.5010 0.020
0.5047 −0.001
0.5065 −0.012
0.5084 −0.019
0.5102 −0.028
0.5121 −0.054
0.5139 −0.066
0.5158 −0.074
0.5199 −0.087
0.5218 −0.109
0.5237 −0.126
0.5255 −0.152
0.5274 −0.192
0.5292 −0.236
0.5311 −0.266
0.5355 −0.331
0.5373 −0.394
0.5392 −0.422
0.5410 −0.480
0.5429 −0.598
0.5447 −0.679
0.5519 −0.853
0.5537 −0.891
0.5556 −0.898
0.5595 −0.955
0.5614 −0.945
0.5632 −0.922
0.5651 −0.904
0.5684 −0.871
0.5698 −0.852
0.5712 −0.827
0.5731 −0.829
0.5760 −0.815
0.5818 −0.792
0.5853 −0.757

2436451 +
0.4500 0.037
0.4521 0.038
0.4540 0.000
0.4559 −0.001
0.4577 −0.026
0.4614 −0.035
0.4630 −0.060
0.4648 −0.077
0.4682 −0.104
0.4697 −0.114
0.4712 −0.136
0.4748 −0.160
0.4764 −0.214
0.4780 −0.235
0.4828 −0.311
0.4851 −0.360
0.4874 −0.412
0.4917 −0.478
0.4946 −0.556
0.4973 −0.589
0.5020 −0.652
0.5045 −0.702
0.5060 −0.754
0.5101 −0.851
0.5124 −0.870
0.5146 −0.876
0.5236 −0.868
0.5261 −0.856
0.5285 −0.833

2436454 +
0.2920 0.069
0.2941 0.063
0.2958 0.067
0.2996 0.057
0.3015 0.061
0.3035 0.071
0.3074 0.071
0.3093 0.070
0.3120 0.058
0.3170 0.032
0.3192 0.016
0.3214 −0.021
0.3260 −0.042
0.3280 −0.060
0.3302 −0.081
0.3350 −0.135
0.3371 −0.189
0.3397 −0.235
0.3442 −0.302
0.3465 −0.354
0.3489 −0.396
0.3538 −0.470
0.3564 −0.505
0.3588 −0.545
0.3629 −0.623
0.3650 −0.674
0.3672 −0.726
0.3716 −0.847
0.3740 −0.866
0.3763 −0.877
0.3801 −0.894
0.3820 −0.885
0.3842 −0.874
0.3878 −0.848

2436463 +
0.3573 0.075
0.3649 0.049
0.3697 0.019
0.3711 0.010
0.3725 0.007
0.3760 −0.052
0.3779 −0.064
0.3797 −0.097
0.3834 −0.139
0.3853 −0.160
0.3872 −0.188
0.3911 −0.243
0.3929 −0.291
0.3948 −0.300
0.3987 −0.345
0.4006 −0.394
0.4024 −0.439
0.4061 −0.481
0.4080 −0.540
0.4098 −0.571
0.4135 −0.627
0.4154 −0.684
0.4172 −0.727
0.4209 −0.814
0.4228 −0.890
0.4246 −0.913
0.4284 −0.945
0.4300 −0.941
0.4318 −0.938
0.4360 −0.920
0.4378 −0.907
0.4397 −0.896
0.4434 −0.878
0.4452 −0.863

2436474 +
0.3656 −0.655
0.3688 −0.696
0.3710 −0.723
0.3763 −0.755
0.3785 −0.771
0.3805 −0.785
0.3850 −0.791
0.3879 −0.802
0.3907 −0.791
0.3962 −0.770
0.3990 −0.738
0.4018 −0.726
0.4080 −0.698
0.4108 −0.684
0.4136 −0.680

2436475 +
0.2807 −0.010
0.2860 −0.085
0.2883 −0.143
0.2905 −0.176
0.2947 −0.246
0.2965 −0.290
0.3008 −0.377
0.3041 −0.427
0.3066 −0.454
0.3118 −0.550
0.3145 −0.602
0.3173 −0.676
0.3225 −0.737
0.3253 −0.760
0.3281 −0.786
0.3333 −0.826
0.3378 −0.807
0.3402 −0.821
0.3451 −0.814

2436486 +
0.2462 −0.261
0.2479 −0.293
0.2498 −0.318
0.2542 −0.388
0.2561 −0.410
0.2584 −0.433
0.2632 −0.494
0.2655 −0.514
0.2681 −0.525
0.2735 −0.550
0.2758 −0.589
0.2780 −0.589
0.2830 −0.620
0.2856 −0.631
0.2878 −0.643
0.2953 −0.654
0.2977 −0.665

2436503 +
0.4091 −0.334
0.4132 −0.409
0.4152 −0.453
0.4194 −0.514
0.4214 −0.541
0.4233 −0.554
0.4274 −0.574
0.4292 −0.580
0.4312 −0.585
0.4358 −0.581
0.4380 −0.598
0.4402 −0.601
0.4445 −0.655
0.4467 −0.682
0.4491 −0.703
0.4544 −0.706
0.4564 −0.720
0.4596 −0.706
0.4633 −0.708
0.4655 −0.700

2436506 +
0.2146 0.062
0.2182 0.070
0.2199 0.061
0.2231 0.020
0.2247 0.006
0.2263 0.013
0.2298 −0.002
0.2316 −0.001
0.2371 −0.041
0.2390 −0.048
0.2405 −0.057
0.2443 −0.090
0.2461 −0.115
0.2481 −0.162
0.2519 −0.180
0.2536 −0.204
0.2552 −0.213
0.2588 −0.296
0.2611 −0.296
0.2670 −0.385
0.2690 −0.449
0.2707 −0.451
0.2767 −0.459
0.2783 −0.480
0.2820 −0.510
0.2839 −0.523
0.2857 −0.548
0.2897 −0.578
0.2914 −0.592
0.2933 −0.607
0.2968 −0.629
0.2987 −0.638
0.3008 −0.663
0.3043 −0.695
0.3061 −0.697
0.3077 −0.701
0.3114 −0.719
0.3138 −0.730
0.3161 −0.727
0.3208 −0.714
0.3236 −0.706
0.3254 −0.700
0.3300 −0.670
0.3320 −0.664

2436514 +
0.3675 −0.301
0.3693 −0.337
0.3712 −0.400
0.3749 −0.438
0.3767 −0.475
0.3786 −0.502
0.3823 −0.550
0.3841 −0.598
0.3860 −0.646
0.3897 −0.736
0.3916 −0.759
0.3934 −0.768
0.3971 −0.787
0.3990 −0.794
0.4008 −0.792
0.4126 −0.787
0.4145 −0.773

2437348 +
0.5407 0.021
0.5469 0.043
0.5537 0.026
0.5603 0.032
0.5671 0.012
0.5826 0.041
0.5886 0.043
0.5941 0.034
0.6013 0.012
0.6138 0.080
0.6284 0.095
0.6355 0.142
0.6424 0.155
0.6502 0.182
0.6582 0.188

2437465 +
0.4645 −0.441
0.4671 −0.470
0.4686 −0.487
0.4716 −0.538
0.4731 −0.568
0.4748 −0.587
0.4782 −0.653
0.4796 −0.672
0.4810 −0.679
0.4843 −0.711
0.4863 −0.707
0.4877 −0.707
0.4908 −0.704
0.4924 −0.707
0.4940 −0.724
0.4972 −0.721
0.4991 −0.709
0.5008 −0.718
0.5045 −0.718
0.5062 −0.707
0.5086 −0.705
0.5128 −0.680
0.5144 −0.685
0.5157 −0.679
0.5191 −0.669
0.5212 −0.674
0.5228 −0.666
0.5262 −0.649
0.5280 −0.644
0.5300 −0.641
0.5368 −0.613
0.5390 −0.603

2437467 +
0.4061 −0.730
0.4106 −0.709
0.4130 −0.700
0.4172 −0.688
0.4193 −0.680
0.4214 −0.677
0.4269 −0.676
0.4290 −0.667
0.4311 −0.660
0.4352 −0.641
0.4373 −0.627
0.4394 −0.613
0.4446 −0.598
0.4478 −0.586
0.4502 −0.575

2437475 +
0.4082 0.027
0.4101 0.035
0.4120 0.011
0.4158 0.012
0.4187 −0.005
0.4205 −0.034
0.4274 −0.087
0.4293 −0.106
0.4313 −0.109
0.4363 −0.154
0.4396 −0.173
0.4417 −0.193
0.4470 −0.248
0.4486 −0.251
0.4509 −0.272
0.4560 −0.359
0.4579 −0.360
0.4598 −0.388
0.4632 −0.430
0.4650 −0.456
0.4672 −0.470
0.4721 −0.528
0.4738 −0.551
0.4757 −0.561
0.4788 −0.595
0.4820 −0.607
0.4879 −0.645
0.4895 −0.646
0.4910 −0.649
0.4955 −0.660
0.4987 −0.655
0.5011 −0.652
0.5063 −0.646
0.5087 −0.637
0.5143 −0.630

2437486 +
0.3806 −0.035
0.3829 −0.073

0.3851 −0.079
0.3889 −0.097
0.3906 −0.118
0.3923 −0.130
0.3967 −0.163
0.3984 −0.190
0.4000 −0.201
0.4039 −0.233
0.4057 −0.240
0.4077 −0.260
0.4116 −0.308
0.4134 −0.323
0.4154 −0.344
0.4194 −0.407
0.4213 −0.425
0.4230 −0.442
0.4264 −0.476
0.4280 −0.481
0.4312 −0.509
0.4355 −0.526
0.4378 −0.535
0.4395 −0.545
0.4413 −0.555
0.4453 −0.578
0.4469 −0.608
0.4485 −0.615
0.4522 −0.619
0.4538 −0.629
0.4561 −0.636
0.4619 −0.635
0.4633 −0.627
0.4647 −0.628
0.4686 −0.628
0.4705 −0.629
0.4728 −0.623
0.4770 −0.616
0.4800 −0.606
0.4816 −0.602
0.4862 −0.589
0.4878 −0.587
0.4909 −0.580
0.4985 −0.541
0.4999 −0.531
0.5022 −0.536
0.5094 −0.521
0.5169 −0.507
0.5218 −0.465
0.5321 −0.410
0.5342 −0.401
0.5364 −0.401
0.5415 −0.382
0.5443 −0.368
0.5469 −0.359

2439391 +
0.4069 −0.030
0.4099 −0.069
0.4155 −0.129
0.4180 −0.143
0.4230 −0.192
0.4256 −0.203
0.4337 −0.327
0.4356 −0.337
0.4405 −0.406
0.4422 −0.443
0.4441 −0.469
0.4493 −0.530
0.4517 −0.561
0.4533 −0.559
0.4577 −0.598
0.4591 −0.603
0.4608 −0.598
0.4641 −0.607
0.4656 −0.637
0.4677 −0.634
0.4710 −0.653
0.4744 −0.669
0.4781 −0.652
0.4817 −0.655
0.4854 −0.652
0.4872 −0.653
0.4887 −0.643
0.4921 −0.627
0.4938 −0.622
0.4954 −0.633
0.4997 −0.616
0.5014 −0.620
0.5031 −0.605
0.5068 −0.607
0.5087 −0.590
0.5103 −0.571

2439402 +
0.4057 −0.336
0.4084 −0.409
0.4140 −0.524
0.4161 −0.567
0.4216 −0.666
0.4244 −0.721
0.4307 −0.789
0.4328 −0.810
0.4390 −0.834
0.4418 −0.849
0.4480 −0.859
0.4508 −0.856
0.4550 −0.838
0.4577 −0.829
0.4626 −0.789
0.4654 −0.776
0.4702 −0.729
0.4723 −0.721
0.4779 −0.699
0.4807 −0.682

2439403 +
0.3119 0.139
0.3133 0.147
0.3147 0.129
0.3189 0.106
0.3209 0.106
0.3230 0.089
0.3265 0.084
0.3286 0.081
0.3300 0.071
0.3348 0.026
0.3369 0.006
0.3383 −0.011
0.3418 −0.043
0.3439 −0.066
0.3460 −0.087
0.3494 −0.127
0.3522 −0.154
0.3536 −0.210
0.3578 −0.307
0.3598 −0.330
0.3619 −0.400
0.3654 −0.501
0.3675 −0.572
0.3689 −0.572
0.3723 −0.602
0.3737 −0.611
0.3751 −0.658
0.3779 −0.683
0.3793 −0.709
0.3814 −0.752
0.3841 −0.785
0.3862 −0.793
0.3876 −0.802
0.3904 −0.808
0.3918 −0.813
0.3937 −0.809
0.3973 −0.786
0.3987 −0.796
0.4001 −0.783
0.4043 −0.765
0.4057 −0.763
0.4071 −0.760
0.4105 −0.742
0.4119 −0.732
0.4140 −0.729
0.4168 −0.716
0.4189 −0.717
0.4203 −0.712
0.4237 −0.711
0.4251 −0.697
0.4265 −0.680

2440494 +
0.5104 0.081
0.5118 0.063
0.5243 −0.029
0.5271 −0.048
0.5306 −0.061
0.5320 −0.083
0.5389 −0.216
0.5431 −0.268
0.5445 −0.262
0.5486 −0.340
0.5500 −0.402
0.5619 −0.548
0.5633 −0.574
0.5688 −0.716
0.5730 −0.734
0.5744 −0.740

2440500 +
0.2607 −0.397
0.2621 −0.420
0.2635 −0.425
0.2663 −0.451
0.2677 −0.471
0.2691 −0.494
0.2718 −0.523
0.2732 −0.548
0.2746 −0.590
0.2774 −0.691
0.2788 −0.685
0.2802 −0.712
0.2829 −0.731
0.2843 −0.729
0.2857 −0.741
0.2885 −0.792
0.2899 −0.783
0.2913 −0.820
0.2940 −0.824
0.2954 −0.813

2440504 +
0.5423 −0.258
0.5437 −0.278
0.5451 −0.299
0.5478 −0.337
0.5492 −0.357
0.5506 −0.365
0.5534 −0.429
0.5548 −0.449
0.5562 −0.500
0.5590 −0.567
0.5604 −0.615
0.5618 −0.634
0.5645 −0.684
0.5659 −0.699
0.5673 −0.719
0.5701 −0.739
0.5715 −0.743
0.5729 −0.755
0.5756 −0.764
0.5770 −0.783
0.5784 −0.783
0.5812 −0.773
0.5826 −0.771
0.5840 −0.770
0.5867 −0.768
0.5881 −0.767
0.5895 −0.768

2440516 +

0.4007	0.014
0.4021	0.008
0.4035	0.010
0.4063	0.012
0.4077	0.012
0.4091	−0.004
0.4118	−0.007
0.4132	−0.012
0.4146	−0.030
0.4174	−0.032
0.4188	−0.038
0.4202	−0.043
0.4229	−0.075
0.4243	−0.094
0.4257	−0.099
0.4285	−0.098
0.4299	−0.107
0.4313	−0.115
0.4340	−0.124
0.4354	−0.129
0.4368	−0.150
0.4396	−0.173
0.4410	−0.201
0.4424	−0.210
0.4451	−0.231
0.4465	−0.249
0.4479	−0.271
0.4507	−0.298
0.4521	−0.304
0.4535	−0.320
0.4576	−0.364
0.4590	−0.373
0.4604	−0.385
0.4632	−0.424
0.4646	−0.434
0.4660	−0.453
0.4688	−0.493
0.4702	−0.507
0.4716	−0.520
0.4743	−0.528
0.4757	−0.528
0.4771	−0.565
0.4799	−0.568
0.4813	−0.585
0.4827	−0.588
0.4854	−0.621
0.4868	−0.640
0.4882	−0.647
0.4910	−0.649
0.4924	−0.651
0.4938	−0.648
0.4965	−0.650
0.4979	−0.660
0.4993	−0.663
0.5021	−0.651
0.5035	−0.655
0.5049	−0.668
0.5076	−0.663
0.5090	−0.643
0.5104	−0.648
0.5132	−0.617
0.5146	−0.617
0.5160	−0.605

2440528 +

0.3188	0.083
0.3202	0.085
0.3216	0.078
0.3244	0.085
0.3258	0.076
0.3272	0.072
0.3300	0.039
0.3314	0.068
0.3328	0.062
0.3355	0.059
0.3369	0.056
0.3383	0.042
0.3411	0.009
0.3425	−0.005
0.3439	−0.009
0.3466	−0.021
0.3480	−0.040
0.3494	−0.044
0.3522	−0.058
0.3536	−0.083
0.3550	−0.106
0.3577	−0.139
0.3591	−0.158
0.3605	−0.165
0.3633	−0.225
0.3647	−0.240
0.3661	−0.255
0.3688	−0.304
0.3702	−0.324
0.3716	−0.341
0.3744	−0.383
0.3758	−0.383
0.3772	−0.399
0.3800	−0.435
0.3814	−0.457
0.3828	−0.467
0.3855	−0.506
0.3869	−0.537
0.3883	−0.554
0.3911	−0.578
0.3925	−0.603
0.3939	−0.618
0.3966	−0.643
0.3980	−0.660
0.3994	−0.676
0.4022	−0.702
0.4036	−0.711
0.4050	−0.713
0.4077	−0.732
0.4091	−0.733
0.4105	−0.745
0.4133	−0.751
0.4147	−0.751
0.4161	−0.754
0.4189	−0.758
0.4203	−0.742
0.4217	−0.739

2440530 +

0.2633	−0.103
0.2647	−0.141
0.2661	−0.167
0.2689	−0.187
0.2703	−0.217
0.2717	−0.236
0.2745	−0.250
0.2759	−0.270
0.2773	−0.297
0.2800	−0.333
0.2814	−0.351
0.2828	−0.369
0.2856	−0.405
0.2870	−0.421
0.2884	−0.454
0.2911	−0.496
0.2925	−0.509
0.2939	−0.529
0.2967	−0.578
0.2981	−0.602
0.2995	−0.627
0.3022	−0.661
0.3036	−0.662
0.3050	−0.676
0.3078	−0.709
0.3092	−0.726
0.3106	−0.745
0.3147	−0.732
0.3161	−0.729
0.3175	−0.730
0.3203	−0.726
0.3217	−0.720
0.3231	−0.721
0.3258	−0.717
0.3272	−0.721
0.3286	−0.720

2440541 +

0.2333	−0.077
0.2354	−0.113
0.2396	−0.197
0.2417	−0.231
0.2458	−0.329
0.2479	−0.362
0.2521	−0.446
0.2542	−0.501
0.2583	−0.561
0.2604	−0.613
0.2646	−0.708
0.2667	−0.732
0.2708	−0.790
0.2729	−0.833
0.2771	−0.850
0.2792	−0.858
0.2833	−0.827
0.2854	−0.817
0.2896	−0.802
0.2917	−0.798

2440676 +

0.5170	0.044
0.5232	0.032
0.5295	−0.009
0.5357	−0.032
0.5378	−0.037
0.5420	−0.058
0.5441	−0.079
0.5482	−0.094
0.5503	−0.118
0.5545	−0.163
0.5566	−0.176
0.5607	−0.208
0.5628	−0.241
0.5670	−0.288
0.5691	−0.330
0.5732	−0.377
0.5753	−0.395
0.5795	−0.471
0.5816	−0.487
0.5857	−0.526
0.5878	−0.536
0.5920	−0.580
0.5941	−0.609
0.5982	−0.645
0.6003	−0.657
0.6045	−0.674
0.6066	−0.673
0.6107	−0.689
0.6128	−0.688
0.6170	−0.673
0.6198	−0.657
0.6226	−0.647

2440707 +

0.5084	0.112
0.5105	0.132
0.5147	0.134
0.5168	0.132
0.5209	0.141
0.5230	0.135
0.5272	0.116
0.5293	0.106
0.5334	0.065
0.5355	0.026
0.5401	−0.011
0.5422	−0.052
0.5452	−0.095
0.5473	−0.122
0.5515	−0.243
0.5536	−0.314

0.5577 −0.410
0.5598 −0.446
0.5640 −0.620
0.5661 −0.724
0.5702 −0.873
0.5723 −0.914
0.5758 −0.959
0.5779 −0.971
0.5821 −0.976
0.5842 −0.973

2440709 +
0.4157 0.151
0.4171 0.160
0.4198 0.156
0.4212 0.138
0.4240 0.111
0.4254 0.110
0.4282 0.107
0.4296 0.081
0.4323 0.089
0.4337 0.076
0.4365 0.042
0.4379 0.032
0.4407 −0.009
0.4421 −0.037
0.4448 −0.035
0.4462 −0.076
0.4490 −0.116
0.4504 −0.129
0.4532 −0.167
0.4546 −0.192
0.4573 −0.259
0.4587 −0.277
0.4615 −0.372
0.4629 −0.406
0.4657 −0.471
0.4671 −0.504
0.4698 −0.603
0.4712 −0.633
0.4740 −0.700
0.4754 −0.730
0.4782 −0.811
0.4796 −0.860
0.4823 −0.900
0.4837 −0.911
0.4865 −0.942
0.4879 −0.961
0.4907 −0.958
0.4921 −0.950
0.4948 −0.943
0.4962 −0.941
0.4990 −0.931
0.5004 −0.924
0.5032 −0.916
0.5046 −0.901
0.5073 −0.894
0.5087 −0.882
0.5115 −0.875
0.5129 −0.855

2440731 +
0.3407 0.010
0.3421 0.008
0.3449 −0.002
0.3463 −0.011
0.3491 −0.056
0.3505 −0.072
0.3531 −0.117
0.3545 −0.156
0.3573 −0.183
0.3587 −0.211
0.3615 −0.255
0.3629 −0.273
0.3656 −0.315
0.3670 −0.352
0.3698 −0.391
0.3712 −0.421
0.3740 −0.446
0.3754 −0.479
0.3781 −0.525
0.3795 −0.544
0.3823 −0.584
0.3837 −0.595
0.3865 −0.623
0.3879 −0.641
0.3906 −0.679
0.3920 −0.692
0.3948 −0.721
0.3962 −0.733
0.3990 −0.759
0.4004 −0.769
0.4031 −0.770
0.4045 −0.771
0.4073 −0.775
0.4087 −0.768

2440751 +
0.3586 −0.079
0.3600 −0.099
0.3642 −0.120
0.3655 −0.150
0.3690 −0.162
0.3704 −0.186
0.3739 −0.211
0.3753 −0.214
0.3788 −0.259
0.3802 −0.280
0.3829 −0.307
0.3843 −0.319
0.3871 −0.359
0.3891 −0.378
0.3919 −0.434
0.3933 −0.446
0.3968 −0.517
0.3982 −0.532
0.4017 −0.596
0.4038 −0.616
0.4072 −0.623
0.4086 −0.635
0.4114 −0.640
0.4128 −0.648
0.4156 −0.655
0.4170 −0.670
0.4197 −0.659
0.4211 −0.667
0.4239 −0.664
0.4253 −0.661
0.4287 −0.673
0.4301 −0.664
0.4329 −0.650
0.4343 −0.647
0.4371 −0.643
0.4385 −0.646
0.4412 −0.640
0.4426 −0.632
0.4454 −0.620
0.4468 −0.613
0.4495 −0.600
0.4510 −0.598

2440780 +
0.4454 −0.164
0.4476 −0.202
0.4517 −0.252
0.4538 −0.287
0.4579 −0.369
0.4600 −0.393
0.4642 −0.475
0.4663 −0.532
0.4704 −0.636
0.4725 −0.709
0.4767 −0.839
0.4788 −0.884
0.4829 −0.958
0.4850 −0.979
0.4905 −0.971
0.4926 −0.945
0.4968 −0.899
0.4989 −0.886

2440821 +
0.4103 −0.279
0.4124 −0.290
0.4172 −0.333
0.4193 −0.360
0.4235 −0.398
0.4256 −0.424
0.4312 −0.502
0.4333 −0.534
0.4430 −0.627
0.4451 −0.655
0.4499 −0.698
0.4520 −0.703
0.4569 −0.740
0.4638 −0.779
0.4659 −0.782
0.4756 −0.734
0.4777 −0.713
0.4846 −0.699
0.4867 −0.661
0.4923 −0.621
0.4944 −0.593
0.5069 −0.500
0.5090 −0.490

2440840 +
0.4597 0.128
0.4624 0.096
0.4638 0.084
0.4652 0.072
0.4680 0.049
0.4694 0.044
0.4708 0.009
0.4735 −0.003
0.4749 −0.028
0.4763 −0.047
0.4791 −0.076
0.4805 −0.096
0.4846 −0.187
0.4860 −0.214
0.4874 −0.234
0.4902 −0.273
0.4916 −0.304
0.4957 −0.367
0.4971 −0.380
0.4985 −0.406
0.5013 −0.470
0.5027 −0.485
0.5041 −0.513
0.5069 −0.549
0.5083 −0.580
0.5097 −0.612
0.5124 −0.671
0.5138 −0.686
0.5152 −0.697
0.5180 −0.718
0.5194 −0.740
0.5208 −0.750
0.5249 −0.766
0.5263 −0.767
0.5291 −0.744
0.5305 −0.736
0.5319 −0.730
0.5346 −0.717
0.5360 −0.716
0.5374 −0.705
0.5395 −0.705
0.5409 −0.696
0.5423 −0.695

2440863 +
0.3764 −0.441
0.3778 −0.477
0.3792 −0.497

0.3833	−0.585	0.3336	−0.832	0.2800	−0.820	0.3541	−0.425	0.2929	−0.204
0.3847	−0.625	0.3350	−0.854	0.2814	−0.812	0.3564	−0.488	0.2979	−0.294
0.3861	−0.665	0.3364	−0.866			0.3575	−0.500	0.3042	−0.387
0.3910	−0.765	0.3392	−0.868	2441249 +		0.3586	−0.527	0.3055	−0.408
0.3931	−0.784	0.3406	−0.862	0.2510	0.094	0.3612	−0.577	0.3094	−0.480
0.3945	−0.804	0.3420	−0.860	0.2524	0.098	0.3624	−0.596	0.3105	−0.508
0.3986	−0.869	0.3448	−0.841	0.2538	0.101	0.3635	−0.628	0.3116	−0.516
0.4000	−0.904	0.3462	−0.840	0.2566	0.107	0.3662	−0.672	0.3172	−0.626
0.4014	−0.919	0.3476	−0.838	0.2580	0.101	0.3673	−0.693	0.3184	−0.639
0.4056	−0.942	0.3503	−0.831	0.2594	0.097	0.3685	−0.713	0.3196	−0.672
0.4070	−0.948	0.3517	−0.826	0.2621	0.100	0.3712	−0.750	0.3227	−0.728
0.4084	−0.953	0.3531	−0.813	0.2635	0.103	0.3728	−0.755	0.3239	−0.738
0.4146	−0.942	0.3559	−0.788	0.2656	0.103	0.3741	−0.767	0.3253	−0.755
0.4160	−0.934	0.3573	−0.782	0.2691	0.099	0.3772	−0.774	0.3287	−0.790
0.4174	−0.922	0.3587	−0.776	0.2705	0.104	0.3785	−0.788	0.3300	−0.796
0.4208	−0.898			0.2719	0.104	0.3798	−0.782	0.3311	−0.801
0.4222	−0.880	2440937 +		0.2747	0.101	0.3830	−0.791	0.3344	−0.796
0.4236	−0.861	0.2216	−0.092	0.2761	0.111	0.3844	−0.794	0.3361	−0.798
0.4299	−0.805	0.2230	−0.114	0.2775	0.121	0.3860	−0.799	0.3372	−0.791
0.4313	−0.783	0.2244	−0.162	0.2802	0.118	0.3893	−0.795	0.3405	−0.790
0.4327	−0.773	0.2272	−0.195	0.2816	0.108	0.3907	−0.794	0.3417	−0.784
		0.2286	−0.221	0.2830	0.113	0.3920	−0.788	0.3431	−0.782
2440925 +		0.2300	−0.234	0.2865	0.124	0.3946	−0.787	0.3463	−0.775
0.2663	0.084	0.2327	−0.272	0.2906	0.160	0.3962	−0.777	0.3475	−0.771
0.2677	0.088	0.2341	−0.284	0.2941	0.166	0.3979	−0.772	0.3485	−0.770
0.2691	0.088	0.2355	−0.314	0.2955	0.161	0.4020	−0.757		
0.2718	0.100	0.2376	−0.356	0.2976	0.161	0.4035	−0.749	2441539 +	
0.2732	0.108	0.2390	−0.386	0.3205	0.030	0.4054	−0.730	0.5023	0.039
0.2746	0.114	0.2404	−0.447	0.3217	0.031			0.5037	0.053
0.2795	0.117	0.2432	−0.501	0.3228	0.033	2441250 +		0.5065	0.037
0.2809	0.115	0.2446	−0.557	0.3256	0.042	0.2309	0.108	0.5078	0.041
0.2823	0.129	0.2460	−0.612	0.3270	0.031	0.2323	0.118	0.5106	0.052
0.2850	0.126	0.2474	−0.658	0.3281	−0.006	0.2378	0.132	0.5120	0.040
0.2864	0.134	0.2488	−0.683	0.3315	−0.032	0.2390	0.142	0.5148	0.040
0.2878	0.123	0.2502	−0.730	0.3330	−0.079	0.2404	0.132	0.5162	0.032
0.3114	−0.170	0.2536	−0.793	0.3339	−0.101	0.2608	0.135	0.5190	0.003
0.3128	−0.225	0.2550	−0.836	0.3367	−0.138	0.2621	0.124	0.5204	−0.024
0.3142	−0.247	0.2564	−0.850	0.3376	−0.148	0.2636	0.121	0.5231	−0.037
0.3170	−0.347	0.2591	−0.861	0.3389	−0.158	0.2684	0.097	0.5245	−0.047
0.3184	−0.367	0.2647	−0.882	0.3413	−0.192	0.2697	0.089	0.5273	−0.053
0.3198	−0.424	0.2675	−0.868	0.3424	−0.212	0.2711	0.080	0.5287	−0.065
0.3225	−0.498	0.2689	−0.862	0.3437	−0.227	0.2757	0.038	0.5314	−0.109
0.3239	−0.546	0.2703	−0.861	0.3462	−0.262	0.2769	0.007	0.5328	−0.131
0.3253	−0.611	0.2730	−0.860	0.3481	−0.299	0.2837	−0.048	0.5356	−0.164
0.3281	−0.698	0.2744	−0.851	0.3494	−0.324	0.2864	−0.094	0.5370	−0.200
0.3295	−0.755	0.2758	−0.845	0.3512	−0.375	0.2901	−0.158	0.5398	−0.225
0.3309	−0.783	0.2786	−0.828	0.3527	−0.414	0.2914	−0.178	0.5412	−0.257

0.5440 −0.319
0.5454 −0.364
0.5481 −0.419
0.5495 −0.489
0.5523 −0.606
0.5537 −0.648
0.5565 −0.771
0.5578 −0.809
0.5605 −0.859
0.5620 −0.874
0.5648 −0.922
0.5662 −0.928
0.5690 −0.952
0.5704 −0.954
0.5731 −0.953
0.5745 −0.949
0.5773 −0.934
0.5787 −0.923
0.5815 −0.895
0.5829 −0.876

2441589 +
0.5604 −0.348
0.5618 −0.359
0.5646 −0.407
0.5660 −0.421
0.5688 −0.458
0.5702 −0.474
0.5729 −0.518
0.5743 −0.553
0.5771 −0.593
0.5785 −0.624
0.5813 −0.665
0.5827 −0.667
0.5854 −0.675
0.5868 −0.689
0.5896 −0.694
0.5910 −0.706
0.5938 −0.709
0.5952 −0.720
0.5979 −0.717
0.5993 −0.707
0.6021 −0.694
0.6035 −0.686
0.6063 −0.666
0.6077 −0.657
0.6104 −0.650
0.6118 −0.644
0.6146 −0.631
0.6160 −0.617

2441591 +
0.4557 −0.221
0.4571 −0.238
0.4598 −0.265
0.4612 −0.281
0.4640 −0.323
0.4654 −0.338
0.4682 −0.354
0.4696 −0.373
0.4723 −0.393
0.4737 −0.423
0.4765 −0.463
0.4779 −0.476
0.4807 −0.509
0.4821 −0.538
0.4848 −0.560
0.4862 −0.590
0.4890 −0.611
0.4904 −0.625
0.4932 −0.641
0.4946 −0.645
0.4973 −0.648
0.4987 −0.661
0.5015 −0.665
0.5029 −0.666
0.5057 −0.670
0.5071 −0.667
0.5098 −0.664
0.5112 −0.667
0.5140 −0.663
0.5154 −0.659
0.5182 −0.651
0.5196 −0.636
0.5223 −0.617
0.5237 −0.613

2441606 +
0.2403 −0.200
0.2414 −0.214
0.2421 −0.237
0.2448 −0.294
0.2458 −0.310
0.2469 −0.345
0.2497 −0.395
0.2507 −0.430
0.2518 −0.472
0.2546 −0.543
0.2553 −0.605
0.2560 −0.629
0.2583 −0.677
0.2590 −0.708
0.2601 −0.732
0.2625 −0.799
0.2636 −0.818
0.2643 −0.842
0.2671 −0.877
0.2681 −0.893
0.2692 −0.900
0.2719 −0.923
0.2726 −0.928
0.2740 −0.937
0.2768 −0.934
0.2782 −0.935
0.2796 −0.920
0.2823 −0.900
0.2831 −0.884
0.2844 −0.872
0.2868 −0.843
0.2879 −0.824
0.2886 −0.816

2441622 +
0.4320 −0.108
0.4334 −0.109
0.4361 −0.144
0.4375 −0.175
0.4403 −0.217
0.4417 −0.233
0.4445 −0.270
0.4459 −0.283
0.4486 −0.329
0.4500 −0.351
0.4528 −0.425
0.4542 −0.458
0.4570 −0.491
0.4584 −0.511
0.4611 −0.557
0.4625 −0.594
0.4653 −0.644
0.4667 −0.660
0.4695 −0.688
0.4709 −0.710
0.4736 −0.731
0.4750 −0.748
0.4778 −0.782
0.4792 −0.827
0.4820 −0.840
0.4834 −0.849
0.4861 −0.855
0.4875 −0.866
0.4903 −0.862
0.4917 −0.869
0.4945 −0.860
0.4959 −0.855
0.4986 −0.849
0.5000 −0.846
0.5028 −0.842

2441772 +
0.5145 −0.050
0.5159 −0.072
0.5187 −0.105
0.5201 −0.126
0.5228 −0.148
0.5242 −0.165
0.5270 −0.185
0.5284 −0.226
0.5312 −0.252
0.5326 −0.270
0.5353 −0.296
0.5367 −0.321
0.5395 −0.368
0.5409 −0.388
0.5437 −0.410
0.5451 −0.438
0.5478 −0.475
0.5492 −0.504
0.5520 −0.559
0.5534 −0.601
0.5562 −0.669
0.5576 −0.693
0.5603 −0.784
0.5617 −0.816
0.5645 −0.835
0.5659 −0.857
0.5687 −0.879
0.5701 −0.880
0.5728 −0.888
0.5742 −0.902
0.5770 −0.894
0.5784 −0.889
0.5812 −0.879
0.5826 −0.871
0.5853 −0.849
0.5867 −0.833

2441803 +
0.4694 −0.151
0.4711 −0.178
0.4738 −0.218
0.4745 −0.221
0.4764 −0.231
0.4771 −0.235
0.4792 −0.239
0.4802 −0.241
0.4819 −0.248
0.4829 −0.255
0.4847 −0.271
0.4861 −0.274
0.4881 −0.282
0.4895 −0.295
0.4914 −0.314
0.4928 −0.324
0.4950 −0.353
0.4964 −0.364
0.4985 −0.380
0.4999 −0.411
0.5020 −0.449
0.5027 −0.458
0.5044 −0.470
0.5055 −0.475
0.5075 −0.481
0.5082 −0.484
0.5099 −0.501
0.5110 −0.517
0.5131 −0.549
0.5141 −0.559
0.5159 −0.580
0.5173 −0.588
0.5194 −0.607
0.5204 −0.619
0.5222 −0.626
0.5232 −0.634
0.5249 −0.641

0.5259 −0.639
0.5277 −0.644
0.5284 −0.651
0.5305 −0.659
0.5319 −0.666
0.5340 −0.669
0.5350 −0.669
0.5367 −0.667
0.5377 −0.659
0.5395 −0.649
0.5409 −0.648
0.5430 −0.653
0.5437 −0.649
0.5458 −0.639
0.5472 −0.641
0.5492 −0.637
0.5506 −0.644
0.5527 −0.640
0.5541 −0.639
0.5561 −0.637
0.5571 −0.636
0.5589 −0.630
0.5603 −0.631
0.5624 −0.631
0.5638 −0.627
0.5659 −0.613
0.5669 −0.610
0.5687 −0.587
0.5701 −0.593
0.5722 −0.577
0.5736 −0.586

2441815 +
0.4055 −0.347
0.4066 −0.367
0.4087 −0.382
0.4101 −0.390
0.4121 −0.410
0.4130 −0.423
0.4151 −0.441
0.4162 −0.453
0.4191 −0.482
0.4205 −0.518
0.4226 −0.552
0.4233 −0.564
0.4260 −0.595
0.4267 −0.607

0.4301 −0.642
0.4312 −0.661
0.4329 −0.674
0.4339 −0.681
0.4364 −0.696
0.4374 −0.699
0.4399 −0.707
0.4409 −0.711
0.4434 −0.713
0.4448 −0.715
0.4475 −0.718
0.4482 −0.720
0.4506 −0.722
0.4517 −0.718
0.4540 −0.709
0.4551 −0.704
0.4579 −0.691
0.4593 −0.688
0.4614 −0.682
0.4620 −0.683
0.4644 −0.672
0.4651 −0.670
0.4677 −0.660
0.4691 −0.649
0.4715 −0.636
0.4726 −0.631
0.4746 −0.623
0.4760 −0.622
0.4781 −0.621
0.4795 −0.614

2441833 +
0.5013 −0.035
0.5027 −0.048
0.5048 −0.061
0.5062 −0.074
0.5082 −0.076
0.5096 −0.077
0.5117 −0.087
0.5131 −0.093
0.5152 −0.123
0.5166 −0.148
0.5187 −0.172
0.5201 −0.202
0.5221 −0.225
0.5235 −0.248
0.5256 −0.273

0.5270 −0.304
0.5291 −0.367
0.5305 −0.410
0.5326 −0.466
0.5340 −0.516
0.5360 −0.569
0.5374 −0.610
0.5395 −0.707
0.5409 −0.738
0.5430 −0.781
0.5444 −0.799
0.5465 −0.846
0.5479 −0.862
0.5499 −0.869

2441835 +
0.4208 −0.088
0.4222 −0.109
0.4246 −0.143
0.4257 −0.159
0.4285 −0.181
0.4299 −0.209
0.4326 −0.249
0.4340 −0.282
0.4368 −0.344
0.4378 −0.376
0.4410 −0.467
0.4420 −0.502
0.4444 −0.634
0.4458 −0.691
0.4482 −0.778
0.4496 −0.837
0.4524 −0.880
0.4538 −0.883
0.4566 −0.905
0.4580 −0.910
0.4594 −0.920
0.4625 −0.920
0.4639 −0.931
0.4667 −0.921
0.4681 −0.922
0.4708 −0.910
0.4718 −0.891
0.4746 −0.873
0.4756 −0.872
0.4788 −0.860
0.4802 −0.855

0.4833 −0.832
0.4847 −0.831
0.4871 −0.826
0.4888 −0.825
0.4913 −0.803
0.4924 −0.796

2441905 +
0.4635 −0.192
0.4649 −0.212
0.4674 −0.244
0.4682 −0.267
0.4704 −0.326
0.4715 −0.353
0.4745 −0.421
0.4757 −0.439
0.4781 −0.519
0.4789 −0.541
0.4813 −0.589
0.4823 −0.620
0.4845 −0.697
0.4856 −0.740
0.4873 −0.780
0.4885 −0.802
0.4915 −0.825
0.4927 −0.840
0.4947 −0.833
0.4960 −0.844
0.4981 −0.849
0.4993 −0.857
0.5016 −0.857
0.5026 −0.860
0.5049 −0.870
0.5059 −0.867
0.5079 −0.868
0.5090 −0.862
0.5113 −0.854
0.5125 −0.848
0.5149 −0.836
0.5159 −0.829
0.5181 −0.817
0.5191 −0.815

2441915 +
0.4497 0.047
0.4508 0.041
0.4529 0.029

0.4539 0.019
0.4564 0.016
0.4574 −0.011
0.4598 −0.022
0.4612 −0.030
0.4640 −0.057
0.4654 −0.067
0.4678 −0.085
0.4688 −0.089
0.4716 −0.128
0.4730 −0.144
0.4754 −0.171
0.4764 −0.197
0.4879 −0.380
0.4890 −0.411
0.4916 −0.461
0.4930 −0.482
0.4952 −0.545
0.4962 −0.566
0.4983 −0.608
0.4994 −0.648
0.5015 −0.715
0.5025 −0.740
0.5047 −0.784
0.5071 −0.812
0.5090 −0.829
0.5119 −0.862
0.5140 −0.877

2441918 +
0.3223 −0.080
0.3237 −0.090
0.3263 −0.101
0.3275 −0.114
0.3296 −0.122
0.3313 −0.137
0.3341 −0.162
0.3355 −0.190
0.3383 −0.240
0.3397 −0.263
0.3421 −0.304
0.3454 −0.354
0.3487 −0.421
0.3515 −0.476
0.3525 −0.494
0.3553 −0.522
0.3560 −0.546

2441933 +
0.5646 −0.039
0.5655 −0.043
0.5674 −0.060
0.5683 −0.066
0.5701 −0.090
0.5710 −0.108
0.5729 −0.125
0.5738 −0.149
0.5757 −0.186
0.5766 −0.194
0.5785 −0.238
0.5794 −0.242
0.5813 −0.307
0.5821 −0.330
0.5868 −0.476
0.5877 −0.499

2441934 +
0.5148 −0.002
0.5176 −0.053
0.5203 −0.122
0.5255 −0.191
0.5262 −0.214
0.5283 −0.250
0.5290 −0.272
0.5315 −0.294
0.5342 −0.332
0.5370 −0.386
0.5398 −0.437
0.5426 −0.470
0.5453 −0.520
0.5481 −0.552
0.5509 −0.610
0.5537 −0.668
0.5565 −0.729
0.5592 −0.761
0.5620 −0.782
0.5651 −0.788
0.5734 −0.792
0.5755 −0.789
0.5780 −0.773
0.5815 −0.758

2441938 +
0.3683 −0.687
0.3697 −0.695
0.3731 −0.699
0.3745 −0.712
0.3776 −0.726
0.3793 −0.736
0.3829 −0.735
0.3846 −0.735
0.3877 −0.714
0.3891 −0.705
0.3933 −0.690
0.3950 −0.688
0.3988 −0.656
0.4005 −0.640

2441939 +
0.2856 −0.188
0.2870 −0.211
0.2891 −0.224
0.2905 −0.250
0.2926 −0.267
0.2940 −0.292
0.2960 −0.326
0.2974 −0.349
0.2995 −0.370
0.3009 −0.405
0.3030 −0.446
0.3044 −0.463
0.3065 −0.484
0.3079 −0.511
0.3099 −0.545
0.3113 −0.580
0.3134 −0.621
0.3148 −0.633
0.3169 −0.663
0.3183 −0.674
0.3204 −0.699
0.3218 −0.715
0.3238 −0.722
0.3252 −0.731
0.3273 −0.746
0.3287 −0.755
0.3308 −0.759
0.3322 −0.762
0.3342 −0.769
0.3356 −0.759
0.3377 −0.762
0.3391 −0.751
0.3412 −0.757
0.3426 −0.749
0.3447 −0.742
0.3461 −0.737
0.3481 −0.726
0.3495 −0.720
0.3516 −0.709
0.3530 −0.699
0.3551 −0.685
0.3565 −0.677

2441949 +
0.2850 −0.308
0.2861 −0.336
0.2884 −0.345
0.2895 −0.368
0.2919 −0.382
0.3037 −0.493
0.3065 −0.521
0.3092 −0.537
0.3120 −0.554
0.3148 −0.569
0.3176 −0.606
0.3202 −0.617
0.3231 −0.631
0.3259 −0.650
0.3287 −0.667
0.3315 −0.673
0.3342 −0.684
0.3370 −0.697
0.3452 −0.674
0.3481 −0.664
0.3509 −0.660
0.3537 −0.652
0.3565 −0.648
0.3592 −0.618
0.3648 −0.604

2441990 +
0.2652 −0.030
0.2666 −0.037
0.2698 −0.042
0.2712 −0.048
0.2745 −0.057
0.2759 −0.080
0.2788 −0.108
0.2802 −0.109
0.2832 −0.154
0.2843 −0.163
0.2870 −0.201
0.2884 −0.212
0.2927 −0.259
0.2950 −0.305
0.2957 −0.330
0.2982 −0.383
0.2996 −0.446
0.3020 −0.513
0.3027 −0.542
0.3048 −0.627
0.3055 −0.687
0.3075 −0.770
0.3082 −0.819
0.3103 −0.835
0.3110 −0.842
0.3131 −0.831
0.3138 −0.835
0.3159 −0.888
0.3166 −0.897
0.3187 −0.926
0.3194 −0.926
0.3214 −0.926
0.3221 −0.928
0.3242 −0.933
0.3249 −0.936
0.3270 −0.930
0.3277 −0.928
0.3302 −0.917
0.3316 −0.914
0.3343 −0.906
0.3357 −0.901
0.3385 −0.891
0.3399 −0.876
0.3427 −0.855
0.3441 −0.843
0.3468 −0.814
0.3482 −0.808

2442147 +
0.4811 0.144
0.4825 0.150
0.4853 0.156
0.4866 0.143
0.4978 0.130
0.4992 0.116
0.5033 0.117
0.5047 0.109
0.5089 0.066
0.5103 0.065
0.5130 0.015
0.5144 −0.002
0.5193 −0.056
0.5207 −0.070
0.5221 −0.097
0.5235 −0.109
0.5269 −0.159
0.5283 −0.175
0.5325 −0.228
0.5339 −0.254
0.5380 −0.328
0.5394 −0.363
0.5422 −0.419
0.5436 −0.465
0.5471 −0.558
0.5485 −0.594
0.5519 −0.701
0.5533 −0.730
0.5568 −0.788
0.5582 −0.810
0.5617 −0.862
0.5631 −0.896
0.5665 −0.911
0.5679 −0.918
0.5721 −0.916
0.5735 −0.912
0.5769 −0.916
0.5783 −0.915
0.5818 −0.905
0.5832 −0.897
0.5860 −0.856
0.5874 −0.835
0.5908 −0.810
0.5922 −0.786
0.5943 −0.758
0.5957 −0.756

2442201 +
0.3729 −0.439
0.3743 −0.478
0.3777 −0.541
0.3791 −0.571
0.3819 −0.614
0.3833 −0.646

0.3861 −0.683
0.3875 −0.704
0.3902 −0.749
0.3916 −0.766
0.3944 −0.789
0.3958 −0.797
0.3993 −0.808
0.4007 −0.811
0.4048 −0.809
0.4083 −0.809
0.4097 −0.805
0.4125 −0.806
0.4139 −0.802
0.4173 −0.800
0.4187 −0.798
0.4215 −0.785
0.4229 −0.762
0.4264 −0.739
0.4278 −0.729
0.4312 −0.725
0.4361 −0.693
0.4375 −0.675
0.4410 −0.641
0.4424 −0.637

2442220 +
0.4285 −0.111
0.4313 −0.139
0.4341 −0.198
0.4355 −0.227
0.4369 −0.259
0.4396 −0.307
0.4410 −0.355
0.4423 −0.392
0.4452 −0.450
0.4466 −0.486
0.4480 −0.519
0.4508 −0.586
0.4522 −0.604
0.4536 −0.632
0.4563 −0.702
0.4577 −0.720
0.4591 −0.755
0.4619 −0.820
0.4633 −0.847
0.4647 −0.863
0.4674 −0.902

0.4688 −0.927
0.4702 −0.933
0.4730 −0.935
0.4744 −0.926
0.4758 −0.916
0.4785 −0.895
0.4799 −0.883
0.4813 −0.866
0.4841 −0.854
0.4855 −0.847
0.4869 −0.837
0.4896 −0.816
0.4910 −0.806
0.4924 −0.801

2442242 +
0.3526 −0.316
0.3535 −0.333
0.3581 −0.449
0.3590 −0.472
0.3609 −0.512
0.3618 −0.522
0.3637 −0.562
0.3646 −0.589
0.3665 −0.621
0.3674 −0.642
0.3693 −0.679
0.3713 −0.700
0.3762 −0.754
0.3781 −0.762
0.3818 −0.777
0.3855 −0.783
0.3873 −0.774
0.3892 −0.765
0.3911 −0.770
0.3929 −0.756

2442260 +
0.4192 −0.102
0.4206 −0.107
0.4234 −0.120
0.4248 −0.122
0.4275 −0.148
0.4289 −0.173
0.4317 −0.214
0.4331 −0.235
0.4360 −0.264

0.4372 −0.290
0.4400 −0.314
0.4414 −0.328
0.4442 −0.352
0.4456 −0.352
0.4484 −0.356
0.4498 −0.351
0.4525 −0.373
0.4539 −0.400
0.4567 −0.431
0.4581 −0.463
0.4605 −0.495
0.4612 −0.514
0.4633 −0.536
0.4643 −0.540
0.4667 −0.568
0.4681 −0.589
0.4706 −0.614
0.4720 −0.619
0.4744 −0.634
0.4758 −0.644
0.4785 −0.646
0.4799 −0.651
0.4824 −0.663
0.4838 −0.682
0.4872 −0.704
0.5063 −0.732
0.5091 −0.726
0.5105 −0.715
0.5130 −0.713

2442269 +
0.4879 −0.153
0.4907 −0.199
0.4917 −0.214
0.4949 −0.252
0.4963 −0.270
0.4987 −0.293
0.4997 −0.316
0.5025 −0.341
0.5039 −0.356
0.5078 −0.391
0.5101 −0.431
0.5113 −0.447
0.5140 −0.465
0.5151 −0.478
0.5175 −0.513

0.5182 −0.533
0.5209 −0.563
0.5216 −0.575
0.5240 −0.624
0.5251 −0.649
0.5276 −0.663
0.5287 −0.671
0.5310 −0.681
0.5321 −0.687
0.5345 −0.689
0.5356 −0.694
0.5380 −0.695
0.5390 −0.699
0.5414 −0.694
0.5425 −0.700
0.5452 −0.702
0.5463 −0.703
0.5490 −0.702
0.5501 −0.701
0.5525 −0.699
0.5536 −0.698
0.5564 −0.697
0.5594 −0.691
0.5601 −0.690

2442279 +
0.4847 0.085
0.4860 0.081
0.4874 0.080
0.4886 0.080
0.4900 0.055
0.4957 0.043
0.4972 0.022
0.4986 0.024
0.4999 0.012
0.5010 −0.017
0.5064 −0.098
0.5074 −0.109
0.5086 −0.139
0.5098 −0.173
0.5109 −0.192
0.5181 −0.344
0.5193 −0.369
0.5203 −0.376
0.5256 −0.528
0.5267 −0.556
0.5278 −0.574

0.5288 −0.598
0.5301 −0.637
0.5351 −0.700
0.5362 −0.719
0.5372 −0.738
0.5383 −0.754
0.5393 −0.775
0.5440 −0.812
0.5450 −0.827
0.5462 −0.824
0.5472 −0.821
0.5484 −0.818
0.5535 −0.796
0.5545 −0.782
0.5554 −0.781
0.5565 −0.773
0.5575 −0.768
0.5585 −0.762

2442303 +
0.3446 −0.174
0.3460 −0.193
0.3487 −0.214
0.3494 −0.224
0.3515 −0.260
0.3522 −0.262
0.3542 −0.290
0.3548 −0.298
0.3570 −0.329
0.3577 −0.336
0.3601 −0.368
0.3607 −0.382
0.3636 −0.450
0.3646 −0.464
0.3672 −0.504
0.3682 −0.537
0.3716 −0.660
0.3736 −0.698
0.3750 −0.742
0.3769 −0.773
0.3783 −0.775
0.3804 −0.782
0.3814 −0.792
0.3834 −0.787
0.3841 −0.790
0.3862 −0.786
0.3869 −0.789

0.3890 −0.798
0.3900 −0.798
0.3921 −0.793
0.3932 −0.799
0.3957 −0.806

2442636 +
0.3606 −0.034
0.3614 −0.033
0.3632 −0.043
0.3639 −0.050
0.3660 −0.048
0.3668 −0.065
0.3689 −0.080
0.3696 −0.071
0.3715 −0.078
0.3760 −0.124
0.3786 −0.136
0.3805 −0.147
0.3814 −0.159
0.3839 −0.194
0.3846 −0.212
0.3864 −0.269
0.3873 −0.287
0.3894 −0.318
0.3904 −0.310
0.3925 −0.319
0.3933 −0.324
0.3962 −0.322
0.3983 −0.324
0.3990 −0.332
0.4011 −0.358
0.4036 −0.383
0.4060 −0.409
0.4115 −0.470
0.4123 −0.470
0.4143 −0.481
0.4152 −0.488
0.4172 −0.485
0.4180 −0.490
0.4204 −0.498
0.4230 −0.517
0.4282 −0.595
0.4291 −0.606
0.4310 −0.627
0.4339 −0.650
0.4346 −0.650
0.4443 −0.715
0.4464 −0.698
0.4472 −0.701
0.4498 −0.670
0.4514 −0.650
0.4522 −0.639
0.4546 −0.619
0.4580 −0.602

2442948 +
0.4872 −0.089
0.4886 −0.100
0.4914 −0.135
0.4928 −0.143
0.4955 −0.169
0.4990 −0.205
0.5004 −0.239
0.5032 −0.261
0.5046 −0.281
0.5079 −0.331
0.5093 −0.350
0.5122 −0.348
0.5136 −0.348
0.5184 −0.388
0.5226 −0.446
0.5260 −0.456
0.5299 −0.487
0.5312 −0.521

2443660 +
0.3501 0.119
0.3541 0.097
0.3590 0.119
0.3637 0.083
0.3672 0.097
0.3754 0.093
0.3798 0.098
0.3846 0.098
0.3899 0.049
0.3955 0.009
0.4003 −0.006
0.4049 −0.026
0.4090 −0.043
0.4212 −0.189
0.4225 −0.211
0.4253 −0.243
0.4268 −0.307
0.4295 −0.369
0.4309 −0.377
0.4335 −0.442
0.4349 −0.508
0.4376 −0.601
0.4391 −0.631
0.4423 −0.765
0.4438 −0.831

2443700 +
0.3944 0.050
0.3958 0.051
0.3985 0.048
0.3999 0.028
0.4041 0.021
0.4083 −0.005
0.4110 −0.049
0.4124 −0.059
0.4152 −0.083
0.4166 −0.094
0.4194 −0.109
0.4208 −0.113
0.4235 −0.143
0.4249 −0.159
0.4277 −0.181
0.4291 −0.196
0.4319 −0.231
0.4333 −0.264
0.4360 −0.278
0.4374 −0.303
0.4402 −0.326
0.4416 −0.328
0.4444 −0.352
0.4485 −0.378
0.4499 −0.401
0.4527 −0.419
0.4541 −0.431
0.4569 −0.474
0.4583 −0.515
0.4610 −0.527
0.4624 −0.539
0.4652 −0.572
0.4666 −0.602
0.4694 −0.656
0.4708 −0.678
0.4735 −0.691
0.4749 −0.704
0.4777 −0.698
0.4791 −0.712
0.4819 −0.708
0.4833 −0.704
0.4860 −0.695
0.4874 −0.689
0.4902 −0.674
0.4916 −0.665
0.4944 −0.660
0.4958 −0.655
0.4985 −0.646
0.4999 −0.642
0.5027 −0.639
0.5069 −0.615
0.5083 −0.600
0.5110 −0.594
0.5124 −0.578

2443720 +
0.4578 −0.368
0.4592 −0.383
0.4615 −0.408
0.4624 −0.430
0.4643 −0.470
0.4652 −0.477
0.4671 −0.509
0.4680 −0.538
0.4708 −0.610
0.4726 −0.685
0.4736 −0.717
0.4754 −0.761
0.4763 −0.776
0.4787 −0.804
0.4800 −0.824
0.4828 −0.857
0.4842 −0.866
0.4870 −0.885
0.4884 −0.888
0.4912 −0.889
0.4925 −0.890
0.4967 −0.868
0.4995 −0.844
0.5009 −0.831
0.5037 −0.814
0.5050 −0.803
0.5078 −0.779
0.5092 −0.774

2443730 +
0.4582 −0.052
0.4610 −0.093
0.4624 −0.129
0.4651 −0.162
0.4665 −0.192
0.4693 −0.272
0.4703 −0.302
0.4730 −0.352
0.4740 −0.385
0.4766 −0.429
0.4778 −0.457

2443732 +
0.3639 0.018
0.3700 −0.091
0.3754 −0.174
0.3770 −0.216
0.3824 −0.362
0.3841 −0.423
0.3938 −0.756
0.3998 −0.908
0.4012 −0.927
0.4052 −0.983

2443743 +
0.3267 −0.088
0.3278 −0.101
0.3300 −0.140
0.3311 −0.161
0.3334 −0.192
0.3344 −0.212
0.3393 −0.267
0.3403 −0.282
0.3424 −0.335
0.3433 −0.352
0.3456 −0.413
0.3491 −0.439
0.3500 −0.444
0.3524 −0.549
0.3534 −0.591
0.3557 −0.636
0.3569 −0.659
0.3598 −0.691
0.3607 −0.709
0.3634 −0.747
0.3662 −0.800

0.3673 −0.812
0.3710 −0.839
0.3734 −0.840
0.3745 −0.835
0.3782 −0.818
0.3809 −0.811
0.3820 −0.799

2443763 +
0.3359 −0.226
0.3368 −0.246
0.3398 −0.284
0.3413 −0.316
0.3449 −0.364
0.3508 −0.437
0.3523 −0.463
0.3555 −0.490
0.3572 −0.523
0.3608 −0.558
0.3626 −0.576
0.3662 −0.611
0.3681 −0.621
0.3709 −0.641
0.3727 −0.657
0.3768 −0.672
0.3811 −0.682
0.3830 −0.685
0.3862 −0.681
0.3880 −0.676
0.3920 −0.666
0.3938 −0.659
0.3971 −0.630
0.3987 −0.627
0.4044 −0.594

2445609 +
0.2835 −0.687
0.2848 −0.711
0.2862 −0.738
0.2875 −0.753
0.2888 −0.779
0.2947 −0.820
0.2960 −0.826
0.2974 −0.835
0.2987 −0.832
0.3000 −0.832
0.3053 −0.829

0.3066 −0.816
0.3080 −0.811
0.3093 −0.813
0.3106 −0.808

2445791 +
0.3595 −0.729
0.3609 −0.725
0.3622 −0.713
0.3635 −0.713
0.3648 −0.700
0.3775 −0.609
0.3789 −0.599
0.3802 −0.592
0.3815 −0.587
0.4101 −0.357
0.4115 −0.353
0.4128 −0.351
0.4142 −0.348
0.4155 −0.343
0.4168 −0.341
0.4182 −0.333
0.4195 −0.330
0.4209 −0.325
0.4222 −0.324
0.4360 −0.324
0.4374 −0.326
0.4387 −0.326
0.4401 −0.324
0.4414 −0.324
0.4427 −0.317
0.4441 −0.313
0.4454 −0.312
0.4468 −0.304
0.4481 −0.302
0.4555 −0.265
0.4568 −0.256
0.4581 −0.246
0.4595 −0.248
0.4608 −0.247
0.4622 −0.238
0.4635 −0.244
0.4648 −0.242
0.4662 −0.243
0.4676 −0.240
0.4733 −0.235
0.4746 −0.231

0.4760 −0.236
0.4773 −0.232
0.4786 −0.228
0.4800 −0.229
0.4813 −0.228
0.4827 −0.227
0.4840 −0.228
0.4853 −0.223
0.5208 −0.120
0.5221 −0.112
0.5234 −0.111
0.5248 −0.108
0.5261 −0.112
0.5275 −0.110
0.5288 −0.104
0.5301 −0.096
0.5315 −0.097
0.5328 −0.096
0.5393 −0.076
0.5407 −0.078
0.5420 −0.075
0.5434 −0.066
0.5447 −0.069
0.5461 −0.063
0.5474 −0.062
0.5487 −0.067
0.5501 −0.060
0.5514 −0.050
0.5589 −0.040
0.5602 −0.038
0.5616 −0.034
0.5629 −0.024
0.5643 −0.024
0.5656 −0.025
0.5669 −0.002
0.5683 0.010
0.5696 0.009
0.5710 −0.001
0.5773 −0.005
0.5787 −0.005
0.5800 −0.005
0.5814 0.006
0.5840 0.019

2445806 +
0.4749 0.103
0.4763 0.099

0.4776 0.077
0.4789 0.071
0.4802 0.065
0.4861 0.045
0.4874 0.038
0.4887 0.026
0.4901 0.035
0.4914 0.016
0.4971 −0.019
0.4984 −0.032
0.4998 −0.062
0.5012 −0.075
0.5025 −0.087
0.5079 −0.129
0.5093 −0.142
0.5106 −0.159
0.5120 −0.165
0.5133 −0.192
0.5191 −0.238
0.5204 −0.252
0.5218 −0.265
0.5231 −0.290
0.5244 −0.309
0.5301 −0.382
0.5314 −0.399
0.5328 −0.422
0.5341 −0.435
0.5355 −0.455
0.5409 −0.533
0.5422 −0.568
0.5436 −0.589
0.5449 −0.614
0.5462 −0.633
0.5513 −0.677
0.5527 −0.689
0.5540 −0.705
0.5554 −0.713
0.5567 −0.725
0.5624 −0.729
0.5637 −0.730
0.5651 −0.728
0.5664 −0.734
0.5678 −0.727
0.5731 −0.711
0.5744 −0.713
0.5757 −0.704
0.5771 −0.711

0.5784 −0.707
0.5835 −0.683
0.5849 −0.677
0.5862 −0.672
0.5932 −0.643
0.5945 −0.641
0.5959 −0.633
0.5972 −0.629

2446193 +
0.4372 −0.201
0.4385 −0.212
0.4398 −0.229
0.4412 −0.241
0.4426 −0.253
0.4480 −0.318
0.4493 −0.328
0.4507 −0.359
0.4520 −0.368
0.4534 −0.389
0.4586 −0.451
0.4599 −0.465
0.4612 −0.492
0.4626 −0.506
0.4639 −0.513
0.4691 −0.571
0.4705 −0.588
0.4718 −0.596
0.4732 −0.617
0.4745 −0.628
0.4803 −0.667
0.4816 −0.673
0.4830 −0.678
0.4843 −0.682
0.4857 −0.689
0.4914 −0.693
0.4927 −0.695
0.4941 −0.686
0.4954 −0.681
0.4968 −0.680
0.5028 −0.671
0.5041 −0.669
0.5055 −0.655
0.5068 −0.658
0.5081 −0.650
0.5136 −0.627
0.5150 −0.615

0.5163 −0.606
0.5176 −0.596
0.5190 −0.578

2447306 +
0.4921 0.147
0.4934 0.144
0.4986 0.157
0.4998 0.152
0.5059 0.123
0.5072 0.131
0.5123 0.126
0.5136 0.103
0.5192 0.071
0.5205 0.053
0.5258 −0.012

0.5271 −0.008
0.5322 −0.079
0.5335 −0.096
0.5387 −0.214
0.5400 −0.224
0.5453 −0.254
0.5465 −0.309
0.5514 −0.413
0.5527 −0.442

2447360 +
0.3676 0.094
0.3689 0.078
0.3745 0.053
0.3758 0.053
0.3809 0.020

0.3821 0.010
0.3870 −0.019
0.3883 −0.018
0.3935 −0.093
0.3948 −0.097
0.3961 −0.121
0.4033 −0.216
0.4047 −0.242
0.4060 −0.264
0.4118 −0.380
0.4131 −0.396
0.4186 −0.621
0.4199 −0.668
0.4252 −0.902
0.4265 −0.923
0.4321 −0.953

0.4334 −0.949
0.4391 −0.944
0.4488 −0.905
0.4501 −0.866
0.4515 −0.867
0.4590 −0.789
0.4645 −0.782
0.4658 −0.769

2447462 +
0.3534 −0.264
0.3544 −0.297
0.3592 −0.308
0.3603 −0.319
0.3666 −0.433
0.3677 −0.445

0.3790 −0.607
0.3801 −0.615
0.3849 −0.673
0.3860 −0.679
0.3936 −0.710
0.3947 −0.712
0.3994 −0.733
0.4005 −0.725
0.4056 −0.712
0.4067 −0.712
0.4131 −0.681
0.4142 −0.669
0.4191 −0.656
0.4202 −0.660
0.4246 −0.634
0.4256 −0.630

Table 5.e Photoelectric differential $R_{\rm C}$ observations of XZ Dra

2447306 +
0.4924 0.159
0.4937 0.176
0.4989 0.169
0.5001 0.172
0.5062 0.158
0.5075 0.157
0.5126 0.152
0.5139 0.137
0.5195 0.102
0.5208 0.097
0.5261 0.048
0.5274 0.043
0.5325 −0.031
0.5338 −0.043

0.5390 −0.128
0.5403 −0.137
0.5456 −0.155
0.5468 −0.188
0.5517 −0.272
0.5530 −0.300

2447360 +
0.3679 0.120
0.3692 0.123
0.3748 0.110
0.3761 0.105
0.3812 0.073
0.3824 0.059
0.3873 0.035
0.3886 0.035

0.3938 −0.032
0.3951 −0.038
0.3964 −0.040
0.4036 −0.120
0.4050 −0.134
0.4063 −0.161
0.4121 −0.268
0.4134 −0.298
0.4189 −0.471
0.4202 −0.487
0.4255 −0.710
0.4268 −0.713
0.4324 −0.734
0.4337 −0.732
0.4394 −0.732

0.4491 −0.679
0.4504 −0.664
0.4518 −0.667
0.4593 −0.600
0.4648 −0.577
0.4661 −0.536

2447462 +
0.3537 −0.150
0.3547 −0.173
0.3595 −0.163
0.3606 −0.225
0.3669 −0.285
0.3680 −0.293
0.3793 −0.429
0.3804 −0.438

0.3852 −0.482
0.3863 −0.499
0.3939 −0.508
0.3950 −0.510
0.3997 −0.525
0.4008 −0.529
0.4059 −0.519
0.4070 −0.510
0.4134 −0.490
0.4145 −0.486
0.4194 −0.487
0.4205 −0.486
0.4249 −0.464
0.4259 −0.450

Table 5.f Photoelectric differential $I_{\rm C}$ observations of XZ Dra

2447306 +
0.4926 0.180
0.4939 0.196
0.4991 0.155
0.5003 0.155
0.5064 0.180
0.5077 0.169
0.5128 0.166
0.5141 0.162
0.5197 0.162

0.5210 0.162
0.5263 0.162
0.5276 0.162
0.5327 0.041
0.5340 0.048
0.5392 −0.016
0.5405 −0.003
0.5458 −0.071
0.5470 −0.047
0.5519 −0.177

0.5532 −0.165

2447360 +
0.3681 0.152
0.3694 0.130
0.3750 0.123
0.3763 0.132
0.3814 0.114
0.3826 0.100
0.3875 0.104

0.3888 0.096
0.3940 0.050
0.3953 0.046
0.3966 0.034
0.4038 −0.035
0.4052 −0.046
0.4065 −0.069
0.4123 −0.163
0.4136 −0.179
0.4191 −0.324

0.4204 −0.292
0.4257 −0.482
0.4270 −0.509
0.4326 −0.503
0.4339 −0.505
0.4396 0.505
0.4493 −0.442
0.4506 −0.447
0.4520 −0.453
0.4595 −0.397

0.4650 −0.393	0.3597 −0.049	0.3806 −0.289	0.3999 −0.339	0.4147 −0.316
0.4663 −0.393	0.3608 −0.064	0.3854 −0.314	0.4010 −0.333	0.4196 −0.306
	0.3671 −0.118	0.3865 −0.339	0.4061 −0.337	0.4207 −0.298
2447462 +	0.3682 −0.111	0.3941 −0.317	0.4072 −0.352	0.4251 −0.275
0.3539 −0.033	0.3795 −0.285	0.3952 −0.350	0.4136 −0.317	0.4261 −0.258
0.3549 −0.076				

CCD Observations

CCD observations were obtained on 5 nights in July–August 2001, with the 60/90/180cm Schmidt telescope at Piszkéstető Mountain Station of the Konkoly Observatory. A Photometrics CCD camera with a thermoelectrically cooled Kodak KAF-1600 1024 × 1536 chip yielded a $19' \times 28'$ field of view, with $1.''0$/pixel resolution. Standard Johnson V filter was used and the total amount of frames were 405. The typical exposition time was between 30 and 15 sec. To the calibration process of the camera and other technical details see Bakos (2000).

Since there were no pattern in the bias images, we applied a simple zero offset value subtraction to the frames determined from their overscan area. Common flat field corrections were carried out using calibration images taken of the sky during twilight. Other corrections were unnecessary.

Finally, aperture photometry (IRAF/DAOPHOT/PHOT) was accomplished to obtain instrumental magnitudes. The relative magnitudes Var−Comp (=TYC 4225_1323_1, the same comparison star used for photoelectric observations) are shown in Table 6. We note here, that the colour system satisfyingly realizes the international one without any transformation (see Benkő *et al.*, 2001). The accuracy of the individual points is estimated to be $\pm 0.^{\rm m}002$ from the IRAF noise statistics.

On $8^{\rm th}$ July 134 frames of the field of XZ Dra were taken with 60 sec exposition time yielding good enough signal-to-noise ratio to measure the fainter stars as well. This enabled us to check the constancy of the neighbouring stars. The ISIS-2.1 program package was applied as a realization of the Image Subtraction Method (Alard & Lupton 1998, Alard 2000) to find possible variable stars. Except XZ Dra, we could not detect variability of any of the stars shown in Fig 1. during this night. Based on the other nights' observations longer term variability of the brighter objects were not found either.

On two nights in July, 2001 we observed XZ Dra with the second small Hungarian Automatic Telescope (HAT-2) during its test run phase. About the HAT project see Bakos (2001a,b) The fully automatized observatory was equipped with a 0.1m diameter, f/10 Maksutov MT0 lens, and an amateur Meade Pictor 416xte CCD camera (512×768 9μm pixels). The system yielded a resolution of $1.''85$ per pixel, and FOV of $\sim 16' \times 24'$. 47 frames of the field of XZ Dra were taken with I filter. After standard bias, dark and skyflat calibration, aperture photometry was performed. The relative instrumental i magnitudes are given in Table 7 (XZ Dra−TYC 4225_1323_1).

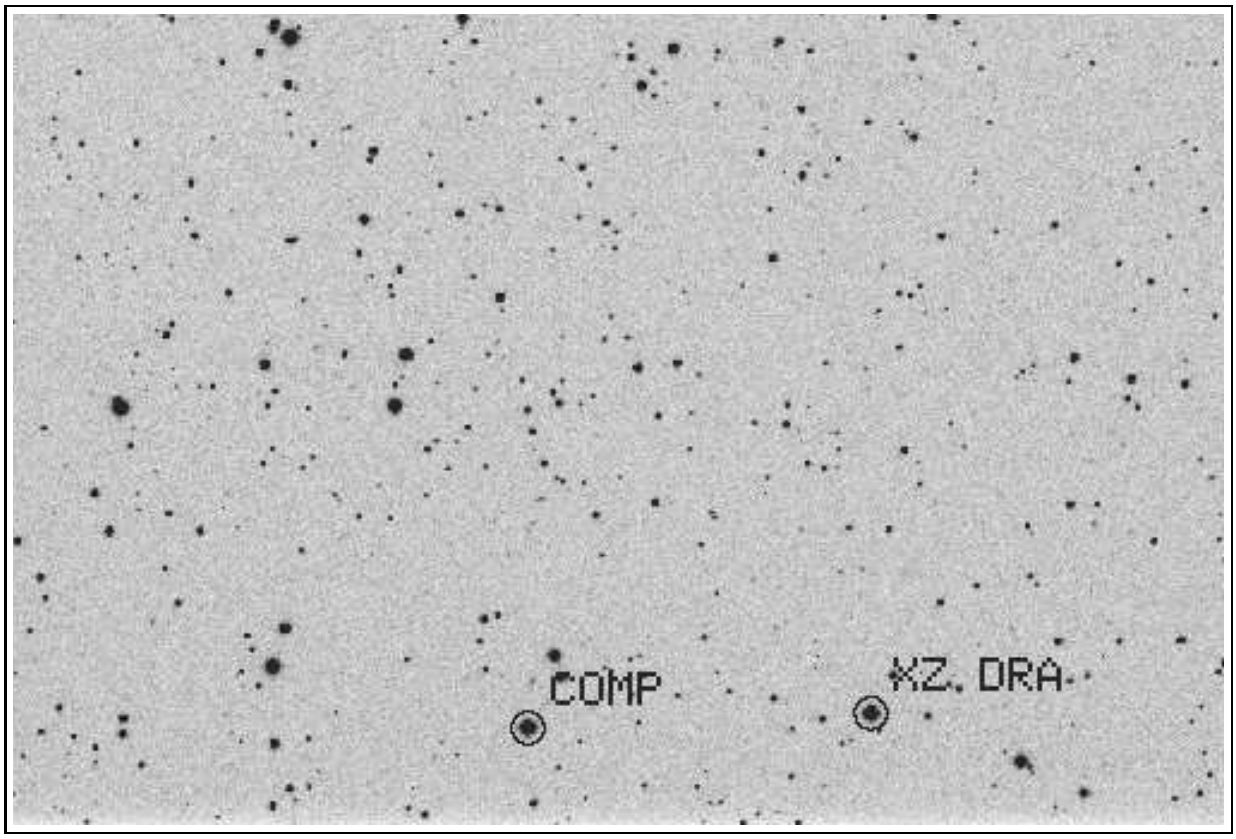

Figure 1: 60 sec exposition V filter CCD frame taken with the Schmidt telescope. XZ Dra and the photoelectric/CCD comparison TYC 4225_1323_1 are marked. North is up, east is to the left.

Table 6. Differential CCD V observations of XZ Dra

2452100 +		0.3947	0.025	0.4201	0.044	0.4464	0.091	0.4702	0.144
0.3699	−0.001	0.3960	0.024	0.4215	0.043	0.4480	0.095	0.4714	0.150
0.3712	−0.004	0.3973	0.023	0.4227	0.043	0.4493	0.093	0.4735	0.153
0.3730	0.002	0.3986	0.024	0.4240	0.046	0.4505	0.100	0.4747	0.152
0.3743	0.006	0.3999	0.023	0.4253	0.044	0.4517	0.101	0.4759	0.155
0.3755	0.006	0.4012	0.023	0.4266	0.048	0.4529	0.104	0.4772	0.157
0.3768	0.004	0.4025	0.022	0.4279	0.050	0.4542	0.107	0.4784	0.158
0.3781	0.008	0.4037	0.024	0.4292	0.051	0.4554	0.112	0.4796	0.160
0.3794	0.009	0.4050	0.026	0.4305	0.057	0.4566	0.108	0.4809	0.161
0.3807	0.013	0.4063	0.026	0.4318	0.057	0.4579	0.116	0.4821	0.165
0.3820	0.013	0.4076	0.026	0.4341	0.065	0.4591	0.116	0.4833	0.161
0.3833	0.014	0.4089	0.026	0.4353	0.066	0.4603	0.124	0.4845	0.168
0.3846	0.018	0.4102	0.028	0.4367	0.066	0.4615	0.123	0.4858	0.165
0.3858	0.015	0.4114	0.032	0.4379	0.070	0.4628	0.129	0.4870	0.168
0.3871	0.020	0.4137	0.034	0.4392	0.068	0.4640	0.138	0.4882	0.167
0.3884	0.019	0.4150	0.035	0.4405	0.069	0.4652	0.143	0.4895	0.171
0.3897	0.017	0.4163	0.038	0.4425	0.084	0.4665	0.136	0.4907	0.169
0.3910	0.022	0.4176	0.034	0.4438	0.075	0.4677	0.141	0.4919	0.165
0.3934	0.019	0.4189	0.040	0.4451	0.083	0.4689	0.148	0.4931	0.164

0.4944	0.172	0.5563	−0.485	0.4962	−0.262	0.4317	0.046	0.4342	−0.094		
0.4956	0.169	0.5574	−0.511	0.4973	−0.277	0.4328	0.044	0.4355	−0.083		
0.4968	0.168	0.5585	−0.537	0.4984	−0.298	0.4339	0.026	0.4368	−0.090		
0.4994	0.162	0.5595	−0.563	0.4995	−0.340	0.4350	0.024	0.4381	−0.085		
0.5006	0.167	0.5606	−0.583	0.5018	−0.411	0.4362	0.002	0.4393	−0.083		
0.5018	0.167	0.5617	−0.601	0.5036	−0.466	0.4373	−0.005	0.4406	−0.083		
0.5031	0.164	0.5630	−0.620			0.4384	−0.018	0.4419	−0.082		
0.5043	0.166	0.5641	−0.640	2452102 +		0.4395	−0.032	0.4432	−0.073		
0.5055	0.159	0.5651	−0.655	0.3412	0.070	0.4406	−0.042	0.5670	0.054		
0.5068	0.157	0.5662	−0.675	0.3423	0.076	0.4417	−0.070	0.5687	0.054		
0.5080	0.153	0.5711	−0.744	0.3434	0.069	0.4428	−0.084	0.5692	0.061		
0.5092	0.147	0.5733	−0.761	0.3445	0.073	0.4440	−0.094	0.5698	0.061		
0.5104	0.143	0.5744	−0.765	0.3456	0.079	0.4451	−0.122	0.5704	0.059		
0.5117	0.138	0.5755	−0.771	0.3468	0.077	0.4462	−0.127	0.5717	0.062		
0.5129	0.134	0.5791	−0.783	0.3479	0.086	0.4484	−0.152	0.5730	0.065		
0.5141	0.125	0.5802	−0.777	0.3490	0.088	0.4495	−0.190	0.5743	0.068		
0.5154	0.116	0.5813	−0.784	0.3501	0.083	0.4518	−0.210	0.5756	0.067		
0.5166	0.108	0.5825	−0.787	0.3512	0.097	0.4529	−0.234	0.5769	0.078		
0.5178	0.104	0.5835	−0.794	0.3523	0.091	0.4551	−0.309	0.5781	0.076		
0.5190	0.089	0.5846	−0.779	0.3534	0.094			0.5802	0.078		
0.5203	0.087	0.5858	−0.782	0.3545	0.096	2452138 +		0.5815	0.085		
0.5215	0.068			0.3556	0.098	0.3953	−0.160	0.5828	0.097		
0.5227	0.056	2452101 +		0.3568	0.097	0.3972	−0.144	0.5841	0.097		
0.5253	0.031	0.4688	0.137	0.3579	0.099	0.3987	−0.143	0.5854	0.100		
0.5265	0.017	0.4702	0.127	0.3590	0.107	0.4013	−0.135	0.5867	0.104		
0.5277	0.005	0.4713	0.128	0.3601	0.108	0.4026	−0.135	0.5880	0.105		
0.5289	−0.015	0.4724	0.119	0.3612	0.107	0.4051	−0.133	0.5892	0.108		
0.5300	−0.025	0.4736	0.110	0.3623	0.110	0.4064	−0.132	0.5905	0.112		
0.5312	−0.043	0.4747	0.111	0.3642	0.120	0.4077	−0.129	0.5918	0.108		
0.5324	−0.053	0.4758	0.099	0.3653	0.114	0.4090	−0.127	0.5931	0.115		
0.5336	−0.073	0.4769	0.082	0.3664	0.115	0.4103	−0.121	0.5944	0.110		
0.5347	−0.087	0.4780	0.087	0.3675	0.120	0.4116	−0.130	0.5957	0.110		
0.5359	−0.099	0.4791	0.066	0.4145	0.164	0.4129	−0.123	0.5970	0.120		
0.5403	−0.180	0.4803	0.058	0.4156	0.167	0.4142	−0.121	0.5982	0.123		
0.5414	−0.204	0.4814	0.049	0.4167	0.154	0.4154	−0.115				
0.5425	−0.222	0.4825	0.037	0.4178	0.155	0.4182	−0.112	2452140 +			
0.5436	−0.249	0.4836	0.017	0.4190	0.143	0.4195	−0.112	0.2984	−0.141		
0.5448	−0.279	0.4847	0.011	0.4201	0.138	0.4208	−0.113	0.2995	−0.143		
0.5459	−0.307	0.4859	−0.019	0.4212	0.139	0.4221	−0.107	0.3014	−0.142		
0.5470	−0.324	0.4870	−0.021	0.4223	0.127	0.4234	−0.102	0.3026	−0.137		
0.5481	−0.343	0.4881	−0.053	0.4234	0.120	0.4247	−0.094	0.3037	−0.136		
0.5492	−0.364	0.4892	−0.073	0.4245	0.114	0.4260	−0.106	0.3048	−0.131		
0.5503	−0.387	0.4903	−0.087	0.4256	0.105	0.4272	−0.097	0.3059	−0.134		
0.5520	−0.407	0.4917	−0.123	0.4267	0.105	0.4285	−0.099	0.3070	−0.125		
0.5531	−0.428	0.4928	−0.147	0.4279	0.088	0.4298	−0.095	0.3081	−0.121		
0.5541	−0.443	0.4939	−0.176	0.4290	0.077	0.4316	−0.091	0.3092	−0.118		
0.5552	−0.468	0.4951	−0.213	0.4306	0.066	0.4329	−0.093	0.3103	−0.125		

0.3114 −0.119	0.3345 −0.091	0.3544 −0.061	0.3757 −0.039	0.3993 0.005
0.3125 −0.122	0.3356 −0.082	0.3555 −0.070	0.3768 −0.037	0.4004 −0.005
0.3137 −0.116	0.3367 −0.083	0.3566 −0.058	0.3779 −0.039	0.4016 0.009
0.3169 −0.111	0.3378 −0.080	0.3578 −0.058	0.3803 −0.034	0.4027 0.006
0.3180 −0.110	0.3389 −0.074	0.3589 −0.056	0.3814 −0.033	0.4038 0.006
0.3191 −0.105	0.3400 −0.076	0.3600 −0.056	0.3824 −0.024	0.4049 0.014
0.3202 −0.107	0.3411 −0.076	0.3611 −0.061	0.3835 −0.024	0.4060 0.017
0.3214 −0.102	0.3428 −0.079	0.3622 −0.058	0.3846 −0.023	0.4071 0.017
0.3225 −0.102	0.3439 −0.078	0.3633 −0.057	0.3857 −0.029	0.4082 0.022
0.3236 −0.096	0.3450 −0.070	0.3644 −0.047	0.3867 −0.020	0.4093 0.014
0.3247 −0.103	0.3461 −0.073	0.3682 −0.044	0.3878 −0.029	0.4104 0.018
0.3258 −0.099	0.3472 −0.072	0.3693 −0.048	0.3889 −0.017	0.4116 0.019
0.3269 −0.092	0.3483 −0.068	0.3703 −0.044	0.3900 −0.013	0.4127 0.026
0.3300 −0.089	0.3494 −0.073	0.3714 −0.043	0.3949 −0.012	0.4138 0.027
0.3311 −0.085	0.3505 −0.067	0.3725 −0.046	0.3960 −0.009	0.4149 0.030
0.3322 −0.088	0.3516 −0.067	0.3736 −0.042	0.3971 −0.007	0.4160 0.030
0.3334 −0.089	0.3528 −0.070	0.3746 −0.037	0.3982 0.007	

Table 7. Differential CCD i observations of XZ Dra

2452124 +	0.4307 −0.334	0.3639 −0.438	0.4119 −0.272	0.4677 −0.101
0.4067 −0.420	0.4349 −0.364	0.3667 −0.426	0.4148 −0.248	0.4706 −0.126
0.4110 −0.398		0.3783 −0.419	0.4254 −0.235	0.4872 −0.056
0.4137 −0.407	2452125 +	0.3850 −0.272	0.4298 −0.212	0.4903 −0.094
0.4162 −0.437	0.3060 +0.198	0.3903 −0.502	0.4352 −0.189	0.4933 −0.044
0.4183 −0.499	0.3179 +0.187	0.3931 −0.470	0.4404 −0.150	0.4996 −0.059
0.4204 −0.359	0.3235 +0.135	0.3959 −0.430	0.4456 −0.156	0.5075 −0.044
0.4224 −0.440	0.3474 −0.190	0.3988 −0.443	0.4519 −0.133	0.5104 −0.027
0.4245 −0.365	0.3530 −0.258	0.4027 −0.201	0.4576 −0.135	0.5133 −0.016
0.4287 −0.401	0.3581 −0.366	0.4071 −0.201	0.4648 −0.144	0.5133 −0.016

Radial Velocity Measurements

During eight nights in 1971 XZ Dra was observed spectroscopically with the 2131 spectrograph at the Cassegrain focus of the 72 inch telescope of the DAO (Dominion Astrophysical Observatory, Canada). 26 spectrograms were obtained in order to determine the radial velocity variation. The spectra, at the dispersion of 60 Å/mm, were taken on baked Eastman Kodak IIaO emulsion. The lines measured and the wavelengths accepted for them were chosen from those adopted at DAO. Standard-velocity stars were observed on some of the nights that spectrograms were obtained of XZ Dra. Velocities of these stars, measured in the adopted wavelength system, showed a satisfactory freedom from systematic errors.

Values of radial velocities of XZ Dra are presented in Table 8 (Col. 2,6). In the table the Julian date of the middle of exposures (Col. 1,5), the internal mean error of the velocities (Col. 3,7) and the number of lines measured (Col. 4,8) are also given.

Table 8. Radial velocities of XZ Dra

HJD 2440000+	$v_{\rm rad}$ [km/s]	σ [km/s]	n	HJD 2440000+	$v_{\rm rad}$ [km/s]	σ [km/s]	n
1078.782	−50.5	3.3	17	1147.933	−59.4	5.3	16
1078.805	−71.1	5.2	17	1147.966	−43.8	5.4	13
1078.829	−65.6	4.4	17	1157.799	−5.1	3.9	16
1097.844	−64.0	5.4	16	1157.845	−22.1	3.8	16
1097.869	−62.7	3.4	17	1157.878	−38.1	4.0	16
1097.898	−63.7	3.5	17	1157.905	−70.8	4.3	14
1097.930	−55.2	3.9	17	1157.930	−62.5	3.9	17
1107.778	−7.0	4.3	17	1168.726	−12.6	7.3	14
1107.837	−55.4	6.6	16	1177.710	−22.5	8.0	9
1107.882	−53.0	3.6	17	1177.909	−58.9	4.0	16
1147.800	−7.4	4.9	16	1186.811	−23.3	8.2	7
1147.862	−40.6	4.5	17	1186.965	−39.6	3.7	14
1147.897	−71.8	3.4	14	1187.009	−49.1	5.1	6

TIMES AND MAGNITUDES OF LIGHT MAXIMA AND O−C VALUES

The times and magnitudes of light maxima from the Konkoly photographic (Table 9.a), photoelectric B, V and CCD (Table 9.b) data were determined from polynomial fits to the data around maxima. The maximum magnitudes were obtain by adopting Struch's (1966) $V = 10.493$, $B = 11.065$ magnitudes for the comparison star.

In Table 10.a and 10.b individual and normal maxima and O−C values derived from all the available published measurements are listed. Both professional and amateur observations are regarded, but only those which have publicly available references. The GEOS RR Lyrae database* lists some further unpublished amateur (visual) observations which we have not included in our compilation. From multicolor observations B data were considered. The only published measurements of XZ Dra that is not included in either of the tables is that of Butler *et al.* (1982). These observations cover the linear part of the descending branch on two successive nights and no unambiguous normal maxima could have been extrapolated from these data.

In each cases when not only maxima timings but the original observations were also given, individual maxima times and normal maxima were independently determined. In Tab 10.a–b these values are given instead of the originally published data. This causes very small if any difference in the cases of individual maxima, but may lead to significantly different normal values.

Individual maxima were determined by polynomial fitting of the data around maximum values with the exception of Batyrev's (1955) measurements, where the times of the brightest magnitudes were taken as estimates of O−C values. Wenske (1982) gave the times of the mean magnitudes on the ascending branch instead of the maxima. These

*http://www.upv.es/geos/

Table 9.a Times and magnitudes of photographic maxima

pg maxima		pg maxima		pg maxima	
HJD 2400000+	[mag]	HJD 2400000+	[mag]	HJD 2400000+	[mag]
28404.476	9.84	29720.532	9.43	34599.395:	9.44
29084.424	9.70	29721.482	9.48	34605.586:	9.69
29113.498:	9.65	29730.543:	9.36	34627.510	9.26
29284.558	9.40	29732.452	9.50	35377.510	9.58
29295.518	9.50	29734.346	9.46	35421.338	9.59
29365.559	9.42	30514.393	9.66	35622.423	9.24
29366.503	9.48	31352.547	9.77	35682.460	9.28
29376.515	9.55	31353.503	9.78	35732.488:	9.94
29377.461	9.57	31700.386	9.31	35756.313	9.50
29378.418	9.61	34234.412:	9.88	35933.580:	9.31
29449.414	9.58	34241.558	9.82	36005.532:	9.45
29458.466	9.71	34253.463	9.57	36007.437:	9.13
29468.460	9.82	34264.432	9.41	36038.395	9.50
29518.499:	9.60	34455.491	9.53	36069.364:	9.59
29519.463	9.53	34476.463	9.38	36077.485	9.29
29520.401	9.71	34486.472	9.22	36087.505	9.44
29527.545	9.76	34488.379	9.05	36100.365:	9.43
29691.469	9.81	34515.531	9.25	36128.458	9.74
29699.568	9.62	34546.502:	9.41	36131.325	9.40
29701.476	9.74	34589.382:	9.42	36142.275	9.58

values were shifted by $0.^{\rm d}027$ (the mean value of the time difference between the timings of the mean magnitude on the ascending branch and the maximum $[\Delta T = \overline{T_{\rm max} - T_{\rm med}}]$ determined from the Budapest photoelectric B observations) to estimate the times of maxima. It has to be emphasized, however, that these transformed values are not true maxima times, since depending on the Blazhko phase, the actual value of ΔT can differ by $\pm 0.^{\rm d}015$ from $0.^{\rm d}027$.

An $8^{\rm th}$ order Fourier fit to the Budapest photographic observations between HJD 2430433 and 2431708 were regarded as a basic normal light curve using $P=0.^{\rm d}4764955$ period. These data cover the whole pulsational period well, and in this interval no definite period change has been observed. The normal maximum of these data was determined to be at HJD=2431244.383, at the mid-time of the observations. This normal epoch corresponds thus to a calculated maximum and not to real observations. All the O−C values were accordingly calculated by using the ephemeris:

$$\mathrm{MaxHJD} = 2431244.383 + 0.^{\rm d}4764955 \times \mathrm{E} \qquad (1)$$

In Table 10.a all the individual maxima timings (Col. 1,5) found in the literature and given in the present paper, O−C values (Col. 2,6), type of detector (Col. 3,7), and references (Col. 4,8) are given.

Normal maxima were determined from measurements of one or two observing season(s) but there were also some cases when only a few nights' (sometimes consecutive)

Table 9.b Times and magnitudes of photoelectric maxima

B maxima		V maxima		B maxima		V maxima	
HJD	[mag]	{HJD}*	[mag]	HJD	[mag]	{HJD}*	[mag]
2400000+				2400000+			
36410.5253	9.951	.5251	9.711	41249.3860	9.891	.3852	9.692
36413.3927	9.941	.3924	9.759	41250.3344	9.886	.3344	9.687
36421.4972	9.992	.4972	9.780	41539.5695	9.702	.5700	9.537
36443.4126	9.996	.4129	9.712	41589.5960	9.980	.5958	9.776
36450.5613	9.795	.5601	9.543	41591.5045	10.010	.5047	9.825
36451.5162	9.836	.5165	9.604	41606.2756	9.711	.2760	9.555
36454.3776	9.794	.3784	9.596	41622.4890	9.850	.4888	9.624
36463.4280	9.750	.4275	9.548	41772.5747	9.769	.5750	9.597
36474.3893	9.935	.3877	9.698	41803.5347	9.996	.5345	9.826
36475.3386	9.883	.3370	9.668	41815.4484	9.967	.4484	9.772
36486.2980:	10.025:	.2980:	9.825:	41833.5500:	9.795:	.5500:	9.620:
36503.4562	10.014	.4550	9.778	41835.4641	9.697	.4643	9.569
36506.3130	10.008	.3145	9.766	41905.5046	9.808	.5050	9.625
36514.4016	9.947	.4006	9.699	41915.5140:	9.805:	.5140:	9.615:
37465.4948	9.903	.4957	9.772	41934.5722	9.919	.5700	9.698
37467.4040:	9.865:	.4050:	9.760:	41938.3821	9.912	.3818	9.756
37475.4946	9.956	.4950	9.834	41939.3350	9.904	.3348	9.731
37486.4665	9.968	.4592	9.860	41949.3367	10.032	.3375	9.804
39391.4767	10.045	.4765	9.831	41990.3254	9.692	.3253	9.560
39402.4404	9.835	.4460	9.638	42147.5715	9.772	.5714	9.575
39403.3939	9.840	.3921	9.688	42201.4016	9.898	.4019	9.678
40500.2947:	9.897	.2930:	9.666	42220.4715	9.768	.4720	9.558
40504.5845	9.949	.5824	9.713	42242.3829	9.935	.3844	9.714
40516.4990	10.062	.4999	9.828	42260.4980:	10.055	.4980:	9.758
40528.4163	9.964	.4160	9.737	42269.5440	10.030	.5452	9.790
40530.3118	9.955	.3118	9.750	42279.5459	9.830	.5466	9.668
40541.2790	9.810	.2783	9.638	42303.3830:	9.906	.3900:	9.690
40676.6093	10.028	.6105	9.806	42636.4427	10.089	.4432	9.778
40707.5803	9.640	.5810	9.516	43700.4801	10.000	.4802	9.783
40709.4894	9.667	.4897	9.539	43720.4906	9.789	.4906	9.604
40731.4080:	9.887	.4070	9.718	43732.4050:	9.665:	.4050:	9.510:
40751.4215	10.018	.4211	9.825	43743.3720	9.864	.3726	9.652
40780.4874	9.707	.4871	9.510	43763.3808	10.018	.3825	9.809
40821.4660	9.967	.4651	9.715	45609.2994	9.808	.2994	9.659
40840.5249	9.933	.5250	9.728	45806.5680	9.922	.5665	9.759
40863.4094	9.682	.4096	9.540	46193.4902	9.999	.4901	9.798
40925.3400	9.787	.3393	9.618	47360.4319	9.684	.4321	9.543
40937.2661	9.769	.2655	9.611	47462.3998	9.976	.4000	9.763
				52100.		.5828	9.706†

*{HJD} denotes the fractional part of HJD. The integer part can be read form the same line in Col. 1,5.

† CCD V observation

observations defined the normal values. The most deviant points were omitted from each data set. The observations were folded by the period given in Eq. (1) and were fitted both vertically (magnitude-shifts to compensate the differences of the different photometric systems) and horizontally (phase-shifts which can be regarded as O−C value) to the basic light curve applying a standard least squares method. In this way we could eliminate the problem of the different magnitude scales, and the effect of the different shapes of the light curves in different wavelengths. The normal maximum times were then calculated at the mean Julian date of the observations by using these overall phase shift values and ephemeris Eq. (1).

In Table 10.b normal maxima timings (Col. 1), O−C values (Col. 2), the first and the last dates of the observations (Col. 3), number of measurements (Col. 4), type of detector (Col. 5), and references (Col. 6) are listed. The references of those data which were taken from the literature and not directly determined from the original observations (due to the lack of published data) are denoted by asterisks both in Table 10.a and 10.b. Maximum times which seems to give erroneous O−C values are in parentheses, independently whether or not they were published as uncertain values.

Table 10.a O−C values calculated from observed maxima[†]

HJD 2400000+	O−C [d]	det.	ref.	HJD 2400000+	O−C [d]	det.	ref.
25850.445:	−0.009	vis	8	27556.327:	0.019	vis	19
25936.241:	0.018	vis	8	27618.277	0.025	vis	38*
26025.343:	0.015	vis	8	27619.230	0.025	vis	38*
26298.360:	0.000	vis	8	27625.418	0.018	vis	38*
26478.488:	0.013	vis	8	27628.270	0.011	vis	38*
(26624.338:	0.055	vis	8)	27629.221	0.009	vis	38*
26835.381	0.011	vis	19	27974.221	0.027	vis	38*
26945.452	0.011	vis	19	27979.450:	0.014	vis	38*
26957.374:	0.021	vis	19	27980.399	0.010	vis	38*
27161.311:	0.018	vis	19	27983.263	0.015	vis	38*
27230.411	0.026	vis	19	27984.218	0.017	vis	38*
27300.450	0.020	vis	41	27994.229	0.022	vis	38*
27301.400:	0.017	vis	41	28003.268	0.007	vis	38*
27302.357	0.021	vis	41	28004.225	0.011	vis	38*
27309.507	0.024	vis	41	28005.183	0.016	vis	38*
27310.465	0.029	vis	41	28395.417	0.001	vis	38*
27311.408	0.019	vis	41	28396.383	0.014	vis	38*
27312.369	0.027	vis	41	28398.275	0.000	vis	38*
27313.314	0.019	vis	41	28399.230	0.002	vis	38*
27324.277	0.022	vis	41	28400.187	0.006	vis	38*
27332.373	0.018	vis	41	28404.476	0.006	pg	39
27353.340	0.019	vis	41	28407.330:	0.001	vis	38*
27354.290:	0.016	vis	41	28409.235	0.000	vis	38*

[†]Reference list can be found at the end of Table 10.b

Table 10.a continued

HJD 2400000+	O−C [d]	det.	ref.	HJD 2400000+	O−C [d]	det.	ref.
29084.424	−0.005	pg	39	34520.291	0.001	vis	6
29113.498:	0.003	pg	39	34546.502:	0.005	pg	39
29284.558	0.001	pg	39	34589.382:	0.001	pg	39
29295.518	0.002	pg	39	34599.395:	0.007	pg	39
29365.559	−0.002	pg	39	34600.352	0.011	vis	6
29366.503	−0.011	pg	39	34605.586:	0.004	pg	39
29376.515	−0.006	pg	39	34612.263	0.010	vis	6
29377.461	−0.013	pg	39	34620.352	−0.002	vis	38
29378.418	−0.009	pg	39	34621.308	0.001	vis	38
29449.414	−0.010	pg	39	34627.510	0.009	pg	39
29458.466	−0.012	pg	39	34627.512	0.011	vis	38
29468.460	−0.024	pg	39	34631.339	0.026	vis	38
29518.499:	−0.017	pg	39	34632.287	0.021	vis	38
29519.463	−0.006	pg	39	34637.522	0.015	vis	38
29520.401	−0.021	pg	39	34638.475	0.015	vis	38
29527.545	−0.025	pg	39	34639.426:	0.013	vis	38
29691.469	−0.015	pg	39	34640.379	0.013	vis	38
29699.568	−0.017	pg	39	34641.338	0.019	vis	38
29701.476	−0.015	pg	39	34644.203	0.025	vis	6
29720.532	−0.018	pg	39	34651.346	0.020	vis	38
29721.482	−0.021	pg	39	34652.298	0.019	vis	38
29730.543:	−0.014	pg	39	34659.440	0.014	vis	38
29732.452	−0.011	pg	39	34662.306	0.021	vis	38
29734.346	−0.023	pg	39	34674.213	0.015	vis	38
30514.393	0.001	pg	39	34680.418	0.026	vis	38
31352.547	0.000	pg	39	34683.285	0.034	vis	6
31353.503	0.003	pg	39	34684.197:	−0.007	vis	38
31700.386	−0.003	pg	39	34943.425:	0.007	vis	38
34234.412:	0.020	pg	39	34945.334	0.010	vis	38
34241.558	0.018	pg	39	34953.443	0.019	pg	5*
34253.463	0.011	pg	39	34973.437	0.000	vis	6
34264.432	0.021	pg	39	34986.305	0.003	vis	6
34338.311	0.043	vis	6	35008.232	0.011	vis	6
34339.238	0.017	vis	6	35377.510	0.005	pg	39
34455.491	0.005	pg	39	35421.338	−0.005	pg	39
34476.463	0.011	pg	39	35622.423	−0.001	pg	39
34486.472	0.014	pg	39	35682.460	−0.002	pg	39
34488.379	0.015	pg	39	35732.488:	−0.006	pg	39
34510.281	−0.002	vis	6	35756.313	−0.006	pg	39
34515.531	0.006	pg	39	35933.580:	0.005	pg	39

Table 10.a continued

HJD 2400000+	O−C [d]	det.	ref.	HJD 2400000+	O−C [d]	det.	ref.
35956.441	−0.006	pe	40	38146.425	0.005	pg	58
36005.532:	0.006	pg	39	38883.539	−0.020	vis	10*
36007.437:	0.005	pg	39	38883.542	−0.017	vis	10*
36038.395	−0.009	pg	39	38945.491	−0.012	vis	10*
36069.364:	−0.012	pg	39	38945.497	−0.006	vis	10*
36077.485	0.008	pg	39	38945.500	−0.003	vis	10*
36087.505	0.022	pg	39	39031.728	−0.021	pe	23
36100.365:	0.016	pg	39	39352.411	−0.019	vis	4*
36128.458	−0.004	pg	39	39391.477	−0.026	pe	40
36131.325	0.004	pg	39	39402.440	−0.022	pe	40
36142.275	−0.005	pg	39	39403.392	−0.023	vis	11*
36289.541:	0.024	pg	58	39403.394	−0.021	pe	40
36410.525	−0.022	pe	40	(39403.419	0.004	vis	11*)
36413.393	−0.013	pe	40	39405.294	−0.027	vis	11*
36421.497	−0.010	pe	40	39405.295	−0.026	vis	11*
36443.413	−0.012	pe	40	39406.262	−0.012	vis	11*
36450.561	−0.012	pe	40	39406.269	−0.005	vis	11*
36451.516	−0.010	pe	40	40384.503	−0.017	pe	57*
36454.378	−0.007	pe	40	40385.462	−0.011	pe	57*
36463.428	−0.010	pe	40	40385.466	−0.007	pe	48*
36474.389	−0.009	pe	40	40386.427	0.001	pe	48*
36475.339	−0.012	pe	40	40434.523:	−0.029	pe	57*
36486.298:	−0.012	pe	40	40435.485	−0.020	pe	57*
36503.456	−0.008	pe	40	40444.539	−0.019	pe	57*
36506.313	−0.010	pe	40	40446.442	−0.022	pe	57*
36514.402	−0.021	pe	40	40456.447	−0.024	pe	57*
36850.340	−0.013	vis	2*	40467.420	−0.010	pe	57*
36851.293	−0.013	vis	2*	40500.295:	−0.013	pe	40
36852.249	−0.010	vis	2*	40504.585	−0.012	pe	40
36899.424	−0.008	vis	2*	40516.499	−0.010	pe	40
37465.495	−0.013	pe	40	40528.416	−0.005	pe	40
37467.404:	−0.010	pe	40	40530.312	−0.015	pe	40
37475.495	−0.020	pe	40	40539.364	−0.017	pe	57*
37486.467	−0.007	pe	40	40541.279	−0.008	pe	40
37914.361	−0.006	vis	47*	40676.609	−0.002	pe	40
37914.365	−0.002	vis	47*	40707.580	−0.004	pe	40
37914.366	−0.001	vis	47*	40709.489	−0.001	pe	40
37914.368	0.001	vis	47*	40731.408:	0.000	pe	40
(37941.365	−0.162	vis	44*)	40751.422	0.001	pe	40
37945.339	0.000	vis	44*	40769.520	−0.008	pe	49*

Table 10.a continued

HJD 2400000+	O−C [d]	det.	ref.	HJD 2400000+	O−C [d]	det.	ref.
40780.487	0.000	pe	40	41595.309	0.014	pe	57*
40812.404	−0.009	vis	12*	41603.415	0.020	pe	57*
40821.466	0.000	pe	40	41604.371	0.023	pe	57*
40840.525	−0.001	pe	40	41606.276	0.022	pe	40
40844.335	−0.003	pe	49*	41612.473	0.024	pe	57*
40851.493	0.008	pe	57*	41622.489	0.034	pe	40
40852.427:	−0.011	pe	57*	41636.288	0.015	pe	57*
40853.388	−0.003	pe	49*	41772.575	0.024	pe	40
40853.393	0.002	pe	57*	41785.425	0.009	pe	57*
40863.409	0.011	pe	40	(41795.390	−0.033	vis	13*)
40916.287	−0.002	pe	57*	41803.535	0.012	pe	40
40925.340	−0.002	pe	40	41815.448	0.012	pe	40
40935.358	0.010	pe	57*	41833.550:	0.008	pe	40
40937.266	0.012	pe	40	41835.464	0.016	pe	40
40955.365	0.004	pe	57*	41895.488	0.001	pe	57*
40966.313	−0.008	pe	57*	41905.505	0.012	pe	40
41074.492	0.007	pe	57*	(41906.499	0.053	pe	57*)
41074.496	0.011	vis	12*	41907.408	0.009	pe	57*
41075.452	0.014	vis	12*	41915.514:	0.014	pe	40
41075.454	0.016	vis	12*	41917.422	0.016	pe	57*
41085.460	0.015	pe	57*	41934.572	0.012	pe	40
41093.558	0.013	pe	57*	41936.468	0.002	pe	57*
41095.950	0.023	pe	46	41938.382	0.010	pe	40
41187.428	0.013	pe	57*	41939.335	0.011	pe	40
41216.490	0.009	pe	57*	41949.337	0.006	pe	40
41229.364	0.018	pe	57*	(41957.421	−0.010	pe	57*)
41240.329	0.023	pe	57*	41987.466	0.015	pe	57*
41249.386	0.027	pe	40	41990.325	0.015	pe	40
41249.393	0.034	vis	12*	42147.572	0.019	pe	40
41250.334	0.022	pe	40	42159.471	0.006	pe	57*
41439.496	0.015	pe	57*	42201.402	0.005	pe	40
41470.480	0.027	pe	57*	42208.548	0.004	pe	57*
41511.448	0.016	pe	57*	42219.517	0.013	pe	57*
41539.570	0.025	pe	40	42220.472	0.015	pe	40
41541.478	0.027	pe	57*	42242.383	0.007	pe	40
41550.518	0.014	pe	57*	(42251.396:	−0.033	vis	13*)
41552.435	0.025	pe	57*	42251.429	0.000	pe	57*
41589.596	0.019	pe	40	42260.498:	0.016	pe	40
41591.505	0.022	pe	40	42269.544	0.008	pe	40
41593.399	0.010	pe	57*	42279.546	0.004	pe	40

Table 10.a continued

HJD 2400000+	O−C [d]	det.	ref.	HJD 2400000+	O−C [d]	det.	ref.
42280.500	0.005	pe	57*	47432.381	0.016	vis	31*
42303.383:	0.016	pe	40	47462.400	0.016	pe	40
42636.443	0.006	pe	40	47470.493	0.009	vis	24*
42698.386	0.004	pe	57*	47471.459	0.022	vis	24*
42710.297	0.003	pe	57*	47471.473	0.036	vis	24*
42739.371	0.011	pe	57*	47480.522	0.031	vis	24*
42840.390	0.013	vis	14*	47612.494:	0.014	vis	32*
42895.181	0.007	vis	18	(47910.277	−0.013	vis	32*)
42896.135	0.008	vis	18	47947.497:	0.041	pe	29
43248.275	0.017	vis	18	47966.535	0.019	vis	24*
43249.202	−0.009	vis	18	48028.484	0.024	vis	24*
43255.391	−0.014	vis	18	48036.100	0.016	pe	29
43256.343	−0.015	vis	18	(48037.507	−0.007	vis	24*)
43257.302	−0.009	vis	18	48096.149:	0.026	pe	29
43260.174	0.004	vis	18	48347.260:	0.024	pe	29
43277.332	0.008	vis	18	48496.410:	0.031	pe	29
43278.276	−0.001	vis	18	48632.212:	0.032	pe	29
43287.342	0.012	vis	18	48829.465	0.016	pg	25*
43297.343	0.006	vis	18	49439.365	0.001	vis	33*
43298.293	0.003	vis	18	(49573.416	0.157	pg	25*)
43308.316	0.020	vis	18	49893.481	0.017	pg	26*
43700.480	0.028	pe	40	49903.494	0.024	pg	26*
43720.491	0.026	pe	40	(49922.577	0.047	vis	25*)
43732.405:	0.028	pe	40	49934.455	0.013	pe	1*
43743.372	0.036	pe	40	49945.417	0.015	pg	26*
43763.381	0.032	pe	40	50079.298	0.001	vis	34*
43795.305	0.031	vis	15*	50247.520	0.020	pg	26*
45280.496	−0.015	vis	9*	50288.510	0.031	vis	35*
45609.299	0.006	pe	40	50331.383	0.020	pg	26*
45806.568	0.006	pe	40	50593.459	0.023	vis	35*
46193.490	0.014	pe	40	50594.405	0.016	vis	35*
(47107.438	0.043	vis	30*)	50727.350	0.019	vis	35*
47180.334	0.035	vis	30*	50756.413	0.016	vis	35*
(47275.572	−0.026	pg	31*)	51080.426	0.012	vis	36*
47276.574	0.023	vis	24*	51362.494	−0.006	vis	37*
47296.582	0.019	pg	31*	51425.402	0.005	vis	37*
47360.432	0.018	pe	40	52100.583	−0.008	ccd	40
47369.502	0.035	vis	24*	52124.418	0.002	ccd	40
47379.505	0.031	vis	31*	52125.365	−0.004	ccd	40
(47391.433	0.047	vis	31*)				

Table 10.b O−C values calculated from normal points

HJD 2400000+	O−C [d]	time range [JD/year]	n	det.	ref.†
(15267.573	0.084	14000−20800		pg	45*)
(20787.670	−0.019	20800−23000		pg	45*)
(23052.533	0.061	23000−25500		pg	45*)
25749.435	−0.002	25503−25951	19	pg	51
25875.718	0.010	25500−29500		pg	45*
25890.481	0.001	25721−26127	71	vis	8
26275.483	−0.005	26001−26506	30	pg	51
26440.374	0.019	26196−26642	65	vis	8
26865.401	0.012	26825−26960	185	vis	19
26957.367	0.014	26928−26985	16	vis	8
26987.397	0.025		248	vis	59*
27230.409	0.024	27161−27556	159	vis	19
27318.566	0.029	27300−27354	94	vis	41
27622.565	0.024	1934		vis	52*
27985.645	0.015	1935	200	vis	53*
28363.503	0.012	1936	179	vis	54*
28501.681	0.006	28356−28784	263	pg	39
28614.618	0.014	27198−29903	562	vis	20*
29287.412	−0.004	29084−29378	789	pg	39
29596.648	−0.014	29449−29734	1162	pg	39
30461.499	−0.002	30433−30514	178	pg	39
31345.396	−0.004	31330−31376	702	pg	39
31703.732	0.007	31700−31708	148	pg	39
33740.789	0.046	33661−33796	11	pg	58
34206.306	0.027	33896−34294	276	pg	39
34338.766	0.021	34335−34339	35	vis	6
34538.886	0.012	34455−34627	306	pg	39
34610.374	0.027	34509−34719	137	vis	6
34641.339	0.020	34599−34686	414	vis	38
34943.431	0.013	34935−34947	62	vis	38
35005.376	0.014	34971−35072	117	vis	6
35399.424	0.000	35377−35421	81	pg	39
35690.563	0.000	35622−35756	147	pg	39
36031.749	0.016	1952−1960	255	pg	50*
36074.626	0.008	35933−36142	388	pg	39
36224.724	0.010	36077−36344	21	pgv	58
36229.489	0.010	36074−36347	32	pg	58
36331.447	−0.002	36041−36518	98	vis	43
36370.511	−0.011	36370−36371		pe	27*
36458.664	−0.009	36410−36514	392	pe	40
36834.629	0.001	36819−36848	18	pg	58

Table 10.b continued

36837.480	−0.005	36819−36848	10	pgv	58
36851.294	−0.012	36850−36852	43	vis	3*
36893.232	−0.005	36876−36904	24	vis	3*
37055.700	−0.022	36728−37228	116	vis	43
37464.537	−0.018	37348−37486	154	pe	40
37728.531	−0.003	37458−37964	129	vis	43
38317.486	0.004	38198−38700	66	vis	43
38634.344	−0.008	38530−38709	47	pg+pe	28,55
39018.393	−0.014	38935−39425	46	vis	43
39399.583	−0.020	39391−39403	106	pe	40
40037.616	−0.015	39675−40420	17	vis	43
40684.715	0.003	40494−40937	600	pe	40
41112.630	0.025	41064−41133	75	pe	46
41249.386	0.027	41249−41250	115	pe	40
41413.296	0.023	41375−41425	114	vis	7*
41550.534	0.030	1972		pg	56*
41802.592	0.022	41539−41990	636	pe	40
41928.372	0.007	1973		vis	42*
41928.374	0.009	1973−1974		vis	21*
42238.581	0.017	42147−42303	280	pe	40
42638.365	0.022		90	vis	17*
42638.366	0.023		75	vis	16*
42725.540	−0.002	42636−42948	63	pe	40
42895.192	0.018	42894−42898	55	vis	18
(43043.337	−0.028		75	vis	17*)
43272.579	0.020	43248−43308	315	vis	18
43717.641	0.035	43660−43763	177	pe	40
45864.703	0.009	45609−46193	193	pe	40
45870.408	−0.004	1984		vis	22*
47376.640	0.025	47306−47462	71	pe	40
48032.770	0.021	47865−48176	49	pe	29
48330.588	0.029	48209−48462	38	pe	29
48742.743	0.016	48519−49019	31	pe	29
52115.368	0.006	52100−52140	405	ccd	40

†1 Agerer & Hübscher (1996), 2 Ahnert (1961a), 3 Ahnert (1961b), 4 Ahnert (1967), 5 Alania (1956), 6 Batyrev (1955), 7 Berdnikov (1977), 8 Beyer (1934), 9 Böhme (1983), 10 Braune & Hübscher (1967), 11 Braune *et al.* (1970), 12 Braune *et al.* (1972), 13 Braune *et al.* (1977), 14 Braune *et al.* (1979), 15 Braune *et al.* (1981), 16 Busch (1976), 17 Busch (1979), 18 Dyachenko (1982), 19 Konkoly vis, 20 Dziewulski (1953), 21 Firmanyuk *et al.* (1975), 22 Firmanyuk *et al.* (1985), 23 Fitch *et al.* (1966), 24 GEOS NC 650, 25 Vandenbroere (1997), 26 Vandenbroere (1998), 27 Geyer (1961), 28 Harding & Penston (1966), 29 ESA (1997), 30 Hübscher & Lichtenknecker (1988), 31 Hübscher *et al.* (1989), 32 Hübscher *et al.* (1990), 33 Hübscher *et al.* (1994), 34 Hübscher & Agerer (1996), 35 Hübscher *et al.* (1998), 36 Hübscher *et al.* (1999), 37 Hübscher *et al.* (2000), 38 Klepikova (1958), 39 Konkoly pg, 40 Konkoly pe & CCD, 41 Lange (1938), 42 Lange *et al.* (1976), 43 Lebedev (1975), 44 Oburka (1965), 45 Payne-Gaposchkin (1954), 46 Penston (1973), 47 Pohl & Kizilirmak (1964), 48 Popovici (1970), 49 Popovici (1971), 50 Satyvaldyev (1962), 51 Schneller (1931), 52 Soloviev (1934), 53 Soloviev (1936), 54 Soloviev (1937), 55 Sturch (1966), 56 Tsessevich (1974), 57 Wenske (1982), 58 Zaleski (1965), 59 Kharadse (1933).

ACKNOWLEDGEMENTS

The extended observational material of XZ Dra has not been congregated without the inspiring interest of Prof. László Detre, the late director of the Konkoly Observatory about Blazhko type RR Lyrae stars. We would like to thank the present and former staff members of Konkoly Observatory especially to Drs. K. Oláh and L. Szabados for taking part in the observations. The continuous help of Oliver Rauch in operating the UMAX PowerLook 3000 scanner under Linux is also acknowledged. This research has made use of the SIMBAD database, operated at CDS, Strasbourg, France, and also that of the GEOS RR Lyrae Database. This work has been partly supported by OTKA grants T30954 and T30955.

REFERENCES

Agerer, F., Hübscher, J., 1996, IBVS 4382
Ahnert, P., 1961a, Mitt. Veränd. Sterne 544
Ahnert, P., 1961b, Mitt. Veränd. Sterne 545
Ahnert, P., 1967, Mitt. Veränd. Sterne 4, 138
Alania, N. F., 1956, Astr. Tsirk. 173, 20
Alard, C., 2000, A&AS 144, 363
Alard, C., Lupton, R. H., 1998, ApJ 503, 325
Bakos, G.Á., 2000, Occasional. Tech. Notes Konkoly Obs., No. 11,
`http://www.konkoly.hu/Mitteilungen/Mitteilungen.html`
Bakos, G. Á., 2001a, in *Small-Telescope Astronomy in Global Scale*,
(Eds. B. Paczyński, W-P. Cheng, W. Ip), ASP Conf. Ser.
Bakos, G. Á., 2001b, `http://www.konkoly.hu/staff/bakos/HAT/`
Balázs, J., Detre, L., 1938, Comm. Konkoly Obs. No 5
Balázs, J., Detre, L., 1941, Astron. Nachr. 271, 231
Batyrev, A. A., 1955, Perem. Zvezdy 10, 292
Benkő, J. M., et al., 2001, in preparation
Berdnikov, N. L., 1977, Perem. Zvezdy Pril. 3, 329
Beyer, M., 1934, Astron. Nachr. 252, 85
Böhme, D., 1983, Mitt. Veränd. Sterne 10, 44
Braune, W., Hübscher, J., 1967, Astron. Nachr. 290, 105
Braune, W., Hübscher, J., Mundry, E., 1970, Astron. Nachr. 292, 185
Braune, W., Hübscher, J., Mundry, E., 1972, Astron. Nachr. 294, 123
Braune, W., Hübscher, J., Mundry, E., 1977, Astron. Nachr. 298, 121
Braune, W., Hübscher, J., Mundry, E., 1979, Astron. Nachr. 300, 165
Braune, W., Hübscher, J., Mundry, E., 1981, Astron. Nachr. 302, 53
Busch, H., 1976, Mitt. Veränd. Sterne 7, 149
Busch, H., 1979, Mitt. Veränd. Sterne 8, 137
Butler, D., Manduca, A., Deming, D., Bell, R. A., 1982, AJ 87, 640
Detre, L., Lassovszky, K., 1939, Comm. Konkoly Obs. No 9
Dyachenko, A. I., 1982, Perem. Zvezdy Pril. 4, 275
Dziewulski, W., 1953, Toruń Bull. 12, 41

ESA, 1997, *The Hipparcos and Tycho Catalogues*, ESA SP–1200
Firmanyuk, B. N., Derevyagin, V. G., Lysova, L. E., 1985, Astr. Tsirk. 1374, 7
Firmanyuk, B. N., Lange, G. A., Tsessevich, V. P., 1975, Astr. Tsirk. 853, 4
Fitch, W. S., Wiśniewski, W. Z., Johnson, H. L., 1966, Comm. Lun. and Planet. Lab., Vol 5, Part 2, No 71
GEOS NC 650
Geyer, E., 1961, Zeitschr. f. Astrophys. 52, 229
Hardie, R. H., 1962, in *Astronomical Techniques, Stars and Stellar Systems* Vol 2 (Ed.: W.A. Hiltner), p 178
Harding, G. A., Penston, M. J., 1966, Roy. Obs. Bull. Ser. E, No 115
Høg, E., Fabricius, C., Makarov, V. V., Urban, S., Corbin, T., Wycoff, G., Bastian, U., Schwekendiek, P., Wicenec, A., 2000, A&A 357, L27
Hübscher, J., Agerer, F., 1996, BAV Mitt. 93
Hübscher, J., Agerer, F., Busch, H., Goldhahn, H., Haßforther, B., Dahm, M., 1999, BAV Mitt. 122
Hübscher, J., Agerer, F., Busch, H., Goldhahn, H., Haßforther, B., Dahm, M., 2000, BAV Mitt. 131
Hübscher, J., Agerer, F., Frank, P., Wunder, E., 1994, BAV Mitt. 68
Hübscher, J., Agerer, F., Haßforther, B., Dahm, M., 1998, BAV Mitt. 113
Hübscher, J., Lichtenknecker, D., 1988, BAV Mitt. 50
Hübscher, J., Lichtenknecker, D., Wunder, E., 1989, BAV Mitt. 52
Hübscher, J., Lichtenknecker, D., Wunder, E., 1990, BAV Mitt. 56
Kharadse, E., 1933, Perem. Zvezdy 4, 139
Klepikova, L. A., 1958, Perem. Zvezdy 12, 164
Lange, G., 1938, Tadjik Annals, Vol 1. Part 2, 3
Lange, G. A., Motrich, V. D., Firmanyuk, B. N., Tsessevich, V. P., 1976, Astr. Tsirk. 900, 5
Lebedev, S., 1975, Perem. Zvezdy Pril. 2, 313
Oburka, O., 1965, Bull. Astr. Inst. Czech. 16, 55
Payne-Gaposchkin, C., 1954, Harvard Ann. 113, No 3, 151
Penston, M. J., 1973, MNRAS 164, 133
Pohl, E., Kizilirmak, A., 1964, Astron. Nachr. 288, 69
Popovici, C., 1970, IBVS 419
Popovici, C., 1971, IBVS 508
Satyvaldyev, V., 1962, Tadjik Bull. 33, 12
Schneller, H., 1929, Astron. Nachr. 235, 85
Schneller, H., 1931, Astron. Nachr. 243, 336
Soloviev, A., 1934, Tadjik Obs. Circ. 3, 2
Soloviev, A., 1936, Tadjik Obs. Circ. 17, 2
Soloviev, A., 1937, Tadjik Obs. Circ. 31, 2
Sturch, C., 1966, ApJ 143, 774
Tsessevich, V. P., 1974, Astr. Tsirk. 811, 1
Vandenbroere, J., 1997, GEOS Circ RR14
Vandenbroere, J., 1998, GEOS Circ RR15
Wenske, K., 1982, BAV Rundbrief 31/4, 81
Zaleski, L., 1965, Acta Astron. 15, 233

COMMUNICATIONS
FROM THE
KONKOLY OBSERVATORY
OF THE
HUNGARIAN ACADEMY OF SCIENCES

MITTEILUNGEN
DER
STERNWARTE
DER UNGARISCHEN AKADEMIE
DER WISSENSCHAFTEN

BUDAPEST–SVÁBHEGY

No. 102.
(Vol. 13, Part 2)

Photometry of RW Draconis at Konkoly Observatory*

Szeidl B., Oláh K., Barlai K., Szabados L.

Konkoly Observatory of the Hungarian Academy of Sciences,
P.O. Box 67, H-1525 Budapest, Hungary

BUDAPEST, 2001

*The data are available in electronic form at
`http://www.konkoly.hu/Mitteilungen/Mitteilungen.html`

ISBN 963 8361 409
HU ISSN 0238-2091
Felelős kiadó: Balázs Lajos

PHOTOMETRY OF RW DRACONIS AT KONKOLY OBSERVATORY

Abstract

We present 2863 photographic observations performed in the years 1952-1957, 373 photoelectric observations made in integrated light in the years 1954-1956, and 4114 V, 3962 B and 63 U observations of RW Dra obtained between 1958 -1975. Times and brightness of maximum light are also given.

Key words: Stars – variable: RR Lyrae; stars – individual: RW Dra – Techniques: photometric

INTRODUCTION

Seventy years ago Dr. Julia Balázs and Prof. L. Detre started a comprehensive study of RR Lyrae stars (Balázs & Detre, 1938). They paid special attention to the stars that showed light curve variation (i.e. Blazhko effect using modern terminology). One of their program stars was RW Dra. Their early study based on more than 6000 photographic observations has already been published (Balázs & Detre, 1952). Since that time the star has been intensively observed both by photographic and photoelectric methods at the Konkoly Observatory. In this paper we publish these observations. A comprehensive investigation of all published data of RW Dra will be published elsewhere.

The variability of RW Dra was discovered by Ceraski (1906) on Moscow plates and the preliminary name 87.1906 was given the star. Blazhko (1907) carried out the first intensive investigation of the light variation of RW Dra. He determined the star's pulsation period and found the evidence for the phase oscillation of light maximum with a period of 41.6 days. A historically important fact is that S. Blazhko was the very first who recognized long period phase oscillation in an RR Lyrae star (namely in RW Dra itself) and the phenomenon is deservedly called Blazhko effect.

OBSERVATIONS

Photographic observations

Photographic photometry was made at the Konkoly Observatory with the 16 cm astrograph from September 10, 1952 through November 23, 1957 on 95 nights. In the years 1952 and 1953 Eastman 40, and in the subsequent years Guilleminot Superfulgur plates were used with either 3 or 4 min. exposure times depending on the sky condition. The plates were measured with the observatory's Cuffey-type iris photometer. The comparison stars and their magnitudes used were taken from the paper of Balázs and Detre (1952). The 2863 photographic observations obtained are presented in Table 2. The time of the observations are converted to HJD. The estimated error of the observations is $0.05-0.10$ magn.

Photoelectric observations in integrated light

The early photoelectric photometry was conducted by L. Detre with the observatory's 60 cm telescope without using any filter. From 1954 an RCA 1P21 photomultiplier tube was employed in the photometer. Although these observations are on an indefinite photometric system, they may be useful in investigating the period changes and the Blazhko effect of RW Dra. The 373 observations published here in the sense variable minus comparison (s. Table 3) were made on 8 nights. The comparison star used was GSC 03885-00893 (=USNO 1425- 08562266), the star labelled e in Balázs and Detre's (1938, 1952) papers.

UBV photometry

The UBV photoelectric observations were carried out with the 60 cm Newton telescope at Budapest from April 24, 1958 till October 15, 1972 and with the 50 cm Cassegrain telescope at Piszkéstető mountain station between August 3, 1973 and February 11, 1975. Before 1963 the mirror of the 60 cm telescope had a silver coating, and an RCA 1P21 multiplier was employed with Schott filters UG1 in U, BG12+GG13 in B and GG11 in V. Thereafter an EMI 9052 B tube with the same filter combinations as in the previous years was used and the mirror was aluminized. The 50 cm telescope was equipped with an unrefrigerated photometer. This photometer contained an EMI 9058 QB multiplier tube and the colour filters matched closely the UBV system: in ultraviolet light UG2, in blue light BG12+GG13 and in yellow light GG11 Schott filters were used. The observations of the variable were reduced in the usual way. The UT values have been converted to HJD. Correction for atmospheric extinction was not applied as the comparison star is very close to the variable. The instrumental observations have been transformed into the UBV system in the traditional way. The comparison star used during the UBV observations was the same as used in the photoelectric observations in integrated light. During 146 nights between 1958 and 1975 4114 V, 3962 B and 63 U observations were collected. Since the star is too faint for our telescopes, U observations were made only on four nights with the 60 cm telescope. The observations are presented in Tables 4, 5 and 6 in the sense variable minus comparison.

TIMES AND BRIGHTNESS OF LIGHT MAXIMUM

For further studies we determined times and brightness of light maxima from our observations. Although the times of light maximum in B and in V may differ from each other, the difference between them is usually less than or is about the error of their determination. Therefore we give the mean values of the times of B and V light maximum. The brightness of the photoelectrically observed maxima is given in differential magnitudes to the comparison star. We wish to continue the investigation of Balázs and Detre (1952) and therefore we also determined the times of the "middle" (at $m=11\overset{m}{.}5$) of the ascending branch of the photographic light curves and the times of two points (at $\Delta m=0\overset{m}{.}0$ and $\Delta m=-0\overset{m}{.}5$) on the ascending branch of the photoelectrically observed light curves. The results of the photographic, the white light and the B and V observations are presented in Tables 1a, 1b and 1c, respectively.

ACKNOWLEDGEMENTS

We are grateful to the late director of the Konkoly Observatory, Prof. L. Detre, who made the early photoelectric observations. We would like to express our thanks to the staff of the Konkoly Observatory for having taken share in the observations. Thanks are due to Dr. J. Benkő and to Mr. A. Holl for their help in preparing the manuscript. This work was partly supported by the Hungarian OTKA Research Grants No. T-30954 and T-30955.

REFERENCES

Balázs, J. and Detre, L. 1938, Budapest Mitt. (Commun. Konkoly Obs.) No.5
Balázs, J. and Detre, L. 1952, Budapest Mitt. (Commun. Konkoly Obs.) No.27
Blazhko, S. 1907, Astron. Nachr. 175.326
Ceraski, W. 1906, Astron. Nachr. 172.96

Table 1: A. Times and brightness of photographic maxima and times of the "middle" (m=11.^{m}5) of the ascending branches

year	t(max) 2400000+	t(m=11.^{m}5)	m(max)	year	t(max) 2400000+	t(m=11.^{m}5)	m(max)
1952	34270.440:	.4233	10.57		35267.	.4815	
1953	34443.	.6030			35283.406		10.86
	34451.580	.5580	10.58		35290.492	.4560	10.88
	34463.541	.5006	10.95		35291.381		10.88
	34486.	.5690:			35299.375:		10.69
	34490.	.5429			35310.462	.4388	10.60
	34502.	.4755			35314.452		10.50
	34514.500:	.4764	10.76:		35318.425	.4008	10.58
	34522.	.4543			35333.443	.4212	11.00
	34565.	.4205			35341.458	.4334	10.89
	34568.	.5131			35345.465	.4360	10.85
	34573.404	.3765	10.60		35358.301		10.80
	34576.487	.4668	10.77		35373.307		10.97
	34580.460	.4327	10.78		35377.307	.2804	10.90
	34596.	.4165			35393.298	.2720	10.52
	34607.524	.4992	10.78		35396.420:		10.60:
	34608.403	.3825	10.48		35408.345:	.3150:	11.40:
	34619.450	.4233	10.80	1956	35601.475	.4496	10.30
	34623.426		10.90		35749.376	.3390	10.88
	34627.414		10.97	1957	35934.559	.5282	10.61
	34636.314	.2765	10.77		35947.367	.3347	10.74
1954	34952.529	.5078	10.90		35982.382	.3565	10.70
	34956.508	.4808	10.91		35988.	.5281	
	34960.512	.4758	11.04		35989.451	.4119	10.78
	34964.510	.4813	10.90		35992.535:	.5073	10.85
	34968.	.4743			36000.	.4948	
	34976.497	.4714	10.68		36004.	.4926	
	34988.430	.4100	10.65		36005.414	.3617	10.87
	34992.402	.3841	10.87		36012.	.4852	
	35016.357	.3328	10.62		36020.469:	.4495	10.20:
	35031.391	.3695	10.63		36066.529	.5059	10.51
	35032.274	.2520	10.56		36074.475	.4482	10.84
	35039.346	.3133	10.96		36087.349	.3225:	10.76
1955	35228.526	.4968	10.40		36098.435	.4072	10.42
	35237.364		10.64		36102.421	.3892	10.42
	35240.456:		10.46		36118.332	.2933	10.90
	35244.433	.3977	10.77		36129.449	.4107	11.16
	35247.522	.4857	10.84		36137.410	.3915	10.90
	35251.528	.4848	10.96		36165.269	.2478	11.06
	35256.409	.3814	10.87				

Table 1: B. Times and brightness of maxima in integrated light and the times of the $\Delta m = 0\overset{m}{.}0$ and $\Delta m = -0\overset{m}{.}5$ points on the ascending branches

year	t(max) 2400000+	t($\Delta m = 0\overset{m}{.}0$)	t($\Delta m = -0\overset{m}{.}5$)	Δm(max)
1954	35032.2786	.2452	.2553	−1.05
1955	35237.3610			−1.31
1956	35694.4661	.4319	.4452	−0.95
	35695.3466	.3266		−0.96
	35706.3977	.3592	.3773	−0.67
	35726.3806	.3446	.3552	−1.14
	35738.3067	.2720	.2827	−1.01

Table 1: C. Times and brightness of photoelectric B and V maxima and the times of the $\Delta B = 0\overset{m}{.}0$, $\Delta V = 0\overset{m}{.}0$ and $\Delta B = -0\overset{m}{.}5$, $\Delta V = -0\overset{m}{.}5$ points of the ascending branches

year	t(max)	t($\Delta m = 0\overset{m}{.}0$)		t($\Delta m = -0\overset{m}{.}5$)		Δm(max)	
	2400000+	in B	in V	in B	in V	ΔB	ΔV
1958	36318.5417	.5160	.5175	.5236	.5265	−1.17	−0.90
	36338.4945	.4538	.4554	.4694	.4728	−0.99	−0.78
	36373.4562	.4189	.4194	.4389	.4446	−0.87	−0.66
	36400.4930	.4639	.4650	.4719	.4746	−1.25	−0.95
	36404.4708	.4323	.4351	.4438	.4490	−1.05	−0.78
	36408.4475	.4083	.4074	.4190	.4228	−0.95	−0.76
	36420.	.3915	.3958	.4132	.4207		
	36431.5245	.4912	.4904	.5031	.5058	−1.08	−0.90
	36447.	.3910	.3916	.4033	.4051		
	36451.4100				.3818	−0.95	−0.70
	36476.2535					−1.25	−0.95
	36514.3455	.3110	.3134	.3280	.3304	−1.12	−0.82
1959	36679.5600	.5287	.5292	.5382	.5412	−1.20	−0.95
	36695.4797	.4373	.4386	.4491	.4540	−1.05	−0.76
	36726.	.4781	.4800				
	36757.5125	.4806	.4816	.4900	.4934	−1.07	−0.86
	36761.5040	.4712	.4719	.4813	.4846	−1.18	−0.90
	36812.433:	.3995	.4004	.4069	.4115	−1.17:	−0.96:
1960	37117.	.5380:	.5410:				
	37134.4562			.4318	.4356	−1.26	−0.99
	37138.4440	.4066	.4095	.4168	.4225	−1.29	−1.00
	37145.5172	.4793	.4805	.4912	.4967	−1.02	−0.79
	37149.4865	.4485	.4485	.4612	.4648	−0.93	−0.67
	37173.4265	.3928	.3948	.4050	.4084	−1.17	−0.89
1961	37467.5375	.4985	.5006	.5094	.5139	−1.33	−0.95
	37468.4235	.3870:	.3875:	.3951	.3985	−1.26	−0.97
	37483.4465:					−1.13	−0.83
	37487.4340:	.3824	.3850	.3945	.4019	−0.98	−0.73
	37490.5350	.4860	.4865	.4990	.5070	−0.94	−0.67
	37494.5300	.4845	.4858	.5010	.5064	−0.94	−0.69

Table 1: C. cont.

year	t(max)	t(Δm=0^m.0)		t(Δm=$-$0^m.5)		Δm(max)	
	2400000+	in B	in V	in B	in V	ΔB	ΔV
1962	37840.4820:	.4403	.4410	.4496	.4527	-1.31	-0.96
	37851.5259	.4925	.4936	.5029	.5063	-1.26	-0.91
	37852.4095	.3772	.3764	.3864	.3920	-1.05	-0.82
	37856.3880					-0.95	-0.67
	37867.4760:	.4286	.4250	.4488	.4520	-0.84	-0.58
	37871.4750	.4275	.4350	.4492	.4621	-0.90	-0.58
	37883.4480	.4041	.4079	.4195	.4259	-1.15	-0.79
	37895.		.3325		.3470		-0.71
	37903.3270				.3109		-0.69
1963	38163.		.3372		.3495		-0.60:
	38236.4150		.3643	.3780	.3950	-0.86	-0.60
	38248.4085	.3726	.3748	.3871	.3956	-0.90	-0.68
	38264.			.3068	.3113		
	38267.4195	.3845	.3857	.3963	.4003	-1.18	-0.86
	38291.3800		.3395		.3524		-0.88
1964	38585.4752	.4364	.4362	.4472	.4504	-1.24	-0.91
	38605.3500				.3392	-0.88	-0.66
	38608.4635	.4158	.4173	.4344	.4400	-0.78	-0.54
	38621.3537			.3234	.3326	-1.04	-0.72
	38636.3782	.3526	.3538	.3601	.3638	-1.31	-0.96
	38655.4275	.3973	.3978	.4068	.4116	-0.95	-0.67
	38664.3245	.2768	.2797	.2893	.2987	-1.00	-0.80
	38668.3055	.2632	.2708	.2796	.2844	-1.10	-0.81
1965	38965.4855	.4480	.4501	.4626	.4678	-1.00	-0.71
	38981.3995	.3565	.3580	.3748	.3877	-0.86	-0.58
	38985.4025	.3696	.3695	.3794	.3850	-0.90	-0.70
	38989.	.3645	.3686	.3763	.3817		
	38993.3975	.3588	.3590	.3705	.3730	-1.12	-0.80
	39028.3755	.3343	.3320	.3536	.3598	-0.85	-0.63
	39056.2523			.2267	.2326	-0.98	-0.73
	39060.2395					-0.98	-0.68
	39064.2318			.2049	.2122	-0.96	-0.69
1966	39264.4195				.404:	-0.87	-0.59
	39267.5275:					-0.80:	-0.53:
	39268.4024	.3629	.3676	.3788	.3864	-0.86	-0.67
	39323.3725	.3347	.3405	.3517	.3597	-0.93	-0.65
	39326.4845			.4560:	.4605	-1.00	-0.79
	39346.3600:			.3376	.3444	-0.96	-0.68
	39349.4612	.4200	.4216	.4337	.4428	-0.86	-0.62
	39373.4270:	.3864	.3864	.3948	.3984	-1.23	-0.93
	39381.3770	.3415	.3415	.3519	.3564	-1.08	-0.83
	39409.3070	.2665	.2660	.2816	.2872	-0.98	-0.73
	39413.3000:	.2497	.2501	.2649	.2687	-1.06:	-0.86:

Table 1: C. cont.

year	t(max)	t(Δm=0$^{\rm m}$.0)		t(Δm=$-$0$^{\rm m}$.5)		Δm(max)	
	2400000+	in B	in V	in B	in V	ΔB	ΔV
1967	39581.5900	.5564	.5569	.5628	.5670	-1.25	-1.02
	39604.6025	.5589	.5643	.5759	.5842	-0.87	-0.66
	39605.4895			.4645	.4722	-0.88	-0.63
	39648.4630			.4319	.4352	-1.04	-0.83
	39667.5080	.4755	.4755	.4817	.4873	-1.32	-0.92
	39710.	.4310	.4294	.4412	.4453		
	39711.3513					-1.09	-0.84
	39714.4410			.4138	.4174	-1.16	-0.81
	39722.405:				.3784	-0.98	-0.77
	39726.40:			.3680	.3735	-1.12	-0.82:
	39738.3860	.3481	.3485	.3598	.3600	-1.13	-0.88
1968	39923.48:					-0.95:	-0.69:
	39942.5595	.5274	.5290	.5363	.5426	-1.19	-0.83
	39978.4319	.3863	.3865	.4096	.4197	-0.81	-0.58
	39985.5388	.5020	.5028	.5146	.5219	-0.96	-0.68
	39993.5075	.4694	.4718	.4807	.4851	-1.07	-0.83
	40012.5125	.4670	.4670	.4812	.4873	-0.91	-0.68
	40067.	.434:	.438:	.4481	.4545		
1969	40338.4945	.4510	.4524	.4676	.4764	-0.84	-0.62
	40354.49:	.4353	.4381	.4512	.4566		
	40357.	.5465	.5490	.5607	.564:		
	40389.4460					-1.05	-0.72
	40420.4270	.3898	.3934	.4036	.4138	-0.85	-0.60
	40436.4150	.3784	.3805	.3908	.4000	-0.97	-0.80
	40439.5215	.4820	.4844	.4946	.5006	-1.02	-0.81
1970	40675.5650	.5178	.5215	.5339	.5414	-1.00	-0.72
	40707.4530	.4097	.4089	.4245	.4265	-0.91	-0.68
	40769.4897	.4558	.4582	.4694	.4745	-0.97	-0.69
	40781.4392	.4106	.4075	.4199	.4213	-1.02	-0.86
	40796.	.4221	.4260	.4392	.4480		
	40807.5680	.5385	.5397	.5500	.5556	-0.95	-0.70
	40859.3984	.3693	.3700	.3838	.3902	-1.05	-0.81
	40867.3575	.3203	.3237	.3346	.3390	-0.99	-0.80
	40883.2900		.2647	.2736		-0.95	-0.70
1971	41035.	.6230	.6245	.6314	.6346		
	41060.	.4525	.4525	.4655	.4705		
	41063.594:	.5550	.5561	.5684	.5732	-1.08:	-0.86:
	41071.5550	.5153	.5160	.5267	.5333	-1.08	-0.80
	41087.4760	.4198	.4252	.4380	.4530	-0.82	-0.65
	41094.	.5408	.5449	.5552	.5595		
	41095.4710	.4274	.4302	.4424	.4483	-1.03	-0.76
	41118.4804					-1.21	-0.91
	41126.46:			.4130	.4270	-0.95:	-0.70:

Table 1: C. cont.

year	t(max)	t(Δm=0$^{\rm m}$.0)		t(Δm=$-$0$^{\rm m}$.5)		Δm(max)	
	2400000+	in B	in V	in B	in V	ΔB	ΔV
1971	41161.4295	.4020	.4032	.4145	.4179	-0.93	-0.72
	41189.3755	.3384	.3404	.3491	.3532	-1.27	-0.94
1972	41529.5128	.4847	.4854	.4948	.4973	-0.99	-0.74
	41537.47:	.4335	.4335	.4475	.4530	-0.89	-0.62
	41538.3595			.332:	.3425	-1.01	-0.73
	41545.4572	.4196	.4236	.4368	.4422	-1.02	-0.76
	41589.3215	.2713	.2783	.2946	.3052	-0.90	-0.65
	41597.3115	.2725	.2733	.2844	.2883	-0.96	-0.77
	41605.2775	.2404	.2387	.2487	.2517	-1.15	-0.89
1973	41898.4800	.4474	.4474	.4567	.4590	-1.19	-0.86
	41949.	.3502	.3513	.3637	.3696		
1974	42126.575:	.5414	.5437	.5532	.5575	-1.07:	-0.79:
	42216.5063	.4730	.4741	.4829	.4868	-1.11	-0.81
	42220.4960	.4640	.4640	.4727	.4756	-1.17	-0.90
	42224.4842	.4479	.4486	.4578	.4609	-1.17	-0.89
	42255.	.4444	.4462	.4588	.4646		
	42256.			.3456	.3562		
	42275.397:	.3635	.3638	.3700	.3732	-1.35:	-0.99:
	42278.4865	.4535	.4543	.4622	.4653	-1.15	-0.86
	42299.	.3016	.3016	.3126	.3175		

Table 2. Photographic observations of RW Dra

2434266 +
0.3237 +12.200
0.3258 +12.310
0.3314 +12.210
0.3334 +12.360
0.3355 +12.300
0.3376 +12.250
0.3397 +12.310
0.3418 +12.260
0.3439 +12.280
0.3459 +12.390
0.3480 +12.400
0.3501 +12.490
0.3522 +12.480

2434270 +
0.3610 +12.280
0.3631 +12.330
0.3652 +12.300
0.3673 +12.250
0.3694 +12.240
0.3714 +12.180
0.3735 +12.350
0.3756 +12.240
0.3776 +12.440
0.3798 +12.420
0.3819 +12.280
0.3839 +12.250
0.3860 +12.280
0.3881 +12.270
0.3902 +12.270
0.3923 +12.280
0.3944 +12.100
0.3964 +12.190
0.3985 +12.250
0.4006 +12.120
0.4027 +12.000
0.4159 +11.720
0.4180 +11.650
0.4200 +11.600
0.4221 +11.580
0.4242 +11.450
0.4263 +11.320
0.4284 +11.160
0.4305 +10.980
0.4325 +10.800
0.4346 +10.640
0.4367 +10.580
0.4388 +10.570

2434443 +
0.5335 +12.080
0.5363 +12.050
0.5391 +12.070
0.5419 +12.030
0.5446 +12.200
0.5472 +12.000
0.5613 +12.010
0.5641 +12.100
0.5669 +12.050
0.5696 +12.050
0.5724 +12.100
0.5752 +12.220
0.5780 +12.050
0.5863 +12.050
0.5891 +12.200
0.5919 +12.000
0.5946 +12.190
0.5974 +11.820
0.6002 +11.720
0.6030 +11.450
0.6058 +11.300
0.6092 +11.170
0.6120 +11.100
0.6148 +10.900
0.6176 +10.810
0.6203 +10.620
0.6231 +10.820
0.6259 +10.700

2434451 +
0.5588 +11.400
0.5616 +11.360
0.5644 +11.000
0.5672 +10.970
0.5699 +10.730
0.5727 +10.750
0.5755 +10.610
0.5783 +10.550
0.5811 +10.550
0.5838 +10.600
0.5866 +10.680
0.5894 +10.610

0.5922 +10.680
0.5949 +10.660
0.5977 +10.700
0.6005 +10.770
0.6033 +10.800
0.6061 +10.880
0.6088 +10.870
0.6116 +10.930
0.6144 +10.950
0.6179 +10.890
0.6206 +11.030
0.6234 +10.960
0.6262 +11.000
0.6290 +11.040
0.6318 +11.070
0.6345 +11.020
0.6373 +11.100
0.6401 +11.150
0.6429 +11.110
0.6456 +11.240

2434455 +
0.5485 +10.900
0.5506 +10.760
0.5527 +10.790
0.5548 +10.750
0.5569 +10.810
0.5589 +10.940
0.5610 +10.930
0.5631 +10.900
0.5652 +10.870
0.5673 +10.960
0.5694 +10.880
0.5714 +10.880
0.5735 +10.860
0.5756 +10.850
0.5778 +10.870
0.5798 +10.860
0.5819 +10.920
0.5839 +10.970
0.5860 +10.950
0.5881 +11.020
0.5902 +11.190
0.5923 +11.270
0.5944 +11.180
0.5964 +11.270
0.5985 +11.340

0.6006 +11.400
0.6027 +11.430
0.6048 +11.390
0.6069 +11.300
0.6089 +11.280
0.6110 +11.390
0.6131 +11.360
0.6152 +11.380
0.6173 +11.460
0.6194 +11.430
0.6214 +11.430
0.6235 +11.520
0.6256 +11.600

2434459 +
0.5141 +11.200
0.5162 +10.880
0.5183 +10.950
0.5203 +10.900
0.5224 +11.080
0.5245 +11.000
0.5266 +10.940
0.5287 +10.960
0.5308 +10.900
0.5328 +10.960
0.5349 +10.890
0.5370 +10.970
0.5391 +10.910
0.5412 +11.020
0.5433 +10.890
0.5453 +10.840
0.5474 +10.900
0.5495 +10.850
0.5516 +10.980
0.5537 +11.100
0.5558 +11.040
0.5578 +11.030
0.5599 +11.050
0.5620 +11.100
0.5641 +11.080
0.5662 +11.190
0.5683 +11.250
0.5703 +11.130
0.5724 +11.140
0.5745 +11.220
0.5766 +11.200
0.5787 +11.200

0.5808 +11.250
0.5828 +11.350
0.5849 +11.300
0.5870 +11.380
0.5891 +11.200
0.5912 +11.280
0.5933 +11.320
0.5953 +11.500
0.5974 +11.470
0.5995 +11.380
0.6016 +11.440
0.6037 +11.420

2434463 +
0.4885 +12.080
0.4906 +12.000
0.4927 +11.980
0.4947 +11.950
0.4968 +11.640
0.4989 +11.520
0.5010 +11.450
0.5031 +11.420
0.5052 +11.380
0.5072 +11.250
0.5093 +11.220
0.5114 +11.170
0.5135 +11.200
0.5156 +11.070
0.5204 +11.120
0.5225 +11.130
0.5246 +10.960
0.5267 +11.030
0.5288 +11.020
0.5309 +10.930
0.5329 +10.980
0.5350 +11.000
0.5371 +10.910
0.5392 +10.920
0.5413 +11.000
0.5441 +10.900
0.5461 +10.970
0.5482 +10.920
0.5503 +10.930
0.5524 +10.980

2434482 +
0.5140 +12.360

0.5168 +12.440
0.5195 +12.400
0.5223 +12.460
0.5251 +12.450
0.5279 +12.310
0.5307 +12.400
0.5334 +12.440
0.5362 +12.500
0.5390 +12.350
0.5445 +12.450
0.5473 +12.370
0.5501 +12.370
0.5529 +12.410
0.5557 +12.360
0.5584 +12.470
0.5612 +12.320
0.5640 +12.460
0.5668 +12.280
0.5695 +12.060
0.5716 +12.110

2434486 +
0.5085 +12.300
0.5113 +12.320
0.5141 +12.280
0.5169 +12.300
0.5196 +12.250
0.5224 +12.380
0.5252 +12.400
0.5280 +12.350
0.5308 +12.330
0.5335 +12.400
0.5363 +12.350
0.5391 +12.430
0.5419 +12.470
0.5446 +12.380
0.5474 +12.300
0.5502 +12.100
0.5530 +12.200
0.5558 +11.920
0.5585 +11.900
0.5613 +12.000
0.5641 +11.850
0.5669 +11.560
0.5696 +11.530

2434490 +
0.5082 +12.500
0.5110 +12.460
0.5138 +12.390
0.5166 +12.400
0.5194 +12.500
0.5221 +12.370
0.5249 +12.470
0.5277 +12.480
0.5305 +12.430
0.5332 +12.080
0.5360 +11.970
0.5388 +11.680
0.5416 +11.570
0.5444 +11.490
0.5471 +11.150
0.5499 +11.040
0.5527 +11.040

2434502 +
0.4662 +11.900
0.4745 +11.540
0.4773 +11.440
0.4801 +11.420
0.4828 +11.180
0.4856 +11.100
0.4884 +11.130
0.4912 +11.140
0.4940 +11.070
0.4967 +11.150
0.4995 +11.020
0.5023 +10.970
0.5051 +11.100
0.5078 +10.960
0.5106 +10.960
0.5134 +10.900

2434514 +
0.3982 +12.050
0.4010 +12.130
0.4038 +12.210
0.4066 +12.180
0.4093 +12.180
0.4121 +12.120
0.4149 +12.100
0.4177 +12.180
0.4204 +12.200

0.4232 +12.230
0.4262 +12.150
0.4288 +12.140
0.4316 +12.140
0.4343 +12.140
0.4371 +12.170
0.4399 +12.210
0.4427 +12.210
0.4454 +12.200
0.4482 +12.110
0.4538 +12.100
0.4566 +12.120
0.4593 +12.180
0.4621 +12.130
0.4649 +12.050
0.4677 +12.050
0.4704 +11.850
0.4732 +11.680
0.4760 +11.500
0.4788 +11.360
0.4816 +11.300
0.4843 +11.080
0.4871 +10.920
0.4900 +10.850
0.4928 +10.870
0.4955 +10.800
0.4983 +10.750

2434522 +
0.3660 +12.170
0.3688 +12.390
0.3715 +12.360
0.3743 +12.350
0.3771 +12.420
0.3800 +12.370
0.3826 +12.340
0.3854 +12.290
0.3882 +12.390
0.3938 +12.390
0.3965 +12.350
0.3993 +12.520
0.4049 +12.490
0.4104 +12.420
0.4132 +12.500
0.4160 +12.400
0.4188 +12.350
0.4243 +12.450
0.4271 +12.400
0.4299 +12.350
0.4326 +12.210
0.4354 +12.200
0.4382 +12.000
0.4410 +12.050
0.4438 +12.000
0.4465 +11.850
0.4493 +11.700
0.4521 +11.560
0.4549 +11.500
0.4576 +11.320
0.4604 +11.240
0.4632 +11.110
0.4660 +10.920
0.4688 +10.900

2434565 +
0.3727 +12.500
0.3755 +12.390
0.3783 +12.360
0.3811 +12.300
0.3838 +12.430
0.3873 +12.510
0.3894 +12.280
0.3922 +12.220
0.3949 +12.170
0.3977 +12.200
0.4005 +12.320
0.4033 +12.110
0.4061 +12.100
0.4088 +12.110
0.4172 +11.620
0.4199 +11.540
0.4227 +11.330
0.4255 +11.300
0.4283 +11.090
0.4311 +10.980
0.4338 +10.950
0.4366 +10.850
0.4394 +10.700
0.4422 +10.780

2434568 +
0.4682 +12.080
0.4709 +12.090
0.4737 +12.140
0.4765 +12.110
0.4793 +12.220
0.4820 +12.360
0.4848 +12.150
0.4876 +12.200
0.4904 +12.120
0.4932 +12.100
0.4959 +12.130
0.4987 +12.000
0.5015 +12.120
0.5043 +12.090
0.5070 +11.820
0.5098 +11.800
0.5126 +11.550
0.5154 +11.260
0.5182 +11.180
0.5209 +11.100
0.5265 +11.000
0.5293 +10.850
0.5320 +10.880
0.5348 +10.800
0.5376 +10.620
0.5404 +10.770
0.5432 +10.680

2434573 +
0.3624 +12.330
0.3652 +12.330
0.3680 +12.150
0.3707 +12.100
0.3735 +11.790
0.3763 +11.420
0.3791 +11.160
0.3819 +11.180
0.3846 +11.030
0.3874 +10.910
0.3902 +10.730
0.3930 +10.720
0.3957 +10.690
0.3985 +10.560
0.4013 +10.700
0.4041 +10.530
0.4069 +10.700
0.4096 +10.630
0.4124 +10.730
0.4152 +10.610
0.4180 +10.720
0.4207 +10.760
0.4235 +10.780
0.4263 +10.830
0.4291 +10.800
0.4319 +10.940
0.4346 +11.010
0.4374 +11.090

2434576 +
0.4261 +12.140
0.4289 +12.100
0.4317 +12.150
0.4344 +12.160
0.4372 +12.300
0.4400 +12.320
0.4428 +12.230
0.4483 +12.280
0.4539 +12.150
0.4567 +12.150
0.4594 +12.000
0.4622 +11.890
0.4650 +11.510
0.4678 +11.440
0.4705 +11.150
0.4733 +11.090
0.4761 +10.980
0.4789 +10.950
0.4817 +10.920
0.4844 +10.760
0.4872 +10.670
0.4900 +10.800
0.4928 +10.880
0.4955 +10.810
0.4983 +10.850
0.5011 +10.850
0.5039 +10.840
0.5067 +10.880
0.5094 +10.850
0.5122 +10.890
0.5150 +10.940
0.5178 +10.940
0.5205 +10.970
0.5233 +11.060
0.5261 +11.030
0.5289 +11.020
0.5317 +11.160
0.5344 +11.200
0.5372 +11.080
0.5400 +11.250

2434580 +
0.3853 +12.360
0.3881 +12.260
0.3909 +12.320
0.3937 +12.320
0.3964 +12.400
0.3992 +12.380
0.4020 +12.350
0.4048 +12.400
0.4103 +12.350
0.4131 +12.170
0.4159 +12.210
0.4187 +12.080
0.4214 +11.910
0.4242 +11.840
0.4270 +11.850
0.4298 +11.610
0.4325 +11.450
0.4353 +11.370
0.4381 +11.420
0.4408 +11.320
0.4438 +11.140
0.4492 +10.830
0.4520 +10.870
0.4548 +10.710
0.4576 +10.780
0.4603 +10.780
0.4631 +10.840
0.4687 +10.780
0.4714 +10.820
0.4742 +10.860
0.4770 +10.880
0.4798 +10.840
0.4825 +10.850
0.4853 +10.990
0.4881 +10.990
0.4909 +10.890

2434596 +
0.3305 +12.280
0.3332 +12.330
0.3360 +12.300
0.3388 +12.170
0.3416 +12.270

0.3444 +12.280
0.3471 +12.160
0.3499 +12.220
0.3527 +12.200
0.3555 +12.320
0.3582 +12.300
0.3610 +12.270
0.3638 +12.210
0.3666 +12.270
0.3694 +12.200
0.3721 +12.310
0.3749 +12.290
0.3777 +12.250
0.3805 +12.220
0.3832 +12.220
0.3874 +12.180
0.3916 +12.300
0.3944 +12.180
0.3971 +12.090
0.3999 +12.240
0.4027 +11.960
0.4055 +11.900
0.4082 +11.820
0.4110 +11.800
0.4138 +11.580
0.4166 +11.500
0.4194 +11.410
0.4221 +11.270
0.4249 +11.220
0.4277 +11.200
0.4305 +11.070
0.4332 +10.950
0.4360 +10.960
0.4388 +10.870
0.4416 +10.700
0.4444 +10.730
0.4471 +10.780

2434599 +
0.4260 +12.370
0.4288 +12.400
0.4316 +12.500
0.4343 +12.430
0.4371 +12.440
0.4399 +12.370
0.4427 +12.400
0.4454 +12.420
0.4482 +12.400
0.4510 +12.430
0.4538 +12.430
0.4566 +12.400
0.4593 +12.370
0.4621 +12.510

2434604 +
0.3191 +12.230
0.3218 +12.290
0.3246 +12.360
0.3274 +12.320
0.3302 +12.370
0.3329 +12.340
0.3357 +12.430
0.3385 +12.390
0.3413 +12.300
0.3441 +12.340
0.3468 +12.450
0.3496 +12.280
0.3524 +12.350
0.3552 +12.390
0.3579 +12.450
0.3607 +12.440
0.3635 +12.480
0.3663 +12.290
0.3691 +12.450
0.3718 +12.250

2434606 +
0.5117 +12.350
0.5145 +12.300
0.5173 +12.380
0.5200 +12.270
0.5228 +12.370
0.5256 +12.380
0.5284 +12.300
0.5312 +12.290
0.5339 +12.320
0.5367 +12.350
0.5395 +12.320
0.5423 +12.390
0.5450 +12.470
0.5478 +12.460
0.5506 +12.460
0.5534 +12.450
0.5562 +12.460
0.5589 +12.430
0.5617 +12.390
0.5645 +12.450
0.5673 +12.410
0.5700 +12.500
0.5728 +12.460
0.5756 +12.450
0.5784 +12.480
0.5812 +12.500
0.5895 +12.420
0.5923 +12.470
0.5950 +12.430

2434607 +
0.4800 +12.100
0.4827 +12.110
0.4855 +11.900
0.4883 +11.780
0.4911 +11.770
0.4939 +11.750
0.4966 +11.570
0.4994 +11.490
0.5022 +11.280
0.5050 +11.370
0.5077 +11.240
0.5105 +11.160
0.5133 +10.980
0.5161 +10.890
0.5189 +10.730
0.5216 +10.760
0.5244 +10.750
0.5272 +10.800
0.5300 +10.810
0.5327 +10.800
0.5355 +10.890
0.5383 +10.830
0.5411 +10.930
0.5439 +10.960
0.5466 +10.980
0.5494 +11.040
0.5522 +10.940
0.5550 +11.070
0.5577 +10.970
0.5605 +11.010

2434608 +
0.3272 +12.150
0.3300 +12.180
0.3327 +12.160
0.3355 +12.250
0.3383 +12.150
0.3411 +12.320
0.3439 +12.200
0.3466 +12.300
0.3494 +12.150
0.3522 +12.240
0.3550 +12.160
0.3577 +12.170
0.3605 +12.100
0.3633 +12.020
0.3675 +12.050
0.3716 +11.880
0.3744 +11.700
0.3772 +11.800
0.3800 +11.720
0.3827 +11.560
0.3855 +11.500
0.3883 +11.220
0.3911 +11.210
0.3939 +11.050
0.3994 +10.600
0.4022 +10.520
0.4050 +10.480
0.4077 +10.460
0.4105 +10.480
0.4133 +10.500
0.4161 +10.590
0.4189 +10.490
0.4216 +10.450
0.4244 +10.560
0.4272 +10.460
0.4300 +10.500

2434619 +
0.3820 +12.240
0.3848 +12.170
0.3876 +12.100
0.3904 +12.200
0.3932 +12.130
0.3959 +12.080
0.3987 +12.180
0.4015 +12.300
0.4043 +12.100
0.4070 +12.020
0.4105 +12.130
0.4126 +12.000
0.4154 +11.900
0.4182 +11.910
0.4209 +11.680
0.4265 +11.260
0.4293 +11.150
0.4320 +11.000
0.4348 +10.910
0.4376 +10.890
0.4404 +10.850
0.4432 +10.840
0.4459 +10.800
0.4487 +10.880
0.4515 +10.720
0.4543 +10.860
0.4570 +10.850
0.4598 +10.800
0.4625 +10.800
0.4653 +10.880
0.4709 +10.950
0.4737 +10.900
0.4765 +10.980
0.4793 +11.060
0.4820 +11.040
0.4847 +10.950
0.4875 +11.050
0.4903 +11.050
0.4932 +11.180
0.4959 +11.200
0.4987 +11.280
0.5015 +11.300
0.5043 +11.330

2434623 +
0.4041 +11.170
0.4069 +11.120
0.4096 +11.000
0.4124 +10.990
0.4152 +10.900
0.4180 +10.900
0.4207 +10.820
0.4235 +10.960
0.4263 +10.840
0.4291 +10.970
0.4319 +10.880
0.4346 +10.970

0.4374 +10.900
0.4555 +11.010
0.4583 +11.100
0.4610 +11.060
0.4638 +11.060
0.4666 +11.070
0.4694 +11.030
0.4721 +11.120
0.4749 +11.210
0.4777 +11.180
0.4805 +11.230
0.4832 +11.350
0.4860 +11.330

2434627 +
0.3816 +11.300
0.3843 +11.350
0.3871 +11.240
0.3899 +11.160
0.3927 +11.100
0.3954 +11.100
0.3982 +11.070
0.4010 +11.100
0.4038 +11.020
0.4066 +11.000
0.4093 +11.050
0.4121 +10.970
0.4149 +10.920
0.4177 +11.000
0.4204 +11.060
0.4232 +10.980
0.4260 +11.060
0.4288 +11.040
0.4316 +11.000
0.4343 +11.020
0.4371 +11.120
0.4399 +11.080
0.4427 +11.110
0.4454 +11.140
0.4482 +11.160
0.4510 +11.160
0.4538 +11.300
0.4566 +11.180

2434636 +
0.2645 +11.800
0.2673 +11.760
0.2700 +11.790
0.2728 +11.610
0.2756 +11.550
0.2784 +11.420
0.2812 +11.280
0.2839 +11.090
0.2867 +11.030
0.2895 +10.970
0.2923 +10.960
0.2950 +10.800
0.2978 +10.850
0.3006 +10.830
0.3034 +10.810
0.3062 +10.830
0.3089 +10.820
0.3117 +10.750
0.3145 +10.760
0.3173 +10.800
0.3200 +10.750
0.3228 +10.800
0.3256 +10.800
0.3284 +10.800
0.3312 +10.810
0.3346 +11.040
0.3367 +10.850
0.3395 +10.900

2434952 +
0.4107 +12.300
0.4163 +12.370
0.4191 +12.360
0.4218 +12.520
0.4246 +12.440
0.4274 +12.340
0.4302 +12.370
0.4329 +12.270
0.4357 +12.310
0.4385 +12.290
0.4413 +12.270
0.4441 +12.300
0.4468 +12.360
0.4496 +12.220
0.4524 +12.240
0.4552 +12.300
0.4580 +12.460
0.4607 +12.340
0.4635 +12.260
0.4663 +12.240
0.4691 +12.220
0.4718 +12.380
0.4746 +12.260
0.4774 +12.430
0.4802 +12.460
0.4829 +12.360
0.4857 +12.260
0.4885 +12.230
0.4913 +12.300
0.4941 +12.230
0.4968 +11.910
0.4996 +11.770
0.5024 +11.660
0.5079 +11.600
0.5107 +11.350
0.5135 +11.290
0.5163 +11.040
0.5191 +11.110
0.5218 +10.940
0.5246 +10.900
0.5274 +10.890
0.5302 +10.910
0.5329 +10.960
0.5357 +11.020
0.5385 +10.910

2434956 +
0.4206 +12.080
0.4235 +12.200
0.4262 +12.120
0.4290 +12.180
0.4318 +12.140
0.4345 +12.140
0.4373 +12.270
0.4401 +12.130
0.4429 +12.220
0.4456 +12.360
0.4484 +12.300
0.4512 +12.330
0.4540 +12.150
0.4568 +12.200
0.4595 +12.300
0.4623 +12.190
0.4651 +12.120
0.4679 +12.080
0.4706 +12.070
0.4734 +12.140
0.4762 +12.090
0.4790 +11.880
0.4818 +11.530
0.4845 +11.370
0.4873 +11.320
0.4901 +11.140
0.4929 +11.090
0.4956 +10.990
0.4984 +10.970
0.5012 +10.960
0.5040 +10.970
0.5068 +10.870
0.5095 +10.910

2434960 +
0.4220 +12.160
0.4248 +12.150
0.4276 +12.120
0.4304 +12.210
0.4331 +12.220
0.4359 +12.200
0.4387 +12.220
0.4415 +12.180
0.4443 +12.260
0.4470 +12.290
0.4498 +12.240
0.4526 +12.250
0.4554 +12.150
0.4582 +12.110
0.4609 +12.020
0.4637 +11.910
0.4665 +11.780
0.4693 +11.640
0.4721 +11.640
0.4748 +11.480
0.4776 +11.440
0.4804 +11.380
0.4831 +11.400
0.4859 +11.380
0.4887 +11.330
0.4915 +11.170
0.4943 +11.110
0.4970 +11.190
0.4998 +11.150
0.5026 +11.100
0.5054 +11.020
0.5081 +11.020
0.5137 +11.020
0.5165 +11.070
0.5193 +11.080
0.5220 +11.090
0.5248 +11.050
0.5276 +11.060
0.5304 +11.170
0.5359 +11.120
0.5387 +11.180

2434964 +
0.4108 +12.200
0.4136 +12.250
0.4164 +12.180
0.4192 +12.150
0.4219 +12.200
0.4247 +12.220
0.4275 +12.340
0.4303 +12.200
0.4330 +12.380
0.4358 +12.280
0.4386 +12.260
0.4414 +12.260
0.4442 +12.380
0.4497 +12.260
0.4525 +12.200
0.4553 +12.200
0.4608 +12.040
0.4636 +12.030
0.4664 +11.890
0.4692 +11.850
0.4719 +11.800
0.4747 +11.610
0.4775 +11.510
0.4803 +11.540
0.4830 +11.480
0.4858 +11.320
0.4886 +11.300
0.4914 +11.320
0.4942 +11.200
0.4969 +11.120
0.4997 +10.960
0.5025 +11.000
0.5053 +10.880
0.5080 +10.890
0.5108 +10.900

0.5136 +10.960

2434968 +
0.4148 +12.270
0.4196 +12.330
0.4245 +12.200
0.4295 +12.330
0.4349 +12.260
0.4398 +12.140
0.4470 +12.190
0.4544 +12.010
0.4599 +11.990
0.4655 +11.840
0.4710 +11.690
0.4766 +11.420

2434976 +
0.3633 +12.300
0.3661 +12.320
0.3689 +12.200
0.3716 +12.200
0.3744 +12.370
0.3772 +12.250
0.3800 +12.290
0.3827 +12.320
0.3855 +12.260
0.3883 +12.330
0.3911 +12.410
0.3939 +12.350
0.3966 +12.280
0.3994 +12.380
0.4022 +12.270
0.4050 +12.360
0.4077 +12.280
0.4105 +12.400
0.4133 +12.400
0.4209 +12.330
0.4237 +12.350
0.4265 +12.330
0.4293 +12.470
0.4320 +12.500
0.4348 +12.450
0.4376 +12.360
0.4404 +12.350
0.4432 +12.470
0.4459 +12.490
0.4515 +12.240

0.4543 +12.410
0.4571 +12.190
0.4598 +11.960
0.4626 +11.830
0.4689 +11.630
0.4716 +11.430
0.4744 +11.420
0.4772 +11.250
0.4800 +11.160
0.4827 +11.010
0.4855 +10.930
0.4883 +10.800
0.4911 +10.630
0.4939 +10.660
0.4966 +10.750
0.4994 +10.710
0.5022 +10.760
0.5050 +10.700
0.5077 +10.770
0.5105 +10.830
0.5133 +10.910
0.5161 +10.840
0.5189 +10.980
0.5216 +11.010
0.5244 +10.970
0.5272 +10.960
0.5300 +11.020
0.5327 +11.010
0.5355 +11.170

2434988 +
0.3603 +12.350
0.3631 +12.390
0.3659 +12.290
0.3687 +12.320
0.3714 +12.350
0.3742 +12.430
0.3770 +12.260
0.3798 +12.350
0.3825 +12.300
0.3853 +12.250
0.3881 +12.330
0.3909 +12.430
0.3937 +12.350
0.3964 +12.300
0.3992 +12.300
0.4020 +12.220

0.4048 +12.130
0.4075 +11.880
0.4103 +11.400
0.4131 +11.150
0.4159 +11.110
0.4187 +10.940
0.4214 +10.840
0.4242 +10.680
0.4270 +10.650
0.4298 +10.710
0.4325 +10.630
0.4353 +10.720
0.4381 +10.680
0.4409 +10.680
0.4437 +10.730
0.4464 +10.760
0.4520 +10.860
0.4548 +10.800
0.4576 +10.850
0.4603 +10.960
0.4631 +10.870
0.4659 +11.070
0.4687 +11.020
0.4714 +11.050
0.4742 +11.150

2434992 +
0.3404 +12.390
0.3432 +12.530
0.3459 +12.280
0.3487 +12.300
0.3515 +12.290
0.3543 +12.170
0.3570 +12.140
0.3598 +12.030
0.3654 +12.060
0.3682 +11.910
0.3709 +11.850
0.3737 +11.690
0.3765 +11.710
0.3793 +11.600
0.3820 +11.490
0.3848 +11.340
0.3876 +11.280
0.3904 +11.120
0.3932 +10.940
0.3959 +10.840

0.3987 +10.860
0.4015 +10.890
0.4043 +10.860
0.4070 +10.910
0.4098 +10.910
0.4126 +10.960
0.4154 +11.070
0.4182 +11.010
0.4209 +11.120
0.4237 +11.090

2435016 +
0.2516 +12.310
0.2544 +12.240
0.2572 +12.200
0.2599 +12.130
0.2627 +12.170
0.2780 +12.350
0.2808 +12.390
0.2835 +12.310
0.2863 +12.200
0.2891 +12.280
0.2919 +12.490
0.2946 +12.200
0.2974 +12.370
0.3002 +12.220
0.3030 +12.250
0.3058 +12.370
0.3086 +12.370
0.3113 +12.320
0.3141 +12.230
0.3169 +12.380
0.3196 +12.200
0.3224 +12.070
0.3252 +12.040
0.3280 +11.770
0.3308 +11.520
0.3335 +11.470
0.3363 +11.290
0.3391 +11.190
0.3419 +11.120
0.3446 +10.900
0.3474 +10.890
0.3502 +10.780
0.3530 +10.590
0.3558 +10.600
0.3585 +10.640

0.3620 +10.790
0.3648 +10.920
0.3676 +10.890
0.3703 +10.820
0.3731 +10.890
0.3759 +10.800
0.3787 +10.910
0.3815 +10.940
0.3842 +10.970
0.3870 +11.040
0.3898 +11.160
0.3926 +11.170
0.3953 +11.270
0.3981 +11.330
0.4009 +11.270
0.4037 +11.330
0.4065 +11.370

2435031 +
0.3100 +12.360
0.3142 +12.460
0.3184 +12.290
0.3225 +12.390
0.3267 +12.290
0.3309 +12.470
0.3350 +12.430
0.3392 +12.430
0.3434 +12.470
0.3475 +12.460
0.3517 +12.200
0.3559 +12.120
0.3600 +12.000
0.3642 +11.860
0.3684 +11.650
0.3725 +11.280
0.3767 +11.000
0.3809 +10.810
0.3850 +10.600
0.3892 +10.650
0.3934 +10.630
0.3975 +10.660
0.4017 +10.700
0.4059 +10.720
0.4100 +10.750
0.4142 +10.760
0.4184 +10.810
0.4225 +10.940

0.4267 +11.020
0.4309 +11.010
0.4350 +11.050
0.4392 +11.080
0.4434 +11.180
0.4475 +11.200
0.4517 +11.190

2435032 +
0.2490 +11.660
0.2518 +11.590
0.2546 +11.360
0.2573 +11.140
0.2601 +11.000
0.2643 +10.700
0.2671 +10.620
0.2698 +10.580
0.2726 +10.560
0.2754 +10.580
0.2782 +10.600
0.2810 +10.600
0.2838 +10.630
0.2865 +10.640
0.2893 +10.700
0.2921 +10.700
0.2948 +10.690
0.2976 +10.720
0.3004 +10.800
0.3032 +10.850
0.3060 +10.940
0.3087 +10.980
0.3115 +10.950
0.3143 +11.000
0.3171 +11.030
0.3198 +11.060
0.3226 +11.000

2435039 +
0.2989 +12.000
0.3017 +11.930
0.3045 +11.900
0.3072 +11.770
0.3100 +11.680
0.3128 +11.520
0.3156 +11.340
0.3184 +11.250
0.3211 +11.180

0.3239 +11.100
0.3267 +11.060
0.3295 +10.970
0.3322 +10.970
0.3350 +11.020
0.3378 +11.000
0.3406 +10.960
0.3434 +10.980
0.3461 +11.020
0.3489 +10.960
0.3517 +10.950
0.3545 +10.950
0.3572 +10.930
0.3600 +10.970
0.3628 +11.000
0.3656 +11.040
0.3684 +11.100
0.3711 +11.050
0.3739 +11.070
0.3767 +11.080
0.3795 +11.170
0.3822 +11.200
0.3850 +11.240
0.3878 +11.110
0.3906 +11.140
0.3934 +11.300
0.3961 +11.230
0.3989 +11.270
0.4017 +11.300
0.4045 +11.420

2435223 +
0.4862 +12.350
0.4890 +12.390
0.4918 +12.300
0.4945 +12.370
0.4973 +12.460
0.5001 +12.450
0.5029 +12.380
0.5057 +12.420
0.5084 +12.370
0.5112 +12.300
0.5140 +12.360
0.5168 +12.360
0.5195 +12.390
0.5223 +12.320
0.5251 +12.400

0.5348 +12.350
0.5376 +12.340
0.5404 +12.400
0.5432 +12.410
0.5459 +12.420
0.5487 +12.360
0.5515 +12.350
0.5543 +12.360
0.5570 +12.310
0.5598 +12.410
0.5626 +12.490
0.5654 +12.460
0.5682 +12.470
0.5709 +12.350
0.5737 +12.500
0.5765 +12.410
0.5793 +12.500
0.5820 +12.410
0.5848 +12.450
0.5876 +12.360
0.5904 +12.370
0.5932 +12.480

2435228 +
0.4473 +12.420
0.4543 +12.470
0.4577 +12.460
0.4647 +12.460
0.4689 +12.450
0.4723 +12.500
0.4758 +12.440
0.4793 +12.320
0.4827 +12.300
0.4862 +12.170
0.4925 +11.740
0.4959 +11.570
0.4994 +11.380
0.5029 +11.100
0.5064 +10.930
0.5098 +10.800
0.5119 +10.650
0.5140 +10.600
0.5158 +10.510
0.5175 +10.550
0.5195 +10.500
0.5216 +10.470
0.5237 +10.420

0.5258 +10.380
0.5279 +10.400
0.5300 +10.390
0.5320 +10.500
0.5341 +10.470
0.5362 +10.460
0.5383 +10.600
0.5404 +10.550
0.5425 +10.630
0.5445 +10.580
0.5466 +10.680
0.5487 +10.700

2435237 +
0.3417 +11.250
0.3438 +11.120
0.3458 +10.940
0.3486 +10.860
0.3507 +10.850
0.3528 +10.790
0.3549 +10.740
0.3569 +10.660
0.3590 +10.680
0.3611 +10.680
0.3632 +10.700
0.3653 +10.640
0.3674 +10.620
0.3694 +10.640
0.3715 +10.720
0.3736 +10.770
0.3757 +10.720
0.3778 +10.780
0.3799 +10.840
0.3819 +10.850
0.3882 +10.800
0.3903 +10.910
0.3924 +10.890
0.3944 +10.900
0.3965 +10.950
0.3986 +10.950
0.4007 +11.000
0.4028 +10.950

2435240 +
0.4455 +10.520
0.4476 +10.510
0.4497 +10.500

0.4518 +10.470
0.4539 +10.480
0.4560 +10.540
0.4580 +10.560
0.4601 +10.490
0.4622 +10.460
0.4643 +10.500
0.4664 +10.490
0.4685 +10.580
0.4705 +10.680
0.4726 +10.690

2435244 +
0.3404 +12.180
0.3432 +12.190
0.3459 +12.200
0.3487 +12.230
0.3515 +12.240
0.3543 +12.300
0.3598 +12.240
0.3626 +12.180
0.3654 +12.170
0.3682 +12.110
0.3709 +12.040
0.3737 +12.120
0.3765 +12.060
0.3793 +12.000
0.3820 +11.900
0.3848 +11.950
0.3876 +11.880
0.3904 +11.740
0.3932 +11.700
0.3959 +11.570
0.3987 +11.490
0.4015 +11.300
0.4043 +11.150
0.4070 +11.080
0.4098 +11.070
0.4126 +10.980
0.4154 +10.850
0.4182 +10.830
0.4209 +10.800
0.4237 +10.820
0.4265 +10.740
0.4293 +10.810
0.4320 +10.790
0.4348 +10.750

0.4376 +10.740
0.4404 +10.800
0.4432 +10.790
0.4459 +10.780
0.4487 +10.790
0.4515 +10.850
0.4543 +10.830
0.4570 +10.910
0.4598 +10.890
0.4626 +10.930
0.4654 +11.000
0.4682 +11.000
0.4709 +11.100
0.4723 +11.060
0.4751 +11.070
0.4779 +11.030

2435247 +
0.4791 +12.200
0.4819 +12.020
0.4846 +11.750
0.4874 +11.630
0.4902 +11.470
0.4930 +11.380
0.4957 +11.260
0.4985 +11.190
0.5013 +11.050
0.5041 +11.000
0.5069 +11.030
0.5096 +10.920
0.5124 +10.910
0.5152 +10.860
0.5180 +10.810
0.5207 +10.840
0.5235 +10.830
0.5263 +10.900
0.5291 +10.880
0.5319 +10.920
0.5346 +10.930
0.5374 +10.890
0.5402 +10.900
0.5430 +10.900
0.5457 +10.890
0.5485 +10.930
0.5513 +10.950

2435251 +
0.4515 +12.120
0.4543 +12.080
0.4570 +12.050
0.4598 +12.000
0.4626 +11.980
0.4654 +12.000
0.4682 +11.920
0.4709 +11.870
0.4737 +11.820
0.4765 +11.700
0.4793 +11.630
0.4820 +11.600
0.4848 +11.480
0.4876 +11.420
0.4904 +11.270
0.4932 +11.250
0.4959 +11.210
0.4987 +11.200
0.5015 +11.110
0.5043 +11.100
0.5112 +11.040
0.5140 +11.050
0.5168 +11.030
0.5195 +11.020
0.5223 +11.000
0.5251 +10.950
0.5307 +10.970
0.5334 +10.980
0.5362 +10.960
0.5390 +10.990
0.5418 +10.980

2435256 +
0.3593 +12.150
0.3621 +12.000
0.3649 +11.800
0.3677 +11.730
0.3704 +11.700
0.3732 +11.650
0.3816 +11.480
0.3843 +11.370
0.3871 +11.220
0.3899 +11.190
0.3927 +11.010
0.3954 +10.940
0.3982 +10.850
0.4010 +10.920
0.4038 +10.900
0.4072 +10.900
0.4100 +10.890
0.4128 +10.880
0.4156 +10.910

2435267 +
0.4286 +12.260
0.4320 +12.200
0.4355 +12.200
0.4390 +12.180
0.4425 +12.250
0.4459 +12.140
0.4494 +12.200
0.4529 +12.120
0.4564 +12.150
0.4598 +12.050
0.4633 +12.020
0.4668 +11.970
0.4702 +11.880
0.4737 +11.820
0.4772 +11.720
0.4807 +11.530
0.4869 +11.200
0.4897 +11.070
0.4925 +10.860
0.4952 +10.710

2435283 +
0.3935 +11.150
0.3962 +11.030
0.3990 +11.000
0.4018 +10.830
0.4046 +10.900
0.4073 +10.840
0.4101 +10.890
0.4129 +10.900
0.4157 +10.940
0.4185 +11.000
0.4212 +10.980
0.4240 +10.970
0.4268 +11.020
0.4296 +11.060
0.4323 +11.070
0.4351 +11.030
0.4379 +11.060
0.4407 +11.020
0.4435 +11.080
0.4455 +11.090
0.4483 +11.090
0.4511 +11.120
0.4539 +11.110
0.4567 +11.120
0.4594 +11.140
0.4622 +11.170
0.4650 +11.180
0.4678 +11.200
0.4719 +11.290
0.4747 +11.240
0.4775 +11.250
0.4803 +11.270
0.4830 +11.310
0.4858 +11.300

2435290 +
0.4309 +12.250
0.4336 +12.130
0.4364 +12.000
0.4392 +11.970
0.4420 +11.980
0.4447 +11.920
0.4475 +11.900
0.4503 +11.780
0.4531 +11.660
0.4586 +11.330
0.4621 +11.230
0.4649 +11.200
0.4677 +11.100
0.4704 +11.040
0.4732 +11.010
0.4802 +11.020
0.4829 +10.900
0.4857 +10.950
0.4885 +10.960
0.4913 +10.950
0.4941 +10.860
0.4968 +10.920
0.4996 +10.870
0.5024 +10.900
0.5052 +10.950
0.5079 +10.940
0.5107 +10.910
0.5135 +10.980
0.5163 +10.910
0.5191 +10.980
0.5218 +11.100
0.5246 +11.100
0.5274 +11.110
0.5302 +11.200

2435291 +
0.3712 +10.880
0.3740 +10.920
0.3768 +10.920
0.3796 +10.880
0.3823 +10.870
0.3851 +10.880
0.3879 +10.900
0.3907 +10.930
0.3962 +11.100
0.3990 +11.150
0.4018 +11.140
0.4046 +11.180
0.4101 +11.220
0.4157 +11.280

2435299 +
0.3753 +10.700
0.3781 +10.720
0.3809 +10.650
0.3836 +10.700
0.3864 +10.780
0.3892 +10.800
0.3920 +10.740
0.3947 +10.820
0.3975 +10.860
0.4003 +10.910
0.4066 +10.950
0.4093 +10.950
0.4121 +11.030
0.4149 +11.020

2435310 +
0.3737 +12.440
0.3765 +12.480
0.3793 +12.400
0.3820 +12.430
0.3848 +12.430
0.3876 +12.390
0.3904 +12.410

0.3932 +12.350
0.3959 +12.450
0.3987 +12.430
0.4043 +12.300
0.4070 +12.340
0.4098 +12.350
0.4126 +12.260
0.4154 +12.340
0.4182 +12.200
0.4209 +12.070
0.4237 +12.020
0.4265 +12.060
0.4293 +11.940
0.4320 +11.860
0.4348 +11.670
0.4376 +11.570
0.4404 +11.410
0.4432 +11.350
0.4459 +11.120
0.4487 +10.840
0.4515 +10.830
0.4543 +10.670
0.4577 +10.700
0.4605 +10.570
0.4633 +10.600
0.4661 +10.650
0.4716 +10.650
0.4744 +10.710

2435314 +
0.3553 +12.400
0.4289 +11.160
0.4317 +11.010
0.4344 +10.950
0.4372 +10.830
0.4400 +10.790
0.4428 +10.700
0.4455 +10.580
0.4483 +10.570
0.4511 +10.500
0.4539 +10.470
0.4567 +10.590
0.4594 +10.610
0.4622 +10.600
0.4650 +10.600
0.4678 +10.680
0.4705 +10.780
0.4733 +10.830
0.4761 +10.870
0.4789 +10.820

2435318 +
0.3446 +12.330
0.3474 +12.240
0.3502 +12.270
0.3530 +12.240
0.3558 +12.330
0.3585 +12.280
0.3613 +12.300
0.3641 +12.350
0.3669 +12.460
0.3696 +12.500
0.3724 +12.480
0.3752 +12.500
0.3780 +12.460
0.3808 +12.440
0.3835 +12.370
0.3877 +12.250
0.3933 +11.920
0.3960 +11.800
0.3988 +11.620
0.4016 +11.420
0.4044 +11.250
0.4072 +11.110
0.4099 +11.000
0.4127 +10.890
0.4155 +10.780
0.4183 +10.670
0.4210 +10.600
0.4238 +10.580
0.4266 +10.600
0.4294 +10.630
0.4321 +10.660
0.4349 +10.700
0.4377 +10.700
0.4405 +10.750
0.4433 +10.740
0.4460 +10.700
0.4488 +10.780

2435333 +
0.3731 +12.170
0.3759 +12.150
0.3787 +12.190
0.3815 +12.230
0.3842 +12.160
0.3870 +12.200
0.3898 +12.240
0.3926 +12.170
0.3953 +12.150
0.3981 +12.120
0.4009 +12.120
0.4037 +12.020
0.4065 +12.000
0.4092 +11.860
0.4120 +11.900
0.4148 +11.750
0.4176 +11.650
0.4203 +11.570
0.4231 +11.410
0.4259 +11.290
0.4287 +11.210
0.4315 +11.220
0.4342 +11.120
0.4370 +11.110
0.4426 +10.970
0.4453 +11.010
0.4481 +11.040
0.4509 +11.070
0.4537 +11.090
0.4565 +11.070
0.4606 +11.100
0.4648 +11.050
0.4676 +11.060

2435341 +
0.3645 +12.420
0.3666 +12.480
0.3687 +12.330
0.3707 +12.300
0.3749 +12.270
0.3791 +12.300
0.3812 +12.150
0.3843 +12.220
0.3871 +12.160
0.3899 +12.150
0.3927 +12.050
0.3954 +12.030
0.3982 +12.060
0.4010 +12.090
0.4038 +12.110
0.4066 +12.080
0.4093 +12.100
0.4121 +12.090
0.4149 +12.000
0.4177 +11.920
0.4204 +11.900
0.4232 +11.820
0.4260 +11.770
0.4288 +11.680
0.4316 +11.600
0.4343 +11.420
0.4371 +11.360
0.4399 +11.280
0.4427 +11.150
0.4454 +11.000
0.4482 +10.970
0.4510 +10.940
0.4538 +10.860
0.4566 +10.900
0.4600 +10.900
0.4628 +10.930
0.4656 +10.900
0.4684 +10.910
0.4711 +10.950
0.4739 +11.000
0.4767 +11.000
0.4795 +11.020

2435345 +
0.4166 +12.070
0.4194 +11.950
0.4249 +11.770
0.4277 +11.710
0.4305 +11.700
0.4332 +11.570
0.4360 +11.410
0.4388 +11.470
0.4416 +11.270
0.4444 +11.240
0.4471 +11.060
0.4499 +10.980
0.4527 +11.050
0.4555 +10.900
0.4582 +10.910
0.4610 +10.820
0.4638 +10.890
0.4666 +10.820
0.4694 +10.930

2435358 +
0.2825 +11.000
0.2853 +11.000
0.2881 +10.840
0.2909 +10.840
0.2964 +10.790
0.2992 +10.830
0.3020 +10.820
0.3047 +10.820
0.3075 +10.840
0.3103 +10.800
0.3131 +10.840
0.3159 +10.880
0.3187 +10.920
0.3214 +10.980
0.3242 +10.960

2435363 +
0.2769 +11.640
0.2797 +11.760
0.2824 +11.800
0.2852 +11.770
0.2880 +11.820
0.2908 +11.890
0.2936 +11.950
0.2963 +12.040
0.2991 +11.930
0.3019 +12.040
0.3047 +12.060
0.3074 +12.170
0.3102 +12.170
0.3130 +12.150
0.3158 +12.220
0.3186 +12.120
0.3213 +12.170
0.3241 +12.170
0.3269 +12.230
0.3297 +12.160
0.3324 +12.170
0.3352 +12.310

2435373 +
0.2894 +11.030
0.2926 +11.110
0.2953 +10.990
0.2981 +11.050
0.3009 +11.000

0.3037 +10.900
0.3064 +10.910
0.3092 +10.960
0.3120 +10.980
0.3148 +11.020
0.3176 +11.010
0.3203 +10.980
0.3231 +10.950
0.3259 +11.060
0.3287 +11.040
0.3314 +11.110
0.3342 +11.070
0.3370 +11.060
0.3398 +11.080
0.3419 +11.100
0.3446 +11.090
0.3474 +11.140
0.3530 +11.080
0.3557 +11.080
0.3585 +11.170

2435376 +
0.2922 +12.310
0.2949 +12.290
0.2977 +12.240
0.3005 +12.270
0.3033 +12.230
0.3061 +12.270
0.3088 +12.280
0.3116 +12.410
0.3144 +12.350
0.3172 +12.320
0.3199 +12.330
0.3227 +12.400
0.3255 +12.360
0.3283 +12.460
0.3311 +12.440
0.3338 +12.400
0.3366 +12.400
0.3394 +12.360
0.3422 +12.440
0.3463 +12.500
0.3491 +12.390
0.3519 +12.410
0.3547 +12.500

2435377 +
0.2485 +12.370
0.2520 +12.420
0.2555 +12.320
0.2589 +12.340
0.2624 +12.350
0.2659 +12.120
0.2700 +11.900
0.2735 +11.720
0.2792 +11.590
0.2839 +11.350
0.2874 +11.230
0.2916 +11.100
0.2950 +11.020
0.2985 +10.970
0.3020 +10.900
0.3055 +10.930
0.3089 +10.900
0.3131 +10.920
0.3166 +10.880
0.3200 +10.960
0.3235 +10.900
0.3270 +11.000
0.3305 +11.000
0.3339 +11.010

2435393 +
0.2360 +12.300
0.2388 +12.420
0.2416 +12.340
0.2444 +12.280
0.2471 +12.180
0.2499 +12.150
0.2527 +12.120
0.2555 +12.000
0.2582 +11.980
0.2610 +11.920
0.2638 +11.840
0.2666 +11.720
0.2694 +11.650
0.2721 +11.510
0.2749 +11.330
0.2777 +11.250
0.2805 +11.110
0.2832 +11.030
0.2860 +10.810
0.2888 +10.760
0.2916 +10.670
0.2943 +10.580
0.2971 +10.520
0.2999 +10.570
0.3027 +10.550
0.3054 +10.590
0.3082 +10.570
0.3110 +10.540

2435396 +
0.2527 +12.400
0.2555 +12.430
0.2582 +12.410
0.2610 +12.360
0.2638 +12.410
0.2666 +12.370
0.2694 +12.500
0.2721 +12.500
0.2749 +12.500
0.2777 +12.430
0.2805 +12.380
0.2832 +12.350
0.2860 +12.520
0.2888 +12.440
0.2916 +12.400
0.2944 +12.490
0.2971 +12.530
0.2999 +12.490
0.3027 +12.360
0.3055 +12.410
0.3082 +12.420
0.3110 +12.450
0.3138 +12.430
0.3166 +12.490
0.3194 +12.490
0.3221 +12.470
0.3249 +12.390
0.3277 +12.580
0.3305 +12.430
0.3332 +12.510
0.3360 +12.540
0.3388 +12.460
0.3416 +12.530
0.3444 +12.480
0.3471 +12.420
0.3499 +12.450
0.3527 +12.410
0.3582 +12.200
0.3610 +12.060
0.3638 +11.890
0.3666 +11.690
0.3694 +11.550
0.3721 +11.420
0.3749 +11.250
0.3777 +11.170
0.3805 +11.030
0.3832 +10.940
0.3860 +10.860
0.3888 +10.720
0.3916 +10.670
0.3944 +10.640

2435404 +
0.2848 +12.340
0.2876 +12.290
0.2904 +12.260
0.2932 +12.190
0.2959 +12.220
0.3633 +10.780
0.3661 +10.840
0.3689 +10.940
0.3716 +10.960
0.3744 +10.970
0.3772 +10.980
0.3800 +11.010
0.3827 +11.050
0.3855 +11.080

2435408 +
0.2360 +12.280
0.2444 +12.390
0.2471 +12.340
0.2499 +12.310
0.2527 +12.250
0.2555 +12.400
0.2582 +12.230
0.2610 +12.300
0.2638 +12.250
0.2666 +12.220
0.2721 +12.180
0.2784 +12.050
0.2812 +11.860
0.2839 +11.860
0.2867 +11.790
0.2895 +11.640
0.2964 +11.610
0.2992 +11.600
0.3020 +11.580
0.3048 +11.580
0.3075 +11.560
0.3131 +11.540
0.3159 +11.450
0.3187 +11.490
0.3207 +11.500
0.3235 +11.400
0.3263 +11.420
0.3291 +11.480
0.3319 +11.460
0.3346 +11.390

2435601 +
0.4486 +11.610
0.4514 +11.230
0.4542 +11.020
0.4569 +10.850
0.4597 +10.800
0.4625 +10.580
0.4653 +10.430
0.4681 +10.350
0.4708 +10.320
0.4736 +10.430
0.4764 +10.360
0.4792 +10.300
0.4819 +10.280
0.4847 +10.370
0.4875 +10.420
0.4903 +10.500
0.4931 +10.540
0.4958 +10.520
0.4986 +10.540
0.5014 +10.630
0.5042 +10.580
0.5069 +10.630
0.5097 +10.710
0.5125 +10.730
0.5153 +10.800
0.5181 +10.900
0.5208 +10.890

2435749 +
0.3056 +12.270

0.3083 +12.200
0.3111 +12.170
0.3139 +12.090
0.3167 +12.060
0.3194 +12.000
0.3222 +11.920
0.3250 +11.960
0.3278 +11.800
0.3333 +11.700
0.3361 +11.550
0.3389 +11.520
0.3417 +11.390
0.3444 +11.400
0.3472 +11.320
0.3500 +11.140
0.3528 +11.140
0.3556 +11.090
0.3583 +10.970
0.3611 +10.980
0.3639 +10.920
0.3667 +10.970
0.3694 +10.920
0.3722 +10.860
0.3764 +10.910
0.3806 +10.900
0.3833 +10.870
0.3861 +10.910
0.3889 +10.950

2435934 +
0.4218 +12.400
0.4253 +12.410
0.4281 +12.370
0.4309 +12.300
0.4336 +12.310
0.4364 +12.330
0.4392 +12.370
0.4433 +12.340
0.4475 +12.400
0.4503 +12.330
0.4531 +12.310
0.4559 +12.300
0.4586 +12.430
0.4614 +12.360
0.4642 +12.300
0.4670 +12.300
0.4697 +12.290
0.4725 +12.330
0.4753 +12.380
0.4781 +12.480
0.4809 +12.470
0.4836 +12.400
0.4864 +12.470
0.4892 +12.390
0.4920 +12.410
0.4947 +12.400
0.4975 +12.470
0.5003 +12.350
0.5031 +12.400
0.5059 +12.510
0.5094 +12.360
0.5122 +12.100
0.5178 +11.850
0.5205 +11.830
0.5233 +11.810
0.5261 +11.600
0.5289 +11.510
0.5317 +11.260
0.5344 +11.130
0.5372 +11.100
0.5400 +11.020
0.5428 +10.890
0.5455 +10.820
0.5483 +10.690
0.5511 +10.670
0.5539 +10.620
0.5567 +10.610
0.5594 +10.600
0.5622 +10.610
0.5650 +10.610
0.5678 +10.660
0.5705 +10.720
0.5733 +10.790
0.5761 +10.790
0.5789 +10.820
0.5817 +10.790
0.5844 +10.810

2435938 +
0.4647 +12.330
0.4668 +12.330
0.4689 +12.380
0.4709 +12.480
0.4765 +12.420
0.4786 +12.460
0.4807 +12.470
0.4827 +12.510
0.4848 +12.530
0.4876 +12.300
0.4897 +12.270
0.4918 +12.120

2435947 +
0.3154 +12.280
0.3182 +12.160
0.3209 +12.130
0.3237 +12.020
0.3265 +11.910
0.3293 +11.720
0.3320 +11.640
0.3348 +11.500
0.3376 +11.310
0.3404 +11.130
0.3432 +10.980
0.3515 +10.830
0.3543 +10.850
0.3564 +10.780
0.3591 +10.750
0.3619 +10.710
0.3647 +10.780
0.3675 +10.750
0.3702 +10.800
0.3730 +10.740
0.3758 +10.800
0.3786 +10.760
0.3814 +10.840
0.3841 +10.860
0.3869 +10.830
0.3897 +10.870
0.3932 +10.880
0.3959 +10.930
0.3987 +10.880
0.4015 +10.920
0.4043 +11.020
0.4070 +10.970
0.4098 +11.020
0.4126 +11.100
0.4293 +11.220
0.4320 +11.290
0.4348 +11.280
0.4376 +11.300
0.4404 +11.410
0.4432 +11.380
0.4466 +11.450
0.4494 +11.480
0.4522 +11.450
0.4550 +11.510
0.4577 +11.540
0.4605 +11.650

2435982 +
0.3447 +12.000
0.3475 +11.840
0.3503 +11.730
0.3531 +11.680
0.3559 +11.530
0.3586 +11.410
0.3614 +11.180
0.3642 +11.030
0.3670 +10.930
0.3697 +10.850
0.3725 +10.780
0.3753 +10.730
0.3781 +10.670
0.3809 +10.680
0.3836 +10.680
0.3864 +10.720
0.3892 +10.680
0.3920 +10.730
0.3947 +10.740
0.3975 +10.810
0.4003 +10.870
0.4031 +10.900
0.4059 +10.990
0.4086 +11.000
0.4114 +11.080
0.4142 +11.030

2435988 +
0.4649 +12.200
0.4677 +12.260
0.4704 +12.240
0.4732 +12.300
0.4760 +12.320
0.4788 +12.230
0.4816 +12.290
0.4843 +12.230
0.4871 +12.280
0.4899 +12.300
0.4927 +12.350
0.4954 +12.300
0.4982 +12.350
0.5010 +12.240
0.5038 +12.300
0.5066 +12.290
0.5093 +12.180
0.5121 +12.050
0.5149 +12.120
0.5177 +11.930
0.5204 +11.770
0.5232 +11.730
0.5260 +11.610
0.5288 +11.390
0.5316 +11.370
0.5343 +11.230
0.5399 +11.010
0.5427 +10.970
0.5454 +10.840
0.5482 +10.960

2435989 +
0.3739 +12.280
0.3767 +12.340
0.3795 +12.370
0.3857 +12.230
0.3885 +12.240
0.3913 +12.360
0.3941 +12.190
0.3968 +12.190
0.3996 +12.020
0.4024 +11.810
0.4072 +11.630
0.4100 +11.620
0.4128 +11.510
0.4156 +11.350
0.4184 +11.330
0.4211 +11.140
0.4267 +11.050
0.4295 +11.000
0.4322 +11.020
0.4350 +10.870
0.4378 +10.870
0.4406 +10.790
0.4434 +10.830
0.4461 +10.800

0.4489 +10.820
0.4628 +10.820
0.4656 +10.810
0.4684 +10.880
0.4711 +10.900
0.4739 +11.010
0.4767 +11.070
0.4795 +11.100

2435992 +
0.4581 +12.420
0.4609 +12.160
0.4637 +12.270
0.4665 +12.410
0.4693 +12.350
0.4720 +12.390
0.4748 +12.370
0.4776 +12.230
0.4804 +12.400
0.4831 +12.250
0.4859 +12.240
0.4887 +12.150
0.4922 +12.040
0.4956 +11.900
0.4984 +11.810
0.5040 +11.600
0.5068 +11.530
0.5123 +11.210
0.5151 +11.160
0.5179 +11.080
0.5206 +11.050
0.5234 +10.890
0.5262 +10.860
0.5290 +10.950
0.5318 +11.000
0.5345 +11.020
0.5373 +11.020
0.5401 +10.920
0.5429 +10.870

2436000 +
0.4399 +12.320
0.4427 +12.340
0.4468 +12.400
0.4559 +12.350
0.4600 +12.260
0.4628 +12.240

0.4663 +12.260
0.4691 +12.240
0.4732 +12.100
0.4760 +12.040
0.4871 +11.660
0.4899 +11.630
0.4935 +11.520
0.4962 +11.400
0.5024 +11.100
0.5060 +11.120

2436004 +
0.4350 +12.230
0.4378 +12.260
0.4406 +12.230
0.4468 +12.250
0.4496 +12.200
0.4524 +12.280
0.4593 +12.190
0.4621 +12.120
0.4649 +12.080
0.4718 +12.000
0.4774 +11.980
0.4829 +11.770
0.4857 +11.720
0.4885 +11.620
0.4934 +11.500
0.4961 +11.400
0.4989 +11.320
0.5038 +11.110
0.5066 +11.080
0.5093 +10.920
0.5149 +10.920
0.5177 +10.800

2436005 +
0.3634 +12.110
0.3662 +12.120
0.3690 +11.960
0.3717 +11.860
0.3759 +11.690
0.3787 +11.680
0.3815 +11.490
0.3877 +11.270
0.3905 +11.170
0.3933 +11.100
0.3960 +10.940

0.3995 +10.940
0.4023 +10.960
0.4051 +10.930
0.4078 +10.890
0.4120 +10.890
0.4148 +10.850
0.4176 +10.870

2436012 +
0.4263 +12.200
0.4291 +12.200
0.4319 +12.290
0.4346 +12.220
0.4374 +12.310
0.4402 +12.440
0.4430 +12.390
0.4464 +12.370
0.4492 +12.300
0.4520 +12.280
0.4548 +12.310
0.4575 +12.300
0.4603 +12.290
0.4631 +12.230
0.4659 +12.070
0.4687 +12.020
0.4770 +11.870
0.4798 +11.790
0.4825 +11.690
0.4853 +11.490
0.4881 +11.260
0.4909 +11.130
0.4937 +11.010
0.4964 +10.840
0.4992 +10.700

2436020 +
0.4118 +12.290
0.4146 +12.330
0.4174 +12.430
0.4201 +12.460
0.4229 +12.350
0.4264 +12.460
0.4292 +12.350
0.4319 +12.260
0.4354 +12.170
0.4382 +12.030
0.4410 +11.850

0.4438 +11.780
0.4500 +11.480
0.4528 +11.350
0.4556 +11.000
0.4611 +10.670
0.4639 +10.340
0.4667 +10.240
0.4701 +10.320

2436023 +
0.4659 +12.390
0.4687 +12.400
0.4714 +12.400
0.4742 +12.360
0.4770 +12.480
0.4798 +12.390
0.4825 +12.480
0.4853 +12.390
0.4881 +12.340
0.4909 +12.460
0.4937 +12.400
0.4971 +12.340
0.4999 +12.300
0.5027 +12.360
0.5055 +12.360
0.5082 +12.420
0.5110 +12.470
0.5138 +12.360
0.5166 +12.360
0.5194 +12.300
0.5221 +12.280
0.5249 +12.300
0.5277 +12.190
0.5305 +12.110
0.5332 +11.990
0.5360 +11.790
0.5388 +11.790
0.5416 +11.660

2436051 +
0.3592 +12.280
0.3620 +12.230
0.3648 +12.360
0.3676 +12.130
0.3703 +12.130
0.3731 +12.180
0.3759 +12.240

0.3787 +12.240
0.3815 +12.190
0.3849 +12.270
0.3877 +12.230
0.3905 +12.200
0.3933 +12.300
0.3961 +12.270
0.3988 +12.290
0.4023 +12.250
0.4051 +12.310
0.4078 +12.270
0.4106 +12.370
0.4134 +12.290
0.4162 +12.270
0.4190 +12.320
0.4217 +12.280
0.4245 +12.370
0.4273 +12.260
0.4301 +12.320
0.4328 +12.350
0.4357 +12.290
0.4384 +12.280
0.4412 +12.240
0.4440 +12.350
0.4467 +12.170

2436054 +
0.3556 +12.180
0.3590 +12.100
0.3618 +12.230
0.3833 +12.130
0.3896 +12.180
0.3924 +12.120
0.3951 +12.290

2436066 +
0.4350 +12.290
0.4378 +12.340
0.4406 +12.390
0.4434 +12.340
0.4461 +12.330
0.4489 +12.250
0.4524 +12.390
0.4560 +12.360
0.4586 +12.290
0.4614 +12.350
0.4642 +12.400

0.4670 +12.460
0.4697 +12.320
0.4725 +12.470
0.4753 +12.410
0.4788 +12.320
0.4816 +12.350
0.4843 +12.350
0.4871 +12.500
0.4899 +12.430
0.4927 +12.430
0.4954 +12.190
0.4989 +11.980
0.5017 +11.800
0.5045 +11.590
0.5072 +11.430
0.5100 +11.300
0.5128 +11.240
0.5156 +11.080
0.5184 +10.800
0.5232 +10.710
0.5260 +10.530
0.5288 +10.510
0.5316 +10.540
0.5343 +10.520
0.5371 +10.560
0.5441 +10.690
0.5468 +10.670
0.5496 +10.760
0.5524 +10.760
0.5552 +10.780
0.5579 +10.820
0.5614 +10.980
0.5642 +11.030
0.5670 +11.120
0.5725 +11.080
0.5753 +11.150

2436074 +
0.4036 +12.400
0.4064 +12.320
0.4091 +12.280
0.4121 +12.340
0.4147 +12.280
0.4175 +12.380
0.4202 +12.330
0.4230 +12.270
0.4258 +12.300

0.4286 +12.330
0.4314 +12.210
0.4341 +12.160
0.4369 +11.990
0.4397 +11.900
0.4425 +11.780
0.4459 +11.610
0.4487 +11.520
0.4515 +11.310
0.4543 +11.090
0.4570 +11.070
0.4598 +10.980
0.4626 +10.940
0.4654 +10.930
0.4682 +10.900
0.4709 +10.830
0.4737 +10.860
0.4765 +10.880
0.4793 +10.850
0.4820 +10.860
0.4848 +10.910
0.4883 +10.890
0.4911 +10.940
0.4939 +11.020
0.4966 +11.050
0.5001 +11.080

2436087 +
0.2836 +12.130
0.2864 +12.180
0.2892 +12.280
0.2920 +12.180
0.2982 +12.090
0.3010 +12.080
0.3038 +12.170
0.3066 +12.180
0.3246 +11.400
0.3274 +11.260
0.3302 +11.100
0.3329 +11.060
0.3371 +10.870
0.3399 +10.940
0.3427 +10.800
0.3447 +10.780
0.3496 +10.760
0.3524 +10.730
0.3552 +10.800

0.3579 +10.830
0.3621 +10.880
0.3649 +10.920
0.3677 +10.920
0.3704 +10.910
0.3746 +11.020
0.3774 +11.020
0.3829 +11.130
0.3871 +11.090
0.3954 +11.100
0.3982 +11.230

2436098 +
0.3214 +12.350
0.3242 +12.350
0.3270 +12.500
0.3298 +12.380
0.3325 +12.460
0.3353 +12.460
0.3381 +12.420
0.3409 +12.420
0.3437 +12.440
0.3464 +12.340
0.3499 +12.420
0.3527 +12.480
0.3555 +12.430
0.3582 +12.490
0.3617 +12.420
0.3645 +12.420
0.3673 +12.320
0.3700 +12.420
0.3728 +12.420
0.3756 +12.430
0.3784 +12.480
0.3812 +12.440
0.3839 +12.420
0.3867 +12.340
0.3895 +12.260
0.3936 +12.320
0.3978 +12.220
0.4006 +12.120
0.4034 +12.030
0.4062 +11.620
0.4096 +11.300
0.4124 +11.280
0.4152 +11.120
0.4180 +10.930

0.4207 +10.700
0.4235 +10.650
0.4263 +10.520
0.4291 +10.500
0.4319 +10.410
0.4346 +10.440
0.4374 +10.390
0.4402 +10.470
0.4430 +10.500
0.4457 +10.530
0.4485 +10.650
0.4513 +10.680
0.4541 +10.640
0.4569 +10.750

2436102 +
0.2611 +12.530
0.2639 +12.580
0.2667 +12.440
0.2694 +12.450
0.2722 +12.560
0.2750 +12.500
0.2778 +12.570
0.2806 +12.550
0.2833 +12.430
0.2861 +12.500
0.2889 +12.530
0.2917 +12.430
0.2944 +12.560
0.2972 +12.500
0.3000 +12.600
0.3028 +12.450
0.3056 +12.610
0.3083 +12.450
0.3111 +12.500
0.3139 +12.500
0.3167 +12.500
0.3194 +12.440
0.3222 +12.430
0.3250 +12.550
0.3278 +12.560
0.3306 +12.550
0.3333 +12.610
0.3361 +12.420
0.3389 +12.560
0.3417 +12.520
0.3444 +12.440

0.3472 +12.560
0.3500 +12.450
0.3542 +12.490
0.3569 +12.540
0.3597 +12.550
0.3625 +12.420
0.3653 +12.490
0.3681 +12.570
0.3708 +12.570
0.3736 +12.460
0.3764 +12.610
0.3792 +12.390
0.3819 +12.060
0.3847 +11.900
0.3875 +11.620
0.3903 +11.450
0.3931 +11.420
0.3951 +11.300
0.3979 +11.140
0.4007 +10.920
0.4035 +10.700
0.4063 +10.610
0.4090 +10.530
0.4118 +10.500
0.4146 +10.510
0.4174 +10.410
0.4201 +10.460
0.4229 +10.400
0.4257 +10.450
0.4285 +10.480
0.4313 +10.480
0.4340 +10.540
0.4368 +10.520

2436115 +
0.2350 +10.650
0.2378 +10.780
0.2406 +10.800
0.2447 +10.910
0.2475 +10.890
0.2503 +10.930
0.2545 +10.920
0.2572 +10.890
0.2611 +10.960
0.2656 +11.040
0.2684 +11.060
0.2715 +11.000

0.2760 +11.010
0.2788 +11.030
0.2816 +11.190
0.2871 +11.160
0.2899 +11.260
0.2941 +11.250
0.2968 +11.370

2436118 +
0.2911 +11.600
0.2932 +11.460
0.2952 +11.430
0.2994 +11.320
0.3015 +11.330
0.3036 +11.350
0.3070 +11.260
0.3091 +11.140
0.3113 +11.090
0.3147 +11.080
0.3168 +11.000
0.3189 +10.950
0.3223 +10.970
0.3244 +10.970
0.3265 +10.910
0.3300 +10.900
0.3320 +10.930
0.3341 +10.870
0.3376 +10.870

0.3397 +10.950
0.3418 +10.970
0.3452 +11.010
0.3473 +11.050
0.3494 +11.050
0.3529 +11.050
0.3550 +11.090
0.3570 +11.130
0.3612 +11.200
0.3633 +11.160
0.3654 +11.130
0.3689 +11.150
0.3709 +11.210
0.3730 +11.160
0.3765 +11.300
0.3786 +11.300
0.3841 +11.240
0.3862 +11.210

2436129 +
0.4087 +11.540
0.4115 +11.490
0.4142 +11.410
0.4170 +11.370
0.4198 +11.250
0.4226 +11.280
0.4253 +11.280
0.4281 +11.260

0.4309 +11.210
0.4337 +11.220
0.4365 +11.220
0.4392 +11.130
0.4420 +11.180
0.4448 +11.210
0.4476 +11.140
0.4503 +11.180
0.4531 +11.130
0.4559 +11.220

2436137 +
0.2813 +12.290
0.2840 +12.240
0.2882 +12.290
0.2910 +12.310
0.2938 +12.370
0.2965 +12.290
0.2993 +12.290
0.3021 +12.270
0.3049 +12.290
0.3076 +12.310
0.3104 +12.290
0.3132 +12.190
0.3160 +12.200
0.3188 +12.240
0.3216 +12.200
0.3243 +12.360

0.3271 +12.320
0.3299 +12.280
0.3326 +12.330
0.3354 +12.270
0.3382 +12.240
0.3410 +12.360
0.3438 +12.210
0.3465 +12.380
0.3493 +12.290
0.3521 +12.370
0.3549 +12.200
0.3576 +12.220
0.3604 +12.270
0.3632 +12.220
0.3660 +12.340
0.3688 +12.280
0.3715 +12.320
0.3743 +12.190
0.3771 +12.150
0.3799 +12.050
0.3826 +11.850
0.3854 +11.710
0.3882 +11.670
0.3910 +11.560
0.3938 +11.440
0.3965 +11.260
0.3993 +10.980
0.4021 +10.810

0.4049 +10.700
0.4076 +10.720
0.4104 +10.700
0.4132 +10.720
0.4160 +10.760

2436165 +
0.2125 +12.250
0.2153 +12.390
0.2181 +12.270
0.2208 +12.280
0.2236 +12.280
0.2264 +12.430
0.2292 +12.360
0.2319 +12.260
0.2347 +12.070
0.2403 +11.760
0.2431 +11.620
0.2458 +11.610
0.2486 +11.520
0.2514 +11.320
0.2542 +11.300
0.2569 +11.270
0.2597 +11.140
0.2625 +11.160
0.2653 +11.130
0.2681 +11.030
0.2708 +11.070

Table 3. Photoelectric differential observations of RW Dra without filter

2435032 +
0.2385 +0.201
0.2408 +0.179
0.2428 +0.110
0.2450 −0.027
0.2462 −0.048
0.2487 −0.139
0.2494 −0.181
0.2520 −0.342
0.2529 −0.385
0.2539 −0.429
0.2548 −0.479
0.2558 −0.531
0.2578 −0.640
0.2588 −0.704
0.2597 −0.762

0.2608 −0.787
0.2616 −0.813
0.2688 −0.975
0.2702 −1.024
0.2714 −0.992
0.2723 −1.001
0.2747 −1.026
0.2756 −1.035
0.2766 −1.045
0.2776 −1.031
0.2784 −1.034
0.2792 −1.035
0.2816 −1.051
0.2825 −1.024
0.2836 −1.029
0.2847 −1.024

0.2858 −1.038
0.2863 −1.017
0.2893 −0.976
0.2905 −0.964
0.2915 −0.969
0.2925 −0.924
0.2934 −0.909
0.2940 −0.922
0.2981 −0.881
0.2993 −0.861
0.3002 −0.853
0.3065 −0.787
0.3077 −0.782
0.3098 −0.743
0.3105 −0.756
0.3130 −0.717

0.3140 −0.731
0.3147 −0.726
0.3156 −0.693
0.3173 −0.670

2435237 +
0.3518 −1.145
0.3525 −1.162
0.3534 −1.205
0.3543 −1.252
0.3548 −1.246
0.3570 −1.285
0.3579 −1.295
0.3587 −1.302
0.3597 −1.303
0.3607 −1.292

0.3632 −1.279
0.3640 −1.300
0.3648 −1.285
0.3658 −1.293
0.3664 −1.290
0.3686 −1.257
0.3697 −1.232
0.3706 −1.219
0.3715 −1.213
0.3722 −1.223
0.3813 −1.119
0.3829 −1.101
0.3847 −1.089
0.3885 −1.036
0.3895 −1.014
0.3906 −1.009

0.3916 −0.988
0.3922 −0.998

2435694 +
0.3622 +0.278
0.3632 +0.265
0.3653 +0.272
0.3661 +0.256
0.3688 +0.258
0.3698 +0.272
0.3709 +0.247
0.3718 +0.276
0.3728 +0.256
0.3738 +0.282
0.3763 +0.262
0.3771 +0.277
0.3779 +0.266
0.3809 +0.264
0.3841 +0.264
0.3852 +0.290
0.3872 +0.291
0.3880 +0.277
0.3888 +0.294
0.3924 +0.318
0.3934 +0.311
0.3944 +0.314
0.3953 +0.325
0.3963 +0.337
0.3992 +0.350
0.4012 +0.361
0.4034 +0.348
0.4073 +0.323
0.4085 +0.331
0.4095 +0.353
0.4112 +0.338
0.4146 +0.305
0.4157 +0.318
0.4168 +0.281
0.4177 +0.278
0.4186 +0.266
0.4194 +0.279
0.4217 +0.263
0.4225 +0.269
0.4233 +0.214
0.4240 +0.212
0.4256 +0.156
0.4277 +0.144

0.4287 +0.113
0.4295 +0.095
0.4302 +0.042
0.4310 +0.049
0.4318 +0.013
0.4351 −0.110
0.4359 −0.128
0.4380 −0.197
0.4389 −0.216
0.4398 −0.236
0.4407 −0.278
0.4429 −0.385
0.4438 −0.440
0.4446 −0.472
0.4457 −0.520
0.4470 −0.587
0.4478 −0.610
0.4509 −0.727
0.4518 −0.760
0.4526 −0.818
0.4534 −0.811
0.4544 −0.825
0.4552 −0.887
0.4575 −0.919
0.4587 −0.918
0.4602 −0.919
0.4617 −0.930
0.4625 −0.940
0.4649 −0.949
0.4658 −0.956
0.4668 −0.949
0.4677 −0.946
0.4686 −0.951
0.4733 −0.942
0.4743 −0.915
0.4752 −0.928
0.4763 −0.931
0.4773 −0.937
0.4784 −0.901
0.4810 −0.898
0.4819 −0.860
0.4827 −0.853
0.4836 −0.889
0.4853 −0.867
0.4890 −0.826
0.4899 −0.808
0.4908 −0.801

0.4918 −0.791
0.4926 −0.798
0.4968 −0.728

2435695 +
0.3269 −0.527
0.3277 −0.532
0.3286 −0.578
0.3295 −0.630
0.3334 −0.753
0.3345 −0.807
0.3354 −0.822
0.3364 −0.837
0.3374 −0.859
0.3383 −0.907
0.3408 −0.937
0.3417 −0.935
0.3425 −0.966
0.3435 −0.952
0.3444 −0.963
0.3454 −0.952
0.3478 −0.951
0.3491 −0.965
0.3501 −0.947
0.3510 −0.954
0.3527 −0.956
0.3560 −0.929
0.3568 −0.934
0.3577 −0.912
0.3586 −0.908
0.3596 −0.916
0.3609 −0.900
0.3636 −0.876
0.3645 −0.871
0.3666 −0.850
0.3676 −0.846
0.3694 −0.851

2435706 +
0.3408 +0.290
0.3428 +0.305
0.3459 +0.257
0.3479 +0.228
0.3496 +0.199
0.3529 +0.135
0.3554 +0.093
0.3578 +0.059

0.3586 +0.018
0.3593 −0.003
0.3602 −0.008
0.3611 −0.081
0.3648 −0.214
0.3660 −0.256
0.3681 −0.340
0.3707 −0.378
0.3716 −0.394
0.3725 −0.405
0.3737 −0.421
0.3748 −0.438
0.3775 −0.494
0.3786 −0.535
0.3796 −0.514
0.3805 −0.562
0.3817 −0.553
0.3847 −0.601
0.3863 −0.612
0.3876 −0.616
0.3897 −0.624
0.3932 −0.660
0.3943 −0.672
0.3956 −0.679
0.3967 −0.660
0.3978 −0.685
0.4045 −0.637
0.4054 −0.646
0.4067 −0.614
0.4077 −0.608
0.4125 −0.609
0.4136 −0.607

2435726 +
0.2970 +0.449
0.2987 +0.438
0.2999 +0.449
0.3009 +0.460
0.3019 +0.448
0.3071 +0.480
0.3082 +0.488
0.3091 +0.503
0.3100 +0.480
0.3109 +0.481
0.3141 +0.463
0.3162 +0.467
0.3173 +0.493

0.3181 +0.487
0.3212 +0.452
0.3220 +0.452
0.3230 +0.441
0.3241 +0.436
0.3259 +0.411
0.3293 +0.379
0.3303 +0.370
0.3313 +0.347
0.3334 +0.309
0.3350 +0.267
0.3388 +0.185
0.3398 +0.155
0.3409 +0.120
0.3419 +0.074
0.3431 +0.065
0.3442 +0.018
0.3478 −0.149
0.3490 −0.184
0.3502 −0.257
0.3513 −0.292
0.3525 −0.363
0.3537 −0.449
0.3568 −0.580
0.3579 −0.616
0.3591 −0.692
0.3602 −0.726
0.3612 −0.768
0.3623 −0.802
0.3659 −0.942
0.3669 −0.960
0.3679 −1.005
0.3690 −1.010
0.3700 −1.037
0.3712 −1.074
0.3746 −1.108
0.3757 −1.128
0.3768 −1.115
0.3780 −1.125
0.3794 −1.146
0.3807 −1.144
0.3854 −1.111
0.3873 −1.103
0.3887 −1.083
0.3900 −1.091
0.3913 −1.076
0.3951 −1.014

0.3962 −0.986 0.4208 −0.721 0.2753 −0.158 0.2988 −0.972 2435742 +
0.3973 −0.984 0.4221 −0.710 0.2783 −0.272 0.3019 −0.988 0.3008 −0.844
0.3984 −0.956 0.4260 −0.670 0.2792 −0.330 0.3029 −1.006 0.3019 −0.832
0.3997 −0.957 0.4274 −0.649 0.2805 −0.361 0.3042 −1.005 0.3032 −0.816
0.4012 −0.930 0.4285 −0.620 0.2818 −0.440 0.3056 −1.010 0.3043 −0.801
0.4051 −0.884 0.4296 −0.602 0.2828 −0.493 0.3067 −1.005 0.3054 −0.803
0.4062 −0.868 0.4306 −0.596 0.2860 −0.633 0.3107 −0.992 0.3083 −0.783
0.4073 −0.853 0.4318 −0.607 0.2872 −0.677 0.3119 −0.997 0.3094 −0.778
0.4088 −0.832 0.4354 −0.566 0.2884 −0.778 0.3130 −0.997 0.3106 −0.766
0.4100 −0.818 0.4374 −0.538 0.2894 −0.812 0.3141 −0.990 0.3120 −0.748
0.4110 −0.827 0.2904 −0.837 0.3152 −0.987 0.3129 −0.729
0.4160 −0.752 2435738 + 0.2942 −0.937 0.3190 −0.981 0.3155 −0.713
0.4173 −0.748 0.2711 +0.057 0.2952 −0.933 0.3201 −0.974
0.4184 −0.717 0.2721 −0.010 0.2963 −0.962 0.3212 −0.946
0.4195 −0.725 0.2731 −0.014 0.2974 −0.953 0.3223 −0.935

Table 4. Photoelectric differential U observations of RW Dra

2438267 + 0.3475 +0.374 0.4114 −0.872 0.4761 −0.954 0.2622 −0.927
0.3725 +0.402 0.3537 +0.063 0.4134 −0.826 0.4782 −1.016 0.2657 −0.886
0.3794 +0.259 0.3593 −0.240 0.4176 −0.764 0.4844 −1.101 0.2733 −0.829
0.3884 +0.036 0.3607 −0.349 0.4197 −0.761 0.4886 −1.122 0.2761 −0.819
0.3964 −0.423 0.3683 −0.943 0.4941 −1.109 0.2830 −0.781
0.4055 −0.818 0.3745 −1.245 2438965 + 0.2865 −0.743
0.4162 −1.151 0.3766 −1.239 0.4379 +0.241 2439056 + 0.2962 −0.641
0.4263 −1.189 0.3850 −1.179 0.4441 +0.108 0.2268 −0.460 0.3032 −0.555
0.4367 −1.024 0.3870 −1.194 0.4518 −0.110 0.2309 −0.729 0.3073 −0.532
0.4457 −0.891 0.3891 −1.193 0.4538 −0.181 0.2379 −0.905 0.3129 −0.527
0.4565 −0.778 0.3961 −1.089 0.4594 −0.423 0.2448 −1.014 0.3164 −0.495
0.3982 −1.039 0.4622 −0.563 0.2476 −1.046 0.3226 −0.448
2438636 + 0.4030 −0.977 0.4670 −0.714 0.2525 −1.068 0.3247 −0.433
0.3412 +0.358 0.4058 −0.936 0.4698 −0.801 0.2552 −1.058 0.3282 −0.383

Table 5. Photoelectric differential B observations of RW Dra

2436318 + 0.5540 −1.095 0.4313 +0.306 0.4816 −0.916 2436373 +
0.4980 +0.513 0.5574 −1.062 0.4337 +0.301 0.4847 −0.959 0.4096 +0.151
0.5008 +0.489 0.5651 −0.998 0.4389 +0.249 0.4877 −0.974 0.4125 +0.109
0.5028 +0.437 0.5686 −0.981 0.4415 +0.202 0.4926 −0.985 0.4161 +0.053
0.5090 +0.242 0.5734 −0.938 0.4439 +0.166 0.4956 −0.995 0.4218 −0.071
0.5151 +0.034 0.5790 −0.895 0.4488 +0.102 0.4982 −0.982 0.4249 −0.139
0.5220 −0.388 0.5824 −0.865 0.4539 +0.002 0.5031 −0.976 0.4280 −0.212
0.5255 −0.630 0.4591 −0.128 0.5058 −0.951 0.4395 −0.516
0.5297 −0.821 2436338 + 0.4617 −0.216 0.5085 −0.941 0.4430 −0.612
0.5373 −1.115 0.4189 +0.382 0.4647 −0.316 0.5135 −0.923 0.4506 −0.814
0.5401 −1.152 0.4216 +0.366 0.4702 −0.514 0.5160 −0.908 0.4555 −0.864
0.5443 −1.156 0.4243 +0.347 0.4732 −0.633 0.5195 −0.881 0.4623 −0.862
0.5512 −1.114 0.4291 +0.328 0.4761 −0.749 0.4687 −0.830

0.4728 −0.807
0.4770 −0.793
0.4839 −0.792
0.4877 −0.761
0.4909 −0.746
0.4968 −0.686
0.4999 −0.650
0.5037 −0.617
0.5093 −0.598
0.5138 −0.582
0.5173 −0.559

2436400 +
0.4304 +0.436
0.4338 +0.443
0.4403 +0.425
0.4431 +0.428
0.4466 +0.412
0.4528 +0.355
0.4593 +0.254
0.4656 −0.098
0.4685 −0.273
0.4712 −0.446
0.4768 −0.804
0.4792 −0.914
0.4811 −0.998
0.4852 −1.128
0.4872 −1.184
0.4900 −1.234
0.4952 −1.245
0.5004 −1.194
0.5067 −1.113
0.5094 −1.076
0.5122 −1.033
0.5178 −0.973
0.5205 −0.954
0.5233 −0.936
0.5289 −0.879
0.5317 −0.856
0.5400 −0.773
0.5428 −0.742
0.5455 −0.717
0.5483 −0.686

2436404 +
0.3908 +0.338
0.3935 +0.345
0.4038 +0.365
0.4071 +0.363
0.4096 +0.336
0.4152 +0.281
0.4180 +0.268
0.4207 +0.248
0.4263 +0.173
0.4291 +0.103
0.4318 +0.028
0.4416 −0.428
0.4437 −0.507
0.4482 −0.664
0.4502 −0.724
0.4523 −0.796
0.4568 −0.944
0.4600 −0.990
0.4624 −1.007
0.4680 −1.045
0.4707 −1.059
0.4735 −1.049
0.4791 −1.033
0.4818 −0.995
0.4846 −0.959
0.4943 −0.899
0.4971 −0.852
0.5027 −0.792
0.5055 −0.769

2436408 +
0.3963 +0.287
0.4018 +0.189
0.4068 +0.067
0.4093 −0.050
0.4116 −0.159
0.4171 −0.421
0.4196 −0.523
0.4224 −0.634
0.4282 −0.784
0.4307 −0.827
0.4400 −0.927
0.4428 −0.947
0.4459 −0.957
0.4520 −0.953
0.4551 −0.929
0.4576 −0.894
0.4622 −0.870
0.4651 −0.868
0.4679 −0.862
0.4744 −0.849
0.4802 −0.818
0.4896 −0.739
0.4918 −0.718

2436420 +
0.3838 +0.142
0.3890 +0.055
0.3941 −0.047
0.3962 −0.105
0.3988 −0.159
0.4040 −0.282
0.4065 −0.350
0.4108 −0.440
0.4153 −0.552
0.4177 −0.600
0.4198 −0.659
0.4241 −0.745
0.4268 −0.807

2436431 +
0.3886 +0.381
0.3914 +0.392
0.3942 +0.395
0.4025 +0.394
0.4053 +0.419
0.4080 +0.425
0.4178 +0.430
0.4205 +0.419
0.4233 +0.414
0.4317 +0.414
0.4344 +0.419
0.4372 +0.424
0.4435 +0.455
0.4462 +0.463
0.4490 +0.487
0.4553 +0.490
0.4580 +0.498
0.4608 +0.484
0.4757 +0.332
0.4784 +0.292
0.4876 +0.095
0.4917 −0.021
0.5052 −0.589
0.5076 −0.728
0.5100 −0.817
0.5132 −0.944
0.5155 −0.992
0.5180 −1.033
0.5209 −1.072
0.5244 −1.097
0.5306 −1.076
0.5332 −1.042
0.5386 −0.974
0.5417 −0.919
0.5445 −0.881

2436447 +
0.3594 +0.339
0.3619 +0.348
0.3642 +0.328
0.3689 +0.343
0.3711 +0.335
0.3737 +0.340
0.3806 +0.270
0.3824 +0.240
0.3868 +0.160
0.3961 −0.210
0.3982 −0.285
0.4048 −0.562
0.4069 −0.605
0.4090 −0.645
0.4137 −0.737
0.4158 −0.766
0.4178 −0.787
0.4218 −0.821
0.4239 −0.862
0.4257 −0.897

2436451 +
0.3833 −0.714
0.3880 −0.786
0.3905 −0.821
0.3928 −0.841
0.3979 −0.900
0.4008 −0.930
0.4039 −0.941
0.4091 −0.950
0.4117 −0.953
0.4142 −0.954
0.4195 −0.943
0.4221 −0.930
0.4247 −0.916
0.4297 −0.883

2436460 +
0.3251 −0.833
0.3279 −0.801
0.3304 −0.735
0.3348 −0.682
0.3372 −0.630
0.3396 −0.609
0.3439 −0.554
0.3465 −0.536
0.3504 −0.485

2436476 +
0.2474 −1.208
0.2510 −1.239
0.2532 −1.245
0.2559 −1.235
0.2610 −1.208
0.2644 −1.182
0.2706 −1.131
0.2732 −1.115
0.2764 −1.086

2436514 +
0.2837 +0.385
0.2855 +0.370
0.2876 +0.369
0.2927 +0.372
0.2968 +0.317
0.3048 +0.142
0.3076 +0.062
0.3121 −0.029
0.3142 −0.070
0.3163 −0.120
0.3229 −0.332
0.3250 −0.412
0.3286 −0.530
0.3304 −0.606
0.3323 −0.675
0.3360 −0.844
0.3378 −0.923
0.3397 −1.006
0.3434 −1.094
0.3452 −1.114
0.3471 −1.101
0.3524 −1.036

2436679 +
0.4898 +0.430
0.4926 +0.434
0.4954 +0.436
0.5009 +0.444
0.5041 +0.460
0.5069 +0.465
0.5124 +0.426
0.5150 +0.411
0.5176 +0.382
0.5232 +0.217
0.5259 +0.106
0.5280 +0.025
0.5332 −0.211
0.5388 −0.531
0.5440 −0.812
0.5461 −0.907
0.5485 −0.989
0.5530 −1.128
0.5550 −1.155
0.5623 −1.194
0.5770 −1.143
0.5803 −1.116
0.5836 −1.082
0.5896 −1.030
0.5923 −0.999

2436695 +
0.3432 +0.305
0.3461 +0.310
0.3565 +0.299
0.3603 +0.307
0.3642 +0.305
0.3721 +0.311
0.3759 +0.302
0.3790 +0.293
0.3860 +0.295
0.3888 +0.293
0.3919 +0.309
0.4013 +0.356
0.4041 +0.353
0.4069 +0.358
0.4124 +0.383
0.4152 +0.379
0.4263 +0.298
0.4319 +0.173
0.4364 +0.035
0.4392 −0.061
0.4416 −0.163
0.4461 −0.334
0.4482 −0.451
0.4506 −0.570
0.4562 −0.790
0.4583 −0.816
0.4603 −0.831
0.4649 −0.904
0.4690 −0.968
0.4735 −1.009
0.4756 −1.025
0.4798 −1.039
0.4840 −1.041
0.4860 −1.038
0.4919 −0.973
0.4940 −0.964
0.4961 −0.937
0.5003 −0.902
0.5044 −0.853
0.5065 −0.818

2436726 +
0.4347 +0.389
0.4400 +0.416
0.4424 +0.423
0.4479 +0.409
0.4507 +0.434
0.4535 +0.433
0.4584 +0.417
0.4604 +0.411
0.4667 +0.286
0.4688 +0.234
0.4749 +0.079
0.4763 +0.043
0.4777 +0.012

2436757 +
0.4305 +0.472
0.4325 +0.467
0.4346 +0.469
0.4430 +0.467
0.4471 +0.481
0.4492 +0.475
0.4513 +0.470
0.4555 +0.481
0.4575 +0.491
0.4596 +0.490
0.4638 +0.472
0.4659 +0.445
0.4680 +0.395
0.4721 +0.295
0.4742 +0.218
0.4763 +0.156
0.4808 −0.004
0.4829 −0.099
0.4850 −0.224
0.4889 −0.445
0.4903 −0.512
0.4917 −0.575
0.4952 −0.715
0.4966 −0.784
0.4979 −0.838
0.5007 −0.942
0.5021 −0.972
0.5035 −1.005
0.5063 −1.038
0.5077 −1.053
0.5091 −1.057
0.5118 −1.068
0.5132 −1.065
0.5146 −1.063
0.5183 −1.060
0.5204 −1.057
0.5225 −1.056
0.5287 −1.018
0.5308 −1.006
0.5343 −0.977
0.5364 −0.960
0.5384 −0.942
0.5426 −0.908

2436761 +
0.4589 +0.378
0.4644 +0.250
0.4668 +0.167
0.4714 −0.014
0.4738 −0.139
0.4762 −0.264
0.4807 −0.487
0.4832 −0.588
0.4856 −0.688
0.4901 −0.864
0.4922 −0.950
0.4943 −1.016
0.4991 −1.144
0.5013 −1.167
0.5038 −1.170
0.5083 −1.149
0.5108 −1.143
0.5131 −1.125
0.5197 −1.073
0.5218 −1.053
0.5245 −1.022
0.5438 −0.838
0.5461 −0.815

2436812 +
0.3782 +0.448
0.3833 +0.425
0.3849 +0.405
0.3894 +0.353
0.3920 +0.310
0.3934 +0.261
0.3977 +0.080
0.3995 −0.004
0.4010 −0.088
0.4049 −0.361
0.4068 −0.478
0.4129 −0.815
0.4154 −0.925
0.4180 −0.991
0.4252 −1.132
0.4270 −1.136
0.4288 −1.151

2437115 +
0.3824 −0.995
0.3841 −0.994
0.3861 −0.985
0.3916 −0.892
0.3931 −0.875
0.3953 −0.851
0.3987 −0.817
0.4007 −0.786
0.4027 −0.757
0.4061 −0.725
0.4085 −0.708
0.4180 −0.626
0.4192 −0.612
0.4207 −0.610
0.4236 −0.585
0.4252 −0.568
0.4267 −0.542
0.4309 −0.510
0.4324 −0.501
0.4342 −0.493
0.4423 −0.442
0.4439 −0.437
0.4523 −0.358
0.4539 −0.350
0.4553 −0.341
0.4603 −0.272
0.4622 −0.263
0.4638 −0.248

2437117 +
0.3740 +0.298
0.3758 +0.293
0.3777 +0.280
0.3816 +0.296
0.3869 +0.295
0.3907 +0.292
0.3925 +0.297
0.3944 +0.308
0.4020 +0.309
0.4038 +0.306
0.4057 +0.315
0.4096 +0.299
0.4110 +0.281
0.4126 +0.282
0.4159 +0.295
0.4203 +0.331
0.4224 +0.341
0.4277 +0.321
0.4295 +0.325
0.4332 +0.328
0.4351 +0.342
0.4370 +0.356
0.4402 +0.358
0.4418 +0.349
0.4437 +0.351
0.4488 +0.343
0.4504 +0.328
0.4541 +0.345
0.4555 +0.347
0.4571 +0.340
0.4626 +0.330

0.4645 +0.316
0.4680 +0.307
0.4694 +0.310
0.4714 +0.309
0.4927 +0.326
0.4944 +0.335
0.4969 +0.361
0.4992 +0.357
0.5006 +0.359
0.5041 +0.405
0.5059 +0.393
0.5073 +0.415
0.5131 +0.435
0.5145 +0.427
0.5200 +0.388
0.5214 +0.372
0.5242 +0.332
0.5256 +0.311
0.5270 +0.295
0.5297 +0.249
0.5308 +0.216
0.5318 +0.189
0.5349 +0.088
0.5361 +0.085

2437134 +
0.3658 +0.365
0.3672 +0.353
0.3686 +0.370
0.3716 +0.345
0.3730 +0.353
0.3744 +0.354
0.3772 +0.335
0.3786 +0.335
0.3800 +0.339
0.3827 +0.357
0.3845 +0.369
0.3859 +0.394
0.3887 +0.408
0.4300 −0.387
0.4341 −0.679
0.4371 −0.825
0.4383 −0.920
0.4390 −0.959
0.4438 −1.091
0.4489 −1.193
0.4508 −1.227
0.4522 −1.249
0.4550 −1.254
0.4563 −1.256
0.4577 −1.262
0.4633 −1.230
0.4647 −1.223
0.4688 −1.197
0.4702 −1.195
0.4769 −1.152
0.4807 −1.125
0.4845 −1.104
0.4866 −1.075
0.4883 −1.056
0.4918 −1.038
0.4934 −1.035
0.5166 −0.846
0.5246 −0.789
0.5267 −0.773
0.5302 −0.749
0.5452 −0.626

2437138 +
0.3554 +0.343
0.3576 +0.331
0.3618 +0.336
0.3637 +0.313
0.3656 +0.291
0.3697 +0.306
0.3729 +0.336
0.3792 +0.369
0.3808 +0.411
0.3831 +0.407
0.3845 +0.362
0.3861 +0.348
0.3889 +0.352
0.3913 +0.347
0.3977 +0.447
0.3991 +0.392
0.4072 −0.048
0.4086 −0.141
0.4116 −0.246
0.4130 −0.307
0.4143 −0.367
0.4181 −0.568
0.4197 −0.638
0.4211 −0.685
0.4255 −0.888
0.4269 −0.953
0.4297 −1.037
0.4311 −1.092
0.4324 −1.127
0.4352 −1.186
0.4366 −1.212
0.4380 −1.230
0.4408 −1.277
0.4422 −1.280
0.4436 −1.285
0.4496 −1.254
0.4510 −1.250
0.4524 −1.233
0.4554 −1.211
0.4567 −1.203
0.4611 −1.188
0.4625 −1.161
0.4639 −1.145
0.4667 −1.113
0.4708 −1.099
0.4739 −1.077
0.4753 −1.044
0.4769 −1.025
0.4802 −0.986
0.4816 −0.978
0.4829 −0.962
0.4857 −0.931
0.4871 −0.909
0.4913 −0.851
0.4927 −0.836
0.4941 −0.832
0.4982 −0.782
0.4996 −0.771
0.5026 −0.748
0.5040 −0.731
0.5054 −0.713
0.5081 −0.703
0.5102 −0.689

2437145 +
0.3589 +0.340
0.3609 +0.338
0.3734 +0.393
0.3762 +0.376
0.3817 +0.402
0.3852 +0.429
0.3880 +0.410
0.3932 +0.370
0.3960 +0.366
0.3984 +0.374
0.4043 +0.352
0.4064 +0.344
0.4092 +0.316
0.4150 +0.300
0.4175 +0.318
0.4330 +0.308
0.4346 +0.323
0.4367 +0.329
0.4408 +0.343
0.4423 +0.382
0.4501 +0.395
0.4522 +0.416
0.4543 +0.403
0.4580 +0.395
0.4594 +0.388
0.4610 +0.375
0.4652 +0.296
0.4673 +0.257
0.4686 +0.240
0.4735 +0.154
0.4756 +0.116
0.4774 +0.042
0.4823 −0.104
0.4837 −0.153
0.4851 −0.224
0.4904 −0.472
0.4918 −0.530
0.4934 −0.593
0.4973 −0.760
0.5004 −0.868
0.5064 −0.973
0.5082 −0.997
0.5103 −1.002
0.5156 −1.008
0.5177 −1.013
0.5198 −0.996
0.5256 −0.984
0.5277 −0.954
0.5321 −0.922
0.5411 −0.810
0.5430 −0.787
0.5446 −0.760
0.5487 −0.713

2437149 +
0.3800 +0.329
0.3814 +0.323
0.3835 +0.350
0.3924 +0.362
0.3939 +0.348
0.3953 +0.370
0.3994 +0.376
0.4008 +0.397
0.4057 +0.423
0.4071 +0.416
0.4085 +0.421
0.4124 +0.414
0.4159 +0.407
0.4177 +0.407
0.4221 +0.384
0.4235 +0.382
0.4284 +0.392
0.4316 +0.369
0.4330 +0.346
0.4367 +0.303
0.4418 +0.189
0.4439 +0.131
0.4501 −0.049
0.4522 −0.154
0.4550 −0.267
0.4594 −0.436
0.4615 −0.517
0.4680 −0.716
0.4717 −0.829
0.4731 −0.852
0.4744 −0.866
0.4777 −0.895
0.4791 −0.898
0.4805 −0.913
0.4844 −0.927
0.4858 −0.929
0.4872 −0.919
0.4904 −0.913
0.4918 −0.908
0.4932 −0.903
0.4976 −0.874
0.4992 −0.873
0.5008 −0.867
0.5041 −0.850
0.5059 −0.846
0.5075 −0.834

0.5115 −0.785
0.5133 −0.774
0.5150 −0.767
0.5193 −0.735
0.5210 −0.709
0.5224 −0.694
0.5256 −0.688
0.5274 −0.668
0.5293 −0.639

2437173 +
0.3420 +0.358
0.3440 +0.379
0.3488 +0.411
0.3506 +0.418
0.3525 +0.416
0.3568 +0.406
0.3586 +0.412
0.3602 +0.424
0.3647 +0.422
0.3668 +0.417
0.3731 +0.389
0.3772 +0.345
0.3816 +0.279
0.3838 +0.248
0.3857 +0.187
0.3929 −0.008
0.3948 −0.062
0.3985 −0.206
0.4005 −0.290
0.4024 −0.383
0.4071 −0.603
0.4090 −0.695
0.4104 −0.740
0.4134 −0.905
0.4149 −0.971
0.4162 −1.010
0.4191 −1.092
0.4223 −1.144
0.4255 −1.156
0.4269 −1.158
0.4282 −1.161
0.4310 −1.151
0.4326 −1.142
0.4353 −1.138
0.4389 −1.115
0.4403 −1.100
0.4417 −1.084
0.4457 −1.034
0.4524 −0.964
0.4546 −0.943
0.4563 −0.929
0.4600 −0.892
0.4625 −0.872
0.4642 −0.850
0.4680 −0.812
0.4698 −0.784

2437175 +
0.3235 −0.189
0.3256 −0.185
0.3277 −0.165
0.3314 −0.111
0.3337 −0.103
0.3358 −0.092
0.3401 −0.079
0.3425 −0.061
0.3448 −0.034
0.3497 −0.008
0.3518 −0.007
0.3594 +0.027
0.3613 +0.046
0.3638 +0.049
0.3690 +0.088
0.3711 +0.096
0.3843 +0.193
0.3864 +0.221
0.3885 +0.246
0.3923 +0.267
0.3944 +0.296
0.3964 +0.296

2437467 +
0.4666 +0.510
0.4707 +0.509
0.4728 +0.487
0.4773 +0.448
0.4794 +0.440
0.4815 +0.410
0.4878 +0.328
0.4898 +0.282
0.4940 +0.156
0.4968 +0.053
0.4998 −0.047
0.5012 −0.092
0.5026 −0.150
0.5060 −0.350
0.5074 −0.412
0.5088 −0.486
0.5137 −0.678
0.5151 −0.745
0.5190 −0.901
0.5204 −0.963
0.5232 −1.051
0.5246 −1.084
0.5259 −1.134
0.5287 −1.210
0.5301 −1.225
0.5315 −1.244
0.5343 −1.281
0.5357 −1.310
0.5371 −1.321
0.5412 −1.316
0.5426 −1.314
0.5454 −1.286

2437468 +
0.3887 −0.106
0.3932 −0.384
0.3946 −0.456
0.3981 −0.672
0.3995 −0.763
0.4009 −0.818
0.4057 −1.003
0.4071 −1.045
0.4113 −1.123
0.4141 −1.173
0.4161 −1.197
0.4175 −1.212
0.4189 −1.212
0.4217 −1.242
0.4231 −1.251
0.4245 −1.257
0.4273 −1.255
0.4300 −1.245
0.4328 −1.229
0.4349 −1.209
0.4418 −1.144
0.4746 −0.784
0.4802 −0.709

2437480 +
0.3857 −0.904
0.3874 −0.909
0.3893 −0.887
0.3950 −0.871
0.3982 −0.840
0.4000 −0.836
0.4046 −0.769
0.4063 −0.760
0.4084 −0.744
0.4119 −0.726
0.4143 −0.700

2437483 +
0.4420 −1.114
0.4437 −1.127
0.4467 −1.120
0.4483 −1.123
0.4499 −1.121
0.4531 −1.113
0.4574 −1.090
0.4608 −1.055
0.4624 −1.031
0.4641 −1.003
0.4678 −0.986
0.4698 −0.942
0.4719 −0.922

2437487 +
0.3748 +0.241
0.3768 +0.158
0.3806 +0.057
0.3819 +0.023
0.3833 −0.026
0.3870 −0.153
0.3882 −0.224
0.3891 −0.248
0.3921 −0.390
0.3947 −0.505
0.3970 −0.583
0.3981 −0.613
0.4014 −0.674
0.4023 −0.700
0.4060 −0.789
0.4074 −0.805
0.4088 −0.840
0.4123 −0.861
0.4136 −0.872
0.4164 −0.902
0.4178 −0.911
0.4190 −0.912
0.4218 −0.941
0.4229 −0.949
0.4280 −0.961
0.4294 −0.966
0.4306 −0.969
0.4331 −0.974
0.4343 −0.970

2437490 +
0.4210 +0.296
0.4226 +0.293
0.4242 +0.285
0.4273 +0.298
0.4294 +0.304
0.4310 +0.318
0.4359 +0.335
0.4372 +0.336
0.4393 +0.370
0.4430 +0.373
0.4446 +0.367
0.4509 +0.370
0.4523 +0.369
0.4641 +0.348
0.4694 +0.276
0.4708 +0.257
0.4722 +0.245
0.4759 +0.198
0.4789 +0.162
0.4828 +0.086
0.4842 +0.064
0.4856 +0.016
0.4893 −0.124
0.4914 −0.196
0.4933 −0.265
0.4974 −0.463
0.4990 −0.505
0.5004 −0.555
0.5035 −0.643
0.5046 −0.683
0.5060 −0.708
0.5090 −0.741
0.5125 −0.788
0.5155 −0.826

0.5185 −0.848
0.5222 −0.880
0.5236 −0.888
0.5250 −0.911
0.5308 −0.941
0.5322 −0.926
0.5338 −0.932
0.5370 −0.941
0.5379 −0.944
0.5389 −0.919
0.5416 −0.938
0.5446 −0.933
0.5465 −0.908

2437494 +
0.4605 +0.355
0.4619 +0.308
0.4771 +0.120
0.4826 +0.027
0.4840 +0.010
0.4854 −0.026
0.4896 −0.085
0.4938 −0.228
0.4969 −0.342
0.4986 −0.388
0.5000 −0.430
0.5038 −0.633
0.5048 −0.668
0.5060 −0.721
0.5124 −0.852
0.5136 −0.859
0.5150 −0.893
0.5183 −0.920
0.5198 −0.917
0.5211 −0.922
0.5234 −0.921
0.5278 −0.935
0.5325 −0.929
0.5339 −0.934
0.5372 −0.927
0.5386 −0.937
0.5399 −0.926
0.5445 −0.891
0.5490 −0.855

2437840 +
0.4261 +0.297
0.4275 +0.302
0.4289 +0.293
0.4324 +0.254
0.4338 +0.217
0.4384 +0.061
0.4398 +0.013
0.4412 −0.043
0.4444 −0.167
0.4458 −0.240
0.4472 −0.354
0.4507 −0.552
0.4521 −0.665
0.4534 −0.747
0.4569 −0.888
0.4583 −0.951
0.4597 −0.995
0.4625 −1.068
0.4639 −1.092
0.4653 −1.101
0.4680 −1.116
0.4696 −1.146
0.4710 −1.182
0.4748 −1.266
0.4761 −1.284
0.4775 −1.296
0.4805 −1.311
0.4819 −1.305

2437851 +
0.4679 +0.490
0.4692 +0.482
0.4706 +0.463
0.4741 +0.424
0.4755 +0.391
0.4769 +0.343
0.4804 +0.253
0.4817 +0.240
0.4866 +0.138
0.4880 +0.104
0.4956 −0.109
0.4970 −0.147
0.4984 −0.227
0.5012 −0.388
0.5026 −0.489
0.5040 −0.612
0.5067 −0.781
0.5081 −0.832
0.5095 −0.910
0.5123 −1.025
0.5137 −1.068
0.5151 −1.112
0.5178 −1.182
0.5192 −1.205
0.5206 −1.216
0.5241 −1.250
0.5255 −1.260
0.5269 −1.258
0.5304 −1.243
0.5317 −1.235
0.5373 −1.191
0.5387 −1.166
0.5401 −1.149
0.5436 −1.112

2437852 +
0.3706 +0.172
0.3719 +0.126
0.3733 +0.102
0.3773 −0.002
0.3789 −0.073
0.3803 −0.178
0.3844 −0.381
0.3858 −0.458
0.3879 −0.594
0.3907 −0.703
0.3921 −0.750
0.4018 −0.990
0.4067 −1.036
0.4080 −1.044
0.4094 −1.042
0.4122 −1.048
0.4157 −1.027
0.4185 −1.012
0.4199 −1.002
0.4219 −1.000
0.4261 −0.966
0.4303 −0.931
0.4317 −0.924
0.4330 −0.912
0.4358 −0.901
0.4379 −0.866
0.4393 −0.849
0.4428 −0.812

2437856 +
0.3748 −0.863
0.3766 −0.893
0.3787 −0.909
0.3827 −0.936
0.3851 −0.953
0.3872 −0.943
0.3912 −0.942
0.3932 −0.941
0.3959 −0.923
0.4219 −0.652

2437867 +
0.4200 +0.148
0.4221 +0.113
0.4242 +0.084
0.4311 −0.063
0.4325 −0.111
0.4339 −0.131
0.4360 −0.187
0.4402 −0.289
0.4422 −0.341
0.4443 −0.385
0.4513 −0.578
0.4534 −0.631
0.4554 −0.688
0.4575 −0.727
0.4624 −0.767
0.4666 −0.804
0.4686 −0.812
0.4763 −0.839
0.4784 −0.834

2437871 +
0.3640 +0.191
0.3655 +0.191
0.3691 +0.193
0.3707 +0.193
0.3725 +0.191
0.3767 +0.194
0.3784 +0.181
0.3799 +0.179
0.3847 +0.174
0.3866 +0.175
0.3885 +0.176
0.3928 +0.200
0.3953 +0.190
0.3970 +0.185
0.4009 +0.181
0.4029 +0.177
0.4048 +0.170
0.4085 +0.191
0.4104 +0.204
0.4161 +0.160
0.4186 +0.128
0.4201 +0.099
0.4239 +0.046
0.4256 +0.027
0.4272 +0.000
0.4304 −0.038
0.4319 −0.050
0.4338 −0.081
0.4370 −0.138
0.4410 −0.252
0.4451 −0.364
0.4467 −0.414
0.4486 −0.490
0.4518 −0.576
0.4534 −0.637
0.4548 −0.670
0.4583 −0.766
0.4601 −0.798
0.4619 −0.818
0.4653 −0.849
0.4668 −0.868
0.4686 −0.883
0.4722 −0.891
0.4740 −0.896
0.4756 −0.904
0.4794 −0.889
0.4813 −0.873
0.4831 −0.871
0.4870 −0.839
0.4892 −0.830
0.4910 −0.828
0.4948 −0.804

2437883 +
0.3665 +0.312
0.3684 +0.300
0.3735 +0.305
0.3751 +0.306
0.3767 +0.305
0.3804 +0.300

0.3838 +0.280
0.3872 +0.255
0.3888 +0.226
0.3904 +0.219
0.3943 +0.185
0.3962 +0.145
0.3981 +0.128
0.4016 +0.067
0.4032 +0.023
0.4051 −0.023
0.4090 −0.152
0.4109 −0.204
0.4124 −0.244
0.4158 −0.354
0.4176 −0.418
0.4194 −0.495
0.4226 −0.668
0.4241 −0.715
0.4255 −0.749
0.4286 −0.854
0.4301 −0.895
0.4316 −0.931
0.4367 −1.032
0.4384 −1.067
0.4416 −1.110
0.4436 −1.126
0.4453 −1.144
0.4488 −1.149
0.4506 −1.141
0.4523 −1.130
0.4560 −1.100
0.4578 −1.082
0.4594 −1.071
0.4629 −1.031
0.4648 −1.021
0.4665 −1.006

2438236 +
0.3653 −0.198
0.3667 −0.233
0.3722 −0.355
0.3736 −0.393
0.3771 −0.480
0.3785 −0.514
0.3806 −0.550
0.3840 −0.589
0.3861 −0.621
0.3875 −0.658
0.3908 −0.701
0.3922 −0.716
0.3950 −0.735
0.3992 −0.780
0.4020 −0.813
0.4041 −0.827
0.4076 −0.848
0.4097 −0.850
0.4118 −0.852
0.4146 −0.859
0.4174 −0.852
0.4188 −0.846
0.4222 −0.850
0.4243 −0.838
0.4257 −0.826
0.4299 −0.809
0.4319 −0.802
0.4333 −0.795
0.4375 −0.767
0.4389 −0.750
0.4403 −0.740
0.4444 −0.711
0.4465 −0.695
0.4479 −0.684
0.4528 −0.664
0.4542 −0.656
0.4576 −0.642
0.4597 −0.630
0.4618 −0.605
0.4674 −0.567
0.4688 −0.556
0.4702 −0.549
0.4730 −0.516
0.4744 −0.505

2438248 +
0.3431 +0.279
0.3451 +0.277
0.3528 +0.240
0.3563 +0.223
0.3597 +0.183
0.3653 +0.134
0.3681 +0.106
0.3708 +0.043
0.3778 −0.151
0.3806 −0.269
0.3847 −0.414
0.3903 −0.611
0.3971 −0.806
0.4034 −0.894
0.4069 −0.902
0.4104 −0.896
0.4181 −0.847
0.4222 −0.816
0.4313 −0.686

2438264 +
0.3064 −0.495
0.3078 −0.539
0.3119 −0.739

2438267 +
0.3579 +0.439
0.3652 +0.379
0.3732 +0.262
0.3746 +0.248
0.3805 +0.128
0.3829 +0.044
0.3843 −0.008
0.3905 −0.191
0.3923 −0.274
0.3971 −0.546
0.3989 −0.660
0.4009 −0.754
0.4065 −1.019
0.4082 −1.062
0.4107 −1.100
0.4173 −1.166
0.4190 −1.173
0.4218 −1.176
0.4374 −1.089
0.4398 −1.066
0.4412 −1.054
0.4464 −1.018
0.4482 −1.009
0.4499 −0.981
0.4572 −0.927
0.4596 −0.919
0.4628 −0.870

2438284 +
0.2692 −1.026
0.2708 −1.034
0.2725 −1.014
0.2791 −1.005
0.2810 −1.012
0.2844 −0.993
0.2863 −0.966
0.2876 −0.974
0.2910 −0.939
0.2924 −0.948
0.2940 −0.940
0.2971 −0.935
0.2983 −0.926
0.2995 −0.880
0.3032 −0.860
0.3043 −0.836
0.3055 −0.819
0.3081 −0.806
0.3092 −0.805
0.3105 −0.802
0.3133 −0.776
0.3145 −0.767
0.3156 −0.746
0.3185 −0.706
0.3196 −0.714
0.3208 −0.689
0.3238 −0.669
0.3250 −0.657
0.3262 −0.635
0.3294 −0.634
0.3305 −0.610
0.3318 −0.573
0.3538 −0.358
0.3559 −0.375
0.3681 −0.233
0.3695 −0.209

2438585 +
0.4341 +0.092
0.4369 −0.022
0.4402 −0.146
0.4416 −0.201
0.4453 −0.409
0.4467 −0.462
0.4507 −0.676
0.4524 −0.759
0.4561 −0.923
0.4578 −0.993
0.4608 −1.056
0.4642 −1.130
0.4685 −1.199
0.4713 −1.235
0.4734 −1.243
0.4768 −1.239
0.4782 −1.233
0.4817 −1.214
0.4831 −1.208
0.4866 −1.186
0.4886 −1.169
0.4928 −1.125
0.4956 −1.076
0.4970 −1.059
0.4998 −1.035
0.5011 −1.016

2438605 +
0.3403 −0.759
0.3432 −0.801
0.3447 −0.831
0.3479 −0.870
0.3494 −0.872
0.3532 −0.866
0.3553 −0.862
0.3592 −0.837
0.3615 −0.832
0.3648 −0.862
0.3669 −0.868
0.3723 −0.810
0.3747 −0.773
0.3780 −0.731

2438608 +
0.4014 +0.242
0.4066 +0.171
0.4097 +0.117
0.4201 −0.090
0.4257 −0.237
0.4288 −0.317
0.4351 −0.526
0.4372 −0.572
0.4424 −0.652
0.4451 −0.672
0.4507 −0.721
0.4545 −0.764
0.4604 −0.777
0.4639 −0.777

0.4729 −0.764
0.4753 −0.760
0.4812 −0.704
0.4840 −0.671
0.4913 −0.586
0.4944 −0.546
0.5073 −0.391
0.5101 −0.344

2438621 +
0.3224 −0.459
0.3332 −0.780
0.3342 −0.803
0.3356 −0.835
0.3370 −0.865
0.3405 −0.923
0.3464 −0.993
0.3474 −0.998
0.3498 −1.031
0.3523 −1.029
0.3537 −1.028
0.3561 −1.024
0.3575 −1.008
0.3603 −0.978
0.3613 −0.961
0.3627 −0.945
0.3655 −0.926
0.3669 −0.897
0.3683 −0.890
0.3710 −0.868
0.3724 −0.836
0.3752 −0.805
0.3773 −0.787
0.3787 −0.773
0.3818 −0.748
0.3835 −0.723
0.3884 −0.705
0.3898 −0.698
0.3946 −0.664
0.3995 −0.633
0.4085 −0.595
0.4099 −0.580

2438636 +
0.3405 +0.306
0.3468 +0.297
0.3523 +0.009
0.3586 −0.385
0.3614 −0.589
0.3704 −1.168
0.3752 −1.290
0.3773 −1.305
0.3843 −1.279
0.3864 −1.267
0.3884 −1.267
0.3905 −1.255
0.3954 −1.221
0.3975 −1.204
0.4023 −1.160
0.4051 −1.132
0.4107 −1.063
0.4127 −1.041
0.4190 −0.992

2438655 +
0.3685 +0.309
0.3698 +0.294
0.3747 +0.257
0.3768 +0.261
0.3810 +0.254
0.3942 +0.088
0.3955 +0.058
0.3990 −0.068
0.4004 −0.166
0.4046 −0.380
0.4087 −0.608
0.4101 −0.646
0.4136 −0.751
0.4150 −0.785
0.4178 −0.864
0.4192 −0.879
0.4219 −0.932
0.4233 −0.942
0.4268 −0.942
0.4282 −0.944
0.4310 −0.929
0.4323 −0.931
0.4351 −0.929
0.4365 −0.912
0.4400 −0.878
0.4414 −0.856
0.4448 −0.812
0.4462 −0.807

2438664 +
0.2536 +0.362
0.2553 +0.353
0.2607 +0.348
0.2641 +0.283
0.2702 +0.170
0.2723 +0.117
0.2771 −0.017
0.2795 −0.066
0.2844 −0.238
0.2865 −0.345
0.2913 −0.590
0.2938 −0.673
0.2990 −0.805
0.3018 −0.859
0.3070 −0.916
0.3101 −0.950
0.3160 −0.976
0.3237 −0.993
0.3264 −0.991

2438668 +
0.2615 +0.025
0.2688 −0.113
0.2709 −0.155
0.2747 −0.315
0.2768 −0.381
0.2817 −0.602
0.2838 −0.709
0.2886 −0.899
0.2924 −1.011
0.2973 −1.053
0.2994 −1.073
0.3042 −1.090
0.3070 −1.088
0.3278 −0.977
0.3296 −0.958

2438965 +
0.4351 +0.245
0.4427 +0.106
0.4462 +0.030
0.4504 −0.064
0.4531 −0.124
0.4580 −0.302
0.4608 −0.419
0.4663 −0.645
0.4691 −0.752
0.4754 −0.915
0.4775 −0.955
0.4830 −0.993
0.4858 −0.988
0.4927 −0.969
0.4962 −0.949
0.5045 −0.915
0.5108 −0.887
0.5156 −0.854
0.5219 −0.799
0.5240 −0.777
0.5302 −0.701
0.5316 −0.684
0.5344 −0.661
0.5358 −0.634

2438981 +
0.3589 −0.056
0.3603 −0.082
0.3645 −0.174
0.3659 −0.207
0.3672 −0.258
0.3700 −0.332
0.3721 −0.413
0.3749 −0.501
0.3763 −0.556
0.3777 −0.628
0.3811 −0.683
0.3832 −0.689
0.3850 −0.705
0.3895 −0.766
0.3909 −0.778
0.3922 −0.813
0.3964 −0.852
0.3985 −0.865
0.4006 −0.866
0.4040 −0.847
0.4054 −0.839
0.4068 −0.840
0.4110 −0.826
0.4131 −0.821
0.4145 −0.813
0.4179 −0.786
0.4193 −0.771
0.4207 −0.764
0.4270 −0.730
0.4298 −0.710
0.4318 −0.690
0.4360 −0.656
0.4374 −0.652
0.4388 −0.625
0.4436 −0.593
0.4457 −0.567
0.4478 −0.542
0.4506 −0.530
0.4527 −0.514
0.4548 −0.503
0.4589 −0.483
0.4603 −0.458
0.4617 −0.441
0.4659 −0.408
0.4672 −0.408
0.4693 −0.381
0.4728 −0.340
0.4749 −0.313
0.4770 −0.286

2438985 +
0.3670 +0.153
0.3690 +0.067
0.3711 −0.091
0.3760 −0.357
0.3781 −0.445
0.3802 −0.534
0.3843 −0.666
0.3864 −0.724
0.3885 −0.788
0.3920 −0.854
0.3940 −0.873
0.3961 −0.886
0.4017 −0.904
0.4045 −0.896
0.4072 −0.879
0.4107 −0.863
0.4128 −0.859
0.4142 −0.849
0.4190 −0.826
0.4239 −0.789
0.4281 −0.782
0.4315 −0.767
0.4343 −0.746
0.4392 −0.725
0.4426 −0.707

0.4454 −0.681

2438989 +
0.3558 +0.271
0.3579 +0.240
0.3614 +0.091
0.3635 +0.053
0.3656 −0.133
0.3690 −0.255
0.3704 −0.286
0.3725 −0.379
0.3808 −0.638

2438993 +
0.3383 +0.383
0.3411 +0.347
0.3487 +0.242
0.3515 +0.186
0.3598 −0.035
0.3633 −0.188
0.3710 −0.529
0.3751 −0.709
0.3821 −0.923
0.3862 −1.029
0.3966 −1.123
0.4022 −1.098
0.4154 −1.043
0.4210 −1.000
0.4251 −0.956
0.4314 −0.886

2439028 +
0.3038 +0.283
0.3114 +0.271
0.3156 +0.249
0.3260 +0.153
0.3343 +0.004
0.3399 −0.128
0.3426 −0.198
0.3496 −0.393
0.3524 −0.487
0.3593 −0.653
0.3614 −0.689
0.3676 −0.800
0.3711 −0.829
0.3781 −0.836
0.3808 −0.826

0.3878 −0.768
0.3927 −0.726
0.3996 −0.682
0.4031 −0.662

2439056 +
0.2254 −0.421
0.2302 −0.659
0.2372 −0.847
0.2441 −0.959
0.2462 −0.967
0.2518 −0.980
0.2545 −0.977
0.2615 −0.939
0.2643 −0.937
0.2719 −0.905
0.2754 −0.889
0.2823 −0.840
0.2851 −0.817
0.2920 −0.724
0.2948 −0.697
0.3018 −0.659
0.3039 −0.638
0.3066 −0.615
0.3122 −0.560
0.3150 −0.542
0.3212 −0.497
0.3240 −0.470
0.3268 −0.447

2439060 +
0.2238 −0.872
0.2252 −0.889
0.2286 −0.933
0.2307 −0.941
0.2321 −0.954
0.2356 −0.958
0.2376 −0.971
0.2390 −0.983
0.2418 −0.971
0.2439 −0.967
0.2460 −0.952
0.2495 −0.937
0.2508 −0.924
0.2522 −0.921
0.2557 −0.909
0.2585 −0.895

0.2613 −0.882
0.2633 −0.868
0.2654 −0.838
0.2710 −0.799
0.2731 −0.771
0.2918 −0.594
0.2932 −0.578
0.2981 −0.517
0.2995 −0.509
0.3008 −0.501
0.3043 −0.448
0.3057 −0.427
0.3071 −0.420
0.3106 −0.403
0.3120 −0.394

2439064 +
0.1999 −0.347
0.2041 −0.474
0.2110 −0.675
0.2138 −0.746
0.2200 −0.868
0.2228 −0.903
0.2277 −0.946
0.2298 −0.950
0.2346 −0.954
0.2436 −0.910
0.2700 −0.645
0.2805 −0.533
0.2818 −0.519
0.2832 −0.496

2439230 +
0.3858 −0.502
0.3872 −0.478
0.3907 −0.446
0.3921 −0.449
0.3948 −0.430
0.3983 −0.390
0.4025 −0.368
0.4039 −0.358
0.4067 −0.343
0.4087 −0.341
0.4115 −0.312
0.4129 −0.310
0.4157 −0.284

2439260 +
0.4734 −0.783
0.4755 −0.771
0.4769 −0.779
0.4797 −0.758
0.4838 −0.726
0.4859 −0.703
0.4887 −0.702
0.4922 −0.668
0.4943 −0.636
0.4956 −0.636
0.5019 −0.576
0.5061 −0.547
0.5095 −0.491
0.5116 −0.478
0.5137 −0.447
0.5172 −0.444
0.5200 −0.419
0.5213 −0.412
0.5276 −0.390
0.5304 −0.363
0.5325 −0.361
0.5359 −0.319
0.5373 −0.341
0.5387 −0.321
0.5505 −0.233
0.5519 −0.195
0.5540 −0.174
0.5582 −0.156
0.5595 −0.132

2439264 +
0.4073 −0.821
0.4094 −0.840
0.4121 −0.855
0.4135 −0.859
0.4156 −0.874
0.4205 −0.861
0.4218 −0.857
0.4239 −0.863
0.4392 −0.785
0.4462 −0.739
0.4472 −0.744
0.4482 −0.735
0.4507 −0.712
0.4528 −0.720
0.4538 −0.718

0.4566 −0.700
0.4580 −0.669

2439267 +
0.5237 −0.792
0.5265 −0.803
0.5293 −0.802
0.5327 −0.795
0.5355 −0.774
0.5369 −0.762
0.5390 −0.759
0.5432 −0.738
0.5452 −0.724
0.5466 −0.726
0.5557 −0.659
0.5598 −0.612

2439268 +
0.3598 +0.082
0.3612 +0.044
0.3646 −0.054
0.3716 −0.289
0.3751 −0.391
0.3778 −0.479
0.3792 −0.512
0.3806 −0.557
0.3841 −0.647
0.3855 −0.687
0.3869 −0.700
0.3910 −0.732
0.3924 −0.766
0.3945 −0.792
0.3980 −0.832
0.3994 −0.841
0.4008 −0.847
0.4042 −0.842
0.4056 −0.844
0.4070 −0.844
0.4112 −0.829
0.4153 −0.812
0.4209 −0.801
0.4230 −0.789
0.4292 −0.743
0.4313 −0.714
0.4334 −0.703
0.4466 −0.606
0.4480 −0.592

0.4903 −0.288
0.4917 −0.266
0.4931 −0.252
0.4973 −0.252
0.4987 −0.246

2439323 +
0.3321 +0.034
0.3419 −0.128
0.3446 −0.193
0.3467 −0.290
0.3516 −0.498
0.3537 −0.578
0.3551 −0.636
0.3585 −0.701
0.3599 −0.734
0.3638 −0.822
0.3676 −0.882
0.3689 −0.901
0.3724 −0.925
0.3745 −0.921
0.3759 −0.913
0.3800 −0.909
0.3814 −0.925
0.3828 −0.923
0.3877 −0.918
0.3898 −0.903
0.3912 −0.882
0.3946 −0.867
0.3967 −0.864
0.3981 −0.849
0.4044 −0.800
0.4058 −0.786
0.4071 −0.780
0.4259 −0.683
0.4273 −0.673

2439326 +
0.3625 +0.183
0.4584 −0.588
0.4597 −0.651
0.4611 −0.684
0.4639 −0.751
0.4653 −0.781
0.4667 −0.811
0.4702 −0.886
0.4716 −0.907

0.4729 −0.931
0.4757 −0.959
0.4778 −0.976
0.4799 −0.988
0.4834 −1.000
0.4847 −0.996
0.4861 −1.011
0.4896 −1.000
0.4917 −1.002
0.4931 −0.987
0.4959 −0.988
0.4972 −0.977
0.4986 −0.971
0.5021 −0.953
0.5035 −0.933
0.5049 −0.915
0.5132 −0.775
0.5160 −0.731
0.5174 −0.714
0.5188 −0.707

2439346 +
0.3311 −0.255
0.3324 −0.323
0.3338 −0.357
0.3366 −0.470
0.3380 −0.513
0.3394 −0.575
0.3422 −0.665
0.3436 −0.706
0.3449 −0.749
0.3477 −0.809
0.3491 −0.853
0.3505 −0.875
0.3533 −0.918
0.3547 −0.943
0.3561 −0.948
0.3588 −0.957
0.3602 −0.962
0.3616 −0.954
0.3644 −0.931

2439349 +
0.4191 +0.029
0.4212 −0.038
0.4261 −0.220
0.4274 −0.265

0.4288 −0.324
0.4330 −0.487
0.4344 −0.531
0.4372 −0.589
0.4386 −0.630
0.4399 −0.657
0.4427 −0.718
0.4441 −0.737
0.4455 −0.761
0.4483 −0.807
0.4497 −0.820
0.4511 −0.829
0.4538 −0.855
0.4552 −0.861
0.4566 −0.857
0.4594 −0.857
0.4608 −0.860
0.4622 −0.867
0.4649 −0.858
0.4663 −0.853
0.4677 −0.856
0.4712 −0.857
0.4726 −0.847
0.4740 −0.840
0.4774 −0.830
0.4788 −0.822
0.4809 −0.819

2439373 +
0.3072 +0.457
0.3103 +0.443
0.3134 +0.431
0.3148 +0.422
0.3162 +0.418
0.3328 +0.409
0.3342 +0.416
0.3356 +0.422
0.3391 +0.450
0.3405 +0.462
0.3419 +0.470
0.3446 +0.483
0.3460 +0.483
0.3474 +0.479
0.3502 +0.487
0.3516 +0.482
0.3551 +0.524
0.3578 +0.542

0.3592 +0.540
0.3669 +0.538
0.3683 +0.507
0.3738 +0.397
0.3752 +0.376
0.3766 +0.350
0.3794 +0.249
0.3808 +0.209
0.3822 +0.166
0.3849 +0.065
0.3863 −0.010
0.3877 −0.064
0.3905 −0.265
0.3919 −0.337
0.3933 −0.406
0.3974 −0.667
0.3988 −0.712
0.4002 −0.749
0.4023 −0.849
0.4037 −0.890
0.4072 −0.996
0.4099 −1.052
0.4113 −1.087
0.4127 −1.118
0.4155 −1.156
0.4169 −1.178
0.4183 −1.194
0.4210 −1.207
0.4224 −1.208
0.4245 −1.226

2439381 +
0.3042 +0.327
0.3070 +0.332
0.3084 +0.344
0.3097 +0.346
0.3125 +0.332
0.3139 +0.323
0.3153 +0.323
0.3181 +0.320
0.3195 +0.324
0.3209 +0.317
0.3236 +0.322
0.3250 +0.298
0.3264 +0.281
0.3292 +0.243
0.3320 +0.177

0.3347 +0.121
0.3403 +0.024
0.3417 −0.006
0.3459 −0.163
0.3472 −0.210
0.3500 −0.373
0.3514 −0.482
0.3528 −0.564
0.3556 −0.680
0.3570 −0.759
0.3584 −0.795
0.3611 −0.882
0.3625 −0.938
0.3639 −0.985
0.3667 −1.038
0.3681 −1.044
0.3695 −1.053
0.3722 −1.058
0.3736 −1.062
0.3750 −1.074
0.3778 −1.078
0.3792 −1.072
0.3806 −1.060
0.3834 −1.042
0.3847 −1.042
0.3861 −1.033
0.3889 −1.010
0.3903 −1.015
0.3917 −1.003
0.3945 −0.958
0.3958 −0.937
0.3972 −0.920

2439409 +
0.2612 +0.156
0.2633 +0.105
0.2647 +0.071
0.2695 −0.098
0.2779 −0.375
0.2793 −0.429
0.2807 −0.494
0.2848 −0.640
0.2862 −0.692
0.2883 −0.745
0.2925 −0.860
0.2945 −0.887
0.2966 −0.912

0.3008 −0.957
0.3029 −0.977
0.3050 −0.979
0.3084 −0.980
0.3105 −0.971
0.3126 −0.970
0.3161 −0.943
0.3182 −0.934
0.3202 −0.921
0.3244 −0.904
0.3258 −0.889
0.3272 −0.881
0.3307 −0.843
0.3327 −0.818
0.3348 −0.796

2439413 +
0.2493 +0.012
0.2542 −0.178
0.2556 −0.228
0.2611 −0.372
0.2625 −0.410
0.2639 −0.475
0.2674 −0.585
0.2694 −0.649
0.2708 −0.692
0.2764 −0.853
0.2778 −0.892
0.2812 −0.936
0.2840 −0.971
0.2854 −0.998
0.2903 −1.033
0.2941 −1.040

2439507 +
0.6014 −1.170
0.6028 −1.153
0.6042 −1.159
0.6077 −1.128
0.6090 −1.116
0.6104 −1.098
0.6139 −1.065
0.6153 −1.049
0.6174 −1.033
0.6222 −0.995
0.6243 −0.974
0.6257 −0.964
0.6306 −0.915
0.6320 −0.898

2439581 +
0.5425 +0.418
0.5439 +0.404
0.5467 +0.333
0.5481 +0.305
0.5508 +0.252
0.5522 +0.195
0.5550 +0.086
0.5564 −0.024
0.5592 −0.225
0.5606 −0.338
0.5626 −0.500
0.5640 −0.587
0.5661 −0.693
0.5675 −0.756
0.5696 −0.816
0.5710 −0.828
0.5745 −0.985
0.5772 −1.116
0.5786 −1.160
0.5807 −1.190
0.5821 −1.200
0.5856 −1.242
0.5876 −1.244
0.5890 −1.249
0.5911 −1.244
0.5925 −1.241
0.5946 −1.236

2439604 +
0.5171 +0.299
0.5185 +0.311
0.5212 +0.308
0.5226 +0.290
0.5254 +0.297
0.5268 +0.274
0.5296 +0.255
0.5358 +0.238
0.5372 +0.228
0.5400 +0.202
0.5414 +0.193
0.5442 +0.164
0.5504 +0.101
0.5546 +0.064
0.5560 +0.032
0.5601 −0.014
0.5650 −0.129
0.5664 −0.175
0.5719 −0.336
0.5733 −0.391
0.5761 −0.506
0.5775 −0.555
0.5803 −0.611
0.5817 −0.643
0.5844 −0.715
0.5858 −0.740
0.5886 −0.784
0.5900 −0.796
0.5942 −0.833
0.5969 −0.846
0.5983 −0.854
0.6011 −0.867
0.6025 −0.861
0.6053 −0.850
0.6067 −0.851
0.6094 −0.842

2439605 +
0.4567 −0.228
0.4608 −0.325
0.4629 −0.386
0.4643 −0.499
0.4657 −0.562
0.4678 −0.634
0.4720 −0.730
0.4740 −0.761
0.4754 −0.788
0.4838 −0.852
0.4851 −0.856
0.4879 −0.867
0.4893 −0.869
0.4928 −0.861
0.4942 −0.852
0.4976 −0.835
0.4997 −0.826
0.5025 −0.807
0.5039 −0.804
0.5074 −0.780
0.5108 −0.763
0.5136 −0.735
0.5150 −0.730
0.5296 −0.630
0.5372 −0.559

2439648 +
0.4309 −0.442
0.4358 −0.697
0.4379 −0.784
0.4400 −0.823
0.4414 −0.853
0.4448 −0.913
0.4462 −0.959
0.4476 −0.971
0.4511 −1.012
0.4525 −1.023
0.4546 −1.031
0.4580 −1.013
0.4601 −1.014
0.4615 −1.032
0.4650 −1.033
0.4664 −1.034
0.4677 −1.029
0.4733 −0.984
0.4761 −0.986
0.4809 −0.919
0.4823 −0.906
0.4844 −0.890
0.4879 −0.859
0.4893 −0.855
0.4955 −0.788
0.4969 −0.761

2439667 +
0.4734 +0.173
0.4748 +0.038
0.4761 −0.072
0.4789 −0.272
0.4803 −0.392
0.4831 −0.649
0.4845 −0.734
0.4873 −0.849
0.4886 −0.919
0.4914 −1.044
0.4956 −1.131
0.4970 −1.160
0.4998 −1.209
0.5011 −1.234
0.5039 −1.261
0.5053 −1.293
0.5081 −1.317
0.5095 −1.314
0.5123 −1.293
0.5136 −1.275
0.5178 −1.234
0.5206 −1.215
0.5220 −1.207
0.5248 −1.188
0.5261 −1.168
0.5289 −1.126
0.5303 −1.103

2439710 +
0.4294 +0.060
0.4328 −0.074
0.4342 −0.174
0.4370 −0.286
0.4384 −0.361
0.4412 −0.500
0.4426 −0.579
0.4453 −0.691
0.4467 −0.737
0.4495 −0.833
0.4509 −0.881
0.4537 −0.938
0.4551 −0.995

2439711 +
0.3412 −1.065
0.3439 −1.072
0.3502 −1.087
0.3516 −1.089
0.3537 −1.092
0.3578 −1.086
0.3592 −1.087
0.3606 −1.076
0.3641 −1.049
0.3676 −1.006
0.3710 −0.986
0.3724 −0.973
0.3738 −0.948
0.3780 −0.903
0.3801 −0.850
0.3814 −0.837

2439714 +
0.4127 −0.454
0.4169 −0.655
0.4196 −0.776
0.4231 −0.889
0.4259 −0.951
0.4287 −1.024
0.4335 −1.111
0.4356 −1.134
0.4377 −1.141
0.4412 −1.146
0.4432 −1.146
0.4446 −1.143
0.4481 −1.111
0.4495 −1.095
0.4509 −1.079
0.4544 −1.042
0.4558 −1.034
0.4571 −1.010
0.4599 −0.981
0.4613 −0.953

2439722 +
0.3717 −0.639
0.3745 −0.710
0.3793 −0.779
0.3807 −0.790
0.3821 −0.809
0.3842 −0.829
0.3863 −0.862
0.3911 −0.927
0.3939 −0.950
0.3967 −0.961
0.4015 −0.974
0.4036 −0.980
0.4050 −0.967
0.4085 −0.903
0.4133 −0.872
0.4154 −0.866
0.4196 −0.877
0.4224 −0.885
0.4245 −0.893
0.4286 −0.867
0.4321 −0.829
0.4349 −0.781
0.4390 −0.719

2439726 +
0.3702 −0.591
0.3716 −0.642
0.3730 −0.703
0.3772 −0.847
0.3786 −0.887
0.3800 −0.917
0.3841 −1.043
0.3855 −1.071
0.3869 −1.095
0.3904 −1.120
0.3918 −1.109
0.3938 −1.092
0.3980 −1.102
0.4022 −1.093
0.4050 −1.093
0.4112 −1.002
0.4154 −0.943
0.4209 −0.839
0.4237 −0.772
0.4258 −0.736
0.4279 −0.703
0.4320 −0.630
0.4348 −0.602

2439738 +
0.3249 +0.379
0.3291 +0.397
0.3305 +0.410
0.3361 +0.359
0.3374 +0.327
0.3465 +0.056
0.3493 −0.031
0.3506 −0.096
0.3555 −0.309
0.3569 −0.394
0.3583 −0.438
0.3618 −0.572
0.3631 −0.639
0.3645 −0.687
0.3673 −0.761
0.3701 −0.844
0.3729 −0.929
0.3749 −0.998
0.3763 −1.035
0.3812 −1.112
0.3833 −1.123
0.3861 −1.134
0.3902 −1.130
0.3923 −1.119
0.3951 −1.086
0.3992 −1.040
0.4006 −1.009
0.4041 −0.977
0.4069 −0.943
0.4083 −0.934

2439923 +
0.4796 −0.944
0.4810 −0.942
0.4852 −0.938
0.4880 −0.933
0.4914 −0.915
0.4942 −0.901
0.4956 −0.897
0.4991 −0.882
0.5005 −0.870
0.5032 −0.849
0.5046 −0.839
0.5074 −0.808
0.5088 −0.804
0.5116 −0.769
0.5130 −0.762
0.5157 −0.748
0.5171 −0.727
0.5199 −0.681
0.5213 −0.660

2439942 +
0.4542 +0.374
0.4556 +0.379
0.4584 +0.365
0.4597 +0.359
0.4625 +0.345
0.4639 +0.330
0.4667 +0.323
0.4681 +0.319
0.4709 +0.333
0.4722 +0.337
0.4750 +0.332
0.4764 +0.325
0.4792 +0.320
0.4806 +0.307
0.4847 +0.335
0.4875 +0.349
0.4889 +0.357
0.4917 +0.320
0.4931 +0.327
0.4959 +0.340
0.4972 +0.324
0.5000 +0.327
0.5014 +0.322
0.5056 +0.336
0.5097 +0.335
0.5125 +0.333
0.5139 +0.313
0.5167 +0.278
0.5181 +0.267
0.5209 +0.246
0.5222 +0.201
0.5250 +0.115
0.5264 +0.056
0.5292 −0.091
0.5306 −0.203
0.5320 −0.254
0.5347 −0.418
0.5361 −0.488
0.5375 −0.567
0.5417 −0.742
0.5431 −0.813
0.5459 −0.923
0.5472 −0.971
0.5486 −1.016
0.5514 −1.110
0.5528 −1.139
0.5542 −1.155
0.5570 −1.182
0.5584 −1.182
0.5597 −1.184
0.5625 −1.179
0.5639 −1.166
0.5653 −1.163
0.5681 −1.148
0.5695 −1.133
0.5709 −1.119
0.5736 −1.102
0.5750 −1.086
0.5764 −1.078

2439978 +
0.3628 +0.277
0.3642 +0.289
0.3669 +0.287
0.3683 +0.272
0.3711 +0.267
0.3725 +0.255
0.3753 +0.206
0.3767 +0.172
0.3794 +0.068
0.3808 +0.050
0.3836 +0.039
0.3850 +0.018
0.3878 −0.021
0.3892 −0.041
0.3933 −0.097
0.3961 −0.142
0.3975 −0.167
0.4003 −0.193
0.4017 −0.221
0.4044 −0.308
0.4058 −0.370
0.4086 −0.472
0.4100 −0.514
0.4128 −0.584
0.4142 −0.615
0.4170 −0.681
0.4183 −0.704
0.4211 −0.742
0.4225 −0.771
0.4253 −0.782
0.4267 −0.787
0.4294 −0.800
0.4308 −0.809
0.4336 −0.808
0.4350 −0.804
0.4378 −0.810
0.4392 −0.800
0.4420 −0.789
0.4433 −0.782
0.4461 −0.776
0.4475 −0.779
0.4503 −0.766
0.4517 −0.750
0.4544 −0.731
0.4558 −0.713
0.4586 −0.693
0.4600 −0.682
0.4628 −0.675

0.4642 −0.650
0.4669 −0.616
0.4683 −0.605

2439985 +
0.4550 +0.286
0.4564 +0.293
0.4592 +0.323
0.4828 +0.244
0.4912 +0.177
0.4967 +0.093
0.5099 −0.238
0.5120 −0.348
0.5148 −0.501
0.5162 −0.536
0.5203 −0.645
0.5217 −0.682
0.5245 −0.789
0.5259 −0.827
0.5287 −0.872
0.5300 −0.905
0.5328 −0.912
0.5342 −0.927
0.5370 −0.946
0.5384 −0.954
0.5412 −0.954
0.5426 −0.949
0.5453 −0.942
0.5467 −0.935
0.5495 −0.898
0.5509 −0.899
0.5537 −0.867
0.5578 −0.846
0.5606 −0.831
0.5620 −0.816
0.5648 −0.776
0.5662 −0.771
0.5689 −0.764
0.5703 −0.752

2439993 +
0.4688 +0.016
0.4702 −0.034
0.4730 −0.191
0.4744 −0.245
0.4772 −0.369
0.4786 −0.427
0.4813 −0.524
0.4827 −0.549
0.4855 −0.641
0.4869 −0.679
0.4897 −0.750
0.4911 −0.771
0.4952 −0.877
0.4980 −0.950
0.5022 −1.026
0.5036 −1.035
0.5084 −1.062
0.5119 −1.053
0.5133 −1.051
0.5161 −1.014
0.5174 −0.993

2440012 +
0.4595 +0.226
0.4630 +0.090
0.4644 +0.054
0.4672 −0.001
0.4686 −0.035
0.4713 −0.128
0.4727 −0.190
0.4762 −0.324
0.4790 −0.413
0.4804 −0.469
0.4831 −0.546
0.4845 −0.614
0.4873 −0.685
0.4887 −0.704
0.4915 −0.753
0.4929 −0.761
0.4956 −0.790
0.4998 −0.833
0.5012 −0.841
0.5040 −0.878
0.5054 −0.875
0.5081 −0.886
0.5095 −0.898
0.5123 −0.908
0.5137 −0.919
0.5165 −0.907
0.5206 −0.898
0.5220 −0.892
0.5248 −0.878
0.5262 −0.875
2440067 +
0.4009 +0.342
0.4023 +0.365
0.4051 +0.348
0.4064 +0.340
0.4092 +0.330
0.4106 +0.302
0.4134 +0.317
0.4148 +0.322
0.4176 +0.289
0.4190 +0.281
0.4217 +0.231
0.4231 +0.212
0.4259 +0.175
0.4273 +0.157
0.4460 −0.427
0.4474 −0.469
0.4502 −0.600
0.4516 −0.638
0.4544 −0.695
0.4558 −0.706
0.4585 −0.710
0.4599 −0.722
0.4627 −0.797
0.4641 −0.844

2440338 +
0.4257 +0.340
0.4270 +0.336
0.4298 +0.309
0.4312 +0.303
0.4340 +0.298
0.4354 +0.279
0.4395 +0.227
0.4437 +0.165
0.4465 +0.115
0.4479 +0.096
0.4507 −0.003
0.4520 −0.024
0.4548 −0.097
0.4562 −0.118
0.4590 −0.182
0.4604 −0.232
0.4632 −0.333
0.4646 −0.393
0.4673 −0.498
0.4687 −0.533
0.4715 −0.640
0.4729 −0.671
0.4757 −0.717
0.4770 −0.720
0.4798 −0.714
0.4812 −0.738
0.4840 −0.767
0.4854 −0.801
0.4882 −0.822
0.4895 −0.823
0.4923 −0.840
0.4937 −0.837
0.4965 −0.839
0.4979 −0.839
0.5007 −0.835
0.5020 −0.831
0.5048 −0.820
0.5062 −0.811
0.5090 −0.802
0.5104 −0.806
0.5132 −0.804
0.5145 −0.798
0.5173 −0.778
0.5187 −0.781
0.5215 −0.764
0.5229 −0.730
0.5257 −0.714
0.5270 −0.702

2440354 +
0.4005 +0.222
0.4019 +0.235
0.4047 +0.211
0.4061 +0.213
0.4089 +0.233
0.4103 +0.229
0.4131 +0.230
0.4145 +0.222
0.4173 +0.228
0.4187 +0.221
0.4214 +0.207
0.4228 +0.197
0.4256 +0.177
0.4270 +0.153
0.4339 +0.051
0.4367 −0.016
0.4381 −0.052
0.4409 −0.156
0.4423 −0.191
0.4492 −0.420
0.4506 −0.471
0.4534 −0.580
0.4548 −0.616
0.4575 −0.689
0.4589 −0.732
0.4617 −0.821
0.4631 −0.866
0.4659 −0.907
0.4673 −0.915
0.4700 −0.918
0.4714 −0.921
0.4742 −0.926
0.4756 −0.936
0.5048 −0.932
0.5062 −0.927

2440357 +
0.4830 +0.335
0.4844 +0.342
0.4872 +0.351
0.4914 +0.343
0.4928 +0.345
0.4955 +0.371
0.4969 +0.385
0.4997 +0.410
0.5011 +0.409
0.5039 +0.409
0.5053 +0.411
0.5080 +0.406
0.5094 +0.395
0.5122 +0.407
0.5136 +0.393
0.5164 +0.389
0.5178 +0.397
0.5219 +0.392
0.5247 +0.371
0.5261 +0.368
0.5289 +0.388
0.5303 +0.377
0.5330 +0.328
0.5463 +0.002
0.5504 −0.088
0.5518 −0.117
0.5546 −0.234

0.5560 −0.290
0.5587 −0.443
0.5601 −0.485

2440389 +
0.4355 −0.975
0.4369 −0.986
0.4390 −1.008
0.4404 −1.027
0.4425 −1.031
0.4439 −1.037
0.4460 −1.042
0.4474 −1.043
0.4494 −1.039
0.4508 −1.037
0.4529 −1.019
0.4564 −0.980
0.4578 −0.971

2440420 +
0.3787 +0.203
0.3814 +0.184
0.3828 +0.159
0.3856 +0.073
0.3870 +0.048
0.3898 −0.002
0.3912 −0.044
0.3939 −0.145
0.3953 −0.209
0.3981 −0.336
0.3995 −0.389
0.4023 −0.454
0.4037 −0.498
0.4064 −0.573
0.4078 −0.610
0.4106 −0.701
0.4120 −0.717
0.4148 −0.757
0.4162 −0.803
0.4189 −0.836
0.4203 −0.838
0.4231 −0.851
0.4245 −0.853
0.4273 −0.854
0.4287 −0.851
0.4314 −0.852
0.4328 −0.849

0.4356 −0.847
0.4370 −0.844
0.4398 −0.838
0.4412 −0.834
0.4439 −0.824
0.4453 −0.812
0.4481 −0.789
0.4495 −0.777
0.4516 −0.748
0.4530 −0.738

2440436 +
0.3412 +0.406
0.3426 +0.403
0.3537 +0.414
0.3551 +0.412
0.3592 +0.371
0.3620 +0.301
0.3634 +0.272
0.3676 +0.225
0.3717 +0.155
0.3759 +0.101
0.3787 −0.009
0.3801 −0.049
0.3828 −0.189
0.3842 −0.272
0.3870 −0.356
0.3884 −0.411
0.3912 −0.537
0.3926 −0.570
0.3953 −0.652
0.3967 −0.689
0.3995 −0.764
0.4009 −0.799
0.4037 −0.841
0.4051 −0.874
0.4078 −0.908
0.4092 −0.930
0.4120 −0.963
0.4134 −0.976
0.4162 −0.969
0.4176 −0.964
0.4203 −0.945
0.4217 −0.931
0.4245 −0.891
0.4259 −0.886
0.4287 −0.874

0.4301 −0.855
0.4328 −0.841
0.4342 −0.833

2440439 +
0.4465 +0.450
0.4479 +0.457
0.4507 +0.434
0.4521 +0.434
0.4549 +0.429
0.4563 +0.432
0.4590 +0.393
0.4632 +0.366
0.4674 +0.340
0.4688 +0.332
0.4715 +0.336
0.4729 +0.326
0.4757 +0.278
0.4771 +0.192
0.4799 +0.092
0.4813 +0.053
0.4840 −0.063
0.4854 −0.157
0.4882 −0.260
0.4896 −0.342
0.4924 −0.444
0.4938 −0.494
0.4965 −0.543
0.4979 −0.584
0.5007 −0.721
0.5021 −0.779
0.5049 −0.851
0.5063 −0.902
0.5111 −0.954
0.5125 −0.954
0.5153 −0.990
0.5167 −1.011
0.5194 −1.023
0.5208 −1.024
0.5236 −1.014
0.5250 −0.994
0.5278 −0.963
0.5292 −0.941
0.5319 −0.919
0.5333 −0.899
0.5361 −0.879
0.5375 −0.874

0.5403 −0.857

2440675 +
0.4954 +0.306
0.4968 +0.281
0.4982 +0.271
0.5010 +0.252
0.5066 +0.220
0.5080 +0.197
0.5094 +0.190
0.5121 +0.144
0.5135 +0.108
0.5149 +0.070
0.5177 +0.003
0.5191 −0.031
0.5205 −0.057
0.5232 −0.103
0.5246 −0.129
0.5260 −0.165
0.5288 −0.310
0.5302 −0.375
0.5316 −0.415
0.5357 −0.571
0.5371 −0.633
0.5399 −0.733
0.5413 −0.767
0.5427 −0.805
0.5454 −0.868
0.5468 −0.895
0.5482 −0.907
0.5510 −0.940
0.5524 −0.967
0.5538 −0.971
0.5566 −0.995
0.5580 −1.001
0.5594 −1.001
0.5621 −0.999
0.5635 −0.991
0.5649 −0.992
0.5677 −0.980
0.5691 −0.974
0.5705 −0.975
0.5732 −0.956
0.5746 −0.947
0.5760 −0.939
0.5788 −0.918
0.5802 −0.908

2440707 +
0.3982 +0.308
0.3996 +0.284
0.4024 +0.219
0.4093 +0.007
0.4107 −0.043
0.4135 −0.114
0.4149 −0.143
0.4176 −0.219
0.4190 −0.266
0.4218 −0.397
0.4232 −0.471
0.4260 −0.552
0.4274 −0.600
0.4301 −0.665
0.4315 −0.705
0.4343 −0.733
0.4385 −0.794
0.4398 −0.804
0.4426 −0.828
0.4468 −0.878
0.4482 −0.888
0.4510 −0.908
0.4524 −0.909
0.4558 −0.911
0.4586 −0.906
0.4600 −0.897
0.4628 −0.869
0.4642 −0.868
0.4669 −0.857

2440769 +
0.4150 +0.398
0.4164 +0.430
0.4192 +0.468
0.4205 +0.464
0.4233 +0.468
0.4247 +0.464
0.4274 +0.461
0.4288 +0.474
0.4316 +0.437
0.4330 +0.384
0.4358 +0.341
0.4372 +0.318
0.4399 +0.308
0.4413 +0.275
0.4441 +0.229

0.4455 +0.233
0.4483 +0.211
0.4497 +0.183
0.4524 +0.099
0.4538 +0.056
0.4566 −0.021
0.4608 −0.153
0.4622 −0.194
0.4649 −0.292
0.4691 −0.486
0.4705 −0.545
0.4747 −0.738
0.4774 −0.812
0.4788 −0.829
0.4816 −0.901
0.4830 −0.931
0.4858 −0.947
0.4872 −0.948
0.4899 −0.968
0.4913 −0.966
0.4941 −0.957
0.4955 −0.956
0.4983 −0.959
0.4997 −0.953
0.5024 −0.941
0.5038 −0.936

2440781 +
0.3932 +0.324
0.3960 +0.309
0.3974 +0.301
0.4002 +0.277
0.4043 +0.212
0.4057 +0.177
0.4084 +0.080
0.4098 +0.025
0.4126 −0.115
0.4140 −0.186
0.4168 −0.334
0.4182 −0.430
0.4210 −0.550
0.4223 −0.597
0.4251 −0.711
0.4265 −0.743
0.4286 −0.787
0.4300 −0.825
0.4328 −0.902

0.4341 −0.942
0.4369 −0.996
0.4383 −1.013
0.4411 −1.012
0.4425 −1.000
0.4453 −0.986
0.4467 −0.985
0.4495 −0.975
0.4509 −0.969
0.4536 −0.975
0.4550 −0.973
0.4578 −0.987
0.4592 −0.984
0.4620 −0.966
0.4634 −0.952
0.4661 −0.918
0.4675 −0.894
0.4703 −0.850
0.4717 −0.842
0.4745 −0.780
0.4759 −0.770

2440796 +
0.4221 −0.007
0.4234 −0.027
0.4262 −0.079
0.4290 −0.154
0.4304 −0.191
0.4332 −0.308
0.4346 −0.334
0.4373 −0.450
0.4387 −0.489
0.4415 −0.566
0.4429 −0.615
0.4457 −0.691
0.4471 −0.750
0.4498 −0.832
0.4512 −0.856

2440807 +
0.5043 +0.357
0.5057 +0.353
0.5084 +0.369
0.5098 +0.378
0.5126 +0.372
0.5140 +0.354
0.5168 +0.349

0.5182 +0.341
0.5209 +0.333
0.5251 +0.302
0.5265 +0.310
0.5293 +0.257
0.5307 +0.255
0.5334 +0.218
0.5348 +0.185
0.5376 +0.016
0.5390 −0.042
0.5418 −0.149
0.5432 −0.182
0.5459 −0.291
0.5473 −0.375
0.5501 −0.510
0.5515 −0.566
0.5543 −0.702
0.5557 −0.756
0.5584 −0.863
0.5598 −0.902
0.5624 −0.925
0.5668 −0.956
0.5682 −0.956
0.5709 −0.940
0.5751 −0.927
0.5793 −0.910

2440859 +
0.3356 +0.428
0.3370 +0.428
0.3426 +0.437
0.3440 +0.431
0.3454 +0.415
0.3481 +0.390
0.3592 +0.247
0.3604 +0.231
0.3618 +0.199
0.3648 +0.106
0.3662 +0.063
0.3676 +0.028
0.3703 −0.029
0.3717 −0.045
0.3731 −0.077
0.3773 −0.229
0.3787 −0.281
0.3814 −0.407
0.3828 −0.464

0.3842 −0.524
0.3877 −0.624
0.3891 −0.677
0.3933 −0.815
0.3947 −0.863
0.3959 −0.896
0.3995 −0.987
0.4009 −1.003
0.4023 −1.036
0.4071 −1.034
0.4085 −1.028
0.4099 −1.012
0.4141 −0.959
0.4155 −0.942
0.4169 −0.937
0.4203 −0.890
0.4217 −0.879

2440867 +
0.3102 +0.307
0.3116 +0.255
0.3165 +0.110
0.3241 −0.136
0.3255 −0.184
0.3304 −0.350
0.3333 −0.457
0.3373 −0.592
0.3387 −0.649
0.3436 −0.788
0.3450 −0.828
0.3498 −0.925
0.3512 −0.960
0.3547 −0.979
0.3568 −0.995
0.3609 −0.977
0.3630 −0.969
0.3693 −0.944
0.3748 −0.899
0.3762 −0.891

2440883 +
0.2550 −0.223
0.2564 −0.232
0.2578 −0.278
0.2605 −0.381
0.2619 −0.410
0.2668 −0.568

0.2682 −0.617
0.2696 −0.652
0.2730 −0.741
0.2744 −0.773
0.2758 −0.806
0.2779 −0.843
0.2793 −0.877
0.2807 −0.906
0.2841 −0.939
0.2855 −0.947
0.2869 −0.944
0.2907 −0.952
0.2921 −0.951
0.2935 −0.951
0.2952 −0.954
0.2966 −0.948
0.2980 −0.945
0.3008 −0.941
0.3022 −0.943
0.3036 −0.931
0.3064 −0.922
0.3078 −0.918

2441035 +
0.5945 +0.403
0.5959 +0.389
0.5969 +0.371
0.5992 +0.373
0.6003 +0.376
0.6015 +0.387
0.6041 +0.370
0.6094 +0.377
0.6106 +0.376
0.6118 +0.338
0.6153 +0.244
0.6180 +0.153
0.6217 +0.061
0.6231 −0.011
0.6245 −0.081
0.6269 −0.232
0.6281 −0.300
0.6296 −0.374
0.6321 −0.553
0.6334 −0.640
0.6347 −0.712
0.6376 −0.881
0.6388 −0.962

0.6401 −1.021
0.6432 −1.103
0.6447 −1.147
0.6460 −1.172

2441060 +
0.3983 +0.386
0.3997 +0.365
0.4023 +0.371
0.4047 +0.338
0.4088 +0.374
0.4100 +0.367
0.4130 +0.425
0.4144 +0.460
0.4179 +0.453
0.4190 +0.469
0.4201 +0.459
0.4237 +0.449
0.4248 +0.474
0.4275 +0.447
0.4288 +0.407
0.4299 +0.392
0.4322 +0.364
0.4374 +0.297
0.4425 +0.270
0.4437 +0.231
0.4450 +0.201
0.4474 +0.173
0.4484 +0.139
0.4503 +0.072
0.4528 +0.011
0.4538 −0.051
0.4548 −0.093
0.4576 −0.188
0.4598 −0.306
0.4625 −0.407
0.4635 −0.442
0.4669 −0.527
0.4681 −0.568
0.4691 −0.600
0.4714 −0.701
0.4724 −0.737
0.4734 −0.770

2441063 +
0.5031 +0.384
0.5042 +0.359
0.5078 +0.343
0.5089 +0.367
0.5115 +0.363
0.5128 +0.365
0.5142 +0.364
0.5168 +0.374
0.5182 +0.360
0.5219 +0.362
0.5232 +0.382
0.5243 +0.362
0.5298 +0.357
0.5311 +0.366
0.5324 +0.352
0.5359 +0.326
0.5371 +0.332
0.5395 +0.317
0.5408 +0.292
0.5420 +0.309
0.5444 +0.265
0.5506 +0.171
0.5542 +0.049
0.5553 −0.030
0.5565 −0.067
0.5604 −0.228
0.5617 −0.275
0.5641 −0.305
0.5652 −0.342
0.5663 −0.412
0.5686 −0.513
0.5698 −0.550
0.5709 −0.624
0.5730 −0.709
0.5741 −0.760
0.5752 −0.820
0.5775 −0.921
0.5786 −0.935
0.5819 −1.025
0.5830 −1.048
0.5867 −1.067
0.5878 −1.074
0.5889 −1.077

2441071 +
0.5156 −0.038
0.5166 −0.096
0.5177 −0.147
0.5200 −0.220
0.5211 −0.236
0.5221 −0.260
0.5242 −0.363
0.5252 −0.399
0.5261 −0.457
0.5288 −0.606
0.5298 −0.653
0.5308 −0.695
0.5340 −0.791
0.5362 −0.844
0.5397 −0.911
0.5408 −0.934
0.5457 −1.015
0.5467 −1.027
0.5502 −1.057
0.5527 −1.078
0.5538 −1.084
0.5564 −1.077
0.5592 −1.068
0.5653 −1.044

2441087 +
0.4114 +0.171
0.4126 +0.135
0.4137 +0.103
0.4179 +0.038
0.4192 +0.000
0.4205 −0.017
0.4229 −0.055
0.4254 −0.112
0.4266 −0.133
0.4278 −0.148
0.4303 −0.232
0.4316 −0.283
0.4328 −0.333
0.4340 −0.380
0.4369 −0.472
0.4393 −0.548
0.4407 −0.572
0.4433 −0.616
0.4453 −0.643
0.4470 −0.660
0.4497 −0.686
0.4520 −0.719
0.4531 −0.724
0.4558 −0.741
0.4571 −0.757
0.4583 −0.761
0.4597 −0.770
0.4621 −0.772
0.4632 −0.774
0.4657 −0.808
0.4681 −0.802
0.4692 −0.815
0.4703 −0.803
0.4715 −0.809
0.4739 −0.814
0.4751 −0.818
0.4763 −0.817
0.4774 −0.813
0.4815 −0.813
0.4840 −0.804
0.4854 −0.805
0.4883 −0.799
0.4897 −0.788
0.4909 −0.778
0.4923 −0.776
0.4950 −0.773
0.4975 −0.741
0.4987 −0.733
0.5013 −0.704
0.5026 −0.700
0.5038 −0.682
0.5049 −0.676

2441094 +
0.5297 +0.197
0.5307 +0.192
0.5317 +0.185
0.5327 +0.164
0.5347 +0.131
0.5360 +0.117
0.5371 +0.094
0.5385 +0.063
0.5396 +0.028
0.5423 −0.038
0.5445 −0.086
0.5457 −0.123
0.5480 −0.219
0.5491 −0.239
0.5511 −0.284
0.5534 −0.388
0.5543 −0.441
0.5554 −0.508
0.5565 −0.561
0.5587 −0.646

2441095 +
0.4170 +0.227
0.4185 +0.194
0.4208 +0.155
0.4232 +0.115
0.4242 +0.096
0.4262 +0.030
0.4284 −0.025
0.4295 −0.067
0.4317 −0.128
0.4328 −0.150
0.4352 −0.230
0.4365 −0.269
0.4376 −0.304
0.4388 −0.361
0.4398 −0.398
0.4423 −0.507
0.4434 −0.537
0.4445 −0.574
0.4458 −0.629
0.4484 −0.697
0.4496 −0.745
0.4631 −0.993
0.4666 −1.017
0.4678 −1.012
0.4688 −1.008
0.4699 −1.013
0.4723 −1.022
0.4735 −1.021
0.4745 −1.023
0.4756 −1.016
0.4779 −1.006
0.4791 −1.004
0.4802 −0.998
0.4814 −0.981
0.4839 −0.958
0.4851 −0.951
0.4865 −0.949
0.4878 −0.939

2441118 +
0.4680 −1.006
0.4694 −1.050
0.4704 −1.090

0.4715 −1.111
0.4735 −1.149
0.4747 −1.181
0.4758 −1.195
0.4770 −1.201
0.4797 −1.211
0.4808 −1.217
0.4819 −1.215
0.4831 −1.207
0.4860 −1.179
0.4876 −1.158
0.4888 −1.131
0.4902 −1.112
0.4927 −1.077
0.4938 −1.063
0.4949 −1.049
0.4960 −1.042
0.4984 −1.010
0.4997 −0.993
0.5011 −0.979
0.5025 −0.969

2441126 +
0.4068 −0.247
0.4082 −0.287
0.4089 −0.322
0.4103 −0.423
0.4137 −0.520
0.4151 −0.529
0.4165 −0.523
0.4179 −0.549
0.4206 −0.626
0.4220 −0.665
0.4234 −0.692
0.4243 −0.721
0.4283 −0.760
0.4297 −0.771
0.4311 −0.789
0.4325 −0.818
0.4345 −0.848
0.4373 −0.876
0.4388 −0.885
0.4470 −0.932
0.4485 −0.934

2441161 +
0.3723 +0.328
0.3734 +0.332
0.3748 +0.341
0.3776 +0.334
0.3801 +0.321
0.3828 +0.321
0.3840 +0.311
0.3852 +0.296
0.3884 +0.270
0.3896 +0.241
0.3909 +0.225
0.3930 +0.207
0.3941 +0.221
0.3953 +0.196
0.3981 +0.109
0.3995 +0.070
0.4008 +0.026
0.4037 −0.050
0.4050 −0.088
0.4063 −0.125
0.4087 −0.221
0.4112 −0.339
0.4134 −0.456
0.4146 −0.508
0.4159 −0.573
0.4195 −0.720
0.4207 −0.767
0.4219 −0.816
0.4256 −0.903
0.4269 −0.918
0.4291 −0.931
0.4305 −0.930
0.4318 −0.933
0.4340 −0.921
0.4356 −0.919
0.4373 −0.910

2441189 +
0.3077 +0.562
0.3091 +0.558
0.3120 +0.520
0.3130 +0.520
0.3141 +0.508
0.3166 +0.467
0.3193 +0.440
0.3208 +0.436
0.3264 +0.379
0.3307 +0.300
0.3321 +0.237
0.3331 +0.165
0.3358 +0.082
0.3370 +0.056
0.3383 +0.007
0.3410 −0.080
0.3423 −0.174
0.3436 −0.275
0.3459 −0.367
0.3471 −0.408
0.3483 −0.470
0.3508 −0.576
0.3521 −0.664
0.3532 −0.704
0.3556 −0.807
0.3569 −0.866
0.3579 −0.900
0.3601 −0.991
0.3611 −1.027
0.3624 −1.051
0.3648 −1.106
0.3661 −1.133
0.3672 −1.157
0.3701 −1.218
0.3714 −1.243
0.3727 −1.262
0.3754 −1.257
0.3766 −1.266
0.3802 −1.248
0.3815 −1.244
0.3829 −1.230
0.3853 −1.221
0.3866 −1.203
0.3877 −1.190
0.3902 −1.169
0.3915 −1.164
0.3927 −1.147
0.3950 −1.127
0.3962 −1.105
0.3978 −1.085

2441529 +
0.4841 +0.033
0.4876 −0.135
0.4917 −0.340
0.4931 −0.396
0.4973 −0.645
0.5001 −0.777
0.5015 −0.826
0.5042 −0.923
0.5056 −0.957
0.5098 −0.982
0.5126 −0.985
0.5140 −0.988
0.5167 −0.976
0.5181 −0.968
0.5209 −0.951
0.5223 −0.931
0.5278 −0.890
0.5306 −0.865
0.5320 −0.854
0.5348 −0.834
0.5362 −0.812

2441537 +
0.4181 +0.377
0.4195 +0.347
0.4222 +0.260
0.4236 +0.211
0.4278 +0.153
0.4306 +0.101
0.4320 +0.047
0.4361 −0.120
0.4389 −0.216
0.4403 −0.257
0.4445 −0.414
0.4472 −0.503
0.4486 −0.554
0.4514 −0.671
0.4528 −0.704
0.4556 −0.778
0.4570 −0.805
0.4597 −0.846
0.4611 −0.858
0.4639 −0.873
0.4653 −0.865
0.4681 −0.879
0.4695 −0.883

2441538 +
0.3347 −0.618
0.3361 −0.644
0.3472 −0.919
0.3486 −0.943
0.3507 −0.982
0.3521 −0.984
0.3556 −1.001
0.3570 −1.002
0.3597 −1.006
0.3611 −1.005
0.3639 −0.990
0.3681 −0.980
0.3694 −0.973
0.3722 −0.966
0.3736 −0.951
0.3764 −0.929
0.3778 −0.904
0.3806 −0.864
0.3820 −0.850
0.3847 −0.827
0.3861 −0.812

2441545 +
0.4039 +0.208
0.4052 +0.197
0.4063 +0.194
0.4082 +0.171
0.4095 +0.176
0.4109 +0.167
0.4143 +0.158
0.4155 +0.100
0.4169 +0.052
0.4197 −0.016
0.4211 −0.038
0.4226 −0.073
0.4253 −0.145
0.4266 −0.191
0.4280 −0.231
0.4307 −0.297
0.4320 −0.330
0.4362 −0.477
0.4377 −0.553
0.4391 −0.607
0.4422 −0.745
0.4436 −0.789
0.4448 −0.837
0.4478 −0.916
0.4492 −0.951
0.4507 −0.976
0.4535 −1.003
0.4548 −1.015

0.4561 −1.015
0.4589 −1.012
0.4602 −1.011
0.4616 −1.000
0.4646 −0.988
0.4661 −0.979
0.4675 −0.968
0.4704 −0.938
0.4719 −0.931
0.4735 −0.918
0.4764 −0.895
0.4778 −0.879
0.4793 −0.871

2441589 +
0.2669 +0.055
0.2683 +0.041
0.2710 +0.007
0.2724 −0.020
0.2752 −0.057
0.2766 −0.077
0.2794 −0.131
0.2808 −0.147
0.2835 −0.187
0.2849 −0.222
0.2877 −0.316
0.2891 −0.360
0.2933 −0.474
0.2960 −0.534
0.2974 −0.567
0.3002 −0.616
0.3016 −0.636
0.3044 −0.682
0.3058 −0.711
0.3085 −0.769
0.3099 −0.794
0.3141 −0.848
0.3169 −0.886
0.3183 −0.889
0.3210 −0.895
0.3224 −0.893
0.3252 −0.893
0.3266 −0.892
0.3294 −0.891
0.3308 −0.881
0.3335 −0.871
0.3349 −0.872
0.3377 −0.852
0.3391 −0.835

2441597 +
0.2641 +0.251
0.2660 +0.166
0.2709 +0.042
0.2727 −0.009
0.2767 −0.151
0.2785 −0.226
0.2802 −0.296
0.2842 −0.486
0.2860 −0.596
0.2876 −0.681
0.2892 −0.717
0.2930 −0.831
0.2947 −0.880
0.2964 −0.886
0.2979 −0.897
0.2996 −0.904
0.3012 −0.932
0.3050 −0.947
0.3067 −0.938
0.3083 −0.958
0.3099 −0.945
0.3116 −0.962
0.3150 −0.953
0.3166 −0.941
0.3182 −0.952
0.3199 −0.941
0.3245 −0.917
0.3261 −0.922

2441605 +
0.2392 +0.053
0.2416 −0.067
0.2443 −0.237
0.2450 −0.301
0.2471 −0.420
0.2481 −0.476
0.2503 −0.589
0.2510 −0.640
0.2531 −0.739
0.2538 −0.759
0.2558 −0.822
0.2568 −0.854
0.2593 −0.939
0.2603 −0.952
0.2628 −0.999
0.2635 −1.015
0.2652 −1.026
0.2659 −1.044
0.2683 −1.067
0.2697 −1.102
0.2718 −1.131
0.2732 −1.146
0.2760 −1.157
0.2770 −1.148
0.2795 −1.150
0.2805 −1.150
0.2829 −1.141
0.2843 −1.134
0.2867 −1.112
0.2877 −1.108
0.2899 −1.093
0.2909 −1.078
0.2940 −1.031
0.2947 −1.017

2441898 +
0.4315 +0.369
0.4373 +0.296
0.4401 +0.240
0.4429 +0.210
0.4456 +0.076
0.4486 −0.096
0.4516 −0.204
0.4548 −0.411
0.4579 −0.580
0.4607 −0.779
0.4635 −0.938
0.4663 −1.031
0.4692 −1.108
0.4719 −1.143
0.4746 −1.159
0.4774 −1.187
0.4802 −1.196
0.4858 −1.178
0.4887 −1.162
0.4917 −1.141
0.4945 −1.108

2441949 +
0.3484 +0.055
0.3513 −0.036
0.3570 −0.220
0.3601 −0.351
0.3633 −0.472
0.3664 −0.618
0.3696 −0.699
0.3735 −0.775
0.3768 −0.806
0.3799 −0.837

2442126 +
0.5298 +0.271
0.5312 +0.224
0.5325 +0.199
0.5337 +0.173
0.5410 +0.020
0.5422 −0.013
0.5434 −0.082
0.5445 −0.118
0.5457 −0.168
0.5513 −0.427
0.5525 −0.469
0.5537 −0.522
0.5548 −0.581
0.5560 −0.648
0.5573 −0.708
0.5585 −0.781
0.5596 −0.817
0.5635 −0.938
0.5647 −0.956
0.5658 −0.984
0.5670 −1.019
0.5680 −1.034
0.5691 −1.039
0.5703 −1.052
0.5714 −1.057
0.5725 −1.066

2442216 +
0.4266 +0.407
0.4281 +0.434
0.4294 +0.442
0.4346 +0.471
0.4355 +0.476
0.4371 +0.486
0.4385 +0.499
0.4437 +0.516
0.4450 +0.505
0.4462 +0.485
0.4476 +0.480
0.4527 +0.450
0.4544 +0.431
0.4559 +0.386
0.4581 +0.357
0.4622 +0.308
0.4635 +0.278
0.4661 +0.234
0.4708 +0.091
0.4723 +0.025
0.4737 −0.032
0.4749 −0.087
0.4803 −0.356
0.4816 −0.432
0.4827 −0.513
0.4840 −0.568
0.4853 −0.626
0.4900 −0.839
0.4913 −0.885
0.4928 −0.939
0.4941 −0.972
0.4956 −1.010
0.4970 −1.014
0.5018 −1.078
0.5034 −1.089
0.5049 −1.097
0.5063 −1.105
0.5076 −1.098
0.5089 −1.101
0.5136 −1.073
0.5149 −1.063
0.5177 −1.032
0.5191 −1.016
0.5256 −0.922
0.5270 −0.916
0.5284 −0.911

2442220 +
0.4523 +0.483
0.4539 +0.442
0.4574 +0.309
0.4591 +0.239
0.4625 +0.083
0.4641 −0.004
0.4677 −0.217

0.4693 −0.296
0.4728 −0.497
0.4735 −0.551
0.4768 −0.754
0.4787 −0.848
0.4818 −0.985
0.4836 −1.035
0.4870 −1.105
0.4886 −1.128
0.4922 −1.158
0.4972 −1.168
0.4987 −1.170
0.5021 −1.152
0.5038 −1.136
0.5077 −1.111
0.5097 −1.105

2442224 +
0.4344 +0.429
0.4359 +0.394
0.4389 +0.293
0.4407 +0.248
0.4442 +0.134
0.4457 +0.072
0.4479 −0.012
0.4493 −0.046
0.4509 −0.122
0.4551 −0.360
0.4572 −0.487
0.4591 −0.589
0.4633 −0.797
0.4664 −0.901
0.4680 −0.936
0.4710 −0.993
0.4726 −1.026
0.4758 −1.072
0.4774 −1.095

0.4808 −1.161
0.4819 −1.163
0.4851 −1.171
0.4886 −1.163
0.4949 −1.134

2442255 +
0.3820 +0.285
0.3879 +0.309
0.3956 +0.344
0.4022 +0.378
0.4083 +0.364
0.4138 +0.340
0.4186 +0.345
0.4228 +0.345
0.4277 +0.319
0.4326 +0.262
0.4426 +0.052
0.4470 −0.105
0.4541 −0.363
0.4599 −0.536
0.4639 −0.638
0.4697 −0.757

2442256 +
0.3459 −0.503
0.3511 −0.696
0.3560 −0.787
0.3618 −0.901

2442275 +
0.3547 +0.297
0.3567 +0.264
0.3582 +0.204
0.3610 +0.093
0.3636 −0.015
0.3658 −0.143

0.3680 −0.344
0.3704 −0.526
0.3730 −0.670
0.3750 −0.786
0.3772 −0.916
0.3795 −1.004
0.3819 −1.089
0.3848 −1.189
0.3862 −1.250
0.3883 −1.284
0.3912 −1.325

2442278 +
0.4482 +0.217
0.4496 +0.170
0.4509 +0.112
0.4524 +0.060
0.4538 −0.061
0.4593 −0.323
0.4607 −0.383
0.4620 −0.479
0.4635 −0.628
0.4648 −0.710
0.4703 −0.926
0.4718 −0.966
0.4732 −0.991
0.4745 −1.012
0.4760 −1.046
0.4811 −1.108
0.4825 −1.128
0.4840 −1.141
0.4854 −1.149
0.4867 −1.150
0.4881 −1.150
0.4947 −1.105

2442299 +
0.2969 +0.174
0.2979 +0.129
0.3009 +0.017
0.3017 −0.008
0.3026 −0.039
0.3055 −0.162
0.3065 −0.215
0.3075 −0.258
0.3085 −0.301
0.3105 −0.405
0.3115 −0.445
0.3125 −0.494
0.3135 −0.562
0.3173 −0.692
0.3184 −0.736
0.3194 −0.768
0.3204 −0.801

2442307 +
0.2698 +0.495
0.2708 +0.458
0.2743 +0.216
0.2754 +0.118
0.2782 +0.001
0.2788 −0.020
0.2812 −0.132
0.2819 −0.178
0.2844 −0.306
0.2879 −0.464
0.2892 −0.526
0.2919 −0.642
0.2929 −0.679
0.2959 −0.771
0.2969 −0.809
0.2999 −0.900
0.3010 −0.925
0.3045 −1.042

0.3055 −1.067
0.3094 −1.108
0.3104 −1.121
0.3142 −1.119
0.3149 −1.114
0.3184 −1.095
0.3237 −1.067
0.3250 −1.063
0.3288 −1.029
0.3337 −0.954

2442454 +
0.6255 +0.290
0.6265 +0.276
0.6278 +0.288
0.6290 +0.295
0.6302 +0.285
0.6359 +0.300
0.6372 +0.295
0.6383 +0.303
0.6394 +0.284
0.6408 +0.294
0.6494 +0.288
0.6508 +0.293
0.6521 +0.273
0.6540 +0.297
0.6549 +0.306
0.6598 +0.289
0.6612 +0.286
0.6630 +0.311
0.6644 +0.313
0.6664 +0.307
0.6713 +0.328
0.6727 +0.299
0.6741 +0.321

Table 6. Photoelectric differential V observations of RW Dra

2436318 +
0.4992 +0.441
0.5018 +0.414
0.5040 +0.405
0.5100 +0.261
0.5130 +0.169
0.5172 +0.010
0.5234 −0.351

0.5276 −0.561
0.5318 −0.755
0.5387 −0.885
0.5429 −0.901
0.5456 −0.881
0.5526 −0.846
0.5561 −0.827
0.5588 −0.831

0.5672 −0.788
0.5713 −0.776
0.5748 −0.735
0.5811 −0.700
0.5845 −0.670

2436338 +
0.4201 +0.293

0.4230 +0.304
0.4255 +0.302
0.4301 +0.267
0.4324 +0.245
0.4349 +0.224
0.4401 +0.205
0.4427 +0.176
0.4500 +0.104

0.4525 +0.060
0.4551 +0.009
0.4603 −0.125
0.4633 −0.213
0.4660 −0.280
0.4715 −0.466
0.4743 −0.535
0.4774 −0.636

0.4832 −0.748
0.4863 −0.753
0.4888 −0.762
0.4942 −0.785
0.4969 −0.776
0.4992 −0.773
0.5045 −0.767
0.5071 −0.745
0.5096 −0.732
0.5173 −0.706
0.5215 −0.686

2436373 +
0.4110 +0.086
0.4144 +0.064
0.4175 +0.019
0.4232 −0.049
0.4263 −0.087
0.4298 −0.149
0.4374 −0.335
0.4412 −0.425
0.4447 −0.498
0.4527 −0.652
0.4638 −0.612
0.4707 −0.589
0.4749 −0.559
0.4791 −0.571
0.4860 −0.574
0.4895 −0.569
0.4923 −0.543
0.4985 −0.474
0.5020 −0.454
0.5048 −0.425
0.5110 −0.381
0.5159 −0.382
0.5190 −0.384

2436400 +
0.4288 +0.373
0.4321 +0.378
0.4352 +0.373
0.4418 +0.360
0.4453 +0.343
0.4483 +0.333
0.4542 +0.289
0.4577 +0.237
0.4607 +0.188
0.4671 −0.111
0.4698 −0.262
0.4726 −0.408
0.4781 −0.657
0.4802 −0.747
0.4820 −0.795
0.4862 −0.876
0.4886 −0.909
0.4914 −0.932
0.4962 −0.944
0.5018 −0.912
0.5080 −0.824
0.5108 −0.793
0.5136 −0.765
0.5192 −0.710
0.5219 −0.690
0.5247 −0.682
0.5303 −0.643
0.5330 −0.607
0.5358 −0.573
0.5414 −0.518
0.5442 −0.497
0.5469 −0.478
0.5504 −0.461

2436404 +
0.3920 +0.336
0.3957 +0.363
0.4056 +0.370
0.4082 +0.359
0.4110 +0.324
0.4166 +0.263
0.4193 +0.248
0.4221 +0.241
0.4277 +0.192
0.4305 +0.149
0.4332 +0.082
0.4402 −0.192
0.4430 −0.285
0.4492 −0.512
0.4513 −0.578
0.4534 −0.602
0.4586 −0.708
0.4610 −0.726
0.4638 −0.746
0.4693 −0.780
0.4721 −0.788
0.4749 −0.775
0.4805 −0.751
0.4832 −0.715
0.4860 −0.682
0.4957 −0.621
0.4985 −0.609
0.5041 −0.535
0.5096 −0.509

2436408 +
0.3977 +0.183
0.4008 +0.137
0.4031 +0.085
0.4080 −0.019
0.4104 −0.089
0.4129 −0.168
0.4182 −0.367
0.4210 −0.459
0.4241 −0.528
0.4293 −0.613
0.4328 −0.682
0.4362 −0.723
0.4443 −0.751
0.4472 −0.758
0.4538 −0.760
0.4563 −0.734
0.4587 −0.693
0.4636 −0.663
0.4665 −0.663
0.4692 −0.659
0.4761 −0.656
0.4814 −0.631
0.4884 −0.604
0.4907 −0.593

2436420 +
0.3855 +0.142
0.3902 +0.078
0.3952 +0.014
0.3976 −0.031
0.4001 −0.090
0.4053 −0.197
0.4095 −0.285
0.4124 −0.334
0.4164 −0.416
0.4187 −0.467
0.4209 −0.509
0.4254 −0.587
0.4280 −0.627

2436431 +
0.3872 +0.322
0.3900 +0.332
0.3928 +0.325
0.4011 +0.312
0.4039 +0.298
0.4067 +0.307
0.4157 +0.320
0.4192 +0.307
0.4219 +0.317
0.4299 +0.353
0.4330 +0.349
0.4358 +0.382
0.4421 +0.455
0.4448 +0.451
0.4476 +0.434
0.4546 +0.463
0.4567 +0.459
0.4594 +0.467
0.4717 +0.370
0.4745 +0.325
0.4772 +0.272
0.4834 +0.132
0.4862 +0.081
0.4900 +0.006
0.5040 −0.434
0.5062 −0.522
0.5087 −0.608
0.5116 −0.704
0.5143 −0.785
0.5167 −0.812
0.5194 −0.843
0.5231 −0.887
0.5264 −0.901
0.5292 −0.868
0.5319 −0.845
0.5344 −0.816
0.5428 −0.653
0.5457 −0.596

2436447 +
0.3583 +0.331
0.3607 +0.336
0.3630 +0.318
0.3654 +0.335
0.3699 +0.280
0.3723 +0.270
0.3833 +0.197
0.3877 +0.113
0.3896 +0.070
0.3924 −0.020
0.3972 −0.207
0.3992 −0.298
0.4013 −0.369
0.4080 −0.586
0.4100 −0.612
0.4148 −0.640
0.4169 −0.641
0.4188 −0.662
0.4228 −0.741
0.4248 −0.782
0.4269 −0.820

2436451 +
0.3822 −0.504
0.3868 −0.576
0.3892 −0.600
0.3917 −0.616
0.3966 −0.664
0.3995 −0.678
0.4025 −0.679
0.4078 −0.695
0.4104 −0.696
0.4130 −0.694
0.4181 −0.684
0.4208 −0.684
0.4234 −0.664
0.4282 −0.634

2436460 +
0.3265 −0.634
0.3292 −0.591
0.3314 −0.557
0.3360 −0.496
0.3384 −0.478
0.3407 −0.468
0.3450 −0.433
0.3481 −0.412
0.3515 −0.403

2436476 +
0.2464 −0.893
0.2501 −0.936
0.2522 −0.944
0.2547 −0.955
0.2592 −0.922
0.2691 −0.872
0.2721 −0.838
0.2747 −0.809

2436514 +
0.2846 +0.372
0.2867 +0.379
0.2889 +0.388
0.2937 +0.357
0.2958 +0.359
0.2979 +0.322
0.3062 +0.166
0.3090 +0.104
0.3132 +0.010
0.3153 −0.053
0.3173 −0.102
0.3218 −0.235
0.3260 −0.379
0.3295 −0.505
0.3313 −0.545
0.3332 −0.600
0.3369 −0.678
0.3388 −0.728
0.3406 −0.783
0.3443 −0.828
0.3462 −0.827
0.3480 −0.804
0.3499 −0.774
0.3533 −0.734

2436679 +
0.4912 +0.461
0.4940 +0.451
0.4968 +0.473
0.5027 +0.480
0.5055 +0.452
0.5082 +0.439
0.5138 +0.404
0.5164 +0.410
0.5190 +0.384
0.5246 +0.220
0.5272 +0.078
0.5292 +0.008
0.5343 −0.242
0.5373 −0.382
0.5402 −0.462
0.5450 −0.639
0.5473 −0.717
0.5497 −0.817
0.5542 −0.901
0.5562 −0.924
0.5632 −0.927
0.5694 −0.895
0.5817 −0.820
0.5854 −0.781
0.5910 −0.715
0.5937 −0.700
0.5963 −0.682

2436695 +
0.3446 +0.243
0.3478 +0.247
0.3513 +0.249
0.3583 +0.263
0.3625 +0.253
0.3663 +0.264
0.3737 +0.258
0.3774 +0.257
0.3808 +0.260
0.3874 +0.254
0.3904 +0.256
0.3930 +0.252
0.4028 +0.341
0.4055 +0.350
0.4083 +0.353
0.4138 +0.363
0.4166 +0.357
0.4194 +0.359
0.4277 +0.272
0.4305 +0.208
0.4333 +0.138
0.4378 +0.035
0.4406 −0.046
0.4426 −0.101
0.4471 −0.256
0.4492 −0.329
0.4520 −0.438
0.4572 −0.593
0.4614 −0.618
0.4659 −0.644
0.4680 −0.664
0.4701 −0.719
0.4746 −0.753
0.4788 −0.760
0.4829 −0.759
0.4871 −0.747
0.4930 −0.693
0.4951 −0.678
0.4971 −0.659
0.5013 −0.634
0.5055 −0.573
0.5076 −0.561

2436726 +
0.4361 +0.417
0.4410 +0.394
0.4434 +0.381
0.4493 +0.375
0.4521 +0.400
0.4549 +0.407
0.4594 +0.419
0.4615 +0.396
0.4698 +0.241
0.4719 +0.198
0.4756 +0.102
0.4770 +0.070

2436757 +
0.4273 +0.455
0.4315 +0.456
0.4336 +0.453
0.4357 +0.463
0.4398 +0.467
0.4440 +0.460
0.4482 +0.461
0.4503 +0.448
0.4523 +0.448
0.4565 +0.459
0.4586 +0.455
0.4607 +0.441
0.4648 +0.411
0.4669 +0.386
0.4690 +0.340
0.4732 +0.236
0.4753 +0.203
0.4773 +0.171
0.4819 −0.009
0.4839 −0.082
0.4896 −0.318
0.4910 −0.397
0.4924 −0.458
0.4959 −0.610
0.4972 −0.669
0.4986 −0.693
0.5014 −0.764
0.5028 −0.782
0.5042 −0.818
0.5070 −0.831
0.5084 −0.853
0.5097 −0.865
0.5125 −0.869
0.5139 −0.853
0.5153 −0.847
0.5194 −0.842
0.5214 −0.834
0.5235 −0.819
0.5277 −0.799
0.5298 −0.784
0.5318 −0.779
0.5353 −0.756
0.5374 −0.738
0.5395 −0.723
0.5437 −0.685

2436761 +
0.4603 +0.351
0.4658 +0.223
0.4679 +0.145
0.4724 −0.019
0.4752 −0.124
0.4773 −0.187
0.4818 −0.384
0.4846 −0.512
0.4866 −0.579
0.4912 −0.735
0.4932 −0.777
0.4957 −0.816
0.5002 −0.880
0.5026 −0.899
0.5049 −0.898
0.5094 −0.888
0.5120 −0.883
0.5180 −0.842
0.5233 −0.797
0.5450 −0.625
0.5473 −0.600

2436812 +
0.3805 +0.410
0.3860 +0.346
0.3910 +0.265
0.3927 +0.216
0.3943 +0.176
0.3987 +0.049
0.4003 +0.013
0.4021 −0.062
0.4058 −0.256
0.4077 −0.337
0.4096 −0.435
0.4138 −0.587
0.4171 −0.716
0.4189 −0.764
0.4260 −0.928
0.4279 −0.944
0.4299 −0.954

2437115 +
0.3833 −0.666
0.3853 −0.651
0.3922 −0.592
0.3940 −0.571
0.3962 −0.555
0.4001 −0.540
0.4020 −0.538
0.4037 −0.521
0.4068 −0.493
0.4098 −0.483
0.4186 −0.436
0.4200 −0.424
0.4213 −0.418
0.4243 −0.385
0.4260 −0.376
0.4275 −0.374
0.4317 −0.334
0.4334 −0.330
0.4368 −0.303
0.4414 −0.282
0.4433 −0.286
0.4447 −0.275

0.4531 −0.205
0.4545 −0.187
0.4561 −0.181
0.4615 −0.148
0.4632 −0.138
0.4645 −0.126

2437117 +
0.3749 +0.214
0.3768 +0.207
0.3786 +0.211
0.3825 +0.231
0.3879 +0.253
0.3916 +0.267
0.3934 +0.263
0.3953 +0.274
0.4029 +0.249
0.4048 +0.232
0.4066 +0.240
0.4103 +0.223
0.4117 +0.214
0.4133 +0.216
0.4168 +0.248
0.4214 +0.263
0.4233 +0.274
0.4270 +0.286
0.4286 +0.281
0.4305 +0.281
0.4342 +0.286
0.4360 +0.281
0.4376 +0.277
0.4409 +0.287
0.4427 +0.296
0.4446 +0.302
0.4494 +0.292
0.4513 +0.300
0.4578 +0.290
0.4617 +0.298
0.4636 +0.288
0.4652 +0.281
0.4687 +0.282
0.4705 +0.296
0.4721 +0.291
0.4918 +0.307
0.4934 +0.312
0.4981 +0.338
0.4999 +0.349

0.5013 +0.350
0.5052 +0.349
0.5066 +0.360
0.5080 +0.379
0.5138 +0.339
0.5152 +0.326
0.5207 +0.314
0.5221 +0.320
0.5249 +0.305
0.5263 +0.298
0.5277 +0.291
0.5302 +0.232
0.5313 +0.225
0.5323 +0.226
0.5344 +0.165
0.5372 +0.114

2437134 +
0.3665 +0.378
0.3679 +0.371
0.3692 +0.370
0.3723 +0.389
0.3737 +0.371
0.3751 +0.357
0.3779 +0.339
0.3793 +0.328
0.3807 +0.326
0.3834 +0.326
0.3852 +0.333
0.3866 +0.352
0.3894 +0.352
0.4334 −0.299
0.4348 −0.425
0.4378 −0.594
0.4387 −0.646
0.4397 −0.682
0.4447 −0.838
0.4463 −0.865
0.4498 −0.927
0.4515 −0.949
0.4529 −0.970
0.4557 −0.983
0.4570 −0.985
0.4584 −0.982
0.4626 −0.953
0.4640 −0.945
0.4654 −0.942

0.4695 −0.916
0.4718 −0.903
0.4737 −0.887
0.4781 −0.860
0.4797 −0.835
0.4820 −0.806
0.4855 −0.781
0.4873 −0.769
0.4890 −0.751
0.4940 −0.723
0.4961 −0.715
0.5145 −0.599
0.5255 −0.537
0.5286 −0.528
0.5315 −0.517
0.5412 −0.460
0.5428 −0.445

2437138 +
0.3565 +0.329
0.3588 +0.356
0.3625 +0.355
0.3646 +0.382
0.3670 +0.371
0.3706 +0.400
0.3722 +0.409
0.3739 +0.424
0.3785 +0.459
0.3799 +0.453
0.3838 +0.360
0.3852 +0.348
0.3868 +0.337
0.3896 +0.367
0.3924 +0.370
0.3984 +0.442
0.3998 +0.385
0.4011 +0.363
0.4065 +0.138
0.4079 +0.068
0.4093 +0.009
0.4123 −0.120
0.4137 −0.191
0.4150 −0.260
0.4190 −0.391
0.4204 −0.442
0.4218 −0.485
0.4262 −0.635

0.4275 −0.666
0.4304 −0.739
0.4317 −0.784
0.4331 −0.814
0.4359 −0.894
0.4373 −0.927
0.4387 −0.952
0.4415 −0.981
0.4429 −0.994
0.4443 −0.993
0.4503 −0.974
0.4517 −0.966
0.4560 −0.956
0.4574 −0.947
0.4588 −0.932
0.4618 −0.897
0.4632 −0.894
0.4646 −0.873
0.4687 −0.850
0.4701 −0.833
0.4715 −0.807
0.4746 −0.772
0.4757 −0.753
0.4809 −0.707
0.4823 −0.686
0.4836 −0.686
0.4864 −0.646
0.4878 −0.625
0.4892 −0.620
0.4934 −0.600
0.4947 −0.581
0.4975 −0.553
0.4989 −0.535
0.5003 −0.539
0.5033 −0.518
0.5047 −0.492
0.5060 −0.492
0.5088 −0.472

2437145 +
0.3596 +0.232
0.3623 +0.257
0.3650 +0.275
0.3720 +0.309
0.3748 +0.307
0.3776 +0.286
0.3838 +0.281

0.3866 +0.297
0.3890 +0.289
0.3974 +0.275
0.3998 +0.264
0.4053 +0.267
0.4074 +0.260
0.4109 +0.236
0.4161 +0.234
0.4189 +0.240
0.4337 +0.252
0.4356 +0.254
0.4379 +0.277
0.4430 +0.292
0.4443 +0.288
0.4510 +0.361
0.4531 +0.368
0.4552 +0.369
0.4587 +0.387
0.4603 +0.378
0.4619 +0.354
0.4661 +0.268
0.4680 +0.229
0.4698 +0.201
0.4744 +0.134
0.4765 +0.089
0.4830 −0.063
0.4844 −0.118
0.4858 −0.166
0.4911 −0.326
0.4925 −0.391
0.4943 −0.434
0.4999 −0.588
0.5018 −0.628
0.5073 −0.720
0.5092 −0.748
0.5112 −0.771
0.5168 −0.788
0.5209 −0.783
0.5247 −0.772
0.5265 −0.745
0.5330 −0.690
0.5348 −0.691
0.5374 −0.653
0.5420 −0.585
0.5436 −0.570
0.5455 −0.571
0.5497 −0.544

2437149 +
0.3807 +0.278
0.3828 +0.278
0.3842 +0.283
0.3931 +0.281
0.3946 +0.277
0.3960 +0.274
0.4001 +0.287
0.4015 +0.295
0.4029 +0.303
0.4064 +0.336
0.4078 +0.350
0.4092 +0.358
0.4133 +0.369
0.4170 +0.402
0.4184 +0.387
0.4214 +0.399
0.4228 +0.395
0.4291 +0.367
0.4323 +0.344
0.4342 +0.320
0.4402 +0.238
0.4427 +0.164
0.4453 +0.076
0.4508 −0.065
0.4536 −0.158
0.4564 −0.225
0.4606 −0.366
0.4631 −0.455
0.4673 −0.566
0.4691 −0.596
0.4724 −0.628
0.4738 −0.626
0.4751 −0.634
0.4784 −0.654
0.4798 −0.654
0.4812 −0.661
0.4851 −0.664
0.4865 −0.662
0.4879 −0.679
0.4911 −0.679
0.4925 −0.670
0.4939 −0.667
0.4985 −0.650
0.4999 −0.661
0.5018 −0.645
0.5050 −0.643
0.5066 −0.635
0.5082 −0.624
0.5126 −0.609
0.5140 −0.604
0.5156 −0.583
0.5203 −0.546
0.5231 −0.526
0.5263 −0.495
0.5284 −0.483
0.5300 −0.462

2437173 +
0.3410 +0.354
0.3429 +0.365
0.3449 +0.381
0.3497 +0.374
0.3514 +0.375
0.3536 +0.383
0.3577 +0.394
0.3600 +0.417
0.3612 +0.429
0.3679 +0.420
0.3699 +0.419
0.3763 +0.367
0.3781 +0.327
0.3848 +0.216
0.3874 +0.173
0.3917 +0.065
0.3939 +0.022
0.3958 −0.021
0.3996 −0.139
0.4014 −0.201
0.4032 −0.288
0.4080 −0.490
0.4098 −0.561
0.4111 −0.619
0.4142 −0.715
0.4156 −0.763
0.4170 −0.808
0.4199 −0.854
0.4231 −0.880
0.4262 −0.884
0.4275 −0.880
0.4289 −0.887
0.4317 −0.876
0.4334 −0.862
0.4362 −0.853
0.4396 −0.823
0.4410 −0.803
0.4428 −0.791
0.4465 −0.767
0.4533 −0.727
0.4555 −0.708
0.4610 −0.657
0.4634 −0.649
0.4650 −0.630
0.4690 −0.620
0.4708 −0.606

2437175 +
0.3244 −0.063
0.3268 −0.029
0.3286 −0.028
0.3328 +0.014
0.3349 +0.031
0.3367 +0.054
0.3413 +0.074
0.3462 +0.105
0.3508 +0.134
0.3529 +0.138
0.3552 +0.161
0.3603 +0.174
0.3626 +0.186
0.3652 +0.191
0.3700 +0.210
0.3721 +0.194
0.3746 +0.227
0.3853 +0.285
0.3874 +0.288
0.3895 +0.306
0.3933 +0.320
0.3975 +0.318

2437467 +
0.4676 +0.463
0.4718 +0.454
0.4739 +0.446
0.4784 +0.423
0.4805 +0.406
0.4825 +0.396
0.4867 +0.368
0.4888 +0.342
0.4909 +0.266
0.4947 +0.154
0.4975 +0.097
0.5005 +0.015
0.5019 −0.040
0.5033 −0.114
0.5067 −0.257
0.5081 −0.303
0.5095 −0.361
0.5130 −0.474
0.5144 −0.521
0.5158 −0.553
0.5183 −0.636
0.5197 −0.688
0.5211 −0.722
0.5239 −0.812
0.5252 −0.832
0.5266 −0.851
0.5294 −0.895
0.5308 −0.909
0.5322 −0.922
0.5350 −0.940
0.5364 −0.943
0.5405 −0.931
0.5419 −0.922
0.5433 −0.918
0.5461 −0.898

2437468 +
0.3901 −0.131
0.3939 −0.306
0.3953 −0.359
0.3988 −0.527
0.4002 −0.586
0.4016 −0.655
0.4078 −0.796
0.4120 −0.868
0.4134 −0.891
0.4156 −0.920
0.4182 −0.950
0.4196 −0.955
0.4224 −0.967
0.4238 −0.968
0.4252 −0.968
0.4280 −0.954
0.4293 −0.941
0.4307 −0.936
0.4366 −0.881
0.4387 −0.865
0.4760 −0.546
0.4813 −0.509

2437480 +
0.3866 −0.570
0.3883 −0.560
0.3911 −0.547
0.3966 −0.530
0.3990 −0.504
0.4018 −0.496
0.4056 −0.451
0.4074 −0.437
0.4131 −0.419
0.4150 −0.410
0.4171 −0.393

2437483 +
0.4429 −0.814
0.4445 −0.830
0.4475 −0.836
0.4491 −0.823
0.4506 −0.802
0.4540 −0.797
0.4581 −0.770
0.4615 −0.742
0.4632 −0.737
0.4649 −0.715
0.4688 −0.705
0.4708 −0.677
0.4729 −0.668

2437487 +
0.3757 +0.232
0.3775 +0.182
0.3812 +0.109
0.3877 −0.079
0.3886 −0.094
0.3896 −0.116
0.3928 −0.225
0.3940 −0.289
0.3951 −0.341
0.3974 −0.412
0.3986 −0.446
0.3995 −0.454
0.4018 −0.499
0.4028 −0.514
0.4039 −0.536

0.4067 −0.577
0.4081 −0.582
0.4095 −0.584
0.4116 −0.584
0.4130 −0.585
0.4143 −0.603
0.4171 −0.633
0.4185 −0.649
0.4197 −0.673
0.4224 −0.713
0.4236 −0.723
0.4252 −0.725
0.4287 −0.728
0.4301 −0.724
0.4310 −0.726
0.4338 −0.724
0.4350 −0.729

2437490 +
0.4218 +0.252
0.4250 +0.252
0.4282 +0.226
0.4302 +0.228
0.4320 +0.248
0.4366 +0.287
0.4384 +0.298
0.4400 +0.294
0.4437 +0.325
0.4456 +0.331
0.4477 +0.342
0.4516 +0.346
0.4532 +0.352
0.4555 +0.350
0.4648 +0.327
0.4660 +0.309
0.4673 +0.295
0.4702 +0.267
0.4715 +0.244
0.4734 +0.236
0.4766 +0.192
0.4780 +0.162
0.4801 +0.118
0.4835 +0.053
0.4849 +0.048
0.4863 +0.024
0.4905 −0.120
0.4923 −0.179

0.4942 −0.269
0.4981 −0.374
0.5011 −0.421
0.5042 −0.455
0.5053 −0.483
0.5065 −0.496
0.5118 −0.553
0.5132 −0.577
0.5162 −0.588
0.5178 −0.607
0.5229 −0.648
0.5243 −0.654
0.5315 −0.673
0.5328 −0.680
0.5345 −0.662
0.5384 −0.649
0.5396 −0.638
0.5421 −0.631
0.5437 −0.633
0.5456 −0.639

2437494 +
0.4612 +0.232
0.4626 +0.252
0.4640 +0.241
0.4764 +0.157
0.4778 +0.133
0.4792 +0.103
0.4833 +0.034
0.4847 +0.016
0.4861 −0.001
0.4931 −0.115
0.4978 −0.254
0.4993 −0.295
0.5007 −0.325
0.5042 −0.426
0.5052 −0.472
0.5070 −0.522
0.5130 −0.628
0.5142 −0.630
0.5156 −0.640
0.5191 −0.664
0.5204 −0.677
0.5215 −0.676
0.5243 −0.677
0.5264 −0.680
0.5285 −0.694

0.5320 −0.695
0.5346 −0.688
0.5379 −0.669
0.5422 −0.663
0.5459 −0.644
0.5498 −0.618

2437840 +
0.4268 +0.231
0.4282 +0.205
0.4296 +0.194
0.4331 +0.161
0.4345 +0.159
0.4359 +0.134
0.4391 +0.071
0.4405 −0.004
0.4419 −0.035
0.4451 −0.148
0.4465 −0.227
0.4479 −0.289
0.4514 −0.452
0.4528 −0.485
0.4541 −0.559
0.4576 −0.696
0.4590 −0.739
0.4604 −0.770
0.4632 −0.794
0.4646 −0.797
0.4660 −0.813
0.4687 −0.849
0.4703 −0.856
0.4717 −0.865
0.4754 −0.901
0.4768 −0.921
0.4782 −0.944
0.4812 −0.958
0.4826 −0.954

2437851 +
0.4686 +0.408
0.4699 +0.385
0.4713 +0.385
0.4748 +0.373
0.4762 +0.361
0.4776 +0.366
0.4810 +0.314
0.4824 +0.280

0.4838 +0.256
0.4873 +0.198
0.4887 +0.143
0.4915 +0.079
0.4963 −0.071
0.4977 −0.141
0.4991 −0.235
0.5019 −0.388
0.5033 −0.419
0.5047 −0.440
0.5074 −0.554
0.5088 −0.627
0.5102 −0.702
0.5130 −0.803
0.5144 −0.839
0.5158 −0.867
0.5185 −0.898
0.5199 −0.907
0.5213 −0.911
0.5248 −0.915
0.5262 −0.916
0.5276 −0.910
0.5310 −0.901
0.5324 −0.887
0.5338 −0.880
0.5394 −0.803
0.5408 −0.782
0.5442 −0.739

2437852 +
0.3712 +0.106
0.3761 +0.011
0.3782 −0.059
0.3796 −0.101
0.3837 −0.263
0.3851 −0.305
0.3865 −0.335
0.3900 −0.424
0.4011 −0.754
0.4025 −0.768
0.4060 −0.803
0.4074 −0.803
0.4087 −0.806
0.4115 −0.830
0.4136 −0.820
0.4178 −0.805
0.4192 −0.795

0.4240 −0.772
0.4254 −0.763
0.4296 −0.704
0.4310 −0.697
0.4324 −0.694
0.4351 −0.659
0.4365 −0.625
0.4386 −0.617
0.4421 −0.576

2437856 +
0.3757 −0.549
0.3775 −0.570
0.3798 −0.612
0.3841 −0.649
0.3860 −0.669
0.3921 −0.670
0.3971 −0.659
0.4032 −0.611
0.4053 −0.589
0.4076 −0.566
0.4207 −0.448

2437867 +
0.4207 +0.095
0.4228 +0.049
0.4249 −0.003
0.4284 −0.065
0.4304 −0.112
0.4332 −0.154
0.4395 −0.283
0.4416 −0.334
0.4436 −0.378
0.4478 −0.457
0.4520 −0.496
0.4540 −0.508
0.4561 −0.520
0.4582 −0.555
0.4617 −0.557
0.4638 −0.554
0.4659 −0.568
0.4679 −0.573
0.4700 −0.571
0.4777 −0.576

2437871 +
0.3633 +0.155

0.3648 +0.146
0.3663 +0.151
0.3700 +0.182
0.3715 +0.179
0.3734 +0.179
0.3776 +0.205
0.3791 +0.196
0.3806 +0.215
0.3857 +0.190
0.3870 +0.203
0.3895 +0.197
0.3961 +0.200
0.3978 +0.192
0.4018 +0.193
0.4039 +0.168
0.4057 +0.153
0.4094 +0.193
0.4111 +0.200
0.4132 +0.197
0.4170 +0.220
0.4194 +0.188
0.4209 +0.171
0.4247 +0.118
0.4263 +0.090
0.4280 +0.086
0.4311 +0.075
0.4328 +0.030
0.4379 −0.046
0.4402 −0.093
0.4419 −0.128
0.4460 −0.203
0.4477 −0.235
0.4494 −0.260
0.4526 −0.332
0.4540 −0.359
0.4557 −0.383
0.4592 −0.451
0.4610 −0.489
0.4628 −0.514
0.4660 −0.543
0.4677 −0.539
0.4695 −0.550
0.4730 −0.581
0.4748 −0.575
0.4765 −0.575
0.4804 −0.565
0.4822 −0.567

0.4839 −0.561
0.4880 −0.550
0.4901 −0.549
0.4919 −0.541
0.4958 −0.519

2437883 +
0.3675 +0.300
0.3693 +0.324
0.3743 +0.318
0.3759 +0.319
0.3776 +0.296
0.3813 +0.281
0.3846 +0.310
0.3880 +0.273
0.3896 +0.267
0.3912 +0.251
0.3952 +0.234
0.3972 +0.213
0.3990 +0.186
0.4023 +0.140
0.4042 +0.108
0.4060 +0.048
0.4099 −0.056
0.4116 −0.115
0.4131 −0.162
0.4166 −0.227
0.4186 −0.285
0.4201 −0.333
0.4233 −0.443
0.4247 −0.468
0.4263 −0.504
0.4293 −0.581
0.4308 −0.624
0.4323 −0.657
0.4357 −0.716
0.4375 −0.735
0.4391 −0.761
0.4427 −0.778
0.4444 −0.783
0.4462 −0.781
0.4497 −0.795
0.4514 −0.796
0.4532 −0.786
0.4568 −0.780
0.4601 −0.759
0.4637 −0.727

0.4656 −0.717
0.4674 −0.714

2437895 +
0.3320 +0.003
0.3337 −0.041
0.3400 −0.284
0.3415 −0.305
0.3431 −0.382
0.3446 −0.421
0.3460 −0.476
0.3476 −0.547
0.3492 −0.584
0.3507 −0.612
0.3522 −0.646
0.3539 −0.669
0.3555 −0.692
0.3575 −0.711
0.3592 −0.713
0.3613 −0.710
0.3638 −0.703
0.3670 −0.702
0.3690 −0.702
0.3708 −0.702
0.3725 −0.713
0.3743 −0.702
0.3758 −0.703
0.3796 −0.713
0.3815 −0.705
0.3835 −0.695

2437903 +
0.2987 −0.207
0.2992 −0.229
0.3004 −0.317
0.3010 −0.341
0.3017 −0.376
0.3031 −0.408
0.3036 −0.417
0.3042 −0.426
0.3059 −0.455
0.3072 −0.471
0.3077 −0.451
0.3095 −0.470
0.3101 −0.485
0.3117 −0.518
0.3123 −0.536

0.3140 −0.572
0.3146 −0.599
0.3158 −0.634
0.3165 −0.641
0.3180 −0.636
0.3186 −0.642
0.3199 −0.657
0.3215 −0.643
0.3230 −0.655
0.3235 −0.668
0.3250 −0.678
0.3256 −0.684
0.3270 −0.688
0.3293 −0.677
0.3300 −0.679
0.3315 −0.678
0.3320 −0.679
0.3334 −0.684
0.3340 −0.667
0.3355 −0.660
0.3362 −0.647
0.3376 −0.651
0.3382 −0.652
0.3397 −0.647
0.3404 −0.635
0.3418 −0.631
0.3425 −0.641

2438163 +
0.3372 +0.000
0.3409 −0.175
0.3438 −0.309
0.3453 −0.379
0.3474 −0.452
0.3490 −0.489
0.3674 −0.593
0.3689 −0.594
0.3733 −0.593
0.3751 −0.587
0.3770 −0.586
0.3785 −0.573
0.3801 −0.577
0.3820 −0.562
0.3835 −0.562

2438236 +
0.3660 −0.033

0.3674 −0.062
0.3715 −0.127
0.3729 −0.178
0.3743 −0.209
0.3778 −0.263
0.3799 −0.299
0.3813 −0.341
0.3854 −0.411
0.3868 −0.422
0.3882 −0.428
0.3915 −0.466
0.3936 −0.485
0.3957 −0.504
0.4013 −0.537
0.4048 −0.560
0.4083 −0.581
0.4111 −0.595
0.4125 −0.597
0.4153 −0.602
0.4181 −0.603
0.4194 −0.601
0.4229 −0.586
0.4250 −0.581
0.4264 −0.580
0.4306 −0.568
0.4326 −0.566
0.4347 −0.543
0.4382 −0.533
0.4396 −0.529
0.4458 −0.488
0.4472 −0.481
0.4486 −0.474
0.4521 −0.441
0.4535 −0.431
0.4549 −0.425
0.4590 −0.411
0.4611 −0.397
0.4632 −0.394
0.4681 −0.362
0.4695 −0.351
0.4709 −0.342
0.4737 −0.323
0.4751 −0.309

2438248 +
0.3438 +0.239
0.3465 +0.247

0.3549 +0.180
0.3583 +0.155
0.3639 +0.129
0.3667 +0.102
0.3694 +0.080
0.3764 −0.034
0.3819 −0.159
0.3958 −0.504
0.4020 −0.639
0.4055 −0.673
0.4090 −0.678
0.4160 −0.676
0.4201 −0.649
0.4243 −0.627
0.4327 −0.559

2438264 +
0.3071 −0.365
0.3085 −0.385
0.3126 −0.555

2438267 +
0.3662 +0.362
0.3683 +0.328
0.3739 +0.281
0.3752 +0.268
0.3815 +0.103
0.3836 +0.056
0.3850 +0.026
0.3916 −0.151
0.3930 −0.198
0.3982 −0.420
0.4020 −0.571
0.4075 −0.754
0.4100 −0.817
0.4121 −0.825
0.4183 −0.857
0.4225 −0.848
0.4284 −0.841
0.4312 −0.820
0.4325 −0.790
0.4384 −0.743
0.4423 −0.716
0.4471 −0.659
0.4489 −0.641
0.4516 −0.635
0.4582 −0.577
0.4607 −0.535
0.4638 −0.519

2438284 +
0.2702 −0.696
0.2717 −0.693
0.2741 −0.695
0.2801 −0.691
0.2819 −0.691
0.2856 −0.688
0.2869 −0.689
0.2883 −0.689
0.2917 −0.682
0.2932 −0.676
0.2950 −0.663
0.2977 −0.669
0.2989 −0.668
0.3003 −0.636
0.3038 −0.612
0.3050 −0.617
0.3062 −0.608
0.3086 −0.587
0.3098 −0.584
0.3111 −0.582
0.3139 −0.558
0.3151 −0.543
0.3163 −0.532
0.3191 −0.509
0.3202 −0.521
0.3215 −0.500
0.3243 −0.478
0.3256 −0.461
0.3268 −0.456
0.3299 −0.423
0.3312 −0.403
0.3324 −0.390
0.3545 −0.237
0.3566 −0.237
0.3688 −0.142
0.3709 −0.135

2438291 +
0.3166 +0.429
0.3173 +0.407
0.3179 +0.389
0.3221 +0.329
0.3227 +0.290
0.3236 +0.293
0.3300 +0.203
0.3308 +0.194
0.3315 +0.196
0.3336 +0.158
0.3346 +0.107
0.3367 +0.040
0.3389 −0.004
0.3398 −0.017
0.3408 −0.040
0.3429 −0.097
0.3440 −0.184
0.3452 −0.242
0.3471 −0.343
0.3478 −0.380
0.3492 −0.409
0.3520 −0.487
0.3527 −0.515
0.3534 −0.561
0.3551 −0.645
0.3561 −0.694
0.3565 −0.707
0.3579 −0.718
0.3586 −0.729
0.3593 −0.754
0.3624 −0.797
0.3627 −0.798
0.3671 −0.838
0.3679 −0.841
0.3697 −0.853
0.3728 −0.867
0.3752 −0.877
0.3762 −0.881
0.3772 −0.873
0.3793 −0.869
0.3804 −0.869
0.3811 −0.870
0.3836 −0.880
0.3841 −0.884
0.3853 −0.864
0.3877 −0.857
0.3895 −0.860
0.3915 −0.855
0.3926 −0.851
0.3933 −0.843
0.3985 −0.807
0.3992 −0.793
0.4065 −0.701
0.4072 −0.698
0.4092 −0.672
0.4100 −0.646
0.4120 −0.613
0.4131 −0.613
0.4138 −0.591
0.4158 −0.593
0.4165 −0.590
0.4183 −0.549
0.4190 −0.527
0.4197 −0.512

2438585 +
0.4350 +0.025
0.4378 −0.043
0.4409 −0.138
0.4425 −0.191
0.4460 −0.342
0.4474 −0.386
0.4512 −0.540
0.4541 −0.598
0.4570 −0.667
0.4585 −0.695
0.4615 −0.734
0.4647 −0.766
0.4678 −0.813
0.4692 −0.832
0.4727 −0.893
0.4740 −0.900
0.4775 −0.900
0.4789 −0.900
0.4824 −0.892
0.4838 −0.880
0.4872 −0.858
0.4893 −0.850
0.4921 −0.829
0.4935 −0.817
0.4963 −0.791
0.4977 −0.788
0.5004 −0.779
0.5018 −0.764

2438605 +
0.3397 −0.520
0.3424 −0.590
0.3439 −0.626
0.3470 −0.649
0.3487 −0.664
0.3524 −0.642
0.3546 −0.630
0.3584 −0.610
0.3605 −0.627
0.3640 −0.660
0.3660 −0.623
0.3705 −0.575
0.3733 −0.559
0.3771 −0.515
0.3792 −0.497

2438608 +
0.4024 +0.127
0.4076 +0.096
0.4104 +0.080
0.4184 −0.015
0.4208 −0.071
0.4271 −0.300
0.4306 −0.390
0.4358 −0.467
0.4430 −0.518
0.4458 −0.515
0.4521 −0.518
0.4555 −0.530
0.4615 −0.543
0.4656 −0.534
0.4736 −0.512
0.4760 −0.513
0.4924 −0.452
0.4958 −0.429
0.5087 −0.345
0.5111 −0.349

2438621 +
0.3235 −0.355
0.3335 −0.503
0.3349 −0.535
0.3363 −0.558
0.3374 −0.574
0.3460 −0.687
0.3467 −0.676
0.3495 −0.704
0.3516 −0.700
0.3530 −0.728
0.3554 −0.723

0.3568 −0.716
0.3596 −0.673
0.3610 −0.664
0.3620 −0.677
0.3648 −0.624
0.3662 −0.629
0.3676 −0.609
0.3703 −0.593
0.3766 −0.541
0.3780 −0.535
0.3811 −0.529
0.3828 −0.511
0.3877 −0.467
0.3926 −0.449
0.3940 −0.451
0.3967 −0.420
0.3981 −0.414
0.4023 −0.410
0.4037 −0.411
0.4078 −0.380

2438636 +
0.3398 +0.288
0.3461 +0.311
0.3509 +0.166
0.3572 −0.154
0.3627 −0.448
0.3711 −0.880
0.3759 −0.953
0.3780 −0.957
0.3836 −0.935
0.3857 −0.923
0.3877 −0.913
0.3898 −0.906
0.3947 −0.884
0.3968 −0.847
0.4016 −0.820
0.4044 −0.798
0.4120 −0.747
0.4183 −0.712

2438655 +
0.3692 +0.220
0.3712 +0.217
0.3754 +0.224
0.3775 +0.237
0.3816 +0.210
0.3921 +0.130
0.3948 +0.083
0.3962 +0.045
0.3997 −0.078
0.4025 −0.180
0.4053 −0.313
0.4094 −0.440
0.4143 −0.569
0.4157 −0.580
0.4185 −0.591
0.4198 −0.612
0.4226 −0.624
0.4275 −0.661
0.4289 −0.657
0.4316 −0.669
0.4330 −0.654
0.4358 −0.651
0.4455 −0.640
0.4469 −0.635

2438664 +
0.2544 +0.388
0.2599 +0.348
0.2631 +0.294
0.2709 +0.205
0.2729 +0.153
0.2782 +0.049
0.2851 −0.142
0.2872 −0.205
0.2924 −0.339
0.2945 −0.384
0.2997 −0.528
0.3028 −0.596
0.3084 −0.673
0.3108 −0.716
0.3167 −0.754
0.3195 −0.773
0.3247 −0.800
0.3275 −0.788

2438668 +
0.2608 +0.120
0.2636 +0.085
0.2695 +0.029
0.2716 −0.020
0.2754 −0.178
0.2775 −0.237
0.2824 −0.415
0.2844 −0.502
0.2900 −0.660
0.2935 −0.745
0.2980 −0.794
0.3001 −0.791
0.3053 −0.802
0.3081 −0.801
0.3285 −0.724
0.3303 −0.716

2438965 +
0.4344 +0.329
0.4386 +0.272
0.4406 +0.208
0.4448 +0.112
0.4497 +0.012
0.4524 −0.049
0.4573 −0.199
0.4601 −0.267
0.4656 −0.457
0.4684 −0.520
0.4747 −0.609
0.4768 −0.626
0.4823 −0.700
0.4851 −0.712
0.4920 −0.705
0.4955 −0.694
0.5011 −0.684
0.5038 −0.676
0.5101 −0.638
0.5143 −0.594
0.5226 −0.524
0.5254 −0.515
0.5282 −0.500
0.5295 −0.490
0.5309 −0.473
0.5337 −0.460
0.5351 −0.442

2438981 +
0.3575 −0.001
0.3596 −0.016
0.3610 −0.042
0.3638 −0.092
0.3652 −0.125
0.3666 −0.171
0.3679 −0.196
0.3707 −0.254
0.3714 −0.260
0.3756 −0.357
0.3770 −0.377
0.3784 −0.396
0.3825 −0.442
0.3839 −0.455
0.3856 −0.478
0.3902 −0.521
0.3916 −0.536
0.3936 −0.553
0.3999 −0.564
0.4013 −0.564
0.4047 −0.558
0.4061 −0.555
0.4082 −0.557
0.4117 −0.573
0.4138 −0.577
0.4152 −0.591
0.4186 −0.588
0.4200 −0.583
0.4221 −0.569
0.4284 −0.547
0.4304 −0.540
0.4350 −0.516
0.4381 −0.486
0.4395 −0.493
0.4450 −0.481
0.4485 −0.451
0.4520 −0.425
0.4534 −0.405
0.4561 −0.389
0.4596 −0.343
0.4610 −0.334
0.4624 −0.324
0.4666 −0.293
0.4679 −0.257
0.4700 −0.235
0.4742 −0.217
0.4763 −0.211
0.4777 −0.199

2438985 +
0.3684 +0.049
0.3704 −0.045
0.3725 −0.109
0.3767 −0.255
0.3788 −0.309
0.3808 −0.376
0.3850 −0.502
0.3871 −0.554
0.3892 −0.586
0.3934 −0.645
0.3954 −0.666
0.3975 −0.679
0.4031 −0.701
0.4058 −0.696
0.4086 −0.689
0.4121 −0.677
0.4135 −0.671
0.4156 −0.654
0.4232 −0.595
0.4246 −0.586
0.4329 −0.530
0.4357 −0.514
0.4406 −0.501
0.4440 −0.477
0.4468 −0.449

2438989 +
0.3552 +0.323
0.3572 +0.271
0.3593 +0.208
0.3642 +0.089
0.3663 +0.069
0.3697 −0.038
0.3711 −0.121
0.3732 −0.228
0.3822 −0.511

2438993 +
0.3397 +0.296
0.3501 +0.214
0.3529 +0.148
0.3612 −0.054
0.3647 −0.152
0.3723 −0.462
0.3765 −0.594
0.3834 −0.723
0.3869 −0.750
0.3939 −0.801
0.3980 −0.798
0.4029 −0.797

0.4071 −0.800
0.4133 −0.775
0.4161 −0.737
0.4223 −0.700
0.4265 −0.671
0.4321 −0.633

2439028 +
0.3017 +0.237
0.3052 +0.239
0.3128 +0.204
0.3170 +0.157
0.3246 +0.082
0.3267 +0.049
0.3350 −0.039
0.3406 −0.136
0.3440 −0.224
0.3503 −0.341
0.3531 −0.393
0.3600 −0.501
0.3628 −0.550
0.3683 −0.592
0.3718 −0.618
0.3788 −0.627
0.3822 −0.607
0.3899 −0.557
0.3934 −0.534
0.4003 −0.504
0.4038 −0.480

2439056 +
0.2247 −0.290
0.2296 −0.422
0.2386 −0.599
0.2434 −0.667
0.2455 −0.673
0.2511 −0.724
0.2532 −0.730
0.2601 −0.710
0.2636 −0.703
0.2705 −0.677
0.2740 −0.651
0.2809 −0.641
0.2844 −0.633
0.2914 −0.584
0.2941 −0.574
0.3011 −0.539

0.3052 −0.465
0.3115 −0.402
0.3136 −0.372
0.3205 −0.339
0.3233 −0.310
0.3261 −0.265

2439060 +
0.2231 −0.580
0.2245 −0.590
0.2279 −0.632
0.2293 −0.647
0.2314 −0.650
0.2349 −0.665
0.2370 −0.665
0.2383 −0.674
0.2411 −0.678
0.2432 −0.676
0.2446 −0.674
0.2488 −0.659
0.2502 −0.655
0.2515 −0.642
0.2550 −0.630
0.2564 −0.619
0.2578 −0.610
0.2606 −0.587
0.2626 −0.585
0.2682 −0.547
0.2703 −0.532
0.2717 −0.520
0.2911 −0.375
0.2925 −0.373
0.2946 −0.347
0.2974 −0.320
0.3002 −0.299
0.3036 −0.291
0.3050 −0.287
0.3064 −0.261
0.3099 −0.251
0.3113 −0.248
0.3126 −0.225

2439064 +
0.2034 −0.336
0.2103 −0.470
0.2131 −0.519
0.2186 −0.574

0.2221 −0.615
0.2263 −0.672
0.2291 −0.690
0.2332 −0.686
0.2430 −0.656
0.2457 −0.645
0.2693 −0.478
0.2707 −0.460
0.2798 −0.371
0.2825 −0.364

2439230 +
0.3865 −0.391
0.3879 −0.379
0.3914 −0.354
0.3928 −0.327
0.3969 −0.294
0.3990 −0.275
0.4032 −0.230
0.4046 −0.222
0.4074 −0.205
0.4094 −0.192
0.4122 −0.190
0.4136 −0.187
0.4164 −0.166

2439260 +
0.4748 −0.555
0.4762 −0.536
0.4783 −0.535
0.4804 −0.519
0.4845 −0.498
0.4873 −0.467
0.4894 −0.456
0.4936 −0.456
0.4950 −0.443
0.5054 −0.432
0.5068 −0.416
0.5102 −0.403
0.5130 −0.354
0.5144 −0.354
0.5186 −0.340
0.5206 −0.335
0.5227 −0.303
0.5290 −0.306
0.5311 −0.299
0.5332 −0.290

0.5366 −0.262
0.5380 −0.256
0.5394 −0.242
0.5456 −0.205
0.5470 −0.163
0.5512 −0.165
0.5526 −0.129
0.5547 −0.121
0.5588 −0.083
0.5609 −0.082

2439264 +
0.4080 −0.532
0.4100 −0.557
0.4128 −0.568
0.4163 −0.577
0.4212 −0.580
0.4232 −0.580
0.4253 −0.571
0.4705 −0.413

2439267 +
0.5244 −0.500
0.5272 −0.504
0.5300 −0.530
0.5320 −0.523
0.5334 −0.530
0.5362 −0.508
0.5376 −0.511
0.5397 −0.511
0.5522 −0.420
0.5570 −0.378
0.5609 −0.343

2439268 +
0.3591 +0.210
0.3605 +0.184
0.3639 +0.103
0.3674 −0.002
0.3709 −0.085
0.3744 −0.199
0.3771 −0.248
0.3785 −0.297
0.3799 −0.327
0.3827 −0.418
0.3848 −0.466
0.3862 −0.508

0.3896 −0.540
0.3917 −0.573
0.3966 −0.632
0.3987 −0.662
0.4001 −0.664
0.4035 −0.662
0.4063 −0.660
0.4105 −0.644
0.4119 −0.638
0.4140 −0.623
0.4181 −0.608
0.4264 −0.576
0.4299 −0.551
0.4452 −0.397
0.4473 −0.375
0.4896 −0.175
0.4910 −0.146
0.4924 −0.139
0.4966 −0.106
0.4980 −0.094

2439323 +
0.3308 +0.134
0.3384 +0.032
0.3432 −0.059
0.3453 −0.110
0.3481 −0.158
0.3523 −0.310
0.3544 −0.368
0.3558 −0.401
0.3592 −0.483
0.3613 −0.545
0.3627 −0.570
0.3669 −0.615
0.3682 −0.633
0.3703 −0.653
0.3731 −0.646
0.3752 −0.639
0.3766 −0.633
0.3807 −0.639
0.3821 −0.630
0.3842 −0.627
0.3891 −0.617
0.3905 −0.607
0.3919 −0.604
0.3974 −0.579
0.4051 −0.540

0.4064 −0.527
0.4245 −0.463
0.4266 −0.466

2439326 +
0.3618 +0.131
0.4590 −0.437
0.4604 −0.512
0.4618 −0.563
0.4646 −0.594
0.4660 −0.623
0.4722 −0.732
0.4736 −0.747
0.4771 −0.770
0.4792 −0.782
0.4806 −0.788
0.4840 −0.780
0.4854 −0.790
0.4868 −0.780
0.4903 −0.776
0.4924 −0.777
0.4938 −0.771
0.4966 −0.766
0.4979 −0.759
0.4993 −0.756
0.5028 −0.727
0.5042 −0.719
0.5104 −0.669
0.5167 −0.590
0.5181 −0.582

2439346 +
0.3318 −0.156
0.3331 −0.184
0.3345 −0.204
0.3373 −0.279
0.3387 −0.345
0.3401 −0.402
0.3429 −0.462
0.3442 −0.493
0.3456 −0.533
0.3484 −0.587
0.3498 −0.609
0.3512 −0.628
0.3540 −0.650
0.3554 −0.679
0.3568 −0.681

0.3595 −0.669
0.3609 −0.679
0.3623 −0.672

2439349 +
0.4205 +0.029
0.4226 −0.023
0.4268 −0.126
0.4281 −0.157
0.4295 −0.200
0.4337 −0.340
0.4351 −0.381
0.4379 −0.427
0.4392 −0.453
0.4406 −0.473
0.4434 −0.508
0.4448 −0.517
0.4462 −0.544
0.4490 −0.568
0.4504 −0.580
0.4518 −0.589
0.4545 −0.600
0.4559 −0.612
0.4573 −0.611
0.4601 −0.620
0.4615 −0.612
0.4629 −0.609
0.4656 −0.602
0.4670 −0.605
0.4684 −0.604
0.4733 −0.582
0.4747 −0.584
0.4781 −0.573
0.4816 −0.558

2439373 +
0.3096 +0.319
0.3110 +0.320
0.3141 +0.312
0.3155 +0.308
0.3183 +0.327
0.3335 +0.475
0.3349 +0.475
0.3363 +0.493
0.3398 +0.477
0.3412 +0.467
0.3426 +0.466

0.3453 +0.464
0.3467 +0.429
0.3481 +0.436
0.3509 +0.450
0.3544 +0.472
0.3558 +0.478
0.3585 +0.506
0.3676 +0.463
0.3704 +0.412
0.3745 +0.316
0.3759 +0.290
0.3773 +0.283
0.3801 +0.203
0.3815 +0.169
0.3856 +0.043
0.3870 −0.024
0.3884 −0.093
0.3912 −0.173
0.3926 −0.243
0.3957 −0.417
0.3981 −0.491
0.3995 −0.538
0.4009 −0.587
0.4030 −0.650
0.4065 −0.747
0.4078 −0.768
0.4106 −0.819
0.4120 −0.863
0.4134 −0.876
0.4162 −0.885
0.4176 −0.892
0.4190 −0.914
0.4217 −0.922
0.4231 −0.919
0.4252 −0.925

2439381 +
0.3049 +0.397
0.3077 +0.388
0.3090 +0.405
0.3104 +0.414
0.3132 +0.403
0.3146 +0.408
0.3160 +0.397
0.3188 +0.385
0.3216 +0.392
0.3243 +0.354

0.3257 +0.339
0.3271 +0.336
0.3299 +0.267
0.3313 +0.248
0.3327 +0.233
0.3410 +0.000
0.3424 −0.032
0.3452 −0.097
0.3466 −0.159
0.3479 −0.205
0.3521 −0.389
0.3535 −0.435
0.3563 −0.494
0.3577 −0.548
0.3590 −0.586
0.3618 −0.673
0.3632 −0.719
0.3646 −0.743
0.3674 −0.760
0.3688 −0.783
0.3702 −0.791
0.3729 −0.812
0.3743 −0.822
0.3757 −0.826
0.3785 −0.828
0.3799 −0.825
0.3813 −0.830
0.3840 −0.820
0.3854 −0.818
0.3896 −0.798
0.3910 −0.807
0.3924 −0.797
0.3952 −0.767
0.3965 −0.758
0.3979 −0.758

2439409 +
0.2619 +0.112
0.2640 +0.050
0.2661 +0.006
0.2702 −0.141
0.2723 −0.185
0.2786 −0.336
0.2800 −0.363
0.2814 −0.393
0.2855 −0.468
0.2890 −0.536

0.2932 −0.601
0.2959 −0.654
0.2973 −0.686
0.3022 −0.707
0.3043 −0.722
0.3057 −0.731
0.3098 −0.715
0.3112 −0.717
0.3175 −0.687
0.3188 −0.672
0.3209 −0.646
0.3251 −0.611
0.3265 −0.601
0.3279 −0.590
0.3320 −0.562
0.3341 −0.556
0.3355 −0.544

2439413 +
0.2486 +0.050
0.2528 −0.069
0.2549 −0.119
0.2597 −0.257
0.2618 −0.317
0.2632 −0.367
0.2667 −0.461
0.2681 −0.488
0.2736 −0.612
0.2757 −0.648
0.2771 −0.665
0.2806 −0.714
0.2826 −0.734
0.2847 −0.764
0.2882 −0.797
0.2896 −0.810
0.2917 −0.832
0.2951 −0.847

2439507 +
0.6021 −0.842
0.6035 −0.849
0.6049 −0.826
0.6084 −0.784
0.6097 −0.759
0.6111 −0.746
0.6146 −0.712
0.6160 −0.701

0.6181 −0.687
0.6229 −0.637
0.6250 −0.626
0.6271 −0.615
0.6313 −0.587
0.6334 −0.568

2439581 +
0.5432 +0.371
0.5446 +0.349
0.5474 +0.261
0.5488 +0.231
0.5515 +0.152
0.5529 +0.132
0.5571 −0.009
0.5599 −0.162
0.5613 −0.214
0.5633 −0.355
0.5647 −0.417
0.5668 −0.494
0.5682 −0.519
0.5703 −0.530
0.5717 −0.576
0.5738 −0.713
0.5752 −0.802
0.5779 −0.928
0.5793 −0.963
0.5814 −0.982
0.5828 −0.988
0.5863 −1.012
0.5883 −1.013
0.5918 −1.009
0.5932 −1.011
0.5953 −1.007

2439604 +
0.5178 +0.328
0.5192 +0.325
0.5219 +0.294
0.5233 +0.298
0.5261 +0.278
0.5275 +0.278
0.5303 +0.287
0.5365 +0.241
0.5379 +0.229
0.5407 +0.224
0.5421 +0.220
0.5469 +0.202
0.5483 +0.200
0.5511 +0.182
0.5567 +0.114
0.5657 −0.025
0.5726 −0.187
0.5740 −0.221
0.5768 −0.280
0.5782 −0.338
0.5810 −0.432
0.5824 −0.468
0.5851 −0.516
0.5865 −0.541
0.5893 −0.591
0.5907 −0.602
0.5935 −0.610
0.5948 −0.617
0.5976 −0.634
0.5990 −0.648
0.6018 −0.648
0.6032 −0.656
0.6060 −0.656
0.6074 −0.643
0.6101 −0.645

2439605 +
0.4553 −0.088
0.4615 −0.212
0.4636 −0.242
0.4650 −0.303
0.4664 −0.363
0.4685 −0.413
0.4726 −0.516
0.4747 −0.541
0.4810 −0.587
0.4844 −0.626
0.4858 −0.628
0.4886 −0.636
0.4900 −0.636
0.4935 −0.630
0.4949 −0.625
0.4983 −0.622
0.5004 −0.621
0.5032 −0.612
0.5046 −0.596
0.5101 −0.577
0.5115 −0.579
0.5143 −0.561
0.5310 −0.461
0.5386 −0.410

2439648 +
0.4302 −0.297
0.4372 −0.578
0.4393 −0.659
0.4407 −0.731
0.4420 −0.779
0.4455 −0.817
0.4469 −0.828
0.4483 −0.833
0.4518 −0.792
0.4532 −0.778
0.4552 −0.769
0.4587 −0.783
0.4608 −0.813
0.4622 −0.819
0.4657 −0.795
0.4670 −0.786
0.4684 −0.781
0.4726 −0.737
0.4747 −0.716
0.4775 −0.698
0.4816 −0.655
0.4830 −0.641
0.4851 −0.624
0.4886 −0.584
0.4900 −0.564
0.4962 −0.529
0.4983 −0.523

2439667 +
0.4741 +0.083
0.4754 +0.029
0.4768 −0.091
0.4796 −0.228
0.4810 −0.315
0.4838 −0.375
0.4852 −0.428
0.4880 −0.550
0.4893 −0.602
0.4935 −0.747
0.4963 −0.808
0.5004 −0.872
0.5018 −0.884
0.5046 −0.908
0.5060 −0.919
0.5088 −0.906
0.5102 −0.906
0.5130 −0.883
0.5143 −0.884
0.5171 −0.887
0.5185 −0.880
0.5213 −0.848
0.5254 −0.793
0.5268 −0.801
0.5296 −0.750
0.5310 −0.728

2439710 +
0.4301 −0.025
0.4335 −0.141
0.4349 −0.183
0.4377 −0.275
0.4391 −0.320
0.4419 −0.395
0.4433 −0.438
0.4460 −0.522
0.4474 −0.550
0.4502 −0.616
0.4516 −0.636
0.4544 −0.708
0.4558 −0.718

2439711 +
0.3405 −0.791
0.3432 −0.800
0.3446 −0.802
0.3495 −0.819
0.3509 −0.833
0.3530 −0.824
0.3571 −0.835
0.3585 −0.821
0.3599 −0.804
0.3634 −0.779
0.3648 −0.777
0.3669 −0.750
0.3703 −0.705
0.3717 −0.686
0.3731 −0.672
0.3766 −0.612
0.3794 −0.597
0.3808 −0.573

2439714 +
0.4162 −0.466
0.4176 −0.501
0.4224 −0.611
0.4245 −0.667
0.4273 −0.706
0.4328 −0.775
0.4342 −0.793
0.4363 −0.801
0.4419 −0.809
0.4474 −0.785
0.4488 −0.780
0.4502 −0.771
0.4537 −0.742
0.4551 −0.724
0.4564 −0.714
0.4592 −0.683
0.4606 −0.687
0.4620 −0.672

2439722 +
0.3710 −0.295
0.3738 −0.397
0.3752 −0.438
0.3786 −0.507
0.3800 −0.535
0.3849 −0.637
0.3904 −0.730
0.3925 −0.739
0.3953 −0.764
0.4002 −0.735
0.4029 −0.714
0.4043 −0.723
0.4078 −0.738
0.4126 −0.756
0.4147 −0.759
0.4210 −0.746
0.4231 −0.716
0.4300 −0.623
0.4335 −0.586
0.4383 −0.517

2439726 +
0.3709 −0.437
0.3723 −0.466

0.3737 −0.507
0.3779 −0.588
0.3793 −0.603
0.3807 −0.632
0.3848 −0.677
0.3862 −0.692
0.3876 −0.727
0.3911 −0.723
0.3925 −0.733
0.3945 −0.779
0.4091 −0.813
0.4119 −0.792
0.4168 −0.716
0.4188 −0.679
0.4251 −0.598
0.4272 −0.592
0.4293 −0.572
0.4355 −0.480

2439738 +
0.3242 +0.398
0.3284 +0.441
0.3298 +0.427
0.3347 +0.417
0.3368 +0.411
0.3388 +0.355
0.3458 +0.120
0.3479 +0.000
0.3500 −0.048
0.3541 −0.260
0.3576 −0.391
0.3611 −0.543
0.3624 −0.621
0.3638 −0.616
0.3666 −0.605
0.3680 −0.637
0.3694 −0.703
0.3722 −0.787
0.3742 −0.826
0.3756 −0.840
0.3798 −0.868
0.3826 −0.875
0.3847 −0.876
0.3888 −0.872
0.3909 −0.863
0.3937 −0.854
0.3979 −0.830
0.3999 −0.808
0.4027 −0.771
0.4062 −0.722
0.4076 −0.726

2439923 +
0.4817 −0.683
0.4845 −0.690
0.4908 −0.687
0.4921 −0.666
0.4949 −0.662
0.4970 −0.661
0.4998 −0.646
0.5012 −0.641
0.5039 −0.604
0.5053 −0.580
0.5081 −0.562
0.5095 −0.550
0.5123 −0.542
0.5137 −0.517
0.5164 −0.502
0.5178 −0.478
0.5206 −0.447
0.5220 −0.437

2439942 +
0.4549 +0.287
0.4563 +0.287
0.4590 +0.306
0.4604 +0.314
0.4632 +0.291
0.4646 +0.289
0.4674 +0.302
0.4688 +0.314
0.4716 +0.349
0.4729 +0.352
0.4757 +0.368
0.4771 +0.363
0.4799 +0.345
0.4813 +0.335
0.4840 +0.333
0.4854 +0.341
0.4882 +0.337
0.4896 +0.341
0.4924 +0.337
0.4938 +0.349
0.4966 +0.339
0.4979 +0.355
0.5007 +0.355
0.5021 +0.349
0.5063 +0.349
0.5090 +0.326
0.5104 +0.329
0.5132 +0.311
0.5146 +0.307
0.5174 +0.294
0.5188 +0.271
0.5216 +0.229
0.5229 +0.215
0.5257 +0.115
0.5271 +0.064
0.5299 −0.035
0.5313 −0.060
0.5327 −0.118
0.5354 −0.221
0.5368 −0.288
0.5382 −0.350
0.5410 −0.444
0.5438 −0.548
0.5466 −0.620
0.5479 −0.666
0.5493 −0.709
0.5521 −0.770
0.5535 −0.798
0.5549 −0.804
0.5577 −0.821
0.5590 −0.827
0.5604 −0.835
0.5632 −0.829
0.5646 −0.818
0.5660 −0.811
0.5688 −0.789
0.5702 −0.780
0.5716 −0.760
0.5743 −0.735
0.5757 −0.729
0.5771 −0.720

2439978 +
0.3635 +0.275
0.3649 +0.274
0.3676 +0.258
0.3790 +0.247
0.3718 +0.253
0.3732 +0.245
0.3760 +0.189
0.3774 +0.139
0.3801 +0.092
0.3815 +0.071
0.3843 +0.030
0.3857 +0.006
0.3885 −0.017
0.3899 −0.018
0.3968 −0.088
0.3982 −0.099
0.4010 −0.138
0.4024 −0.170
0.4051 −0.223
0.4065 −0.251
0.4093 −0.294
0.4107 −0.327
0.4135 −0.392
0.4149 −0.413
0.4176 −0.454
0.4190 −0.485
0.4218 −0.535
0.4232 −0.536
0.4260 −0.559
0.4274 −0.570
0.4301 −0.577
0.4315 −0.576
0.4343 −0.579
0.4357 −0.566
0.4385 −0.552
0.4399 −0.544
0.4440 −0.526
0.4468 −0.516
0.4482 −0.523
0.4510 −0.507
0.4524 −0.494
0.4551 −0.471
0.4565 −0.472
0.4593 −0.445
0.4607 −0.436
0.4635 −0.409
0.4649 −0.400
0.4676 −0.386
0.4690 −0.376

2439985 +
0.4557 +0.379
0.4571 +0.391
0.4599 +0.395
0.4613 +0.381
0.4835 +0.283
0.4926 +0.178
0.4974 +0.099
0.4988 +0.069
0.5030 −0.005
0.5050 −0.051
0.5113 −0.291
0.5127 −0.371
0.5155 −0.450
0.5176 −0.468
0.5210 −0.478
0.5224 −0.512
0.5252 −0.595
0.5266 −0.635
0.5294 −0.653
0.5307 −0.675
0.5335 −0.676
0.5349 −0.671
0.5377 −0.673
0.5391 −0.673
0.5419 −0.673
0.5432 −0.663
0.5460 −0.657
0.5474 −0.650
0.5502 −0.647
0.5516 −0.646
0.5571 −0.617
0.5585 −0.616
0.5627 −0.591
0.5655 −0.576
0.5669 −0.572
0.5696 −0.563
0.5710 −0.561

2439993 +
0.4695 +0.103
0.4709 +0.025
0.4737 −0.081
0.4751 −0.120
0.4792 −0.303
0.4820 −0.412
0.4834 −0.466
0.4862 −0.528
0.4876 −0.580

0.4904 −0.647
0.4918 −0.672
0.4959 −0.734
0.5001 −0.793
0.5029 −0.823
0.5042 −0.827
0.5077 −0.827
0.5098 −0.819
0.5126 −0.812
0.5140 −0.796
0.5168 −0.762

2440012 +
0.4602 +0.198
0.4616 +0.142
0.4637 +0.085
0.4679 −0.015
0.4692 −0.043
0.4720 −0.123
0.4734 −0.141
0.4755 −0.226
0.4769 −0.269
0.4797 −0.316
0.4811 −0.336
0.4838 −0.399
0.4852 −0.441
0.4880 −0.517
0.4894 −0.541
0.4922 −0.567
0.4936 −0.585
0.4963 −0.611
0.4977 −0.620
0.5019 −0.639
0.5047 −0.655
0.5061 −0.663
0.5088 −0.677
0.5102 −0.677
0.5130 −0.671
0.5144 −0.668
0.5172 −0.668
0.5186 −0.652
0.5213 −0.651
0.5227 −0.646
0.5255 −0.634
0.5269 −0.631

2440067 +
0.4016 +0.411
0.4030 +0.406
0.4058 +0.389
0.4071 +0.404
0.4099 +0.377
0.4113 +0.375
0.4141 +0.340
0.4155 +0.313
0.4183 +0.286
0.4196 +0.291
0.4238 +0.240
0.4266 +0.208
0.4280 +0.191
0.4467 −0.247
0.4481 −0.291
0.4509 −0.380
0.4523 −0.405
0.4551 −0.514
0.4564 −0.540
0.4592 −0.533
0.4606 −0.530
0.4634 −0.574
0.4648 −0.593

2440338 +
0.4264 +0.344
0.4277 +0.329
0.4305 +0.316
0.4319 +0.310
0.4347 +0.288
0.4388 +0.245
0.4402 +0.229
0.4430 +0.187
0.4444 +0.164
0.4472 +0.112
0.4486 +0.083
0.4514 +0.014
0.4527 +0.009
0.4555 −0.058
0.4569 −0.084
0.4597 −0.149
0.4611 −0.169
0.4639 −0.223
0.4652 −0.247
0.4680 −0.323
0.4694 −0.378

0.4722 −0.434
0.4736 −0.452
0.4764 −0.499
0.4777 −0.527
0.4805 −0.524
0.4819 −0.526
0.4847 −0.531
0.4861 −0.538
0.4888 −0.584
0.4902 −0.589
0.4930 −0.608
0.4944 −0.613
0.4972 −0.614
0.4986 −0.612
0.5014 −0.596
0.5055 −0.580
0.5069 −0.578
0.5097 −0.570
0.5111 −0.549
0.5138 −0.539
0.5152 −0.523
0.5180 −0.512
0.5194 −0.502
0.5222 −0.499
0.5236 −0.488
0.5264 −0.464
0.5277 −0.462

2440354 +
0.3998 +0.296
0.4012 +0.285
0.4040 +0.251
0.4054 +0.240
0.4082 +0.262
0.4096 +0.278
0.4124 +0.254
0.4138 +0.244
0.4166 +0.223
0.4180 +0.225
0.4207 +0.229
0.4221 +0.218
0.4249 +0.198
0.4263 +0.176
0.4291 +0.126
0.4305 +0.112
0.4332 +0.082
0.4360 +0.040

0.4374 +0.012
0.4402 −0.023
0.4416 −0.080
0.4485 −0.270
0.4499 −0.310
0.4527 −0.385
0.4541 −0.416
0.4568 −0.500
0.4582 −0.523
0.4624 −0.577
0.4652 −0.634
0.4666 −0.654
0.4693 −0.680
0.4707 −0.697
0.4735 −0.698
0.4749 −0.698
0.5041 −0.692
0.5055 −0.692

2440357 +
0.4851 +0.293
0.4879 +0.331
0.4893 +0.383
0.4921 +0.400
0.4935 +0.395
0.4962 +0.426
0.4976 +0.412
0.5018 +0.410
0.5046 +0.439
0.5060 +0.438
0.5087 +0.412
0.5101 +0.402
0.5129 +0.397
0.5143 +0.392
0.5171 +0.389
0.5185 +0.373
0.5254 +0.388
0.5268 +0.391
0.5296 +0.341
0.5310 +0.332
0.5337 +0.310
0.5470 +0.049
0.5484 +0.009
0.5525 −0.092
0.5553 −0.176
0.5567 −0.238
0.5594 −0.332

0.5608 −0.380

2440389 +
0.4362 −0.678
0.4376 −0.681
0.4397 −0.706
0.4411 −0.718
0.4432 −0.708
0.4446 −0.722
0.4467 −0.722
0.4480 −0.723
0.4501 −0.722
0.4515 −0.714
0.4536 −0.707
0.4550 −0.681
0.4571 −0.663
0.4585 −0.653

2440420 +
0.3794 +0.221
0.3821 +0.178
0.3835 +0.175
0.3863 +0.115
0.3877 +0.082
0.3919 +0.021
0.3946 −0.013
0.3960 −0.047
0.3988 −0.145
0.4002 −0.190
0.4030 −0.279
0.4044 −0.329
0.4071 −0.422
0.4085 −0.460
0.4113 −0.467
0.4127 −0.484
0.4155 −0.529
0.4169 −0.565
0.4196 −0.580
0.4210 −0.585
0.4238 −0.585
0.4252 −0.587
0.4280 −0.586
0.4294 −0.585
0.4321 −0.585
0.4335 −0.582
0.4363 −0.564
0.4377 −0.565

0.4405 −0.566
0.4419 −0.557
0.4446 −0.551
0.4460 −0.542
0.4488 −0.537
0.4502 −0.524
0.4523 −0.521
0.4537 −0.500

2440436 +
0.3419 +0.354
0.3433 +0.370
0.3544 +0.354
0.3599 +0.307
0.3627 +0.264
0.3641 +0.236
0.3669 +0.202
0.3683 +0.190
0.3752 +0.073
0.3766 +0.050
0.3794 +0.057
0.3808 +0.013
0.3835 −0.064
0.3849 −0.134
0.3891 −0.273
0.3919 −0.347
0.3933 −0.373
0.3960 −0.411
0.3974 −0.414
0.4002 −0.516
0.4016 −0.552
0.4044 −0.620
0.4058 −0.664
0.4085 −0.738
0.4099 −0.771
0.4127 −0.791
0.4141 −0.798
0.4210 −0.787
0.4224 −0.768
0.4252 −0.742
0.4266 −0.724
0.4294 −0.717
0.4308 −0.711
0.4335 −0.674
0.4349 −0.649

2440439 +
0.4472 +0.431
0.4486 +0.445
0.4514 +0.440
0.4570 +0.400
0.4597 +0.375
0.4611 +0.366
0.4639 +0.310
0.4653 +0.300
0.4695 +0.263
0.4722 +0.238
0.4736 +0.237
0.4764 +0.219
0.4778 +0.190
0.4806 +0.152
0.4820 +0.095
0.4847 −0.007
0.4861 −0.073
0.4889 −0.155
0.4903 −0.224
0.4931 −0.280
0.4945 −0.316
0.4972 −0.375
0.4986 −0.408
0.5014 −0.531
0.5028 −0.610
0.5056 −0.693
0.5070 −0.712
0.5118 −0.761
0.5132 −0.764
0.5160 −0.777
0.5174 −0.783
0.5201 −0.802
0.5215 −0.813
0.5243 −0.813
0.5257 −0.802
0.5285 −0.764
0.5299 −0.749
0.5326 −0.739
0.5340 −0.741
0.5368 −0.724
0.5382 −0.723
0.5410 −0.705

2440675 +
0.4961 +0.206
0.4975 +0.195
0.5017 +0.200
0.5031 +0.188
0.5045 +0.178
0.5073 +0.178
0.5087 +0.135
0.5101 +0.128
0.5128 +0.086
0.5142 +0.089
0.5156 +0.080
0.5184 +0.040
0.5198 +0.019
0.5212 +0.010
0.5239 −0.052
0.5253 −0.073
0.5267 −0.103
0.5295 −0.200
0.5323 −0.295
0.5350 −0.368
0.5364 −0.393
0.5378 −0.420
0.5406 −0.491
0.5420 −0.516
0.5461 −0.635
0.5475 −0.661
0.5489 −0.668
0.5517 −0.692
0.5531 −0.691
0.5545 −0.700
0.5573 −0.707
0.5587 −0.719
0.5601 −0.721
0.5642 −0.706
0.5656 −0.706
0.5684 −0.691
0.5698 −0.688
0.5712 −0.686
0.5739 −0.680
0.5753 −0.673
0.5795 −0.637
0.5809 −0.626

2440707 +
0.3989 +0.205
0.4003 +0.167
0.4030 +0.114
0.4044 +0.089
0.4100 −0.021
0.4114 −0.064
0.4142 −0.157
0.4156 −0.177
0.4183 −0.256
0.4197 −0.306
0.4225 −0.397
0.4239 −0.420
0.4267 −0.508
0.4280 −0.526
0.4308 −0.559
0.4322 −0.569
0.4350 −0.607
0.4364 −0.623
0.4392 −0.630
0.4405 −0.638
0.4433 −0.648
0.4447 −0.653
0.4475 −0.681
0.4489 −0.670
0.4517 −0.670
0.4530 −0.668
0.4551 −0.677
0.4565 −0.664
0.4607 −0.670
0.4635 −0.659
0.4676 −0.628
0.4690 −0.617

2440769 +
0.4157 +0.295
0.4171 +0.314
0.4198 +0.384
0.4212 +0.453
0.4240 +0.439
0.4254 +0.474
0.4281 +0.464
0.4295 +0.461
0.4323 +0.423
0.4337 +0.383
0.4379 +0.313
0.4420 +0.260
0.4448 +0.231
0.4462 +0.208
0.4490 +0.166
0.4504 +0.147
0.4531 +0.112
0.4545 +0.081
0.4573 +0.026
0.4615 −0.106
0.4629 −0.135
0.4656 −0.190
0.4670 −0.240
0.4698 −0.343
0.4712 −0.385
0.4740 −0.492
0.4754 −0.521
0.4781 −0.609
0.4795 −0.637
0.4823 −0.658
0.4865 −0.688
0.4879 −0.689
0.4906 −0.690
0.4920 −0.680
0.4948 −0.681
0.4962 −0.671
0.4990 −0.662
0.5004 −0.652
0.5031 −0.643
0.5045 −0.638

2440781 +
0.3939 +0.203
0.3967 +0.195
0.3981 +0.184
0.4009 +0.136
0.4023 +0.110
0.4050 +0.068
0.4064 +0.021
0.4091 −0.060
0.4133 −0.221
0.4147 −0.280
0.4175 −0.400
0.4189 −0.430
0.4230 −0.545
0.4258 −0.611
0.4272 −0.634
0.4293 −0.687
0.4307 −0.710
0.4334 −0.763
0.4348 −0.803
0.4376 −0.854
0.4390 −0.857
0.4418 −0.830
0.4432 −0.815

0.4460 −0.805
0.4474 −0.790
0.4502 −0.788
0.4516 −0.779
0.4543 −0.805
0.4557 −0.820
0.4585 −0.817
0.4599 −0.814
0.4627 −0.801
0.4641 −0.787
0.4668 −0.746
0.4682 −0.720
0.4710 −0.680
0.4724 −0.666
0.4752 −0.615
0.4766 −0.611

2440796 +
0.4214 +0.074
0.4227 +0.040
0.4255 +0.005
0.4269 −0.018
0.4297 −0.037
0.4311 −0.066
0.4339 −0.195
0.4352 −0.220
0.4380 −0.319
0.4394 −0.347
0.4436 −0.422
0.4464 −0.480
0.4477 −0.501
0.4505 −0.532
0.4519 −0.545

2440807 +
0.5050 +0.346
0.5064 +0.353
0.5091 +0.340
0.5133 +0.324
0.5147 +0.335
0.5175 +0.335
0.5189 +0.341
0.5230 +0.330
0.5258 +0.316
0.5272 +0.306
0.5300 +0.296
0.5314 +0.267
0.5341 +0.240
0.5355 +0.205
0.5383 +0.078
0.5397 −0.009
0.5425 −0.063
0.5439 −0.078
0.5466 −0.144
0.5480 −0.220
0.5508 −0.290
0.5550 −0.474
0.5564 −0.539
0.5591 −0.622
0.5605 −0.651
0.5631 −0.692
0.5675 −0.698
0.5689 −0.709
0.5716 −0.685
0.5730 −0.693
0.5758 −0.672
0.5772 −0.668
0.5800 −0.654
0.5814 −0.638

2440859 +
0.3349 +0.425
0.3363 +0.416
0.3447 +0.397
0.3488 +0.360
0.3597 +0.214
0.3611 +0.189
0.3625 +0.154
0.3655 +0.087
0.3669 +0.065
0.3683 +0.049
0.3710 −0.014
0.3724 −0.051
0.3738 −0.068
0.3766 −0.132
0.3780 −0.171
0.3794 −0.197
0.3821 −0.288
0.3835 −0.315
0.3849 −0.361
0.3884 −0.454
0.3898 −0.489
0.3912 −0.550
0.3940 −0.631
0.3952 −0.657
0.3966 −0.690
0.4002 −0.789
0.4016 −0.807
0.4030 −0.806
0.4078 −0.780
0.4092 −0.753
0.4106 −0.736
0.4148 −0.675
0.4162 −0.656
0.4176 −0.642
0.4210 −0.604
0.4224 −0.586

2440867 +
0.3109 +0.265
0.3172 +0.164
0.3186 +0.148
0.3248 −0.023
0.3269 −0.104
0.3311 −0.250
0.3347 −0.366
0.3380 −0.485
0.3394 −0.510
0.3443 −0.644
0.3457 −0.665
0.3505 −0.734
0.3519 −0.762
0.3561 −0.796
0.3575 −0.801
0.3616 −0.784
0.3644 −0.763
0.3707 −0.720
0.3755 −0.684

2440883 +
0.2557 −0.116
0.2571 −0.126
0.2598 −0.163
0.2612 −0.175
0.2661 −0.306
0.2675 −0.339
0.2689 −0.376
0.2723 −0.452
0.2737 −0.508
0.2751 −0.560
0.2772 −0.601
0.2786 −0.604
0.2800 −0.645
0.2834 −0.680
0.2848 −0.681
0.2862 −0.679
0.2900 −0.678
0.2914 −0.679
0.2928 −0.682
0.2945 −0.674
0.2959 −0.681
0.2973 −0.678
0.3001 −0.676
0.3015 −0.674
0.3057 −0.656
0.3071 −0.663
0.3085 −0.655

2441035 +
0.5952 +0.385
0.5964 +0.408
0.5975 +0.394
0.5998 +0.368
0.6009 +0.381
0.6021 +0.358
0.6070 +0.354
0.6100 +0.325
0.6113 +0.317
0.6175 +0.168
0.6187 +0.153
0.6224 +0.072
0.6252 −0.013
0.6274 −0.101
0.6287 −0.197
0.6300 −0.251
0.6328 −0.414
0.6340 −0.478
0.6353 −0.538
0.6381 −0.637
0.6394 −0.696
0.6408 −0.727
0.6440 −0.821
0.6454 −0.869
0.6466 −0.898

2441060 +
0.3977 +0.398
0.3992 +0.370
0.4030 +0.323
0.4041 +0.360
0.4082 +0.336
0.4095 +0.353
0.4108 +0.353
0.4138 +0.422
0.4150 +0.421
0.4161 +0.428
0.4184 +0.411
0.4206 +0.403
0.4232 +0.409
0.4243 +0.384
0.4256 +0.399
0.4293 +0.354
0.4305 +0.351
0.4340 +0.349
0.4350 +0.345
0.4391 +0.303
0.4404 +0.279
0.4445 +0.230
0.4456 +0.215
0.4479 +0.162
0.4489 +0.127
0.4522 +0.017
0.4533 −0.014
0.4543 −0.058
0.4569 −0.113
0.4593 −0.140
0.4620 −0.175
0.4631 −0.211
0.4640 −0.253
0.4663 −0.329
0.4674 −0.384
0.4686 −0.428
0.4710 −0.515
0.4719 −0.548
0.4729 −0.574

2441063 +
0.5037 +0.337
0.5048 +0.332
0.5072 +0.324
0.5095 +0.326
0.5121 +0.332
0.5136 +0.311
0.5148 +0.312
0.5176 +0.321

0.5198 +0.298
0.5249 +0.324
0.5318 +0.336
0.5330 +0.357
0.5354 +0.348
0.5366 +0.355
0.5377 +0.322
0.5402 +0.304
0.5415 +0.288
0.5427 +0.270
0.5512 +0.162
0.5523 +0.123
0.5548 +0.023
0.5573 −0.032
0.5598 −0.073
0.5611 −0.100
0.5623 −0.135
0.5647 −0.166
0.5658 −0.194
0.5669 −0.247
0.5704 −0.411
0.5715 −0.442
0.5736 −0.498
0.5746 −0.566
0.5757 −0.594
0.5780 −0.643
0.5792 −0.673
0.5803 −0.701
0.5838 −0.765
0.5849 −0.792
0.5873 −0.836
0.5883 −0.845
0.5894 −0.842
0.5918 −0.845
0.5930 −0.857

2441071 +
0.5160 −0.022
0.5171 −0.040
0.5182 −0.069
0.5206 −0.135
0.5216 −0.156
0.5226 −0.170
0.5247 −0.271
0.5257 −0.318
0.5266 −0.348
0.5293 −0.394
0.5303 −0.428
0.5313 −0.441
0.5346 −0.530
0.5368 −0.581
0.5392 −0.649
0.5402 −0.673
0.5414 −0.698
0.5462 −0.746
0.5473 −0.759
0.5485 −0.761
0.5508 −0.792
0.5533 −0.797
0.5543 −0.794
0.5571 −0.799
0.5597 −0.796
0.5647 −0.783

2441087 +
0.4120 +0.123
0.4131 +0.111
0.4154 +0.097
0.4187 +0.076
0.4200 +0.067
0.4210 +0.049
0.4222 +0.032
0.4249 +0.005
0.4260 −0.017
0.4272 −0.029
0.4284 −0.054
0.4322 −0.108
0.4334 −0.150
0.4346 −0.184
0.4377 −0.244
0.4388 −0.289
0.4413 −0.328
0.4438 −0.367
0.4464 −0.415
0.4475 −0.434
0.4503 −0.462
0.4514 −0.482
0.4525 −0.496
0.4537 −0.509
0.4565 −0.527
0.4577 −0.542
0.4605 −0.578
0.4627 −0.591
0.4638 −0.619
0.4663 −0.633
0.4687 −0.645
0.4698 −0.639
0.4709 −0.651
0.4720 −0.648
0.4745 −0.633
0.4758 −0.648
0.4823 −0.631
0.4835 −0.633
0.4847 −0.620
0.4861 −0.631
0.4903 −0.599
0.4916 −0.592
0.4029 −0.602
0.4956 −0.594
0.4969 −0.600
0.4982 −0.587
0.4993 −0.585
0.5019 −0.555
0.5033 −0.558
0.5044 −0.549

2441094 +
0.5293 +0.157
0.5302 +0.138
0.5312 +0.141
0.5322 +0.131
0.5331 +0.116
0.5353 +0.104
0.5366 +0.074
0.5380 +0.067
0.5391 +0.085
0.5402 +0.057
0.5429 +0.040
0.5440 +0.015
0.5451 +0.000
0.5463 −0.027
0.5486 −0.096
0.5496 −0.122
0.5505 −0.137
0.5516 −0.186
0.5549 −0.324
0.5560 −0.364
0.5571 −0.395
0.5595 −0.502

2441095 +
0.4177 +0.229
0.4191 +0.216
0.4202 +0.204
0.4215 +0.190
0.4237 +0.165
0.4247 +0.150
0.4257 +0.129
0.4268 +0.093
0.4290 +0.035
0.4301 +0.009
0.4312 −0.046
0.4322 −0.071
0.4333 −0.096
0.4382 −0.258
0.4393 −0.297
0.4404 −0.333
0.4429 −0.386
0.4440 −0.417
0.4463 −0.471
0.4489 −0.511
0.4502 −0.547
0.4637 −0.732
0.4649 −0.737
0.4673 −0.744
0.4684 −0.750
0.4694 −0.759
0.4705 −0.763
0.4729 −0.761
0.4740 −0.754
0.4751 −0.751
0.4785 −0.740
0.4796 −0.736
0.4808 −0.731
0.4820 −0.731
0.4846 −0.719
0.4958 −0.713
0.4872 −0.696
0.4883 −0.686

2441118 +
0.4686 −0.804
0.4699 −0.832
0.4709 −0.855
0.4720 −0.875
0.4741 −0.889
0.4753 −0.889
0.4763 −0.898
0.4775 −0.911
0.4802 −0.905
0.4813 −0.913
0.4825 −0.912
0.4837 −0.897
0.4867 −0.887
0.4882 −0.876
0.4894 −0.858
0.4908 −0.851
0.4932 −0.829
0.4943 −0.812
0.4954 −0.803
0.4990 −0.776
0.5004 −0.774
0.5017 −0.760
0.5031 −0.737

2441126 +
0.4075 −0.078
0.4096 −0.179
0.4110 −0.219
0.4144 −0.343
0.4158 −0.358
0.4172 −0.351
0.4186 −0.347
0.4213 −0.403
0.4227 −0.442
0.4258 −0.493
0.4290 −0.523
0.4304 −0.543
0.4318 −0.571
0.4332 −0.582
0.4353 −0.615
0.4367 −0.633
0.4380 −0.634
0.4395 −0.642
0.4463 −0.681
0.4476 −0.688
0.4487 −0.688

2441161 +
0.3742 +0.269
0.3753 +0.279
0.3782 +0.281
0.3807 +0.272
0.3834 +0.302

0.3846 +0.290
0.3857 +0.282
0.3890 +0.255
0.3903 +0.246
0.3915 +0.262
0.3936 +0.230
0.3947 +0.195
0.3959 +0.147
0.4002 +0.067
0.4016 +0.041
0.4043 −0.039
0.4058 −0.074
0.4069 −0.118
0.4107 −0.276
0.4117 −0.296
0.4140 −0.360
0.4153 −0.402
0.4165 −0.458
0.4189 −0.534
0.4201 −0.573
0.4213 −0.606
0.4237 −0.662
0.4250 −0.691
0.4263 −0.705
0.4286 −0.711
0.4298 −0.718
0.4311 −0.709
0.4334 −0.702
0.4348 −0.696
0.4362 −0.690

2441189 +
0.3085 +0.496
0.3095 +0.509
0.3106 +0.499
0.3124 +0.472
0.3148 +0.452
0.3173 +0.424
0.3187 +0.406
0.3197 +0.379
0.3201 +0.371
0.3259 +0.324
0.3271 +0.318
0.3286 +0.302
0.3327 +0.208
0.3338 +0.192
0.3364 +0.128
0.3376 +0.109
0.3390 +0.039
0.3415 −0.026
0.3430 −0.095
0.3441 −0.155
0.3465 −0.250
0.3476 −0.298
0.3490 −0.345
0.3515 −0.440
0.3526 −0.489
0.3538 −0.524
0.3563 −0.617
0.3574 −0.674
0.3606 −0.768
0.3618 −0.815
0.3631 −0.845
0.3655 −0.861
0.3666 −0.873
0.3677 −0.876
0.3708 −0.917
0.3721 −0.926
0.3732 −0.936
0.3760 −0.938
0.3772 −0.942
0.3785 −0.935
0.3808 −0.926
0.3822 −0.908
0.3835 −0.913
0.3859 −0.906
0.3871 −0.896
0.3908 −0.860
0.3922 −0.849
0.3933 −0.837
0.3956 −0.807
0.3970 −0.789
0.3985 −0.778

2441529 +
0.4848 +0.021
0.4883 −0.114
0.4924 −0.316
0.4938 −0.348
0.4966 −0.485
0.4980 −0.534
0.5008 −0.607
0.5049 −0.691
0.5091 −0.735
0.5105 −0.745
0.5133 −0.744
0.5147 −0.739
0.5188 −0.728
0.5216 −0.701
0.5237 −0.684
0.5272 −0.651
0.5313 −0.609
0.5327 −0.587
0.5355 −0.567
0.5369 −0.564

2441537 +
0.4202 +0.303
0.4229 +0.246
0.4243 +0.241
0.4271 +0.185
0.4313 +0.044
0.4327 +0.010
0.4354 −0.040
0.4396 −0.184
0.4410 −0.214
0.4438 −0.266
0.4452 −0.312
0.4479 −0.358
0.4493 −0.398
0.4521 −0.486
0.4535 −0.511
0.4563 −0.555
0.4577 −0.575
0.4604 −0.590
0.4618 −0.596
0.4646 −0.612
0.4660 −0.615
0.4688 −0.616
0.4702 −0.622

2441538 +
0.3354 −0.323
0.3368 −0.341
0.3396 −0.414
0.3438 −0.542
0.3452 −0.574
0.3493 −0.669
0.3514 −0.705
0.3528 −0.706
0.3563 −0.725
0.3577 −0.735
0.3604 −0.723
0.3618 −0.722
0.3646 −0.721
0.3660 −0.695
0.3688 −0.692
0.3701 −0.678
0.3729 −0.648
0.3743 −0.645
0.3785 −0.586
0.3813 −0.548
0.3827 −0.534
0.3854 −0.531
0.3868 −0.516

2441545 +
0.4046 +0.201
0.4057 +0.198
0.4070 +0.212
0.4089 +0.199
0.4103 +0.208
0.4116 +0.199
0.4149 +0.171
0.4161 +0.153
0.4176 +0.132
0.4219 +0.023
0.4233 +0.001
0.4259 −0.048
0.4273 −0.078
0.4288 −0.106
0.4315 −0.161
0.4328 −0.215
0.4339 −0.247
0.4370 −0.324
0.4399 −0.435
0.4428 −0.520
0.4443 −0.569
0.4457 −0.607
0.4485 −0.667
0.4500 −0.696
0.4515 −0.719
0.4542 −0.742
0.4554 −0.754
0.4568 −0.756
0.4595 −0.754
0.4609 −0.757
0.4623 −0.747
0.4654 −0.714
0.4668 −0.706
0.4712 −0.674
0.4726 −0.653
0.4742 −0.643
0.4772 −0.618
0.4786 −0.606
0.4800 −0.593

2441589 +
0.2676 +0.139
0.2690 +0.131
0.2717 +0.096
0.2731 +0.067
0.2759 +0.039
0.2773 +0.021
0.2801 −0.030
0.2815 −0.067
0.2842 −0.127
0.2856 −0.154
0.2884 −0.190
0.2898 −0.214
0.2926 −0.262
0.2940 −0.280
0.2967 −0.336
0.2981 −0.359
0.3009 −0.410
0.3023 −0.448
0.3051 −0.498
0.3065 −0.518
0.3092 −0.554
0.3106 −0.583
0.3134 −0.616
0.3148 −0.636
0.3176 −0.642
0.3190 −0.645
0.3217 −0.637
0.3231 −0.643
0.3259 −0.634
0.3273 −0.638
0.3342 −0.609
0.3356 −0.604
0.3384 −0.584
0.3398 −0.573

2441597 +
0.2651 +0.182

0.2668 +0.153
0.2718 +0.052
0.2736 −0.012
0.2776 −0.126
0.2794 −0.192
0.2817 −0.260
0.2851 −0.407
0.2868 −0.446
0.2884 −0.495
0.2900 −0.560
0.2938 −0.636
0.2956 −0.676
0.2972 −0.685
0.2988 −0.714
0.3004 −0.725
0.3021 −0.736
0.3059 −0.772
0.3075 −0.757
0.3091 −0.775
0.3107 −0.763
0.3124 −0.768
0.3158 −0.761
0.3174 −0.768
0.3191 −0.735
0.3206 −0.738
0.3253 −0.719
0.3269 −0.710

2441605 +
0.2399 −0.040
0.2419 −0.129
0.2426 −0.177
0.2446 −0.234
0.2453 −0.247
0.2474 −0.322
0.2506 −0.445
0.2513 −0.494
0.2534 −0.568
0.2541 −0.593
0.2565 −0.664
0.2572 −0.677
0.2596 −0.717
0.2610 −0.753
0.2631 −0.787
0.2638 −0.811
0.2655 −0.835
0.2662 −0.850

0.2690 −0.865
0.2700 −0.865
0.2725 −0.865
0.2739 −0.877
0.2767 −0.885
0.2774 −0.885
0.2802 −0.888
0.2809 −0.886
0.2836 −0.869
0.2850 −0.855
0.2870 −0.865
0.2884 −0.854
0.2902 −0.828
0.2916 −0.822
0.2943 −0.803
0.2954 −0.794

2441898 +
0.4317 +0.358
0.4375 +0.325
0.4406 +0.266
0.4433 +0.227
0.4461 +0.049
0.4490 −0.093
0.4519 −0.228
0.4552 −0.389
0.4581 −0.468
0.4611 −0.585
0.4637 −0.721
0.4665 −0.765
0.4694 −0.771
0.4721 −0.795
0.4750 −0.823
0.4777 −0.854
0.4803 −0.858
0.4863 −0.829
0.4890 −0.811
0.4919 −0.794
0.4947 −0.768

2441949 +
0.3486 +0.072
0.3511 +0.006
0.3532 −0.064
0.3568 −0.158
0.3599 −0.251
0.3631 −0.320

0.3661 −0.416
0.3698 −0.507
0.3733 −0.581
0.3766 −0.617
0.3797 −0.646

2442126 +
0.5287 +0.239
0.5306 +0.216
0.5319 +0.192
0.5331 +0.164
0.5405 +0.047
0.5416 +0.028
0.5428 +0.009
0.5439 −0.007
0.5451 −0.037
0.5506 −0.249
0.5519 −0.297
0.5531 −0.347
0.5543 −0.408
0.5554 −0.447
0.5567 −0.480
0.5579 −0.511
0.5590 −0.559
0.5630 −0.679
0.5641 −0.691
0.5652 −0.710
0.5664 −0.735
0.5675 −0.748
0.5685 −0.764
0.5697 −0.764
0.5708 −0.769
0.5720 −0.777
0.5731 −0.780

2442216 +
0.4260 +0.384
0.4272 +0.390
0.4287 +0.411
0.4337 +0.410
0.4351 +0.411
0.4364 +0.422
0.4379 +0.429
0.4432 +0.395
0.4444 +0.391
0.4455 +0.407
0.4469 +0.387

0.4520 +0.382
0.4536 +0.382
0.4552 +0.380
0.4567 +0.347
0.4615 +0.273
0.4628 +0.256
0.4641 +0.242
0.4654 +0.229
0.4702 +0.106
0.4714 +0.065
0.4730 +0.030
0.4743 −0.010
0.4796 −0.178
0.4809 −0.238
0.4822 −0.311
0.4834 −0.357
0.4847 −0.420
0.4895 −0.599
0.4907 −0.631
0.4919 −0.666
0.4934 −0.715
0.4948 −0.727
0.4963 −0.754
0.5011 −0.801
0.5027 −0.809
0.5041 −0.812
0.5069 −0.814
0.5083 −0.811
0.5130 −0.798
0.5142 −0.801
0.5156 −0.799
0.5170 −0.788
0.5234 −0.735
0.5248 −0.725
0.5264 −0.715
0.5277 −0.706

2442220 +
0.4521 +0.361
0.4541 +0.302
0.4572 +0.214
0.4589 +0.166
0.4619 +0.075
0.4643 −0.022
0.4675 −0.166
0.4691 −0.220
0.4725 −0.386

0.4737 −0.433
0.4766 −0.528
0.4783 −0.591
0.4815 −0.663
0.4833 −0.714
0.4867 −0.789
0.4884 −0.812
0.4919 −0.863
0.4938 −0.893
0.4969 −0.898
0.4983 −0.905
0.5019 −0.886
0.5035 −0.872
0.5066 −0.857
0.5093 −0.846

2442224 +
0.4342 +0.340
0.4357 +0.320
0.4386 +0.294
0.4405 +0.255
0.4440 +0.138
0.4455 +0.090
0.4477 +0.032
0.4490 −0.023
0.4507 −0.092
0.4554 −0.252
0.4569 −0.329
0.4586 −0.412
0.4630 −0.575
0.4662 −0.663
0.4678 −0.699
0.4708 −0.788
0.4723 −0.810
0.4755 −0.853
0.4772 −0.867
0.4806 −0.885
0.4817 −0.884
0.4849 −0.886
0.4884 −0.889
0.4920 −0.873
0.4945 −0.862

2442255 +
0.3815 +0.301
0.3876 +0.295
0.3952 +0.298

0.4017 +0.303
0.4135 +0.295
0.4183 +0.314
0.4225 +0.314
0.4274 +0.276
0.4323 +0.245
0.4369 +0.184
0.4421 +0.111
0.4467 −0.019
0.4537 −0.208
0.4593 −0.342
0.4635 −0.473
0.4693 −0.630

2442256 +
0.3455 −0.309
0.3508 −0.477
0.3557 −0.648
0.3615 −0.734

2442275 +
0.3544 +0.239
0.3565 +0.198
0.3586 +0.153
0.3608 +0.120
0.3634 +0.014
0.3656 −0.073
0.3671 −0.167
0.3701 −0.343
0.3727 −0.469
0.3748 −0.571
0.3770 −0.661
0.3793 −0.739
0.3817 −0.830
0.3837 −0.877
0.3860 −0.930
0.3881 −0.958
0.3910 −0.976

2442278 +
0.4478 +0.177
0.4492 +0.163
0.4505 +0.149
0.4520 +0.103
0.4534 +0.035
0.4590 −0.188
0.4604 −0.254
0.4617 −0.312
0.4630 −0.394
0.4645 −0.481
0.4700 −0.643
0.4715 −0.672
0.4729 −0.707
0.4742 −0.723
0.4756 −0.749
0.4808 −0.808
0.4821 −0.820
0.4836 −0.844
0.4850 −0.861
0.4864 −0.867
0.4877 −0.859
0.4944 −0.823

2442299 +
0.2966 +0.081
0.2977 +0.059
0.3004 +0.034
0.3014 +0.009
0.3024 −0.015
0.3053 −0.116
0.3063 −0.135
0.3073 −0.161
0.3083 −0.209
0.3103 −0.298
0.3113 −0.329
0.3122 −0.369
0.3132 −0.401
0.3171 −0.479
0.3181 −0.513
0.3199 −0.552

2442307 +
0.2694 +0.475
0.2705 +0.420
0.2733 +0.266
0.2747 +0.166
0.2775 +0.071
0.2785 +0.049
0.2809 −0.057
0.2816 −0.099
0.2840 −0.188
0.2851 −0.220
0.2872 −0.303
0.2885 −0.337
0.2916 −0.455
0.2926 −0.518
0.2952 −0.580
0.2966 −0.622
0.2996 −0.703
0.3003 −0.728
0.3038 −0.808
0.3052 −0.835
0.3087 −0.852
0.3097 −0.862
0.3135 −0.859
0.3145 −0.848
0.3177 −0.821
0.3191 −0.828
0.3233 −0.798
0.3246 −0.792
0.3281 −0.753
0.3295 −0.753
0.3330 −0.695

2442454 +
0.6262 +0.220
0.6272 +0.232
0.6284 +0.223
0.6297 +0.220
0.6352 +0.209
0.6366 +0.219
0.6376 +0.229
0.6390 +0.223
0.6401 +0.214
0.6470 +0.212
0.6484 +0.203
0.6500 +0.225
0.6515 +0.235
0.6533 +0.234
0.6543 +0.233
0.6588 +0.246
0.6609 +0.236
0.6623 +0.255
0.6637 +0.251
0.6654 +0.272
0.6706 +0.277
0.6716 +0.261
0.6734 +0.261

Communications from the
Konkoly Observatory
of the Hungarian
Academy of Sciences

Mitteilungen
der Sternwarte der
Ungarischen Akademie
der Wissenschaften

Budapest–Svábhegy

No. 103
(Vol. 13, Part 3)

The Interaction of Stars with their Environment II.

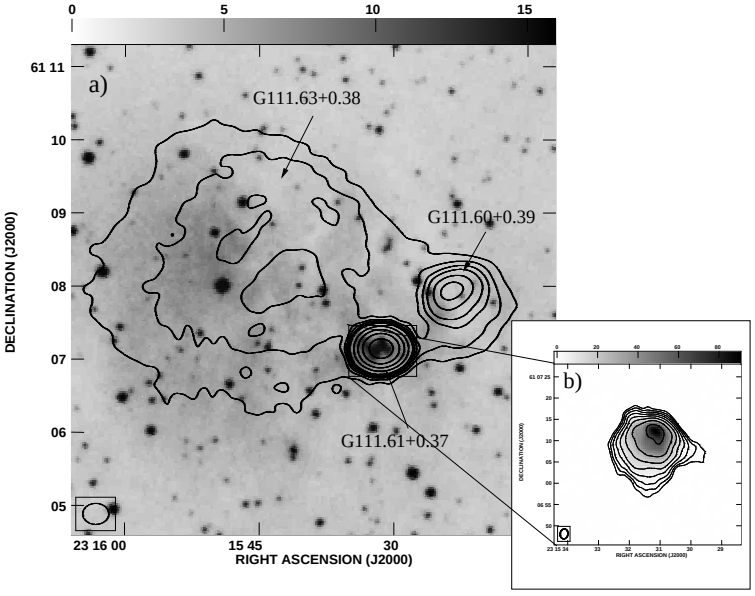

Proceedings of the workshop held at the Eötvös Loránd
University, Budapest, Hungary, 15–18 May, 2002

Budapest, 2003

EDITORS:

Csaba Kiss, **Mária Kun**
Konkoly Observatory of the Hungarian Academy of Sciences
P.O. Box 67, H-1525 Budapest, Hungary

and **Vera Könyves**
Astronomy Department, Eötvös Loránd University
P.O. Box 32, H-1518 Budapest, Hungary

ISBN 963 8361 41 7
HU ISSN 0238-2091
Responsible publisher: Lajos G. Balázs

Contents

Young Stars

(Post-)Main-Sequence Stars

Winds and Bubbles

Processes on Galactic Scales

PREFACE

The first workshop and spring school organized by the Department of Astronomy of the Loránd Eötvös University and Konkoly Observatory was held in 1996 at Visegrád, Hungary. The second conference of the series followed it six years later in Budapest. During this six years several new aspects of this field of research emerged. The mid- and far-infrared detectors of ISO opened new windows on the great variety of phenomena related to the interactions between stars and their environment. New types of objects came into the foreground, such as circumstellar environments of brown dwarfs and very cold cloud cores.

Participants from nine countries, mainly students, attended the workshop, whose topics embraced a wide scale of phenomena accompanying the life of the stars, from protostellar winds and disks through the effects of pulsating stellar atmospheres on the surrounding gas and dust to circumstellar envelopes of Wolf-Rayet and post-AGB stars.

We hope that the two volumes of 'Interactions of Stars with their Environment' published by Konkoly Observatory will be followed by further issues on this intriguing and amazing field of astronomy.

We are grateful to the Astronomy Department of the Eötvös Loránd University for the hospitality during the conference and to the Hungarian Research Found (OTKA) for the financial support.

These proceedings could not have been published without the financial resources provided by Dr. L. Szabados and Dr. L.V. Tóth (OTKA #T029013 and #T043773). Their help is highly appreciated.

The Editors

Star Formation

Multivariate Separation of Cosmic Components

L.G. Balázs
Konkoly Observatory of the Hungarian Academy of Sciences
P.O. Box 67, H-1525 Budapest, Hungary
E-mail: balazs@konkoly.hu

Abstract

Observing and storing the photons of the incoming radiation from the Cosmos typically give a data cube defined by $(\alpha, \delta, \lambda)$. It is easy to translate this data structure into the formalism of multivariate statistics. A common problem in the multivariate statistics is whether the stochastic variables described by observed properties are statistically independent or can be described by a less number of hidden variables. This is the task of factor analysis. Forming groups from cases having similar properties according to the measures of similarities or the distances is the task of cluster analysis. We demonstrated in three cases how these technics can be used for separating physically independent cosmic components projected onto the same celestial area by chance.

1. Introduction: Nature of astronomical information

The information we receive from Cosmos is predominantly in the form of electromagnetic radiation. An incoming plain wave can be characterized by the following quantities:

$$\underline{n}\,(direction),\ \lambda\,(wavelength),\ polarization.$$

These physical quantities determine basically the possible observational programs:

1. Position $\Longrightarrow$ astrometry
2. Distribution of photons with $\lambda \Longrightarrow$ spectroscopy
3. Number of photons $\Longrightarrow$ photometry
4. Polarization $\Longrightarrow$ polarimetry
5. Time of observation $\Longrightarrow$ variability
6. Distribution of photons in data space $\Longrightarrow$ statistical studies

In the reality, however, not all these quantities can be measured simultaneously. Restriction is imposed by the existing instrumentation.

By observing and storing the photons of the incoming radiation typically we get a data cube defined by $(\alpha, \delta, \lambda)$. The measuring instrument has some finite resolution in respect to the parameters of the incoming radiation. Consequently, the data cube can be divided into cells of size of the resolution. The astronomical objects can be characterized by isolated domains on the α, δ plane. A real object can be more extended than one pixel in this plane. Each pixel in the α, δ plane can have a set of non-empty cells according to the different λ values. A list of non-empty pixels can be ordered into a matrix form having columns of properties (α, δ, and the set of λs) and rows referring to the serial number of objects. This structure is called the 'Data Matrix' which is the input of many multivariate statistical procedures.

Table 1: Structure of the Data Matrix: m means the number of properties and n runs over the cases.

α_1	δ_1	λ_{11}	λ_{12}	$\cdots$	λ_{1m}
α_2	δ_2	λ_{21}	λ_{22}	$\cdots$	λ_{2m}
$\vdots$	$\vdots$	$\vdots$	$\vdots$	$\ddots$	$\vdots$
α_n	δ_n	λ_{11}	λ_{12}	$\ldots$	λ_{nm}

2. Brief summary of multivariate methods

2.1. Factor Analysis

A common problem in the multivariate statistics is whether the stochastic variables described by different properties are statistically independent or can be described by a less number of physically important quantities behind the data observed. The solution of this problem is the subject of the factor analysis.

Factor analysis assumes a linear relationship between the observed and the background variables. The value (factor scores) and number of background variables, along with the coefficients of the relationship (factor loadings) are outputs of the analysis. The basic model of factor analysis can be written in the following form:

$$X_j = \sum_{k=1}^{p} a_{jk} F_k + u_j \qquad , \qquad (j = 1, \cdots, m). \tag{1}$$

In the formula above X_j means the observed variables, m is the number of properties, p is the number of hidden factors (normally $p < m$), a_{jk} denotes the factor loadings, F_k the factor scores, and u_j-s are called individual factors. The individual factors represent those parts of the observed variables which are not explained by the common factors.

A common way to solve the factor problem uses the Principal Components Analysis (PCA). PCA has many similarity with the factor analysis, however, its basic idea is different. Factor analysis assumes that behind the observed ones there are hidden variables, less in number, responsible for the correlation between the observed ones. The PCA looks for uncorrelated background variables from which one obtains the observed variables by linear combination. The number of PCs is equal to those of the the observed variables. In order to compute the PCs one has to solve the following eigenvalue problem:

$$\underline{R}\,\underline{a} = \lambda\,\underline{a} \tag{2}$$

where $\underline{R}$, $\underline{a}$ and λ mean the correlation matrix of the observed variables, its eigenvector and eigenvalue, respectively. The components of the $\underline{a}$ eigenvectors give the coefficients of the linear relationship between the PCs and the observed variables. The PC belonging to the biggest eigenvalue of $\underline{R}$ gives the most significant contribution to the observed variables. The PCs can be ordered according to the size of the eigenvalues. In most cases the default solution of the factor problem is the PCA in the statistical software packages (e.g. BMDP, SPSS). Normally, if the observed variables can be described by a less number of background variables (the starting assumption of the factor model) there is a small number of PCs having large eigenvalue and their linear combination reproduce fairly well the observed quantities. The number of large eigenvalues gives an idea on the number of the hidden factors. Keeping only those PCs having large eigenvalues offers a solution for the factor model. This technique has a very wide application in the different branches of observational sciences. For the astronomical context see Murtagh & Heck (1987).

The factor model can be used successfully for separating cosmic structures physically not related to each other but projected by chance on the same area of the sky. We will return to the details later on when dealing with case studies.

2.2. Cluster Analysis

Factor analysis is dealing with relationships between properties when describing the mutual correlations of observed quantities by hidden background variables. One may ask, however, for the relationship between cases. In order to study the relationship between cases one have to introduce some measure of similarity. Two cases are similar if their properties, the value of their observed quantities, are close to each other.

"Similarity", or alternatively "distance" between l and k cases, is a function of two X_j^l, X_j^k set of observed quantities (j is running over the properties describing a given case). Conventionally, if $l = k$, i. e. the two cases are identical, the similarity $a(X_j^l, X_j^k) = 1$ and the distance $d(X_j^l, X_j^k) = 0$. The mutual similarities or distances of cases form a similarity or distance matrix.

Forming groups from cases having similar properties according to the measures of similarities and the distances is the task of cluster analysis. There are several methods for searching clusters in multivariate data. There is no room here to enter into the details. For the astronomical context see again (Murtagh & Heck, 1987). Typical application of this procedure is the recognition of celestial areas with similar properties, based on multicolor observations. The procedure of clustering in this case is a searching for pixels on the images taken in different wavelengths but having similar intensities in the given colors.

In the following we try to demonstrate how these procedures are working in real cases.

3. Case studies

3.1. Separation of the Zodiacal Light and Galactic Dust Emission

The IRAS mission covered the whole sky in four (12, 25, 60, 100 μm) wavelengths. In particular, the 12 and 25 micron images were dominated by the thermal emission of the Zodiacal Light (ZL) having a characteristic temperature around 250 $K\hbar$. The contamination of the Galactic Dust thermic radiation by the ZL is quite serious close to the Ecliptic. Assuming that both radiation are coming from optically thin media the observed infrared intensities are sums of those coming from these two components. We may assume furthermore the distribution of the intensity of thermal radiation on the sky coming from the Galactic component has some similarities when observed at the given wavelengths and the same holds also for the ZL. Identifying the radiation coming from these two physically distinct components with the hidden variables in Eq.

Table 2: Results of factor analysis. There are two large eigen values indicating the presence of two important factors. The last two columns of the table give the a_{jk} factor coefficients for Eq. (1). (Balázs et al., 1990)

eigenvalue	cum. percent.	Variable	1. factor	2. factor
2.4818	62.0	F_{12}	0.9637	0.2089
1.3910	96.8	F_{25}	0.9917	0.0458
0.1003	99.3	F_{60}	0.3625	0.9044
0.0268	100.0	F_{100}	0.0409	0.9819

(1) and the incoming intensity with the observed ones the separation of the ZL and the Galactic radiation can be translated into the general framework of factor analysis.

In the case of the IRAS images the $\underline{R}$ correlation matrix has a size of 4×4 by cross correlating the four (12, 25, 60 and 100 μm) images. We selected a field of $15^\circ \times 15^\circ$ (corresponding to 512×512 pixels) in Perseus close to the ecliptic, containing the California Nebula, IC 348 and the Pleiades.

Solving Eq. (2) for this case we got the results summarized in Tab. 2. One can infer from this table that there are two large eigenvalues indicating the presence of two important factors. The last two columns of the table give the a_{jk} factor coefficients for Eq. (1). The first factor dominates the radiation at 12 and 25 μm while the second one does it at 60 and 100 μm. Computing the factor values from the observed data (the measured 12, 25, 60 and 100 μm intensities) one gets the two images as shown in Fig. 1, along with the originals (Balázs et al., 1991).

In order to define regions of similar physical properties we performed cluster analysis in the $\{F_1; F_2\}$ factor plane. These two factors define a two-dimensional subspace in the four-dimensional color space. The 1-st factor almost fully explains the 25 micron flux, which is heavily dominated by the Zodiacal Light and therefore represents its influence in different colors. The second factor, in contrast, describes the effect of the radiation coming from the galactic dust which produces most of the 100 micron emission. Performing cluster analysis altogether 10 regions were defined, however this figure was arbitrary. The result is given in Fig. 2. The basic features of this plot are the two 'fingers' pointing upwards and nearly horizontally. These 'fingers' may be identified with the Zodiacal Light (dominating F_l) and the galactic radiation (dominating F_2).

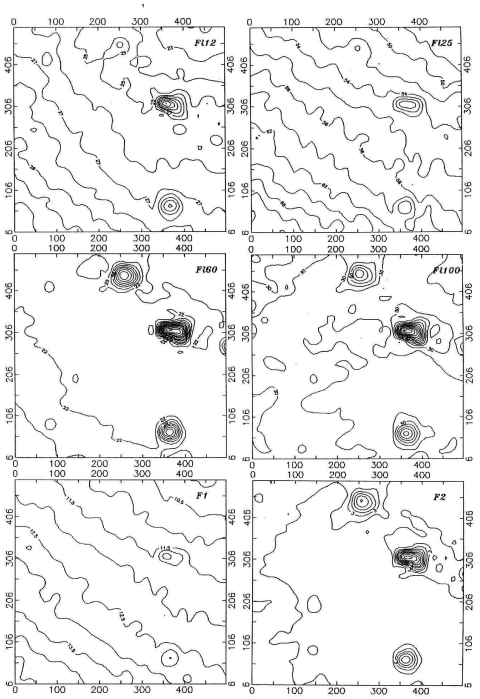

Figure 1: Input IRAS (12, 25, 60, and 100μm) images of the factor analysis and the resulted two factor pictures. The coordinates are measured in pixels. The objects are the California Nebula, IC 348 and the Pleiades, in descending order. Note the strong trend in F_1 representing the ZL while F_2 displays the Galactic component (Balázs et al., 1991).

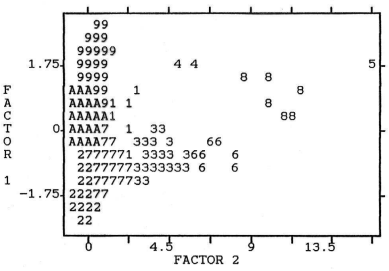

Figure 2. Character plot of regions (clusters) of similar properties in the $\{F_1; F_2\}$ factor plane. The identical symbols mean physically similar regions. The basic features of this plot are the two 'fingers' pointing upwards and nearly horizontally. These 'fingers' may be identified with the Zodiacal Light (dominating $Factor\,1$) and the galactic radiation (dominating $Factor\,2$) (Balázs et al., 1990).

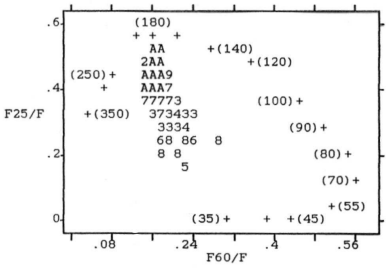

Figure 3. Distribution of duster members in the $\{F25/F; F6O/F\}$ plane. The coding of dusters is the same as in Fig. 2. The loci of dust low $\alpha = 1$ radiations of different temperatures are marked with crosses. The numbers in parentheses are the respective temperatures. Note that the wedge-shaped distribution of symbols representing real measurements points towards dust temeratures of about 40K and 200K (Balázs et al., 1990).

The dust emission is basically thermal. We computed the total infrared emission by adding the fluxes in the four bands:

$$F = F_{12} + F_{25} + F_{60} + F_{100} \tag{3}$$

Assuming a dust emission law in the form of $B(T)/\lambda^{\alpha}$ where $B(T)$ is the black body (BB) radiation at T temperature, λ the wavelength and α depends on the physical properties of the emitting dust, we put $\alpha = 1$. However, recent studies of the far infrared radiation of the ZL with the ISO satellite indicate nearly BB radiation (Leinert et al., 2002), i.e $\alpha = 0$. The specification of α influences the numerical results obtained, of course, but our goal is only to demonstrate the link between the statistical procedure and the physical quantities.

The F_i/F ratios (i is 12, 25, 60 or 100) depend only on T if a region determined by one characteristic temperature. Supposing the validity of the dust emission law given above we computed the loci of such regions in Fig. 3, marked with crosses the sources of different temperatures in the line of sight. As a consequence, the real points in Fig. 3 are not on the theoretically computed line but deviate from it according to the relative intensity of superimposed sources of different temperatures. Keeping the same coding of sources as in Fig. 2 one gets a wedge-shaped distribution of symbols representing real measurements pointing towards dust temperatures of about 40 K and 200K. This distribution can be obtained from the superimposed ZL and Galactic sources with these characteristic temperatures.

4. Separation of HI components in the field of L1780

The next case study refers to L1780, a small dust cloud at a high galactic latitude. By analyzing the profile of the HI 21 cm line it was difficult to separate the object from the background since the velocity of the cloud was very close to those of the background.

The cloud was observed with the 100 m telescope at Effelsberg at 209 positions in 82 channels. Formulating the problem of separation with the phraseology of the multivariate statistical analysis we had 209 cases and 82 properties.

Performing PCA yielded 7 eigenvalues > 1 and they were accepted as significant factors. In order to get clear-cut factor pattern we made Varimax rotation. This procedure makes use of the fact that factors are determined only up to an orthogonal transformation. Varimax rotation is an orthogonal transformation

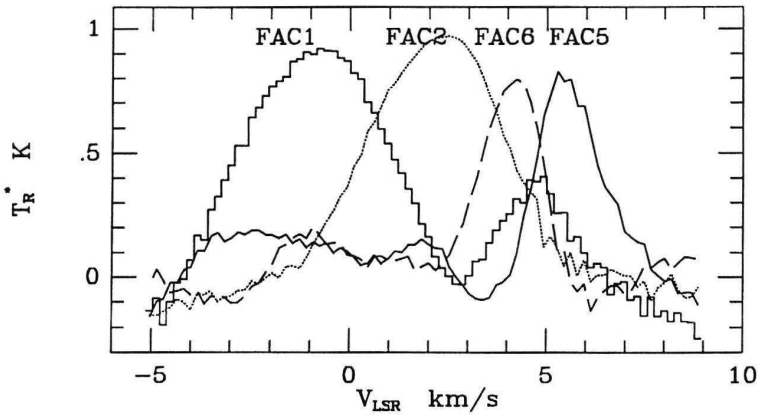

Figure 4: Results of factor analysis in L1780. The factor coefficients are displayed as functions of the channels calibrated to the velocity in the line of sight. Beside the strongest factor (FAC1), the main HI background component, those are displayed which give excess emission in the field of L1780 (FAC2, FAC5, FAC6) (Tóth et al., 1993).

which maximizes the variance of the factor coefficients and usually gives a dominant factor in each observed variables. This dominant factor makes easier to identify the factors with real physical entities.

Inspecting the pictures obtained from the factor scores we found that FAC2, FAC5 and FAC6 indicated excess HI radiation that could be associated with L1780. On the contrary, FAC1, FAC3, FAC4 and FAC7 described the background. The contributions of the different factors to the channel maps are displayed in Fig. 4. Summing up the factors related to the cloud gives the amount of HI associated to L1780 (Tóth et al., 1993).

Using the computed factors associated with the cloud we calculated the HI 21 cm spectra in some characteristic positions of L1780 along with the background as seen in Fig. 5. Note that the difference of the HI spectra across the cloud (i.e. the difference between he position a and c) indicates large scale internal motions.

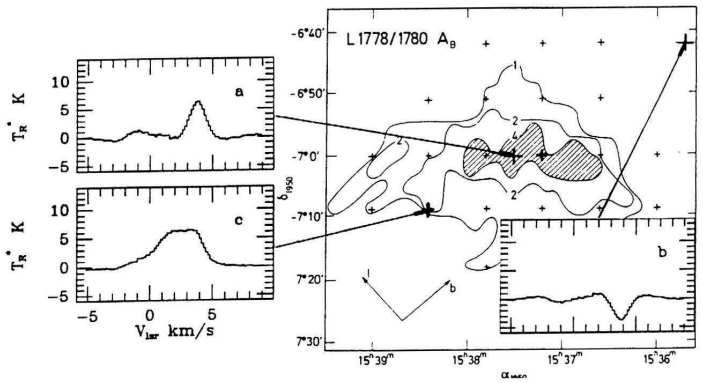

Figure 5: Distribution of the dust in L1780 as obtained from the optical extinction (A_B). The HI spectra in the inserts give velocity profiles at some characteristic parts of the cloud (a, c) and the background (b), respectively. Note that the difference of the HI spectra across the cloud (i.e. the difference between the positions a and c indicates large scale internal motions (Tóth et al., 1993).

5. Multivariate study of the Cepheus Bubble

The Cepheus Bubble was discovered in the IRAS maps (Kun et al., 1987) as a ring about 10 deg. in diameter around Cep OB2 joining several known star forming regions (S140, IC1396, S134, etc). The association of the ring with the star forming regions with known distances (between 800-900 pc) enabled one to estimate the true geometric diameter to be 140-160 pc. The dust responsible for the radiation detected by IRAS, however, is only a tiny fraction of the total mass which is mostly in the form of HI. In order to calculate the mass and internal kinematics of the bubble one of the best choice was to use neutral hydrogen observations. The integrated map of the HI channel intensities clearly showed a ring coinciding with those in the IRAS maps (Fig. 6). We used 43 HI channel maps of the region from the Dwingeloo HI sky survey (Burton & Hartman, 1994) in the [–38 km/s; +10 km/s] range.

Inspection of the channel maps (Fig. 5), starting at –38 km/s and moving towards positive radial velocities, revealed a ring structure starting at –30 km/s, becoming dominant in the [–18 km/s; –10 km/s] range and fading away

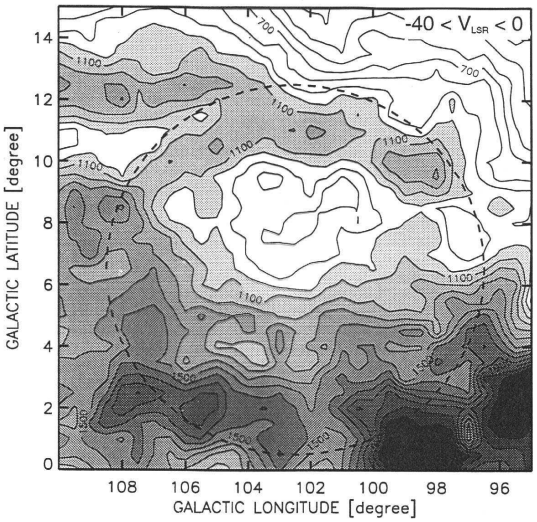

Figure 6: Integrated column density of the HI in the region of the Cepheus Bubble. A dashed circle indicates the outer boundary of the infrared ring (Ábrahám et al., 2000).

afterwards (Fig. 8). In order to separate the HI associated with the Bubble we performed factor analysis based on PCA which yielded 6 main components (see Tab. 3). The factor coefficients, similarly to the case of L1780, could be calibrated for radial velocity and are displayed in Fig. 9. The Figure clearly shows that each factor dominates a certain velocity range. Usage of the images made up from the factor scores (Fig. 10) enabled us to identify the factors in terms of different physical entities of the HI distribution. The main body of the bubble appeared in factor 2 whereas factor 3 and 5 are strong on the area where factor 2 is weak. These factors can be interpreted as different slices of an expanding shell. Identification of the factors with different physical entities of the neutral hydrogen enabled us to separate the HI associated with the Bubble and determine its mass and age (Ábrahám et al., 2000).

6. Conclusions

1. The nature of astronomical information is well suited for multivariate studies.

2. The typical procedures of multivariate methods (factor analysis, cluster analysis) can be applied succesfully for studying different structures in the

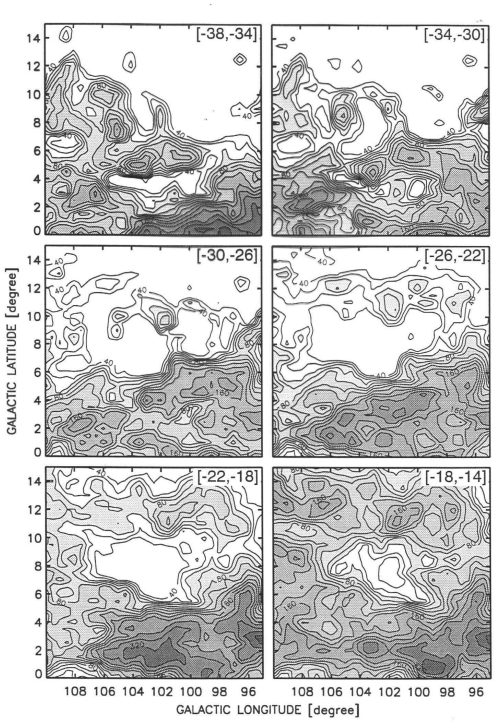

Figure 7: HI channel maps of the Cepheus Bubble in the [-38 km/s; -14 km/s] range. The ring structure appears at -26 km/s and increases in dominance at less negative velocities (Ábrahám et al., 2000).

data cubes.

3. There is no straightforward way to assign physically meaningful objects to the formal statistical results (actually this is one of the basic problems).

4. Special care is needed to separate "ghosts". In some cases physically related structures can be splitted into different mathematical structures.

5. The best results can be expected for problems where the basic mathematical assumptions (e.g. linearity and orthogonality at PCA models) are also physically meaningful.

6. A basic advantage is the existence of professional statistical packages (SPSS, SAS, S-plus, etc.)

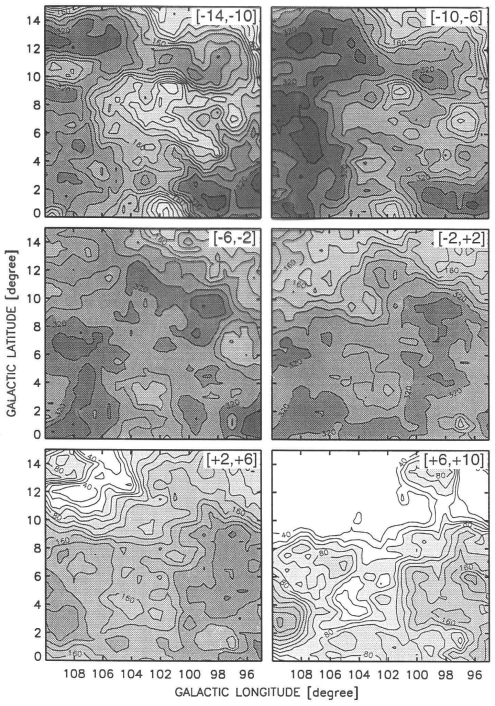

Figure 8: HI channel maps of the Cepheus Bubble in the [-14 km/s; +10 km/s] range. The ring structure fades away towards less negative velocities and completely disappears (Ábrahám et al., 2000).

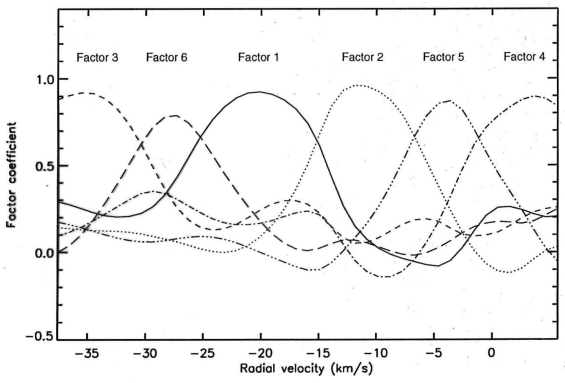

Figure 9: Dependence of the factor coefficients on the radial velocity in the Cepheus Bubble. Each factor dominates a certain range of radial velocities. The 2nd strongest factor can be associated with the main body of the ring (Ábrahám et al., 2000).

Table 3: Results of the factor analysis on the HI data of the Cepheus Bubble. There are 6 eigenvalues > 1 reproducing 95.4 % of the total variance of the data.

PC	Eigenvalue.	Pct. of Var. [%]	Cum.Pct. [%]
1	20.41	47.5	45.5
2	7.80	18.3	65.8
3	5.87	13.7	79.5
4	3.41	7.9	87.4
5	1.87	4.3	91.8
6	1.56	3.6	95.4
7	0.66	1.5	96.7
8	0.52	1.2	98.1
⋮	⋮	⋮	⋮
43	0.00	0.00	100.0

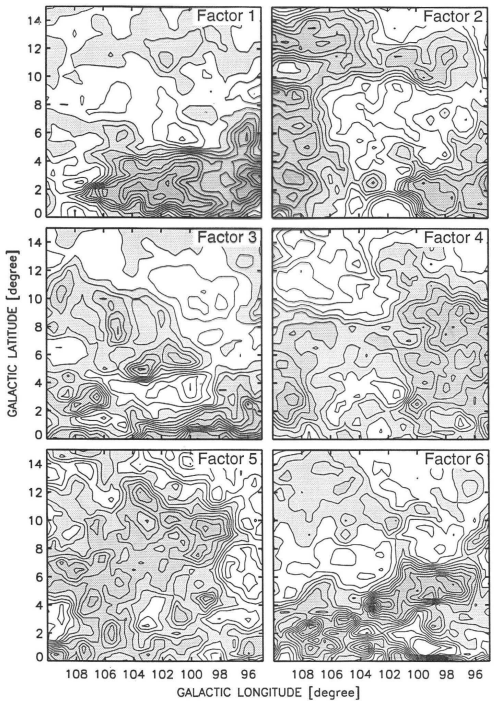

Figure 10: Images made up from the factor scores in the Bubble. The 2nd strongest factor gives the main body of the ring. Images of factors 3 and 5 are strong on the area where factor 2 is weak. These factors can be interpreted as different parts of an expanding shell (Ábrahám et al., 2000).

Acknowledgements

The author is indebted to Dr. Gábor Tusnády (Rényi Institute of Mathematics, Budapest) for the comprehensive discussions in the theory and practice of multivariate statistical methods.

References

Ábrahám, P., Balázs, L.G., Kun, M., 2000, A&A, 354, 645

Balázs, L.G., Kun, M., Tóth, V., 1990, in 'The Galactic and Extragalactic Background Radiation', IAU Symposia No. 139, eds. S. Bowyer & C. Leinert, Kluwer Academic Publishers, Dordrecht, Holland, p.214

Balázs, L.G., Tóth, L.V., 1990, in the 'Physics and Composition of Interstellar Matter', eds. J. Krelowski & J. Papaj, Institute of Astronomy Nicolaus Copernicus University, Torun , p.135

Burton, W.B., Hartmann, D., 1994, A&ASS, 217, 189

Kun, M., Balázs, L.G., Tóth, I. 1987, A&ASS, 134, 211

Leinert, C., Ábrahám, P., Acosta-Pulido, J., Lemke, D., Siebenmorgen, R., 2002, A&A, 393, 1073

Murtagh, F., Heck, A., 1987, "Multivariate data analysis", Astrophysics and Space Science Library, Dordrecht: Reidel

Tóth, L.V., Mattila, K., Haikala, L., Balázs, L.G., ASP Conf. Ser. Vol. 52, 'Astronomical Data Analysis Software and Systems II', eds. R.J. Hanisch et al., p.462

Low-Mass Star Formation Induced by the Orion–Eridanus Bubble

M. Kun[1], **S. Nikolić**[2]

[1]Konkoly Observatory
H-1525 Budapest, P.O. Box 67, Hungary
E-mail: kun@konkoly.hu
[2]Onsala Space Observatory
S-439 92 Onsala, Sweden
E-mail: silvana@oso.chalmers.se

Abstract

During a spectroscopic survey performed with the Nordic Optical Telescope in La Palma we found five classical T Tauri stars in the small, high latitude molecular clouds associated with the reflection nebula IC 2118. The star-forming clouds are located at the outer boundary of the Orion star forming region, at a mean galactic latitude of -28°. Their positions in space and cometary shapes suggest their interaction with the Orion SFR. Using spectroscopic and near-infrared photometric data we determined the positions of the newly discovered pre-main sequence stars in the HRD. Comparison of the results with evolutionary models has shown that the masses of these stars are between 0.3–0.8 $M_{\odot}$ and their ages are close to 10^6 yrs. They are roughly coeval and significantly younger than the known WTTS of the same region. We conclude that the birth of the molecular clouds and the stars was probably induced by the interaction of the Orion–Eridanus Bubble with some small, diffuse high-latitude HI clouds.

KEYWORDS: *ISM: supershells, high-latitude molecular clouds, Orion–Eridanus Bubble, star formation–stars: pre-main sequence*

1. Introduction

The Orion–Eridanus Bubble is a giant supershell blown by the high-mass stars of the oldest subgroup of the Orion OB1 association, Orion OB1a (Brown et al., 1995). Its present radius is about 140 pc, and has a mean expansion velocity of $\sim$40 km s^{-1}. It shows up as a fragmented HI shell with angular extent more than 40°, associated with several Hα loops and filaments, including the Barnard Loop. The interior of the bubble is filled with low density ionized gas which is traced by soft X-ray emission and by ultraviolet absorption lines in the spectra of background stars. This large volume of tenuous gas surrounding Orion OB1

is often referred to as *Orion's cloak* (Cowie, 1982). The total mass of the HI shell is estimated to be about $2.3 \times 10^5\,M_\odot$, and its kinetic energy is about 3.7×10^{51} erg (Brown et al., 1995). The supershell expands into the surrounding interstellar medium, thereby creating favorable circumstances for induced star formation. Identification of individual interstellar features associated with the bubble, hovewer, requires careful study of distances of the objects in question, because the size of this supershell is comparable with its distance from us.

The reflection nebula IC 2118 near Rigel (*Witch head nebula*) is a region associated with the nearest wall of the supershell. Its galactic coordinates are $205^\circ \leq l \leq 210^\circ$, $-30^\circ \leq b \leq -25^\circ$. The distance of the nebula from the Sun is 210 ± 20 pc (Kun et al., 2001).

In this case the well-known distance of the illuminating star makes it possible to determine the distance of the illuminated clouds. Molecular clouds associated with IC 2118 were described by Yonekura et al. (1997) and Kun et al. (2001). The wind-blown appearance of the bright reflection nebula and the cometary shapes of the associated molecular clouds suggest that the region is dynamically influenced by the association Orion OB1: though the main source of illumination is Rigel, the heads of the cometary clouds point towards the north-east, to the centre of the association. This morphology suggests the scenario in which the HI clouds have been compressed from the direction of Orion OB1. The association, however, is some 150 pc more distant than IC 2118. Therefore the interaction of these objects is probably mediated by the high pressure of the bubble surrounding the association.

Objective prism search for Hα emission stars in the region of IC 2118 suggested that low-mass stars might have been born in these high-latitude molecular clouds (Kun et al., 2001). In this paper we present the results of spectroscopic observations that confirm the presence of pre-main sequence stars in the molecular clouds associated with IC 2118.

2. Observations

We observed the spectra of stars selected as possible Hα emission objects in objective prism Schmidt plates in January 2001 with ALFOSC (*Andalucia Faint Object Spectrograph*) on the Nordic Optical Telescope in La Palma. Using grism 8 with a 1 arcsec slit provided a spectral resolution $\lambda/\Delta\lambda \approx 2200$ in the wavelength interval 5800–8300 Å. This spectral region contains both the Hα and the LiI λ6708 lines, crucial for identification of T Tauri type stars, as well as several absorption features suitable for spectral classification (Kirkpatrick et al.,

1991). Spectra of helium and neon lamps were observed before and after each stellar observation for wavelength calibration. For spectral classification purposes we observed a series of spectroscopic standards. We reduced the spectra using the standard IRAF routines. Spectral and luminosity classes were determined using the criteria established by Kirkpatrick et al. (1991) and Martín & Kun (1996).

3. Results

We found five stars closely confined to the clouds which have shown several characteristics of pre-main sequence nature, as well as two stars having weak Hα emission ($EW(H\alpha)$ <5 Å) but no Li I absorption. Figure 1 displays the distribution of the pre-main sequence stars identified during the spectroscopic survey with respect to the molecular clouds, and Fig. 2 shows their spectra, normalized to the continuum. Several emission lines attributed to circumstellar matter can be observed in the spectra, such as the [O I] lines at 6300 and 6360 Å, [N I] at 6583 Å, [S II] at 6717 and 6731 Å, as well as the emission lines of neutral helium at 5875 Å and 6678 Å.

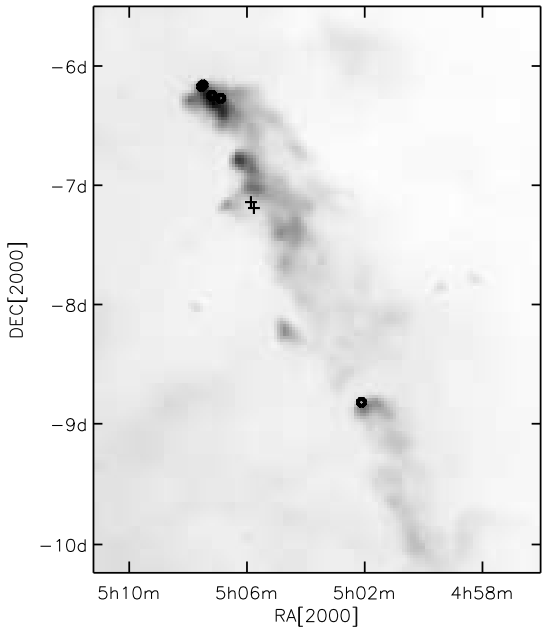

Figure 1: Location of classical T Tauri stars (circles) and weak-line Hα emission stars (crosses) with respect the molecular clouds indicated by the distribution of 100 μm emission observed by IRAS in the region of IC 2118.

Table 1: T Tauri stars in IC 2118

2MASS	Sp.T.	J	$J-H$	$H-K$	$W(\mathrm{H}\alpha)$	$W(\mathrm{LiI})$
0502063−085046	M2IV	10.987	0.782	0.441	−60.72	0.28
0506030−071547	M4V	11.535	0.538	0.285	−4.11	0.03
0506091−071239	M3V	10.888	0.557	0.246	−0.97	0.00
0506535−061712	K7IV	11.182	1.255	0.754	−112.35	0.53
0507115−061509	M0V	13.009	1.730	1.225	−293.20	1.19
0507301−061015	K5IV	10.839	1.254	0.963	−79.35	0.37
0507306−061059	K7IV	10.127	1.081	0.743	−13.47	0.41

J, H, and K magnitudes of the pre-main sequence stars were obtained from the 2MASS Second Incremental Survey Catalog (IPAC, 2000). We used these data to place the stars on the Hertzsprung–Russell diagram. Table 1 shows the 2MASS identifications, spectral types, J, H, and K magnitudes, Hα and LiI equivalent widths of the new pre-main sequence objects. Figure 3 displays their positions on the $(H-K)$ vs. $(J-H)$ color-color diagram together with the lines indicating the position of zero-age main-sequence, the giant branch, direction of the interstellar reddening and the locus of classical T Tauri stars determined by Meyer et al. (1997).

In order to place the stars on the HRD their effective temperatures and bolometric luminosities are to be determined. T_{eff} comes from the spectral type, according to *e.g.* Kenyon & Hartmann (1994), whereas L_{bol} can be determined from the near-infrared photometric data. For this purpose we make the widely used assumption that the total emission of our target stars in the J band originates from the photosphere (e.g. Hartigan et al., 1994). Thus the color index $J-H$ can be written as

$$J-H=(J-H)_0+E_{\mathrm{CS}}(J-H)+E_{\mathrm{IS}}(J-H),$$

where $(J-H)_0$ is the true photospheric color of the star, $E_{\mathrm{CS}}(J-H)$ is the color excess due to the emission from the circumstellar disk in the H band, and $E_{\mathrm{IS}}(J-H)$ is the color excess originating from the interstellar extinction in the H band.

The locus of unreddened T Tauri stars in the $H-K$ vs. $J-H$ color-color diagram (Meyer et al., 1997) allows us to determine $E_{\mathrm{IS}}(J-H)$, the interstellar

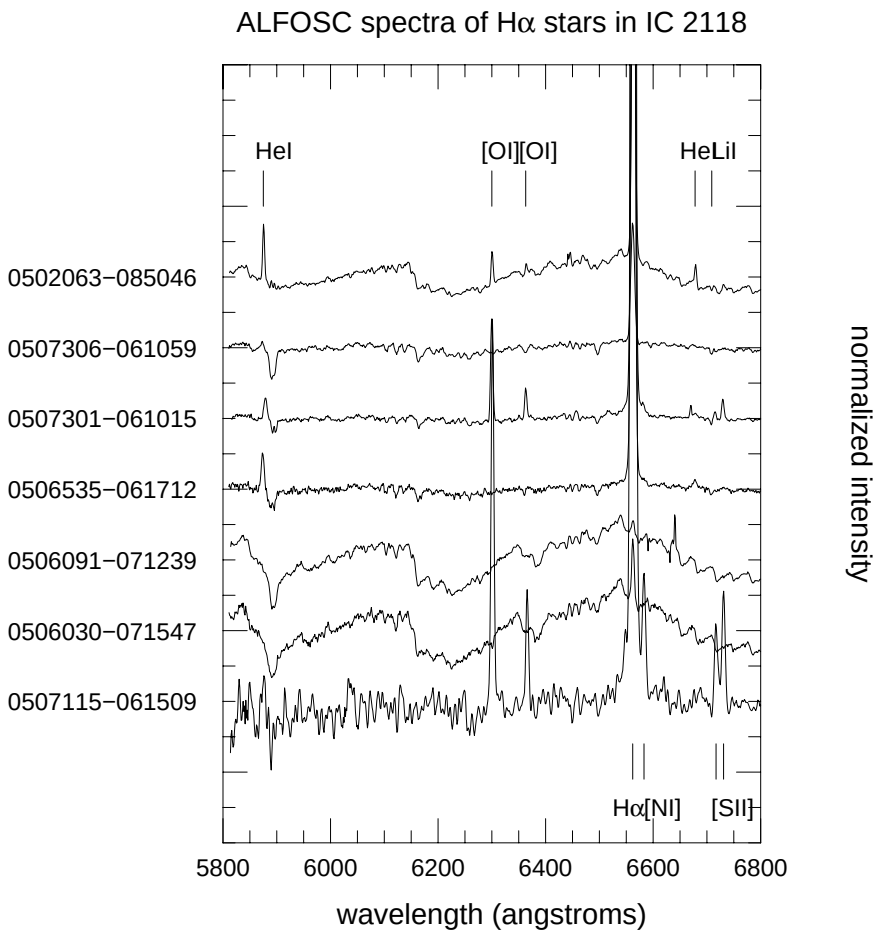

Figure 2: Spectra of the new pre-main sequence stars in IC 2118 in the wavelength region 5800–6800 Å.

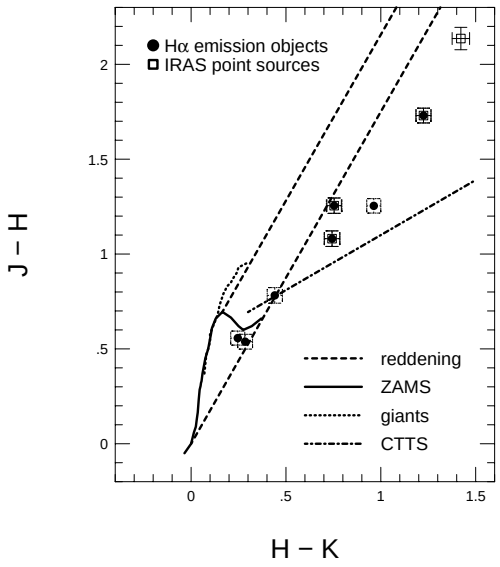

Figure 3: Positions of the T Tauri stars in IC 2118 in the $J-H$ vs. $H-K$ diagram. Loci of zero-age main sequence, giant branch, and classical T Tauri stars, as well as the slope of interstellar reddening are indicated.

component of the $E(J-H)$ color excess. The bolometric luminosities of the stars were derived by using the interstellar extinction law $A_{\rm J} = 2.65 \times E_{\rm IS}(J-H)$, given by Rieke & Lebofsky (1985) and the bolometric corrections tabulated by Hartigan et al. (1994).

The positions of our target stars in the HRD are shown in Fig. 4 together with evolutionary tracks and isochrones given by D'Antona & Mazzitelli (1994) (model 1). It can be seen that the masses of these stars are in the 0.3–0.8 $M_\odot$ interval, and they are grouped along the isochrone corresponding to a mean age of 10^6 years, comparable to the age of the youngest subgroup of Orion OB1.

4. Conclusions

We found five classical T Tauri stars in the molecular clouds associated with IC 2118. We estimated their masses and ages, and found them to be nearly coeval, at a mean age of 10^6 yrs. Our results suggest that the T Tauri stars associated with IC 2118 are significantly younger and less massive than most of the weak-line T Tauri stars discovered by ROSAT (Alcalá et al., 1998) in the Orion–Eridanus region. Both the small, high-latitude clouds and the low-mass stars in them have most probably been produced by the interaction of the Orion–Eridanus Bubble with diffuse HI clouds.

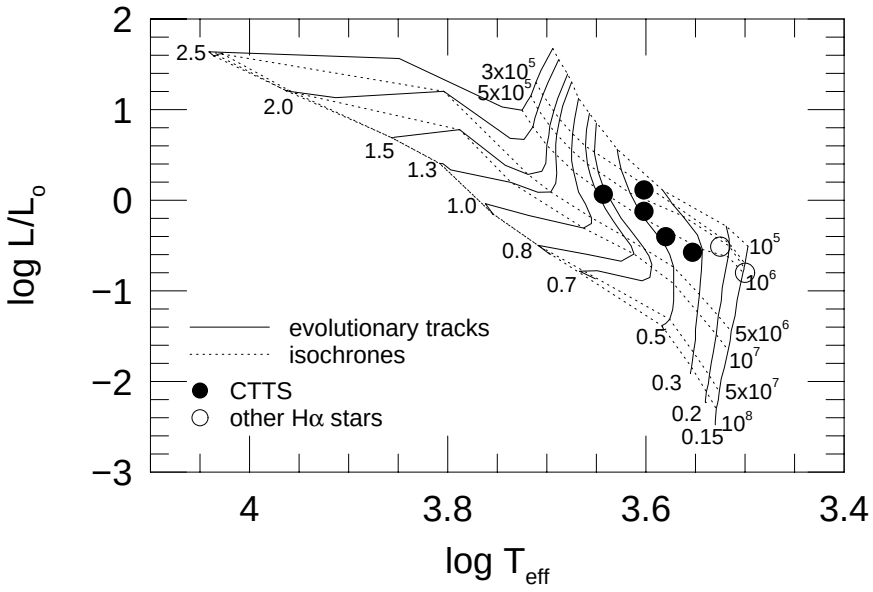

Figure 4: The T Tauri stars of IC 2118 in the HRD. Solid lines indicate the isochrones and dashed lines show the evolutionary tracks from D'Antona & Mazzitelli's (1994) model 1.

Acknowledgements

This work is based on observations with Nordic Optical Telescope operated on the island of La Palma jointly by Denmark, Finland, Iceland, Norway, and Sweden, in the Spanish Observatorio del Roque de los Muchachos of the Instituto de Astrofisica de Canarias. The data presented here have been taken using ALFOSC, which is owned by the Instituto de Astrofisica de Andalucia (IAA) and operated at the Nordic Optical Telescope under agreement between IAA and the NBIfAFG of the Astronomical Observatory of Copenhagen. This research has been supported by the Hungarian grants OTKA T022946 and T034584, and also partly funded by the Ministery of Science and Technology of Serbia grant P1191.

References

Alcalá, J.M., Chavarria-K. C., Terranagra, L., 1998, A&A 330, 1017
Brown, A.G.A., Hartmann, D., Burton, W., 1995, A&A 300, 903
Cardelli, J., Clayton, G.C., Mathis, J., 1989, ApJ 345, 245
Cowie, L.L., 1982, Symposium on the Orion Nebula to Honor Henry Draper, eds. A.E. Glassgold, P.J. Huggins, E.L. Schucking, Ann. NY Acad. Sci. 395, p.17
D'Antona F. & Mazzitelli I. 1994, ApJS 90, 467
Hartigan P., Strom K.M., Strom S.E., 1994, ApJ 427, 961
Hartmann, D., Burton, W.B., 1997, Atlas of Galactic Neutral Hydrogen, Cambridge Univ. Press
Kenyon, S.J., Hartmann, L., 1994, ApJS 101, 117
IPAC 2000, The 2MASS Second Incremental Catalog, URL:"http://www.ipac.caltech.edu
Kirkpatrick, J.D., Henry, T.J., McCarthy, D.W., 1991, ApJS 77, 417
Kun, M., Aoyama, H., Yoshikawa, N., Kawamura, A., Onishi, T., Yonekura, Y., Fukui, Y., 2001, PASJ 53, 1063
Martín, E.L., Kun, M., 1996, A&AS 116, 467
Meyer, M.R., Calvet, N., Hillenbrand, L.A. 1997, AJ 114, 288
Rieke, G.H., Lebofsky, M.J., 1985, ApJ 288, 618
Yonekura, Y., Hayakawa, T., Mizuno, N., Mine, Y., Mizuno, A., Ogawa, H., Fukui, Y., 1999, PASJ 51, 837

Study of Pre-Main Sequence Stars Born in LDN 1251

M. Eredics[1], **M. Kun**[2]

[1] Eötvös Loránd University
H-1518 Budapest, P.O.Box 32., Hungary
[2] Konkoly Observatory of the Hungarian Academy of Sciences
H-1525 Budapest, P.O.Box 67.
E-mail: eredicsm@astro.elte.hu, kun@konkoly.hu

Abstract

We observed the spectra of Hα emission stars in the molecular cloud L1251 using the CAFOS spectrograph on the 2.2 m telescope of Calar Alto Observatory. We found 7 pre-main sequence stars born in the cloud and determined their spectral and luminosity classes. These spectroscopic data, supplemented with near-infrared (JHK) magnitudes allowed us to place these stars in the HR diagram. This paper discusses the evolutionary status of star formation in LDN 1251.

1. Introduction

Observational studies of dark clouds aimed at finding low mass star formation and the evolutionary status of young stellar objects have a long history. Observations of Lynds 1251, a part of the Cepheus Flare, located at 300±30 pc Kun (1998) from the Sun have shown this region to be forming low-mass stars at high efficiency. Several Hα emission stars, probable pre-main sequence stars born in LDN 1251, have been found here (Grasdalen et al. 1973; Kun & Prusti 1993). In this paper, we present the spectral and luminosity classes for 8 pre-main sequence candidates. The placement of the stars on the Hertzsprung–Russell diagram allows a conservative estimate of the age of LDN 1251 as well.

2. Results

We studied the spectra of 8 Hα emission star candidates in the molecular cloud LDN 1251 and determined their spectral types. Spectral types can be estimated using the strength of molecular bands and presence of atomic lines. The observed stars are late-K and M type objects, therefore we set them against G, K, M standards observed with the same resolution, and Pickles' (1998) spectral flux

library data. Spectral types were estimated using the depths of several molecular bands at λ7000–7200 Å (Kirkpatrick et al.1991) and the Na I at λ5890 Å and λ5896 Å.

Hα emission and Li I absorption are the most important indicators of youth of solar type stars. We measured the equivalent width of Hα and Li I λ6707 Å. We found that all but one our programme stars show Hα and Hβ emission, and the emission lines show inverse P Cygni profile except in Hα 1. We found neither Hα emission nor Li absorption in the spectrum of Hα 41. This star is probably a foreground object not related to the cloud, therefore we omitted it from further studies. Li I absorption was neither detected in the spectrum of Hα 2 due to the low S/N. We also identified the forbidden lines [OI] $\lambda\lambda$ 6300Å 6364Å in the spectra of Hα 1, Hα 44 and Hα 45, and [SII] at $\lambda\lambda$ 6717Å 6731Å in Hα 1. He I emission is also present in most spectra. Fig. 1 shows the observed spectra in the wavelength region 5800–7800 Å. The $J-H$ vs. $H-K$ two-colour diagram is presented in Fig. 2.

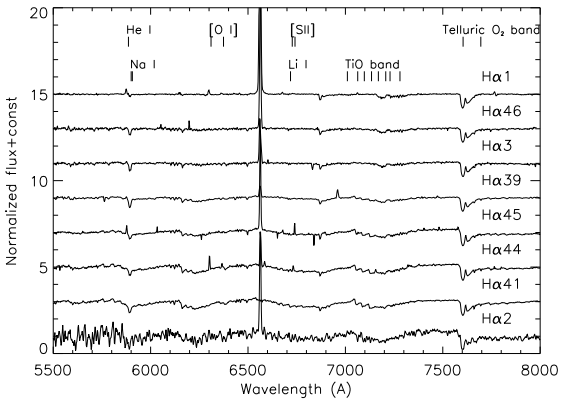

Figure 1: Spectra of the PMS stars in L 1251 in the wavelength region 5800–7800 Å.

In order to place the stars in the HRD we estimated their effective temperatures and bolometric luminosities. Effective temperatures can be obtained directly from the spectral types of the stars Hartigan et al. (1994). The J, H and K magnitudes of the stars were used to determine the bolometric luminosities with the assumption that the whole flux at 1.25μm (J band) comes from the stellar photosphere. Then $J - M_{\rm J} = 5 \log r - 5 + A_{\rm J}$ and $M_{\rm bol} = M_{\rm J} + BC_{\rm J}$ were used, where $r = 300 \pm 30$ pc is the distance of LDN 1251 Kun (1998), $A_{\rm J} = 2.635 E_{\rm J-H}$ is the interstellar absorption in the J band Rieke & Lebofsky (1985), and $BC_{\rm J}$ is the bolometric correction (Hartigan et al. 1994). The results

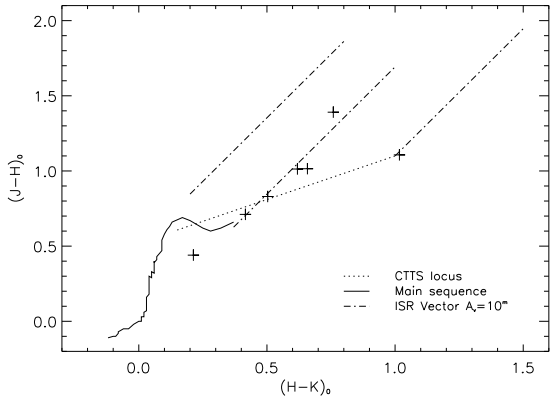

Figure 2: Positions of the T Tauri stars in L 1251 in the $J-H$ vs. $H-K$ diagram. Loci of zero-age main sequence and classical T Tauri stars, as well as the slope of interstellar reddening are indicated.

Table 1: Results of spectroscopy and photometry

Hα	Sp	EW[Å]		J–H	H–K	$\log T_{eff}$	$\log(L/L_\odot)$	M	age
star	±1	[Hα]	[Li I]					[$M_\odot$]	[Myr]
1	K5	-96.07	0.24	1.391	0.759	3.643	0.668	0.6	0.2
2	M2$\leq$	-42.18	–	1.013	0.619	$\leq$3.580	≤ -0.205	$\leq$0.4	0.7
39	M0	-5.90	0.35	1.015	0.658	3.580	-0.325	0.4	1
3	K7	-24.35	0.41	–	–	–	–		
41	M2	–	–	0.440	0.213	–	–	–	–
44	M1.5	-12.12	0.30	0.711	0.416	3.553	-0.687	0.4	2
45	M1	-37.22	0.26	0.830	0.503	3.562	-0.445	0.4	1
46	K5	-60.22	0.35	1.107	1.017	3.643	-0.077	0.8	2

of spectroscopy and photometry are shown in Table 1, and the positions of the programme stars in the HRD are displayed in Fig. 3.

3. Conclusions

We examined basic spectroscopic properties and near-infrared data of 8 pre-main sequence star candidates in the cloud LDN 1251. We confirmed the pre-main sequence nature of 7 of them. All the seven pre-main sequence stars are low mass (0.3-0.8 $M_\odot$) objects, and their spectra show classical T Tauri features. The Li absorption in the spectra and their positions in the HRD indicate that they are young objects, having ages of 1–2 million years. By the estimated age of Hα 46 we think that the cloud is at least 2×10^6 yr old. The inverse P Cygni profile in the Hα emission (except Hα 1) suggests that gathering of mass from

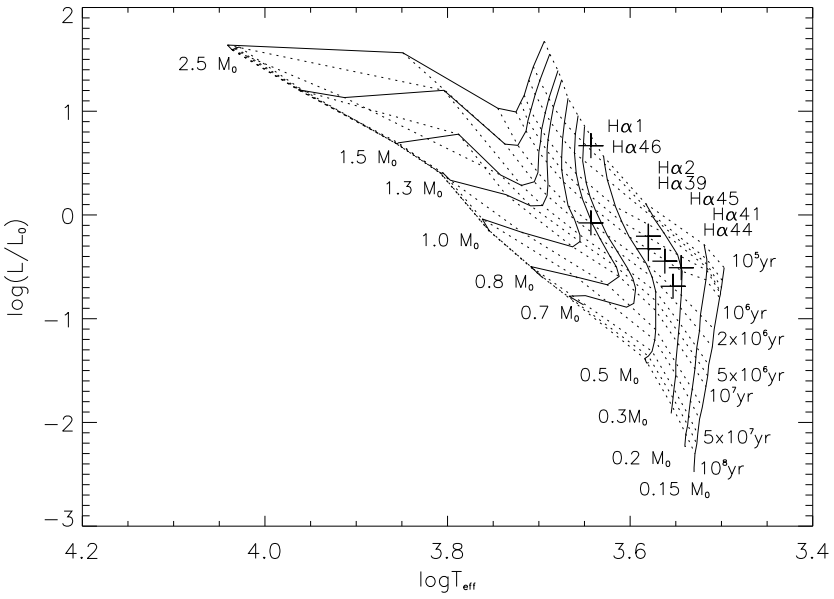

Figure 3: The T Tauri stars of L 1251 (crosses) in the HRD. Dotted lines indicate the isochrones and solid lines show the evolutionary tracks from D'Antona & Mazzitelli's (1994) model 1.

the accretion disks has not been finished in the Hα stars yet.

Acknowledgements

This research is based on spectroscopic observations obtained in the German-Spanish Astronomical Centre, Calar Alto, operated by the Max-Planck-Institute for Astronomy, Heidelberg, jointly with the Spanish National Commission for Astronomy, as well as on near-infrared observations taken at TIRGO (Gornergrat, Switzerland). TIRGO is operated by CAISMI-CNR Arcetri, Firenze, Italy. We acknowledge support by the OTKA grant T034584.

References

D'Antona, F., Mazzitelli, I., 1994, ApJS 90, 467
Grasdalen, G.L., Kuhi, L.V., Harlan, E.A., 1973, PASP 85, 193
Hartigan, P., Strom, K.M., Strom, S.E., 1994, ApJ 427, 961
Kirkpatrick, J.D., Henry, T.J., McCarthy, Jr., D.W., 1991, ApJS 77, 417
Kun., M., 1998, ApJS 115, 59
Martín, E.L., Kun., M., 1996, A&AS 116, 467
Kun., M., Prusti, T., 1993, A&A 272, 235
Meyer, M.R., Calvet, N., 1997, AJ 114, 288
Pickles, A.J. 1998, PASP 110, 863
Rieke, G.H., Lebofsky, M.J., 1985, ApJ 288, 618

Near-Infrared Study of Large Bok Globules

T. Khanzadyan

Armagh Observatory
College Hill, Armagh BT61 9DG, Northern Ireland, UK
E-mail: tig@star.arm.ac.uk

Abstract

We present results from a near-infrared study of CB 3, CB 34, CB 39 and CB 54 as a part of an ongoing project, which is set to determine how Bok globules form, evolve and disperse.

Our observations have revealed the presence of active star formation in CB 3, CB 34 and CB 54, by the discovery of new knots in the H_2 1-0 S(1) emission line images.

We have discovered no indication of star formation in the Bok globule CB 39 which may suggest that this globule is in an early stage of evolution. Meanwhile the globules CB 3, CB 34 and CB 54 are obviously in their later stages of evolution.

Keywords: *infrared: ISM – stars: formation – ISM: jets and outflows – ISM: clouds*

1. Bok Globules

Bok globules are dark patches on the sky against the background of stars, which have small angular extent and were stated as possible sites of star formation (Bok & Reilly, 1947). This statement has been confirmed recently by the work of Yun & Clemens (1990), who actually found manifestations of active star-formation in some globules.

The Catalouge of Northern Bok Globules has been published by Clemens & Barvainis (1988, hereafter CB88). The average catalogue members are small ($\approx$0.7 pc in diameter), with average masses of $\approx 10\,M_\odot$ and nearby ($d \leq 600$ pc; Bok, 1977; Leung, 1985; Launhardt & Henning, 1997). But CB88 contains some objects (e.g. CB 3, CB 34, CB 39, CB 54, CB 205) which are situated beyond 1 kpc and therefore are bigger in size ($\approx$2 pc) and larger in mass up to $120\,M_\odot$ in the case of CB 205 (Launhardt & Henning, 1997; Huard et al., 2000).

The importance of Bok globules is that they are sites of low-mass star formation (see Yun & Clemens, 1990; Khanzadyan et al., 2002). This is very important, because if there are some 10^5 globules in our Galaxy (Clemens et al., 1991), and we assume an average lifetime of 10^6 yrs and mass of $10\,M_\odot$ for them

(Launhardt & Henning, 1997), then a total mass of $10^{10}\,M_{\odot}$ could be processed through them during the lifetime of the Galaxy. This leads us to the conclusion that many field stars including our Sun, as well as T-Tauri stars may find their origin in Bok globules (Yun et al., 1997; Launhardt & Henning, 1997).

LBG vs. SBG: Large Bok Globules (LBGs) are sites for multiple and high-mass star formation, which tends to be a continuous process rather than a relatively instantaneous event like star formation in Small Bok Globules (SBGs) (Knee & Sandell, 2000; Motte et al., 1998). In LBGs powerful outflows, ejected from protostars interact with the globule material and are detectable even at the outskirts. In contrast to SBGs, which are nearby, outflows are not detected due to low column density and big outflow extent. So by detecting outflows from LBGs we are able to trace them back to the globule and associate with protostars (Khanzadyan et al., 2002).

2. Observations and Data Reduction

Observations of Bok globules were carried out during the nights of 7-10 December, 2000 using the Omega Prime (Bizenberger et al., 1998) infrared camera installed on the Calar Alto 3.5m telescope, Almeria, Spain. Omega Prime is equipped with a Rockwell 1024 × 1024 pixel HAWAII array detector. It provides a pixel scale of 0.4 arcsec/pixel and a total field of view of 6.8 × 6.8 arcmin^2 on the sky. Table 1 summarizes the observations.

Table 1: Log of the observations.

Object Name	R.A. (2000)	Decl. (2000)	Observed in Filters	seeing (arcsec.)
CB 3	$00^h28^m46^s$	$+56°42'06''$	K_s, H_2	1.5, 1.4
CB 34	$05^h47^m02^s$	$+21°00'10''$	J, H, K_s, H_2	1.5, 1.4, 1.2, 1.8
CB 39	$06^h02^m00^s$	$+16°31'00''$	K_s, H_2	1.7, 1.4
CB 54	$07^h04^m21^s$	$-16°23'18''$	J, H, K_s, H_2	1.5, 1.7, 1.6, 1.9

The data reduction and mosaicing proceeded through standard routines using several IRAF packages. In the later stage several packages from STARLINK software, such as CCDPACK and KAPPA, has been used for comparison of results and for correcting the array defects (Khanzadyan et al., 2002).

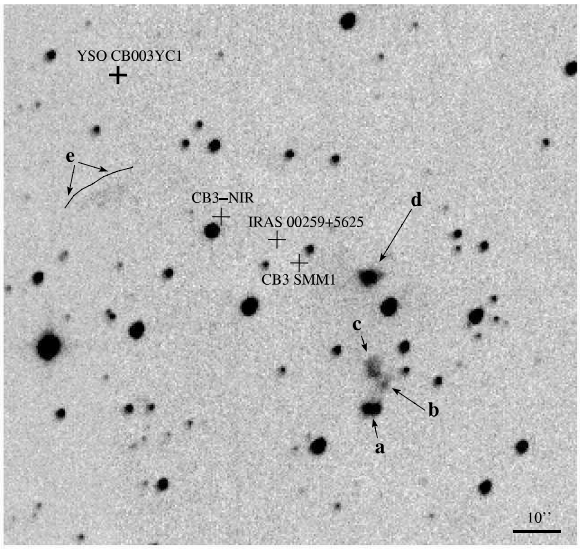

Figure 1: The central part of globule CB 3 in H_2 + cont. Newly found objects are labeled by letters **a** to **e**. The relative positions of several known sources are indicated on the image. The total integration time of this frame is 1120 seconds.

3. Results and Discussion

We found new H_2 excited objects in CB 3 marked by letters **a** to **e** in Fig. 1. The globule is excluded from the Bok globule study by Launhardt & Henning (1997) due to its large distance and mass, although it has a mass of $\approx$110 $M_\odot$, whereas CB 34 and CB 205, which are included, have masses of $\approx$80 $M_\odot$ and $\approx$120 $M_\odot$ (Huard et al., 2000).

CB 34 displays extremely well aligned chains of knots extending from sub-millimetre cores till the outskirts of the cloud, where they disappear without any trace of terminating bow shocks, due to lower density there (see Fig. 2).

CB 39 has several VLA sources in it and does not show any outflow activity (see Fig. 3), which may suggest relatively early stage of evolution.

The new near-infrared knots in CB 54 prove the active nature of cloud and indicate the advanced stage of its evolution (see Fig. 4).

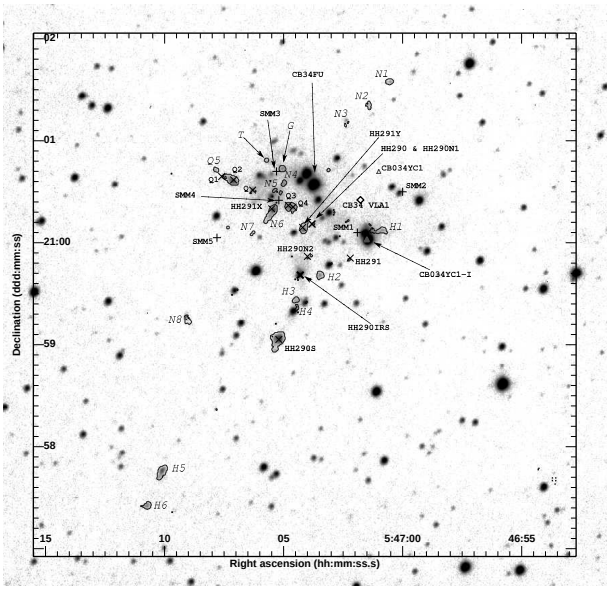

Figure 2: The central part of CB 34 in H_2. Total integration time of this frame is 3800sec. Crosses are SMM objects from Huard et al. (2000) and the asterixs are HH objects and H_2 knots discovered by Moreira & Yun (1995). CB34 VLA1 is marked by a diamond (Yun et al., 1996). The YSOs CB034YC1 and CB034YC1-I (triangles) are from Yun & Clemens (1994). Our discovered objects are indicated as chains of letters H and N as well as G and T. A further Q knot has been found – Q5.

4. Summary

CB 3, CB 34 and CB 54 are in advanced stage of evolution. We have discovered outflows from all of them by detecting their interaction with their environment.

We discovered no indication of active star formation in CB 39, which may suggest that the globule is in an early stage of evolution.

We suggest to classify CB 3 as a typical member of LBGs and therefore to connect it to the main evolutionary scenario of Large Bok Globules, if it exists.

Is there any sequence of LBGs and SBGs? Possibly LBGs are separate group of objects and should be treated apart from SBGs.

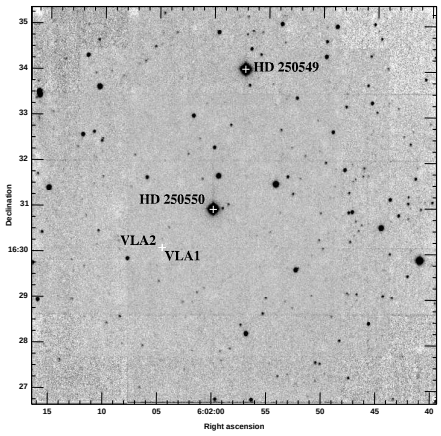

Figure 3: CB 39 in H_2 with total integration time of 1120 seconds.

Acknowledgements

Research at Armagh Observatory is grant-aided by the Department of Culture, Arts and Leisure for Northern Ireland.

References

Bizenberger, P., McCaughrean, M.J., Birk, C., Thompson, D., Storz C., 1998, SPIE 3354, 825
Bok, B.J., Reilly, E.F., 1947, ApJ 105, 255
Bok, B.J., 1977, PASP 89, 597
Clemens, D.P., Barvainis, R.E., 1988, ApJS 68, 257
Clemens, D.P., Yun, J.L., Heyer, M.H., 1991, ApJS 75, 877
Huard, T.L., Weintraub, D.A., Sandell, G., 2000, A&A, 362, 635
Khanzadyan, T., Smith, M.D., Gredel, R., Stanke, T., Davis, C.J., 2002, A&A 383, 502
Knee, L.B.G., Sandell, G., 2000, A&A 361, 671
Launhardt, R., Henning, Th., 1997, A&A 326, 329
Leung, C.M., 1985, Protostars and Planets II, eds. Black, D.C. & Matthews, M.S., Univ. of Arizona Press, Tucson, p.104
Moreira, M.C., Yun, J.L., 1995, ApJ 454, 850
Motte, F., Andre, P., Neri, R., 1998, A&A 336, 150

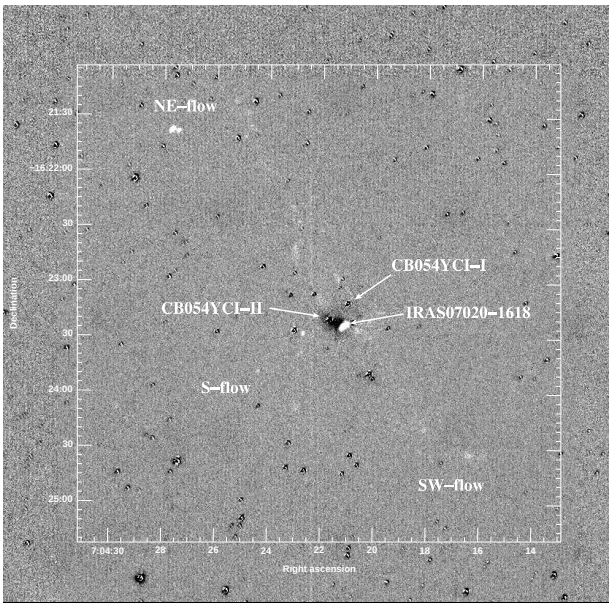

Figure 4: CB 54 in H_2-Continuum. Total integration in H_2 is 2700 seconds.

Yun, J.L., Clemens, D.P., 1990, ApJ 365, L73
Yun, J.L., Clemens, D.P., 1994, ApJS 92, 145
Yun, J.L., Moreira, M.C., Torrelles, J.M., Afonso, J.M., Santos, N.C., 1996, AJ 111, 841
Yun, J.L., Moreira, M.C., Alves, J.F., Storm, J., 1997, A&A 320, 167

Cold Dust in Luminous Star-Forming Regions

O. Krause, R. Vavrek, U. Klaas, L.V. Tóth, D. Lemke, M. Stickel

Max-Planck-Institut für Astronomie
Königstuhl 17, D-69117 Heidelberg, Germany
E-mail: okrause@mpia.de

Abstract

Using the 170 μm ISOPHOT Serendipity Survey (ISOSS) we are searching for high-mass star forming regions. Our sample consists of cold and luminous ISOSS sources coinciding with embedded young stellar objects detected by the MSX, 2MASS and IRAS infrared surveys. The large amount and low temperature of gas and dust, which has not been dispersed, indicates a recent beginning of the ongoing star formation. (Sub)millimeter and infrared follow-up observations confirmed the early evolutionary stage in two candidate regions.

Keywords: *stars: formation – ISM: clouds, dust – instrument: ISO, ISOPHOT*

1. Searching for the earliest stages of high-mass star formation

Massive stars form in clusters and the initial conditions for their birth are expected to be found in dense ($N(H_2) \sim 10^6$ cm^{-3}), cold (T $\sim$ 15 K) and massive (M $\sim$ 5000 $M_\odot$) molecular cloud cores (Evans et al. 2002). Due to the short evolutionary time scales of high-mass star formation such objects are rare. Since the spectral energy distributions of these cloud cores are expected to peak beyond 100 μm, far-infrared and (sub)millimeter continuum surveys are well suited for their identification.

The 170 μm ISOPHOT (Lemke et al. 1996) Serendipity Survey (ISOSS, Bogun et al. 1996) is the largest high spatial resolution survey performed in the far-infrared beyond the IRAS 100 μm band. In order to discover very young star forming regions and their parental clouds, we selected luminous and compact sources with a flux ratio $S_{170\mu m}/S_{100\mu m} > 2$ from the ISOSS data base. These criteria imply a high mass and low temperature of the cold ISM in the objects. Since the clustered mode of massive star formation commonly involves young stellar objects of different evolutionary stages, we require the presence of embedded compact sources with a thermal infrared excess as indicated by the 2MASS and MSX infrared surveys. The latter criterion avoids the confusion

with cold interstellar cirrus, which becomes severe at 170 μm. About 200 sources have been identified using our method and we present here results from follow-up observations of two objects.

2. Multi-wavelength follow-up observations of cold ISOSS sources

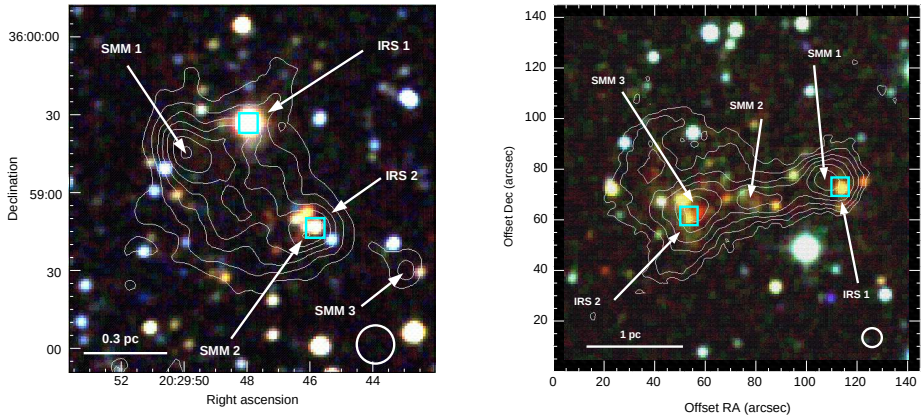

Fig 1: 850 μm and 450 μm continuum maps of the two ISOSS sources 20298+3559 (left) and 04225 (right), overlaid onto a JHK near-infrared composite from 2MASS. While the 1.5 arcmin ISOPHOT beam provided an integral flux measurement, our SCUBA observation resolve compact dust condensations (SMM1, SMM2 and SMM3) surrounded by extended envelopes. Young stellar objects detected by the MSX-satellite are marked (IRS1 and IRS2). The ellipse indicates the position of a very cold (T_{dust} = 11 K) cloud core in ISOSS20298+3559.

Ground-based 450 μm, 850 μm and 1.2mm continuum observations with high spatial resolution have been obtained with the SCUBA bolometer array at the JCMT on Mauna Kea, Hawaii, and MAMBO at the IRAM 30m telescope on Pico Veleta, Spain (Fig. 1). The IRAS and ISOPHOT data near the peak of thermal dust emission in combination with the proper sampling of the Rayleigh-Jeans part from the SCUBA/MAMBO observations allow a precise color temperature determination of the involved dust components (Fig. 2). In order to compare the physical conditions derived from our dust continuum, ammonia molecular line measurements reflecting the gas phase ISM have been performed at the 100m telescope in Effelsberg. For the characterization of the photosphere

and circumstellar environment of the embedded young stellar objects, we have performed spectroscopy with the TWIN spectrograph at the 3.5m telescope on Calar Alto in combination with diffraction-limited mid-infrared imaging using MAX at UKIRT on Mauna Kea. Fig. 3 presents our dereddened energy distribution for the source ISOSS20298+3559-IRS1.

3. ISOSS20298+3559 – A young star forming region

Our follow-up observations confirmed the presence of cold and massive molecular cloud cores. The peak column densities, average dust temperatures and total masses of the central regions of the two sources presented in Fig. 1 are $n(H_2) = 2 \cdot 10^{22} cm^{-2}, T_{dust} = 16K$ and $M = 120 M_\odot$ for ISOSS20298+3559 and $n(H_2) = 3 \cdot 10^{23} cm^{-2}, T_{dust} = 17K$ and $M = 4700 M_\odot$ for ISOSS04186. ISOSS20298+3559 is associated with an optical dark cloud complex in the Cygnus X giant molecular cloud (Krause et al. 2002). Several very young embedded objects have been detected, the most luminous one is the Herbig B2e star IRS1 ($M_\star = 6.5 M_\odot$) with a luminosity of 2200 $L_\odot$ and an age of less than 40000 years as derived from evolutionary tracks. SMM1 and SMM3 are two candidate Class 0 objects of intermediate mass. The externally heated cloud core with a mass of 50 $M_\odot$ is gravitationally bound and a good candidate for a massive pre-protostellar core. A star formation efficiency of 14 % was determined for the region.

4. Outlook

Follow-up observations showed evidence for the low age of star forming regions with red FIR colors ($S_{170\mu m}/S_{100\mu m} > 2$) detected by the ISOPHOT Serendipity Survey. All objects so far have been selected to contain near- and mid-infrared sources being signposts for ongoing clustered star formation. We plan to extend our sample of cold ISOSS sources without evidence for stellar counterparts but only coinciding with molecular clumps detected by carbon-monoxide ^{12}CO, ^{13}CO and CS line surveys. These objects are expected to be further candidates for studies of the earliest stages of massive star formation.

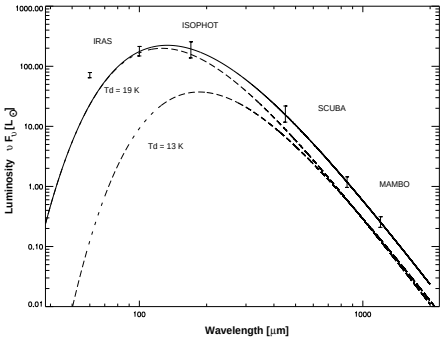

Fig. 2: Spectral energy distribution of ISOSS20298+3559. The total flux density is well described by optically thin thermal radiation of two single temperature modified blackbodies ($\epsilon \propto \lambda^{-2}$) corresponding to the cold cloud core and the warmer envelope with dust temperatures of $T_{dust} = 13 \pm 2K$ and $T_{dust} = 19 \pm 2K$ respectively.

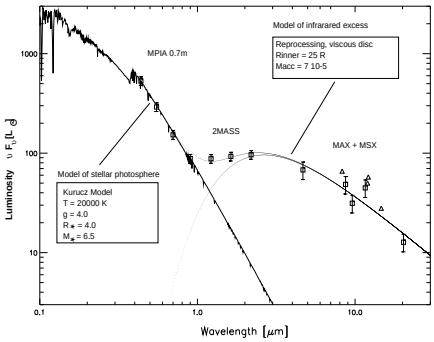

Fig. 3: Dereddened spectral energy distribution of the Herbig B2 star ISOSS20298+3559-IRS1. Our model of the system consists of the stellar photosphere (Kurucz model with $T_{eff} = 20000$ K, log g = 4) and an optically thick, viscous accretion disc, in agreement with the observations obtained with the MPIA 0.7m telescope and MAX at UKIRT.

Acknowledgements

The ISOPHOT Data Centre at MPIA is supported by Deutsches Zentrum für Luft- und Raumfahrt e.V. (DLR) with funds of Bundesministerium für Bildung und Forschung, grant No. 50QI0201. OK thanks the Wernher von Braun-Stiftung zur Förderung der Weltraumwissenschaften e.V. for financial support.

References

Bogun, S., Lemke, D., Klaas, U., et al., 1996, A&A 315, L71

Evans, N.J. II, Shirley, Y.L., et al., 2002, Proc. "Hot Star Workshop III: The earliest phases of massive star birth", ed. P.A. Crowther, ASP Conference Series, in press

Krause, O., Lemke, D., Vavrek, R., et al., 2002, Proc. "Galactic star formation across the stellar mass spectrum", ed. J. De Buizer & van der Bliek, ASP Conference Series, Vol. 287, p.174

Lemke, D., Klaas, U., Abolins, J., et al., 1996, A&A 315, L64

Cold Clouds in Cepheus Flare - Methods and Preliminary Results

Z. Kiss[1], L.V. Tóth[1,2]

[1]Astronomy Department, Eötvös Loránd University
H-1518 Budapest, P.O.Box 32., Hungary
[2]Max-Planck-Institut für Astronomie
Königstuhl 17, D-69117, Heidelberg, Germany
E-mail: Z.Kiss@astro.elte.hu, L.V.Toth@astro.elte.hu

Abstract

We study the physical parameters of the interstellar medium in the Cepheus Flare Region. We investigated the large scale dust temperature and density distribution based on COBE DIRBE, IRAS and ISOSS data. We give optical B band extinction maps of 26 subregions covering ≈ 25 square degrees. We found several opaque spots on the extinction maps, examined their optical, infrared and radio properties. We selected the suspected pre-protostellar clouds in order to perform further detailed studies in the near future. Many of dense clouds we found have very low DIRBE temperature ($T < 15\,K$) and former ^{13}CO and NH_3 detection. The majority of the objects seem to be starless, one third of them show ongoing star formation.

1. Introduction

We intend to gather and analyse multiwavelength data on nearby low mass star forming regions focusing on the phases when no embedded stellar object is seen. Low mass star formation is expected in low and moderate mass (from ten to few hundred solar masses) clouds, in dense ($n(H_2) > 10^3\,cm^{-3}$) and cold ($T \approx 10\,K$) cores. These dense cold cloud cores are optically thick for the visible light and can be identified as obscuring spots on optical images in case of nearby ones. On the other hand they are optically thin for their own quasithermal emission, which has a spectral maximum in the far infrared between 100 and 200μm wavelength. This FIR radiation can efficiently cool the clouds and also helps us to reveal these clouds. In this paper we use the optical extinction and FIR emission data to explore the clouds of the Cepheus Flare.

2. Data processing

We used the Lynds Catalogue of Dark Nebulae (Lynds, 1962) to select the most interesting subregions of the Cepheus Flare, catalogued earlier as dense regions from optical data. The high resolution parts of our studies were made on these subregions. We computed the DIRBE FIR colour temperature and optical depth map of the whole region, defined opaque objects based on extinction maps of subregions and gave the DIRBE temperature at the position of object defined. The high resolution IRAS (HIRES) maps were made for all subregions. We examined the FIR properties of clouds and the relations between FIR and optical features.

2.1. Optical data

To draw extinction maps in the region we considered 26 selected subregions having dark optical clouds of LDN catalog. The fields of these subregions are 1x1 degree sized. Extinction maps were computed via performing star counts (Dickman, 1978) on a $3'$ grid up to 18 mag using the USNO A2.0 catalog data.

Reference counts for unobscured fields were obtained from the galaxy model by Wainscoat et al. (1992) using a FORTRAN programme written by L. Balázs. The actual value of extinction in magnitudes can be obtained according to the following formula:

$$A = \frac{1}{b} log \left(\frac{N_{ref}}{N} \right) \tag{1}$$

where N is the actual count, N_{ref} is the modelled reference count and b is the slope of the modelled $logN(m)$ function. We defined the clouds as ellipses surrounding the 2 mag contours. We estimated cloud masses by the formula given by Dickman:

$$M = (\alpha_c d)^2 (N_{\mathrm{H}_2}/A_V) \mu \sum_i A_V^i \tag{2}$$

where α is the size of a grid cell in radians, d is the distance to the cloud, (N_{H_2}/A_V) is the considered ratio of H_2 column density and the visual extinction, μ is the average mass of particles in the cloud and A_V is the actual visual extinction. Distance data were taken form Hilton & Lahulla (1995).

2.2. Infrared data

For infrared studies we used the data of COBE DIRBE at 60, 100, 140 and 240 μm, IRAS (HIRES) at 60 and 100 μm and ISOSS at 170 μm.

The COBE DIRBE maps having low (≈ 0.7 degree) resolution give the basis of IRAS data ($\approx 4'$ resolution) calibration at 60 and 100 μm as well as the dust temperature and optical depth determination at 100, 140 and 240 μm. The IRAS 60 and 100 μm data were used for further calibration to obtain the high resolution ($90''$) HIRES maps. The fields of high resolution maps are the same as the extinction map fields. The ISOSS data were calibrated by the DIRBE data interpolated to 170 μm. The interpolation, the temperature and the optical depth were computed assuming that the dust emission follows a modified Planck function with $\beta = 2$.

We computed 100 and 170 μm FIR colour excesses defined as $E_{100} = I_{100} - I_{60}/\theta_{60-100}$ and $E_{170} = I_{170} - I_{100}/\theta_{100-170}$ using the values of galactic cirrus $\theta_{60-100} = 0.21$ and $\theta_{100-170} = 0.28$. These quantities are related to the actual dust temperatures, which are typically in the 10–20 K range. High colour excess values are good tracers of cold matter mainly at the longer wavelengths. This way we obtained high resolution maps of temperature distribution of the subregions. We computed the the characteristic values of defined quantities for all of our dense objects.

2.3. Other data

We examined the presence of ^{13}CO clouds from the Nagoya survey (Yonekura et al., 1997), NH_3 detections (Benson & Myers, 1989), YSOs and Hα (Kun, 1998) emission stars within the boundaries of clouds defined above.

3. Results

Using the method described above we defined 61 dense objects in the region possessing extinction value greater than 2 mag. According to DIRBE data these objects are cooler than the 18 K cirrus emission; the coldest ones have temperatures below 15 K. The higher resolution FIR colour excess maps also show low temperatures for our objects. There are some warmer objects with known embedded heating sources, showing notably high extinction and molecular emission (e.g. LDN 1174, LDN 1251). We determined the mass of each cloud and found that they are in the range of ten to some hundred solar masses, which is expected for low mass star forming clouds. Two third (41) of the objects defined are apparently starless, half of them (21) are remarkably cold according to the colour excess maps. Some of them show molecular emission, these are the best candidates for early phase star forming clouds with no embedded point-like object.

4. Conclusions

We studied the multiwavelength features of dark clouds in the Cepheus Flare region. Our methods allowed us to distinguish between the clouds with ongoing star formation, staying at an early phase of prestellar collapse and non-star-forming cloudlets, considering optical and infrared data. We found a number of early phase star forming cloud candidates without any detectable embedded point-like object. However, there are areas in the region without any optically catalogued dense clouds, where the molecular emission in ^{13}CO or the high FIR excess suggest notably high density and low temperature. This inspires us to extend the study to the whole area of the region, in order to find a complete sample of these objects for detailed examination.

Acknowledgements

We would like to thank Lajos Balázs, Mária Kun and Péter Ábrahám for their useful help. This research has made use of USNOFS Image and Catalogue Archive operated by the United States Naval Observatory, Flagstaff Station (http://www.nofs.navy.mil/data/fchpix/). This work was funded by the OTKA, project no. T034998.

References

Benson, P.J., Myers, P.C., 1989, ApJS 71, 89
Dickman, R.L., 1978, AJ 83, 363
Hilton, J., Lahulla, J.F., 1995, A&AS 113, 325
Kun, M., 1998, ApJS 115, 59
Lynds, B.T., 1962, ApJS 7, 1
Wainscoat, R.J., Cohen, M., Volk, K., Walker, H.J., Schwartz, D.E., 1992, ApJS 83, 111
Yonekura, Y., Dobashi, K., Mizuno, A., Ogawa, H., Fukui, Y., 1997, ApJS 110, 21

Indication of Star Formation Trigger on Cold Clouds†

L.V. Tóth[1], S. Hotzel[1], O. Krause[1], D. Lemke[1], Cs. Kiss[2], A. Moór[2]

[1]Max-Planck-Institut für Astronomie
Königstuhl 17, D-69117 Heidelberg, Germany
E-mail: lvtoth@mpia-hd.mpg.de
[2]Konkoly Observatory of the Hungarian Academy of Sciences
H-1525 Budapest, P.O.Box 67., Hungary

Abstract

We investigated the role of trigger mechanisms in the low mass star formation process. Star bearing and pre-protostellar cloud cores were searched as very cold objects of the ISO Serendipity Survey. We compared the distribution of cold starless cores VCCs to the distribution of FIR loops found on IRAS images. The distribution of VCCs follows the large scale ISM density distribution described by the FIR loops. Assuming that the 30pc-200pc scale trigger effects are reflected in the loop/shell structures, this result suggest a link between these effects and the VCCs.
Keywords: *ISM: clouds – dust, extinction – ISM: molecules – Infrared: ISM: continuum – Surveys*

1. Introduction

Our galaxy forms stars on a low enough rate to allow the existence of 10% ISM in spite of the fact that high fraction of the ISM is stored in Jeans unstable clouds. As a solution for the Zuckerman-Evans (1974) paradox, all sorts of support mechanisms were introduced in the 70s. This led to the magnetic field regulated star formation theory. Numerical simulations late last century showed that magnetic braking is not an important support for interstellar cloud cores. Recent observational and modelling evidence suggests that actually there is no need for support since the clouds indeed collapse almost on free-fall time scale. This lowers the importance of star formation trigger mechanisms. Ten years ago those were still thought to be responsible for setting the location and/or timing and/or efficiency of star formation.

†Based on observations with ISO, an ESA project with instruments funded by ESA Member States (especially the PI countries: France, Germany, the Netherlands and the United Kingdom) and with the participation of ISAS and NASA.

One of the major unknown factors in theories of star formation is a detailed observational determination of the initial conditions of the collapse phase that forms a protostar. The pre-protostellar (or prestellar for short) core phase (Ward-Thompson et al. 1994) is believed to be the stage of star formation that precedes the formation of a protostar and hence should represent observationally the initial conditions of protostellar collapse. Some recent observations have even indicated that the Initial Mass Function (IMF) of stars may be determined before the protostellar collapse phase (see eg. Motte et al. 2001). It is thus important to know whether trigger plays an important role in the early (collapse) phase of cloud core evolution, prior to star formation.

Tracing trigger in the galactic ISM we use large FIR structures seen widely on IRAS FIR images. We compiled the first catalogue of FIR Loops which will be briefly discussed here. It is important to check the distribution of gravitationally bound starless cloud cores i.e. pre-protostellar cores whether it follows the large scale ISM density distribution. One has to collect a statistical sample of cloud cores well sampling both the on-loop and off-loop class. We then compare the physical parameters of both classes. Comparing the numbers in the two classes already allows us to draw a statement on the trigger effect of the process responsible for the creation of the loops. We evaluate the ISO Serendipity Survey (ISOSS) data which cover 15% of the sky with serendipitous slews observed at 170 μm with the ISOPHOT camera (Lemke et al. 1996) in board of ISO. We will discuss the parameters of ISOSS cores and their relation to the FIR loops.

2. What we know on low mass star formation

2.1. Tracers and efficiency

We outline important aspects of low mass star formation research, and give observational examples. First of all we list the most common indicators of recent low mass star formation. Various observational and theoretical results on the efficiency of star formation are also given below. Our selection of examples of low mass star formation is biased towards cases where trigger is apparent or expected. The trigger is considered strong when the star formation efficiency is increased.

Tracers of (low mass) star formation:

- Hα emission line stars. Star formation in the L134 complex: few$\times 10^6$ years old Hα stars around L1780, whose formation may be triggered by winds from the Sco-Cen-Lup association (Martin & Kun 1996).

- IRAS point sources as YSOs. Selection criteria were given by eg. Emerson (1987), statistical study of the "whole" IRAS Point Source Catalog was carried out by Prusti et al. (1992). Apparently the YSO distribution is not random.
- NIR point sources with $> 3\%$ NIR excess (Lada 1992)
- bipolar molecular outflows (Bally, 1982, Sato & Fukui 1989)
- cold molecular cloud cores as NH_3 (1,1) density peaks. The most cited NH_3 survey for dense cores in dark clouds (Benson & Myers 1989) indicates a physical association of young type IRAS sources and $T_{kin} \approx 10\,\mathrm{K}$ cold, and $n(\mathrm{H_2}) > 10^4 \mathrm{cm}^{-3}$ dense cloud cores.
- very cold, $T_d \approx 10\,\mathrm{K}$ dust, found in cloud cores eg. in B35 by Lada et al. (1981) and in L1172 by Ladd et al. (1991).

Regulation of star formation - theory: Most of the molecular clouds in the Galaxy are Jeans' unstable, which results in a star-formation rate of $130 < SFE < 400\,\mathrm{M_\odot yr}^{-1}$ (see, e.g., Evans 1991). But this number is two orders of magnitude higher than the average Galactic star-formation rate over the last few Gyr (see, e.g., Scalo 1986). It was generally believed that magnetic fields play a crucial role in supporting the clouds (Mouschovias & Spitzer 1976; Nakano & Nakamura, 1978). A magnetized cloud is virial stable when $M_v > 10^3 \mathrm{M_\odot}$. As it has recently been claimed, magnetic brake (e.g. ambipolar diffusion) cannot prevent local collapse for much longer than the global free-fall time (Heitsch et al., 2001). Does turbulence control the star formation? Is there a still larger scale trigger? Radiation driven implosion (RDI) shapes the clouds: gas condensations in molecular clouds irradiated by an O star and the cloud will have a cometary shape after re-expansion in $\approx 10^6$years (recently e.g. Kessel-Deynet & Burkert, 2002).

Increased efficiency of star formation - observations: The star formation efficiency (SFE) seems to vary with time and location. Large variations of SFE were observed in L1630 where all the massive cores contain regions with densities of at least $10^5\,\mathrm{cm}^{-3}$. The cores with rich embedded clusters (with high SFE), tend to be larger (i.e. to have larger areas of detectable CS($J = 5 \rightarrow 4$) emission) than those without clusters and with low SFE (Lada et al., 1997). It is strange, however, that in the Rosette molecular cloud a majority (65%) of the high-mass ^{13}CO clumps ($M > 450\,\mathrm{M_\odot}$) are not associated with any embedded cluster. The cluster formation may be triggered by the ionization fronts from the nearby HII region associated with NGC 2244 (Phelps & Lada, 1997). The distribution of

YSOs or embedded like IRAS point sources of the Upper Cep-Cas follows a large loop shell (Pásztor et al., 1993) YSOs in L1251 indicate 5% SFE and an age gradient (Kun & Prusti 1993). A shock travelled through L1251 according to Tóth & Walmsley (1996). A few times 10^6 years old Hα stars around L1780 are related to a slowly expanding old SNR shell (Tóth et al., 1995; Martin & Kun, 1996). Cometary clouds RNO 6 and RNO 6NW with embedded IR point sources are cases of formation of intermediate mass stars triggered by RDI according to Bachiller et al. (2002). Star formation propagates with a speed of $1\,\mathrm{kms}^{-1}$, as it can be inferred from the average separation and age difference of aligned cores in the Eagle nebula. Cloud P contains "core b", "core a", and the NIR source P1, with an average projected separation of < 0.1 pc. These objects most likely correspond to a starless core, a Class 0 object, and a Class I object, respec-tively. The age difference is then roughly 10^5 yr. The apparent propagation speed is a little slower than the shock propagation speed of $1.3\,\mathrm{kms}^{-1}$ (White et al., 1999). Conclusion: O5 star is triggering star formation in Cloud P.

2.2. Cold interstellar matter

Star formation occurs in dense cores within molecular clouds (e.g. Williams et al., 2000), although study of such regions was hampered for many years by their very large optical depths at near-infrared and optical wavelengths. It is only since the opening up of the far-infrared and submillimetre regimes that astronomers have been able to study molecular clouds in detail. Density enhancements of the interstellar medium far enough from heat sources and sources of moment can cool efficiently, which leads to collapse. Detailed study of the cold and very cold phase ISM and many pre-stellar cores is central to our understanding of star formation.

Cold interstellar matter (CISM) was introduced in the three phase ISM model of McKee & Ostriker (1977) with density and temperature of $n(\mathrm{H}) = 42\mathrm{cm}^{-3}$ and $T_{kin} \leq 80$K and with a volume filling factor of $\approx 2\%$. The CISM as appears in FIR, is mostly cirrus. At high galactic latitudes it has a temperature of $T_d = 17.5$K (Dwek et al., 1997; Lagache et al., 1998). The ISM gets very cold at shielded regions, efficiently cooled by FIR and mm-lines. It forms molecular clouds ($T_{kin} = 20$K), and starless cloud cores ($T_{kin} = 10$K). The dust is also cold in these clouds and cloud cores. Thus they may be located by excess of FIR relative to 60μm surface brightness. The dust temperature in the very cold ISM is $T_d \leq 15$K (Laureijs et al., 1991; Boulanger et al., 1998; Lagache et al., 1998). An example of FIR radiation of CISM in other galactic disks is given by Haas et al. (1998).

The dust radiation models account for FIR-NIR-optical-UV radiation (e.g. Desert et al., 1990). They assume three components: PAHs and VSGs ($a <$ 10nm, $\lambda \leq 60\mu$m) and large grains (inferred from optical). As simulations show, the heating-cooling instabilities in clouds may lead to collapse (Clarke & Pringle, 1997; Burkert & Lin, 2000). The very cold cloud cores are thought to be the results of such instabilities, and were found to be related to star formation.

IRAS Loops in the 2nd Galactic Quadrant: In order to study the role of trigger in star formation we have carried out a search for interstellar bubble tracers i.e. loops. To achieve a high angular resolution we analysed IRAS maps instead of eg. HI surveys. Due to its low opacity the $100\,\mu$ radiation of dust is useful in a search for both diffuse and dense ISM. All IRAS ISSA maps of the 2nd galactic quadrant were searched for arc-shape bright regions. Our eye-biased search resulted over 150 loops (loop is a $> 60\%$ complete ring with significant surface brightness excess over its surroundings). These FIR loops bear point sources of all types. At intermediate galactic latitudes, the surface density of the TTau-like IRAS point sources is two times higher on the loops than elsewhere whereas the ISM column density is only 50% higher towards the loops than elsewhere (see Kiss et al. 2002).

3. ISO observations and data analysis

ISOSS: The coldest cloud cores are believed to be in the phase of thermal instability induced collapse, and will eventually form low mass stars. The most relevant recent survey to find these objects is the ISO Serendipity Survey (Bogun et al., 1996; Stickel et al., 1998; Tóth et al., 2000). Below we summarize what we have to know on ISOSS and the ISOSS very cold cores (VCCs).
ISOSS - the measurement: Slews between pointed observations of ISO were used to scan the sky with ISOPHOT's C200 array in a broad wavelength band centred at $170\,\mu$m. The slew paths are unpredictable and curved in order to avoid the forbidden regions near Sun and Earth.
ISOSS Calibration Accuracies (errorbars): Photometric accuracy of 30% can be achieved (Müller et al., 2002). Pointing $rms < 1'$, rms reproducibility error is $< 15\%$ as measured at scan crossings (Stickel et al., 2000).

ISOSS very cold cores (VCC): Besides the ISOSS extragalactic point source catalogue (Stickel et al. 1998) the galactic FIR objects were also studied resulting a number of candidate pre-protostellar cores. Very cold (< 15K),

fairly bright (> 6Jy) ISOSS/IRAS sources were located. Their optical associates on DSS2 are mostly opaque cloud cores in cloud complexes or in isolated dark clouds. There are associated NIR point sources seen usually around, but not "inside". As mm spectroscopy followups (CO, CS, NH_3 lines with Effelsberg-100m, Parkes-64m, IRAM-30m telescopes) revealed, these cold ISOSS sources are associated with dense parts of molecular clouds. In Chamaeleon (Tóth et al., 2000), the $I(170)$-excess clouds have $T_{\rm col}$(dust) < 14 K with a 3% area filling factor. The $I(170)$ and $I(100)_{\rm cold}$ FIR surface brightnesses are well correlated, and $I(170)$ is correlated up to $A_V = 7$ mag with the NIR based extinction. The very cold ISOSS sources were found to be cloud cores and thus were named as very cold cloud cores (VCCs). There are 14 VCCs with $T_d \approx$ 12K in the Cepheus region. these VCCs are inside $A_{\rm V} > 3$ mag dark clouds, and mostly associated with $T_{kin} \approx 10$ K NH_3 cores.

4. Relating very cold cores to FIR loops

The distribution of VCCs, which are candidate pre-protostellar cores, is compared to the distribution of FIR loops (Kiss et al. 2002). The FIR loops are most likely projections of 3D bubble shells, as shown by a statistical investigation of the apparent shapes. These are the most prominent features of the nearby (2kpc) interstellar medium on 30–200 pc scales. Thus these shells are considered to be proper tracers of large scale trigger effects. The investigation is limited to the 2^{nd} galactic quadrant which is, however, the region with best sky coverage fraction in the ISOSS database. The resuls of the comparison are:

- 89 VCCs are inside the 2nd Galactic Quadrant
- the VCCs appear within $-40° < b < 30°$ (limited b range)
- the FIR loop shells cover 32% of total sky area within $-40° < b < 30°$
- 70 of the 89 VCCs (79%) are associated with loops, 34 are on loops
- only 6 VCCs are seen inside a loop and 2 VCCs are far from loops

We conclude that the formation of the ISOSS VCCs is likely triggered by the same physical processes which formed the large shells seen as FIR loops. Is it a weak trigger only i.e. modifying the location of otherwhise spontaneous star formation by moving the ISM into shells, or may the high pressure events directly trigger cloud collapses? Further investigation of individual VCCs may answer to this question.

Acknowledgements

We acknowledge the valuable comments by Prof. Kalevi Mattila. The ISOPHOT project and Postoperation Phase was funded by the Deutsche Agentur für Raumfahrtangelegenheiten (DARA, now DLR), the Max-Planck-Gesellschaft, the Danish, British and Spanish Space Agencies and several European and American institutes. Members of the Consortium on the ISOPHOT Serendipity Survey (CISS) are MPIA Heidelberg, ESA ISO SOC Villafranca, AIP Potsdam, IPAC Pasadena, Imperial College, London.
This research was partly supported by the OTKA F-022566 grant and by the Academy of Finland through grants No. 158300 and 173727 and received HAS-JSPS support of Hungarian-Japanese exchange.
This research has made use of the Digitized Sky Survey, produced at the Space Telescope Science Institute, NASA's Astrophysics Data System Abstract Service, the Simbad Database, operated at CDS, Strasbourg, France.

References

Bachiller, R., Fuente, A., Kumar, M.S.N., 2002, A&A 381. 168
Bally, J., 1982, ApJ 261, 558
Benson, P.J. & Myers, P.C., 1989, ApJS, 71, 89.
Bogun, S., Lemke, D., Klaas, U., et al., 1996, A&A 315, L71
Burkert, A., Lin, D.N.C., 2000, ApJ, 537, 270
Clarke, C.J. & Pringle, J.E., 1997, MNRAS 288, 674
Desert, F.-X., Boulanger, F., Puget, J.-L., 1990, A&A 237, 215
Dwek, E., Arendt, R.G., Fixsen, D.J., et al., 1997, ApJ 475, 565
Emerson, J.P., 1987, "IRAS and star formation in dark clouds", in: Star forming regions, IAUS 115, p.19
Evans, N.J.II., 1991, ASP Conf.Ser., 20, 45
Heitsch, F., MacLow, M.M., Klessen, R.S., 2001, ApJ 547, 280
Foster, P.N.; Chevalier, R.A., 1993, ApJ 416 303.
Haas, M., Lemke, D., Stickel, M., et al., 1998, A&A 338, 33
Harjunpää, P., Liljeström, T., Mattila, K., 1991, A&A 249, 493.
Henriksen, R., André, P., Bontemps, S., 1997, A&A 323, 549.
Hotzel, S., 2001, PhD Thesis, Heidelberg.
Hotzel, S., Harju, J., Juvela, D., et al., 2002, A&A 391, 275
Kessel-Deynet, O. & Burkert, A., 2002, RMxAC 12, 25
Kiss, Cs., Moór, A., Tóth, L.V.: Catalogue of IRAS Loops in the 2nd Galactic Quardant, URL:*http://astro.elte.hu/IRASLoops/IRASLoops.html*
Kun M., 1998, ApJS 115, 59
Kun, M. & Prusti, T. 1993 A&A 272. 235

Lada, C.J., Thronson, H.A.Jr., Smith, H.A., et al., 1981, ApJ 251, 91
Ladd, E.F., Adams, F.C., Fuller, G.A., et al., 1991, ApJ, 382, 569
Lada, E.A., 1992, ApJ 393, 25
Lada E.A., Evans, N.J. II, Falgarone, E., 1997 ApJ 488, 286
Lagache et al. 1998, A&A 333, 709
Laureijs, R. J.; Clark, F. O.; Prusti, T., 1991, ApJ 372, 185
Lemke D., Klaas U., Abolins J., et al., 1996, A&A 315, L64
Lynds, B.T., 1962, ApJS, 7, 1.
Martin, E.L. & Kun, M., 1996, A&AS 116. 467
McKee, C.F. & Ostriker, J.P., 1977, ApJ 218, 148
Motte, F. André, P., Ward-Thompson, D., Bontemps, S., 2001, A&A 372, L41
Mouschovias, T.C., & Spitzer, L., 1976, ApJ, 210, 326.
Müller, T.G., Hotzel, S., Stickel, M, 2002 A&A 389, 665
Nakano, T., & Nakamura, T., 1978, PASJ 30, 681
Pásztor, L., Toth, L.V., Balazs, L.G., 1993, A&A 268, 108
Phelps, R.L.& Lada, E.A., 1997 477, 176
Prusti, T., Adorf, H.-M., Meurs, E.J.A., 1992 A&A 261, 685
Reach, W.T., Dwek, E., Fixsen, D.J., et al., 1995, ApJ 451, 188
Sato, F. & Fukui, J. 1989, ApJ
Scalo, J.M., 1986 FCPh 11, 1
Stickel, M., Bogun, S., Lemke, D., et al., 1998, A&A, 336, 116.
Stickel, M., Lemke, D., Klaas U., et al., 2000, A&A 359, 865
Tóth, L.V., Walmsley, C.M., 1996 A&A 311, 981
Tóth, L.V., Hotzel, S., Krause, O., et al., 2000, A&A, 364, 769
Ward-Thompson, D., Scott, P.F., Hills, R.E., Andre, P., 1994, MNRAS 268, 276.
Ward-Thompson, D., André, P., Kirk, J.M., 2002, MNRAS 329, 257
Wheelock, S.L., Gautier, T.N., Chillemi, J., et al., 1994, IRAS sky survey atlas: Explanatory supplement. JPL Publication 94-11, IPAC, JPL
White, G.J., Nelson, R.P., Holland, W.S., et al., 1999, A&A 342, 233
Whitworth, A., Summers, D., 1985, MNRAS 214, 1.
Whitworth, A.P., Ward-Thompson, D., 2001, ApJ 547, 317.
Williams, J.P., Blitz, L., McKee, C.F., 1999, Protostars and Planets IV, 97.
Yonekura, Y., Dobashi, K., Mizuno, A., et al., 1997, ApJS 110, 21.

PDRs in Star Forming Regions

M.E. Lebrón[1], L.F. Rodríguez[2], S. Lizano[2]

[1]Max Planck Institut für Radioastronomie
Auf den Hügel 69, D-53121, Bonn, Germany
[2]Universidad Nacional Autónoma de México - Unidad Morelia
Apdo. Postal 3-72, Morelia, Michoacán, México
E-mail:[1]mlebron@mpifr-bonn.mpg.de

Abstract

The molecular gas can be photodissociated if it is exposed to intense far-ultraviolet (FUV) radiation. Intermediate and high mass stars generate enough flux in the FUV range to produce a significant photodissociation region (PDR) around them. In order to characterize the PDR that forms near these regions high resolution infrared and centimeter wavelength observations are required. Current centimeter-wave telescopes/interferometers offer the required spatial resolution to detect and to study in detail the PDRs in star forming regions. We present a short review of observations of PDRs and discuss the particular case of G111.61+0.37.

KEYWORDS: *ISM: HII regions, clouds – Radio lines: ISM – ISM: Individual objects: G111.61+0.37*

1. Introduction

Young massive stars not only form HII regions but also create significant photodissociated regions and the radiation field excites various transitions in the surrounding molecular material. In the last 25 years many theoretical works were done on PDRs (e.g. Hill & Hollenbach, 1978; Roger & Dewdney, 1992; Bertoldi & Draine, 1996; Hollenbach & Tielens, 1997; Díaz-Miller et al., 1998; Gorti and Hollenbach, 2002). PDRs of young massive stars are simply the intermediate region between the HII region and the quiescent molecular gas. For better illustrate the PDRs produced by young massive stars a simple diagram is shown in Fig. 1. The ionizing photons form an HII region close to the star, while the photodissociating photons penetrate more into the cloud generating, first, a zone where the hydrogen is neutral (HI zone), and then a molecular excited zone. The carbon is ionized deeper than the HI zone into the cloud. The PDR ends when all the oxygen is contained in O_2 and CO molecules (for details about PDRs see the review of Hollenbach & Tielens, 1997).

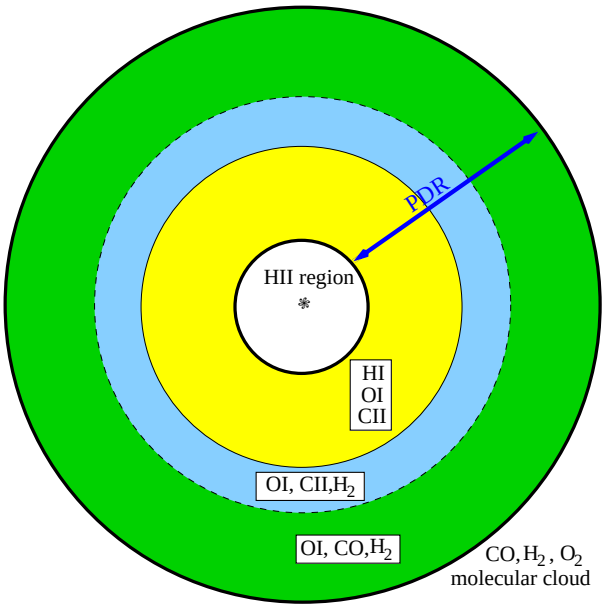

Figure 1: Diagram of a photodissociated region formed around a young massive star that also forms an HII region. The PDR starts with the HI zone where the hydrogen is in neutral phase, carbon is ionized and oxygen neutral. The zone of ionized carbon (CII) extends deeper into the cloud where the hydrogen is already molecular but the oxygen is still neutral. The last zone corresponds to the neutral oxygen (OI), that goes even deeper into the cloud, where the carbon is already contained in CO molecules. The PDR ends when all the oxygen is contained in O_2 and CO molecules.

The main coolants of the PDRs are [CII] 158 μm, [OI] 63 μm lines, CO rotational lines, flourescent H_2 lines, dust continuum emission and PAH features. The FIR and millimetric emission of PDRs are used to determine their physical parameters (e.g. Liu et al., 2001; Vastel et al., 2001). Because of the low angular resolution of FIR telescopes ($\sim$1 arcmin), it is not possible to study in detail the kinematic and the spatial distribution of PDR in compact sources (e.g. star-forming regions). Although the main coolants are in the IR band, PDRs also emit in the cm wavelength range.

The radio emission of PDRs is detected in the 21 cm HI line, and also in carbon recombination lines (e.g. Wyrowski et al., 1997; Lebrón & Rodríguez, 1997; Gómez et al., 1998; Wyrowski et al., 2000). The lines at cm wavelengths are weaker than the IR lines, but with the high spatial and spectral resolution that can be achieved with radio telescopes/interferometers, the observation of radio lines are a valuable tool for studying the kinematics of PDRs in compact sources. An example of a detailed study of the neutral region of the PDR in a star-forming region was done in G111.61+0.37 (Lebrón et al., 2001). The compact HII region G111.61+0.37 was studied in the HI 21cm line (that traces the neutral region of the PDR), ammonia transitions (1,1) and (2,2) (that trace

the dense molecular gas) and the recombination line H92α (that traces the HII region) with the VLA interferometer.

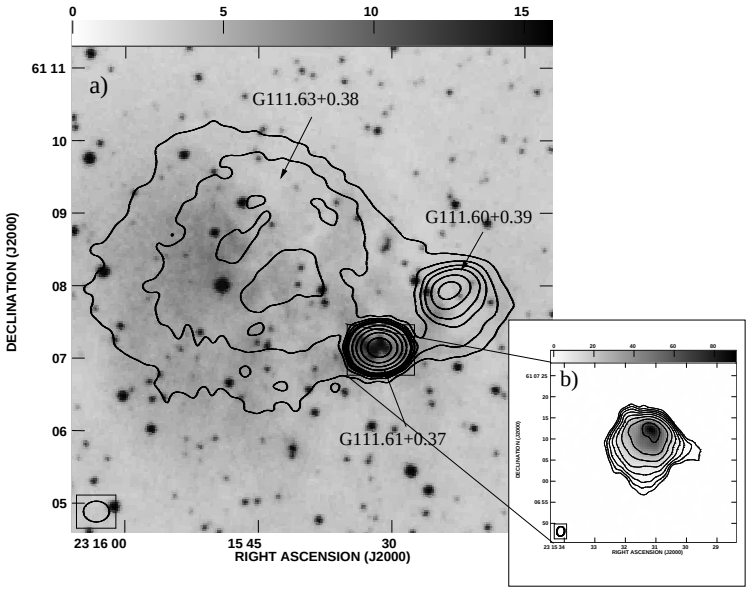

Figure 2: (**a**) 1.4 GHz continuum emission in Sharpless 159 (contours). G111.61+0.37 is located in the center of the map. The background image is the red POSS plate of the region. (**b**) 3.6 cm continuum emission of G111.61+0.37. The continuum emission shows a cometary shape distribution.

2. The PDR in G111.61+0.37

G111.61+0.37 (hereafter called G111.61) is a compact HII region in the Sharpless 159 region at a distance of 3.1 kpc (Brand & Blitz, 1993). Fig. 2a shows a continuum map at 1.4 GHz (contours) of the Sharpless 159 region. G111.61 is the brightest source in the region and is associated with the IR source IRAS 23133+6050. The cometary shape of the continuum emission in G111.61

(see Fig. 2b) is due to a champagne flow of the ionized gas (Lebrón et al., 2001; Kurtz et al., 1994).

The photodissociated region in G111.61 was detected in the 21cm line of HI. The HI spectra of G111.61 shows absorption and emission features (see Fig. 3), being the absorption ones the most prominent. Nevertheless, the emission feature is of our particular interest.

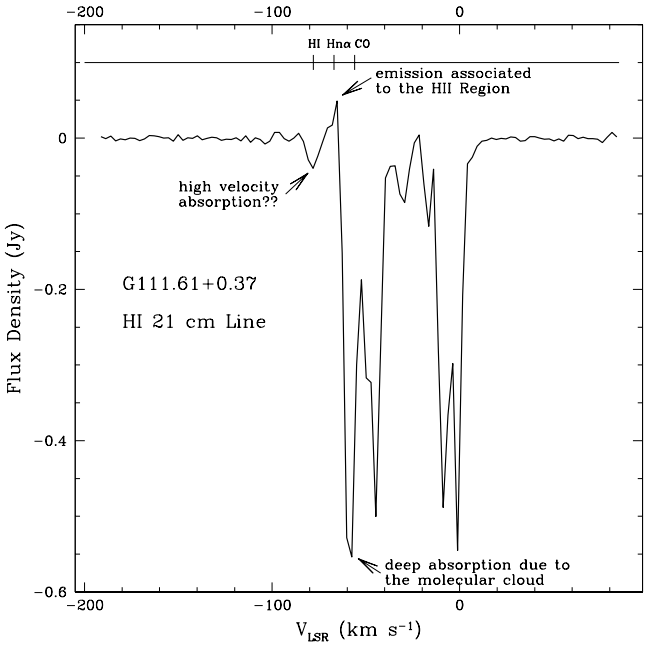

Figure 3: HI 21cm line spectrum of G111.61+0.37.

A contour map of the integrated HI emission between -58 and -67 km s^{-1} (emission feature) is shown in Fig. 4. The HI in emission (continuous line contours) is compact ($25'' = 0.4$ pc) and located next to G111.61. The HI in emission appears to the SE of G111.61. This asymmetry in the emission distribution is interpreted as a consequence of density gradients in the molecular gas. Sizes of PDRs have strong dependence on the density of the molecular gas (Díaz-Miller et al., 1998).

In the case of G111.61 we found dense molecular gas (density $> 10^6$ cm^{-3}), located to the NW of the HII region (see Fig. 5). This dense gas is confining the

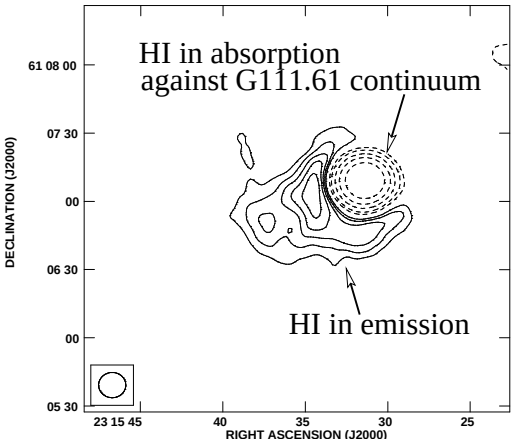

Figure 4: HI 21cm velocity-integrated map of G111.61+0.37. The line emission was integrated between -58.6 to -68.9 km s^{-1}. The continuous line contours show the HI in emission, while the dashed-line contours show the HI in absorption. The contour levels are -100, -50, -25, -12, -9, -6, -4, 4, 5, 6, 7, 8, and 9 $\times$ 1.1 mJy beam^{-1}.

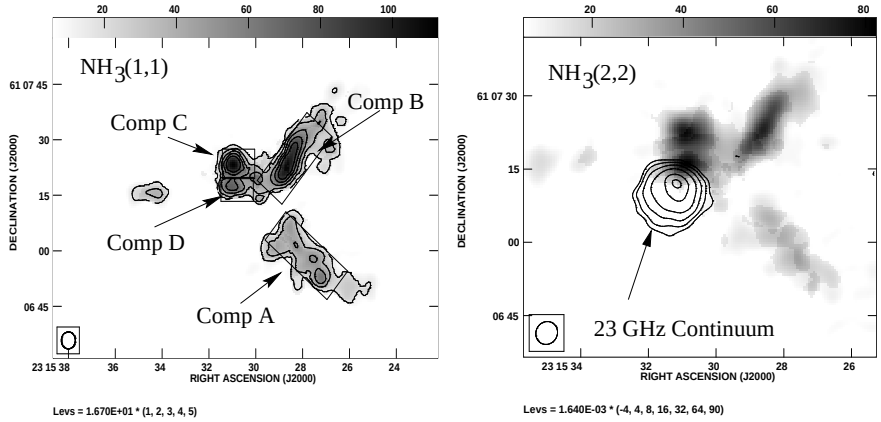

Figure 5: NH_3(1,1) and (2,2) velocity-integrated line maps (grey scale) and 23 GHz continuum map of G111.61+0.37 (contours on right panel). Component D is located near the HII region and is hotter than the other ammonia clumps. Clump D is confining the HII region and the PDR in the NW direction.

HII region in the NW direction (Lebrón et al., 2001). The expected size for a PDR that developes in a medium of density greater than 10^5 cm^{-3} is $<$0.03 pc

(Díaz-Miller et al., 1998). Such small structures could not be detected with the HI observations dicussed here. No PDR was detected between the HII region and the dense molecular gas (traced by ammonia), but a prominent HI zone extends into the low density molecular gas.

The HI emission observed in G111.61 is a clear example of the neutral region of a PDR in a massive star-forming region. The structure of the PDR is also shaped by the molecular environs like the HII region. The determined column density and mass of the HI emission are 5.9 $\times$ 10^{20} cm^{-2} and 0.8 $M_{\odot}$, respectively (a T_{ex} of 300 K was assumed).

3. Conclusions

In this paper we presented the results of the HI 21 cm line observations of the star-forming region G111.61+0.37. The neutral zone of the PDR is bigger than the HII region. The spatial distribution of the HI emission also suggests a density gradient in the molecular gas. This result is confirmed by ammonia observations. The spatial resolution that can be obtained in the cm wavelength range permits the study the PDRs in compact sources.

References

Bertoldi, F., & Draine, B. 1996, ApJ, 458, 222
Brand, J., & Blitz, L. 1993, A&A, 275, 67
Díaz-Miller, R.I., Franco, J., Shore, S.N., 1998, ApJ, 501, 192
Gómez, Y., Lebrón, M., Rodríguez, L.F., Garay, G., Lizano, S., Escalante, V., Cantó, J., 1998, ApJ, 503, 297
Gorti, U, Hollenbach, D.J. 2002, ApJ, 573, 215
Hill, J. K., & Hollenbach, D.J. 1978, ApJ, 225, 390
Hollenbach, D.J., & Tielens, A.G.G.M., 1997, ARA&A, 35, 179
Kurtz, S., Churchwell, E., Wood, D.O.S., 1994, ApJS, 91, 659
Lebrón, M.E., & Rodríguez, L.F. 1997, Rev. Mexicana Astron. Astrofis., 33, 165
Lebrón, M.E., Rodríguez, L.F., Lizano, S. 2001, ApJ, 560, 806
Liu, X.-W., Barlow, M.J., Cohen, M., Danziger, I.J., Lou, S.-G., Baluleau, J.P., Cox, P., Emery, R.J., Lim, T., Peguignot, D. 2001, MNRAS, 323, 343
Roger, R.S., Dewdney, P.E., 1992, ApJ, 385, 536
Vastel, C., Spaan, M., Ceccarelli, C., Tielens, A.G.G.M., Caux, E. 2001, A&A, 376, 1064
Wyrowski, F., Schilke, P., Hofner, P., Walmsley, C.M., 1997, ApJ, 487, L171
Wyrowski, F., Walmsley, C.M., Goss, W.M., Tielens, A.G.G.M., 2000, ApJ, 543, 245

Reducing and Analyzing Chemical Networks

D. Semenov[1], D. Wiebe[2], Th. Henning[3]
[1]Astrophysical Institute and University Observatory
Schillergäßchen 2-3, 07745 Jena, Germany
E-mail: dima@astro.uni-jena.de
[2]Institute of Astronomy of the RAS
Pyatnitskaya St. 48, 109017 Moscow, Russia
[3]Max Planck Institute for Astronomy
Königstuhl 17, 69117 Heidelberg, Germany

Abstract

A new efficient method allowing the reduction of the number of species and reactions in chemical networks is outlined. We applied it to the UMIST 95 astrochemical database in order to find a subset of species and reactions governing the evolution of carbon monoxide under conditions, typical of dense molecular clouds. We succeeded in isolation of such a tiny set for the pure gas-phase chemistry which gives the reliable estimation of the CO abundances under a wide range of the gas temperatures, densities, and visual extinctions. We showed that the reduction is only modest when gas-grain interactions and surface reactions are taken into account.
Keywords: *astrochemistry – stars: formation – molecular processes – ISM: molecules – ISM: abundances*

1. Introduction

Nowadays large progress is achieved in modelling of the chemical and dynamical evolution of various astrophysical environments, like protostellar cores or protoplanetary disks. Still the coupled self-consistent chemical and dynamical modelling of such objects is beyond the capabilities of modern computers. The main reason is that typical chemical networks used in astrophysical simulations contain hundreds of species involved in thousands of reactions. Their accurate handling together with hydrodynamical calculations requires enormous computational efforts.

However, in many cases only a few species are of the main interest for an astronomer. For instance, the most important species for the evolution of magnetized interstellar clouds are few dominant ions, as mainly their abundances regulate the ionization degree. Then it seems intuitively clear that one may neglect some of "exotic" species, like long carbon chains, in order to speed up the calculations and still have reasonable estimations on the degree of ionization.

Notwithstanding, the qualitative considerations of this kind require a rigorous mathematical analysis to be proven.

Ruffle et al. (2002) made a first attempt to apply such a method – objective technique developed in other scientific community – for the reduction of astrochemical networks. They were able to discriminate among about 200 species only 33 which are necessary to follow the evolution of CO abundances within accuracy of 30% at $t > 10^5$ years in static translucent regions. In the paper of Rae et al. (2002) the same reduction technique has been applied to identification of reduced networks governing the fractional ionization in molecular clouds under a wide range of physical circumstances. It has been found that one has to keep about thirty species from the entire set of more than two hundred species in order to predict the ionization degree without significant errors.

In this paper, we introduce a new reaction-based method of reduction which allows to reduce *simultaneously* the number of species and reactions in chemical networks. Using this reduction technique, we perform an analysis of the UMIST 95 database of chemical reactions in order to select species and reactions that are needed for accurate estimations of carbon monoxide abundances under conditions of dense molecular clouds. Our special aim is to investigate the possibility to reduce the chemical networks when complicated gas-grain interactions and dust surface reactions are taken into account beside the common gas-phase reactions.

2. Chemical Model

The detailed description of our chemical model is given in the paper of Wiebe et al. (2002). Here, we briefly summarize its main features.

We take into account gas-phase reactions, gas-grain interactions, and dust surface reactions. The species set and gas-phase reaction rates are taken from the UMIST 95 database (Millar et al. 1997). Dust surface reactions are adopted from Hasegawa et al. (1992). The desorption energies of the surface species are taken or estimated from Hasegawa & Herbst (1993). The gas-grain interactions include the following physical processes: accretion of neutral species onto dust grains, their desorption due to the thermal evaporation and cosmic ray heating, and dissociative recombination of ions on grain surfaces.

Two chemical networks are investigated, namely, the pure gas-phase network consists of electron, 12 atoms, 137 molecules, and 245 ions (in total 395 species) involved in 3864 gas-phase reactions and the gas-grain network having additional 148 surface species, 729 gas-grain and 192 dust surface reactions.

The probability of species to stick on the dust surfaces is assumed to be 0.3 for all ions and all neutral species except for H, He, and H_2. The sticking coefficient of the atomic hydrogen is estimated from the expression given in Hollenbach & McKee (1979), Equation (3.7). Sticking probabilities for helium and molecular hydrogen are assumed to be zero.

We consider the gas density $n_{\rm H} = 10^7$ cm^{-3} and fix gas and dust temperatures to 10 K. No photoprocessing by the interstellar UV radiation is assumed ($A_V \geq 10$). Dust grains are considered as silicate-like spheres having a uniform size 0.1 micron, density 3 g cm^{-3}, and 10^6 surface sites for adsorption. Dust is assumed to constitute 1% of the gas density by mass.

We use well-known "high metal" and "low metal" initial abundances (see, for instance, Lee et al. 1998). The "high metal" means standard solar composition with a modest depletion of 2 for S and stronger depletions of $\sim 10 - 100$ for Si and metal atoms. The "low metal" values contain additional depletion factors of 100 for each of these elements. The abundances of He, C, N, O, S, Si, Na, Mg, and Fe are taken from Aikawa et al. (1996). For P and Cl we take the values from Grevesse & Sauval (1998) and use the same depletion factors as for Fe. We suppose that only these atomic neutral species and molecular hydrogen are present at initial time $t = 0$.

3. Reaction-based Reduction Technique

The new method of reaction-based reduction allows us to select from the entire network only those species and reactions that are *necessary* to compute abundances of chosen (*important*) species with a reasonable accuracy.

The basic idea of this reduction technique is to search for the production and destruction reactions, critical for the evolution of the important species, and determine their relative importance. It can be done by the analysis of the sensitivity of the net formation (or loss) rate of given species in respect to the presence of particular reactions at a certain time.

Below we briefly outline the algorithm of our reduction approach.

First, one runs the chemical model with the full network for certain physical conditions in order to obtain abundances of all species in the network during the entire evolutionary time.

Then, important species for which reduction will be made, are specified. The algorithm estimates weights of all species $w_{\rm s}$ and reactions $w_{\rm r}$ in order to quantify their significance for the evolution of the important species at a particular time moment by the following iterative process:

1. During the first iteration, weights of important species are set to 1 and weights of all other species and all reactions are set to 0;

2. For the iteration i and the current species s_i all relevant formation and destruction reactions are found and their weights $w_{\rm r}^i$ are specified as

$$w_{\rm r}^i(j) = \max\{w_{\rm r}^{i-1}(j),\ \frac{k_j n_{r_1}(j) n_{r_2}(j)}{\sum\limits_{l=1,N_{\rm r}(i)} k_l n_{r_1}(l) n_{r_2}(l)} w_{\rm s}(i)\} \qquad (1)$$

   Here k_j is the rate of jth reaction, $n_{r_1}(j)$ and $n_{r_2}(j)$ are the abundances of the first $r_1(j)$ and second $r_2(j)$ reactants in the jth reaction, respectively, $N_{\rm r}(i)$ is the amount of the reactions having s_i as a reactant or a product, and $w_{\rm s}(i)$ is the weight of the species s_i;

3. Consequently, a new set of species, those found at that iteration to be related to the evolution of the important species and not considered in previous iterations, is formed. Their weights $w_{\rm s}$ are estimated as the maximum possible values of the weights $w_{\rm r}$ of the reactions they are involved in.

The iterations are finished when all species and all time steps are passed. Then one easily obtains a reduced chemical network from the full network by choosing only those reactions, that have weights above a predefined cut-off threshold.

We assume that if there is a difference greater than 30% in abundances of the important species computed with the full and reduced networks for any time moment, then the cut-off is readjusted to a new, smaller value, and the last step is repeated. Utilizing this rather strong selection criterion for the reduced networks, we preserve ourself from introducing severe computational errors in abundances of the important species.

4. Chemistry of Carbon Monoxide

We follow the approach described in the previous section to build the gas-phase and gas-grain reduced networks for CO. The carbon monoxide is chosen as the only important species to be used with the reaction-based reduction technique.

In the case of the purely gas-phase chemistry in a dense cloud the main chemical processes for the evolution of CO are the following. At very early

evolutionary stages, $t < 10^2$ years, key formation processes are the neutral-neutral reactions of oxygen with various light carbon-bearing molecules, like CH and CH_2. Later, CO is formed due to destruction of OCS, H_2CO, and CO_2 by the cosmic ray induced UV photons. The removal of CO during the entire evolutionary time is controlled by the cosmic ray ionization and destruction due to the cosmic ray induced UV photons.

The evolution of carbon monoxide under such circumstances is shown in Figure 1 (left panel). As can be clearly seen, in the absence of the gas-grain interactions the evolution of CO is rather simple – its abundance is rapidly increasing till the chemical equilibrium value of about 10^{-4} (in respect to the amount of hydrogen nuclei) is reached at $\sim 3\,10^3$ years. The rest (and most!) of the evolutionary time the abundance of carbon monoxide remains almost a constant. Remarkably, there is no difference between the high and low metallicity cases.

Applying our reduction approach, we found that one may keep from the entire set of 395 species and 3864 reactions only 8 species involved in 9 reactions in order to accurate estimation CO abundances for all 10^7 years of the evolution. The corresponding reduced network is given in Table 1. The size of this network is so small that the computational time which is needed to solve the relevant system of the ordinary differential equations (ODE) is negligible, less than a second. Still the uncertainties of the resulting abundances do not exceed 15% during the entire evolutionary time.

This extraordinary result demonstrates the power of our reduction technique and explains why there is no difference between the high and low metallicity cases. The reason is that the evolution of these 8 necessary species (see Table 1) depends only on the total amount of H, C, and O available in the gas phase at $t = 0$. As the initial abundances of these atoms are exactly the same for both metallicities, it leads to the nearly identical values of CO abundances for all $0 - 10^7$ years.

It is interesting to examine if such extremely small amount of necessary species and reactions is caused by merely favorable circumstances or it is due to the nature of the CO chemistry itself. In the latter case, the relevant reduced network must reproduce accurately the abundances of carbon monoxide in a range of the physical conditions.

We discovered that this network is functional within accuracy of 50% under the following circumstances:

$$10^4 \text{ cm}^{-3} \leq n_{\rm H} \leq 10^{10} \text{ cm}^{-3},\ T \leq 250 \text{ K},\ A_{\rm V} \geq 1$$

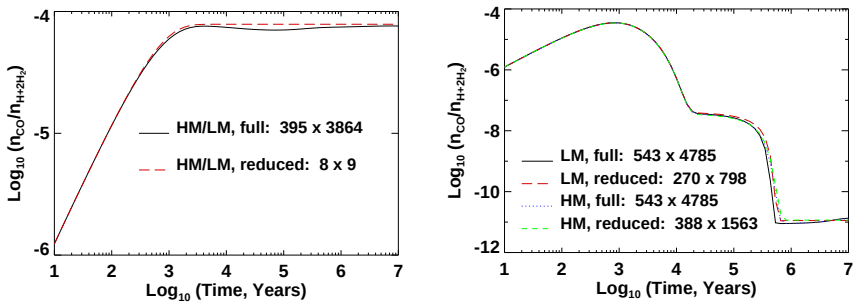

Figure 1: The evolution of CO in a dense cloud computed with the full and reduced networks in the case of the purely gas-phase chemistry (**left panel**) and the gas-grain chemistry involving the surface reactions (**right panel**). The "HM" and "LM" mean high and low metallicity cases, respectively. The sizes of the chemical networks are indicated as "$N_1 \times N_2$", where N_1 is the number of chemical species and N_2 is the number of reactions.

It implies physical conditions, typical of dense and translucent interstellar clouds and "hot cores" of molecular clouds. Thus one may use essentially the same tiny set of species and reactions in order to follow the evolution of CO in the case of the purely gas-phase chemistry in a very wide range of conditions. Compared to the similar network obtained by Ruffle et al. (2002), that has 33 species involved in 116 reactions and is valid for $n_{\rm H} \sim 10^3$ cm^{-3}, $A_{\rm V} = 4-10$, and $t > 10^5$ years our network is much smaller and still is applicable under a much wider range of the physical circumstances.

The situation is more complicated from the chemical point of view when the gas-grain interactions and the dust surface reactions are taken into account. The accretion of species onto the grain surfaces is efficient at high gas density, $n_{\rm H} = 10^7$ cm^{-3}, leading to significant amount of mantle material. Then the quantum tunneling of H and H_2 and thermal hopping of other atoms and light molecules drive the rich surface chemistry, which results in production of heavier species, mostly complex organic molecules. Occasional impulse heating of the dust grains by the energetic cosmic ray particles returns some of the surface species back to the gas phase. All these processes alter the gas-phase chemistry in a high degree.

The evolution of carbon monoxide in this case is shown in Figure 1 (right

Table 1: Reduced network for CO (DENS model)

1 $H + CH_2 \rightarrow CH + H_2$	6 $O + C_2H \rightarrow CO + CH$
2 $H_2 + C \rightarrow CH_2 + PHOTON$	7 $H_2 + CRP^a \rightarrow H + H$
3 $C + CH_2 \rightarrow C_2H + H$	8 $CH + CRPHOT^b \rightarrow C + H$
4 $O + CH \rightarrow CO + H$	9 $CO + CRPHOT \rightarrow C + O$
5 $O + CH_2 \rightarrow CO + H + H$	

[a]"CRP" is an abbreviation for "cosmic ray particle",
[b]"CRPHOT" means "CRP-induced UV photon"

panel). The abundance of the gas-phase CO is increasing at early evolutionary times, till the maximum value of $n_{CO}/n_H \sim 10^{-4}$ is reached at $t \sim 10^3$ years. Then, accretion of CO molecules onto the grains becomes efficient and its abundance in the gas phase is decreasing. The bump on the curve at $t \sim 10^4 - 10^6$ years is due to the influence of the surface reactions as they become quite important at these times. Finally, the equilibrium value $n_{CO}/n_H \approx 10^{-11}$ is reached after about 10^6 years of evolution. Again, as in the previous case, there is no difference between the high and low metallicities.

Our method of reduction is able to select two sets of 388 species and 1563 reactions for the high metallicity case and 270 species and 798 reactions for the low metallicity case. The relevant computational speed gains are only about factors of 3 and 15 for the former and latter cases, respectively. The accuracy of the predicted CO abundances is better than 15% during the entire evolutionary time.

The number of necessary species and reactions is high due to perplexity of the chemical processes in this model. Indeed, the selectivity criterion of the reduction method recognizes many of the surface reactions to be important, so they remain in the reduced chemical network. Consequently, it leads to larger amount of necessary reactions and species compared to the case of the purely gas-phase chemistry.

There is a large ($> 50\%$) difference between the number of the species found to be necessary in the high metallicity case compared to the low metallicity case. The reason is that the reduced networks with smaller amounts of species cannot be used in the calculations because the relevant ODE systems are too stiff to be solved in reasonable time. This is a common situation when the surface reactions are taken into account as they have far too high kinetic rates compared to the gas-phase chemical reactions.

5. Conclusions

We have developed a robust technique to reduce the amount of species and reactions in the chemical networks. It is shown that by utilizing this method the size of the gas-phase chemical network used to compute CO abundances in the dense clouds can be significantly reduced. We have found that such reduction is of no practical use when the gas-grain interactions and the surface chemistry are taken into account since the relevant computational time gains are about factors a few only.

Acknowledgements

DS was supported by the German *Deutsche Forschungsgemeinschaft, DFG* project "Research Group Laboratory Astrophysics" (He 1935/17-1), the work of DW was supported by the INTAS grant YS 2001-1/91 and the RFBR grant 01-02-16206.

References

Aikawa, Y., Miyama, S.M., Nakano, T., Umebayashi, T., 1996, ApJ 467, 684
Grevesse, N., Sauval, A.J., 1998, Space Sci. Rev. 85, 161
Hasegawa, T.I., Herbst, E., Leung, C.M., 1992, ApJSS 82, 167
Hasegawa, T.I., Herbst, E. 1993, MNRAS 263, 589
Hollenbach, D., McKee, C.F., 1979, ApJSS 41, 555
Lee, H.-H., Roueff, E., Pineau des Forêts, G., Shalabiea, O. M., et al., 1998, A&A 334, 1047
Millar, T.J., Farquhar, P.R.A., Willacy, K., 1997, A&AS 121, 139
Rae, J.G.L, Bell, N., Hartquist, T.W., et al., 2002, A&A 383, 738
Ruffle, D.P., Rae, J.G.L., Pilling, M.J., et al., 2002, A&A 381, L13
Wiebe, D., Semenov, D., Henning, Th., 2002, A&A, in preparation

Chemistry in Star-Forming Regions: Making Complex Modelling Feasible

D. Wiebe[1], D. Semenov[2], Th. Henning[3]

[1]Institute of Astronomy of the RAS
48, Pyatnitskaya str., Moscow 119017, Russia
[2]Astrophysical Institute and University Observatory
Schillergäßchen 2-3, 07745 Jena, Germany
[3]Max Planck Institute for Astronomy
Königstuhl 17, 69117 Heidelberg, Germany
E-mail: dwiebe@inasan.rssi.ru

Abstract

In this paper we discuss possible ways to reduce the chemical reaction network for the situations when the accurate abundances are only needed for a limited number of species to compute, for example, such dynamically important factors as the ionisation degree or molecular cooling. We show that it is possible to reduce the number of reactions and species so that the computational time in some astrophysically interesting situations will be reduced by orders of magnitude without appreciable loss of accuracy. For example, to model magnetised dark clouds, self-consistently estimating the ionisation degree with the UMIST 95 database, one only needs to retain about 100 of 395 species with the computational time cut by a factor of a hundred. In the case of dynamical modelling with changing density, extinction, UV-intensity, temperature etc., the reduced chemical network may help to distinguish between feasible and non-feasible tasks.
Keywords: *molecular processes – ISM: molecules – ISM: abundances*

1. Introduction

One of the main problems of the star formation studies is the absence of easily detectable emission from molecular hydrogen, which is the most abundant molecule in molecular clouds that are sites of star formation. Gas motion in star-forming clouds, pre-stellar, protostellar, and young stellar objects (YSO) is essentially motion of H_2 molecules. Yet we have to infer this motion observing far less abundant species.

Molecular diagnostics has now developed into effective tool for the investigation of interstellar clouds. It allows to determine physical conditions in the ISM, may help to elucidate the evolutionary state of different objects (through

the concept of chemical clock), and even sheds some light on the problem of life origins (through observations of complex organic molecules). However, species that are used as tracers for the study of the star formation are not necessarily well mixed with molecular hydrogen and thus with bulk gas. To relate observed distributions of trace molecules to that of molecular hydrogen, the modelling of the chemical evolution of the region under investigation seems to be inevitable.

There are more than 120 species that are known now to exist in the ISM. As they do not form a closed chemical system, one has to assume that many other chemical species are present there that are not (yet) observable. A typical chemical network used in the modelling of the ISM, like the UMIST 95 database (Millar et al. 1997), consists of hundreds of species and thousands of reactions. Differential equations of chemical kinetics that describe time-dependent molecule production and destruction rates are usually stiff and require special methods of solution, implemented, e.g., in LSODE and DVODE packages. Solving of these equations is a demanding computational task even for the fixed relevant physical conditions (density, temperature, extinction, etc.). But interferometric observations that are now becoming abundant allow not only to determine the chemical composition of a particular object but also reveal its detailed chemical structure. To confront these data with theoretical predictions one has to model the chemical evolution at least in several points across the object with the physical conditions that vary, in general, not only in space but also in time.

One way to do this is to place the chemical model over the pre-computed dynamical model. However, it is sometimes necessary to model the chemical and dynamical evolution of the ISM self-consistently in order to take into account a feedback that chemistry has on dynamics either through heating and cooling processes that depend on abundances of certain molecules or through chemically determined ionisation degree (Ciolek & Mouschovias 1993). This makes the situation more complicated.

Even in the case of a static cloud or a cloud with the pre-defined dynamics, modelling of its detailed chemical structure is very time-consuming, if one recalls the number of parameters that can be varied. It seems to be clear that self-consistent coupling of the full-fledged chemical model to the (more or less) full-fledged dynamical model is next to impossible, even with ever-increasing computational power.

2. Motivation and Reduction Model

While one can only guess if the chosen chemical network contains all the needed species and all the needed reactions, the natural question to ask is if we really need all this information. To compare results of chemical modelling with observational data one usually needs to compute abundances of a few selected molecules (like CO, NH_3, CS, HCN, etc.) without spending much computational time on the accurate predictions about, say, complex carbon chains. To model thermal balance in a cloud self-consistently it is in most situations enough to have accurate abundances of CO which is a major molecular coolant in interstellar clouds (Glassgold & Langer 1973). Ionisation degree is determined not by the entire species set but only by a few dominant ions that are involved in a handful of chemical reactions. Intuitively, it seems obvious that in such cases the number of species and reactions can be significantly reduced. However, for now attempts to use abridged chemical networks have been mainly based on a more or less qualitative arguments, without accurate mathematical consideration (e.g. Gerola & Glassgold 1980; Shematovich et al. 1997; Desch & Mouschovias 2001).

So, we can formulate the following task: to reduce the number of species and reactions into a subset that is necessary in a particular situation using mathematically proven arguments that will ensure reliability of the reduced network. Ruffle et al. (2002) and Rae et al. (2002) made the first attempt of this kind found in the astronomical literature. They used methods developed in different branches of science to reduce networks used in modelling of combustion processes. They show that it is possible to isolate species and reactions governing the CO abundance and the ionisation degree at the conditions typical of diffuse illuminated clouds. Their reduced network for CO contains 33 species involved in 116 reactions and is valid for $n_{\rm H} \sim 10^3$ cm^{-3} and $A_{\rm v} = 4 - 10$.

In this paper we present a similar approach to the chemical network reduction and check it for a wider range of physical conditions. We utilise two methods that we refer to as species-based reduction and reaction-based reduction. With these two methods we built reduced networks needed to compute electron and CO abundances for the conditions typical of diffuse ($n_{\rm H} \sim 10^3$ cm^{-3}) and dense ($n_{\rm H} \sim 10^7$ cm^{-3}) molecular clouds. We assume no photoprocessing by interstellar UV photons, implying obscured regions with $\rm A_V > 10$. We consider both purely gas-phase chemistry and gas-phase chemistry coupled to the surface chemistry with two different sets of initial abundances usually referred to as high and low metallicities (e.g. Lee et al. 1998).

We use the UMIST 95 rate file for the gas-phase reactions. Rates for surface

reactions are taken from Hasegawa et al. (1992) and Hasegawa & Herbst (1993). As surface chemistry is included here for illustration purposes only, the rate equation approach is used to model these reactions, even though its validity is now questioned. Gas-phase network consists of 395 species (including electrons) taking part in 3864 reactions. All 148 neutral species but helium and molecular hydrogen are allowed to stick to dust grains where they are involved in 192 surface reactions. Gas-dust connection is realized through accretion and desorption processes. Desorption energies are taken from Hasegawa & Herbst (1993) or interpolated from their data.

The species-based reduction rests upon the first part of the Ruffle et al. (2002) technique and consists of choosing species that are important in a particular context and then selecting from the entire network only those species that are necessary to compute abundances of important species with reasonable accuracy. The analysis is based on sensitivities B_i defined in Ruffle et al. (2002) as

$$B_i = \sum_{j=1,N'} \left(\frac{n_i}{g_j} \frac{\partial f_j}{\partial n_i} \right)^2 , \quad (1)$$

where n_i is the abundance of ith species, N' is the current number of important and necessary species,

$$f_j = G_j - L_j$$

is the net rate of the jth species abundance change expressed as the difference between the net gain G_j and loss L_j rates, and

$$g_j = \max(G_j, L_j).$$

With these definitions, the quantity in parentheses gives the normalised rate of jth species abundance change due to those reactions only that involve ith species. B_i value thus gives a measure of the relative importance of the ith species. The important feature of B_i values pointed out by Ruffle et al. (2002) is the clear cutoff between species with large B_i and small B_i. Before the first step the reduced set contains only important species. Then B_i values are computed for all species from the full network, and those of them, having B_i above the cut-off threshold, are added to the reduced network, and the process starts over. If after the current iteration no new species are added to the reduced network, the process stops.

In the reaction-based method analysis starts from reactions that govern the abundance of important species. All reactions in the entire network are assigned weights according to the influence they have on the abundance of an important

species. Then, only those reactions are selected that have weights above some cut-off parameter that is selected on the basis of the requested accuracy. Only those species are included in the reduced network that participate in selected reactions. Details on the algorithm of the reaction-based reduction are given in Semenov et al. (2003).

3. Ionisation Degree

To build the reduced chemical network that could be used to compute ionisation fraction in molecular clouds we adopted the following approach. First, the model was computed with the full chemical species set. Then, with the abundances of all species corresponding to $t = 0 - 10^7$ years, we estimated which of them are needed to estimate the abundances of dominant ions. Finally, we checked the reduced networks by comparing the ionisation degrees computed with the full and reduced networks.

In a purely gas-phase chemistry case, at $n_{\rm H} = 10^3$ cm^{-3} and high initial metal abundances, the dominant ions during most of the computational time are S^+ and Mg^+. By considering only ionised sulphur as an important species in species-based approach we can reduce the number of species from 395 to 123 and to achieve the computational speed gain of order of 25, but at the expense of $\sim$ 20% uncertainty at times approaching 10^7 years. If we consider both dominant ions to be important species, the number of species in the reduced set is 126, and the computational gain is almost the same with the uncertainty less than 10%. With the reaction-based reduction technique, we choose electron to be the only important species. In this case the number of necessary chemical reactions can be reduced from 3864 to 111 and the number of species from 395 to 58. The computational gain exceeds 500.

The low metallicity case is more complicated from the chemical point of view since in the absence of abundant metals the role of dominant electron suppliers goes to complex species involved in a more diverse chemistry. At this low density gas-dust connections are not important again. In the diffuse cloud case, the dominant ion is H_3^+ most of the time, however it alone does not determine the ionisation degree with enough accuracy. Errors are negligible at earlier times when the chemistry is relatively simple, however, after 10^4 years the error grows significantly, exceeding a factor of 3 at the end of computation. To account for later chemistry, one has to take into account another important ion, HCO^+. When these two species are designated as important, errors do not exceed 15% during entire computational time in the case of species-based

approach. However, due to the perplexed chemical connections of the two ions, the species set reduction is only modest in this case. About one hundred species can be excluded from the set with the reduction of the computational time by a factor of 3 (if errors like 200% cannot be afforded). The reaction-based algorithm is better suited for such situation. From the complicated chemistry involving H_3^+ and HCO^+ it is able to isolate 169 most important reactions, simultaneously reducing the number of species to 73. The speed gain in this case approaches 500, as in the high metallicity case.

Inclusion of accretion and desorption processes, as well as surface reactions, into the diffuse cloud model does not lead to any noticeable changes, primarily because the density is so low that it prevents the effective gas-grain interactions.

When no gas-dust interaction is taken into account, the case of dense cloud ($n_H = 10^7$ cm^{-3}) at high metallicity is qualitatively similar to the low-density case. The difference between high and low metallicity cases is much smaller for a dense cloud than for a diffuse cloud. In a denser environment, such chemically active ions as H_3^+ and HCO^+ are much less abundant, and metal ions dominate the ionisation degree both in high and low metallicity cases. As a result of this similarity, in a dense cloud reduced species sets are nearly the same both for high and low metallicity, with similar errors and computational gains.

The situation changes drastically, when gas-dust connection is taken into account. In high metallicity case, at early stages of the evolution the dominant ions are the same as in diffuse medium, i.e., metals. However, after 10^4 years the metal depletion becomes important, and the dominant ions are H_3^+ and HCO^+. Basically, a dense cloud at high metallicity with accretion and desorption processes behaves similarly to the low metallicity diffuse cloud.

In the low metallicity case, which is more diverse from the chemical point of view, difference between initial and final stages of the cloud evolution (separated by the moment when depletion takes over) is so prominent that the reduced network estimated from the final abundances is not valid at earlier phase, at $t < 10^4$ years, leading to a factor of 2 errors, even though it still predicts later abundances with much better accuracy (less than 20%). In order to take the two different stages into account, we build the reduced set for two times, $t \sim 10^3$ years and 10^7 years, and then use the combined set during the entire time span.

The addition of surface chemistry changes the evolution of the ionisation degree somewhat, but in the absence of effective desorption mechanisms these changes are not strong enough to affect the list of necessary species, so that it is possible to use the same reduced sets as in the case when only accretion and desorption are taken into account, with similar accuracy and computational

gain. Both methods are able to remove about two hundred species from the entire network with the gas-grain interaction (remember that the full network consists of 542 species in this case). This reduction provides the decrease of the computational time by a factor of a few. The greatest speed gain (~ 8) in the model with surface reactions included is achieved with the reaction-based technique due to its ability to remove not only excessive species but excessive reactions as well.

4. Carbon Monoxide

Reduction results for CO are more impressive if no surface chemistry is taken into account. For both metallicities and both cloud densities, the reduced set consists of no more than 35 species and provides accuracy better than 20%. Even though we build reduced sets for each of the considered models separately, it is possible to use a common reduced set for all of them with error less than 100%. This is true both in the case of the purely gas-phase chemistry and in the case when accretion and desorption processes are taken into account. The resulting speed gain is very large. In fact, while it takes about 5 minutes to run the full model, with the reduced network time needed to compute the CO abundance is lost in technical operations (like input/output etc.).

The reduction is most effective in a dense cloud. The reaction-based method shows that 8 species and 9 reactions completely determine the CO abundance when only gas-phase reactions are taken into account (for more details see Semenov et al., 2003).

The situation changes drastically again if surface reactions are switched on. In this case the species-based reduction is less effective. The reduced set contains about 340 species and produces overabundance of CO at later times, when depletion becomes important. The species-based reduction has the disadvantage of not being able to include properly surface molecules. To obtain reasonable results one has to add manually surface species that serve as sinks for surface CO, that is, CO_2 and HCO. The computational gain is only about 2. When surface reactions are taken into account, reaction-based reduction provides modest computational gain, too, though somewhat larger than species-based reduction, with more controllable accuracy and without the need of manual corrections. The speed gain is only about 3 in the high metallicity case, but reaches 16 in the low metallicity case.

So, the species-based reduction is an effective tool for constructing limited chemical networks in situations that do not involve surface chemistry. When

surface reactions are taken into account, species-based reduction is not that effective and reliable. The reaction-based method gives more impressive results.

5. Conclusions

We show that purely gas-phase chemical networks can be significantly reduced to compute electron and CO abundances in dark clouds. The computational gain varies from a few tens up to the point where the computational time needed for chemical modelling is lost in service operations. If the surface chemistry is included, both methods are only able to accelerate the computation by a factor of a few.

Acknowledgements

DS was supported by the German *Deutsche Forschungsgemeinschaft, DFG* project "Research Group Laboratory Astrophysics" (He 1935/17-1). Work of DW was supported by the INTAS grant YS 2001-1/91 and the RFBR grant 01-02-16206.

References

Ciolek, G.E., Mouschovias, T.Ch., 1993, ApJ 418, 774
Desch, S.J., Mouschovias, T.Ch., 2001, ApJ 550, 314
Glassgold, A.E., Langer, W.D., 1973, ApJ 179, 147
Gerola, H., Glassgold, A.E., 1978, ApJS 37, 1
Hasegawa, T.I., Herbst, E., Leung, C.M., 1992, ApJS 82, 167
Hasegawa, T.I., Herbst, E., 1993, MNRAS 263, 589
Millar, T., Farquhar, P., Willacy, K., 1997, A&AS 121, 139
Rae, J.G.L., Bell, N., Hartquist, T.W., et al., 2002, A&A 383, 738
Ruffle, D.P., Rae, J.G.L., Pilling, M.J., Hartquist, T.W., Herbst, E., 2002, A&A 381, L13
Shematovich, V., Wiebe, D., Shustov, B., 1997, MNRAS 292, 601
Semenov, D., Wiebe, D., Henning, Th., 2003, "Reducing and Analyzing Chemical Networks", Comm. Konkoly Obs. 103, proc. of the conf. "The interaction of stars with their environment II.", eds. Cs. Kiss et al., p.59

Molecular Emission from G345.01+1.79

S.V. Salii[1], A.M. Sobolev[1], N.D. Kalinina[1] S.P. Ellingsen[2], D.M. Cragg[3], P.D. Godfrey[3], P. Harjunpää[4], I.I. Zinchenko[5]

[1]Astronomical Observatory of Ural State University
620083, Ekaterinburg, Lenin str. 51, Russia
E-mail: Svetlana.Salii@usu.ru, Andrej.Sobolev@usu.ru
[2]University of Tasmania, Hobart, Australia
[3]Monash University, Clayton, Australia
[4]Helsinki University, Helsinki, Finland
[5]Institute of Applied Physics, N.Novgorod, Russia

Abstract

We present SEST observations of G345.01+1.79 in maser and 'quasi-thermal' lines of CH_3OH, lines of SiO, CS and some other shock tracing molecules. For the first time weak methanol maser emission was detected at frequencies 165.05 and 165.06 GHz. The observed 'quasi-thermal' CH_3OH and SiO (2-1) lines display pronounced blue wings confined to the G345.01+1.79(S) position. Velocities of CH_3OH and OH maser features lie well within the wing. So, there is a high probability that interaction of the wind from the young star with ambient material is responsible for the creation of masers and production of the blue non-gaussian wing. Comparison of velocities for 'quasi-thermal' and maser lines shows that the bow shock velocity relative to the bulk of cloud material is about 10 kms^{-1}. So, most probably we are dealing with the first clear example of an ultracompact HII region moving through a molecular cloud. Modelling of CH_3OH 'quasi-thermal' emission and consideration of maser profiles shows that the cloud material is greatly inhomogeneous.
Keywords: *stars: formation – ISM: clouds – ISM: molecules – radio lines*

1. Introduction

The southern molecular cloud G345.01+1.79 (hereafter G345) shows various signs of interaction of young massive stars with their environment.

G345 displays strong emission in methanol (CH_3OH), hydroxyl (OH) and water vapor (H_2O) maser transitions (Caswell et al., 1995b; Caswell & Haynes, 1983; Caswell et al., 1983; Braz & Epchtein, 1983). VLBI observations have shown that the source contains 2 Class II CH_3OH maser sites, G345(S) and G345(N), according to Norris et al. (1993) notation. Positions of OH masers

coincide with those of CH_3OH masers in G345(S) (Caswell, 1997; Caswell et al., 1995b). H_2O masers in G345 are situated apart from IRAS point source and near infrared sources (NIR) (Testi et al., 1994). They presumably correspond to the sites containing young stellar objects (YSO) at the stages preceding formation of ultracompact HII regions (UCHII)(Cesaroni et al., 1997). Observations by Testi et al. (1994) have shown that the G345(S) OH maser site is situated at the edge of a strong NIR source coincident in position with IRAS16533-4009. Infrared spectrum obtained by Volk et al. (1991) indicates that this source is an UCHII. Interferometry by Caswell (1997) places CH_3OH and OH masers in G345(S) on the western side of UCHII radio continuum image.

2. Observations

The observations were made in October 1997 and March 1999 with the SEST(Swedish-ESO Submillimetre Telescope, La Silla, Chile). The molecular cloud was mapped in SiO(2-1), CH_3OH $5_K - 4_K$ and $C^{34}S$(5-4) lines. Altogether 54 positions were observed with a $20''$ spacing. Direction ($\alpha_{1950.0} = 16^h53^m19.7^s$, $\delta_{1950.0} = -40°09'46''$) toward the methanol maser cluster G345(S) was chosen as a map center. A number of additional lines were observed toward this position. Full list of observed lines includes 32 lines of CH_3OH and the lines of SiO, HCN, HCO^+, DCN, $C^{34}S$, $C^{33}S$, $C^{18}O$, ^{13}CO, H_2S, and SO at frequencies around 80, 86, 88, 96, 110 156, 165, 216 and 241 GHz.

3. SiO

The SiO(2-1) and (5-4) lines peak at V_{LSR} about –15 kms^{-1}. They exhibit asymmetric wing emission extending from about –50 kms^{-1} on the blue-shifted side to +10 kms^{-1} on the red-shifted side. In the SiO(5-4) spectrum the blue wing is more pronounced while the intensity of this line is lower. The SiO(2-1) spectrum towards the map center is shown in Fig.1.

Velocity channel maps for the SiO(2-1) emission over the range –50→ 10 kms^{-1} are shown in Fig.2. The wing emission in four ranges corresponding to high-velocity and low-velocity blue-shifted wings ($-50 \rightarrow -25$ kms^{-1} and $-25 \rightarrow -18$ kms^{-1}, respectively), and low- and high-velocity red-shifted wings ($-12 \rightarrow -8$ kms^{-1} and $-8 \rightarrow 10$ kms^{-1}, respectively) are shown as contour maps. The distribution of the line core emission ($-18 \rightarrow -12$ kms^{-1}) is shown as a grey scale image in each panel.

SiO emission from the quiescent gas ($-18 \rightarrow -12$ kms^{-1}) peaks near the

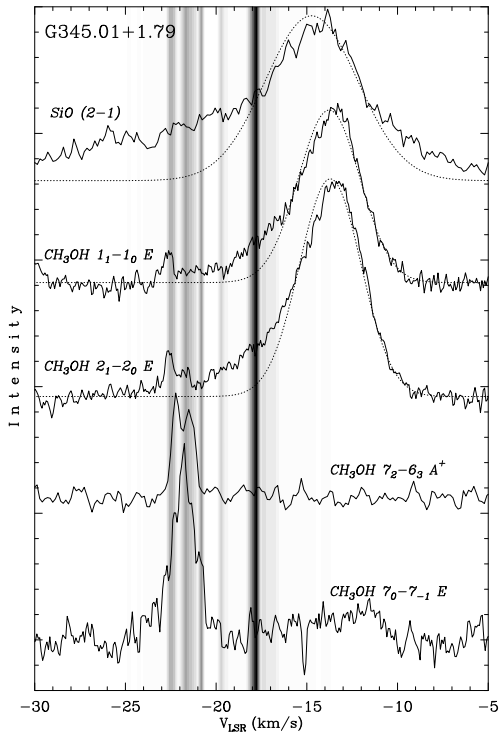

Figure 1: Non-gaussian wings in the spectra of SiO (2-1) and CH_3OH quasi-thermal lines and weak CH_3OH maser lines toward G345(S). Intensity of SiO (2-1) line is 0.6 K, intensities of the CH_3OH lines are listed in the table. Spectrum of the CH_3OH $5_1 - 6_0$ A^+ maser line is shown by shades of grey

methanol maser cluster G345(N). The low-velocity wing emission ($-25 \rightarrow -18$ and $-12 \rightarrow -8\,\mathrm{kms}^{-1}$) is extended. The emission in the low-velocity blue wing is more extended and the intensity maximum is located $10''$ west of G345(N), while emission in the low-velocity red wing peaks $30''$ east of G345(N).

The high-velocity blue-shifted wing emission ($-50 \rightarrow -25\,\mathrm{kms}^{-1}$) is clearly concentrated to the western side of the map and the intensity maximum lies at $(20'', 20'')$, i.e., about $30''$ west of G345(N). Weak high-velocity red-shifted emission ($-8 \rightarrow 10\,\mathrm{kms}^{-1}$) arises predominantly east of G345(N). Separate blue- and red-shifted high-velocity wing emission regions suggest the presence of a bipolar molecular outflow. Its central source is probably located near G345(N) and its projected position angle in the plane of the sky is close to 90°.

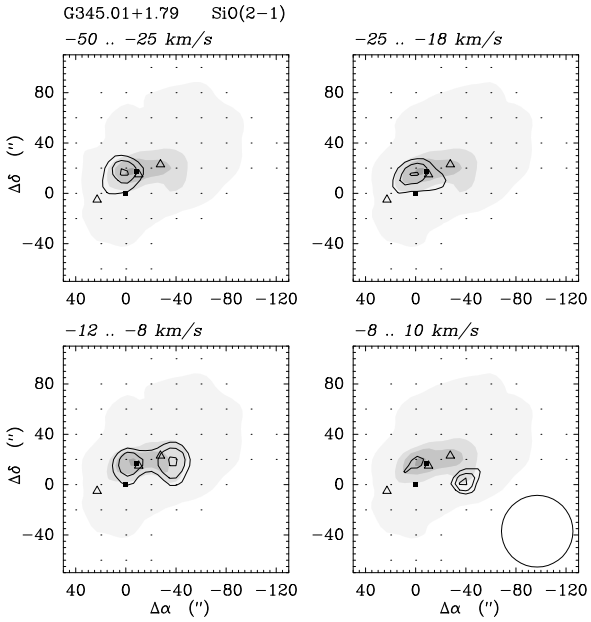

Figure 2: Channel maps of the SiO line wing emission (contours) superimposed on the line core emission (grey scale). The locations of 6.7 GHz methanol maser sites G345(S) and G345(N) are marked by filled squares, and locations of H_2O masers (Caswell et al., 1983) are marked by open triangles. The half power beam size is shown in the lower right panel

4. Methanol

Distribution of methanol emission in G345 resembles that of SiO. However, CH_3OH lines are considerably narrower indicating that turbulent motions are more developed in SiO abundant regions.

CH_3OH lines manifest strong and extended non-gaussian wings (see Fig.1). The blue wing is most pronounced at the map center. Noteworthy that velocities of components of the brightest CH_3OH maser ($5_1 - 6_0$ A^+ at 6.7 GHz) toward G345(S) correspond to velocities of the blue wing of the CH_3OH and SiO lines (Fig.1).

One remarkable feature of the G345(S) maser site is that the maser spots show clear increase in V_{LSR} with the distance from the center of UCHII (Norris et al., 1993). Such a velocity pattern corresponds well to the motions of matter in the wake of the bow shock produced by the movement of UCHII ionizing star toward the observer (Van Buren et al., 1990; Raga et al., 1997).

Other feature of G345(S) is that maser spots show dramatic increase in the ratio of fluxes of 6 GHz and 12 GHz methanol maser lines (hereafter F6 and F12, respectively) with the distance from UCHII center. Indeed, comparison

Table 1 CH_3OH weak maser components of molecular cloud G345.01+1.79

Frequency MHz	Transition	Area $Kkms^{-1}$	V_{LSR} kms^{-1}	ΔV_{LSR} kms^{-1}	T_A^* K
86903.06	$7_2 - 6_3 A^+$	0.46(0.02)	-21.82(0.03)	1.33(0.06)	0.33
156488.95	$8_0 - 8_{-1} E$	4.33(0.13)	-19.08(0.10)	3.33(0.22)	1.22
156602.42	$2_1 - 3_0 A^+$	1.32(0.13)	-20.62(0.10)	2.56(0.27)	0.49
156828.51	$7_0 - 7_{-1} E$	3.06(0.07)	-21.78(0.02)	1.76(0.05)	1.66
157048.62	$6_0 - 6_{-1} E$	3.98(0.12)	-21.11(0.05)	2.96(0.11)	1.27
157178.97	$5_0 - 5_{-1} E$	4.72(0.13)	-21.24(0.04)	2.88(0.10)	1.54
157246.10	$4_0 - 4_{-1} E$	3.82(0.12)	-21.73(0.04)	2.99(0.13)	1.20
165050.19	$1_1 - 1_0 E$	0.06(0.01)	-22.64(0.06)	0.60(0.14)	0.09
165061.16	$2_1 - 2_0 E$	0.12(0.02)	-22.46(0.09)	1.12(0.23)	0.10
216945.60	$5_1 - 4_2$ E	0.27(0.14)	-20.45(0.92)	3.29(1.57)	0.08

with spectra from Caswell et al. (1995a,b) show that F6/F12 is about 0.35 for the –23.8 kms^{-1} feature and increases to more than 150 for the –18 kms^{-1} feature.

From the point of view of Class II CH_3OH maser modelling given in Sobolev et al. (1997a,b) such an F6/F12 behavior for the bright maser spots can be explained by the increase of UCHII emission dilution, decrease in hydrogen number density and increase of maser beaming with the distance from UCHII center. Increase of dilution of UCHII emission with offset is straightforward. However, the difference in F6/F12 is too big to be explained by this effect alone. So, we think that the phenomenon is borne by combined action of mentioned factors. This is likely to take place since the increase of offset from the head of bow shock is followed by 1) increasing CH_3OH column density of less dense material and 2) increasing ratio of radial to tangential dimensions of emitting region which brings higher beaming.

In order to elucidate the situation with weaker Class II CH_3OH masers in G345(S) we performed observations of methanol maser candidates.

In the 10 lines listed in the table we detected components with velocities –24 – –20 kms^{-1} which are about 10 kms^{-1} lower than velocities of the quasi-thermal methanol lines. At the same time they show good agreement with velocities of maser features observed in Class II maser lines (Fig.1). The lines are narrow and we believe that they are really masers despite their quite low intensities. Our observations borne clear detection of new weak methanol masers at 165.05 and 165.06 GHz and marginal detection of maser at 216.9 GHz.

Maser modelling presented in Sobolev et al. (1997b) shows that different maser lines may form in different regimes. This is in accordance with our observations displaying noticeable difference in the line profiles shown in Fig.1.

Thus, observations of weaker methanol maser lines indicate that the physical conditions in G345(S) maser formation region are strongly inhomogeneous.

5. Non-LTE modelling of methanol emission

The LVG modelling of methanol emission at map center position provides much better fit than the rotational diagram (see Fig.3) indicating that excitation of methanol lines in this object exhibits great departures from LTE. Moreover, considerations of the previous sections provide evidence that molecular material in G345 is greatly inhomogeneous.

So, we dared to make a step further in order to investigate possible variation of parameters of cloud constituents. In order to do that we applied 2-component LVG modelling of quasi-thermal emission in methanol lines. Fig. 3 clearly shows that the 2-component modelling provides much better fit to observational data. Results of this modelling demonstrate inhomogeneity of molecular material in G345 and will be described in a separate paper.

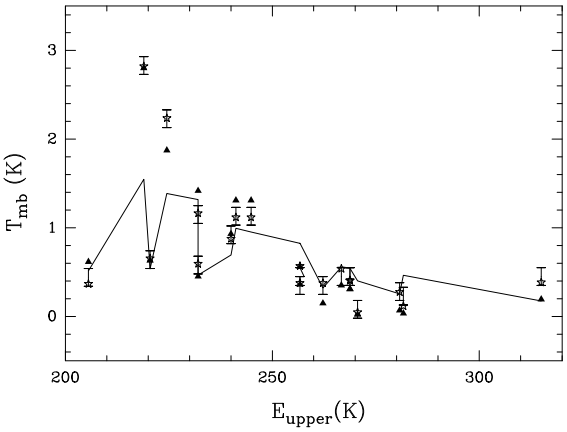

Figure 3: Results of LVG modelling of emission in 'quasi-thermal' methanol lines from map center position. Error bars show observed intensities; solid line connects intensities of rotational diagram; triangles show intensities of the best 1-component LVG fit and stars show intensities from 2-component LVG modelling

6. Conclusions

The G345.01+1.79 cloud was observed in a number of molecular lines. For the first time a weak methanol maser emission in the lines at 165.05 and 165.06 GHz was detected. Maser component in the 216.94 GHz line was marginally detected.

Presence of extended emission of shock tracing molecules shows that the molecular material in the cloud is greatly affected by the passage of shock waves.

Analysis of SiO line emission indicates possible presence of an outflow.

Consideration of the data on methanol and hydroxyl masers in G345(S) maser site suggests that these masers are formed in the region affected by the passage of bow shock borne by interaction of the wind from the young star moving toward the observer with material of the bulk of the G345 cloud. This hypothesis explains observed maser spectra and velocity pattern of maser spots.

LVG modelling of methanol line emission and consideration of methanol maser line profiles show that the molecular material in G345 is greatly inhomogeneous.

Acknowledgements

Studies were supported by INTAS, RFBR and ARC.

References

Braz, M.A., Epchtein, N. 1983, A&AS 54, 167
Caswell, J.L., 1997, MNRAS 289, 203
Caswell, J.L., Batchelor, R.A., Forster, J.R., Wellington, K.J., 1983, Austral.J.Phys. 36, 401
Caswell, J.L., Haynes R.F., 1983, Austral.J.Phys. 36, 361
Caswell, J.L., Vaile, R.A., Ellingsen, S.P., Norris, R.P., 1995a, MNRAS 274, 1126
Caswell, J.L., Vaile, R.A., Ellingsen, S.P., et al., 1995b, MNRAS 272, 96
Cesaroni, R., Felli, M., Testi, L., et al., 1997, A&A 325, 725
Norris, R.P., Whiteoak, J.B., Caswell, J.L., et al., 1993, MNRAS 412, 222
Raga, A.C., Mellema, G., Lundqvist, P., 1997, ApJS 109, 517
Sobolev, A.M., Cragg, D.M., Godfrey, P.D., 1997a, A&A 324, 211
Sobolev, A.M., Cragg, D.M., Godfrey, P.D., 1997b, MNRAS 288, L39
Testi, L., Felli, M., Persi, P., Roth, M., 1994, A&A 288, 634
Van Buren, D., MacLow, M.M., Wood, D.O.S., Churchwell E., 1990, ApJ 353, 570
Volk, K., Kwok, S., Stencel, R.E., Brugel, E., 1991, ApJS 77, 607

Young Stars

ISOPHOT Observations of the Circumstellar Environment of Young Stars

P. Ábrahám

Konkoly Observatory of the Hungarian Academy of Sciences
H-1525 Budapest, P.O. Box 67, Hungary
E-mail: abraham@konkoly.hu

Abstract

ISOPHOT, the photometer on-board the *Infrared Space Observatory*, provided new photometric and spectrophotometric data on a number of pre-main sequence stars in the 2.5–200μm wavelength range. We review the capabilities of ISOPHOT for observing YSOs, briefly report on several projects related to Herbig Ae/Be, T Tau, and FU Ori-type stars, and describe our plans for compiling a homogeneous and easy-to-use photometric catalogue of all young star observations perfomed by ISOPHOT.

Keywords: *Star formation: Herbig Ae/Be stars, T Tau stars, FU Ori stars – Circumstellar matter: accretion disks – instrument: ISO, ISOPHOT – observations: photometry, spectrophotometry*

1. Introduction

In the early phases of their evolution stars are intimately linked to their environment. The spatial and density structure of their circumstellar disk/envelope can be traced by thermal emission of the dust component at infrared wavelengths. 15 years after the successful IRAS mission the *Infrared Space Observatory* (ISO, Kessler et al., 1996) provided new infrared data on the Young Stellar Object (YSO) population during its 28 months cryogenic phase.

Four years after the ISO mission, however, only part of this rich database is published and many observations are still waiting for analysis in the public ISO Archive*. This is also true for ISOPHOT, the imaging photo-polarimeter on-board ISO (Lemke et al., 1996). In many cases the original observers stopped working on their data because (i) the consolidation of the instrumental calibration took several years (and is still on-going for certain observing modes) and this timescale did not fit into the publication plan of the observers; (ii) the necessary exposure time per object turned to be longer than was anticipated prior the mission thus the target list of the proposals had to be cut back seriously.

*www.iso.vilspa.esa.es/IDA

For some proposals of statistical nature the original scientific goal became unrealistic and the observers were not interested in analysing a limited number of individual sources instead of evaluating statistical samples. All these data are freely downloadable now from the ISO Archive for analysis and publication.

In this contribution we discuss ISOPHOT observations of YSOs, with the hope of triggering new interest in the analysis of the archive data. First we review the main technical parameters of ISOPHOT, with special emphasis on the possibilities which could bring new type of information on YSOs. Then, as example, I report on several on-going or finalized YSO projects I was involved in. Finally, future plans are summarized concerning the publication of all YSO-related ISOPHOT data in a photometric catalogue. This catalogue could also be of great help in designing observations for future infrared space missions.

2. ISOPHOT's capabilities for observing YSOs

For a general description of the ISOPHOT instrument we refer to the ISOPHOT Handbook (Laureijs et al. 2002). In this section we discuss only those instrumental aspects which turned to be of special importance for YSO observations.

Photometry: multi-filter observations. The four photometric points of IRAS at 12, 25, 60, and 100μm were useful in identifying YSO candidates but were not sufficient to constrain models on morphology, mass and temperature distribution, heating mechanism and chemical composition. ISOPHOT was designed to provide SEDs in the 3.6–200μm range with much finer spectral sampling. The observer could select up to 24 filters, some of them centred on specific wavelengths, e.g. on PAH emission feaures. In practice typically not more than 4–10 filters were used (with higher preference for the broad-band continuum as well as the IRAS-compatible filters) due to time limitations. Because of the large variety of selectable observing modes, detectors, filters, and apertures, a single accuracy figure cannot be derived for ISOPHOT.

Photometry: spatial resolution. Though the mirror diameters of IRAS and ISO were identical (60 cm), ISOPHOT's design allowed to reach higher spatial resolution. It was a great advantage in observations of YSOs which are often located within dense molecular clumps. ISOPHOT's higher spatial resolution at far-infrared wavelengths was crucial to reduce contamination by the clumps' emission and obtain more precise photometry of the central source.

Shortward of 100 micron a series of apertures was available, and the one matching best the Airy-disk could be selected by the observer. In the 60–105μm range a 3×3 mini-camera could be used, whose pixel size of 43.5″×43.5″ was larger than ideal for matching the PSF (FWHM: 21″ at 60μm, 37″ at 105μm), but it represented a significant improvement compared to the 100 micron detectors of IRAS (3′×5′). At $\lambda > 105\mu$m a 2×2 camera with pixel sizes of 89″×89″ was available. Its angular resolution – dictated again by the pixel size rather than by the PSF – was 1.5′×1.5′, in the order of the IRAS 100 micron detector. Unfortunately, in many observations larger than ideal apertures were used and confusion within the beam remained one of the main limiting factors for the accuracy of far-infrared ISOPHOT observations.

There were a number of observations intended to resolve the extended envelopes of selected YSOs. Most of these measurements, however, utilized the PHT32 (oversampled) observing mode which suffered from serious instrumental problems and is still difficult to calibrate. On the other hand, observations in other modes were able to measure the size of small extended sources of 30–60″.

Mid-infrared spectrophotometry of YSOs is a good tool to detect – in addition to the continuum due to photospheric emission or to radiation of the inner warm part of the accretion disk – broad spectral features like the one of amorphous silicate around 9.7μm, the set of features attributed to PAHs (3.3, 6.3, 7.7, 8.6, 11.3μm), interstellar ices towards deeply embedded objects, the signature of crystalline silicate, etc. The grating spectrophotometer ISOPHOT-S covered simultaneously the 2.5–4.9μm and 5.8–11.6μm ranges with a spectral resolution of about 100, and delivered low-resolution spectra of young objects too faint for the higher resolution ISO-SWS instrument.

Far-infrared mapping. Star forming regions as well as the environment of YSOs could be mapped with the two far-infrared cameras. Especially the $\lambda > 100\mu$m maps are unique and provide information on molecular cloud structure, on the initial phases of star formation, and on the distribution of cold dust in the vicinity of more evolved YSOs.

Polarimetry. For completeness we mention the polarimetric capability of ISOPHOT which was used only occasionaly for young stellar objects. An example for such a programme which searched for polarization towards NGC 7538 IRS9, HH 100 IR, and L1551 IRS5 at 25 micron was presented by Wright & Laureijs (1999).

Simultaneous SED. The possibility to observe the full 3.6–200μm SED and obtain mid-infrared spectrophotometry quasi-simultaneously (within a timescale of 1-2 hours) was important for some projects looking for temporal variation of the infrared emission. As an example we refer to Sect. 3.4 where photometric observations of five FU Ori-type stars are presented.

3. ISOPHOT observations of young stars

A number of ISOPHOT observing programmes were initiated to obtain detailed SEDs of young stars. The results are usually compared with model predictions; first of all with the expected spectral shape of a geometrically-thin, optically-thick circumstellar disk ($\lambda F_\lambda \propto \lambda^{-4/3}$). Deviations from this shape are interpreted in terms of structural changes in the circumstellar matter: deficiency at near-infrared wavelengths may indicate an inner hole while a too high far-infrared flux (which is typically the case) is the signature of a flared outer disk or of an envelope. Low-density gaps dynamically cleared by companions cause dips in the SED at the corresponding wavelengths.

3.1. Far-infrared photometry of Herbig Ae/Be stars

Herbig Ae/Be stars represent the pre-main sequence evolutionary phase of intermediate mass (2–8 $M_\odot$) stars. We observed 7 of these stars to deduce the structure of their circumstellar matter from the SEDs (Ábrahám et al. 2000). Since Herbig Ae/Be stars are often embedded in dense molecular clumps ISOPHOT's higher spatial resolution at far-infrared wavelengths was crucial to reduce contamination by the clumps' emission. Fig. 1 presents our results for two stars.

The SED of LkHα 233, composed of ISOPHOT and IRAS photometry as well as data from the literature, can be described by a power-law in the 5–60μm range. The peak of the SED was predicted at around 100μm by the earlier IRAS measurement, but our 90μm photometry showed that the larger beam of IRAS was contaminated at this wavelength and the circumstellar region of LkHα 233 contains mainly material warmer than 90 K (see Fig. 1). A high resolution ISOPHOT scan at 150μm (not presented here) supports this result by detecting only the clump with no indication for the star. These results fully support a geometrically thin accretion disk model for LkHα 233 as proposed by Leinert et al. (1993).

The other Herbig Ae/Be star, MWC 1080, shows a completely different SED: the flux density is constant in the mid-infrared but the spectrum exhibits a steep raise starting between 20 and 25μm as revealed by the ISOPHOT data

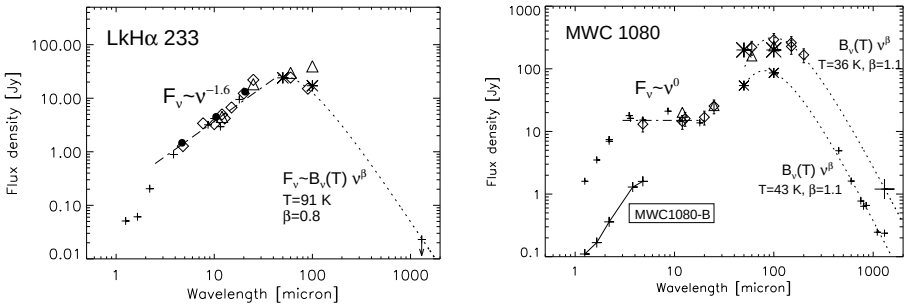

Figure 1: Spectral energy distributions of 2 Herbig Ae/Be stars. *Diamonds:* ISOPHOT; *dots:* UKIRT/MAX; *triangles:* IRAS; *small plus signs and asterisks:* ground-based and KAO observations of small beam size; *large plus signs and asterisks:* ground-based and KAO observations of large beam size (from Ábrahám et al. 2000).

points at these two wavelengths. The strong emission peak centred at 100μm has been thought to originate from the circumstellar region of the star. The typical temperature of the emitting material, however, is almost the same in the large 3′ beam of ISOPHOT and in the smaller ∼20″ aperture used in several KAO and SCUBA observations. The lack of temperature gradient towards the central source indicates that the heating of the emitting dust is independent of MWC 1080, and is more likely due to the embedded cluster of stars seen on K-band images around the Herbig star. Thus models of the circumstellar structure of MWC 1080 do not have to reproduce the far-infrared peak of the SED which is to a large extent unrelated to the central source. The true far-infrared spectrum of MWC 1080 at $\lambda > 20\mu$m cannot be determined from our observations because it would require a significantly higher spatial resolution than available at the moment.

3.2. Circumstellar structure of T Tauri stars

In an on-going project we are studying 34 T Tauri-type stars by analysing their 3.6–200μm SEDs composed of 8–12 ISOPHOT photometric bands. More than half of the sample consists of binary stars. Our goals are twofold: (1) taking advantage of the unprecedented filter coverage of ISOPHOT we determine a detailed SED and compare it with models, e.g. the ones proposed by Chiang & Goldreich (1997); (2) in a young binary system the evolution of the circumstellar disks may depend on the separation and the orbits of the components. Sorting

the binaries in our sample according to the separation of their components and looking for systematic changes in the shape of their SEDs we could shed some light on the size and structure of the circumstellar disks in binary systems. Since the flux density of T Tau stars typically varies within one order of magnitude in the whole infrared range, this comparison requires photometric accuracies around 10% which is a challenge even to the present calibration of ISOPHOT. On the other hand contamination in the beam is less problematic than in the cases of Herbig Ae/Be stars, since T Tau stars are usually not able to heat up their environment creating an extended emitting area around the source.

In Fig. 2 we present some preliminary results. The SED of AK Sco, a binary system, is an example for a rather typical case: the infrared excess emission follows a power-law in the 15–60μm range and peaks around 60μm. At longer wavelengths the emission drops quickly demonstrating the lack of a significant amount of cold dust in the system. The environment of MWC 863 is probably different from that: the emission peak at 20μm indicates a higher average dust temperature, i.e. the outer part of the accretion disk seems to be completely missing. The SED of LkHα 332-20 is virtually very noisy. However, the high flux around 10μm originates from a strong silicate emission feature, and the alternation of peaks and dips at 25, 60, and 100μm are reproduced by the earlier IRAS data, too. Thus the relatively low 60μm emission might be a signature of a low-density ring in the disk.

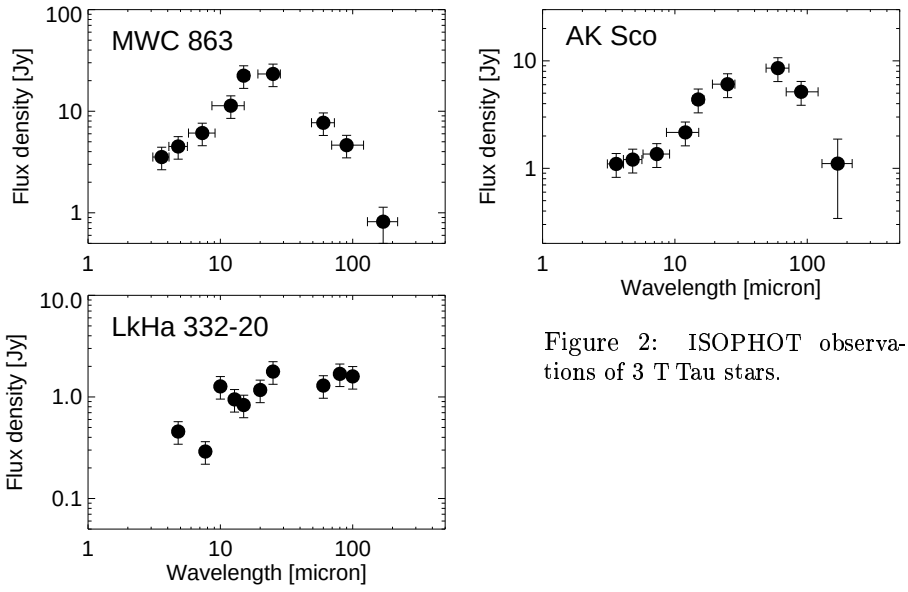

Figure 2: ISOPHOT observations of 3 T Tau stars.

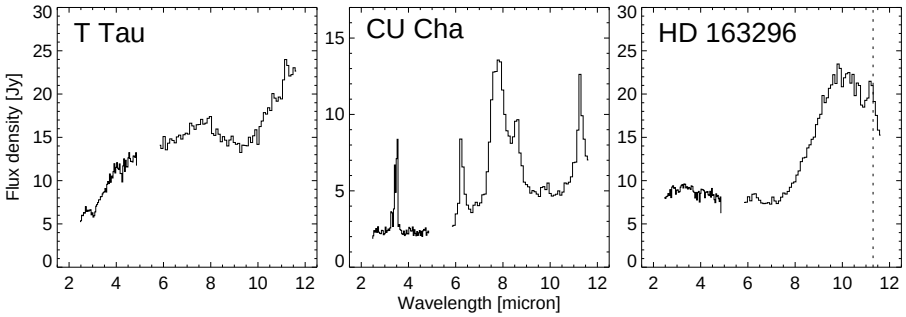

Figure 3: Mid-infrared spectrophotometry of 3 YSOs. T Tau exhibits a strong silicate absorption at 10μm, probably due to the infrared component T Tau-S. CU Cha, an A0-star, emits enough UV photons to excite PAH molecules. In HD 163296 the weak emission feature at 11.3μm on top of the strong 10μm amorphous silicate emission was also observed by ISO-SWS and is attributed to the presence of crystalline silicate.

3.3. Mid-infrared spectrophotometry of YSOs

During the ISO mission the ISOPHOT-S subinstrument performed about 90 observations on YSOs. We are working on an atlas including all these measurements. The atlas will contain 23 observations of embedded objects, 26 spectra of T Tau stars, 17 intermediate-mass pre-main sequence stars, as well as repeated observations of several FU Ori, EX Lup, and UX Ori-type objects. Fig. 3 shows three spectra as examples.

3.4. Evolution of FU Ori-type stars as seen by ISOPHOT

An FU Ori outburst is defined as a dramatic increase in the brightness of a T Tauri-type star (ΔV=4–6 mag). Since the phenomenon is connected to the circumstellar medium (probably caused by the increased accretion rate) the infrared emission spectrum is also expected to change during and after the outburst. The wavelength dependence of the change – which has never been observed before – provides crucial information on this physics of the phenomenon.

We studied 5 FU Ori stars and compiled their SEDs from the ISOPHOT data supplemented with other (2MASS, MSX, etc.) observations performed during the ISO mission (1995-98). These SEDs were compared with 15 years earlier ones derived from the IRAS photometry as well as from ground-based observations carried out around 1983. In 3 cases no difference between the two epochs was seen within the measurement uncertainties, but in one case the

shorter wavelength part of the spectrum ($\lambda \leq 20\mu$m) has decreased by a factor of 2, and in the 5th case a marginal fading was observed. The definite case (V1057 Cyg) shows wavelength-independent fading below 20μm, indicating that the energy source of the inner part of the disk is more re-processed starlight than accretion luminosity. We plan to analyse also similar observational sequences of several other FU Ori and EX Lup type stars.

4. Future work

At Konkoly Observatory we plan to collect and publish all YSO observations of ISOPHOT in a photometric catalogue which, together with the ISOPHOT-S spectral atlas, could be part of ISOPHOT's heritage in the field of star formation. In the catalogue also size of the objects and predicted confusion noise will be included. The database will serve as input catalogue for proposals for future infrared instruments like SIRTF and Herschel.

Acknowledgements

This work has been partly supported by Hungarian Research Fund (OTKA T037508). P.Á. acknowledges the support of the Bolyai Fellowship.

References

Ábrahám, P., Leinert, Ch., Burkert, A., et al., 2000, A&A 354, 965
Chiang, E.I., Goldreich, P., 1997, ApJ 490, 368
Kessler, M.F., Steinz, J.A., Anderegg, M.E., et al., 1996, A&A 315, L27
Laureijs, R.J., et al., 2002, The ISO Handbook Vol. IV, ESA SAI-99-069/Dc, Ver.2.0
Leinert, Ch., Haas, M., Weitzel, N., 1993, A&A 271, 535
Lemke, D., Klaas, U., Abolins, J., et al., 1996, 1996, A&A 315, L64
Wright, C.M., Laureijs, R.J., 1999, ESA-SP 435, 49

Mid-infrared Observations of Brown Dwarfs and their Disks: First Ground-based Detection

D. Apai[1,2], I. Pascucci[1,2], Th. Henning[1,2], M.F. Sterzik[3], R. Klein[2], D. Semenov[2], E. Günther[4], B. Stecklum[4]

[1] Max Planck Institute for Astronomy
Königstuhl 17, Heidelberg, D-69117 Germany
E-mail:[1]apai@mpia-hd.mpg.de
[2] Astrophysical Inst. and University Obs. Jena
Schillergässchen 2-3, D-07745 Jena, Germany
[3] European Southern Observatory
Alonso de Cordova 3107, Vitacura, Casilla 19001, Santiago 19, Chile
[4] TLS Tautenburg
Sternwarte 5, D-07778 Tautenburg, Germany

Abstract

We present the first mid-infrared (MIR) detection of a field brown dwarf (BD) and the first ground-based MIR measurements of a disk around a young BD candidate. We prove the absence of warm dust surrounding the field BD LP 944-20. In the case of the young BD candidate Cha Hα2, we find clear evidence for thermal dust emission from a disk. Surprisingly, the object does not exhibit any silicate feature as previously predicted. We show that the flat spectrum can be explained by an optically thick flat dust disk.

KEYWORDS: *accretion, accretion disks — circumstellar matter — stars: individual (LP 944-20, Cha Hα2) — stars: low-mass, brown dwarfs*

1. Introduction

Brown Dwarfs (BDs) occupy the substellar mass domain. Having masses lower than 75 M_{Jup}, they are unable to burn hydrogen steadily. Although their presence has been already predicted in the sixties by Kumar (1963), their low luminosity delayed their discovery until 1995, when Nakajima et al. (1995) announced the first detection of a BD orbiting the nearby M-dwarf star Gl229A. Recently, the large-scale near-infrared (NIR) surveys 2MASS and DENIS – complemented by optical data – substantially increased the number of known field BDs. Additionally, deep NIR surveys of star-forming regions revealed hundreds of young BD candidates.

In spite of the rapidly growing number of known BDs (Basri, 2000), we do not know if they form like planets or like stars. Proposed scenarios include the straightforward star-like formation via fragmentation and disk accretion (Elmegreen, 1999), the ejection of stellar embryos (Reipurth & Clarke, 2001) from multiple systems and the formation in circumstellar disks like giant planets. The presence of disks and their properties are crucial in distinguishing between the various scenarios: a truncated disk (size of a few AU) would support the ejected stellar embryo hypothesis, a non-truncated one is the sign of stellar-like accretion, while BDs formed like planets should have no dust around them.

In the case of BDs, NIR data are not necessarily a good tracer of disk emission because they are strongly affected by molecular bands of the cool BD atmosphere. Since the emission of warm (100 - 400 K) circumstellar dust peaks around 10 μm, mid-infrared (MIR) excess emission – arising from dust grains close to the star – is the best tool to search for circumstellar disks. The MIR regime is best accessed by space-born telescopes, the last of which was the Infrared Space Observatory (ISO), operating between 1995 - 1998. However, the majority of BDs has been discovered too late to be targeted by ISO.

Up to now, only few BDs with MIR excess are known. These objects, identified in the ISOCAM archive, are located in the Cha I or in the ρ Ophiuchi star-forming regions (Persi et al., 2000; Comerón et al., 1998). Their substellar nature has been deduced from comparing NIR and optical measurements to evolutionary models (Comerón et al., 1998, 2000).

Natta & Testi (2001) proposed a model based on scaled-down disks around pre-main-sequence stars to explain the measured spectral energy distributions (SEDs).

In this paper we present results from our TIMMI2 MIR imaging campaign. Our aim was to detect MIR excess emission and thus to probe the presence of warm circumstellar dust around BDs. We targeted seven very close field BDs of various ages and a young BD candidate in the Cha I star-forming region. Our observations are the first data in the wavelength region of the silicate feature.

2. Observations

We carried out deep MIR observations with the 3.6m/ESO Telescope at La Silla (Chile) using the TIMMI2 camera (Reimann et al., 2000) in 2001 November and December. The targets were seven field BDs and a young BD in the Cha I star-forming region. From the closest field BDs, we selected those which seemed to be the youngest based on their brightness and spectral type.

We used the 9.8 μm filter, where the instrument is the most sensitive, to search for disk emission. In the case of the detected field BD we also complemented the 9.8 μm measurement with 5 and 11.9 μm observations; the BD detected in the Cha I region was also observed at 11.9 μm. We applied long exposure times (typically 2 hrs in each filter) in order to reach the $\sim$10 mJy sensitivity limit of the instrument. Extensive testing of the pointing accuracy shows a typical error not larger than 1.5" towards the Cha I star-forming region. This excludes any confusion with other sources.

3. Results

3.1. Field Brown Dwarfs

Among the seven targeted nearby field BDs, only the object LP 944-20 could be detected. The 3 σ upper limit of the flux density for the other sources is 15 mJy at 9.8 μm. As one of the youngest (475–650 Myr) and closest (5 pc) field BDs (Tinney, 1998), LP 944-20 was the most promising of our targets. Based on its optical spectrum, its spectral type is equal to or later than M9V (Kirkpatrick et al., 1997). Its classification as a BD has been confirmed by the presence of lithium in its photosphere (Tinney, 1998). Excellent atmospheric conditions and a long integration time led to the *first detection of a field BD in the MIR*. The fluxes measured at 5, 9.8 and 11.9 μm are 39 mJy, 24 mJy, and 22 mJy, respectively. These measurements correspond to more than 5 σ detections in each filter. We estimate a photometric error smaller than 15% for each measurement.

3.2. Cha Hα2

In contrast to the older field BDs, we found clear evidence for excess MIR emission in the case of the much younger (2 - 4.5 Myr) BD candidate Cha Hα2. The observed fluxes are 17$\pm$2 and 21$\pm$3 mJy at 9.8 and 11.9 μm, respectively. The object is close to or in the substellar domain, depending on its exact age (Comerón et al., 2000). There is some evidence that Cha Hα2 is actually a close binary with the components in the substellar domain (Neuhäuser et al., 2002).

4. Discussion

4.1. Field Brown Dwarfs

The non-detection of the six field BDs proves the lack of significant amount of warm dust around older field BDs. These data clearly show that the disk dissipation time is below a few 100 Myr, consistent with recent measurements of BDs in the young σ Orionis cluster (Oliveira et al., 2002). Even the detection of the closest target, the 475-650 Myr old LP 944-20, confirms this hypothesis. Compared to a simple blackbody with $T_\star$=2300 K, $R_\star$=0.1 $R_\odot$, D=5 pc (Tinney, 1998), it is clear that our measurements show no MIR excess, but the photospheric flux of the BD itself.

4.2. Disk Models for Cha Hα2

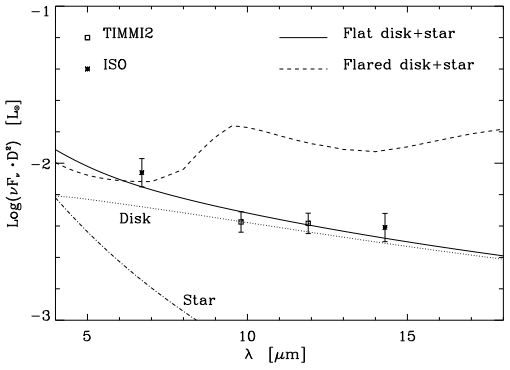

Figure 1: Modelled spectral energy distribution of a flat and a flared disk compared to the observations. Asterisks: ISOCAM measurements at 6.7 and 14.3 μm (20% error bars), while the squares are our TIMMI2 measurements at 9.8 and 11.9 μm (15% error bars).

Modelling the MIR excess emission of Cha Hα2 lead to a surprising result: the SED, plotted in Fig. 1 could be explained by an optically thick, flat disk but not by a T Tauri-like flared one. Fig. 2 shows the schematics of the two different models. A detailed description of the modelling is given in Pascucci et al. (2002).

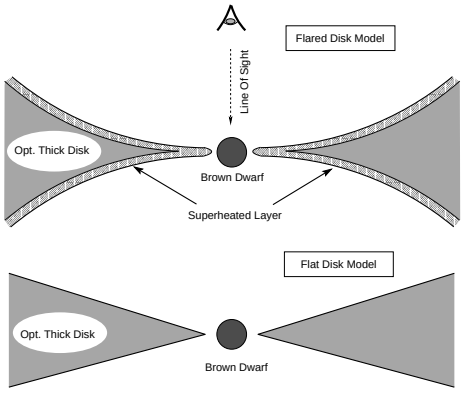

Figure 2: Cross sections of the flared and the flat disk model. The shaded area represents the optically thin superheated layer in the flared disk. This region is the source of the silicate emission feature. The flat disk lacks this disk atmosphere.

5. Summary

Our ground-based measurements represent a new way of probing the properties of disks around BDs, exploring their spectral energy distribution and therefore constraining model prescriptions. We prove the absence of the previously predicted silicate emission feature in the case of the face-on disk around the young BD-candidate Cha Hα2, one of the three known BD-candidates with MIR excess. An optically thick flat disk provides a perfect match to our data. Because no evidence for disks around older field BDs could be detected, disk dissipation times must be shorter than a few 100 Myr. Our results suggest that newborn BDs have disks like young, low-mass stars, but also indicate unexpected differences in their disk geometry. A detailed description of this work can be found in Apai et al. (2002).

References

Apai, D., Pascucci, I., Henning, Th., Sterzik, M. F., Klein, R., Dimitri, S., Günther, E., Stecklum, B., ApJ 573, L115

Basri, G., 2000, ARA&A 38, 485

Comerón, F., Rieke, G. H., Claes, P., Torra, J., Laureijs, R. J., 1998, A&A 335, 522

Comerón, F., Neuhäuser, R., Kaas, A.A., 2000, A&A 359, 269

Elmegreen, B.G., 1999, ApJ, 522, 915

Kirkpatrick, J.D., Henry, T.J., Irwin, M.J., 1997, AJ 113, 1421

Kumar, S.S., 1963, ApJ 137, 1121

Nakajima, T., Oppenheimer, B.R., Kulkarni, S.R., Golimowski, D.A., Matthews, K., Durrance, S.T., 1995, Nature 378, 463

Natta, A., Testi, L., 2001, A&A 376, L22

Neuhäuser, R., Brandner, W., Alves, J., Joergens, V., Comerón, F., 2002, A&A 384, 999

Oliveira, J.M., Jeffries, R.D., Kenyon, M.J., Thompson, S.A., Naylor, T. 2002, A&A 382, L22

Pascucci, I., Apai, D., Semenov, D., Henning, Th., 2003, Comm. Konkoly Obs. 103, proc. of the conf. "Interaction of Stars with their Environment II.", eds. Cs. Kiss et al., p.99

Persi, P., Marenzi, A.R., Olofsson, G., et al., 2000, ApJ 357, 219

Reipurth, G., Clarke, C., 2001, AJ 122, 432

Reimann, H.-G., Linz, H., Wagner, R., Relke, H., Kaeufl, H. U., Dietzsch, E., Sperl, M., Hron, J., 2000, in: "Optical and IR Telescope Instrumentation and Detectors", eds. M. Iye & A.F. Moorwood, ESO, Vol. 4008, 1132

Tinney, C.C. 1998, MNRAS 296, L42

Metamorphosis of a BD Disk: Flared Becomes Flat

I. Pascucci[1,2], D. Apai[1,2], Th. Henning[1,2], D. Semenov[2]

[1] Max Planck Institute for Astronomy
Königstuhl 17, Heidelberg, D-69117 Germany
[2] Astrophysical Inst. and University Obs. Jena
Schillergässchen 2-3, D-07745 Jena, Germany
E-mail:[1] pascucci@mpia-hd.mpg.de

Abstract

We conducted mid-infrared observations of the brown dwarf candidate Cha Hα2. We find that the predicted silicate feature does not appear in its spectral energy distribution (SED). In order to interpret the lack of this feature, we carried out analytical calculations adopting both flared and flat disk geometries. We show that, independently of the chosen parameter set and chemical composition, the flared disk model cannot explain the measured fluxes. On the contrary, the SED emerging from a flat disk fits well the observations.

Keywords: *accretion, accretion disks – circumstellar matter – stars: individual (Chamaeleon Hα2) – stars:low mass, brown dwarfs*

1. The importance of Brown Dwarf disks

Brown Dwarfs (BDs) occupy the substellar mass domain. Having masses lower than 75 M_{Jup}, they are unable to burn hydrogen steadily. In spite of the rapidly growing number of known BDs (Basri, 2000), we do not know if they form like planets or like stars. Proposed scenarios include:

▷ star-like formation via fragmentation and disk accretion (Elmegreen, 1999)
▷ ejection of stellar embryos from multiple systems (Reipurth & Clarke, 2001)
▷ formation in circumstellar disks like giant planets.

The presence of disks and their properties are crucial in distinguishing between the various scenarios: a truncated disk (size of a few AU) would support the ejected stellar embryo hypothesis, a non-truncated one is the sign of stellar-like accretion, while BDs formed like planets should have no dust around them.

Since the emission of warm (100 - 400 K) circumstellar dust peaks around 10 μm, mid-infrared (MIR) excess emission - arising from dust grains close to the star - is the best tool to search for circumstellar disks. Up to now, only few BD candidates with MIR excess have been identified in the ISO archive, all of

them located in the Cha I star-forming region (Persi et al., 2000). Their spectral energy distribution (SED) have been interpreted by Natta & Testi (2001) using a model based on scaled-down disks around pre-main-sequence stars. They followed the Chiang & Goldreich disk geometry which has been rather successful in describing SEDs of T Tauri and Herbig Ae/Be stars (Chiang & Goldreich, 1997).

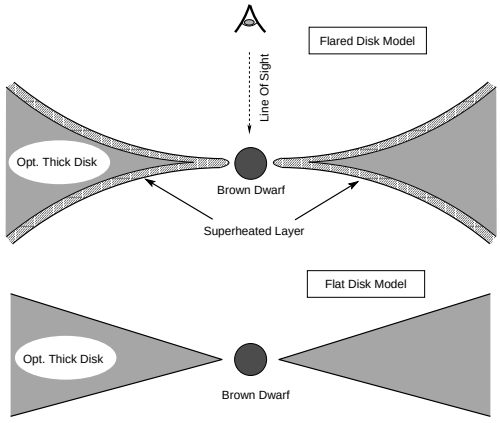

Figure 1: Cross sections of the flared and the flat disk model. The shaded area represents the optically thin superheated layer in the flared disk. This region is the source of the silicate emission feature. The flat disk lacks this disk atmosphere.

2. The flared disk model

The main assumption of the Chiang & Goldreich model is the flaring of the disk, which introduces a superheated surface layer, called the disk atmosphere (see Fig. 1). The major components of this model are: the star, the optically thin disk atmosphere and the optically thick disk interior. In the MIR the stellar radiation is well approximated by a black body, while the optically thick disk emission is given by a power law $F_\nu \propto \lambda^{5/3}$. A simple analytical formula (Natta et al., 2000) is used to describe the optically thin disk atmosphere, which is producing a strong silicate emission around 9.6 μm (Si-O stretching mode).

3. Towards the flat disk model

We observed the BD candidate Cha Hα2 at 9.8 and 11.9 μm using the TIMMI2 camera at the 3.6m/ESO Telescope at La Silla, Chile. Since we find the same

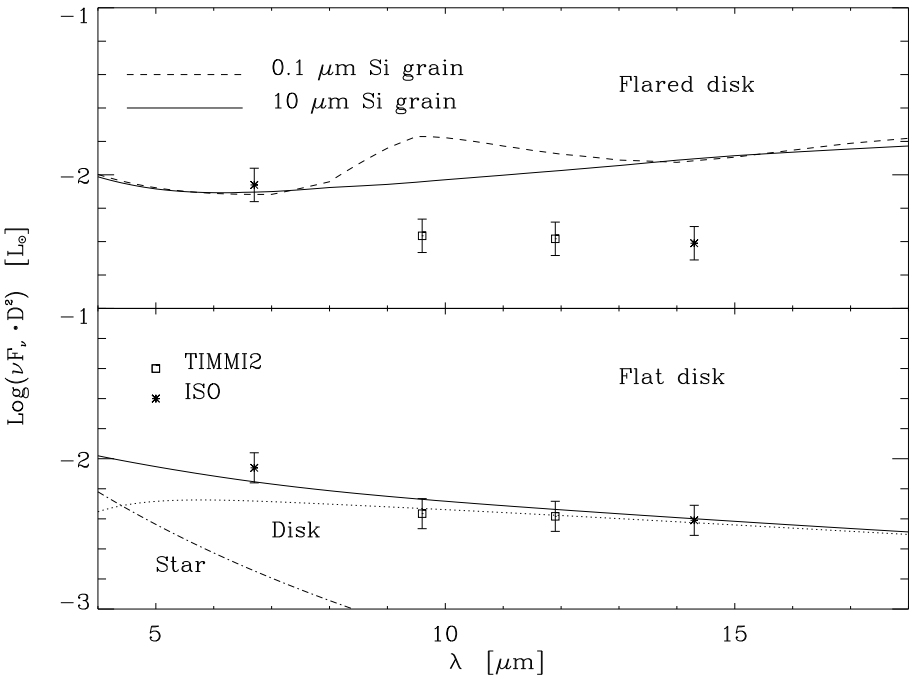

Figure 2: Upper panel: Modelled SED of a flared disk using two different silicate grain sizes. The silicate feature appears in emission for small 0.1 μm grains. The squares and the stars are measurements from TIMMI2 and ISO. Lower panel: Best fit model for an optically thick flat disk. The parameters of the model are as follows: D= 160 pc, $T_\star$ = 2550 K, $M_\star$ = 0.08 $M_\odot$, $L_\star$ = 0.035 $L_\odot$, R_{in} = 4.5 $R_\star$, R_{out} = 100 AU.

flux densities at the peak and on the wing of the feature, we exclude the presence of any silicate feature. This contradicts the prediction of Natta & Testi (Natta & Testi, 2001). We find that changing the disk geometry (inner and outer radii, scale height, inclination) is insufficient to fit the flared model. Altering the optical properties (or composition) of the dust grains has a stronger effect: the absence of the silicate feature could be explained by the lack of this dust component or the presence of large grains (radii larger than 5 μm). However, we stress that the power law continuum, predicted by the flared model, does not fit our data.

A much simpler and more straightforward solution is the assumption that

the BD is surrounded by an optically thick flat disk. We assume a power law disk with a surface density of $\Sigma \propto R^{-3/2}$ and a temperature of $T \propto R^{-3/4}$, typical of reprocessing and viscous disks (Shu, 1990). Since this disk is entirely optically thick, its SED is independent of the dust properties. The model does not show any feature. The continuum of a power-law flat disk has the observed slope. In Fig. 2 we compare the measurements with model predictions.

4. Conclusion

We prove that the lack of the silicate feature in the SED of the BD candidate Cha Hα2 cannot be explained by a T Tauri-like flared disk geometry. Our calculations show that an optically thick flat disk model reproduces the observations.

References

Basri, G., 2000, ARA&A 38, 485
Chiang, E.I., Goldreich, P., 1997, ApJ 490, 368
Elmegreen, B. G., 1999, ApJ 522, 915
Natta, A., Meyer, Michael R., Beckwith, Steven V. W., 2000, ApJ 534, 838
Natta, A., Testi, L., 2001, A&A 376, L22
Persi, P., Marenzi, A.R., Olofsson, G., et al., 2000, A&A 357, 219
Reipurth, B., Clarke, C., 2001, AJ 122, 432
Shu, F. H., 1990 in The Physics of Star Formation (Kluwer)

The Influence of External UV Radiation on the Evolution of Protostellar Disks

S. Richling[1], H.W. Yorke[2]

[1]Institute for Theoretical Astrophysics
University of Heidelberg, Tiergartenstr. 15, D-69121 Heidelberg
E-mail: richling@ita.uni-heidelberg.de
[2]Jet Propulsion Laboratory, California Institute of Technology
MS 169-506, 4800 Oak Grove Drive, Pasadena, CA 91109
E-mail: Harold.Yorke@jpl.nasa.gov

Abstract

We investigate the interaction of an external UV radiation field with protostellar disks of low-mass stars using 2D radiation hydrodynamical simulations. The disks are gradually destroyed via photoevaporation as the UV photons heat the gas in the outer layers of a disk to thermal escape velocities. Beside the UV flux and the luminosity of the stellar wind from the central star, the evolutionary state of the star-disk system at the onset of the external illumination determines the size and the form of the ionized envelope and the resulting spectral appearance of the object. Disks irradiated before one free-fall time after the collapse of the parental molecular cloud lose much of the associated material during the first 10^4 yr of evolution. The star-disk systems remain extremely small in comparison to star-disk systems first irradiated at later evolutionary phases, where the central objects are more massive and much of the clouds mass is already bound in the accretion disk. These results suggest that an early UV illumination favors the formation of low-mass cluster members.
Keywords: *circumstellar matter – hydrodynamics – HII regions – line: formation – radiative transfer – stars: formation*

1. Numerical Methods

We follow the evolution of protostellar disks under the influence of an external radiation field (Fig. 1.) by means of a 2D radiation hydrodynamics code. The code assumes axial symmetry and solves the hydrodynamical equations on nested grids (Yorke & Kaisig, 1995). The transfer of direct UV photons is calculated along lines of sight centered at the star located outside the computational domain. Diffuse UV photons originating from the recombination of hydrogen into the ground state and from scattering on dust grains are treated with the

flux-limited diffusion approximation. Simultaneously, we determine the ionization of hydrogen and carbon. A detailed description of the code is given in Richling & Yorke (1998, 2000).

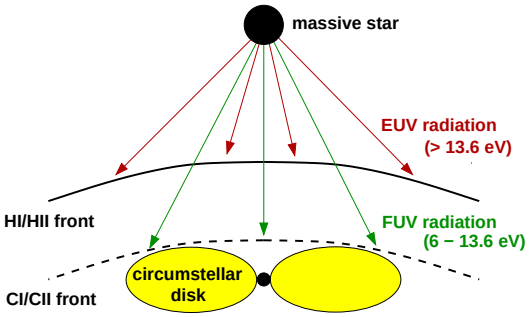

Figure 1: The ionizing radiation of a massive star interacts with a protostellar disk nearby. Both UV components are important.

In a second step, we use the density and temperature distribution of the gas and the velocity field obtained with the hydrocode to calculate emission line maps, continuum maps and spectral energy distributions via a ray-tracing procedure (Kessel et al., 1997). These diagnostic radiative transfer calculations allow us a direct comparison with observations.

2. Ionized Envelope and Micro-Jets

The calculations start with star-disk systems resulting from collapse simulations (Yorke & Bodenheimer, 1999). After the initial launch of a neutral disk wind by FUV photons, the carbon ionization front envelopes the densest parts of the disk. The hydrogen ionization front is prevented from reaching the disk surface by the interaction with the neutral wind and finally forms an envelope with the typical head-tail structure (Fig. 2a). This structure is the natural outcome of our self-consistent simulations and its properties are comparable to the proplyds observed in the Orion Nebula. The size of the ionized envelope and the photoevaporation rate of the disk depend on the distance from the ionizing star. Disks exposed to a UV radiation field are expected to survive no longer than several 10^5 years (Hollenbach et al., 2000; Richling & Yorke, 2000).

If we consider an isotropic stellar wind emerging from the protostar within the disk, we are able to reproduce another feature of proplyds. The spherically symmetric stellar wind is hydrodynamically focused into a jet due to the pressure of the neutral disk wind. The opening angle of the counter-jet is wider, because the neutral wind on this side of the disk shadowed from direct UV photons is

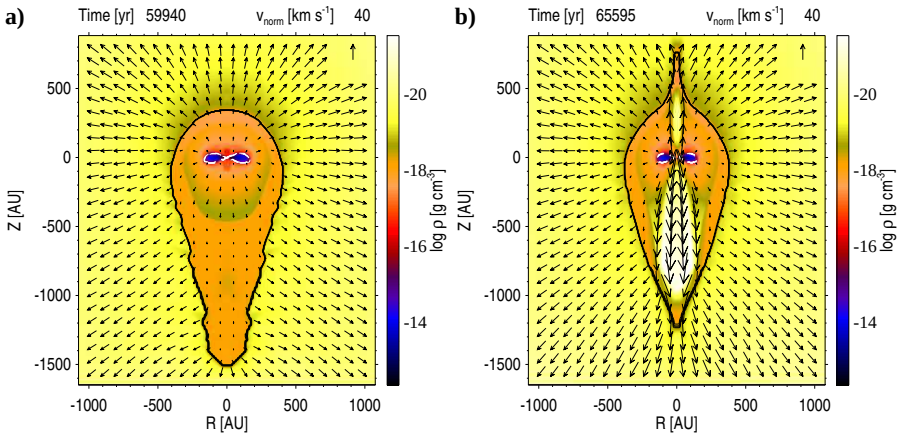

Figure 2: Density distribution, velocity field (arrows), hydrogen ionization front (black contour lines) and carbon ionization front (white contour lines) of a protostellar disk illuminated by an external UV radiation field. a) without a stellar wind b) with an isotropic stellar wind of 100 km/s.

less powerful. The jet changes the form of the ionized envelope as shown in Fig. 2b. In the corresponding emission line maps, the finger in the ionization front appears as a spike emerging from the objects head resembling the micro-jets extending from several proplyds in the Orion Nebula (Fig. 3).

3. The Evolutionary State of the Protostellar Disk

Table 1: Starting models: Elapsed time t since the beginning of collapse, disk radius $r_{\rm d}$ and mass of the protostar $M_\star$ are given.

Model	$t/10^3\,{\rm yr}$	$t/t_{\rm ff}$	$r_{\rm d}/{\rm AU}$	$M_\star/M_\odot$
Y	107	0.5	130	0.64
M	240	1.2	640	0.94
O	438	2.2	1700	1.14

Massive stars evolve relatively fast and reach the main-sequence when low-mass cluster members may still be in earlier phases of evolution. In order to investigate the effect of UV illumination during earlier phases of a protostellar collapse we used three star-disk models at different evolutionary phases all

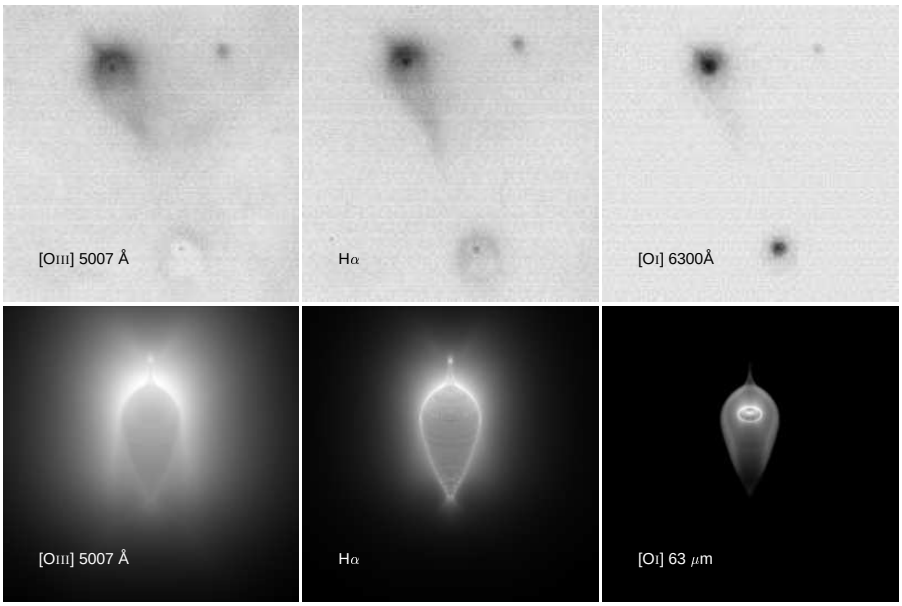

Figure 3: First row: Observed emission line maps of the proplyd HST 2 in M42 (Bally et al., 1998, Fig. 7a). Second row: Calculated emission line maps of the numerical result shown in Fig. 2b. The length of the object is $\sim$ 1500 AU which is about twice as large as HST 2.

resulting from a single collapse simulation of a 2 $M_\odot$ rotating molecular cloud (Table 1).

Fig. 4 shows continuum maps of the three models after 5×10^4 yr of external UV illumination. In the first row are 2 cm radio maps of the whole object. They trace the free-free emission of the dense ionized gas around the head-tail envelope. In the second row are 100 μm maps of an inner part of the domain as indicated in the radio maps. They show the dust emission of the disk itself. The evolution of the mass and the radius of the disk are shown in Fig. 5.

Model Y is younger than one free-fall time of the parental molecular cloud core. Most of the material in its environment is ionized and swept away with the ionized wind during the first 10^4 yr of the evolution. Only a small object remains which will be photoevaporated relatively quickly. The older the starting model the larger is the ionized envelope and the length of the tail. Since the

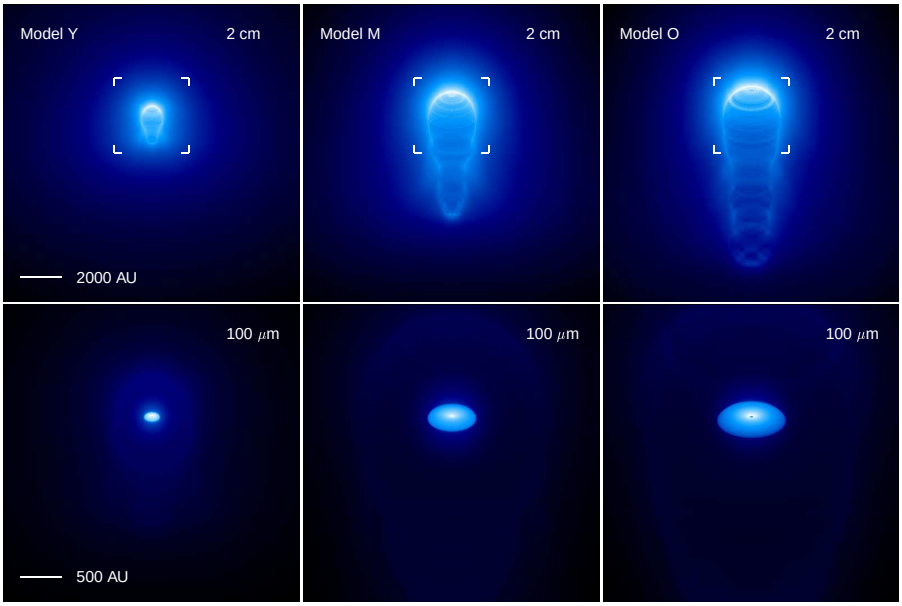

Figure 4: Continuum maps of the models Y, M and O (see Table 1) after 5×10^4yr of external UV illumination.

photoevaporation rate depends on the surface of the disk, model M will survive longer than model O because model O has a larger disk radius during the first 10^5 yr of evolution.

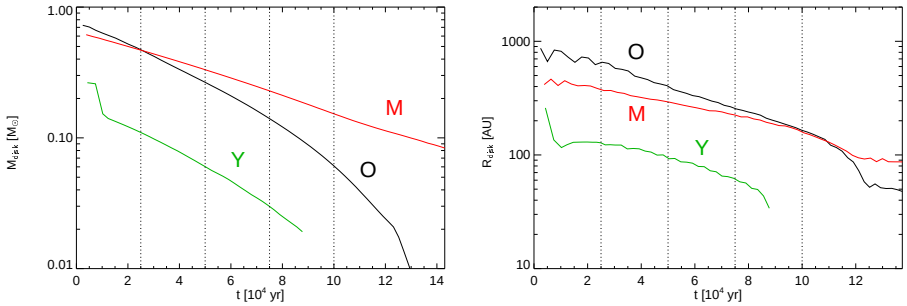

Figure 5: Evolution of mass and radius of the disk.

4. Conclusions

The photoevaporating disk model can explain the observed features of proplyds, e.g. the head-tail structure, the stand-off of the ionization front and the appearance of micro-jets. Photoevaporation is an important disk dispersal mechanism with a time scale of several 10^5 yr which is an upper limit for the time available for planet formation.

The evolutionary state of the protostellar disk at the time when the external UV illumination begins also determines the size and the spectral appearance of the resulting object. UV irradiation during early phases of a protostellar collapse removes the material that otherwise would be accreted onto the disk and finally onto the protostar itself. Thus, an early UV illumination favors the formation of low-mass cluster members and possibly is a mechanism for brown dwarf and brown dwarf disk formation.

Acknowledgements

This work is supported by the Deutsche Forschungsgemeinschaft and by the National Aeronautics and Space Administration (NASA) under grant NRA-99-01-ATP-065. Portions of this research were conducted at Jet Propulsion Laboratory, California Institute of Technology.

References

Bally, J., Sutherland, R.S., Devine, D., Johnstone, D., 1998, AJ 116, 293
Hollenbach, D., Yorke, H.W., Johnstone, D., 2000, in: Protostars & Planets IV, eds. V. Mannings, et al., University of Arizona Press, Tucson, p.401
Kessel, O., Yorke, H.W., Richling, S., 1998, A&A 337, 882
Richling, S., Yorke, H.W., 1998, A&A 340, 508
Richling, S., Yorke, H.W., 2000, ApJ 539, 258
Yorke, H.W., Bodenheimer, P., 1999, ApJ 525, 330
Yorke, H.W., Kaisig, M., 1995, Comp. Phys. Comm. 89, 29

ISO Observations of the Infrared Continuum of the Herbig Ae/Be Stars

D. Elia, F. Strafella, L. Campeggio

Dipartimento di Fisica - Università di Lecce
Via per Arnesano C.P. 193 I-73100 Lecce - Italy
E-mail:[1]eliad@le.infn.it

Abstract

We present a study of the whole sample of the Herbig Ae/Be stars observed with the spectrometers on board of the Infrared Space Observatory (ISO/ESA). These objects have been studied not only by means of their infrared continuum emission but also with respect to all the available photometric data, collected from the optical region to the radio wavelengths. The global spectral energy distributions (SEDs) have been compared with the results of radiative transfer calculations, that have been made in the framework of a circumstellar (CS) model. The results of the selection of the best models allow us to infer on the relationship between the geometry of the CS matter distribution and the evolutionary stage of these objects.
Keywords: *stars: pre-main sequence – circumstellar matter – infrared: stars*

1. Observations, data reduction and results

The ISO data archive has been searched for Short Wavelength Spectrometer (SWS) and Long Wavelength Spectrometer (LWS) observations related to Herbig AeBe stars (HAeBe stars hereinafter). We found 36 objects (out of 108 stars recognized in Thé et al. (1994)), which are listed in Table 1.

Table 1: The observed sample of HAeBe stars

LkHα 198	Z CMa	He 3-1191	WW Vul
V376 Cas	HD 97048	HD 150193	BD +40°4124
Elias 3-1	HD 100546	CoD -42°11721	LkHα 224
AB Aur	HD 104237	HD 163296	PV Cep
MWC 480	IRAS 12496-7650	MWC 297	HD 200775
HD 34282	HD 141569	MWC 300	V645 Cyg
HD 36112	HD 142666	TY CrA	LkHα 234
CQ Tau	HD 144432	R CrA	LkHα 233
MWC 137	HR 5999	HD 179218	MWC 1080

The SWS spectra we discuss here were taken in the range 2.3–45 μm with low resolution ($\lambda/\Delta\lambda \sim 250$) and a typical field of view increasing with wavelength from $14'' \times 20''$ to $20'' \times 33''$ (De Graauw et al., 1996), while the LWS spectra were obtained in the range 43–196.7 μm, $\lambda/\Delta\lambda \sim 200$, (Clegg et al., 1996). In the LWS spectral range the instrumental beam size is $\sim 80''$ so that in some cases (12 objects) the observations were carried out also at an off-source position to account for the contamination due to the local background.

The raw SWS and LWS data were processed using version 10 of the off-line pipeline, which produced series of repeated spectral scans, each composed of 12 and 10 subspectra for SWS and LWS, respectively. These correspond to different spectral ranges, that are arranged to be partially overlapping. The data were further reduced and analysed in subsequent steps:

- removing bad points (glitches, residual detectors responsivity drifts);
- averaging of the many scans obtained on each subspectrum;
- removing of the low-frequency fringes, whose presence affects particularly the LWS spectra (Swinyard et al., 1998).
- smoothing of averaged spectra (SWS only).

Whenever possible, the off-source LWS spectra were subtracted from the corresponding on-source data. Notwithstanding accurate data reduction, the subspectra obtained appear in many cases not perfectly overlapping together, probably because of the variation of the beam size with the wavelength (De Graauw et al., 1996; Swinyard et al., 1998). In Fig. 1. we show examples of two reduced source spectra.

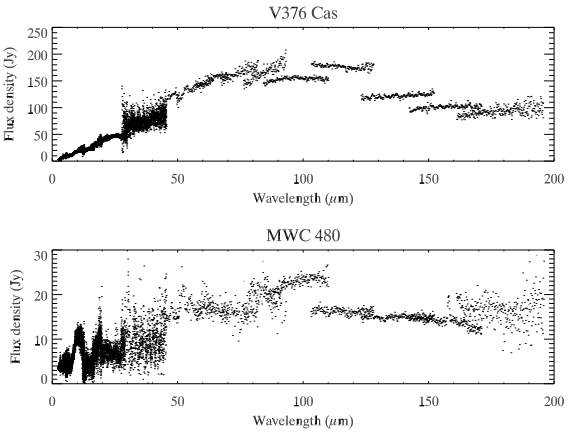

Figure 1: ISO spectra. Both sources show a good continuity between SWS and LWS fluxes despite the different beamsizes involved. On the other hand they clearly present discontinuities in the LWS respective subspectra.

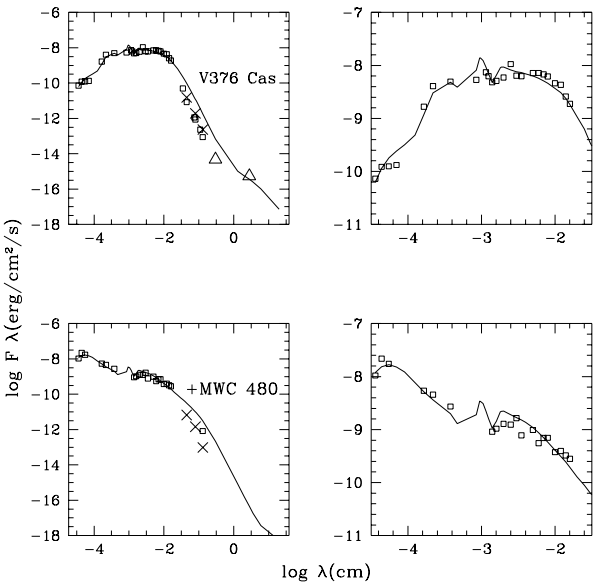

Figure 2: Spectral fits. Computed SEDs (solid line) are superimposed on the observed fluxes (circles, triangles are upper limits). Crosses represent submillimetric model fluxes corrected for diffraction effects due to the instrumental beamsize.

2. Model calculation and comparison with observations

The SEDs emerging from CS envelopes have been computed by means of a model based on a spherical geometry of the circumstellar environment. The model is characterized by a density distribution $n(r)$ around a central star and by the presence of an HII region whose radius is determined by the ionizing luminosity of the central star. A temperature profile $T(r)$ is also considered for the dust component while for the gas we assumed $T = 10^4$ K in the HII region. The gas emission processes considered in the radiation transfer are: free-free, free-bound and electron scattering, while for the dust component the emissivity is computed on the basis of the "astronomical silicate" defined by Draine & Lee (1984). Cases with a modified dust emissivity (at $\lambda > 20\mu$m) have also been computed to take into account the fact that in star forming regions the average dust grain size can be larger than in the diffuse IS medium and consequently the opacity can be described by a $k \propto \lambda^{-\beta}$ law; in our case, $\beta = 1.2$, 0.8, 0.6 (see Pezzuto et al. (1997) for a more complete model description). In addition we also consider:

1) the possible presence of cavities in the CS envelope as can be evacuated by the strong stellar wind associated with the PMS phases;

2) the possibility of two different density distributions describing the inner and outer parts of the envelope, respectively.

A large set of synthetic spectra has been computed; for each object we searched for the best fit with the observed fluxes. Such a comparison, made by means of a "chi square like" method, allows the selection of the best models for each object. In doing this we considered not only the spectral fit but also the consistency of the model fluxes with the spectral type estimated for the star, the distance, and the observed visual absorption. An example of the results obtained is presented in Table 2. and shown in Figure 1..

Table 2: Fit parameters and correspondent observables

Source	β	q	p	n_0	Spectral type		A_V (mag)			Distance (pc)	
				(cm^{-3})	Calc.	Obs.	CS	IS	Obs.	Calc.	Obs.
V376 Cas	1.2	0.5	0.8	$3{\cdot}10^8$	B5	B5 (1)	4	2.5	2.9-5.2 (3,4)	724±32	600 (3)
MWC 480	0.6	0.6	1.3	$3{\cdot}10^{10}$	A3	A3 (2)	1	0	0.25-0.4 (5,6)	101±5	131 (5)

NOTES: V376 Cas was fitted with a simple spherical model, MWC 480 with a model considering also two polar cavities.
REFERENCES TO THE TABLE: 1. Herbig & Bell (1988); 2. Jaschek et al. (1991); 3. Hillenbrand et al. (1992); 4. Pezzuto et al. (1997); 5. van den Ancker et al. (1998); 6. Miroshnichenko et al. (1999).

References

Clegg, P.E., Ade, P.A.R., Armand, C., et al., 1996, A&A 315, L38
De Graauw, T., Haser, L.N., Beintema, D.A., et al., 1996, A&A 315, L49
Draine, B.T., Lee, H.M., 1984, ApJ 285, 89
Herbig, G.H., & Bell, K.R., 1988, Lick Obs. Bull., 1111
Hillenbrand, L.A., Strom, S.E, Vrba, F.J., Keene, J., 1992, ApJ 397, 613
Jaschek, M., Jaschek, C., Andrillat, Y., 1991, A&A 250, 127
Miroshnichenko, A., Ivezić , Z., Vinković, D., & Elitzur, M., 1999, ApJ, 520, L115
Pezzuto, S., Strafella, F., Lorenzetti, D., 1997, ApJ 485, 290
Swinyard, B.M., Burgdorf, M.J., Clegg, P.E., Davis, G.R., Griffin, M.J., Gry, C., Leeks, S.J., Lim, T.L., Pezzuto, S., Tommasi, E., 1998. In: Proc. SPIE, A.M. Fowler (Ed.), Vol. 3354, p.888
Thé, P.S., de Winter, D., Pérez, M.R., 1994, A&AS 104, 315
van den Ancker, M.E., de Winter, D., Tjin A Djie, H.R.E., 1998, A&A 330, 145

(Post-)Main-Sequence Stars

Cepheid Variables and the Circum/Interstellar Matter

L. Szabados
Konkoly Observatory
H-1525 Budapest XII, P.O.Box 67., Hungary
E-mail: szabados@konkoly.hu

Abstract

Various aspects of the relation of classical Cepheids and inter- and circumstellar matter are summarized. Emphasis is given to the question of mass loss from Cepheids and to the role of these pulsating variables in revealing the recent star formation history in their neighbourhood.
Keywords: *Cepheids, reflection nebulae, Stars: chromospheres*

1. Introduction

Classical Cepheids are fundamental objects in astronomy. Being regular radial pulsators, a number of relationships exist between their physical and phenomenological properties. One of them, the period-luminosity (P-L) relationship is instrumental in establishing the cosmic distance scale. In addition to their cosmological role as primary distance indicators, Cepheids serve as astrophysical laboratories for studying structure of post-main sequence stars, hydrodynamics of stellar atmosphere of supergiants, and for checking evolutionary model calculations.

Since Cepheids fall into the mass range of 4-12 $M_{\odot}$, their evolution is rather fast. When they enter the instability strip of the HR diagram and perform radial oscillations, they are old enough that no close connection with the remnants of the star forming cloud is expected, but still too young that mass loss characteristic of late stages of stellar evolution can be expected. Study of mass loss is, however, an interesting topic of Cepheid research for various aspects:
– The circumstellar matter results in reddening and dimming the brightness of the Cepheid, therefore a due extinction correction has to be applied when determining the absolute magnitude of the individual Cepheids.
– The effect of pulsation on the outer region and the atmospheric structure also deserves study. The question is whether the structure of the pulsating atmosphere is different from that of non-pulsating stars located at the same point of the HR diagram.
– Cepheids are unique objects in the sense that their mass can be determined

by various methods, each of them being independent of the others. When comparing the mass predicted by the stellar evolution theory with the mass values determined from various characteristics of stellar pulsation, the evolutionary masses used to be notoriously and significantly larger than the others implying a major mass loss before and/or during the Cepheid phase of evolution (see Cox (1980) for a review). This discrepancy was finally resolved when the new radiative opacities were calculated (Rogers & Iglesias, 1992), but the mass loss from the pulsating atmosphere has remained an important and unsolved issue.

2. Mass loss from Cepheids – multiwaveband studies

According to the theoretical calculations pulsation may result in significant mass loss for Cepheids, predicting mass-loss rates 7×10^{-9} and 2×10^{-7} $M_\odot$ yr^{-1} , for 5 and 7 $M_\odot$ stars respectively (Willson, 1988). Moreover, Willson & Bowen (1984) pointed out that while the star is in the Cepheid phase, mass loss could prolong its lifetime within the instability strip by as much as 5-50 times.

Is there any evidence of mass loss during or prior to the Cepheid phase? The most convincing evidence for mass loss would be the direct detection of the escaped matter. Assuming Pop. I chemical composition, about 1-2% of the mass should be in a form of heavy elements which can form dust grains. These grains could be detected in the IR-region. Several Cepheids show modest mid-IR excess, mainly at 25 μm which could arise from dust with temperatures near 150 K. For these stars the IR excesses are consistent with mass-loss rates of $10^{-8} - 10^{-9} M_\odot$ yr^{-1}, which is really a very low value (McAlary & Welch, 1986). The analysis of the IRAS data also showed that the infrared excess is independent of the pulsation period. This implies that the mass-loss process is largely independent of the size or effective temperature of the Cepheid.

If the outflowing material is hot enough, the ionized matter can be detected by observing its radio emission. VLA observations of 5 very bright Cepheids gave no positive detection at 5 GHz, only resulted in upper limits of the radio radiation, from which upper limits for the ionized mass-loss rates could be derived (Welch & Duric, 1988). These upper limits are an order of magnitude smaller than the calculated values. If Cepheids are indeed losing mass at a rate as high as predicted theoretically, the material must not be ionized.

In addition to the presence of infrared excess, stellar wind may be observed by blueshifted absorption features in lines such as Hα, Ca II H&K and Mg II h&k. The broad emissions of the Mg II resonance lines are particularly sensitive indicators of circumstellar absorption. IUE long-wavelength spectra provide suffi-

ciently high resolution in the 2800 Å region to be able to resolve discrete absorption components. Unfortunately, there are only five classical Cepheids bright enough that could be observed by the IUE in high resolution mode (Schmidt & Parsons, 1984a). The profile of the Mg II h&k line of ζ Geminorum shows two distinct high-velocity blueshifted components near the surface escape velocity which persists for most of the pulsation cycle (Deasy, 1988). The UV spectrum of the 35-day Cepheid l Carinae indicates a mass outflow whose velocity exceeds the escape velocity at the surface. Deasy calculated a mass-loss rate of about $10^{-10}\,M_{\odot}\,\mathrm{yr}^{-1}$ for ζ Gem, and 3 times larger value for l Car.

3. Chromospheric emission in Cepheids

It is an obvious task to search for possible differences between the outer regions of pulsating and stable stars appearing at the same location of the H-R diagram.

As to the chromosphere, the question is whether the observable emission is due to a solar type chromosphere or it is caused by a pulsational shock that propagates through the upper atmosphere of the Cepheid. Shock-induced emission is expected during and just after the brightness maximum because this is the phase when the shock reaches the outer layers of the stellar atmosphere. In the case of a solar type chromosphere the heating is due to some mechanical flux originating in the convection zone, therefore the emission of this origin is more probable during the coolest phases of the pulsational cycle.

The profiles of the Mg II lines in solar-temperature stars are complex and composed of several components. The high-resolution IUE-spectra of Cepheids often show double emission features separated by the circumstellar absorption component (Schmidt & Parsons, 1982, 1984a,b). The general trend in the temporal variation of the total flux of h and k lines is that Mg II turns on rather suddenly and then declines during most of the cycle. The fact that some Mg II absorption components move differently from the photosphere supports the view that they originate at least several tenths of a stellar radius above it. The chromosphere of Cepheids is heterogeneous over the stellar surface and is likely composed of a number of rising and falling columns. The available data are, however, insufficient to decide whether the chromospheric activity is the result of internal convection or it is caused by a shock generated by the pulsation. In any case, for some Cepheids blueshifted chromospheric UV-lines have been observed (Schmidt & Parsons, 1984a) indicating velocities exceeding the surface escape velocity (about 100 km/s).

Hot corona can be studied by X-ray observations. At the sensitivity level of

Einstein, no X-ray emission was detected from three bright Cepheids, δ Cephei, β Dor, and ζ Gem (Böhm-Vitense & Parsons, 1983). A decade later, ζ Gem was reobserved with the more sensitive equipment on board of ROSAT (Sasselov, 1994). No X-ray flux was detected at the upper limit five times lower than previously observed, indicating that classical Cepheids do not have any hot plasma in their upper atmosphere. This means that chromospheric heating is possible in the Cepheid atmospheres but the global envelope pulsation inhibits coronal heating.

4. Cepheids in reflection nebulae

Two classical Cepheids – RS Puppis and SU Cassiopeiae – are connected with reflection nebulae (van den Bergh, 1966). RS Pup is embedded centrally in such a nebula while SU Cas is displaced from the neighbouring nebula but the Cepheid together with some other field stars illuminate the dust particles in their vicinity. These two Cepheids are particularly important because the embedding or nearby reflection nebula offers an independent means for determining their distance, therefore the P-L relation can be calibrated.

A thorough investigation of the region around SU Cas revealed additional reflection nebulae near this Cepheid and from the study of the stars in this region a loose association was discovered (Turner & Evans, 1984). The core group members are at a distance of 258 ± 3 pc and have ages of about 120 million years. The derived luminosity for SU Cas is in agreement with the luminosity obtained from the P-L relation assuming fundamental mode pulsation. It is intriguing, however, that the trigonometric parallax determined from the Hipparcos data places SU Cas at a distance of 433 pc (but the uncertainty is about 100 pc). Moreover, from their Baade-Wesselink analysis, Milone et al. (1999) concluded that SU Cas is pulsating in the first overtone mode.

The reflection nebula surrounding RS Puppis is circularly symmetric around the centrally placed Cepheid. The nebular arcs in these concentric ring structures are higher density regions of reflecting material. In his pioneering study, Havlen (1972) searched for and was able to point out the brightness variations of several nebular features due to the light echo corresponding to the 41.4 day periodicity of the stellar pulsation. The nebulosity varies with the same period as the Cepheid but with a phase delay, owing to the finite light travel time across the nebulosity. It should be emphasized that his study was based on photographic observations, and in spite of the limited accuracy and sensitivity, Havlen could follow the effect of the light echo of the Cepheid on the brightness

of the dust cloud.

The phase difference between the stellar and the nebular variations depends on the linear dimensions of the nebulosity, and a comparison of the linear and angular sizes allows a geometrical determination of the distance to the Cepheid. It would be high time to repeat this study using CCD detectors which are more sensitive and allow to carry out more precise photometry.

In addition, Mayes et al. (1985) pointed out that significant variability is expected in the surface brightness distribution of the reflection nebulosity at IR wavelengths due to variable heating accompanying the effective temperature changes of RS Pup over a pulsation cycle. This infrared echo of the Cepheid variability in the surrounding nebulosity offers a similar but independent method for distance determination. Unfortunately this method has not been applied in practice in lack of dedicated far-infrared observations of this region.

The discrete rings around RS Pup must reflect the nature of the mass ejection process because it is difficult to explain such structure in terms of continuous mass-loss mechanism. The spacing between the successive rings is fairly regular: about 20,000 AU (Deasy, 1988). This is consistent with the regularly repeating phases of intense mass loss from RS Pup whose mass is about 12 $M_{\odot}$. Havlen (1972), however, pointed out that regularly ejected bubbles contradict the generally accepted stellar evolutionary models.

Later calculations performed by **?** showed that pulsationally driven mass loss – even if it is small – reduces the rate of the period change for all masses. According to their evolutionary models mass loosing Cepheids spend more time in the instability strip. A mass loss rate of $10^{-7} M_{\odot}$/yr results in 2-5 times longer crossing time for a 5 $M_{\odot}$ Cepheid, and the rate of period change decreases by a similar factor. Fernie (1984) compared the observed secular period changes of Cepheids with the theoretical values predicted by the evolutionary models of Becker et al. (1977). The observed changes are consistently smaller than the theoretical values which may be evidence of weak mass loss during the Cepheid phase.

5. Effects of binarity on the behaviour of the Cepheids

Presence of a companion may have important consequences on the circumstellar region around the Cepheid. It is known from the evolutionary models that epizodes of intense mass loss may occur during evolution of binary stars (Hilditch, 2001). The effects of the companion, however, have been usually neglected in the Cepheid research in spite of the fact that more than 60 per cent of the

classical Cepheids belong to binary or multiple system (Szabados, 1995).

For example, it is difficult to separate the free-free emission in the mid-IR produced by the hot chromosphere surrounding a Cepheid from the free-free emission which occurs in binary systems consisting a Cepheid and a hot companion where the emission is generated by the stellar wind in the vicinity of the hot component.

Among the key issues related to Cepheids in binaries one can mention searching for traces of current or pre-Cepheid mass loss. Further important problems, e.g. calibration of the P-L relation, theoretical and observational study of period changes or possible nonradial modes excited by the companion, and search for white dwarf companions are not related to the circumstellar matter.

6. Cepheids as tracers of recent star formation history

Cepheids also serve as indicators of star formation occurred in the recent past. Here I refer to two examples. 1. Evidence of propagating star formation in the Large Magellanic Cloud based on the period distribution of Cepheids. 2. The other example shows how the motion of the interaction point of two spiral arms in M31 can be followed with using Cepheids.

About 1800 Cepheids have been analysed based on the data obtained by the MACHO microlensing experiment (Alcock et al., 1999) by comparing the theoretical and observed period-frequency distributions. The main factors that determine the period distribution of Cepheids in a galaxy are: the star formation rate, the initial mass function, metallicity of the galaxy, stellar evolution prior to and during the Cepheid phase, and the location of the instability strip. Evolutionary tracks indicate when a star of a particular mass will be at a given position in the H-R diagram. Pulsation models give the position of the instability strip, and the pulsation period of the star within the strip.

It has been revealed that a significant burst in star formation occurred one hundred million years ago. During the last 10^8 years the central region of this star formation moved from SE to NW along the bar of the LMC. From the regional period distribution of Cepheids Alcock et al. (1999) concluded that the metal content does not change along the bar of the LMC. They were also able to deduce the time scale of the star formation from the period distributions, they derived the mid-epoch and the duration of the star formation epizodes along the bar.

Taking into account the distance of the LMC (assuming a value of 50 kpc), even the velocity could be calculated at which the star formation peak has been

propagating in the bar. It took about 40 million years to reach the northern end of the bar from the southern one, which can be converted into a velocity of about 100 km/s. This large velocity is an independent evidence supporting the finding that star formation was triggered tidally during the last passage of the LMC close to the Milky Way about 150 million years ago.

The star formation history in the superassociation NGC 206 in the Andromeda nebula was studied by comparing the neutral hydrogen emission map, the location and distribution of blue stars and the Cepheid variables (Magnier et al., 1997). It has been pointed out that NGC 206 is located at the intersection of two spiral arms, suggesting that the interaction between spiral arms is responsible for the enhanced level of star formation. The motion of the interaction point can be followed from the distribution of Cepheids. In that study Cepheids were used as age indicators, based on the relationship: $\log A = 8.4 - 0.6 \log P$, where A is the age of Cepheids in years, P is the pulsation period in days.

It is noteworthy that Cepheids are much more frequent in the regions south of NGC 206 where the number ratio of Cepheids/blue stars exceeds 0.5, while in the bulk of the galaxy the ratio of Cepheids to blue stars (for which $B-V < 0.2$ mag) is smaller than 0.2. These blue stars represent the upper part of the main sequence, where stars with ages younger than 30 million years are found.

This difference in number ratio of Cepheids to blue stars can be explained in terms of a region in which star formation is enhanced. In the southern part of M31 the star formation activity has moved during the past $\sim$100 Myr relative to the spiral arm structure seen today. According to this explanation, NGC 206 represents the most recent phase of the enhanced star formation.

The motion of the enhanced star formation can be calculated from the displacement of the region with amply occurring Cepheids relative to NGC 206 and their age difference. Assuming a typical age of 90 Myr for the bulk of these Cepheids, 30 Myr for NGC 206, and an angular distance of 0.15 degrees between the centers of the two groups of different ages, which corresponds to $\sim$1900 pc at the distance of M31, the relative velocity is about 32 ± 15 km/s.

Acknowledgements

This research has been supported by the Hungarian grants OTKA T029013 and T034584. The author is indebted to Dr. Mária Kun for her remarks leading to a considerable improvement of the paper.

References

Alcock, C., Allsman, R.A., Alves, D.R., et al., 1999, AJ 117, 920
Becker, S.A., Iben, I., Tuggle R.S., 1977, ApJ 218, 633
Böhm-Vitense, E., Parsons, S.B., 1983, ApJ 266, 171
Brunish, W.M., Willson, L.A., 1989, in: "The Use of Pulsating Stars in the Fundamental Problems of Astronomy", Proc. IAU Coll. 111, ed. E.G. Schmidt (Cambridge, CUP), p.252
Cox, A.N., 1980, ARA&A 18, 215
Deasy, H., 1988, MNRAS 231, 673
Evans, N.R., Jiang, J.H., McAlary, C.W., Campins, H., 1993, AJ 106, 726
Fernie, J.D., 1984, in: "Observational Tests of Stellar Evolution Theory", Proc. IAU Symp. 105, eds. A. Maeder & A. Renzini (Dordrecht: Reidel), p.441
Havlen, R.J., 1972, A&A 16, 257
Hilditch, R.W., 2001, An Introduction to Close Binary Stars, Cambridge, CUP
Magnier, E.A., Prins, S., Augusteijn, T., et al., 1997, A&A 326, 442
Mayes, A.J., Evans, A., Bode, M.F., 1985, A&A 142, 48
McAlary, C.W., Welch, D.L., 1986, AJ 91, 1209
Milone, E.F., Wilson, W.J.F., & Volk K. 1999, AJ 118, 3016
Rogers, F.J., Iglesias, C.A. 1992, ApJS 79, 507
Sasselov, D.D., 1994, RMxA&A 29, 215
Schmidt, E.G., Parsons, S.B., 1982, ApJS 48, 185
Schmidt, E.G., Parsons S.B., 1984a, ApJ 279, 202
Schmidt, E.G., Parsons, S.B., 1984b, ApJ 279, 215
Szabados, L. 1995, in: "Astrophysical Applications of Stellar Pulsation", Proc IAU Coll. 155, eds. R.S. Stobie & P.A. Whitelock, ASP Conf. Ser. 83 (San Francisco: ASP), p.357
Turner, D.G., Evans, N.R. 1984, ApJ 283, 254
van den Bergh, S., 1966, AJ 71, 990
Welch, D.L., Duric, N., 1988, AJ 95, 1794
Willson, L.A., 1988, in: "Pulsation and Mass Loss in Stars", eds. R. Stalio & L.A. Willson, Kluwer, p. 285
Willson, L.A., Bowen, G.H., 1984, Nature 312, 429

Spectrophotometric Signature of Circumstellar Matter around 89 Her

L.L. Kiss[1], K. Szatmáry[1], J. Vinkó[2]
[1]Astron. Obs. and Dept. of Experimental Physics, University of Szeged
[2]Dept. of Optics and Quantumelectronics, University of Szeged
H-6720 Szeged, Dóm tér 9, Hungary
E-mail: l.kiss, k.szatmary, vinko@physx.u-szeged.hu

Abstract

The bright supergiant and suspected binary star 89 Herculis is studied with help of infrared and optical spectroscopy. The high-resolution sodium D profiles suggest multiple velocity structure of circumstellar clouds. Astrophysical parameters are derived by fitting model spectra in the infrared region. Our results are in agreement with the recently emerged view of the system based on radio and infrared observations. We also discuss photometric and radial velocity variations concluding that pulsations are barely detectable in velocity data. This behaviour is likely to be caused by the spectral line profile distorsions due to circumstellar envelope.
Keywords: *stars: semiregular stars – stars: individual: 89 Her*

1. Introduction

89 Her = V441 Her = HD 163506 = IRAS 17534+2603 is a bright (V = 5.43 mag) supergiant star of spectral type F2 Ibe. This star shows a light change due to semiregular pulsation (SRd type) with P = 65 d and A $\leq$ 0.1 mag. Both the period and the amplitude of the light curve are unstable. So far there is no widely accepted explanation of the mechanism that drives this variability. As many other supergiant stars, 89 Her has circumstellar dust shells due to episodic mass loss. Changes in these shells with time can presumably be revealed by the average brightness of the star. The photoelectric V light curve was analysed with Fourier and wavelet methods earlier (Szatmáry and Kiss 1997).

The radial velocity practically does not vary with the photometric period, although Percy et al. (2000) found a broad peak in the frequency spectrum at 60-70 days. 89 Her is a spectroscopic binary with P_{orb}=288 d.

According to the commonly accepted view of 89 Her, it is a post-AGB star which evolves to a central star of a planetary nebula. The observed circumstellar envelope proves this scenario. This envelope was ejected a few thousand years ago, although there are some signs (mainly spectroscopic pieces of evidence) that

sudden mass-losses occured in the last few decades too. On the other hand, the physical properties of the star are very uncertain. Neither its mass nor luminosity are known with acceptable accuracy. We obtained near-infrared spectra in the Ca-triplet regime. Fitting the hidrogen Paschen-lines with ATLAS9 models, we have obtained $T_{\rm eff} = 6000$ K and $\log g = 0.5$, as a preliminary result. This may confirm the supergiant status of the star.

The period study has revealed a 288 day variation in the light curve which is probably caused by the orbital motion: the varying distance means varying optical path in the circumstellar cloud. This periodicity cannot be detected in the color curve, hence the cloud in the line-of-sight is very homogeneous. The orbital parameters of the 89 Her system (Waters et al. 1993) are: $P_{\rm orb} = 288.36$ d, $e = 0.189$, K=3.09 km s^{-1}, $a_1 \sin i = 12 \times 10^6$ km, $f(M_2) = 0.0008\,M_\odot$. If we assume a mass of $0.6\,M_\odot$ for the primary, the most probable mass of the secondary is between 0.08 and $0.15\,M_\odot$. Adopting a luminosity for the primary of $3000\,L_\odot$, the radius is about $43\,R_\odot$ for an effective temperature of 6500 K.

2. Spectroscopic observations

High resolution optical spectroscopy was carried out on eight nights in 1996 and three nights in 1997 at the David Dunlap Observatory. We used the 1.88 m telescope equipped with the echelle spectrograph. The studied wavelength region was between 6200–6600 Å in 1996 and 5860–6660 Å in 1997. The resolution ($\lambda/\Delta\lambda$) is about 30000, while the typical S/N ratio is around 150-200.

A sample spectrum is shown in Fig. 1. The studied wavelength range covers the strong sodium D doublet and the Hα line. The latter shows very characteristic P Cygni-profile, usually attributed to a strong stellar wind. Other P Cygni-profiles are present, too, while the spectrum is fairly rich in very narrow emission lines. Several absorption lines make the spectrum partially similar to that of the "normal" stars. The general appearance suggests that even in the optical ranges the star is barely visible through the circumstellar nebula.

A question arises: how can we derive stellar radial velocities from such spectra? There are very few pure absorption lines originating in the stellar photosphere, the majority of spectral lines is disturbed by one or more emission components. It looks almost impossible to separate stellar and circumstellar contributions. Therefore, we conclude that earlier radial velocity data from medium-resolution spectra should be carefully re-analysed.

Some interesting conclusions are based on simple comparisons of different spectral lines. First, we compare the strongest sodium doublet and the Hα line

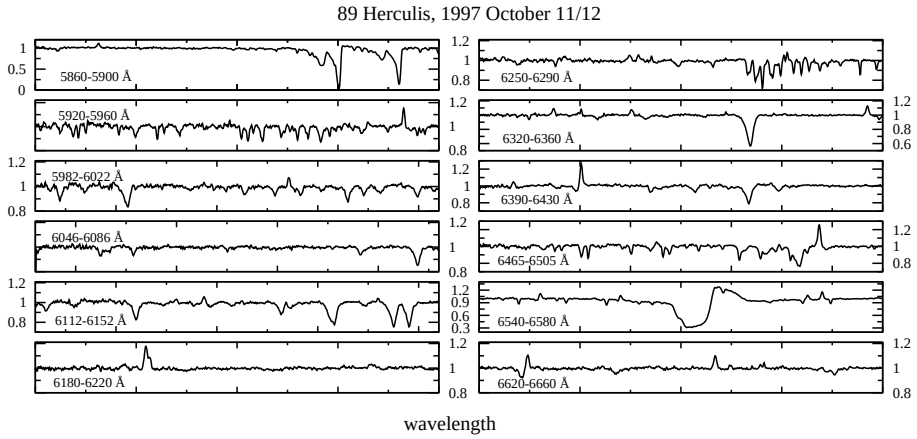

Figure 1: A sample spectrum of 89 Herculis taken in 1997. Note the different scaling of the vertical axes in different subpanels.

(Fig. 2). The two components of the doublet have very similar substructures. They are likely to originate in discrete circumstellar shells with different expansion velocities. The close similarity to the velocity structure of the Hα line strengthens the idea that the weaker components of the doublet originate at 89 Her indeed, not in the intervening interstellar matter. One can identify a shell with $v_{exp} \approx 85\,km\ s^{-1}$, while a weaker feature is unambiguously present with $v_{exp} \approx 140\,km\ s^{-1}$.

Second, two metallic P Cygni-profiles were compared with a pure Si II absorption line and sodium D1 line. It is interesting, that the emission components of the P Cygni-profiles coincide with the minimum of the absorption line, while the sodium D is displaced relative to all lines by more than $+10\,km\,s^{-1}$.

Finally, three narrow emission lines are compared (Fig. 2). The radial velocities of the emission peaks are in very good agreement, however, the seemingly pure emission lines have companion absorption components at $\sim$–$120\,km\,s^{-1}$. Our conclusion is that the optical spectrum of 89 Her is extremely complex due to the presence of circumstellar matter. A future investigation should address the various components of the whole system (a pulsating post-AGB star, a secondary companion of unknown nature, a thick circumstellar nebula with discrete velocity structures) and their contributions to the observed spectrum.

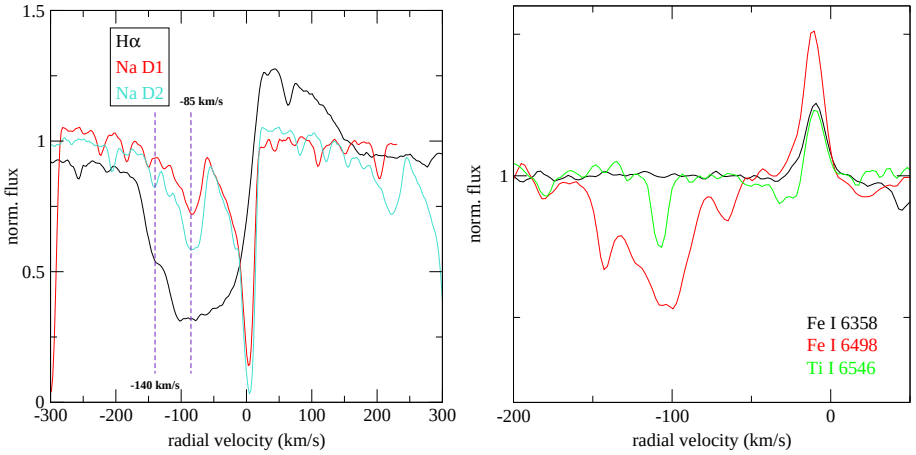

Figure 2: Left: A comparison of the strongest spectral lines. A main expansion velocity of 85 km s^{-1} is suggested by the absorption minimum of the hydrogen P Cygni-profile and the secondary components of the sodium doublet. A weaker feature is also present at –140 km s^{-1}. Right: A comparison of three seemingly pure emission lines. Although the absorption features look similar, the Fe I 6498 and Ti I 6546 lines are in that spectral region which is strongly affected by the atmospheric telluric lines.

Acknowledgements

This work was supported by the Hungarian OTKA grants No. T032258 and T034615, the "Bolyai János" Research Scholarship of LLK from the Hungarian Academy of Sciences and FKFP Grant 0010/2001.

References

Percy, J.R., Bakos, A.G., Henry, G.W., 2000, PASP 112, 840
Szatmáry, K., Kiss, L.L., 1997, IAPPP Comm. No. 67, 66
Waters, L.B., Waelkens, C., Mayor, M., Trams, N.R., 1993, A&A 269, 242

Winds and Bubbles

Stellar Driven Flows in Multi-Phase media

J.E. Dyson
Department of Physics and Astronomy
University of Leeds, Leeds, LS2 9JT, UK

Abstract

After a brief overview of the evolution of flows driven by winds and explosions in single phase media, we briefly describe some of the features of mass injection. We then describe recent work on mass injection into wind-blown bubbles and supernova remnants. We make some final remarks on shocks in multi-phase media.

1. Introduction

Most flows in diffuse astrophysical sources are driven by the injection of mass, momentum and energy. This injection can be impulsive e.g. flows driven by stellar explosions such as novae and supernovae or can be continuous e.g. flows driven by stellar winds and radiation fields. Of course these are not mutually exclusive and in some situations, this distinction is not clear cut. So, for example, a sequence of impulsive events (e.g. supernovae) may often be reasonably approximated as a continuous wind with a mean power of the supernova energy divided by the characteristic time between explosions.

The literature on these flows is vast and just a very few classic papers are mentioned here. Flows driven by the action of stellar UV radiation were classified by Kahn (1954); supernovae induced flows were studied by Shklovskii (1962) and flows driven by fast stellar winds by Pikel'ner (1968). We will here deal only with the latter two types of flow. A useful overview of a variety of problems associated with shock propagation has been given by Bisnovatyi-Kogan & Silich (1995).

2. A brief overview of the evolution of flows in single phase media

2.1. Supernova remnants

In the initial free expansion phase, a forward shock is driven into the supernova site surroundings at velocity $V_s \cong$ constant, so the shock radius $R_s \propto t$, where t is the time. An accelerating reverse shock propagates into the supernova

ejecta. When the mass swept up by the forward shock is O(10) times the ejected mass, the remnant enters the Sedov-Taylor stage of evolution in which only the forward shock remains. Radiation losses are negligible and the remnant evolves with time as $R_s \propto t^{2/5}$, $V_s \propto t^{-3/5}$. Eventually, radiation losses remove thermal energy from all except the very hot interior and the remnant enters the 'pressure-driven snowplough' regime during which $R_s \propto t^{2/7}$ and $V_s \propto t^{-5/7}$. Depending on circumstances, the hot interior may eventually cool and the resulting 'momentum-driven snowplough' evolves as $R_s \propto t^{1/4}$, $V_s \propto t^{-3/4}$. A very comprehensive overview of supernova remnant evolution is given by Truelove & McKee (1999).

2.2. Wind driven interactions

As in the supernova driven interaction, there are two shocks generated, a forward one into the ambient gas and a reverse shock into the ejecta (i.e. the wind). However, the continuous wind means that the reverse shock never collapses onto the stellar surface and the 'two-shock' flow pattern first described by Pikel'ner (1968) moves outwards in the stellar frame. The flow depends largely on the thermal behaviour of the shocked wind. If this wind behaves adiabatically, the outwards shock is driven by the pressure of the shocked wind and the flow is often referred to as 'energy' driven. In that case the outer shock evolves as $R_s \propto t^{3/5}$, $V_s \propto t^{-2/5}$. On the other hand, if the shocked wind cools quickly, the flow is driven by the wind momentum and, unsurprisingly, is then referred to as 'momentum driven'. In that case the outer shock evolves as $R_s \propto t^{1/2}$, $V_s \propto t^{-1/2}$. The type of flow that occurs is determined effectively by the wind velocity. Roughly for wind speeds less than 100 kms^{-1} or so momentum driven flows occur and energy driven flows occur if the wind speed is higher (e.g. Dyson, 1984). So, at least in single phase media, the very fast ($\geq$ few hundred kms^{-1}) winds from stars such as OB stars, Wolf-Rayet Stars and planetary nebula nuclei set up energy driven flows. Winds from YSOs (Young Stellar Objects) which are slower ($\approx$ hundred kms^{-1}) produce either momentum driven flows or energy driven flows since the transition is extremely sharp (Dyson, 1984). Flows can evolve from one type into another dependent on temporal variations in wind power output and/or spatial variations in the ambient density. A thorough treatment is given by Koo & McKee (1992a) and Koo & McKee (1992b).

3. Why study flows in multi-phase media?

Practically every diffuse astronomical source consists of 'cool' clumps embedded in a 'hot' substrate. These include stellar envelopes ejected in the late stages of stellar evolution, molecular clouds and star forming regions and the nuclear regions of active galaxies. Mass from the clumps can be picked up by the global flow initiated by any of the mechanisms above and the resulting dynamics, physics and chemistry of this global flow are thereby altered. The back reaction on the flow may also affect the mass injection mechanism.

There are several ways of injecting material into a flow. The photoevaporation of clumps depends on the presence of an ionizing radiation field. Conduction from cool clumps to the hot substrate may occur; depending on circumstances the inverse may also happen. Clumps can be shredded when overrun by shock waves and the clump material added to the global flow. Finally, simple hydrodynamic ablation via the Bernoulli effect may also happen.

A wide variety of problems involving mass injection have been studied in the literature. A far from exhaustive (though biased) selection includes: the internal dynamics of Wolf-Rayet nebulae (e.g. Hartquist et al., 1986; Arthur et al., 1993, 1994, 1996); ultra-compact HII regions (e.g. Dyson, 1994; Dyson et al., 1995; Lizano et al., 1996); planetary nebula jets (Redman & Dyson, 1999); supernova remnants (McKee & Ostriker, 1997).

4. The scales involved in mass-addition

There is a distinct hierarchy of spatial scales involved in the mass-pick up process. On the smallest scales, mass is accelerated in boundary layers towards full integration with the global flow. Because the global flows are directional, there is the tendency for the accelerated material to be stretched in the flow direction-these are the intermediate scale 'tail' features. The integration of the swept-up material into the global flows takes place on these scales. Finally, the largest scale is the flow itself. Provided there is suitable diagnostic emission or absorption, these various structures can be investigated in astronomical sources giving information on processes that are either difficult or impossible to study under terrestrial laboratory conditions.

5. Remarks on tails

Tail features are interesting for (at least) two reasons. Firstly they provide some of the most intriguing examples of morphology (e.g. the tails in the Helix Nebula NGC 7293, and those of the Orion PROPLYDs). Secondly, it is over these scales in which the integration of the picked up material into the global flow finally takes place and the efficiency of this integration (i.e. the coupling between the global flow and the picked up material) depends on the tail morphology. Very clearly, there is much better coupling if the tails are broad rather than thin, although the number of clumps per unit volume also plays a role. It is worth noting here that all the work discussed later assumes that the mass injection and assimilation into the global flow occurs over length scales much shorter than those associated with the global flows. Thus the likely coarse grain nature of real flows is ignored.

There are in fact several ways of generating visible tail structures. Although we are here concerned with real tails (in the sense that they contain real moving material), what appear observationally to be tails can be formed by the shadowing of radiation fields (e.g. van Berkblom & Arny, 1972; Cantó et al., 1998). The hydrodynamic formation of tails has been discussed on a phenomenological basis by Dyson et al. (1993). These authors considered the way gas liberated from a long-lived source interacted with a uniform stream of gas. There are in principle four possible basic interactions since the source and stream gas can be subsonic or supersonic. Dyson et al. (1993) concluded that wide tails are generated whenever a supersonic stream interacts with either subsonic or supersonic source material or a subsonic stream interacts with supersonic source material. They thus suggested that long thin tails are produced only if a subsonic stream interacts with subsonic source gas. This statement needs the caveat that in addition, any viscous energy dissipation in the tail must be balanced by radiative cooling (Hartquist et al., 1996).

This basic premise has been supported by numerical calculations (Falle et al., 2001) which looked at the interaction of subsonic and supersonic streams with subsonic source material. The wind was assumed to behave adiabatically and the stream gas isothermally. The subsonic-subsonic interaction gave a long thin tail.

An important related problem under study is the interaction of winds with distributed sources and the question of whether a global shock is formed or whether individual shocks occur around individual sources. Some important work has been done on the interaction of global shocks with multiple clumps (Poludnenko et al., 2002), but in these calculations, the clumps are destroyed

by the shocks.

Since the forms of intermediate scale structures depend on the Mach numbers of the global flows, and they in turn determine the coupling between the source and the flow, it is clear that self-consistent flows really need to be studied. In the next sections we will consider a step in this direction by investigating the flows that can be produced with distributed mass loading terms.

6. Mass injection into stellar wind driven flows

Pittard et al. (2001a) and Pittard et al. (2001b) have constructed similarity solutions that describe adiabatic wind-blown bubble evolution with mass loading. Although similarity solutions are rather specialised, they do give some insight into the problems they attempt to describe. The basic equations are the usual conservation of mass, momentum and energy with an appropriate mass injection term added to the continuity equation, specified according to the mode of mass injection.

For conductive (saturated Spitzer) injection, the volume mass injection rate is proportional to $T^{5/2}$, where T is the temperature. For hydrodynamic ablation, the prescription given by Hartquist et al. (1986) is used. In this, the mass injection rate is proportional to M^{γ}, where γ takes the value of 0 if the flow is supersonic relative to the clumps and 4/3 if the flow is subsonic. M is the flow Mach number. We specify the inter-clump density as $\rho = \rho_0 r^{\beta}$. A spatial dependency of the mass injection is included through a term r^{λ}.

In the case of hydrodynamic ablation, the similarity variable is $x = rQ^{1/(5+\lambda)}\dot{E}^{-1/(5+\lambda)}t^{-2/(5+\lambda)}$, and for conductive injection $x = rQ^{1/(10+\lambda)}\dot{E}^{-1/(10+\lambda)}t^{-7/(10+\lambda)}$. Here, Q is the constant of proportionality in the mass injection term, $\dot{E}$ is the energy injection rate and t is the time. In the usual way, the coupled partial differential conservation equations reduce to a set of ordinary differential equations. In order to do this, there is the requirement that $\lambda = (2\beta - 5)/3$ in the ablation case and $\lambda = (5 + 7\beta)/3$ in the conductive case.

To summarise the results:

i) Hydrodynamic ablation. Substantial mass loading of wind-blown bubbles occurs over a wide range of λ. If $\lambda \leq -2$, the bubble mass is larger than that of the swept up shell. The profiles of the flow variables are significantly altered under conditions of large mass loading. In contrast to cases with little mass loading, the density and temperature increase and the velocity and Mach numbers drop. As expected, mass loading of the wind strongly reduces

the Mach number of the inner shock (c.f. Williams et al., 1995). Indeed the wind can mass-load sufficiently to go through a sonic point and thus avoid a termination shock altogether. Importantly, depending on circumstances, the flow may have anything from none to several sonic points. (Note that the mass loading is determined so as to be self-consistent with the Mach number of the local flow).
ii) Conductive evaporation. As before, substantial mass loading can occur over a wide range of λ. Here though the bubble mass is larger than that of the swept-up shell if $\lambda \geq 4$. With high mass loading, the average density of the shocked region is larger, the deceleration of the flow is shallower and the temperature of the shocked wind rapidly decreases. The shocked wind region can be entirely subsonic, entirely supersonic or have one or sometimes two sonic points. For a given value of λ and ratio of the radii of the inner and outer shocks, there is a maximum value of the mass loading that can occur.

These solutions give some idea of the complexities produced when mass injection occurs in stellar wind driven bubbles. It is clear that the effects of mass injection are such that the results on bubble dynamics and evolution obtained from calculations in smooth media (e.g. for planetary nebulae) should be viewed with caution.

7. Mass injection into supernova remnants

As in the case of stellar wind driven bubbles, by far the majority of investigations do not include the effects of mass addition. Cowie et al. (1981) numerically modelled the effects of a supernova explosion on medium where discrete clouds are embedded in a lower density substrate. The cloud material is thermally evaporated into the remnant. There have been various similarity solutions derived where, as above for the wind-blown bubbles, clouds are treated as continuously distributed mass injection sources. McKee & Ostriker (1997), Chièze & Lazareff (1981) and White & Long (1991) assumed that conductive evaporation drives mass injection. (Dyson & Hartquist, 1987) assumed that material is hydrodynamically ablated into remnants according the prescription given in Section 6. Arthur (1994) made a preliminary numerical study of the effects of hydrodynamic mass loading due to hydrodynamic ablation on supernovae remnants in the adiabatic case. Arthur & Henney (1996) used numerical simulations of mass loaded supernova remnants to explain the excess soft X-ray emission in bubbles in the Large Magellanic Cloud.

Mass loaded supernova remnants are important in a variety of contexts. A

remnant propagating inside a molecular cloud propagates through a multiphase medium with a complex structure partly determined by the interaction of the progenitor star or neighbouring stars with the cloud. The range of the remnant in the cloud is a significant factor in the importance of the remnant for e.g. sequential star formation. On larger scales, the collective effects of supernova explosions drive galactic superwinds (e.g. Chevalier & Clegg, 1985; Heckman et al., 1990; Suchkov et al., 1996) showed that the superwind in the starburst galaxy M82 must be mass loaded to account for the observed X-ray emission. This necessary mass injection can be supplied by conductive or ablative cloud evaporation in the core of M82 (Hartquist et al., 1997). The ranges of individual remnants are affected by mass loading; clearly these in turn affect the global wind dynamics. Quite accurate approximations, confirmed by appropriate numerical modelling, are available to describe remnant evolution in smooth media (Cioffi et al., 1988; Truelove & McKee, 1999, and references therein). These approximations represent unified solutions for remnant evolution in the early (Truelove & McKee, 1999) and later (Cioffi et al., 1988) stages. Such solutions have the convenient property that only one simulation need be performed for each regime to determine the evolution of all remnants with the same form of initial ejecta and ambient medium density. In principle these solutions could be used to study problems where multiple supernova events occur and where it would be inconvenient to model each individual event. Since, as noted above, mass loaded remnants are important in a variety of contexts, it is useful to have similar approximations available for the mass loaded case.

Dyson et al. (2002) have calculated the evolution of supernova remnants in which mass loading takes place by hydrodynamic ablation. A related calculation where mass loading takes place by conductive evaporation has been made by Pittard et al. (2002). The basic equations are as in Section 6 with the addition that radiative cooling (assumed to be collisional ionization equilibrium cooling) is added to the energy equation.

In all cases studied, once mass loading becomes significant, the internal structures of remnants deviate appreciably from the structures of standard remnants with no mass loading. The distribution of the remnant energy between thermal and kinetic also changes from that of standard remnants.

In the case where mass injection is hydrodynamic, most significantly, the ranges of supernova remnants (defined at the time they have retained 50% of the initial explosion energy), are strongly influenced by the mass added. For example, a remnant that is heavily mass loaded can affect less than 1% of the volume which would be affected by a standard remnant with the same energy and evolving in a medium with the same ambient density. Clearly ranges are

very seriously affected. It is worth noting that there are significant differences between the evolution of remnants where the prescription for mass loading of Hartquist et al. (1986) is used and where a constant (i.e. Mach number independent) injection rate is assumed only once cooling has occurred. Up to this stage, the differences, given the uncertainties in the physics, are negligible.

The situation is very different when mass addition takes place by thermal evaporation. The reason is straightforward; this latter mass injection is very temperature sensitive and the internal temperature structure can change dramatically spatially and temporally during remnant evolution. Moreover, conductively driven mass loading has a built in limitation mechanism. Mass addition tends to result in lower temperatures that reduce the mass loading rates. Once the interior temperatures of remnants drop below about 10^7K, mass addition rates decrease very sharply. Thus the main differences between these mass loaded models and standard models occur in the earlier stages of evolution. The later stages, where swept up gas dominates in either case, are rather similar.

The main differences between the ablation and conductively loaded remnants are that at late times, the former are dominated by added mass and most of the energy is thermal; the latter are dominated by swept up mass and kinetic energy. Ablation loaded remnants evolve more quickly and reach all dynamical stages earlier than conductively loaded remnants. At any given age, they tend to be more massive and smaller than equivalent remnants that are conductively mass loaded.

8. Discussion

Although the effects of mass addition to flows have been studied at some level for over two decades, it is evident that an enormous range of investigations still remains. In part, this is due to increasing observational data (e.g. on superwinds) which demand the inclusion of mass loading for their interpretation. In part there are fundamental processes associated with mass injection and the assimilation of the injected mass into global flows that remain badly understood. For example, there is evidence that clumps in molecular clouds may be magnetically supported but little work has been done on the photoionization of magnetised clouds. There are even more basic problems that need elucidation. Williams & Dyson (2002) have made a study of the structure of shock waves in two-phase media where simple assumptions were made for the dynamical coupling between a tenuous hot phase and a dense cool phase. The results, even for these simple models, show very important changes from standard shocks,

since the 'shocks' now are resolved regions where the two components interact. Another important question is what determines whether global shocks are set up in flows or whether individual shocks around injection sources predominate. Mass loaded flows will continue to provide gainful employment for astronomers and astrophysicists for some time.

Acknowledgements

I am grateful to my many collaborators for doing most of the work presented here. They are Jane Arthur, Rob Coker, Sam Falle, Tom Hartquist, Julian Pittard, Matt Redman, Robin Williams. I would also thank the organisers of this second meeting for their kind invitation to give a talk in such a marvellous country.

References

Arthur, S.J., Dyson, J.E., Hartquist, T. W., 1993, MNRAS 261, 425
Arthur, S.J., Dyson, J.E., Hartquist, T. W., 1994, MNRAS 269, 1117
Arthur, S.J., Henney, W.J., 1996, ApJ 457, 752
Arthur, S.J., Henney, W.J., Dyson J.E., 1996, A&A 313, 897
Bisnovatyi-Kogan, G. S., Silich, S.A., 1995, Rev. Mod. Phys. 67, 661
Cantó, J., Raga, A., Steffen, W., Shapiro, P., 1998, ApJ 502, 695
Chevalier, R., Clegg, A., 1985, Nature 317, 44
Chièze, J.P., Lazareff, B., 1981, A&A 95, 194
Cioffi, D.F., McKee, C.F., Bertschinger, E., 1988, ApJ 334, 252
Cowie, L.L., McKee, C.F., 1977, ApJ 211, 135
Cowie, L.L., McKee, C.F., Ostriker, J.P., 1981, ApJ 247, 908
Dyson, J.E., 1984, A&SS 106,181
Dyson, J.E., 1994, in: Lecture Notes in Physics 431, *Star Formation and Techniques in Infrared and mm-wave Astronomy*, Ray, T.P., Beckwith, S.V. (eds.), Springer Verlag, Berlin, p.93
Dyson, J.E., Arthur, S.J., Hartquist, T.W., 2002, A&A 390, 1063
Dyson, J.E., Hartquist, T.W., 1987, MNRAS 228, 453
Dyson, J.E., Hartquist, T.W., Biro, S., 1993, MNRAS 261,430
Dyson, J.E., Williams, R.J.R., Redman, M.P., 1995, MNRAS 277, 700
Falle, S.A.E.G., Coker, R.F., Pittard, J.M., Dyson, J.E., Hartquist, T.W., 2001, MNRAS 329, 670
Hartquist, T W., Dyson, J.E., Pettini, M., Smith, L.J., 1986, MNRAS 221, 715
Hartquist, T.W., Dyson, J.E., Williams, R.J.R., 1996, A&SS 235, 165
Hartquist, T.W., Dyson, J.E., Williams, R.J.R., 1997, ApJ 482, 182
Heckman, T.M., Armus, L., Miley, G.K., 1990, ApJS 73, 833

Kahn, F.D., 1954, BAIN 12, 187
Koo, B.C., McKee, C.F., 1992a, ApJ 388, 93
Koo, B.C., McKee, C.F., 1992b, ApJ 388, 102
Lizano, S., Cantó, J., Garay, G., Hollenbach, D., 1996, ApJ 468, 739
McKee, C.F., Ostriker, J.P., 1997, ApJ 218,148
Pikel'ner, S.B., 1968, Ap. Lett. 2, 97
Pittard, J.M., Dyson, J.E., Hartquist, T.W., 2001a, A&A 367, 1000
Pittard, J.M., Hartquist, T.W., Dyson, J.E., 2001b, A&A 373, 1043
Pittard, J.M., Arthur, S.J., Dyson, J.E., Falle, S.A.E.G., Hartquist, T.W., Knight, M.I., Pexton, M., 2002, A&A (submitted)
Poludnenko, A.Y., Frank, A., Blackman, E.G., 2002, in: *Mass outflow in Active Galactic nuclei: New Perspectives*, ASP Conference Series Vol. 255, eds. Crenshaw, D.M., et al., p.285
Redman, M.P., Dyson, J.E., 1999, MNRAS 302, L17
Shklovskii, I.S., 1962, Sov. Ast. 6, 162
Suchkov, A.A., Berman, V.G., Heckman, T.M., Balsara, D.S., 1996, ApJ 463, 528
Truelove, J.K., McKee, C.F., 1999, ApJS 120, 299
van Berkblom, D., Arny, T.T., 1972, MNRAS 156, 91
White, R.L., Long, K.S., 1991, ApJ 373, 543
Williams, R.J.R., Hartquist, T.W., & Dyson J.E., 1995, ApJ 446, 759
Williams, R.J.R., Dyson, J.E., 2002, MNRAS 331, 1

The Breakout of Protostellar Winds in the Infalling Environment

F.P. Wilkin

Instituto de Astronomía, UNAM
Apdo. Postal 3-72 (Xangari), 58089 Morelia, Michoacán, Mexico
E-mail: f.wilkin@astrosmo.unam.mx

Abstract

The time of protostellar wind breakout may be determined by the evolution of the infalling flow, rather than any sudden change in the central engine. I examine the transition from pure infall to outflow, in the context of the inside-out collapse of a rotating molecular cloud core. I have followed numerically the motion of the shocked shell created by the impact of a stellar wind and infalling gas. These fully time-dependent calculations include cases both where the shell falls back to the stellar surface, and where it breaks out as a true outflow. Assuming a wind launched from the protostellar surface, the breakout time is determined in terms of the parameters describing the wind ($\dot{M}_w$, V_w) and collapsing cloud core ($a_\circ$, Ω). The trapped wind phase consists of a wind sufficiently strong to push material back from the stellar surface, but too weak to carry the heavy, shocked infall out of the star's gravitational potential. To produce a large-scale outflow, the shocked material must be able to climb out of the star's gravitational potential well, carrying with it the dense, swept-up infall.

KEYWORDS: *circumstellar material–ISM: jets and outflows–stars: mass-loss–stars: pre-main-sequence*

1. Introduction

Because essentially all known protostellar or pre-main sequence objects show evidence of winds, jets, or outflows, the current thinking is concentrated on a picture of simultaneous infall and outflow, in which infall and accretion occur towards the protostellar equatorial regions, and a wind breaks out along the poles (e.g. André et al., 1993). Yet early thinking on the stages of young stellar evolution identified a phase in which infall directly strikes the protostellar surface, with no outflow present (Shu et al., 1987), no clear examples are known of such protostars. In this contribution I consider limits on the timescale for purely-accreting objects in the context of the standard model of inside-out collapse

from a molecular cloud core. The mathematical formulation is a generalization of Wilkin & Stahler (1998), dropping the assumptions of normal force balance and quasi-stationarity to permit full time-dependence and dynamical expansion (or collapse).

2. Description of the Infall, Wind, and Protostar

The inside-out collapse of a singular, isothermal sphere yields a mass accretion rate $\dot{M}_i = 0.975\, a_\circ^3/G$ at the center (Shu, 1977). Here $a_\circ$ is the isothermal sound speed in the cloud core. At the origin is a protostar whose mass grows linearly in time $M_* = \dot{M}_i\, t$, where t is the time since the start of collapse. In the presence of initial, solid-body rotation, the infall is distorted, and accretion occurs preferentially onto the circumstellar disk (Ulrich, 1976; Cassen & Moosman, 1981; Terebey et al., 1984). The natural length scale of the distortion is the centrifugal radius R_{cen}, which grows as t^3. I turn on a wind at the stellar surface, of radius R_*, and numerically determine whether it can halt infall and escape. At early times, $R_{cen} \ll R_*$ and the accretion is nearly isotropic, making breakout of the wind difficult. At late times, when $R_{cen} \gg R_*$, escape becomes easy along the poles.

For simplicity, the wind is assumed isotropic and of constant speed V_w, and mass-loss rate $\dot{M}_w$. The wind and infall collide supersonically, and a shocked shell forms. Low speeds imply rapid cooling and a geometrically thin shell. The dynamics of such time-dependent, thin shells has been discussed in detail by Giuliani (1982). I include the inputs of mass and momentum from infall, the wind, and the gravitational force due to the protostar.

3. The Trapped Wind Stage

For a given evolutionary time and ratio $\alpha \equiv \dot{M}_w/\dot{M}_i$, I determine the minimum wind speed necessary to break out of the infalling flow. Fig. 1 shows an example calculation of a shell that fails to escape and falls back to the star. In this case, a modest increase in wind speed dramatically changes the outcome, permitting breakout of the shell from the infall region. I solved the problem in dimensionless form, which reduces the parameter space from six (R_*, $\dot{M}_w$, V_w, $a_\circ$, Ω, t) to three dimensions (nondimensional time τ, wind speed ν, and α). As a result, the parameter space has been fully explored. Fig. 2 shows the critical wind speed for breakout. When the wind ram pressure exceeds the infall ram pressure at the stellar surface, the wind may initially push the shell upwards. But if the

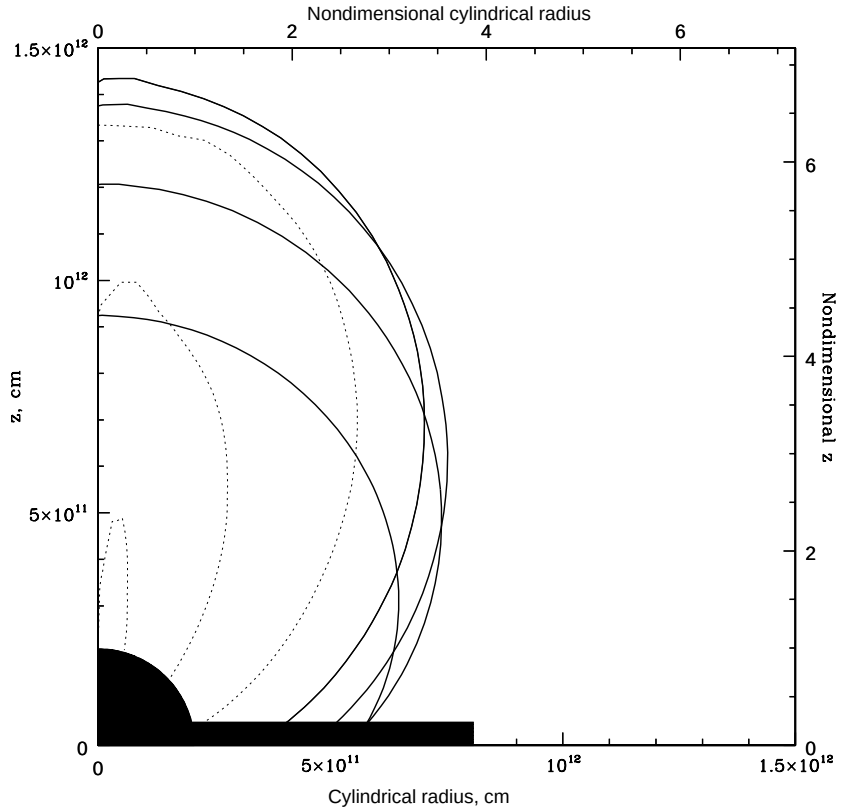

Figure 1: Time-evolution of a failed outflow. The solid curves show the initial rise, while dotted curves show the subsequent recollapse. The protostellar age since core formation is 3.8×10^4 years. The shapes correspond to equal time intervals of 0.016 years. The size of the centrifugal radius is indicated by the disk. Lengths are in cm on the left and bottom axes, and in units of the stellar radius on the remaining axes.

wind speed is less than the critical speed, the shell stalls and falls back. This is the trapped wind stage. In Fig. 3, its duration is the time between the dashed (ram pressure balance) curve and the solid one (critical wind speed) for a given ratio $\alpha \equiv \dot{M}_w/\dot{M}_i$.

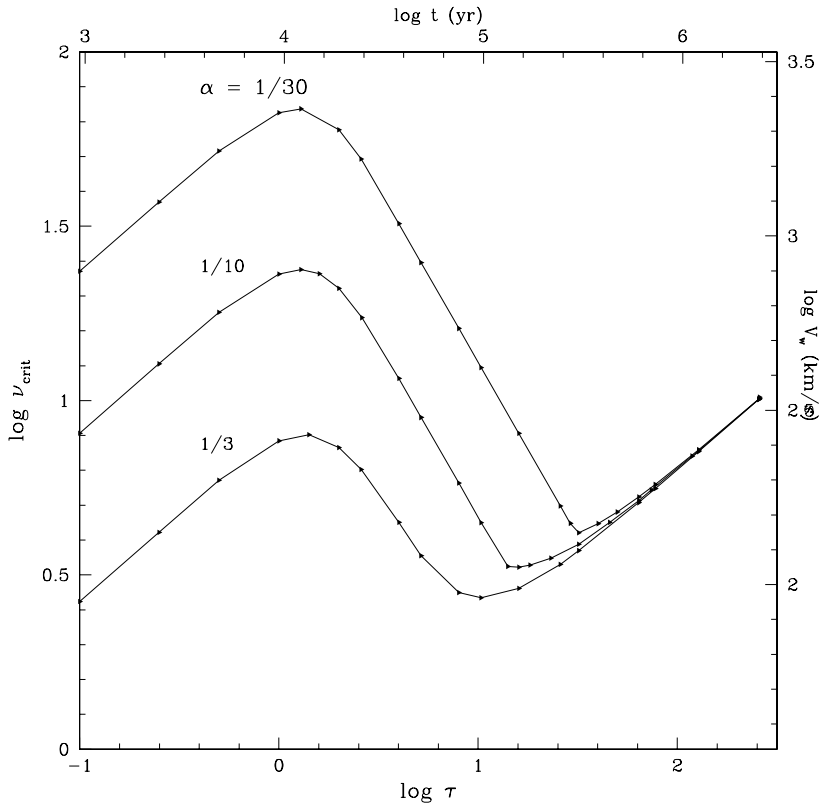

Figure 2: Minimum breakout wind speed versus evolutionary time. The three loci correspond to three ratios, α, of the wind mass loss to infall accretion rate. For a given α, the region above the curve corresponds to breakout, while that below the curve corresponds to recollapse. The power-law increase in v_{crit} at early and late times is associated with the increasing gravitating mass of the protostar.

4. Discussion

The results of Figs. 2 and 3 may be easily scaled to apply to *anisotropic* winds, by comparing to an equivalent, isotropic wind having the same mass and momentum loss rates along the z-axis. Indeed, at early times, the evolution is

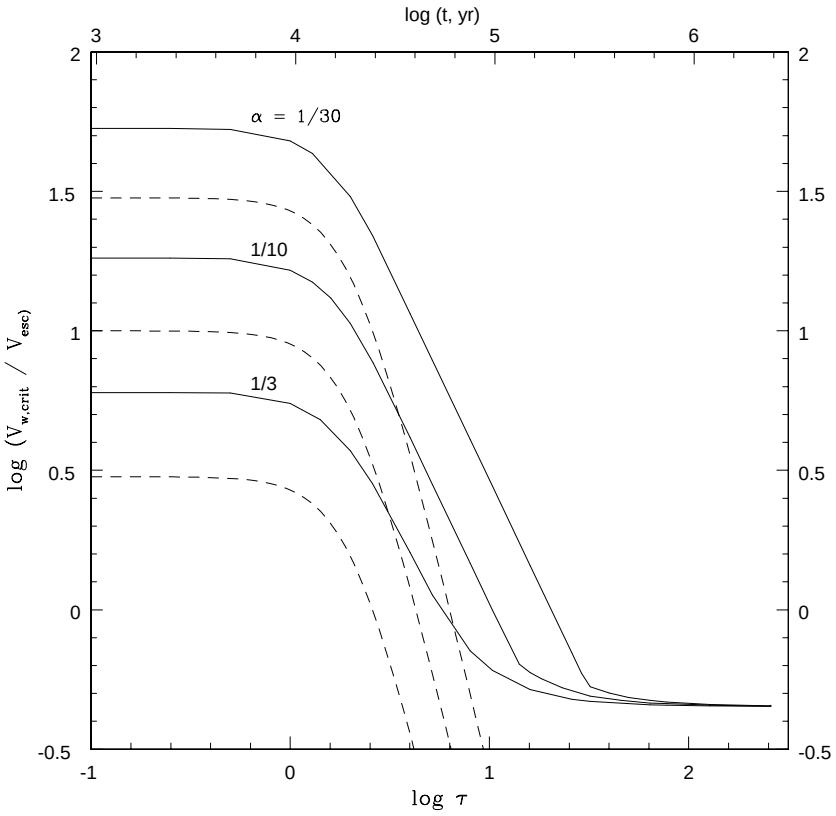

Figure 3: Critical wind speed for breakout (solid curves), in units of the free-fall (escape) speed, as a function of evolutionary time. The corresponding α-values are shown, as well as the wind speed necessary for ram pressure balance at the stellar surface (dashed curves). Assuming wind launch conditions $V_w/V_{esc} = const.$ (i.e. following a horizontal line in this figure), evolution begins at the left edge of the plot with the wind unable to advance beyond the stellar surface until the line intersects the appropriate dashed curve. Then the "trapped wind" phase lasts until the line intersects the corresponding solid curve for breakout. For example, for $V_w/V_{esc} = 1.6$, we follow a horizontal line at $\log(V_w/V_{esc}) = 0.2$. The trapped wind phase begins at $t \approx 19\,000\,yr$, while breakout occurs only at $t \approx 38\,000\,yr$, indicating a substantial duration for the trapped wind stage.

primarily determined by the momentum loss rate of the wind in this direction. At late times, it is the wind speed rather than momentum loss rate that determines breakout. It is hoped that these semi-analytic results will inspire more detailed exploration of this problem with fully radiative hydrodynamic simulations. The existing literature (e.g. Frank & Noriega-Crespo, 1994) on this is not immediately comparable because they have used a different density law which is self-similar, unlike that of Cassen & Moosman. Moreover, I argue that initial conditions with wind velocity much greater than the critical velocity are unphysical, as such a strong wind would have broken out at an earlier time, unless the wind itself evolves strongly with time.

Strong collimation of wind by anisotropic infall is not seen in the current calculations, although further exploration of this issue is forthcoming. I note that numerical simulations demonstrating strong collimation due to the circumstellar density asymmetry (e.g. Delamarter et al., 2000) have assumed a much more asymmetric density field than that used here.

Acknowledgements

I am grateful to the Observatoire de la Côte d'Azur for a Henri Poincaré Fellowship and to the Département Fresnel, UMRS 5528 for hosting my postdoctoral stay in France. I also thank CONACyT/México for financial support and S. Stahler for encouragement in this work.

References

André, P., Ward-Thompson, D., Barsony, M., 1993, ApJ 406, 122
Cassen, P., Moosman, A., 1981, Icarus 48, 353
Delamarter, G., Frank, A., Hartmann, L., 2000, ApJ 530, 923
Frank, A., Noriega-Crespo, A., 1994, A&A 290, 643
Giuliani, J.L., 1982, ApJ 256, 624
Shu, F.H., 1977, ApJ 214, 488
Shu, F.H., Adams, F.C., Lizano, S., 1987, ARAA 25, 23
Terebey, S., Shu, F.H., Cassen, P., 1984, ApJ 286, 529
Ulrich, R.K., 1976, ApJ 210, 377
Wilkin, F.P., Stahler, S.W., 1998, ApJ 502, 661

VLA Observations of WR6: A Search for an Anisotropic Wind

M.E. Contreras[1], L.F. Rodríguez[1], E.M. Arnal[2]

[1]Inst. de Astronomía, UNAM, Apdo.Postal 3-72, Morelia, Mich. 58089, México
[2]Inst. Argentino de Radioastronomía, C.C. 5, 1894 Villa Elisa, Argentina
E-mail: m.contreras@astrosmo.unam.mx

Abstract

The interaction between a stellar wind and its surrounding ISM can create HI cavities or bubbles. In particular, WR 6 shows a very large ovoidal HI bubble around it, whose shape cannot be explained in terms of the standard interstellar bubble theory and may require an anisotropic wind. We have studied this possibility using 3.6-cm VLA observations. We found no firm evidence supporting that WR 6 has a strong anisotropic wind. We conclude that our results are consistent with a classic thermal wind. Under this assumption we have determined the source size, its brightness temperature and its mass loss rate.

Keywords: *Radio Continuum: Stars – Stars: Wolf-Rayet, Individual (WR6) – Stellar Winds*

1. Introduction

Strong winds from massive stars are moving supersonically with respect to the ambient gas, creating a so-called bubble or cavity. Because of their strong stellar winds Wolf-Rayet stars are the best candidates to form an HI cavity around them. Some studies have been carried out to examine the HI distribution around WR stars and to analyze the dynamics and energetic interactions between their stellar wind and the interstellar medium.

Arnal & Cappa (1996) examined the distribution of HI around WR 6. They concluded that the HI bubble is not expanding and that if the standard hydrodynamic stellar wind-blown bubble theory is to be retained in its original form, the most likely explanation is that the central star has a non-isotropic stellar wind.

2. Observations

We present four sets of observations taken with the Very Large Array (VLA) at 3.6-cm. The first observing run was carried out on July 25, 1996. At this epoch

the array was in the D configuration giving the lowest angular resolution. The next three observing runs were made on November 25, December 21, 1996 and on January 12, 1997. During these epochs the array was in the A configuration giving an angular resolution of $\sim 0\farcs2$. The amplitude and phase calibrators were the same for all runs, 1328+307 and 0646-306, respectively. Bootstrapped flux densities for the phase calibrator as well as for WR 6 obtained from each observing run are shown in Table 1.

Table 1: Derived Flux Densities

Observing Run	**0646-306** S_ν [Jy]	**WR 6** S_ν [mJy]
July 25, 1996	0.804 ± 0.006	1.56 ± 0.03
November 26, 1996	0.867 ± 0.005	1.62 ± 0.03
December 21, 1996	0.875 ± 0.005	1.35 ± 0.03
January 12, 1997	0.880 ± 0.004	1.38 ± 0.03

The data analysis and reduction were performed using AIPS and following the standard VLA procedures for editing, calibrating and imaging.

3. Discussion

The presence of an anisotropic wind in WR 6 is important because it could be or could have been in the past related to the elongated HI bubble observed by Arnal & Cappa (1996) at a large scale. It was then important to resolve angularly the source both to detect any possible deviation from the spherical symmetry and to measure the brightness temperature that could help determine if the source has a classical thermal wind. Unfortunately, since the source is not clearly resolved in any of the data sets and it is fairly weak, it was not possible to determine its dimensions directly from our 3.6-cm maps (see Fig. 1).

However, White & Becker (1982) have shown that it is possible to determine the size of a source directly from the u, v data, assuming a spherically symmetric source. Besides, Escalante et al. (1989) have shown that for a marginally resolved wind source the observed flux density depends linearly on the projected

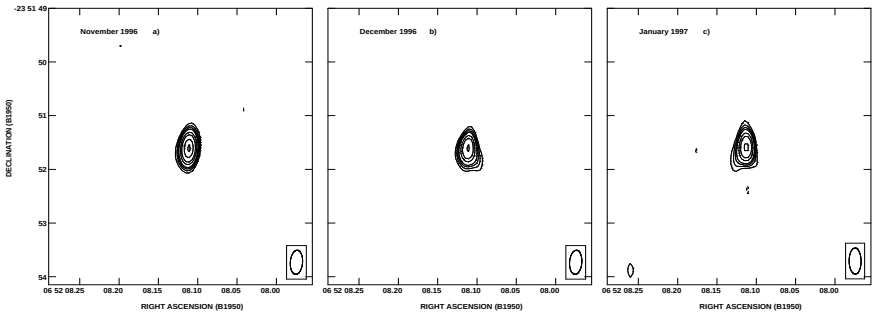

Figure 1: VLA CLEANed 3.6-cm maps for the three high resolution data sets. The maps were obtained with an intermediate *(u,v)* data weight (ROBUST=0). In all three maps the source appears practically unresolved (see beams at right bottom cormer).

baseline separation. Thus, it is possible to determine the source size by making a linear fit to the data in the u, v plane and furthermore to determine its brightness temperature from the same fit. A least squares fit was applied to the real part of all our high angular resolution data using the following equation:

$$V(b) = S_\nu \, (1 - A\, b) \tag{1}$$

where b is the projected baseline separation, given in wavelengths, S_ν is the total flux density, and A is the fitted slope. In our case we have obtained the following values for the slope and the total flux density: $A = 4.6 \pm \times 10^{-7}$ and $S_\nu = 1.52 \pm 0.03$ mJy. Thus, the angular diameter of the source within which half of the flux density is originated can be obtained from the equation:

$$\left[\frac{\theta}{''}\right] = 1.19 \times 10^5 \; A \tag{2}$$

while the brightness temperature is obtained from the relation:

$$\left[\frac{T_B}{10^4 \; K}\right] = \left[\frac{9.48 \times 10^{-15}}{A^2}\right] \; \left[\frac{S_\nu}{mJy}\right] \; \left[\frac{\lambda}{cm}\right]^2 \tag{3}$$

Both relations were derived by Escalante et al. (1989). Then using these expressions we obtained the angular size and the brightness temperature for

WR 6: $\theta = 0\farcs06 \pm 0\farcs01$ and $T_B = 9000 \pm 2500°K$. The angular size corresponds to a dimension of $\sim$ 100 AU at an assumed distance of 1.8 kpc. As we can see, the brightness temperature value is consistent with a classical thermal wind. Additional evidence comes from the spectral index $\alpha = 0.8 \pm 0.2$, obtained from the average of our observations and the 6-cm value of Hogg (1982). Finally, we have obtained the mass loss rate, $\dot{M} = 2.8 \pm 1.0 \times 10^{-5} M_\odot$ yr^{-1}, using the formulation of Panagia & Felli (1975) and a terminal wind velocity of 2700 km s^{-1}.

Then, regarding the main goal of our study, we have not found any firm evidence supporting the possibility of WR 6 having an anisotropic wind, at least one that is evident at scales of $0\farcs2$ or larger. Therefore we cannot provide evidence for a relation between an anisotropy in the stellar wind and the ovoidal shape of the HI cavity. Instead, our data appear consistent with an isotropic thermal wind. Besides, comparing the four flux densities that we have (Table 1), we found no clear evidence for large variability ($\leq$ 15%), in approximately 6 months.

Acknowledgements

We want to thank G. Koenigberger for valuable comments. MEC and LFR acknowledge the support from DGAPA-UNAM and CONACyT-México.

References

Arnal, E.M., Cappa, C.E., 1996, MNRAS 279, 788
Escalante, V., Rodríguez, L.F., Moran, J.M., Cantó, J., 1989, RevMexAA 17, 11
Hogg, D.E., 1982 in IAU Symp. 99, Wolf-Rayet Stars: Observations, Physics and Evolution, eds. C.W.H. de Loore & A.J. Willis, Dordrecht, Reidel, p.221
Panagia, N., Felli, M., 1975, A&A 39, 1
White, R.L., Becker, R.H., 1982, ApJ 262, 657

Multiwavelength Study of the Cas OB5 Supershell

A. Moór, Cs. Kiss

Konkoly Observatory of the Hungarian Academy of Sciences
H-1525 Budapest, P.O. Box 67 , Hungary
E-mail: moor@konkoly.hu

Abstract

We present the results of a multiwavelength study of a large, expanding shell around the Cas OB5 association. Based on the analysis of HI, CO and infrared data the main parameters of the shell were determined. We estimated the total mass in the shell to be $\approx 7.5 \times 10^5 M_\odot$.
Keywords: *ISM:bubbles-ISM:individual(Cas OB5)*

1. Introduction

It is well known that large shell-like structures are relatively common in the disk of spiral galaxies. While the formation of medium size bubbles can be explained by the influence of a single SN event or the stellar wind of massive stars, the size of the largest galactic structures are exceeded by a few orders of magnitude than that created by single event. It is established that these large shells are formed by the energy release of massive stars in OB associations, may be created by impacts of high velocity clouds or its energy input may connect with Gamma-Ray Burst events.

In the last decades several neutral hydrogen shells were investigated apparently related to galactic OB associations (e.g. Cep OB2 (Kun et al., 1987); Orion OB1 (Brown et al., 1995); Perseus OB1 (Cappa & Herbstmeier, 2000)). In our study we investigated the ISM in the vicinity Cas OB5. In this area a large elongated HI shell was found by Fich (1986) with a center position of $l = 117.5°, b = 1.5°$. It was suspected that some SN events occured in the pre-rarified medium of the HI shell and these supernovae actively engaged in enlarging the HI shell. Schwartz (1987) found a far infrared ring ($l = 118°, b = 2°$, diameter $= 5°$) close to the HI shell defined by Fich. Using the diffuse infrared emission originating from this region Kiss et al. (2003, in prep.) identified a far infrared loop GIRL 117+01 at a position similar to Schwartz's. We used HI, CO and infrared data to determine the important parameters of this shell.

2. HI data analysis

In order to study the distribution of HI gas in the environment of Cas OB5, we analyzed the HI emission in the region $108° \leq b \leq 127°$ and $-7° \leq b \leq 9°$ over the velocity interval from $-100\,\mathrm{kms}^{-1}$ to $+30\,\mathrm{kms}^{-1}$. The data were obtained from the Leiden–Dwingeloo HI survey (Hartmann et al., 1997).

Our investigation revealed a large HI shell in the velocity range $[-60\,\mathrm{kms}^{-1} \leq v \leq +3\,\mathrm{kms}^{-1}]$ surrounding the OB association. The projected image of the loop extends to $\sim 8.5°$ in both directions. In Fig. 1 we display the distribution of the neutral hydrogen emission integrated within the velocity range above.

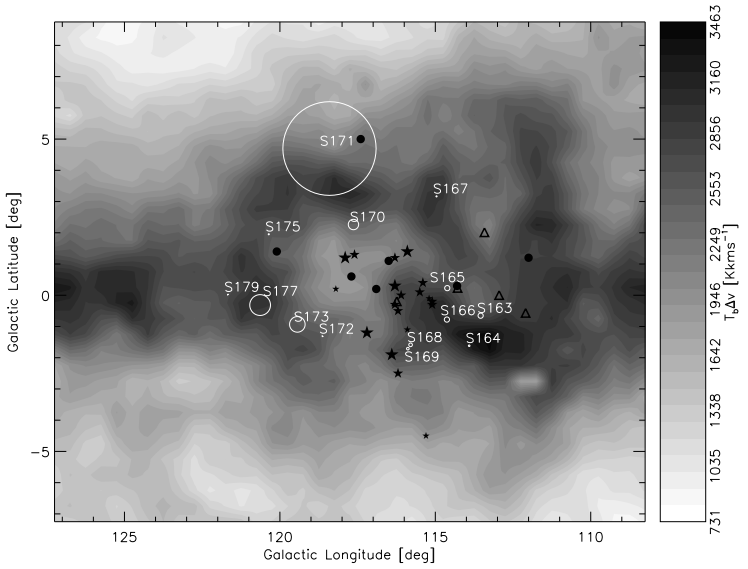

Figure 1: The integrated HI emission map through the velocity range $-60\,\mathrm{kms}^{-1}$ to $+3\,\mathrm{kms}^{-1}$. The displayed Sharpless HII regions are indicated by circles, whose diameter show the mean angular extent of the objects. The star symbols denote the members of the association while the filled circles and triangles mark the SNRs and pulsars respectively

On the basis of the distance to Cas OB5 and HII regions (Sharpless, 1959) encircling the structure we applied a distance of 2.5 kpc for the shell. We assumed that the HI emission is optically thin. After the removal of the background we determined the mass of the HI shell by summing up the column densities of the individual points associated with the shell. This yielded a mass of $M_{sh} \sim 6.3 \times 10^5 M_\odot$. The approaching side of the shell is twice as massive twice as the receding one. This feature sets the true systemic velocity of the center of the expansion to $v_{LSR} \approx -38 kms^{-1}$ and provides a momentum-weighted expansion velocity (Ábrahám et al., 2000) of $v_{eff} \approx 20 kms^{-1}$.

3. Molecular gas in the shell

Heyer et al. (1998) found several large voids of CO emission in the integrated intensity images produced by the FCRAO CO Survey of the Outer Galaxy and demonstrated that there is no extended emission within these voids at a level > 50 mK. One of the most prominent voids is centered at $l = 117.6°, b = 0.0°$ and coincides with the Cas OB5 shell.

In order to estimate the molecular gas mass in the shell we used the Outer Galaxy Survey Cloud Catalog compiled by Heyer et al. (2001). To find the clouds associated with the structure we cut the HI data cube for subsequent 5 kms^{-1} wide slices and searched for clouds in the given velocity range in the shell area. In the velocity interval $v \leq -20 kms^{-1}$ the CO emission originates from the Local Arm therefore we did not consider these clouds in the following.

Using the parameters of the associated clouds (Heyer et al., 2001) and based on the assumption that these clouds have the same distance as the shell we were able to derive the mass of the molecular shell. We estimate the total molecular gas mass to be $\sim 1.2 \times 10^5 M_\odot$. It should be noted that this method has significant uncertainties since the CO 1-0 line is usually optically thick in molecular clouds.

4. Infrared data

The Cas OB5 shell can be identified in the COBE/DIRBE maps of this region. In order to determine the dust mass in the shell we used the 100 and 240μm COBE/DIRBE data. Assuming ν^2 emissivity law we calculated the dust surface density following the method by Hildebrand (1983). The total cold dust mass of the structure was derived by summing up the surface density values of the appropriate COBE/DIRBE pixels. This resulted in $9.5 \times 10^3 M_\odot$.

5. Summary

We investigated the ISM in the vicinity of the Cas OB5 association based on HI, CO and infrared data, and we identified a large shell at each different wavelength. The whole structure is at a distance of 2.5 kpc and is about 190 pc in radius. The expansion velocity of the shell is $\sim 20\,\mathrm{kms}^{-1}$. The total swept up mass is $\sim 7.5 \times 10^5 \mathrm{M}_\odot$

Acknowledgements

This work has been partly supported by the Hungarian Research Fund (OTKA T-034998).

References

Ábrahám, P., Balázs, L.G., Kun, M., 2000, A&A 354, 645
Brown, A.G.A., Hartmann, D., Burton, W.B., 1995, A&A 300, 903
Cappa, C.E., Herbstmeier, U., 2000, AJ 120, 1963
Fich, M., 1986, ApJ 303, 465
Hartmann, D., Burton, W. B., 1997, Atlas of Galactic Neutral Hydrogen, Cambridge: Cambridge Univ. Press
Heyer, M.H., Brunt, C., Snell, R.L., et al., 1998, ApJS 115, 241
Heyer, M.H., Carpenter, J.M., Snell, R.L., 2001, ApJ 551, 852
Hildebrand, R.H., 1983, QJRAS 24, 267
Kun, M., Balázs, L.G., Tóth, I., 1987, Ap&SS 134, 211
Schwartz, P.R., 1987, ApJ 320, 258
Sharpless, S., 1959, ApJS 4, 257

Processes on Galactic Scales

Chemodynamical Modeling of Dwarf Galaxy Evolution

P. Berczik[1], G. Hensler[2], Ch. Theis[2], R. Spurzem[3]

[1]Main Astronomical Observatory, Ukrainian National Academy of Sciences
Zabolotnoho Str., 27, 03680, Kiev, Ukraine.
E-mail: berczik@mao.kiev.ua
[2]Institut für Theoretische Physik und Astrophysik, University of Kiel,
Olshausenstr. 40, 24098 Kiel, Germany.
[3]Astronomisches Rechen-Institut,
Mönchhofstraße 12-14, 69120 Heidelberg, Germany.

Abstract

We present our recently developed 3-dimensional chemodynamical code for galaxy evolution. It follows the evolution of all components of a galaxy such as dark matter, stars, molecular clouds and diffuse interstellar matter (ISM). Dark matter and stars are treated as collisionless N-body systems. The ISM is numerically described by a smoothed particle hydrodynamics (SPH) approach for the diffuse (hot) gas and a sticky particle scheme for the (cool) molecular clouds. Additionally, the galactic components are coupled by several phase transitions like star formation, stellar death or condensation and evaporation processes within the ISM. As an example here we present the dynamical, chemical and photometric evolution of a star forming dwarf galaxy with a total baryonic mass of $2 \times 10^9 M_\odot$.
Keywords: *computational methods: SPH, chemodynamics – evolution of galaxies: dwarf galaxy evolution*

1. Introduction

Since several years smoothed particle hydrodynamics (SPH, Monaghan, 1992) calculations have been applied successfully to study the formation and evolution of galaxies. Its Lagrangian nature as well as its easy implementation together with standard N-body codes allows for a simultaneous description of complex dark matter-gas-stellar systems (Navarro & White, 1993; Mihos & Hernquist, 1996). Nevertheless, until now the present codes lack processes that are based on the coexistence of different phases of the interstellar medium (ISM), mainly dissipative, dynamical and stellar feedback, element distributions, etc. We have therefore developed a 3d chemodynamical code which is based on our single phase galactic evolutionary program (Berczik, 1999, 2000).

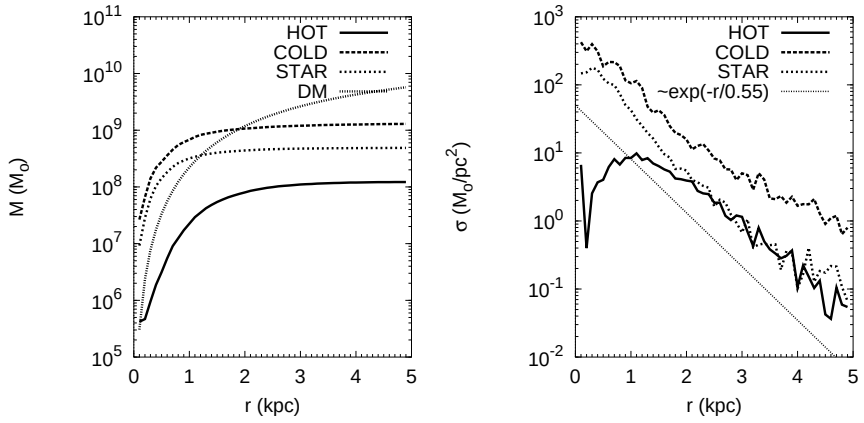

Figure 1: Radial distribution of the cumulative mass (left) and the surface density (right) for the different components in the central region of the model galaxy after 1 Gyr.

This code includes many complex effects such as a multi-phase ISM, cloud-cloud collisions, a drag force between different ISM components, condensation and evaporation of clouds (CE), star formation (SF) and a stellar feedback (FB). This code is a further development of our single phase galactic evolutionary program (Berczik, 1999, 2000) including now different gaseous phases. The more detailed description of the new code and the full list of the interaction processes between all gaseous and stellar phases will be presented in a more comprehensive paper by Berczik et al. (2002). Here we just briefly describe some basic features and effects.

In our new (multi-phase gas) code we use a two component gas description of the ISM (Theis et al., 1992; Samland et al., 1997). The basic idea is to add a cold (10^2 – 10^4 K) cloudy component to the smooth and hot gas (10^4 – 10^7 K) described by SPH. The cold clumps are modelled as N-body particles with some "viscosity" (Theis & Hensler, 1993) (cloud-cloud collisions and drag force between clouds and hot gas component). The cloudy component interacts with the surrounding hot gas also via condensation and evaporation processes (Cowie et al., 1981; Köppen et al., 1998). In the code we introduce also star formation. The "stellar" particles are treated as a dynamically separate (collisionless) N-body component. Only the cloud component forms the stars. During their evolution, these stars return chemically enriched gas material and energy to

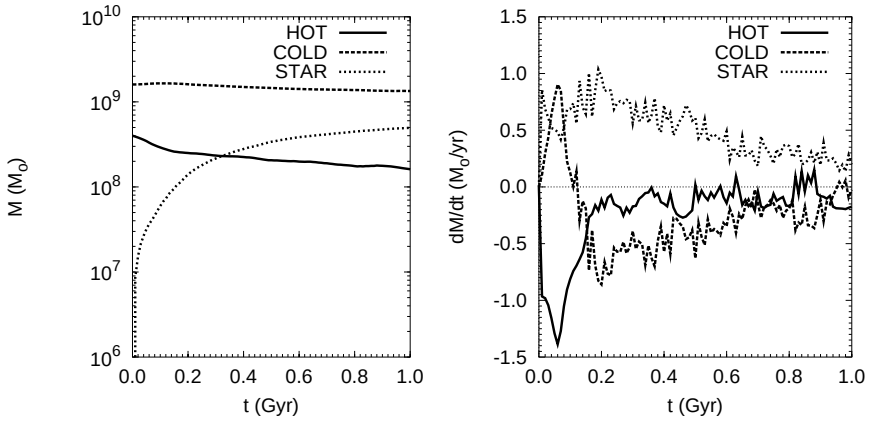

Figure 2: Temporal evolution of the mass (left) and mass exchange rate (right) for the different components of the model galaxy.

both gaseous phases.

2. Basic ingredients of the code

For the parametric description of the cold clumps in the code we use the mass *vs.* radius relation for clouds based mainly on observations and also some theoretical work in this direction (Larson, 1981; Solomon et al., 1987; Maloney, 1990):

$$h_{\rm cl} \simeq 50 \cdot \sqrt{\frac{m_{\rm cl}}{10^6\ {\rm M}_\odot}}\ \ {\rm pc}$$

This parametrization has already successfully been applied for the description of the cloudy medium of the ISM in Theis & Hensler (1993) and Samland et al. (1997).

The basic mechanism for the mass exchange between "cold" and "hot" gaseous phases is a condensation *vs.* evaporation (CE) of the cold cloud clumps. In our code we follow the prescription of these processes using the model proposed in Cowie et al. (1981) and Köppen et al. (1998). In this model the basic parameter controlling the process of CE is σ_0, which gives the ratio between a typical length scale of electron thermal conduction and the cloud size (compare also McKee & Begelman (1990); Begelman & McKee (1990)). If the cloud is small

or has a high temperature the conduction length may exceed the cloud size ($\sigma_0 > 1$) and conductive evaporation is limited by saturation. On the other hand, if the temperature of the cloud becomes very low or its size very large, the cooling length scale becomes shorter than the cloud size and condensation substitutes evaporation. For simplicity and as in Cowie et al. (1981) we just use here $\sigma_0 = 0.03$ as transition value from evaporation to cooling, although a more detailed physical description should invoke the cooling or field length (McKee & Begelman, 1990; Begelman & McKee, 1990). In total the rate at which "cold" clouds evaporate their own material to the surrounding "hot" gas or acquire mass by condensation from the surrounding gas is

$$\frac{dm_{\rm cl}}{dt} = \begin{cases} 0.825 \cdot {\rm T}^{5/2}\, h_{\rm cl}\, \sigma_0^{-1} & \sigma_0 < 0.03 \quad \textbf{Condensation} \\ -27.5 \cdot {\rm T}^{5/2}\, h_{\rm cl}\, \Phi & 0.03 \le \sigma_0 \le 1.0 \quad \textbf{Evaporation} \\ -27.5 \cdot {\rm T}^{5/2}\, h_{\rm cl}\, \Phi\, \sigma_0^{-5/8} & \sigma_0 > 1.0 \quad \textbf{Saturated Evap.} \end{cases}$$

where we have used $\Phi = 1$ (no inhibition of evaporation by magnetic fields) and

$$\sigma_0 = \left(\frac{{\rm T_{hot}(K)}}{1.54 \cdot 10^7} \right)^2 \frac{1}{\Phi\, n_{\rm hot}({\rm cm}^{-3})\, h_{\rm cl}({\rm pc})}$$

In our model the first important dynamical effect in the list of interactions between the two gaseous phases is cloud dragging (DRAG). For this reason we use the prescription proposed in the papers by Shu et al. (1972); Bisnovatyi-Kogan & Sunyaev (1972):

$$\frac{d\mathbf{p}_{\rm cl}}{dt} = C_{\rm DRAG} \cdot \pi h_{\rm cl}^2\, \rho_{\rm hot}\, |\, \mathbf{v}_{\rm cl} - \mathbf{v}_{\rm hot}\, |\, (\mathbf{v}_{\rm cl} - \mathbf{v}_{\rm hot})$$

The drag coefficient $C_{\rm DRAG}$ represents the ratio of the effective cross section of the cloud to its geometrical one $\pi h_{\rm cl}^2$ and is set to 0.5. A value of order unity for $C_{\rm DRAG}$ has the physically correct order of magnitude for the forces exerted by a pressure difference before and after a supersonic shock wave (Courant & Friedrichs, 1998).

The second important dynamical effect during the evolution of the cloudy medium is a cloud *vs.* cloud collisions (COLL). These processes can also significantly reduce the kinetic energy of the cloudy system. As a first approach for these processes we assume that in each collision the colliding clouds lose only 10 % of their kinetic energy.

Stars inject a lot of mass, momentum and energy (both mechanical and thermal) into the galactic system through supernova (SN) explosions, planetary

nebula (PN) events and stellar wind (SW). The gas dynamics then strongly depends on the star formation (SF) and feedback (FB) processes.

Stars are supposed to be formed from collapsing and fragmenting cold gaseous clouds. Some possible SF criteria in numerical simulation have been examined (Katz, 1992; Navarro & White, 1993; Friedli & Benz, 1995). In our code we use the "standard" Jeans instability criterion inside the cloud particle, with randomized efficiency for SF. As a first step we select the cloud particles with:

$$h_{\rm cl} \; > \; \lambda_{\rm J} \; \equiv \; c_{\rm cl} \sqrt{\frac{\pi}{G \; \rho_{\rm cl}}}$$

Next, we calculate the maximum SFR from the whole Jeans mass $M_{\rm J}$ converted from the cloud to star particle during the $\tau_{\rm cl}^{\rm ff}$ time inside the Jeans volume $V_{\rm J}$:

$$\frac{d\rho_*^{\rm max}}{dt} \; \equiv \; \frac{M_{\rm J}}{\tau_{\rm cl}^{\rm ff} \; V_{\rm J}} \; = \; \frac{4}{3} \sqrt{\frac{6 \; G}{\pi}} \; \cdot \; \rho_{cl}^{3/2}$$

where: $\tau_{\rm cl}^{\rm ff} \; \equiv \; \sqrt{\frac{3 \; \pi}{32 \; G \; \rho_{\rm cl}}}$. We set the actual SFR in each current act of SF by randomizing these maximum SFRs:

$$\frac{d\rho_*}{dt} \; = \; \mathbf{RAND} \; (0.1 \; \div \; 1.0) \; \cdot \; \frac{d\rho_*^{\rm max}}{dt}$$

Every new "star" particle in our SF scheme represents a separate, gravitationally bound star formation macro region i.e. Single Stellar Population (SSP). The "star" particle is characterized by its own time of birth $t_{\rm SF}$ which is set equal to the moment of particle formation. We assume that in the moment of creation the "star" particle, the individual stars inside our macro "star" particle are distributed according to the Initial Mass Function (IMF) by Kroupa et al. (1993).

During the evolution, these "star" particles return the chemically enriched gas to surrounding "gas" particles due to SNII, SNIa, PN events. As a first approach, we consider only the production of ^{16}O and ^{56}Fe. The "star" particles return to ISM also the energy due to the SW, SNII, SNIa, PN processes. The total energy released by "star" particles is calculated at each time step and distributed (in the form of thermal energy) between the neighbouring ($N_B = 50$) "gas" particles.

The code also includes the photometric evolution of each "star" particle, based on the idea of the SSP (Bressan et al., 1994; Tantalo et al., 1996). At each time step, absolute magnitudes: M_U, M_B, M_V, M_R, M_I, M_K, M_M and M_{BOL} are defined separately for each "star" particle. The spectro-photometric

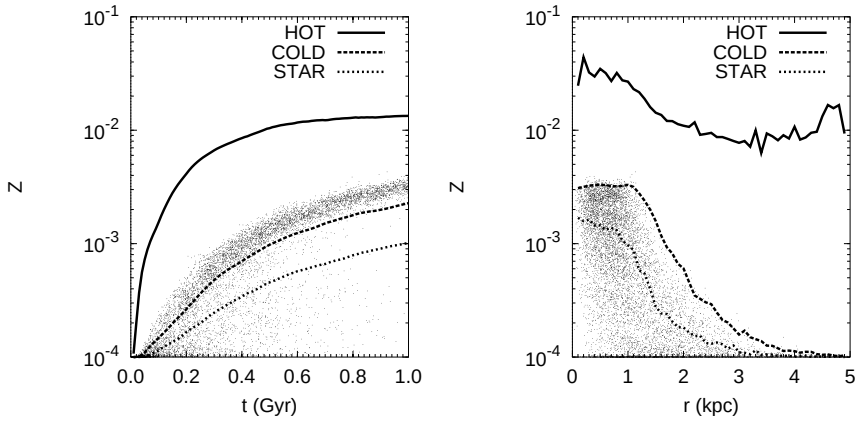

Figure 3: Temporal evolution of the metallicities (left) and their radial distribution after 1 Gyr (right). Individual metallicities of newly born stars are marked by dots.

evolution of the overall ensemble of "star" particles forms the Spectral Energy Distribution (SED) of the galaxy.

As a test of our new code, we calculate the evolution of an isolated star forming dwarf galaxy. The initial total gas content of our dwarf galaxy is 2×10^9 $M_\odot$ (80 % "COLD" + 20 % "HOT" which is placed inside a fixed dark matter halo with parameters $r_0 = 2$ kpc and $\rho_0 = 0.075$ $M_\odot/pc^3$ (Burkert, 1995). With these parameters the dark matter mass inside the initial distribution of gas (20 kpc) is $\simeq 2 \times 10^{10}$ $M_\odot$. We set the initial temperatures on 10^3 K for the cold gas and on 10^5 K for the hot gas. For the initial gas distribution we use a Plummer-Kuzmin disk with parameters a = 0.1 kpc and b = 2 kpc (Miyamoto & Nagai, 1975). The gas initially rotates in centrifugal equilibrium around the z-axis.

We choose the dwarf galaxy as an appropriate object for our code, because in this case even with a relatively "small" number of cold "clouds" ($\sim 10^4$) we achieve the required physical resolution for a realistic description of individual molecular clouds ($\sim 10^5$ $M_\odot$) as a separate "COLD" particle. In the simulation we use $N_{hot} = 10^4$ SPH and $N_{cold} = 10^4$ "COLD" particles. After 1 Gyr more than 10^4 additional stellar particles are created.

3. First results

After a moderate collapse phase the stars and the molecular clouds follow an exponential radial distribution, whereas the diffuse gas shows a central depression as a result of stellar feedback (Fig. 1). The metallicities of the galactic components behave quite differently with respect to their temporal evolution as well as their radial distribution (Fig. 3). Especially, the ISM is not well mixed at any stage.

In Fig. 1 we present the mass and surface density distribution of the different components in the central region of the model after 1 Gyr of evolution. In the region up to $\approx$ 2 kpc the baryonic matter dominates over the DM. The surface density of the stars can well be approximated by an exponential disk with a scale length of 0.55 kpc. In the distribution of hot gas we see a central "hole" ($\approx$ 1 kpc), as a result of gas blow-out from the center mainly due to SN explosions but not for the cold gas. This result disagrees with the model by Mori et al. (1999) where a density hole is caused by their single gas-phase treatment.

In Fig. 2 we present the evolution of the mass and the mass exchange rate of the different components. The SFR (i.e. dM_{STAR}/dt) peaks at a value of 1 $M_\odot yr^{-1}$ after 200 Myrs. Afterwards it drops to 0.2 $M_\odot yr^{-1}$ within several hundred Myrs. After 1 Gyr the stellar mass has already reached 5×10^8 $M_\odot$. Another interesting feature is the behaviour of the hot gas phase mass exchange. After the initial violent phase of condensation an equilibrium is established which gives a hot gas fraction of about 10% of the total gas mass.

The metal content of the diffuse gas and the clouds differ significantly over the whole integration time (Fig. 3). Due to SNII and SNIa events, the metallicity of the hot phase exceeds that of the clouds by almost one order of magnitude. The clouds mainly get their metals by condensation of the hot phase. The central metallicity plateau (up to 1 kpc) of the cold component is explained by the fact, that condensation of metal-enriched material does not work efficiently in that region. This signature agrees well with the observed abundance homogeneity in dIrrs over up to 1 kpc (e.g. in I Zw 18: Izotov, 1999). Moreover, the conditions in the centre lead mainly to evaporation of clouds which also prevents the mixing with the metal enriched hot gas.

Acknowledgements

The work was supported by the German Science Foundation (DFG) with the grants 436 UKR 18/2/99, 436 UKR 17/11/99 and the SFB439 (subproject B5) at the University of Heidelberg. P.B. is grateful for the hospitality of the Astronomisches Rechen-Institut

(Heidelberg) where the main part of this work has been done. The calculation has been computed with the GRAPE5 system at the Astronomical Data Analysis Center of the National Astronomical Observatory, Japan. R.Sp. acknowledges support by the German-Japanese cooperation grant 446 JAP 113/18/0-2.

References

Begelman, M.C., McKee, C.F., 1990, ApJ 358, 375
Berczik, P., 1999, A&A 348, 371
Berczik, P., 2000, Ap&SS 271, 103
Berczik, P., Hensler, G., Theis, Ch., Spurzem, R., 2002, A&A, in prep.
Bisnovatyi-Kogan, G.S.,Sunyaev, R.A., 1972, SvA 16, 201
Bressan, A., Chiosi, C., Fagotto, F., 1994, ApJ 94, 63
Burkert, A., 1995, ApJ 447, L25
Courant R. & Friedrichs K.O., 1998, in "Supersonic Flow and Shock Waves" (Appl. Math. Sciences Vol. 21), Springer-Verlag, Berlin, Heidelberg, p.325
Cowie, L.L., McKee, C.F., Ostriker, J.P., 1981, ApJ, 247, 908
Friedli, D., Benz, W., 1995, A&A 301, 649
Izotov, Y.I., 1999, Proc. XVIII. Rencontre de Moriond, Les Arc, *Dwarf Galaxies and Cosmology*, eds. T.X.Thuan et al., Edition Frontiere, Gif-sur-Yvette
Katz, N., 1992, ApJ 391, 502
Kroupa, P., Tout, C., Gilmore, G., 1993, MNRAS, 262, 545
Köppen, J., Theis, Ch., Hensler, G., 1998, A&A, 331, 524
Larson, R.B., 1981, MNRAS 194, 809
Maloney, P., 1990, ApJ 349, L9
McKee, C.F., Begelman, M.C., 1990, ApJ 358, 392
Mihos, J.C., Hernquist, L., 1996, ApJ 464, 641
Miyamoto, M., Nagai, R., 1975, PASJ 27, 533
Monaghan, J.J., 1992, ARA&A 30, 543
Mori, M., Yoshii, Y., Nomoto, K., 1999, ApJ 511, 585
Navarro, J.F., White, S.D.M., 1993, MNRAS 265, 271
Samland, M., Hensler, G., Theis, Ch., 1997, ApJ 476, 544
Shu, F.H., et al., 1972, ApJ 173, 557
Solomon, P.M., Rivolo, A.R., Barrett, J., Yahil, A., 1987, ApJ 319, 730
Tantalo, R., Chiosi, C., Bressan, A., Fagotto, F., 1996, A&A 311, 361
Theis, Ch., Burkert, A., Hensler, G., 1992, A&A 265, 465
Theis, Ch., Hensler, G., 1993, A&A 280, 85

Milky Way Parameters by the Results of N-body Simulation

A.V. Khoperskov, N.V. Turina
Sternberg Astronomical Institute
119992, Universitetskij pr., 13, Moscow, Russia
E-mail:[1]khopersk@sai.msu.ru,[2]tiurina@sai.msu.ru

Abstract

The results of N-body experiments modelling the disc of our Galaxy are presented. We used the suggestion, that the disc at all radii is on the threshold of gravitational stability. This suggestion sets some limits on dynamic and kinematic parameters of the main subsystems of the Galaxy (disc, bulge and halo). In the solar neighborhood the upper bound of surface density is calculated as $58\,M_\odot/\mathrm{pc}^2$. We came to the conclusion, that the local minimum of the rotation curve in the region $6\,\mathrm{kpc} < r < 10\,\mathrm{kpc}$ is not the result of mass distribution, but may arise from local dynamic processes or another factors, that can cause non-circular motion. Using the observed stellar velocity dispersion and suggesting that the bar in the Milky Way is long-living, we conclude that the central maximum on the rotation curve cannot be explained by the strongly concentrated core of the bulge. The best agreement between model parameters and observed data is reached for an exponential scale length of the disc of 3 kpc. The total disc mass does not exceed $M_d = 4.5 \cdot 10^{10}\,M_\odot$. The relative halo mass in the sphere $r < R_\odot = 8$ kpc should exceed 80 % of disc mass.
KEYWORDS: *galaxies: Milky Way, N-body, bar, rotation curve*

1. Some problems of Milky Way

Rotation curve is one of the most important characteristics of any galaxy. Stars rotate more slowly than gas ($V_* < V_{gas}$, where $V_{gas}(r)$ is the rotation velocity of gas and young stars and $V_*(r)$ relates to the old stars' component). Circular rotation curve $V_c(r)$ is a parameter that enables us to obtain the distributions of gravitation potential and mass. There are many papers presenting rotation curves of stellar and gaseous components of the Milky Way, obtained from observations (Fig.1). Different rotation curves were obtained for various populations of the galactic disc: CO, HI regions, H_α-emission regions, classical cepheids, OB-associations, planetary nebulae and AGB-stars (different symbols and lines in the Fig. 1).

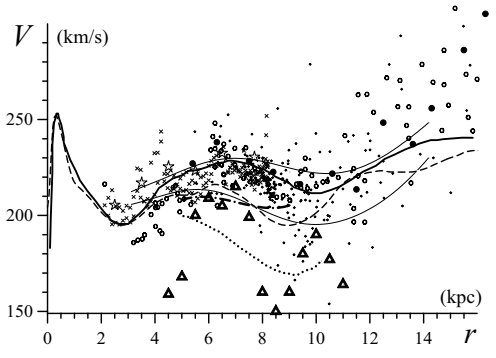

Figure 1: Rotation curves of the Milky Way, taken from different works (for details see Khoperskov & Tiurina, 2002).

Two major features are common for most of them: 1) local depression of the rotation velocity in the region $6\,\mathrm{kpc} < r < 10\,\mathrm{kpc}$ (local minimum of $V(r)$); 2) inner maximum of the rotation velocity near to the centre ($r \simeq 0.3$ kpc). These features may be caused either by mass distribution, or by some dynamic factors.

Spiral galaxies usually consists of two main components: a spherical subsystem (halo, bulge, core) and a disc subsystem (stellar and gaseous discs). Photometric data allow us to model each S-galaxy as disc+bulge system only, but the flatness of the rotation curve at far periphery enforce us to include a halo. If we use rotation curve only for modelling mass distribution of a galaxy, there will be a variety of models, because there is a well known ambiguity in interpretation: we can take low-mass disc and massive halo and bulge or low-mass spherical subsystem and massive disc, the observed rotation curve will be equally well explained in all these cases.

Photometric data give us radial and vertical scales for the distribution of brightness in disc and bulge, but there are some other parameters (like unknown M/L ratio), that give us a freedom for choosing the optimal model for mass distribution. The ambiguity disappears if we assume that the stellar disc of the galaxy is near the threshold of gravitational stability and has a minimum (for this stable state) stellar velocity dispersion c_r. So if we have constructed dynamic model, which would explain observed rotation curves of gas and stellar discs, dispersion of stellar velocities and other observed structural parameters (for example, height scale, scale length), it is possible to calculate the masses of disc and halo separately.

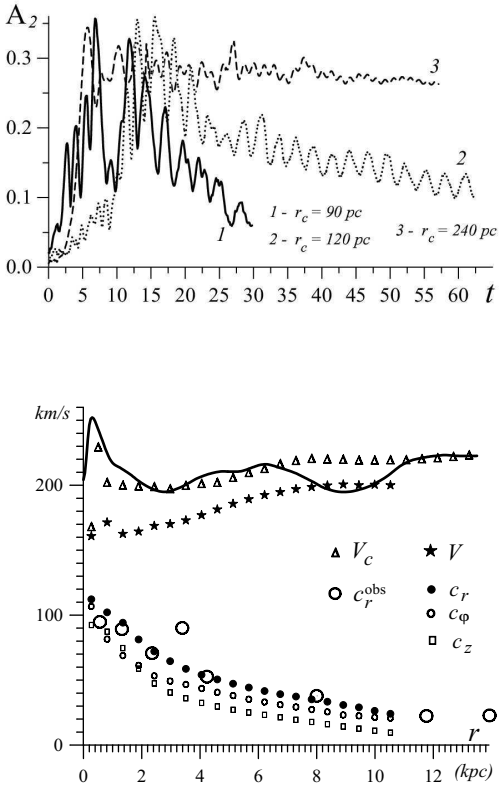

Figure 2: The results of dynamic simulation. (**a**) The evolution of Fourier-harmonics amplitude of the bar-mode in models with different core scales r_c. The decrease of amplitude at small r_c indicate the bar decay. (**b**) The radial distributions of velocity and velocity dispersion in the best model

2. Dynamic simulation of Milky Way

We used dynamic modelling of N-body, using Tree-code ($10^5 \div 5 \cdot 10^5$ particles) and Particle-Particle algorithms ($N = (1 \div 4) \cdot 10^4$). We studied the dynamic evolution of the self-gravitating 3D-disc, weakly unstable initially, which was embedded into the potential of the "rigid" spherical subsystem (halo, bulge, core). During the evolution there is a disc heating (increasing of the velocity dispersion) from the initial unstable state. The disc comes to the stationary state at the end of evolution. For this model disc, which possesses a minimum value of stellar velocity dispersion at a given radius, we compare all its parameters, like surface density, radial, vertical and azimuthal dispersions, disc scales of height and length with the observed ones. In particular, we came to the conclusion,

that if we try to explain the central maximum of Milky Way rotation curve (see Fig.1) by presence of the concentrated core, it would be impossible to create a long-lived bar (Fig.2a) in this dynamic model. The physical mechanism of bar destruction in the presence of a concentrated core is similar to activity of a central massive black hole (Hasan & Norman, 1990).

The presence the of local dip in circular rotation velocity V_c in the region $r \simeq 6 \div 10$ kpc contradicts observed kinematic data of the ratio of velocity dispersions $c_r/c_\varphi = 1.58$ (Dehnen & Binney, 1998) and the results of our dynamic simulation.

The dynamic model that best satisfies the data sets of observations, gives the following parameters of the main components: **bulge** with mass $M_b \leq 1.2{\cdot}10^{10} M_\odot$ and scale of core $r_c \geq 200$ pc; **disc** with full mass $M_d = 4.4{\cdot}10^{10} M_\odot$ and surface density in Solar neighborhood $\sigma_\odot \leq 58 M_\odot/\mathrm{pc}^2$, radial scale 3 kpc and scale height $z_0 = 0.5$ kpc; **halo** with the relative mass $\mu = M_h/M_d \geq 0.87$ at $r < R_\odot$ and $\mu \geq 1.6$ at 4 radial scales ($\sim$ 12 kpc). The ratio between the circular velocity of the disc component V_c^{disc} and the complete circular velocity V_c at the radius $r = 2.2L = 6.6$ kpc is equal to $V_c^{disc}/V_c = 0.73$.

Acknowledgements

This work has been partly supported by the grant 01-02-17597 (RFFI) and Federal programme (40.022.1.1.1101, 01.02.02).

References

Dehnen, W., Binney, J.J., 1998, MN, 298, 387
Hasan, H., Norman, C., 1990, ApJ, 361, 69
Khoperskov, A.V., Tiurina, N.V., 2002, Astr. Rep.

Kinematic Properties of Young Subsystems and the Rotation Curve of Our Galaxy

M.V. Zabolotskikh, A.S. Rastorguev, A.K. Dambis

Sternberg Astronomical Institute
119992, Universitetskij pr., 13, Moscow, Russia
E-mail: zabolot@sai.msu.ru

Abstract

The maximum-likelihood analysis is applied to space velocities of 113 classical Cepheids with periods longer than 9 days, 89 young open clusters with ages less than 40 Myr, 102 blue supergiants, 200 HII-regions and 150 HI radial velocities. We used the distance scales of objects balanced by the statistical-parallax technique. The kinematic properties of young subsystems have been derived (solar motion components, velocity-ellipsoid axes). The rotation curve is constructed from radial velocities of all objects on the galactocentric distances 2-14 kpc for short ($R_0 = 7.5$ kpc) and long ($R_0 = 8.5$ kpc) distance scale.
Keywords: *Galaxy: kinematics, rotation curve, open clusters, Cepheids, blue supergiants, HI, HII*

1. Introduction

The parameters of the Galactic rotation curve were determined by many authors, but it should be pointed out that these parameters depend first on the correctness of the adopted distance scale of objects under study. Objects with known distances – classical Cepheids, open star clusters (OSC), and OB-associations – allow the rotation curve to be determined only out to heliocentric distances of 4-5 kpc, whereas HI and HII kinematic data allow constructing the rotation curve over a wider interval of galactocentric distances. The main problem of using the hydrogen data is that the distances of giant molecular clouds (GMC) and, consequently, those of HII-regions, are determined from their single hot exciting stars whose distance scale is prone to random and systematic errors. Therefore, our goal is to refine the distance scales of young subsystems and to construct the rotational curve of our Galaxy.

2. Observational Data

Our sample included 89 young OSC with $\log T < 7.6$ and heliocentric distances determined by Dambis (1999) by fitting Kholopov's (1980) ZAMS with allowance for evolutionary deviations based on Geneva-group isochrones (Maeder and Meynet 1991). The radial velocities of cluster members were determined by Glushkova based on published data and can be found in the paper by Rastorguev et al. (1999). The proper motions of clusters were computed from those of their member stars found in the HIPPARCOS catalog (Baumgardt et al. 2000).

We also used 113 classical Cepheids with periods $P > 9^d$ and heliocentric distances computed using the fundamental-mode period-luminosity relation of Berdnikov et al. (1996): $\langle M_K \rangle_I = -5.46^m - 3.52^m \log P$ in accordance with the procedure described therein. An earlier statistical-parallax analysis (Rastorguev et al. 1999) showed that the sample of Cepheids with shorter periods is not homogeneous in terms of pulsation mode and may be contaminated by first-overtone pulsators. We used published Cepheid radial velocities and HIPPARCOS proper motions. Young OSC and long-period Cepheids make up a kinematically homogeneous reference sample consisting of 176 and 142 objects with radial velocities and proper motions, respectively, including 124 objects with space velocities.

We performed a separate analysis of a blue supergiant sample consisting of 102 stars with heliocentric distances tied to the OSC distance scale (Dambis 1990). The proper motions of supergiants adopted from the HIPPARCOS catalog, and radial velocities from the catalogs of Barbier-Brossat and Figon (2000) and WEB (Duflot et al. 1995).

Brand and Blitz (1993) published the distances and radial velocities for a total of 206 HII-regions. We selected 203 of these objects with spectroscopic or photometric distances inferred from their exciting stars. The radial velocities of HII-regions were determined from the CO (2.6-mm) radio lines of their associated molecular clouds. We did not include three HII-regions in the final list because of their large residual velocities relative to the provisional rotation-curve solution. The catalog mentioned above also gives standard errors of individual distances and line-of-sight velocities.

We adopted 150 tangent-point radial velocities of HI clouds from Fich et al. (1989). Note that published HI and HII radial velocities are traditionally corrected for the solar motion relative to the standard apex assumed to coincide with the local standard of rest (LSR), and therefore we first converted them into heliocentric radial velocities.

3. Method of Analysis

We used the techniques of maximum-likelihood and statistical parallax (including its simplified version) to compute the kinematic parameters and refine the distance scales involved. See Murray (1983) for a description of the principal ideas of the statistical-parallax method used in this paper. The tangential velocity of a star is computed from its proper motion and distance and therefore depends on the adopted distance scale, whereas radial velocities are distance independent. The distance scale factor is defined as $p = r_o/r_t$, where r_o is the adopted distance and r_t is the true distance. The gist of the method consists of reconciling the fields of radial and tangential velocities in terms of some model of the field of systematic motions and ellipsoidal distribution of residual velocities.

The residual velocity of a star can be written in the following form: $\Delta\mathbf{V} = \mathbf{V}_{obs} - \mathbf{V}_{sun} - \mathbf{V}_{rot}$, where $\mathbf{V}_{obs}$ is the observed space velocity; $\mathbf{V}_{sun}$ is the mean heliocentric velocity of the sample studied; $\mathbf{V}_{rot}$ is the contribution of Galactic differential rotation. Residual space velocities are usually assumed to have a three-dimensional normal distribution: $f(\Delta\mathbf{V}) = (2\pi)^{-3/2} |L_{obs}|^{-1/2} \{-0.5\Delta\mathbf{V}^T \times L_{obs}^{-1} \times \Delta\mathbf{V}\}$, where the matrix of covariance L_{obs} contains the ellipsoidal velocity distribution, errors of distances, radial velocities and proper motion and influence of errors of distances on the systematic velocities. We inferred the unknown parameters by using the maximum-likelihood method or in other words by minimizing the function $\mathrm{LF} = -\sum_{i=1}^{N} \ln f(\Delta\mathbf{V})$. To compute the parameter errors we used the method proposed by Hawley et al. (1986).

The simplified version of the statistical-parallax technique (as used, e.g., by Feast et al. 1998) based on reconciling the kinematic parameters inferred separately from radial velocities and proper motions. Thus it is well known that Oort's constant A inferred from proper motions is much less sensitive to the adopted distance scale than is the value of the same constant inferred from radial velocities. This allows not only the kinematic parameters to be determined but also the distance scale of objects under study to be refined. When refining the distance scale by reconciling the values of Oort's constant A we set $p = 1$.

4. Results and Discussion

First, we applied the maximum-likelihood method to our sample of Cepheids and OSC. Because the galactocentric distance of Sun R_0 and the distance scale

are correlated with each other, we performed our computations with two most commonly adopted values – $R_0 = 7.5$ and 8.5 kpc. We determined the angular velocity of galactic rotation from space velocities of Cepheids and OSC and then used it to construct the Galactic rotation curve based on the radial velocities of all objects considered. The dispersion of the inferred absolute magnitude is equal to $\sigma_M = 0.15^m$ for sample of Cepheids and OSC and $\sigma_M = 0.38^m$ for sample of blue supergiants. It should be noted that the study of the kinematics and space distribution in the disk of other galaxies showed the exponential decrease of surface brightness and velocity dispersion with galactocentric distance (Bottema 1993). But the real accuracy of the computed rotational curve allows us to get rid of this effect.

Table 1 lists the distance scale factors for our samples estimated by the statistical-parallax technique and its simplified version. We analyzed the problem of systematic differences between the distance scale factors given by this two methods. One hundred numerical simulations have shown that the distance scale factor is on the average equal to 1 from both methods and p_1 and p_2 are correlated with each other. We cannot unambiguously choose between the two approaches to the distance scale refinement. It is logical to associate the short and long distance scales with $R_0 = 7.5$ and $R_0 = 8.5$ kpc. In other words $p = 0.96 \rightarrow R_0 = 7.5$ kpc and $p = 0.84 \rightarrow R_0 = 8.5$ kpc for Cepheids+OSC sample and $p = 1.09 \rightarrow R_0 = 7.5$ kpc and $p = 0.97 \rightarrow R_0 = 8.5$ kpc for the blue supergiants sample.

Table 1. Distance scale factors estimated by the statistical-parallax technique (p_1) and by simplified version (p_2).

R_0, kpc	p_1, Cepheids+OSC	p_2, Cepheids+OSC	p_1, Supergiants	p_2, Supergiants
7.5	0.86	0.96	1.09	0.97
8.5	0.84	0.97	1.09	0.97
errors	±0.05	±0.09	±0.08	±0.16

The only way to match the distance scales of HII and stars is to compare the first derivatives of angular velocities inferred from radial and space velocities for gas and stars, respectively. In the result $p = 0.95$ for $R_0 = 7.5$ kpc and $p = 0.90$ for $R_0 = 8.5$ kpc. The good agreement between mean heliocentric velocity components of different young-object samples allows us to construct the rotation curve over a sufficiently wide interval of galactocentric distances, 2 – 14 kpc, using radial velocities of both stars and gas (see Fig. 1, 2). The resulting local centroid velocity and Oort's constant A

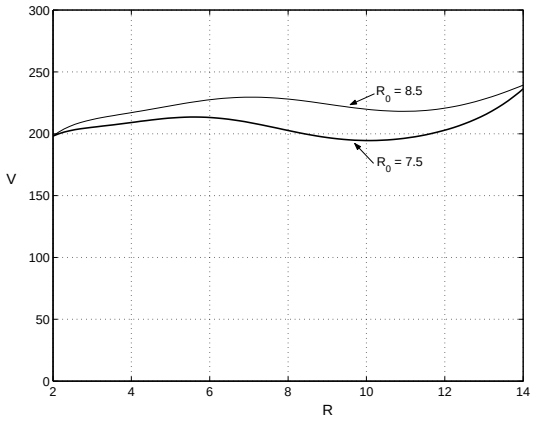

Figure 1: Galactic rotation curve $V(R)$ for the short (R_0 = 7.5 kpc) and long (R_0 = 8.5 kpc) distance scales

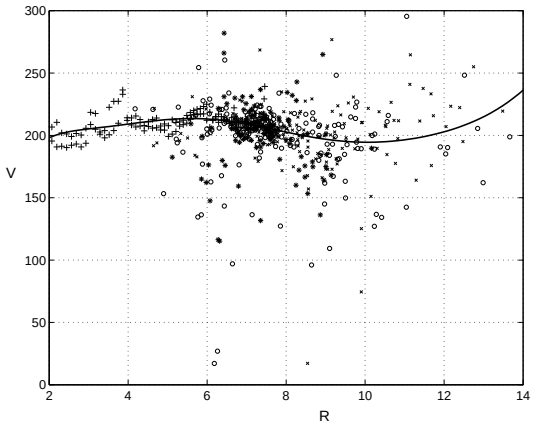

Figure 2: Galactic rotation curve $V(R)$ for the short distance scale (R_0 = 7.5 kpc) with young-object data points ("+" - HI, "×" - HII, "o" - Cepheids+OC, "*" - blue supergiants)

are equal to $V(R_0) = (206 \pm 10)$ kms^{-1}, $A = (17.1 \pm 0.5)$ kms^{-1}kpc^{-1} and $V(R_0) = (226 \pm 12)$ kms^{-1}, $A = (15.4 \pm 0.6)$ kms^{-1}kpc^{-1} for the short and long distance scale, respectively. We computed the velocity ellipsoid axes separately for Cepheids and OSC, supergiants and gas (see Table 2). We see that the axial ratio of the Cepheids and OSC velocity ellipsoid obeys closely to the Lindblad formula, whereas for the gas $\sigma_u \approx \sigma_v$.

Table 2. Heliocentric velocity components and velocity ellipsoid axes for the young object sample (* - fixing parameters).

	σ_u, kms^{-1}	σ_v, kms^{-1}	σ_w*, kms^{-1}	u_0, kms^{-1}	v_0, kms^{-1}	w_0*, kms^{-1}
Cepheids+OSC	13.30	7.59	7.55			
errors	±1.79	±0.41	–			
Supergiants	14.17	10.00	5.13			
errors	±0.51	±2.12	–	−9.17	−12.98	−7.25
HII	6.71	7.19	5.0			
errors	±0.60	0.93	–			
HI	6.60	6.05	5.0			
errors	–	±0.34	–	±0.48	±0.78	–

Acknowledgements

The work was supported by the Russian Foundation for Basic Research (grants nos. 01-02-06012, 00-02-17804, 99-02-17842, 01-02-16086, 02-02-16677, and 02-02-06593) and the Council for the Support of Leading Scientific Schools (grant no. 00-15-96627).

References

Barbier-Brossat, M., Figon, P., 2000, A&AS 142, 217

Baumgardt, H., Dettbarn, C., Wielen, R., 2000, A&AS 146, 251

Berdnikov, L.N., Vozyakova, O.V., Dambis, A.K., 1996, Astron. Lett. 22, 838

Bottema, R., 1993, A&A 275, 16

Brand J., Blitz, L., 1993, A&A 275, 67

Dambis, A.K., 1990, Sov. Astron. Lett. 16, 224

Dambis, A.K., 1999, Astron. Lett. 25, 7

Duflot, M., Figon, P., Meyssonnier, N., 1995, A&AS 114, 269

Feast, M., Pont, F., Whitelock, P., 1998, MNRAS 298, L43

Fich, M., Blitz, L., Stark, A.A., 1989, ApJ 342, 272

Hawley, S.L., Jeffreys, W.H., Barnes, III, T.J., L. Wan, 1986, ApJ 302, 626

Kholopov, P.N., 1980, Sov. Astron. 24, 7

Maeder F., Meynet, G., 1991, A&AS 89, 451

Murray, C.A., 1983, Vectorial Astrometry (A. Hilger, Bristol)

Rastorguev, A.S., Glushkova, E.V., Dambis, A.K., Zabolotskikh, M.V., 1999, Astron. Lett. 25, 595

The HIPPARCOS and TYCHO Catalogues, European Space Agency, 1997, ESA SP-1200

Published by the Konkoly Observatory of the Hungarian Academy of Sciences
Budapest, 2003

COMMUNICATIONS
FROM THE
KONKOLY OBSERVATORY
OF THE
HUNGARIAN ACADEMY OF SCIENCES

MITTEILUNGEN
DER
STERNWARTE
DER UNGARISCHEN AKADEMIE
DER WISSENSCHAFTEN

No. 104

(Vol. 13, Part 4)

Detre Centennial Conference

Proceedings

edited by: L. G. Balázs, L. Szabados, and A. Holl

BUDAPEST, 2006

COMMUNICATIONS
FROM THE
KONKOLY OBSERVATORY
OF THE
HUNGARIAN ACADEMY OF SCIENCES

MITTEILUNGEN
DER
STERNWARTE
DER UNGARISCHEN AKADEMIE
DER WISSENSCHAFTEN

No. 104

(Vol. 13, Part 4)

Detre Centennial Conference

Proceedings

edited by: L. G. Balázs, L. Szabados, and A. Holl

BUDAPEST, 2006

Cover design: Detre Örs Hunor

ISBN 963 8361 42 5
HU ISSN 0238-2091
Felelős kiadó: Balázs Lajos

Contents

Foreword

The Astronomical Research Institute of the Hungarian Academy of Sciences commemorated the 100th anniversary of the birth of László Detre on 19th April, 2006. On the cosmic scale one hundred years is but a blink of an eye, but in the life of a research institute in Central Europe it is a very long time indeed, and the mere fact of its continued existence is, in itself, no mean achievement. In this context, existence does not not only mean having a pleasant building standing in a park in a pleasant area in the Buda Hills on a road named after its founder, behind a fence, displaying, for all to see, a board showing that this is indeed the Astronomical Research Institute of the Hungarian Academy of Sciences, but also that the creation of its founder is still an internationally acknowledged scientific workshop, producing work well up to the prevailing international standards. In Central Europe this cannot be taken for granted in our century. During this time the country (and within it the Institute – better known as the Konkoly Observatory) has managed to survive two World Wars, two revolutions, one world-wide economic crisis (and quite a few smaller ones), five changes of the political regime, and many smaller mishaps, not to be listed here.

As a scientist and the director of the institute, László Detre played a decisive role in the fact that our institute, despite all of the mishaps of the history in Central Europe, is respected worldwide. He was the most prominent representative of Hungarian astronomy in the 20th century. He got his PhD degree in Berlin (1929), having there such outstanding professors as Albert Einstein and Max Planck. Returning to Hungary he got a position at the Konkoly Observatory, Budapest, where he was active until his death in 1974.

He recognized that a small country, like Hungary, could carry out internationally high level research in the field of time-dependent astrophysical processes. Following his initiative, the mountain station at Piszkéstető was established and he passed away in 1974, just before the completion of the 1 m RCC telescope, the largest astronomical telescope in Hungary so far. There are no branches in the recent astronomical research in Hungary which do not go back to his organizational work.

Since László Detre played a significant role in the whole astronomical research in Hungary, the appropriate celebration of his centenary was a scientific colloquium giving a comprehensive overview of his scientific activity and its effect lasting until now. As he was member of the Hungarian Academy of Sciences we organized this colloquium under its auspices.

Although László Detre's scientific activity and achievements are well known abroad, he remained faithful to his country all the time and he did not leave it even in the hardest times. For him, his Hungarian nationality was very important and he emphasized it many times.

Taking into account all these circumstances, our Academy hosted a memorial colloquium on the significance of the work of László Detre on April 20, 2006. All the speakers knew him personally and remember him as a person who played a decisive role in their scientific career. A significant aim of the colloquium was to present a comprehensive overview also for young people who had no opportunity to know him personally.

This dedicated issue of the Communications from the Konkoly Observatory contains the talks presented at the memorial colloquium. We are thankful to our Academy for hosting the colloquium and to the speakers for their valuable contributions.

Lajos G. Balázs
Director

LÁSZLÓ DETRE

19 April 1906, Szombathely – 15 October 1974, Budapest

- 1924: Final exam in the Premonstratensian Secondary School in Szombathely
- 1924-1929: Studies at the Pázmány Péter University (Budapest) and Friedrich Wilhelm University (Berlin)
- 1929: PhD degree (Friedrich Wilhelm University)
- 1929-1974: Staff member in the Konkoly Observatory
- 1943-1974: Director of the Konkoly Observatory
- 1946-1949, 1955-1973: Corresponding member of the Hungarian Academy of Sciences
- 1961-1974: Editor of the Information Bulletin on Variable Stars
- 1964-1968: Head of the Department of Astronomy at the Loránd Eötvös University
- 1967-1970: President of the IAU Commission 27 (Variable Stars)
- 1968-1974: Honorary Professor of the Loránd Eötvös University
- 1970: State Prize awarded
- 1973-1974: Ordinary member of the Hungarian Academy of Sciences

László Detre and the Konkoly Observatory

Lajos G. Balázs

Konkoly Observatory of the Hungarian Academy of Sciences
P.O. Box 67, H-1525 Budapest, Hungary
balazs@konkoly.hu

Prelude

In the seventh decade of the XIXth century changes occurred in astronomy, amounting to a revolution. Gustav R. Kirchhoff and Robert W. Bunsen discovered spectral analysis, which is the method whereby it is possible to draw valid inferences about the composition and physical properties of the emission source from its spectrum. Until then astronomy was to do mainly with measuring the time, the determination of the geographical position of earthly locations, that is with cartography and navigation or with mathematics through the study of celestial mechanics (for example Karl Friedrich Gauss was nominally earning his emoluments as the director of Göttingen Observatory).

The introduction of spectrum analysis into astronomy made it possible to study those physical processes, which produce the electromagnetic radiation observed through the telescopes. The epoch-making importance of this discovery was immediately recognized by Miklós Konkoly Thege, who decided right from the beginning to adopt observational astrophysics as the primary objective of his private observatory at Ógyalla established in 1871. He made regular observations of sunspots, organized a network for the observation of meteors, studied the structural changes visible on the surface of planets, and measured the spectra of some bright comets and stars. He was not satisfied with simply observing the phenomena, he also attempted to analyze them and find their explanation.

The 1860-1870s saw the beginning of the systematic study of stellar spectra. The Ógyalla Institute took the study of the spectra of stars brighter than 7.5 magnitude, and observable between $-15°$ and $0°$ of declination as its contribution to the programme. Between the years 1882-1885, the lion's share of the work was done by Radó Kövesligethy, who was working at the institute as a graduate trainee, on secondment from the University of Vienna, where he was completing his studies. Later he became a professor at the University of Pest, acquiring a world-wide renown as an authority on seismology.

With the passing of the years, Konkoly became increasingly worried about the future of his institute. On the one hand, he was apprehensive – and rightly so – that after his death his stellarium may share the fate of similar initiatives in Hungary, that is falling standards and general decrepitation. On the other hand, he also appreciated the fact, that

his financial resources were insufficient to finance a modern observatory in competition with the outside world, mainly America. Nationalisation appeared to be the only solution. He has already mooted a plan to this effect in the eighties, but it was not before 1899 that, using his parliamentary influence (in the interim he also became an MP), he could realize his intention. After the signing of the necessary papers on 16 May, 1899, the observatory became state property on 20 May, 1899. There were some people of the opinion, that Konkoly's timing was intentional. 21 May, 1899 was the fiftieth anniversary of Buda's liberation from the Austrians during the Hungarian War of Independence, that set the final seal on the sad fate of the observatory on St. Gellért's Hill.

The new National Observatory (full name: Royal Hungarian Astrophysical Observatory of the Konkoly Foundation) selected astronomical photometry as its principal field of exploration. Konkoly chose photometry as the principal field of study for his observatory because at the end of the XIXth century it became more and more obvious that, in the field of spectroscopy, even the state-financed establishment would be unable to keep pace with the rapidly growing observatories operating in the wealthy Western countries. To be able to employ the methods of photometry, it was necessary to establish a system of reference, covering the whole celestial sphere, which could serve as etalon for future measurements. The direction of this program went to the observatory of Potsdam, near Berlin. It was an international effort, and Ógyalla undertook to collect data on more than two thousand stars brighter than 7.5th magnitude, in the segment of declination $-10°$ to $0°$. Photometry was applied not only for creating the system of reference, but also for the study of stars of variable brightness. Konkoly realized that time passes equally fast for the rich and the poor, so, in some fields of study, the advantage of rich, well endowed observatories can be cancelled out, and more modestly equipped observatories could remain competitive. For this reason, the study of variable stars was chosen, in addition to contributing to the photometric reference system, as the primary task of the institute. This decision was to be the main determining factor in the further operation of the observatory.

At the First World War's end Hungary was also buried under the ruins of the defunct Austro-Hungarian empire, and both Ógyalla and the observatory found themselves under alien rule. By the end of 1918 the relevant ministries began to discern the victors' plans for the new Europe, so the Ministry of Education ordered the dismantling and repatriation of all the instruments and equipment in the state's possession. By January 1919 all the dismantled material was safely back in Hungary.

In 1921 the Hungarian government, acting on the recommendation of the Minister of Education, Dr. József Vass, accepted plans for a far-reaching program for the promotion of education and science. The observatory on the Svábhegy (Schwabian Hills) was built under the aegis of this programme. Budapest's local government voted to place twelve acres of land at the disposal of the state government with the proviso, that it may only be used for the building of the new observatory. Construction works started in the autumn of 1921, and one year later observations already started in the first dome. The order for the 24 inch reflector, sent originally to Heyde, but cancelled because of the war, was renewed. The installation of another dome was completed with the financial support of the Budapest local government in 1928. So, in the company of a 16 cm refractor from Ógyalla (in another, smaller dome), and of a meridian instrument, which was used among other things for providing accurate time-signals for the railways, the reincarnated Konkoly institute could also start its scientific work.

Next year, in 1929, László Detre joined the scientific staff of the institute.

Years of study

László Detre was born on April 19, 1906 in Szombathely (Steinamanger). His father, Dr. János Dunst (Detre changed his name in 1933) was a city councillor who died when Detre was only 2 years old. His mother educated him on her very modest widow pension. He studied in the secondary school of the Premonstratensers of Szombathely and had taken his final examination in 1924. Already in these years he showed a very keen interest in natural sciences and in the age of 13 he founded a study circle of natural sciences in his school. Above all, he was a skilled mathematician and he won a Hungarian contest in mathematics. As a consequence he was admitted to the Eötvös Collegium and studied at the Pázmány Péter University of Budapest between 1924-29. After completing three years at this University, he received a fellowship at the Friedrich-Wilhelm University in Berlin.

At that time this University had excellent professors in astronomy, mathematics and physics. According to Detre's university record he studied astronomy from Paul Guthnick, Ernst Kohlschütter and August Kopff. Albert Einstein and Max Planck were his professors in theoretical physics.

The 1920s were famous for the birth of quantum mechanics which made some kind of a revolution in physics. At the same time astronomy also experienced a revolutionary change. Following Hubble's discovery, the concept of the large stellar islands in the Universe, like our Milky Way, became widely accepted. These new results gave a new stimulus to the statistical studies of the space distribution of the stars.

László Detre made acquaintance with these studies in Berlin and prepared his PhD theses on stellar statistics under the leadership of A. Kopff and E. Kohlschütter. He defended his Theses on July 25, 1929. His dissertation was published as the first issue of the institute's communications series (*Fig. 1*).

Before starting the regular work in the institute at the Svábhegy, he made six-month study trips in Vienna and Kiel.

Research fellow at Svábhegy

The science of astrophysics, born in the last three decades of the XIXth century continued its explosive growth all through the subsequent decades. This rate of growth was almost compatible with the growth of physics itself. In the 1920s it was proved by observational astronomy that stars tend to agglomerate in gigantic clusters (galaxies), and these galaxies are getting further away from each other at a rate proportional to their distance. This is a direct consequence of the relativistic models of the universe. The dynamic exploration of galaxies – including our own Milky Way system – also took place at an ever accelerating pace. The list of these achievements would not be complete without mentioning theoretical investigations on the internal structure of the stars, and their confirmation by observations.

Stars of variable brightness are important members of the family of stars. One of their important sub-groups is formed by those stars, whose changes of light emission are caused by oscillations propagating in the body of the star itself. When the oscillations reach the stellar surface, they cause a characteristic pattern of light changes, which carry important information about the internal structure of the stars. The first comprehensive treatment of this subject was the book written by Sir Arthur Eddington. He showed that the pulsation period of a star (P) and its average density (ρ) are related by a simple

A KONKOLY-ALAPITVÁNYÚ BUDAPEST-SVÁBHEGYI M. KIR.
ASZTROFIZIKAI OBSZERVATÓRIUM CSILLAGÁSZATI ÉRTEKEZÉSEI
I. kötet. 1. füzet

ÜBER DIE
RÄUMLICHE VERTEILUNG DER STERNE

VON

LADISLAUS DUNST

INAUGURAL-DISSERTATION
ZUR ERLANGUNG DER DOKTORWÜRDE
GENEHMIGT
VON DER PHILOSOPHISCHEN FAKULTÄT DER
FRIEDRICH-WILHELMS-UNIVERSITÄT ZU BERLIN

Referenten: Professor Dr. A. Kopff.
Professor Dr. E. Kohlschütter.

Tag der mündlichen Prüfung: 25. Juli 1929.

BUDAPEST, 1929

Figure 1: Cover page of the first issue of the institute's communications series containing Detre's PhD Theses on the space distribution of stars.

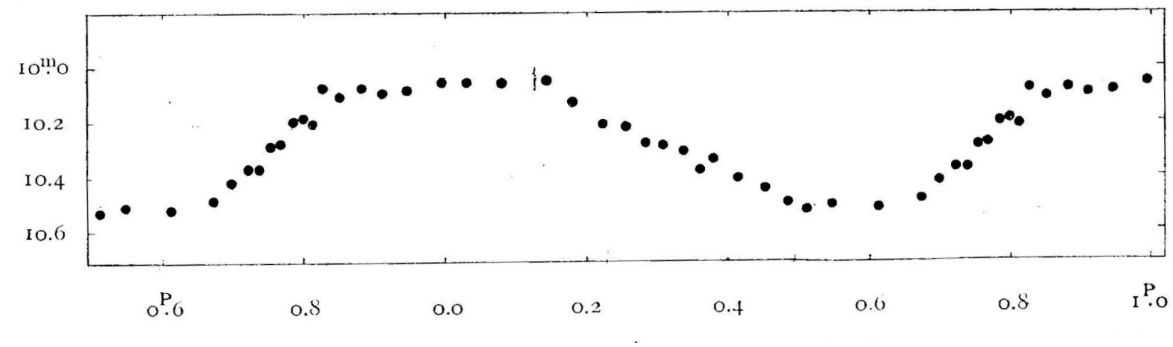

Figure 2: Light curve of RU Piscium as published in the Astronomische Nachrichten in 1931.

formula: $P\sqrt{\rho} = C$, where C is constant within the limits of the theory. Variable stars of short (0.5-1 day) period undergo several tens of thousands of periods during a generation. So their period can be measured to the accuracy of 10^{-5} s. Consequently, the processes, which would take several millions of years to complete, can cause an observable difference in the star's period in only a few decades. Research papers, devoted to the study of period changes caused by the evolution of stars, started to appear in the 1930s.

The Astronomische Gesellschaft, which was dominated by the Germans, held its 1930 General Meeting in Budapest, where some of the leading lights of the Anglo-Saxon astronomical community were also invited. Arthur Eddington was one of those invited, and he, according to the testimony of contemporary photographs, also paid a visit to the observatory in the Svábhegy. We do not know whether they discussed Eddington's new theories about the pulsation of variable stars and their observable consequences, but we know that, with the work of László Detre and later Júlia Balázs in the 1930s, the study of period and light curve variations of short period, RR Lyrae type pulsating variable stars, became one of the most important research fields of the institute at the Svábhegy.

It soon became obvious that the problem was not as simple as it first appeared, because there exist some period changes which cannot be attributed to the passage of time and the ageing of the star. The first task was to eliminate those from the changes studied. The study of variable stars provided decades of work for the institute, and it is still going strong.

I think it is not by chance that Detre changed his research field from stellar statistics to the study of period changes of short periodic pulsating variables. His first paper on this subject was published on the RR Lyrae star RU Piscium in 1931 in the Astronomische Nachrichten (*Fig. 2*). Detre used visual photometry in this work obtained with a Graff photometer attached on the 24 cm Heyde refractor (*Fig. 3*). In 1933 the visual technique was changed onto photographic observations. The 16 cm Merz was replaced by a 19 cm Cook refractor equipped with a 6 inch astrograph for photographic observations (*Fig. 4*). This instrument became the main observing facility for the further variable star research in the institute.

The photographic observation of globular clusters was another new departure for the institute which was initiated by Detre, made possible by the installation of the 24 inch telescope. In these clusters, hundreds of thousands of stars, among which there are many variable ones, are squeezed together in a relatively small volume. This makes it possible to record quite a few hundred variable stars on a single photographic plate. During the 1930s the globular clusters became very important. From their spatial distribution it became

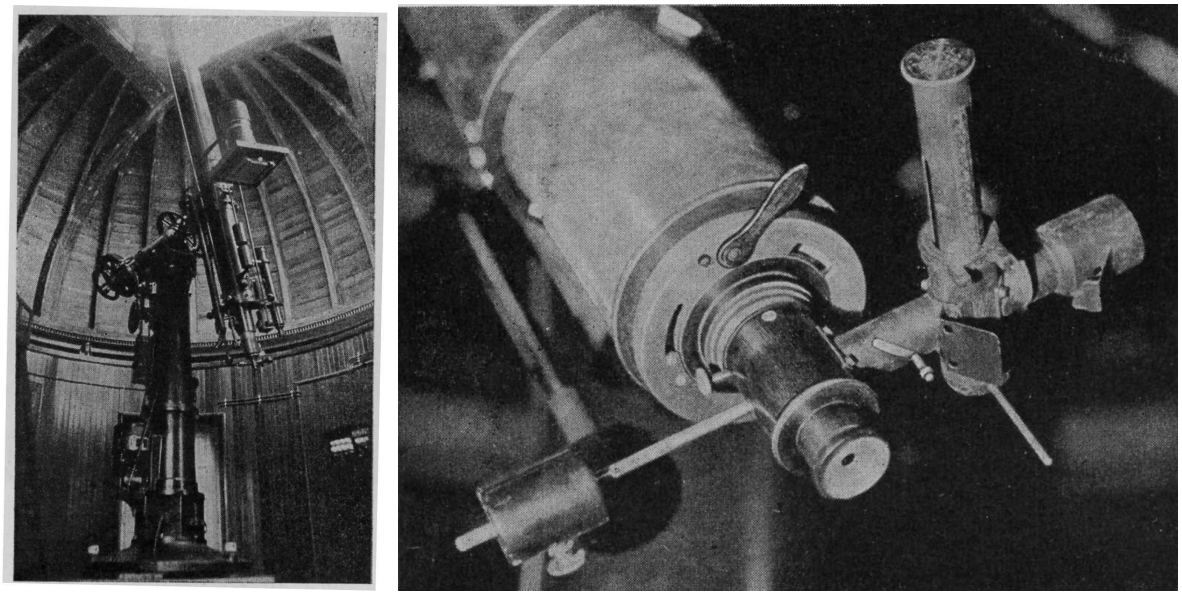

Figure 3: The 20 cm Heyde refractor of the institute (left) and the Graff visual photometer attached to the telescope (right).

possible to deduce the location and distance of the center of our Milky Way system. Subsequent studies revealed that, according to our present knowledge, these clusters are the oldest objects in the Universe, and their age is an excellent clue as to the verification of modern models of cosmological theories.

László Detre as director of the institute

On December 31, 1943 László Detre was appointed director of the institute.

The institute in the Svábhegy did not survive WWII without serious consequences. From 1943 onwards conditions rapidly deteriorated. Most of the periodicals and scientific publications published abroad failed to arrive. From the summer of 1944 the allied air offensive became more and more dangerous. On the top of Csillebérc, in the close neighbourhood of the institute, an AA battery was installed and, as it was a legitimate target, the director was, not unreasonably, worried about suffering collateral damage, should the allied flyers attempt a counterstroke. The 24 inch mirror was dismantled, but with the smaller telescopes observations continued until the early days of December, 1944. On the 25th of December, 1944 the institute was occupied by Soviet troops, specifically by a battery of field artillery, with the strength of about six hundred soldiers and one hundred horses. The soldiers were billeted in the main building, the domes were used as stables for the horses and as field kitchens.

Three days after the occupation Detre reached an agreement with the Soviet command, to the effect that the library and some of the laboratories were declared 'off limits' and free from billeting. When I was a young researcher, I heard some rumors about one of the Soviet officers having been a fellow astronomer and that the quick and favorable response to the institute's request was due to his intervention. While we were preparing for the centenary of the institute in 1999, I tried to verify this story, but I could not find anybody either to confirm or to deny it.

Today it is with pride that we show our library to our visitors, and the exemption

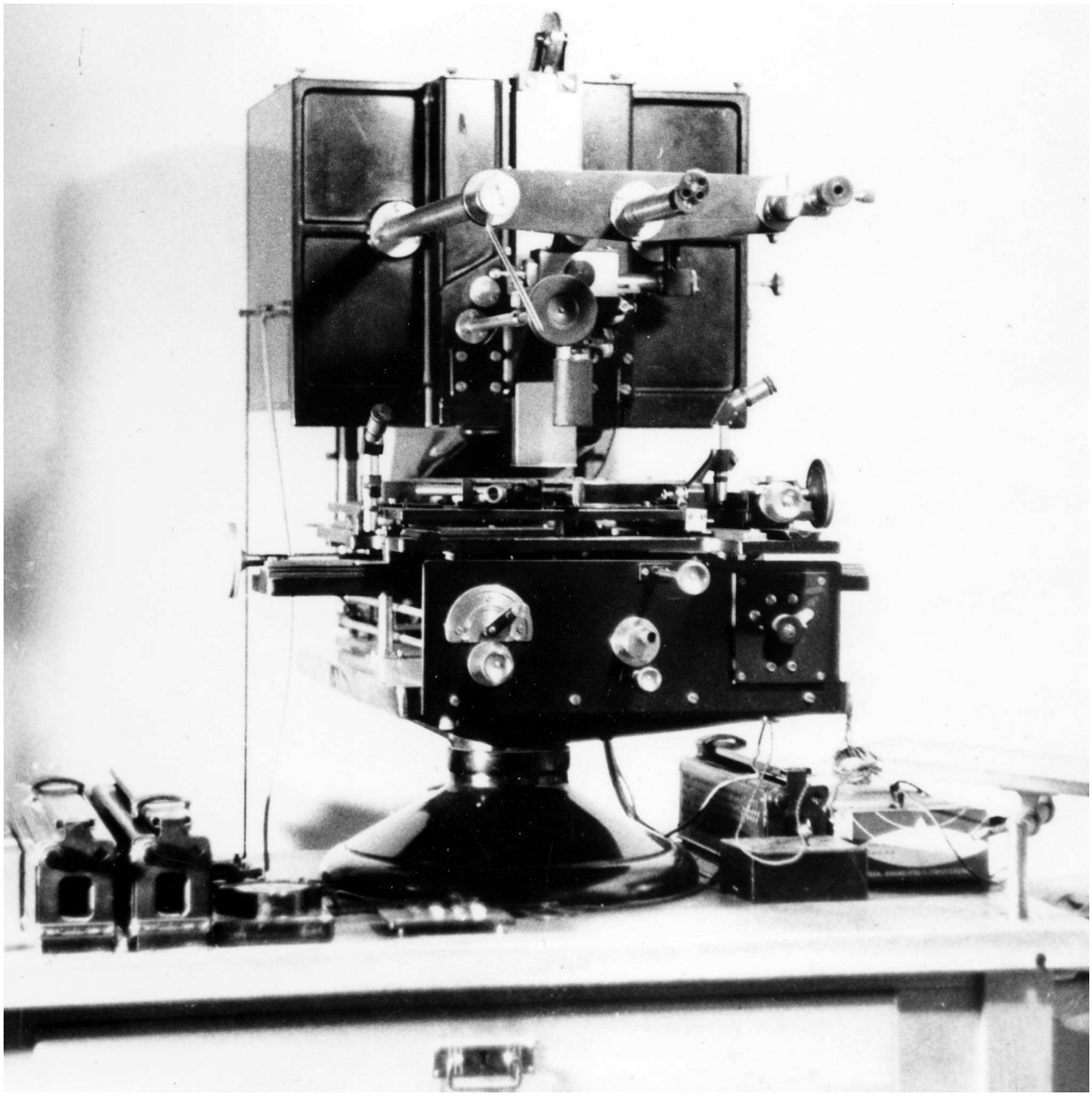

Figure 4: Photometer used for measuring the plates obtained with the 6 inch astrograph.

from billeting was a decisive factor in this. In spite of the turbulent history of Central Europe, complete sets of all the important astronomical publications (the Astronomische Nachrichten from 1823, the Astronomical Journal from 1851, etc.) can be found in our library. Publications not received during the war were successfully replaced soon. Thanks to the Rockefeller Foundation, the library received the missing volumes of the Astrophysical Journal and Astronomical Journal of 1941-46 and 1941-47 years, respectively.

As an acknowledgement of his internationally respected scientific results, László Detre was elected a corresponding member of the Hungarian Academy of Sciences in 1947.

In 1946 a decision was made on establishing a department of solar physics. For making heliophysical observations a photo-heliograph and Konkoly's 25 cm telescope were installed. The regular observations were started in March 1950. The whole solar disc and those parts covered with spots and prominences were regularly observed photographically. Based on their observations, the members of the department informed the National Meteorological Service by phone, when it was necessary, on the development of the solar activity. Beside the observations the statistical investigations made a significant part of the activity of the department. In 1957 a decision was made on moving the Department of Solar Physics into Debrecen where it started to work on January 1, 1958 as an independent institute on a location provided by the Kossuth Lajos University of Sciences.

Astronomical Institute of the Hungarian Academy of Sciences

At the foundation on the Svábhegy the institute belonged to the Ministry of Cultural Affairs but after that it joined the "Collection University" and in 1934 the Pázmány Péter University of Sciences. In 1948 the Ministry of Cultural Affairs received it back again. On the occasion of changing the political system, in 1948 a decision was made on establishing a network of research institutes, independent of the universities and organized within the framework of the Hungarian Academy of Sciences. On February 1, 1951 according to the 10/1951/I.6./M.T. decree of the Council of Ministers the Academy took over the institute under the name of Astronomical Institute of the Hungarian Academy of Sciences (widely known as the Konkoly Observatory abroad). Two departments were formed at the astronomical institute of the Academy: the astrophysical and the heliophysical.

After WWII the advance of astrophysics re-started at a very fast pace indeed. One of the most decisive factors in its advance was the appearance of radio astronomy. The discovery of the theoretically predicted radiation of the neutral hydrogen at the wavelength of 21 cm was its first great achievement. The appearance of computers also produced revolutionary changes. The traditional field of astronomy, optical observations were also significantly influenced by these changes. The giant 5 m reflector at Mt. Palomar started its operations in 1949. There was another reflector there with 180 cm mirror diameter. This telescope of the type Schmidt has a wide field of view (6.5°). With this instrument, the mapping of the whole firmament (up to about 21st magnitude) was completed in a few years. The result of this work, the Palomar Sky Atlas served as a starting point for many important explorations.

This rapid advance resulted in a dilemma for Hungarian astronomy. The problem was to find a compromise between the challenges presented by these advances, and the impoverished state of the Hungarian economy. One element of the solution was the introduction of photoelectric photometry. In the field of optical astronomy, the photoelectric multiplier played the leading role. In comparison with the conventional photographic plate, which

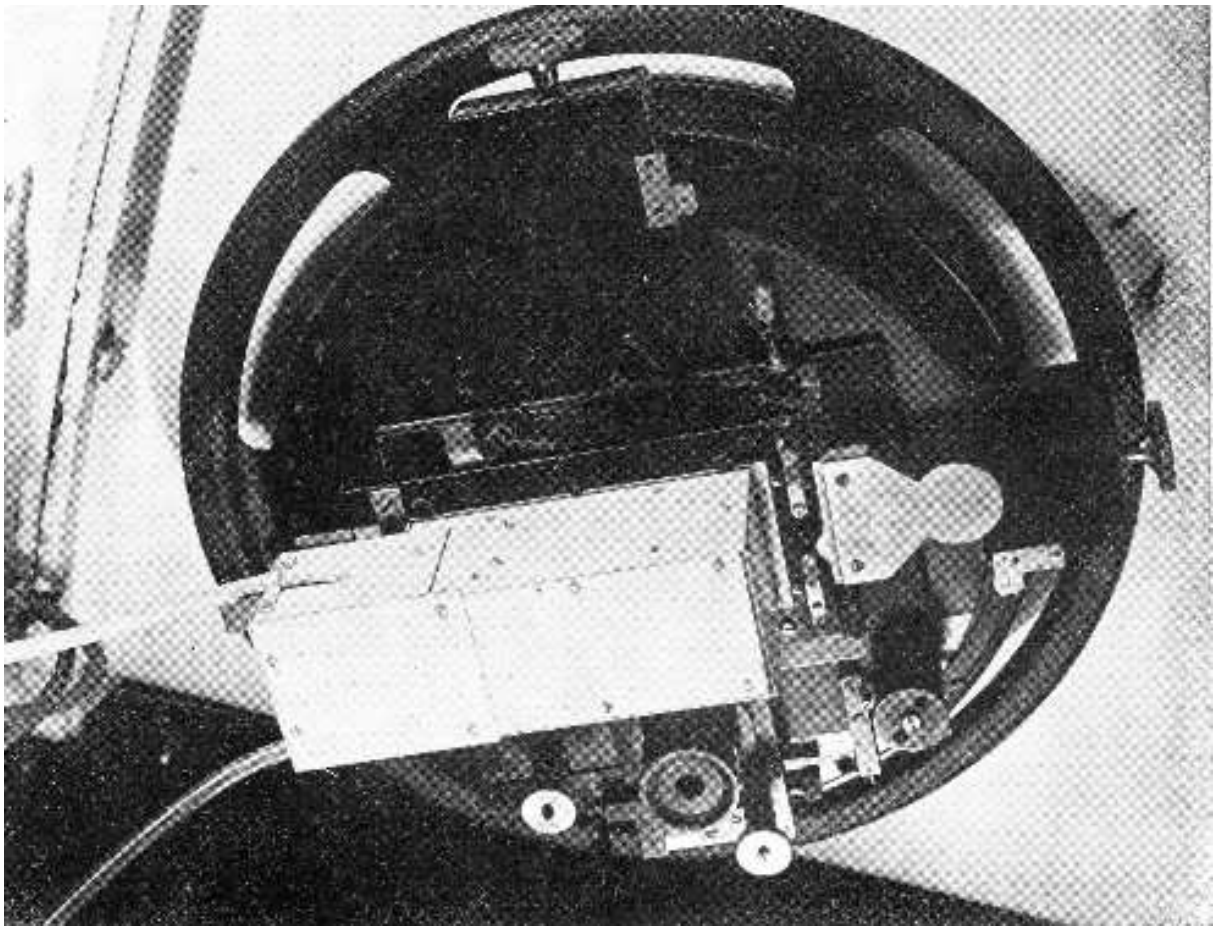

Figure 5: Photoelectric photometer attached on the Newtonian focus of the 60 cm telescope. The instrument used the 1P21 tube obtained from H. Shapley in 1948.

had the disadvantages of a less than one per cent quantum efficiency and the non-linear characteristics of its light sensitivity, the new instrument had a high quantum efficiency, linear characteristics and a much reduced level of noise.

After the war the institute and the firm 'TUNGSRAM Ltd.' conducted some joint experiments to develop a photomultiplier for astronomical purposes, but these failed to yield the desired results. In 1948 the then director of the institute, László Detre, received a 1P21 type multiplier from Harlow Shapley. This equipment made it possible to build a new photometer, which, fitted to the 24 inch telescope, enabled the institute to carry on with its work using really state-of-the-art technology (*Fig. 5.*). The first results were published on the photoelectric observations of the 1950 eclipse of ζ Aurigae in the No. 29 issue of the communications of the institute (*Fig. 6.*).

In 1954 they obtained a further 1P21 tube enabling them to observe down to 13th magnitude. Following the suggestion of the Dutch astronomer Theodor Walraven they rebuilt the amplifier of the photometer in 1955. Two further 1P21 tubes arrived in 1956 and László Detre received a further amplifier as a gift on the occasion of his visit in Leiden which made it possible to establish another photometric observing site based on a 25 cm reflector, so photoelectric photometry became one of the routine methods of observation.

Putting on orbit the first artificial satellite of the Earth in 1957, a new era started in the technical civilization which naturally had an impact on astronomical research.

MITTEILUNGEN
DER
STERNWARTE
DER UNGARISCHEN AKADEMIE
DER WISSENSCHAFTEN

ИЗВЕСТИЯ
АСТРОНОМИЧЕСКОЙ
ОБСЕРВАТОРИИ
АКАДЕМИИ НАУК
ВЕНГРИИ

BUDAPEST—SZABADSÁGHEGY

Nr. 29.

PHOTOELECTRIC OBSERVATIONS OF THE 1950 ECLIPSE OF ZETA AURIGAE

by

L. DETRE and T. HERCZEG

The eclipse of the B-type component in the remarkable binary system ζ Aurigae occured for the last time in 1950 August and September. On this occasion observations were secured with a photoelectric photometer attached to the 24-inch reflecting telescope of the Budapest Observatory. The photoelectric equipment was an R. C. A. multiplier phototube with a d. c. amplifier and with a galvanometer of low sensitivity. The multiplier phototube was presented us by Dr. *H. Shapley*, Director of the Harvard Observatory, at the Zürich meeting of the I. A. U., 1948. The equipment will be described in another paper of this series.

Figure 6: The first published result based on photoelectric measurements carried out in the Konkoly Observatory

The Astrosoviet (Astronomical Council) of Moscow asked our institute to participate in the observations necessary for computing the orbits and donated 40 telescopes for visual observations well suited for installing a satellite tracking station. Besides Budapest such stations were installed in Baja, Miskolc and Szombathely which did not belong to the Academy, the professional coordination, however, was carried out by the institute. Following Detre's initiative, the station of Baja joined the institute but the others kept their independence.

In the field of artificial satellites the cooperations were realized within the framework of the INTERCOSMOS. In 1965 COSPAR had already two Hungarian members. The first computer program made in the institute in 1961 was related to the motion of the artificial satellites.

In 1970 László Detre received a State Award.

New station at Piszkéstető

The building of the observation station on Piszkéstető was a decisive impact of Detre's activity on the institute's life. The story of the Piszkéstető station had its commencement in the 1950s.

After the change of regime in 1948, a decision was made to set up of a network of research institutes under the general guidance of the Hungarian Academy of Sciences. One of the spectacular steps in this programme was the establishment of the Central

Research Institute for Physics. Following a decision made by the Council of Ministers, the Observatory in the Svábhegy also became part of this scientific network. In the context of the programme of extensive investment in science, it also became feasible for the institute to make a substantial capital investment.

At the beginning of the 1950s the improvements made to Budapest's public lighting and its increasing pollution made any further development of the observational facilities in the Svábhegy observatory pointless. In the early 1950s the Academy approved the acquisition of a wide angle telescope of the Sonnenfeld type, and the order was placed with Zeiss of Jena. Shortly afterwards the order was cancelled and a new order was placed for another wide angle telescope of the Schmidt type. This Schmidt telescope has a 900 mm mirror and a 600 mm correction plate, which makes her exactly half the size of the Mount Palomar Telescope, its sister, commissioned a few years earlier. The telescope was supplemented by the planned purchase of a 600 mm objective-prism, which was only marginally smaller than her biggest, 800 mm companion, the instrument installed at Hamburg. With the Schmidt telescope, Hungarian astronomy came again to possess a world-class instrument.

The Council of Ministers allocated nine million Hungarian Forints to astronomy. The construction of the new observatory started in 1958, at Piszkéstető, which is the third highest peak in the Mátra Mountains, 100 km NE from Budapest. The telescope itself became operational in 1962.

The development of astrophysics, that started after WWII, gained considerable momentum by the 1960s. In this, one of the decisive factors was the infusion of the revolutionary new microelectronics into the realms of astrophysics. With the appearance of electronic computers, numerical simulations (or modelling) became feasible. This enabled the scientists to replace their analytical approximations with more exact quantitative models, whose results could be directly compared to observational results. The turn of the 1950s saw the birth of models describing the evolution of stars. One of the interesting achievements of modelling techniques was, that with their help it was possible to verify the Hertzsprung-Russell diagram, which was discovered early in the century and relates the surface temperature of the stars to their absolute luminosity. Curve-fitting using these models can also yield the age of the cluster and its distance from Earth. The number of open, or galactic, clusters in our Milky Way system is estimated as several thousand. The examination of the HRD of these clusters is one of the important investigations carried out with the new telescope at Piszkéstető.

Perhaps the most spectacular touchstone of the stellar evolution theories was the theoretical clarification of the background to the explosion of supernovae. One of the most important problems concerning this subject is the determination of the stellar mass necessary to end up as a supernova. As the last supernova observed in our galaxy was observed by Kepler, our up-to-date knowledge must be based on observations of extragalactic supernovae. With the systematic survey of extragalactic events we might get a reasonable picture of the frequency of such events. With its 5° field of view, the Schmidt telescope at Piszkéstető is capable of regularly surveying areas rich in galaxies. It was in 1964 that the first supernova was observed. This was followed by the finding of 48 more, so it was at Piszkéstető, where almost ten per cent of the known supernovae were discovered in the era of photographic supernova patrols.

The Schmidt telescope also made the observation of special stars possible, such as the flare stars, showing sudden increases of light emission occasionally, or young stars at the beginning of their existence, showing a significant emission in the Hα line. The distribu-

tion of stars showing Hα emission yields important supporting data for the investigation of physical processes, occurring in molecular clouds active in the formation of new stars. In 1966 the Mátra station's instrument park was enriched by a Cassegrain-type telescope of 50 cm mirror diameter. The attachment of a photometer, developed within the institute, made it possible to utilize the favorable conditions prevailing around the Mátra station also in the field of photoelectric photometry.

At Piszkéstető the last and largest capital investment was the acquisition of an RCC telescope of 1 m diameter. In the beginning, the telescope was operated using CAMAC modules and a TPAi minicomputer, which were developed by the Central Research Institute for Physics. They were used for digitally positioning the telescope and collecting and storing the observed data. The telescope, augmented by the photoelectric photometer – developed by the institute – was in all respects up to contemporary world standards.

Unfortunately, László Detre did not live to see the inauguration of the RCC telescope at the end of 1974 since he died weeks before, on October 15.

International relationships

The institute had traditionally good relationship with German astronomy. Until 1942 it issued a summary report on the annual work to the Vierteljahrsschrift published by the Astronomische Gesellschaft.

Following the World War I to compensate the international reputation of the AG, the Anglo-Saxon powers established the International Astronomical Union (IAU). Since Hungary was fighting on the defeated side, its researchers were excluded, along with the Germans. Our relationship to the IAU was normalized only after the World War II. Although there were some efforts to establish American relationships (e.g. on the occasion of a longer study visit of Károly Lassovszky, later director of the institute), the young researchers typically had fellowships at German institutes. Of course, there were some efforts on the part of the scientists to remove this discrimination. The AG had its general assembly on August 8-12, 1930 in Budapest with the participation of several distinguished scientists from Anglo-Saxon countries (e.g. Arthur Eddington, Otto Struve).

The international relations of the institute were changed drastically after the war. As an opening of the new era, László Detre was admitted to the IAU, as the first Hungarian astronomer. After the change of the political system in 1948 international relations started preferring the Soviet Union. Until this time Hungarian astronomers had little contact with their Soviet colleagues, but then it changed drastically. Short and longer study trips to the Soviet Union became regular. In 1950 Boris V. Kukarkin, having an international reputation in the field of variable star research, suggested to start a cooperation in the main research field of the institute. In 1952 the Institute of Theoretical Astronomy of Leningrad requested us to cooperate in the precise determination of positions of minor planets having uncertain ephemerides. Even in this year a third scientific department of the institute was founded under the leadership of István Földes. The Department of Positional Astronomy and Stellar Statistics, however, stopped its operation after two years, since due to the recession of the economy, the reduction of the staff was ordered in the institute. This was solved by putting an end to the young department in 1954 (by dismissing the head and two coworkers).

Due to the bilateral cooperation agreements between the Academies of the socialist countries, personal contacts also became possible in astronomy. As a natural consequence,

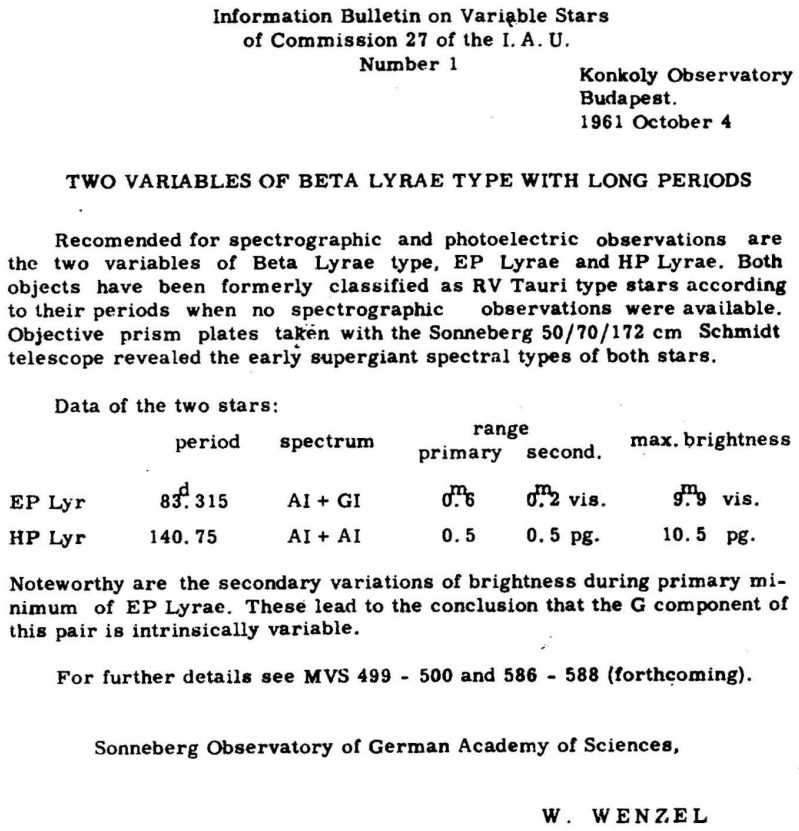

Information Bulletin on Variable Stars
of Commission 27 of the I. A. U.
Number 1

Konkoly Observatory
Budapest.
1961 October 4

TWO VARIABLES OF BETA LYRAE TYPE WITH LONG PERIODS

Recomended for spectrographic and photoelectric observations are the two variables of Beta Lyrae type, EP Lyrae and HP Lyrae. Both objects have been formerly classified as RV Tauri type stars according to their periods when no spectrographic observations were available. Objective prism plates taken with the Sonneberg 50/70/172 cm Schmidt telescope revealed the early supergiant spectral types of both stars.

Data of the two stars:

	period	spectrum	range primary	range second.	max. brightness
EP Lyr	$83^d.315$	AI + GI	$0^m.6$	$0^m.2$ vis.	$9^m.9$ vis.
HP Lyr	140.75	AI + AI	0.5	0.5 pg.	10.5 pg.

Noteworthy are the secondary variations of brightness during primary minimum of EP Lyrae. These lead to the conclusion that the G component of this pair is intrinsically variable.

For further details see MVS 499 - 500 and 586 - 588 (forthcoming).

Sonneberg Observatory of German Academy of Sciences,

W. WENZEL

Figure 7: The first issue of the IBVS in 1961

not only our researchers travelled to these countries but a high number of colleagues visited our institute from there. In 1959 an opportunity was presented to establish contacts with Chinese astronomers. In the framework of this, the institute donated a photoelectric equipment to the Observatory of Nanjing. In order to strengthen the cooperation with Romanian astronomers, an 1P21 photoelectric multiplier was donated.

Starting in the second half of the fifties, the cold war started to turn milder and in the life of the institute an apparent sign for it was Detre's participation at the general assembly of the IAU in Dublin in 1955. The 27th Commission of the IAU (Variable Stars) supported the widening of the international cooperations in a special resolution.

A very high reputation of the Hungarian variable star research and the work of László Detre, was an international conference held in 1956 August 23-28 in Budapest dealing predominantly with period and light curve variations of RR Lyrae and δ Cephei stars.

The revolution in 1956 shocked the institute dramatically. The migration wave following the revolution resulted in the leave of three excellent researchers (Tibor Herczeg, Imre Izsák, and István Ozsváth) who started their career with great promise. Although, they were soon replaced by young people starting out on a career but the loss of their expertise had a long lasting effect on the institute.

It was an important milestone of the international appreciation when the IAU commissioned our institute to edit and publish the Information Bulletin on Variable Stars, on

the occasion of the participation of László Detre at the IAU General Assembly in Berkeley in 1961 (*Fig. 7.*).

There were two further events of international importance in the life of the institute in the last years of Detre's directorship in which he played a leading role. In 1968 the Hungarian Academy of Sciences hosted an IAU colloquium on non-periodic phenomena in variable stars in Budapest. Following the initiative of Soviet astronomers, the scientific academies of the socialist countries signed a cooperation agreement on the physics and evolution of stars in 1974.

One has to pay special attention to the agreement with the Armenian Academy of Sciences. It was quite uncommon that a member republic of the Soviet Union established international relationships getting round Moscow. This agreement obviously was a tribute of Victor Ambartsumian, the president of the Armenian Academy of Sciences and an astronomer of very high international reputation. He visited our institute many times and also had a good personal relationship with László Detre and our researchers. Following this cooperation agreement, signed in 1968, the Armenian and Hungarian astronomers had a very tight contact until the collapse of the Soviet Union.

Epilogue

On the occasion of Detre's centenary, the drawing of conclusions and the recapitulation of the lessons learned is almost inevitable. Many of us are having our minds exercised by the problem of trying to find the source of strength that kept our institute in existence, in spite of the trials and tribulations it was exposed to. How typical was this of the intellectual and scientific life in Hungary? An important element of the success was the finding of a 'window of opportunity' between the international scientific challenges and the material resources of Hungary, but this is not the whole secret.

There is also an independent factor behind the success, which may be called the human factor. It is a loose concept and may include everything that happens inside us and influences our decisions, but remains invisible to the contemporary onlookers and even to history. I have been struck by an idea, found in the writings of István Bibó[1], that there is no natural law which could guarantee success in the development of human societies. The evolution of any social structure is a possibility, which can be achieved by making the right decisions, but the other outcome is also possible.

During the years of Detre's activity, the institute was faced with many crises, but managed to survive them successfully. Does this fact have a special meaning for the intellectual life of Hungary? It is my firm belief that the answer is an unqualified 'yes'. The other important question, which may be even more important than the first one is: Where to go and how to get there. Science will be one of the most important defining factors of any future society. The Hungarian society must develop the inner strength to answer this challenge. What this answer will be, and how effective it will be, is also going to be a determining factor for the future of the Konkoly Observatory, but the heritage of László Detre's work has a significant impact on it.

[1]István Bibó, Hungarian social scientist, one of the spiritual fathers of the Hungarian revolution in 1956

Variable star research at the Konkoly Observatory The first 75 years

Dedicated to László Detre's memory at the 100th anniversary of his birth

Béla Szeidl

Konkoly Observatory of the Hungarian Academy of Sciences
P.O. Box 67, H-1525 Budapest, Hungary

Introduction

It is now evident that at some level, the light output of stars, including our Sun, varies over different length of time. Little wonder that the investigation of variable stars has a special place in astronomy. Almost all of our knowledge of stellar interior come from the study of pulsating variables. The observed surface luminosity, radius and colour variations probe into the stellar interiors in much the same spirit as in terrestrial seismology. The fact, that the light curve parameters and periods of pulsating stars are closely related to their physical state and are well measurable renders them as excellent calibration objects.

The study of other types of variable stars has also large impact on our knowledge about the physics of stars. The eclipsing variables tell us information about the size and mass of the stars. The observations of variable young objects enlighten the process of birth of stars and draw picture on the interaction between stars and interstellar matter. The cataclysmic variables (dwarf novae and their violent relatives, the novae and supernovae) are clue objects in a number of astrophysical problems. Stellar activity manifests itself in luminosity variability in a broad spectral range from X-ray to radio wavelength. The rapid rotation and the convective atmosphere of the cool-surfaced stars render the operation of dynamo possible, producing a magnetic field that drives spot formation and other phenomena of stellar activity. Spotted stars allow to directly measure the stellar rotation, even the differential rotation.

The start of the systematic study of variable stars goes back to the mid-19th century when F. W. A. Argelander's epoch-making paper was published in Schumacher's Jahrbuch

(1844). At that time only one and a half dozen stars of this type were known. This appeal for observing variable stars incited astronomers all over the world. By the end of the 19th century almost one thousand variables were already known mainly due to the rapid development of the photographic technique.

The light variation caused by eclipses of two stars orbiting each other was easy to explain as it was mainly an optical and mechanical problem. The understanding of the physics of intrinsic variables, however, proved to be more difficult. The pulsation theory was put forward as a hypothesis for discussion by H. Shapley[1] and soon the hypothesis for discussion to the rank of major astrophysical theory by A. S. Eddington[2]. The explanation of light variation of cataclysmic and related objects required more knowledge about energy production of stars and became reality only half a century later.

In the second half of the 19th century the observers in Hungary were rather interested in the objects of the Solar System, the planets and comets, so little wonder that records of star observations made here can hardly be met from this time. The first variable star observations in Hungary were made in 1879 by Friedrich Schwab, a German mechanician who worked for a while in our country[3]. Afterwards, apart from Miklós Konkoly's scarce spectroscopic observations no variable star research of scientific value was carried out in Hungary until the beginning of the 20th century.

Ó-Gyalla, after the nationalization

In 1899 Miklós Konkoly Thege handed over his private observatory at Ó-Gyalla to the Hungarian state. It was, indeed, a mile-stone in the history of the Hungarian astronomy. An institute run by the state had greater possibilities and a more prosperous future.

Konkoly Thege was keenly interested in the bodies of the Solar System, planets, comets, and meteors and was a passionate pioneer of photography and spectroscopy. Soon after the foundation of his private observatory regular sunspot observations had been performed. The change in the status of the observatory, however, necessitated the reconsideration of the scientific program and, in conformity with the scientific attitude of that time, a shifting of stress set in toward the study of the physics of stars. In view of the modest optical instruments available then at Ó-Gyalla, the photometric observation of variable stars was chosen as the principal program (Tass 1904b) but, of course, the traditional work had also been pursued. The 6 and 10 inch refractors of the observatory were used for the photometry. In 1901 and 1902 a wedge photometer manufactured in Töpfer's workshop in Potsdam was put to use for stellar brightness measurements. In order to eliminate the disturbing illumination of the scale of the wedge, its position was registered[4]. Later, from 1902, Zöllner-type photometers were mostly used for brightness measurements. The small Zöllner-type photometer was also acquired from O. Töpfer, in 1903. This photometer was then further developed in the workshop of Ó-Gyalla. Instead of paraffin flame (that was used before) an electric lamp provided the artificial star.

The variable star observations in Ó-Gyalla started on the evening of September 19, 1900. The permanent staff members of the observatory, baron Béla Harkányi, Antal

[1]Astrophys. J., 40, 448, 1914

[2]Mon. Not. RAS, 79, 2 and 177, 1918

[3]P. Brosche & E. Zsoldos: Zwischen Handwerk und Wissenschaft: Friedrich Schwab (1858-1931), in: Beiträge zur Astronomiegeschichte, Acta Historica Astronomiae, 18, 182, 2003

[4]The flash of wit that a device should be used to register the wedge position instead of direct reading came from Jenő Gothard (Zeitschrift für Instrumentenkunde Jg. 1887, S. 347)

Tass and Lajos Terkán took part in the ambitious program. Later Emil Czuczi and Zsigmond Fejes joined forces with the principal observers for a while. Harkányi, Tass, and Terkán selected the program stars very carefully. They consulted with S. C. Chandler's "Third Catalogue of Variable Stars"[5], E. Hartwig's "Ephemeriden veränderlicher Sterne" regularly published in the "Vierteljahrsschrift der Astronomischen Gesellschaft" and E. C. Pickering's list published in a note on "Cooperation in observing variable stars"[6]. Of course, the selection of program stars was confined by the limited efficiency of the modest instruments and the latitude of the observatory.

The unfavorable air conditions in the surrounding of Ó-Gyalla very often made the observations difficult. Three rivers, Zsitva, Nyitra, and Vág met near Ó-Gyalla, and the Danube streamed close to it. Due to the frequent fog it rarely happened that photometric observations could be carried out on some consecutive nights.

Between September 19, 1900 and January 2, 1903, 22 variables such as miras, δ Cephei type stars, eclipsing variables, and a nova were observed on 116 nights with the wedge photometers. During this period 425 observations were collected.

Between April 12, 1903 and November 16, 1908, the Zöllner-photometer was used for the photometry of variables. On the whole 1870 observations were obtained on 372 nights. 129 variable stars, mostly miras, red semi-regular stars, cepheids and eclipsing variables were on the list of observation. After 1908 only sporadic observations (5 nights in 1909, one night in 1910 and 8 nights in 1913) could be made, for the principal observers (A. Tass and L. Terkán) had other task, the photometric survey of the southern sky from 0° to 15° southern declination was undertaken, a continuation and extension of the "Potsdam Durchmusterung" to the South. This program was only partly executed, the visual photometry of all stars of the BD down to the magnitude 7.5 in the zone from 0° to 10° southern declination had been carried out and published (Tass & Terkán 1916).

The variable star observations were published in a series of papers (Tass 1904a, 1904b, 1905b, 1906, 1908a, 1908b, Terkán 1905). While observing the program stars two stars were suspected to be variable. In Cassiopeia, near T Cas, the 8th magnitude star BD+54°49 (=190.1904 Cas) was one of the variable candidates (Tass 1905a, 1905c). J. G. Hagen[7], however, doubted its variability. It is worth mentioning that later the star was identified as Bamberg variable BV328 and classified as an eclipsing variable with a period of 0.602625 day and amplitude of 0.3 magn.[8]. The fact, however, is that neither the Hipparcos photometry nor the NSVS[9] prove the variability of the star with an amplitude larger than 0.03 magn.

Tass had hard luck with his other discovery, too. He noted that the star BD+22°1576 in Gemini, close to the program star R Gem, varied in brightness (Tass 1905d) and it received later the variable star name TW Gem. The observations of C. Payne-Gaposchkin[10], however, gave no indication of variability. R. Prager[11] summarized the behaviour of the M3 III type star as of small range and irregular, if it were variable at all.

On February 21, 1901 14^h40^m GMT Th.D. Andersson[12] discovered a $2\overset{m}{.}7$ bright new

[5]Astron. J., 16, 145, 1896

[6]Astron. Nachrichten, 154, 405, 1901

[7]Astron. Nachrichten, 168, 11, 1905

[8]W. Strohmeier & R. Knigge, Veröffentl. Bamberg, 5, Nr. 6, 1960; W. Strohmeier, Inf. Bull. Var. Stars, No. 26, 1963

[9]P. R. Wozniak, W. T. Vestrand, C. W. Akerlof et al., Astron J., 127, 2436, 2004

[10]Harvard Ann., 118, No. 15, 1952

[11]Geschichte und Literatur des Lichtwechsels der Veränderlichen Sterne, 1, 109, 1936

[12]Astron. Nachrichten, 154, 363, 1901

star in Perseus. The new bluish-white variable received the provisional name 3.1901 Per and later the official variable star name GK Persei. On February 19, the star was invisible (fainter than 11^m magn.) and attained to its maximum brightness of about $0\overset{m}{.}0$ around February 23. The observers at Ó-Gyalla (b. B. Harkányi, A. Tass, and L. Terkán) immediately commenced the observations of the new star on the first clear night (*Fig. 1*). Between February 28 and December 29, 1901 294 brightness measurements were made on 63 nights. The observations had been interrupted only in May and June, when the constellation Perseus was near the Sun, and in September due to technical problems. At the end of 1901 the star's brightness became fainter than 7th magnitude, the attainable limit of the 16 cm refractor with the wedge photometer. Throughout the observations the comparison stars were taken from the Potsdam Durchmusterung (Harkányi 1901a, 1901b, 1903). The Ó-Gyalla observations were in very good agreement with other observers' results indicating the high accuracy of the Ó-Gyalla photometry. The nova, during its descending phase, showed fast light fluctuations with amplitudes of 1-2 magn. This behaviour, first observed in GK Per is a characteristic feature of cataclysmic variables with rapid development. Nova GK Per is one of the best observed novae and the typical representative of its class.

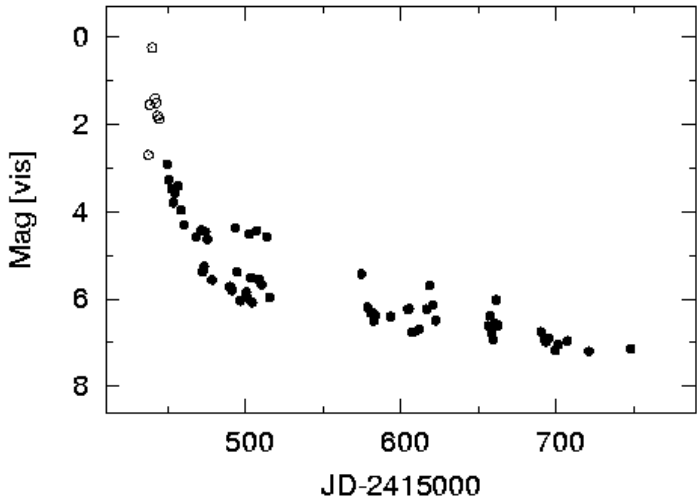

Figure 1: The nightly mean observations of GK Persei (Nova Per 1901) made at the Ógyalla observatory between 1901 February 28 and December 29 (filled circles). The nova, during its descending phase, showed fast, large light fluctuations. The observations of other observers before February 28 are also indicated (open circles).

Tass took part in the observations of another nova, too. Nova Aquilae 3 (=7.1918 Aql) was discovered on June 8, 1918 by L. Courvoisier[13]. The same night F. Schwab[14] estimated its brightness as 1st or 2nd magn. and remarked that is was "in Zunahme", still brightening. It attained the maximum brightness of -0.3 magn. on June 9. Tass (1918) observed the nova on June 14, 15, 16 and made 7 estimates both with the wedge and the Zöllner photometers on the 16 cm refractor. During these three nights the nova had been continuously fading from 0.74 to 2.18 magn.

[13]Astron. Nachrichten, 207, 17, 1918
[14]Astron. Nachrichten, 207, 17, 1918

One hundred years ago the explanation of light variation of stars was certainly known only for the class of eclipsing variables. Little wonder, that the staff of Ó-Gyalla Observatory of Konkoly's Foundation actively took part in the observations of bright eclipsing variables. Terkán (1906a, 1906b) analyzed his photometry of β Lyrae obtained with the Zöllner photometer between July 14 and November 26, 1905 and determined the orbital elements of the system. This kind of investigation proved the applicability of the photometry for solving astrophysical problems, e.g. determining the size and mass of the stars.

At the very beginning of the 20th century, in line with the rapid development in physics (both experimental and theoretical) intensive investigations started around the world in order to get better insight into the problems of radiation and temperature (colour) of stars. At the same time, the use of photographic photometry just entered into astronomical application. This kind of investigations and works also started in Ó-Gyalla (Harkányi 1910, Terkán 1904, 1910). Terkán (1910, 1926) made an attempt at determining the colour and temperature variation of the eclipsing variables β Lyrae and β Persei.

The promising research was interrupted, the World War I broke out and the observatory got into a desperate situation. The comprehensive compilation of the variable star observations obtained at Ó-Gyalla could only be published later (Tass 1925). In consequence of the peace treaties, after the war Ó-Gyalla had belonged to Czechoslovakia, thus the staff left for and most of the instruments were transferred to Budapest. The Royal Hungarian Observatory of Konkoly's foundation found its new home on Svábhegy, a hill near Budapest.

The Start at Budapest-Svábhegy

In spite of the severe condition of the country, the Konkoly's Foundation reviewed in its new home near Budapest on Svábhegy, at an altitude of 470 m. The construction of the main building and domes was completed by 1929. The new 60 cm Newton-Cassegrain reflector was erected in a dome of 10 m diameter. The 20 cm Heyde refractor brought from Ó-Gyalla was housed in a 5 m dome and furnished with a new Graff-type wedge photometer. In 1932, the observation of bright stars using the Zöllner photometer attached to the 15 cm refractor that was also transferred from Ó-Gyalla to Budapest, was finished. Then, this telescope was dismantled and was replaced by a 17 cm Cook refractor from Kiskartal, from the private observatory of the Podmaniczky family. A 16 cm astrograph was fitted out to this telescope on purpose to start photographic photometry.

The scientific programs were essentially the same as those carried out at Ó-Gyalla. So, astrophotometry became the principal activity, with special emphasis on the photometry of variable stars. The regular observation of the Sun and shooting stars was, however, given up.

The visual observations of variable stars were already commenced with the Heyde refractor in 1929 and had been kept up as long as for 7 years, until 1936. Two ambitious astronomers, László Detre and Károly Lassovszky performed the variable star observations. Lassovszky took his doctor's degree at Pázmány University, Budapest in 1920 and then joined the staff of the reviving Konkoly Observatory. During time of the setting up of the observatory, he developed his knowledge at different North American and European astronomical institutes. Detre defended his doctoral dissertation at the Friedrich-Wilhelm University, Berlin in 1929 and, immediately after his returning, he started the research

work at the observatory. Lassovszky took interest in eclipsing binaries in the first place, while Detre was keenly interested in pulsating variables. Nevertheless, both of them had either type of variables on their observing list. These years were very productive, a number of papers had been published mostly in the journal Astronomische Nachrichten. Detre and Lassovszky made the visual observations very carefully. Repeatedly, they checked the calibration of the wedge by measuring the stars of the North Polar Sequence or Pleiades. They found that the wedge-constant was not stable from night to night, therefore the sequence "variable + comparison stars" was chosen with great care. The linearity of the wedge, however, remained, which facilitated the reduction of the measurements. The main source of error of the Graff-type wedge photometer was, however, the inequality in the structure of the natural and artificial stellar images. The natural images heavily depended on the air conditions during the night (Lassovszky 1933c, Detre 1934c).

During the seven years, Detre and Lassovszky observed more than thirty stars visually and obtained more than 12000 observations. As mentioned Lassovszky was rather specialized in eclipsing binaries. He made extensive visual observations of four eclipsing variables. KR Cygni (Lassovszky 1936a) was observed on 81 nights and 1225 brightness estimates were obtained, while for AT Pegasi (Lassovszky 1935b) 1060 observations were collected during 59 nights. Similarly, for AB Persei (Lassovszky 1934) 718 visual observations were made on 115 nights, and for SV Tauri (Lassovszky 1938) 1260 observations during 100 nights. AT Peg, AB Per, and SV Tau are Algol type variables, while KR Cyg is of β Lyrae type. Lassovszky made an attempt at deriving the orbital parameters, furthermore the size of these stars. Of course, these results are outdated, but his photometry is still of high value and is used for studying these stars' period changes. In 1931 Lassovszky (1931b) made a short scientific visit to Babelsberg Observatory and measured some variables exposed on Ernostar plates with the 40 cm astrograph, but the observations were scarce to do rigorous investigation. Nevertheless, he discovered a new variable (Lassovszky 1931a,c), that received the preliminary name 381.1931 And, later the final name AP Andromedae. Then he made a series of exposures on Ernostar plates with the 40 cm astrograph and was able to derive the type and the period of the new variable. It proved to be an Algol type eclipsing variable with a period of 1.59 days. The star was, however, too faint for the Heyde refractor at Svábhegy, Budapest, and it could not be observed visually (Lassovszky 1932a).

Detre observed visually only one eclipsing binary, SV Cam (Detre 1932c, 1933b). During 34 nights he obtained 489 visual observations with the Heyde refractor. Some forty years later this star turned out to be a very interesting object. It is not only an eclipsing binary, one of its components is an active, spotted star. The visual observations, as a matter of course, did not reveal this behaviour.

Over and above the eclipsing variables, Detre and Lassovszky had 6 RR Lyrae stars and 8 Cepheids on their list of visual photometry. Detre observed SW Andromedae (Detre 1934c) on 38 nights (550 observations), W Canum Venaticorum (Detre 1935b) during 55 nights (369 observations), RZ Cephei (only the times of light maximum were published, Detre 1931, Balázs & Detre 1938) on 39 nights (590 estimates), XZ Draconis on 20 nights (344 observations) and RU Piscium (Detre 1934a) on 37 nights (472 observations). Of these RR Lyrae stars only short discussions about the period changes were published, since in 1934 Detre and his co-worker, Júlia Balázs decided to carry out a more detailed and thorough investigation of RR Lyrae stars (see next chapter). Here I only mention

one result that shows how accurate Detre's visual observations were: several observers[15] thought that W CVn had light curve variations and short period waves were superimposed on the light curve. Detre's data, however, exhibited strictly repetitive character of light variation of the star. Several decades later, J. Tremko[16] investigated this variable and found that the star had stable and smooth light curve.

The visual observations of cepheids provided useful data to study the changes in periods of these stars. Both Detre and Lassovszky took part in the work and they collected 2515 observations for 8 cepheids. The program stars were YZ Aurigae (Detre 1935c, on 121 nights 239 observations), RW Cassiopeiae (Lassovszky 1932b, on 103 nights 520 observations), SZ Cassiopeiae (Detre 1933a, on 100 nights 344 observations), XY Cassiopeiae (Detre 1932a, on 87 nights 325 observations), SZ Cygni (Lassovszky 1933a, on 90 nights 265 observations), VY Cygni (Lassovszky 1933c, on 79 nights 240 observations), Z Lacertae (Lassovszky not published, on 93 nights 309 observations) and RR Lacertae (Lassovszky 1935a, on 92 nights 273 observations). Here only I mention two results. Lassovszky showed that the light curve variation of RW Cas suggested by M. Beyer[17] was not real. The data used by Beyer were inhomogeneous, simply they were obtained by different colour sensitive instruments (Detre & Lassovszky 1939). Detre investigating the behaviour of XY Cas presented arguments in favour of smooth changes in the period of the star rejecting the sudden change as propounded by L.V. Robinson[18].

The accurate visual observations of Detre and Lassovszky proved the constancy of some stars that were supposed to be variable by previous observers. These stars are X Canum Venaticorum (Detre 1932b), TV Cygni (Lassovszky 1933b), TW Geminorum (Detre 1936b), TZ Herculis (Detre & Lassovszky 1934b, Detre 1936b) and UY Herculis (Detre & Lassovszky 1934b, Detre 1936b).

Among the program stars there were several stars classified as semi-regular variables. The visual observations of two of them were published. UZ Aurigae was observed on 146 nights and 350 observations were obtained (Detre 1934b, 1935a). UU Herculis was also intensively observed, on 135 nights 517 estimates were made (Detre & Lassovszky 1934a, Detre 1936b). Some 50 years later this star turned out to be a very interesting object with alternating periods and it has been recognised that this supergiant star is a representative of a new class of variables.

The summary of the visual photometry carried out with the wedge photometer on the 20 cm Heyde refractor of Konkoly Observatory is found in one of the observatory's publications (Detre & Lassovszky 1938).

Károly Móra was associate professor at the Astronomy Department of Pázmány University, Budapest and took active part in the work of the observatory. In the middle of thirties he joined the staff of the observatory and became its director in 1936. He published important papers on R Scuti, an RV Tau-type variable (Móra 1930, 1934). This star's variability was discovered by E. Pigott[19] in 1795 and since that time a great number of observations had been published. Móra collected more than 13000 observations of R Scuti from different sources, from publications and archives, and even unpublished

[15]E. Zinner, Astron. Nachrichten, 190, 379, 1912; ibid 202, 233, 1916; N. Bougoslawski, Astron. Nachrichten, 229, 203, 1927; F. C. Jordan, Allegh. Publ., 7, 1, 1929; L. V. Robinson, Harvard Bull., 876, 1930

[16]Mitteilungen Budapest, No. 67, 1974

[17]Astron. Nachrichten, 252, 85, 1934

[18]L. V. Robinson, Harvard Bull., No. 872, 1930

[19]Philosophical Transactions of the Royal Society, London, p. 133, 1797

data were included through correspondence. In this way, he was able to follow the star's behaviour throughout almost 340 pulsation cycles. Móra's work became significant half a century later when it was recognized that the star's pulsation was determined by low dimensional chaos.

Lassovszky, following the tradition of Ó-Gyalla, observed the bright Nova 605.1936 = CP Lac on 9 nights. The nova was discovered by A. V. Nielsen[20] on June 18, 1936, while on board "Strathaird" as a member of the eclipse-trip in Mediterranean.

The observations of Lassovszky were made on the nights June 20, 21, 22, 23, 25, 27, July 5, 6, and 7, with a Zeiss Petzval-7 cm Astrocamera on Eastman plates. During the two weeks of observation the photographic brightness of the nova dimmed from $2\overset{m}{.}40$ to $5\overset{m}{.}92$ (Lassovszky 1936b,c).

Detre's last visual observations were performed during a scientific visit in München (Detre 1942). Using the 10.5 inch telescope of the Universitäts-Sternwarte, München with a wedge photometer, he studied the brightness difference of binary components. Between the Right Ascensions 15^h and 0^h30^m and Declinations $-8°$ and $+47°$, he measured 173 pairs from the Aitken's catalogue[21] of visual binaries and 37 ones from other sources. On the whole he made 11570 estimates.

The RR Lyrae program

At the end of the 19th century, a great number of short period variable stars were discovered in globular clusters. Soon the first field variable star of this type was also discovered by W. P. Fleming[22] in the constellation Lyra. The star RR Lyrae has become the prototype of the class of variables of this type. The number of discovered RR Lyrae stars grew rapidly. At the beginning of the thirties, the number of known RR Lyrae stars brighter than 12^m was already several dozens.

In 1907 S. Blazhko[23] made an interesting discovery. He found that no constant period could satisfy the times of light maxima of RW Draconis (=87.1906 Dra), an RR Lyrae type star discovered in those days. He had to postulate periodic changes in the fundamental period with a secondary period of 41.6 days. Later Blazhko[24] carried out further studies on RR Lyrae stars and found that XZ Cygni changed its light curve from cycle to cycle with a secondary period of 57.4 days.

The striking changes in the maxima of the light curves of RR Lyrae that turned out to be periodic was first stated by H. Shapley[25] some 90 years ago. He obtained a secondary period of 40 days and an amplitude of 37 minutes for the time oscillation of the median magnitude of the ascending branch. This results were fully confirmed by E. Hertzsprung[26] in 1922.

Apart from the discoveries mentioned above, several observers fancied that other RR Lyrae stars also had irregularities, non-repetitive features, changing light curves, short term or sudden period changes etc. As the observational accuracy left much to be desired,

[20]IAU Circ., No. 594, 1936

[21]R. G. Aitken, New General Catalogue of Double Stars within 120° of the North Pole. 1-2., Carnegie Inst. Washington, 1932

[22]E. C. Pickering, Harvard Circ., No. 54, 1901

[23]Astron. Nachrichten, 175, 325, 1907

[24]Annales de l'Observatorie de Moscou, 2-me série, Vol. VIII. No.2, 1922

[25]Astrophys. J., 43, 217, 1916

[26]Bull. Astron. Netherl., 1, 139, 1922

the observed and published irregularities were often doubtful. L. Detre strongly advised that the visual photometric observations were subject to significant systematic errors that could bring about ostensible light curve variations (Detre 1934c). Likely, the disputable irregularities stimulated Detre to conduct a systematic survey of "short periodic cepheids" and to scrutinize these objects. At that time, all pulsating stars with periods shorter than one day were called short period cepheids and no distinction was drawn between δ Scuti and RR Lyrae type stars. The very short periodic pulsating stars with period less than a quarter of a day, nowadays called HADS and SX Phe type stars also captivated Detre's interest.

In the thirties, the photographic photometry was the most simple technique that provided accurate observations exempt from systematic personal errors and could be carried out in small institutes with modest instruments. Therefore, Detre and his associate, Júlia Balázs (his wife to be) decided to execute a comprehensive photographic observing program of RR Lyrae stars. An astrograph fitted out with a photographic doublet of Zeiss (16 cm diameter, f/14) and a Rosenberg type micro-photometer were at their disposal. They tested different kinds of emulsions, measured the limiting magnitude at different exposure times and the field correction by measuring a number of stars in Selected Areas, North Polar Sequence, Pleiades and Coma Berenices. Their experience was that under favorable conditions $0\overset{m}{.}01$-$0\overset{m}{.}02$ accuracy could be achieved, an accuracy that certainly hit the target set by themselves. The program and the results in general were described in several papers (e.g. Balázs 1963, Balázs & Detre 1961b, Detre 1957, 1960, 1965a, 1966a, 1967, 1970a, 1973).

The first variable photographed was XZ Cygni on July 20, 1934 and the last one VZ Herculis on July 8, 1958. During 24 years more than 50 variables were observed and about 60000 exposures were made on more than 3800 photographic plates. The exposition times were chosen between 30 sec and 5 min depending on the brightness of the stars. Several fellows, such as Imre Csada, Loránt Dezső, István Földes, István Guman, Tibor Kolbenheyer, and others joined forces with J. Balázs and L. Detre for a short while.

Detre always made great efforts to improve the accuracy of observations. During the General Assembly of IAU held in Zürich, in 1948, he received an 1P21 photoelectric multiplier tube from H. Shapley as a present. The experiments with this tube were started in December 1, 1949 (*Fig. 2*). The photometer was attached to the 60 cm telescope at its Newtonian focus. The measurements revealed some defects of the equipment, the stability and linearity of the amplifier were not always granted. The troubles with the electronics seemed insolvable since during the post-war and cold war time good-quality electronic parts were not to be had in Hungary. In the long run, Th. Walraven helped to overcome the difficulties. He gave an amplifier to the observatory constructed by himself. Then the photoelectric photometry of variable stars had been carried out unbroken until the eighties, when the reconstruction of the telescope and dome was started. The 60 cm mirror of the telescope was first aluminized in 1962 and afterwards, the three-colour (UBV) observations were routinish running. Later, on the mountain station of the observatory a 50 cm Cassegrain telescope was put into operation. The photometer to this telescope was constructed at the observatory's workshop by Géza Virághalmy.

In the photoelectric observations almost all staff members of the observatory took part. The list of program stars of the photoelectric photometry was essentially the same as was chosen for photographic photometry in 1934.

In the course of observations, it promptly turned out that a variable was misclassified as an RR Lyrae star, or in reality, it was an eclipsing or a variable of an other type or a

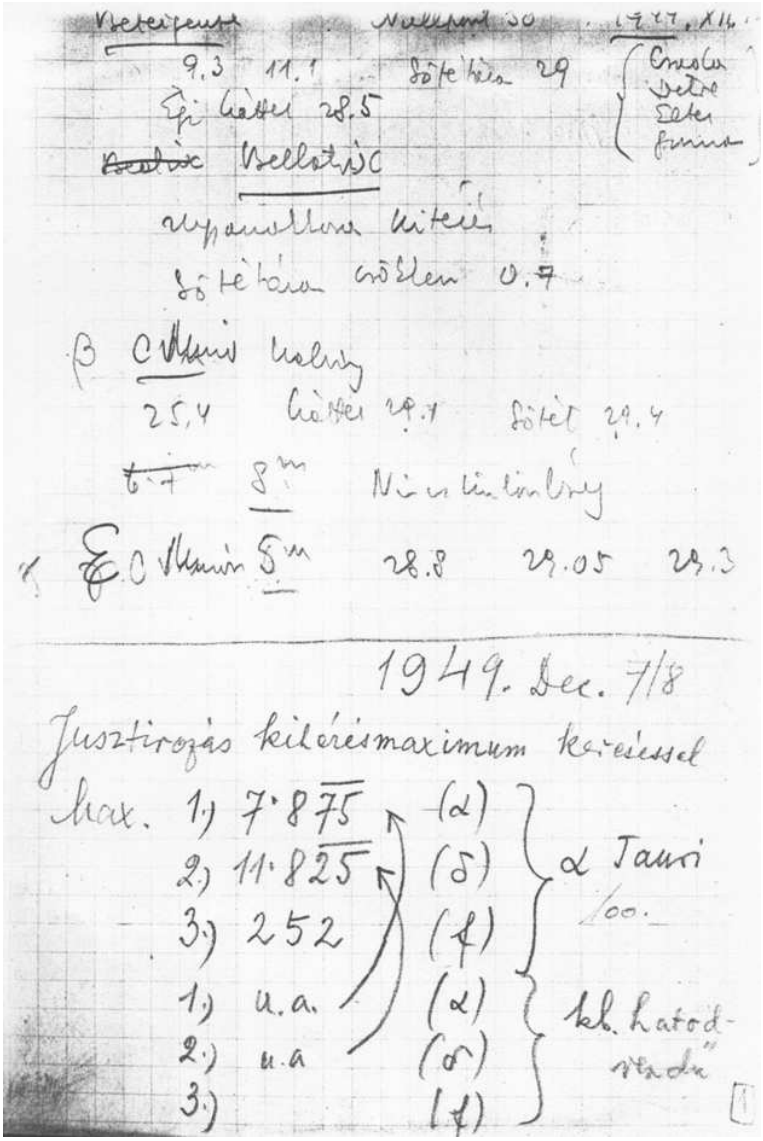

Figure 2: The start of the photoelectric observations at the Konkoly Observatory: First page of the log-book.

non-variable star. In this case, the observations and analysis had been published and the object was crossed out of the program.

The first object that was scrutinized within the scope of the RR Lyrae program was AV Pegasi. 217 observations were obtained during five nights in 1935 and neither light curve variations nor short term period changes were detected (Balázs 1935).

In the pulsation of VZ Herculis secular period change and light curve modulation were found by N. F. Florja[27]. In order to investigate the reality of these findings, 335 exposures of this star were made on 12 nights in 1935. Júlia Balázs' result contrasted with that of Florja. She found no modulation in the light curves of the star. The height of light maxima was constant within the accuracy of photographic observation (Balázs 1936a).

The variability of RR Leonis was discovered in 1907. During the subsequent 30 years, a great number of both visual and photographic observations of the star were obtained. The

[27]Leningrad Bull., 4, 1934

different observers[28] gave dissimilar light curve's amplitudes, and some of them referred to short term period changes. At the Konkoly Observatory 247 photographic observations of this star were secured during six nights in 1936. The investigation of the data unambiguously showed that RR Leo was a single periodic RR Lyrae star and its period was subject to only very slow secular change (Balázs 1937a).

BH Pegasi was also thought to be an RR Lyrae star with variable light curve by F. Lause[29]. In order to investigate the possible modulation of the light variation 249 observations with 3-5 minute exposures were obtained on 16 nights in the years 1934-1936. The results clearly refuted Lause's suggestion, BH Peg had a stable light curve. There was a very strong long lasting hump on the rising branch, probable this feature deceived the visual observers (Balázs 1937b).

DH Pegasi was observed on six nights in 1935 and 465 photographic observations were obtained. The star is of RRc type and has a stable character (Balázs 1937c).

The behaviour of AA Aquilae was also questionable. Both K. Bohlin[30] and N. Ivanov[31], based on their visual observations stated that this RR Lyrae star had strong light curve variations. As the inference drawn from visual photometry was many times not real, photographic photometry of the star was carried out at the Konkoly Observatory on 14 nights in the years 1935-1936. In all, 211 observations were obtained and six light maxima were well measured. The heights of light maxima were constant within the errors of photographic photometry. Neither light curve variations nor noticeable period changes were found (Balázs 1938).

In order to study the very short period pulsating variable RV Arietis, a number of photographic observations were made. One of the stars used as comparison proved to be variable in brightness. The new variable 624.1936Ari discovered by Detre received the final name RW Ari, a typical RRc star with a period of 0.3543 day (Detre 1937a, 1937b).

RU Piscium is also an RRc type star. There were hints in the literature on the unusual period behaviour of the star. Between 1936-1942, on the whole, 759 photographic observations were made and analyzed by Loránt Dezső (1945, 1949). He did not find any modulation in the light curve, only the period of RU Psc varied slowly. He suspected that this variation was periodic (with a period of three years and an amplitude of 0.0002 day). Later on, J. Tremko[32] pointed out that the variation in period of the star was more complicated and the existence of light curve modulation with a secondary period of 28.8 days was possible.

Although the variability of VZ Pegasi was discovered in 1921, and was considered as an eclipsing variable, only in the fifties S. Kato[33] suspected that the variable was in truth, an RR Lyrae star. To be sure of its real character, it was ranged among the RR Lyrae program stars. Photoelectric observations of three nights revealed that the star belonged to the homogeneous group of RRc type variables showing no sign of light curve variation (Barlai & Szeidl 1965).

---

[28]C. Martin & H. C. Plummer, Mon. Not. RAS, 81, 458, 1921
F. C. Jordan, Allegh. Publ., 7, 34, 1929
P. Th. Oosterhoff, Bull. Astron. Netherl. 6. 39, 1930
L. V. Robinson, Harvard Bull. No. 867, 1930
L. B. Allen & F. F. Marsh, Harvard Bull. No. 888, 1932
[29]Astron. Nachrichten, 245, 333, 1932; ibid 249, 380, 1933
[30]Astron. Nachrichten, 221, 195, 1923; ibid 224, 403, 1925
[31]Astron. Nachrichten, 223, 287, 1924; ibid 228, 143, 1926
[32]Mitteilungen Budapest, No. 55, 1964
[33]Tokyo Astronomical Bull., Ser. II, No. 110, 1958

From his visual observations A. A. Batyrev[34] came to the conclusion that the RRab star AN Serpentis had strong light curve variation with a period of 22.94 days. On the one hand, this result was uncertain because of the large scatter of the visual observations, on the other hand, the short modulation period, if true, would make AN Ser an interesting object. Therefore, the photoelectric observations of the star were commenced at the Konkoly Observatory in 1967. Between 1967 and 1971 some 980 observations were obtained during 17 nights (Szeidl 1968b, Kanyó & Szeidl 1974). The results were disappointing, AN Ser was a single periodic RRab star.

AT Andromedae represented a similar case. O. V. Tchumak[35] stated that this star had strong light curve variation with a secondary period of 82.75 days. More than 1300 photoelectric observations were obtained at the Konkoly Observatory during 18 nights in 1974 and 1975 but no light curve variation was detected (Oláh 1974).

Those objects are also worth mentioning, which were erroneously classified as RR Lyrae stars and the Konkoly observations revealed their true nature.

The variability of WZ Cephei was discovered and mistakenly classified as an RRc star by H. Schneller[36]. Júlia Balázs obtained 206 photographic observations on eight nights in 1935 and showed that the star was, in fact, a W UMa type eclipsing binary (Balázs 1936c). L. Detre supplemented J. Balázs data with 208 measurements (five nights in 1939-1940) and analyzed the light curve and derived the system parameters (Detre 1940).

WY Tauri was also classified as an RR Lyrae star by A. S. Williams[37], the discoverer of the star's variability. Therefore, the variable was included in the list of program stars. From some nights' observations it was clear that the star was not of RR Lyrae type but a β Lyrae type eclipsing variable (Balázs 1936b). In order to analyze the light variation, additional observations were made (altogether 403 measurements on 16 nights during the years 1935, 1936, 1937 and 1939) and the period and light curve parameters, furthermore the system constants have been determined (Balázs & Detre 1940).

The classification of ZZ Persei was also questionable. K. Nakamura[38] suspected RR Lyrae, while V. M. Bodokia[39] suggested β Lyrae type light variations. 60 photographic observations were obtained in 1935 which did not show any noticeable variations within the error of measurements (about $0\overset{m}{.}02$-$0\overset{m}{.}03$), so the star could be regarded as constant (Lovas 1952).

A. G. Lange[40] suggested that AV Vulpeculae was an RR Lyrae star resembling AC Andromedae. 489 observations were obtained and the star proved to be a long period irregular variable (Guman 1952).

The Second Edition of GCVS (1958) classified both AT Herculis and BP Vulpeculae as RR Lyrae variables. AT Her was observed photoelectrically on 9 nights in 1960 but no light variation was detected. According to the spectrum, the star is of K0 V spectral type and is certainly not an RR Lyrae variable. The variability is questionable at all (Illés 1963). The photoelectric photometry of BP Vul was carried out during 11 nights in September and October 1959. It turned out that it is, in reality, an Algol type eclipsing binary (Illés 1960).

[34]Peremennye Zvezdy, 12, 137, 1957; ibid 15, 278, 1964
[35]Peremennye Zvezdy, 15, 569, 1965
[36]Astron. Nachrichten, 233, 41, 1928
[37]Mon. Not. RAS, 87, 172, 1926
[38]Kyoto Bull., 8, 10, 1922
[39]Abastumani Bull., 1, 1937
[40]Astron. Tsirk., No. 20, 1943

A summary of the photometry of RR Lyrae stars made at the Konkoly Observatory until 1956 was presented by Detre at the Variable Star Colloquium held in Budapest, 23-28 August, 1956 (Detre 1957). Likewise, Detre gave a review on the photoelectric observations of RR Lyrae stars with stable light curve carried out at the Konkoly Observatory at the first Bamberg Variable Star Colloquium (Detre 1960). Here, he gave an account of an interesting connection between the length of the stillstand on the rising branch and the amplitude of RR Lyrae stars.

At first, the photoelectric observations were made only in two colours, then from the beginning of the sixties in three colours. These observations made the investigation of the position of RR Lyrae stars in the colour-colour and colour-magnitude diagrams possible. Such an investigation was made for the variables of ω Centauri based on photographic photometry (Geyer & Szeidl 1965, 1970).

The Blazhko effect

Since S. Blazhko was the very first to notice the periodic oscillation in the phase of light maximum of an RR Lyrae star (namely of RW Draconis) we refer to this periodic variation as Blazhko effect. Later H. Shapley demonstrated that the phase oscillation was accompanied by the periodic variation in the shape of the light curve and in the height of maxima with the same period in RR Lyrae.

In truth, the investigation of the amplitude and phase modulation of RR Lyrae stars, the Blazhko effect, has brought in the international reputation of the Konkoly Observatory. The results of these investigations have been published in a series of papers.

The planned research and the preliminary list of program stars were described in one of the first publications (Balázs & Detre 1938). The first program star to be studied in detail, was RW Draconis. During 143 nights in the years 1936-1938, 1941, 1942, 1944, 1945, 1947-1952 taken as a whole, 7210 photographic observations were obtained at the Konkoly Observatory. The old visual observations from 1907 made the investigation of long term variations in both the fundamental and the Blazhko period possible. The changes in the characteristics of Blazhko effect could also be studied. The amplitudes of both the phase and the amplitude modulation were the largest in 1937, 0.085 day $\approx$ 2 hours and $1\overset{\mathrm{m}}{.}0$, respectively. The amplitudes of modulation were much smaller after 1937, e.g. in 1941, 0.04 day $\approx$ 1 hour and 0.5 magn., respectively. The striking change in the effect had to take place around 1938-1939, but that time no observations of the star were made at the Konkoly Observatory. Fortunately, observations of RW Dra were obtained at the Leiden Observatory in 1938. These unpublished observations were placed at J. Balázs and Detre's disposal and it became clear that the sudden decrease in the effect took place in 1938 (*Fig. 3*).

Making use of unpublished photoelectric observations, the changes in both the main and secondary periods could be investigated for a time span of 60 years. The very strong change in the amplitude of the effect in 1938 was accompanied by a very large sudden change in both periods. These variations were anticorrelated, the O$-$C diagrams were mirror images to each other.

The photographic observations obtained at the Konkoly Observatory also made the detection of a small amplitude 120 day period (almost three times of the conspicuous 41.6 day Blazhko period) possible. This longer period variation clearly came in sight when the Blazhko effect was stronger than average. The investigation of the long term variation

in the phase modulation revealed a 7.4 year period, that could be barely noticed in the O−C diagrams of the pulsation and Blazhko periods (Balázs 1957, Balázs, & Detre 1938, 1952, 1962).

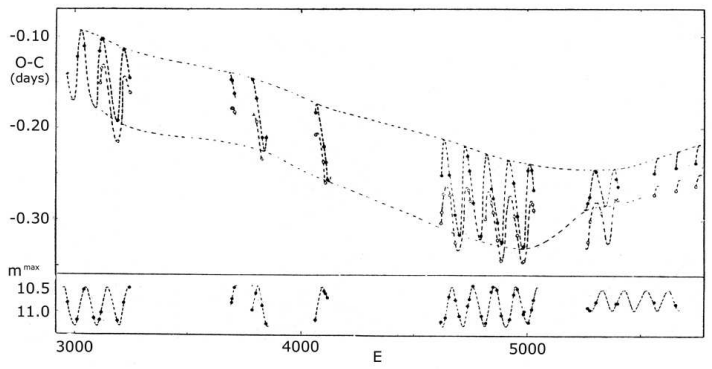

Figure 3: Sudden change in the Blazhko effect of RW Draconis in 1939 (after J. Balázs 1957).

The RR Lyrae stars with light curve modulation were usually observed only in a very limited phase interval of the pulsation period, during minimum, ascending branch and maximum light. J. Balázs and Detre carried out a comprehensive study of the Blazhko star AR Herculis: they covered the whole pulsation cycles at different phases of the secondary period, so thus they were able to construct the so-called light surfaces, the light curves at different fixed Blazhko phases. (More exactly, they gave the $m(\Phi, \Psi)$ brightness of the star in tabulated form, where Φ is the phase of the pulsation and Ψ is the phase of the modulation.) In this way, the study of the Blazhko effect on the whole pulsation cycle became possible. These results aroused the interest of variable star researchers, even Leon Campbell and Luigi Jacchia spent one page expounding these results in their well-known book The Story of Variable Stars (The Harvard Books on Astronomy, eds.: H. Shapley and B. J. Bok, 1941).

The phase modulation of light maximum of the 0.470 day period RR Lyrae star, AR Herculis was first noted by S. Blazhko[41], but apart from the scarce, mostly visual observations no serious investigation was devoted to the star before 1935. This is why J. Balázs and Detre decided to study it intensively. The photographic observations based on their investigation were made during 81 nights between 1935 and 1939. In all, 3363 observations were obtained and scrutinized.

The amplitude of the light variation varied between 0.90 and 1.77 photographic magnitudes during the 31.5 day Blazhko cycle, while the amplitude of the time oscillation of light maximum was 0.06 day $\approx$ one hour and a half (*Fig. 4*). During the modulation cycle the brightness of maximum was nearly the least when the momentary pulsation period was the longest (Balázs & Detre 1939).

Twenty years later Iván Almár repeated the investigation of AR Herculis on new extended photographic and photoelectric data sets. During the years 1946, 1948-1953, 1955-1957, 3511 photographic observations were obtained during 117 nights and, in the years 1958 and 1960, 1141 photoelectric measurements were made. These new data revealed that a 90.8 day period was also present (2.87 times longer than the 31.5 day Blazhko

[41]Leningrad Eph. of short period Ceph., 1932

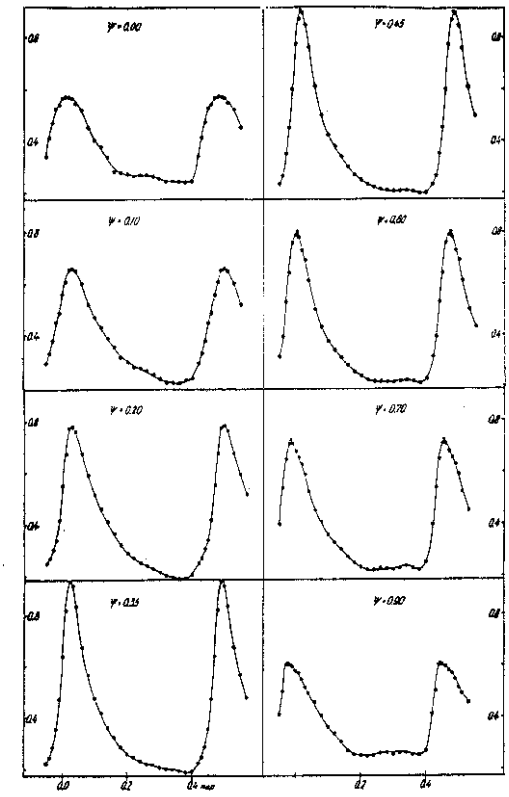

Figure 4: Light curves (light surfaces) of AR Herculis at different Blazhko phases (after Balázs & Detre 1939).

period). A comparison with the previous studies showed that in spite of the strong variations in the Blazhko effect during the decades the brightness of the brightest maximum in the modulation cycle practically had not changed and the form of the relation between the brightness and phase oscillation of light maximum was essentially the same for the different observing seasons. The amplitudes of the brightness and the phase oscillation of light maxima were subject to strong long term variations and between these variations no connection was found.

The new photometry and the published data made the investigation of the secular changes in both the fundamental and the modulation periods possible. Both of them exhibited perceptible changes: the pulsation period changed rather irregularly, the O−C diagram of the Blazhko period resembled a sine-like curve. Between the changes of the two periods no connection could be revealed (Almár 1961).

One of the most favorite Blazhko stars at the Konkoly Observatory was RR Lyrae itself. During the decades a large amount of observations of RR Lyr had been obtained by different observers at different sites, but the results were contradictory. H. Shapley[42] found a 40 days long modulation period, while A. de Sitter[43] gave a value of 38.21 days for it. T. E. Sterne[44] hinted at the possibility that de Sitter's result was affected by the selection of data. In order to clear up the matter in dispute, the star was intensively observed at the

[42]see footnote 25
[43]Bull. Astron. Inst., 6, 215, 1932
[44]Harvard Circ., No. 387, 1934

Konkoly Observatory. During 27 nights in the years 1935, 1938, 1939, and 1941 as a whole, 6512 photographic observations were made. Their own observations and several thousand data (mostly photographic) published by 18 observers were reanalyzed. It became evident that in 1899 (at the discovery of the variability of RR Lyr) the modulation period was around 40.5 days and increased to 41 days up to 1943. During that time interval the pulsation period showed irregular changes. The amplitudes of oscillation in times and heights of maxima were fairly large around the end of the thirties: 0.055 day $\approx$ one hour and 20 minutes and 0.33 photographic magnitude (Detre 1943, Balázs, & Detre 1943, 1962).

The light curve variation of RW Cancri was discovered by S. Blazhko[45] in 1922 and he derived a modulation period of 87 days. The variable was also ranged among the program stars of J. Balázs and Detre. In the years 1938-1940 and 1950, 1210 photographic observations were collected at the Konkoly Observatory during 44 nights and 40 light maxima were observed. In the course of the analysis of the data RW Cnc proved to be one of the most interesting Blazhko stars. During the Blazhko cycle the brightness of light maxima changed between $10\overset{m}{.}74$ and $11\overset{m}{.}80$, while that of the minimum between $12\overset{m}{.}55$ and $12\overset{m}{.}34$. The highest maximum was always preceded by the deepest minimum, so thus the extreme values of amplitude of the light variation were 1.81 and 0.54 photographic magnitude. Such a large amplitude variation had never been observed previously in any other Blazhko star. Two modulation periods were present $P_{B1} = 29.9$ days and $P_{B2} = 91.1$ days, that were increasing. The fundamental period showed both increasing secular and cyclic variations with a suspected 25 year cycle length (Balázs & Detre 1950).

One of the most puzzling Blazhko stars is SW Andromedae. H. Shapley[46] stated that strong light curve variations were present, but no other visual observer mentioned it. Detre's visual observations showed $0\overset{m}{.}07$ scatter in light maximum, that proved if Blazhko effect had existed in the star at all, it diminished to below the detectable limit. In order to reveal the real behaviour of the star 915 photographic observations were made on 23 nights in the years 1936, 1937, 1941, 1942, 1951 and 1952. These observations, however, could only be used to study the changes in the fundamental period, the accuracy of the photographic observations did not allow tracing the light curve variation. The pulsation period was steadily decreasing with a rate of 2 seconds in a century. The earlier assumption of an abrupt change in the period could not be confirmed.

In 1950 and 1953, 864 additional photoelectric observations were obtained on 22 nights. It was noticed that the length of the stillstand on the rising branch of SW And was changing with a period of 36.83 days, while the height of maximum varied $0\overset{m}{.}03$ at the very most. This kind of light curve variation of SW And probably represents a specific type of Blazhko effect (Balázs & Detre 1954).

All the previous visual and photographic observers indicated that RV Ursae Majoris showed well-perceptible strong light curve variations, but were unable to establish the regularity of these variations.

In the years 1936, 1937, 1946-1952, 1229 photographic observations were obtained during 27 nights. From 1955 May to 1957 July RV UMa was observed photoelectrically on 35 nights and 1008 data were collected. The considerable part of the photoelectric observations were made in 1957, in all, 21 maxima were observed in that year, so thus the modulation period could easily be determined. The variable exhibited strong amplitude

[45] Astron. Nachrichten, 216, 103, 1922
[46] Mon. Not. RAS, 81, 209, 1921

modulation, while the phase modulation of maximum was rather small. The variations could accurately be described by the combination of the 0.4680 day fundamental period with a secondary period of 90.1 days. The same periods were apparent in the earlier visual and photographic observations. Having used all the published observations, the O−C diagrams for both periods could be constructed. These diagrams contain cycles of the same length, but of opposite phase (Balázs & Detre 1957).

The investigation of RV Ursae Majoris proceeded at the Konkoly Observatory after 1957. In the years 1958, 1959, 1961-1965, 1968, and 1969, 5966 photoelectric observations (2378 in V, 2627 in B, and 961 in U band) were obtained on 150 nights.

As for the period changes the previous results were confirmed on a longer time base, the O−C diagrams of the pulsation and modulation periods run opposite in phase. During the Blazhko cycle there was no significant change in light curve in the phase interval 0.35-0.55. It was, however, a rather surprising discovery that, around phase 0.94, there was a point on the ascending branch that did not show any significant oscillation either (Kanyó 1976a).

Y Leonis Minoris was a known Blazhko variable. D. J. Martynov[47] derived its modulation period as $P_B = 33.4$ days. As the successive Blazhko cycles differed from each other both in shape and length, J. Balázs decided to reanalyze the published data, and came to the conclusion that the star had a second modulation period of 82.2 days, with a smaller amplitude ($0\overset{m}{.}25$) and phase (0.016 day) modulation. The pulsation period was increasing and also showed a cyclic variation with a period of 7.7 years (Balázs 1955).

The search for light curve modulated RR Lyrae stars and determination of the accurate Blazhko periods were also an important part of the program.

M. Beyer[48], from his visual observations, suspected that XZ Draconis had light curve variation. Its photographic observation was commenced by J. Balázs in 1936. Using some observations obtained up to 1940, the Blazhko period turned out to be 76 days (Balázs & Detre 1941). The star has been kept observing photographically and photoelectrically later on.

V. P. Tsessevich[49] observed strong light curve variation in the RR Lyrae star DL Herculis and gave the modulation period as 49.1 days. Some 750 photoelectric observations were made of this star at the Konkoly Observatory on more than ten nights in 1963 and it turned out that the real value of the Blazhko period was 33.6 days. The modulation amplitude of the phase and height of light maximum were more than 0.02 day ≈ half an hour and about $0\overset{m}{.}3$ in blue light, respectively (Szeidl 1963).

The earlier photographic observations made at the Konkoly Observatory indicated that Z Canum Venaticorum had Blazhko effect. The star was photoelectrically measured at the observatory in 1964 and almost 500 observations were made on 12 nights. From the analysis of these data the Blazhko period proved to be 22.75 days, a surprisingly short secondary period for a star with a fairly long, 0.6538 day pulsation period. The height of the light maximum varied $0\overset{m}{.}45$ in B and $0\overset{m}{.}38$ in V during the modulation cycle, while the amplitude of the phase oscillation of maximum was 0.04 day ≈ one hour (Kanyó 1966).

AR Serpentis was investigated by V. P. Tsessevich[50] who gave the element of its light variation and found strong fluctuation in the period, suggesting the presence of the Blazhko effect. In 1967, some 960 photoelectric observations were obtained in blue and

[47]Engelhardt Obs. Bull., 18, 1940
[48]Astron. Nachrichten, 252, 85, 1934
[49]Odessa Isv., 3, 257, 1953
[50]Astron. Tsirk., No. 353, 3, 1966

yellow lights on 15 nights and a Blazhko period of about 105 days could be derived. The star possessed extremely strong light curve variation, the amplitude of the phase oscillation of maximum exceeded 0.12 day ≈ three hours, while the light amplitudes varied between $0^m.41$ and $1^m.09$ in V and $0^m.49$ and $1^m.32$ in B light (Szeidl 1967).

W. S. Fitch, W. Z. Wisniewski, and H. L. Johnson[51] observed a large sample of RR Lyrae star, among them TT Cancri as well. The observed light maxima differed from each other indicating that TT Cnc was a Blazhko star. From 1967 December up to 1968 April 1080 photoelectric observations were obtained in UBV colours. During this time interval 13 light maxima were observed. The modulation period turned out to be 89 days. The amplitudes of phase modulation of maximum light was 0.035 day ≈ 50 minutes and of the variations in height of light maxima were $0^m.30$ in V and $0^m.35$ in B light, respectively (Szeidl 1968a).

Inspired by a notice of L. J. Robinson[52] on a possible Blazhko effect in the light variation of SZ Hydrae, photoelectric observations were commenced by S. Kanyó at Catania Observatory during a scientific visit in order to determine the length of its secondary period. Although only four maxima could be observed, their favorable distribution in phase enabled the determination of the secondary period: $P_b = 25.8$ days (Kanyó 1970).

All the studies on Blazhko effect were focused on RRab stars. It was a question if RRc stars could also possess the effect. Detre observed TV Bootis, an RRc star, photoelectrically on several nights in 1955 and found that this star also showed light curve variation with a period of 33.5 days (Detre 1965b).

The globular clusters usually contain great number of RR Lyrae stars (e.g. Messier 3 contains over 200), therefore, their study is particularly suitable for determining statistical properties of Blazhko variables. It was concluded from the study of the variables in M3 that about 25-30% of the RRab stars showed the effect. A statistics of field RRab stars led a (less reliable) frequency of 15% (Szeidl 1965, 1973, 1976). As to the Blazhko stars in M3, another interesting observation was that for stars exhibiting variable light curves, the largest modulation amplitudes fitted the period-amplitude diagram valid for RRab stars with single period (Szeidl 1965). A definite negative correlation was found between the noise of pulsation period and the length of the Blazhko period (Kanyó 1976b).

During the years considerable knowledge accumulated at the Konkoly Observatory on the RR Lyrae stars with Blazhko effect. From time to time, it was summarized and published in review papers (Detre 1954, 1956a, 1957, 1962a, Szeidl 1976). In one of the reviews, Detre made an interesting observation. He arranged H. W. Babcock's[53] measures of the magnetic field intensity of RR Lyrae according to the phases of the pulsation and the Blazhko period. There was no correlation with the pulsation period, but a separation of positive and negative values was apparent in the course of the 41 day secondary period. Brightest maxima coincided with the largest negative, lowest maxima with the largest positive values of field intensity. As the number of the magnetic observations was small, the correlation could not be considered definitive (Detre 1962a).

Júlia Balázs propounded the oblique pulsator model as an explanation for Blazhko effect almost fifty years ago (Balázs 1960). If the magnetic axis inclines to the rotation axis of the pulsating star, then, depending on the geometry and the strength of the magnetic field, the Blazhko effect may have a natural explanation. If this hypothesis holds, then the Blazhko period equals to the rotation period. During the years, competitive theories

[51] Commun. Lunar and Planetary Lab., No. 71, Vol. 5, Part 2, 1966

[52] Peremennye Zvezdy, 16, 62, 1966

[53] Astrophys. J. Suppl., 3, 141, 1958

have been advanced but we still lack for understanding of the Blazhko effect.

The situation became more complicated, when the 4-year cycle of RR Lyrae was discovered. After discussing and publishing their early photographic observations of RR Lyrae (Balázs & Detre 1943) its observation was kept on photographically, then photoelectrically from 1950. It seemed that the intensity of Blazhko effect had irregularly changed during the years. Detre wanted to mention it as an example for non-periodic effects in his introductory talk at the IAU Colloquium "Non-periodic Phenomena in Variable Stars" (Detre 1969c).

While preparing the figure of phase and amplitude modulation of RR Lyrae for different years by the author of the present review at Detre's request, it became conspicuous that the effect almost disappeared in the years 1963 and 1967, suggesting that the Blazhko effect might have a 4-year cycle. A very intensive observation of the star was started in 1969 and the transition between the new and old cycles was observed in 1971. At the end of the old 4-year cycle the phase variations during the 41-day Blazhko cycle died down almost completely and then, the new cycle started with a rapid increase of the amplitude. The amplitude of the maximum-variations was only $0\overset{m}{.}07$ at the end of the old cycle, and then very rapidly became as large as $0\overset{m}{.}16$ during 1971 and increased to $0\overset{m}{.}27$ in 1972. The beginning of the new cycle was accompanied by a phase shift of 10 days, about a quarter in the phase of the 41-day Blazhko cycle (*Fig. 5*).

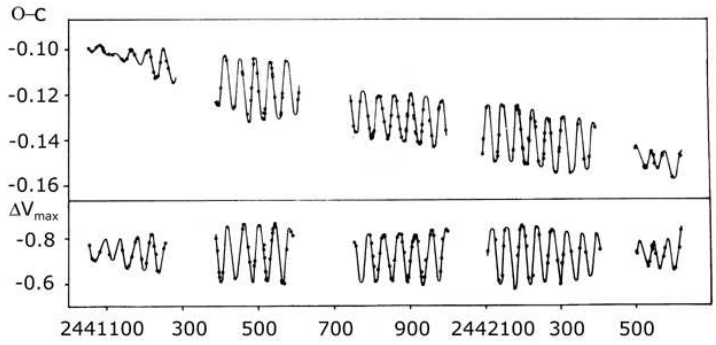

Figure 5: A whole 4-year cycle of RR Lyrae (after Szeidl 1976).

The Konkoly Observatory had almost forty thousand unpublished observations of RR Lyrae in 1972. Supplemented by others' photoelectric observations (1947: Th. Walraven[54], 1953: R. H. Hardie[55], 1955: P. Broglia & A. Masani[56], 1958-1959: G. Cocito & A. Masani[57], 1961-1962: B. Onderlicka & M. Vetesnik[58], 1962-1964: G. W. Preston, J. Smak, & B. Paczynski[59]) the 4-year (more exactly 4.3-year) cycle could be traced back to 1944 (Detre & Szeidl 1973a,b).

These results were fully confirmed by new observations, the transition from the old to the new cycle was also observed in 1975, and the phase discontinuity in the 41-day period was again about 10 days (Szeidl 1976).

[54]Bull. Astron. Netherl., 11, 17, 1949
[55]Astrophys. J., 122, 256, 1955
[56]Contr. Oss. Astr. Milano-Merate, Nuova Serie, No. 105, 1957
[57]Contr. Oss. Astr. Torino, Nuova Serie, No. 27, 1960
[58]Astron. Inst. Univ. Brno (Czechoslovakia) Publ., No. 8, 1968
[59]Astrophys. J. Suppl., 12, 99, 1965

The identification of the 4-year cycle with magnetic cycle was very tempting and later it become the subject of heated debate.

Period Changes

W. Ch. Martin's[60] discovery, that the periods of the RR Lyrae stars in ω Centauri are predominately increasing, aroused the variable star astronomers' interest. Well it was thought that the O−C diagrams were simply accumulated evolutionary changes in the periods. Little wonder, then that the deviations of the epoch of variable stars from the linear elements were represented by second order equations, where the coefficients of the second order terms were supposed to describe the progressive changes in the periods. It was hoped that these coefficients would give some informations on the rate and direction of evolution of horizontal branch stars through the instability strip and would provide a strong test of the theory of stellar evolution. The study of RR Lyrae stars in globular clusters seemed to be particularly promising: at the same time, the period changes of a large sample of homogeneous group of RR Lyre stars could be investigated.

In 1937 L. Detre commenced the study of RR Lyrae stars of globular clusters M3 and M15 at the Konkoly Observatory. Later M. Lovas started the observation of RR Lyrae stars in M5 in 1951, and M56 and M92 were also included into the program. During the years 1937-1966 more than one thousand photographic plates were made on these clusters with the 60 cm Newton telescope. The plates were taken by Júlia Balázs, Katalin Barlai, L. Detre, G. Kulin, M. Lovas, I. Ozsváth, and B. Szeidl.

I. Izsák started investigating the period changes of the RR Lyrae stars in M15. The preliminary results were presented in the 1956 Budapest variable star conference (Izsák 1957). In the course of this study three new variable stars were discovered in M15 (Izsák 1952).

Between 1937-1951 115 plates of M56 were taken with 20 minutes exposure time. Júlia Balázs started analyzing the variables in this cluster. Comparing eight pairs of plates, she discovered two new variables (Balázs 1952a).

The study of period changes of RR Lyrae stars in M3 was started by I. Ozsváth. A short account on the preliminary results was given also at the 1956 variable star meeting (Ozsváth 1957).

For the final investigation of the variables of M3, 214 plates obtained at Budapest and 17 plates supplied by the Hamburg Observatory were used. 121 variables were measured with the microphotometers of the Konkoly Observatory and 13 variables (that could not be measured owing to crowding effect) were estimated. Out of the 134 objects measured, there were one red semiregular variable and one W UMa type eclipsing binary (RV CVn), a foreground star. As a whole, O−C diagrams of 125 RR Lyrae stars have been constructed, for most of them (116) for almost a 70 years timebase. Considering only the variables observed since Bailey's discoveries, the O−C diagrams could be fitted by a straight line for 8, by a positive parabola for 23 and by a negative parabola for 25 variables. No systematic trend was found in the direction of period changes. About half of the O−C diagrams could not be approximated by quadratic formulae. As a rule, the variables with secondary period had very complicated O−C diagrams. It was also an interesting observation that several RR Lyrae stars (both RRab an RRc) had sine-like O−C diagrams.

A review on the period changes of RR Lyrae stars in globular clusters was given by

[60]Leiden Ann., 17, Part 2, 1938

Szeidl at the IAU Symposium on Variable Stars and Stellar Evolution held in Moscow in 1974. There were doubts about the character of the changes, whether the periods were relatively constant (apart from slow secular evolutionary changes) for long time intervals followed by brief intervals of spontaneous, abrupt changes or, whether the variations were relatively smooth. Two field RR Lyrae stars which were on the Konkoly Observatory's program provided examples for both cases. The period of RR Leonis (Balázs & Detre 1949) had increased smoothly, but the rate of change was not at all constant. On the other hand, the period of RR Geminorum changed suddenly around JD 2428900 within a brief interval. It was originally hoped that the period variations would depend on the positions in the colour-magnitude diagram, this expectation, however, was not fulfilled. We could not find any connection between the position of a star and its period change either in M3 or in M15. The final conclusion was that it was impossible to attach any evolutionary significance to the observed period change of an RR Lyrae star. Likely, ω Centauri is the only exception, in which some evidence for evolution effects may be present (Szeidl 1975).

L. Detre made an attempt at investigating the period changes of field RR Lyrae stars, but the sample was too small for drawing statistically significant conclusion (Detre 1955, 1970b). These studies, however, showed that, over and above evolutionary changes, some kinds of other effects exerted significant influence on the period causing period changes of different amount and of different direction.

Júlia Balázs and L. Detre called attention to mechanisms which were not connected closely with the physics of the star and could produce apparent period changes. If a variable moves as compared with the observers (even if in straight line with constant velocity) its observed period changes in consequence of the Doppler effect. In the case of constant velocity, the period is apparently increasing (Detre 1969b, 1970b). In a paper on period changes in variables and evolutionary paths in the Hertzsprung-Russell diagram Júlia Balázs and L. Detre applied the theory of random walk to the O−C diagrams of pulsating variable stars. If the period has random fluctuations, noise with σ standard deviation, then the O−C diagrams are random walks due to the cumulative nature of the fluctuations and do not represent real period changes. It was found that σ was an important parameter of variable stars and correlated with the rapidity of evolution (Balázs & Detre 1965).

Other pulsating variables

- δ Scuti variables

In the early days (in the thirties) δ Scuti stars were not distinguished from RR Lyrae stars, so it is not a wonder that they were also on the observing list at the Konkoly Observatory.

Immediately after the discovery of the variability of 391.1934 Aqr = CY Aquarii, its photographic photometry was commenced by J. Balázs and Detre. During nine nights in 1934, almost 200 observations were obtained and the elements of the light variation were derived. Nine maxima were observed that pointed to single periodic nature of the star (Balázs & Detre 1934, 1935). Later, it was observed photoelectrically that confirmed the previous results (Detre & Chang 1960).

Previous observers of XX Cygni referred to its light curve variations. Analyzing more

than 300 photographic observations obtained in 1936, no sign of secondary periodicity was found (Detre 1936a).

Based on his visual observations, A. G. Lange[61] stated that RV Arietis exhibited irregular variations. About 300 photographic observations made in 1935-1936 during 16 nights revealed the star's real nature: a short period pulsating star (Detre 1936c, 1936d, 1936e, 1937b). Later, Detre succeeded in disclosing the double mode behavior of the star and determined its secondary period making use of the accurate photoelectric observations of P. Broglia and E. Pestarino[62] (Detre 1956b). It turned out that this variable belonged to the subgroup of AI Velorum stars. In order to get more accurate periods and the period ratio, new observations were made during nine nights in the years 1951, 1953, 1954, 1955, and 1956. As a whole, 261 photographic observations of RV Ari were obtained and discussed (Balázs 1956).

In the thirties, the question of multimode stellar pulsation aroused the interest of the variable star astronomers and captivated Detre's interest, too. He analyzed the photoelectric data set of δ Scuti obtained by E. A. Fath[63] and interpreted the star's secondary period as interference of two oscillations with close frequencies (Detre 1941).

At the Konkoly Observatory the observation of δ Scuti stars has proceeded forth photoelectrically (Detre 1957). I. Guman (independently from W. Fitch) discovered that VZ Cancri was also a double mode variable. He observed the star photoelectrically between April, 1951 and February 1954, and collected more than 1200 observations on 24 nights. The measurements were made without filter. The light curve variation and the differences in height of the 26 observed maxima were conspicuous. According to both the periods and the light variations the star behaved resembling AI Velorum and SX Phoenicis (Guman 1955a).

The variability of SZ Lyncis was discovered by C. Hoffmeister[64] and H. Schneller[65] classified it as a short period RR Lyrae star. In 1962 February and March 600 photoelectric B and V observations were collected and the period was derived. It was shown that the star was a single periodic dwarf cepheid (Gefferth & Szeidl 1962).

V. P. Tsesevich[66] called the attention to the possible light curve variation of the Bamberg variable BV92[67] = AE Ursae Majoris. More than one thousand photoelectric observations in two colours were made between January and April 1974 on 12 nights. The observed 18 maxima allowed to determine both the fundamental and first overtone periods. The period ratio 0.773 was very characteristic of the radially pulsating double mode δ Scuti stars. The light curve variations of AE UMa proved to be very strong, during a modulation cycle the height of maxima varied almost $0\overset{m}{.}3$ while the phase of maxima almost 10 minutes (Szeidl 1974).

- *AC Andromedae*

Soon after P. Guthnick and R. Prager[68] discovered the variability of BD+47°4104 (= 9.1927 And) it became evident that the star (soon receiving its variable star name, AC

[61] Tadjik Tsirk., 4, 1935
[62] Mem. Soc. Astr. Ital., 26, 429, 1955
[63] Lick Obs. Bull., No. 479, 1935; Lick Obs. Bull., No. 487, 1937
[64] Astron. Abh. (Erg.-H. zu den AN), 12, 21, 1949
[65] Astron. Nachrichten, 286, 102, 1961
[66] Astron. Tsirk., 775, 1973
[67] E. Geyer, R. Kippenhahn, & W. Strohmeier, Kleine Veröff. Bamberg, Nr. 11, 1955
[68] Astron. Nachrichten, 229, 455, 1927

And) is a unique variable. Through intensive observation, N. T. Florja[69] could derive the type of variability and periods of AC And. He could describe the light variation as superposition of two oscillations with periods 0.525 day and 0.711 day, and he interpreted this result in such a way that two RR Lyrae stars optically coincided with each other. Later, G. Münch[70] refuted this assumption on the basis of spectroscopic observations and suggested that AC And was rather of AI Vel type.

Little wonder, that the strange behavior of this star aroused L. Detre's interest and in 1935 he included AC And into the observing program of the Konkoly Observatory. Between 1935 and 1954, 5670 photographic observations were obtained that were later analyzed by I. Guman.

In order to get a real picture about the nature of the light variation of AC And, the star's intensive photoelectric photometry started in 1958 at the observatory. For the year 1962 Detre organized a campaign, too (Detre 1962b). In the long run, AC And was observed photoelectrically on a total on 78 nights in the years 1958, 1960, 1961, and 1962 and more than 10000 observations were secured in the Johnson U, B, and V bands. The analysis was, however, restricted to the 4662 yellow magnitudes, and revealed that AC And had its fundamental and first and second overtone radial pulsation modes, all excited and nonlinearly coupled. This variable star was found to have a mass of $M = 3.1 M_{Sun}$ and to be a high-mass analog of the δ Scuti stars, in the hydrogen-shell-burning and helium-core-contraction stage of evolution (Fitch & Szeidl 1976).

- Cepheids

In order to test the photoelectric photometer, L. Detre observed bright cepheids, such as FF Aql, η Aql, SU Cas, TU Cas, δ Cep, X Cyg, SU Cyg, S Sge, and T Vul, but these observations have not been published.

The long period cepheid CY Cas was investigated on Moscow archive plates and its period was corrected (Almár 1959).

The beat period cepheid TU Cassiopeiae was intensively observed by Erzsébet Illés in 1960-62 and by L. Szabados after 1971. The light-surface at different beat phases was constructed and the variation of the periods was studied (Illés 1968, Illés & Szabados 1976).

The Observatory's new photometer on the 50 cm Cassegrain telescope was put into operation in 1972. The instrument equipped with a UBV photometer made the expansion of the observatory's program possible. The observations of northern cepheids brighter than 12^{m} were started in 1972. One of the purposes of this observational program was the search for beat cepheids. One new double mode cepheid was discovered: BQ Serpentis had two periods, $P_0 = 4.271$ days fundamental and $P_1 = 3.012$ days first overtone, and $P_1/P_0 = 0.705$ period ratio (Szabados 1976a). Some results of the survey as by products were achieved right away. V445 Cas was wrongly classified as a cepheid, it is in reality an eclipsing variable of β Lyrae type (Szabados 1974a). V361 Per was catalogued as probable cepheid. It turned out to be an early type irregular variable (Szabados 1974b). The Bamberg variable BC Dra was assigned to cepheid. In truth, the star is an RR Lyrae variable of long (0.720 day) period (Szabados et al. 1976). J.D. Fernie and J.C.

[69] Astron. Zhurnal, 14, 1, 1937
[70] Astrophys. J., 114, 546, 1951

Hube[71] reported BD+56°2806 as a probable cepheid. The observations showed that it was, indeed, a cepheid with short period (Szabados 1976b).

In 1966, S. Demers and J. D. Fernie[72] called attention to the strange behavior of the Population II cepheid RU Camelopardalis. The observations of this star started at the Konkoly Observatory already in August 1966 (Detre 1966b, Detre & Szeidl 1967, Detre 1969a, Szeidl 1969b).

- *β Cephei type*

RS Sextantis was identified as "related to the β Canis Majoris stars" by A.B. Underhill[73]. The projected velocity of rotation of RS Sex turned out to be fairly high, 260 km/s (Almár 1968).

- *Red variables*

On the plates taken for the RR Lyrae program, variable stars of other types may be found and could be investigated. BT Lyrae appeared on the plates (close to their edge) taken on the globular cluster M56 and its measurements showed that there were departures from regularities and the form of successive maxima and minima strongly varied. The period could be corrected to $P = 167.85$ days (Balázs 1952a). ST Draconis is near RW Dra. E. Hartwig[74] found it to be variable, but conformity with the photographic observations it proved to be constant within some hundredth of magnitude (Balázs 1952b).

On the plates taken for the study of AC And, two other variables could be found and measured. AI Andromedae is a Mira type variable and showed strong period variation (Guman 1952, 1955b). BE Andromedae is an M6 type semiregular variable. Its average period was newly determined, 157 days as against the previous value of 137 days, but the actual periods showed large fluctuations (Guman 1955b).

- *Cataclysmic variables and flare stars*

Nova Herculis 1963 was discovered by E. Dahlgren[75] on February 6, 1963. This object was observed at the Konkoly Observatory in three colours from February 9, 1963 to October 2, 1964. During 43 nights more than 900 observations were made and spanned almost 8^m of the brightness decrease. Rapid fluctuations in brightness and colour had been found (Almár & Illés 1966).

One of the light outbursts of the very interesting object Rosino-Zwicky near M88 was detected on plates taken by the observatory's 60/90 cm Schmidt telescope for the supernova search program. The object brightened by 6 magnitudes from the middle of March to the beginning of April 1965 (Lovas 1965). In the course of the flare statistics program, a new U Geminorum star was found in Cancer (Jankovics 1973).

The observatory took part in the photoelectric monitoring of flare stars. AD Leonis was observed and events were recorded (Szeidl 1969a, Barlai et al. 1972).

---

[71] Astrophys. J., 168, 437, 1971
[72] Astrophys. J., 144, 440, 1966
[73] The Early Type Stars, D. Reidel Publ. Co. Dordrecht, p. 259, 1966
[74] Astron. Nachrichten, 177, 70, 1908
[75] BAV Rundbrief, 12, 3, 1963

- Binary stars

Although the observatory's main program was the study of intrinsic variables, some eclipsing and spectroscopic binaries were also investigated.

On the plates made for studying AV Vul, the β Lyrae type variable, CD Vulpeculae could also be measured. The amplitude of the primary minimum was about 1^m, and that of the secondary minimum about $0\overset{m}{.}4$ (Guman 1951).

The long period eclipsing binaries Z Aurigae and 32 Cygni were photoelectrically measured (Detre & Herczeg 1952, Herczeg 1956a, 1956b).

The orbits of visual and spectroscopic binaries were also discussed in several papers (Batten & Szeidl 1972, Herczeg 1957a, 1957b).

In 1959, K. K. Kwee[76] organized an international campaign of observations of VW Cephei. In the frame of this program during seven nights in 1959 more than 1000 photoelectric observations were secured in U, B, V, and R bands (Detre & Kanyó 1961). In connection with this program photoelectric observations obtained previously at the observatory (in 1950, 1952, and 1959) were also published and discussed (Balázs & Detre 1961a).

Attempt was made to interpret the O−C diagrams of four eclipsing binaries (W Delphini, Z Draconis, TX Herculis, and RV Lyrae) with the effect of a hypothetical third body, and the mass functions and orbital elements were determined (Illés & Almár 1963a,b)

Putting into operation the 50 cm Cassegrain telescope, more telescope time was at disposal of the staff and the starting of new programs become possible.

The regular photoelectric observations of minima of eclipsing variables were commenced in 1973 (Patkós 1975, 1976).

Epilogue

In this review I made an attempt to summarize the results of variable star research at the Konkoly Observatory published until 1976. This date was chosen for the simple reason as I tried to stress the results and achievements "in which László Detre had a hand". Of course, there were research works commenced before 1976 and concluded and published later on. Here I quote only some examples.

The old photographic observations of AC And were measured and analyzed[77]. The photographic and photoelectric observations of nine single mode RR Lyrae stars (AT And, SU Dra, TW Her, VZ Her, RR Leo, TT Lyn, AV Peg, AR Per, and TU UMa)[78] and the Blazhko stars RW Dra[79], XZ Dra[80], and RR Lyr[81] were published and the basic parameters of the light curves (e.g. times of maximum light) were also given. Still we have old photographic (from the 1930-1950s) and photoelectric observations (from the 1950-1960s) of RR Lyrae stars not yet elaborated.

The period changes of single mode high amplitude δ Scuti stars (CY Aqr, YZ Boo, XX Cyg, DY Her, EH Lib, SZ Lyn, and DY Peg) were investigated also making use of the

[76]Resolution on co-operative programs, IAU Comm. 42 Transactions of IAU, vol. 10, p. 638, 1958

[77]I. Guman, Budapest Mitt., Nr. 78, 1982

[78]K. Oláh & B. Szeidl, Budapest Mitt., Nr. 71, 1978; B. Szeidl, K. Oláh, & A. Mizser, Budapest Mitt., Nr. 89, 1986

[79]B. Szeidl, K. Oláh, K. Barlai, & L. Szabados, Budapest Mitt., Nr. 102, 2001

[80]B. Szeidl, J. Jurcsik, J.M. Benkő, & G. Bakos, Budapest Mitt., Nr. 101, 2001

[81]B. Szeidl, E. F. Guinan, K. Oláh, & L. Szabados, Budapest Mitt., Nr. 99, 1997

old photographic and photoelectric observations of the observatory[82]. The photoelectric observations obtained in the fifties and sixties were also included in the study of double mode HADS (RV Ari and AE UMa)[83].

The behaviour of the peculiar W Vir type star, RU Cam had been followed from 1966 during 16 years. The unique data set covered almost continuously the light variation for that time interval[84].

In the frame of the photographic observational program of RR Lyrae stars in globular clusters, a great number of plates were taken with the 60 cm telescope on different clusters from 1937 up to 1966. Measurements of variables in M15 were accomplished[85], but the investigation of RR Lyrae stars in M5 is still the task for the future.

In this review I have not alluded to two subjects, although both belong to the field of variable stars. In order to make the most the 60/90 cm Schmidt telescope, L. Detre initiated the search for extragalactic supernovae (Detre 1974) and for flare stars in galactic clusters[86]. The motive for setting aside these subjects was that the aim of the searches was the study of the frequency of supernovae and flare stars and not the study of physics of their variability.

The variable star research at the Konkoly Observatory had new perspective when the development of its mountain station was completed in 1975. The new 1 m RCC telescope was right away furnished with an uncooled UBV, and later on with a refrigerated photon-counting UBV(RI)$_C$ photometer[87], that made the broadening of the field of variable star research at the Konkoly Observatory possible. Based on the three photometric telescopes (60 cm Newtonian at Budapest, Svábhegy, 50 cm Cassegrain and 1 m RCC at Piszkéstető mountain station) the author of this review initiated the study of all types of variables in classical instability strip of HRD and of the phenomena of stellar activity. The 1 m telescope also proved to be an ideal equipment for the investigation of variables in globular clusters, to pursue our classical program. Large number of photographic plates were exposed on M3, M5, and M15 before the CCD era.

The variable star research at the Konkoly Observatory well-founded by L. Detre during his life has always had international reputation and the variable star community of the observatory has always taken active part in the international co-operation. Since 1961 the Information Bulletin of Variable Stars, the official publication of the IAU Commissions 27 and 42 has been issued by the observatory. The editors and co-editors were/are L. Detre (1961-1974), B. Szeidl (1968-1990), L. Szabados (1983-2000), Katalin Oláh (1990-) and Johanna Jurcsik (2000-). L. Detre and B. Szeidl fulfilled the duty of presidency of the IAU Variable Star Commission in the years 1967-1970 and 1985-1988, respectively. The observatory organized three international conferences on variable stars before 1976:

- Konferenz über veränderliche Sterne, Budapest, 23-28 August 1956
- Non-periodic Phenomena in Variable Stars, IVth Colloquium on Variable Stars, Budapest, 5-9 September 1968

[82]H.A. Mahdy & B. Szeidl, Budapest Mitt., Nr.74, 1980; B. Szeidl & H. A. Mahdy, Budapest Mitt., Nr.75, 1981; B. Szeidl, Budapest Mitt., Nr.84, 1983

[83]B. Szeidl & G. Virághalmy, Budapest Mitt., Nr. 98, 2000; M. D. Pócs & B. Szeidl, Astron. Astrophys., 368, 880, 2001; M. D. Pócs, B. Szeidl, & G. Virághalmy, Astron. Astrophys., 393, 555, 2002

[84]B. Szeidl, K. Oláh, L. Szabados, K. Barlai, & L. Patkós, Budapest Mitt., Nr. 97, 1992

[85]K. Barlai, Budapest Mitt., Nr. 92, 1989

[86]This program was carried out in cooperation with the Byurakan Observatory, Armenia

[87]The photometers to the 50 cm Cassegrain and 1 m RCC telescopes were designed and built by G. Virághalmy.

- Multiple Periodic Variable Stars, IAU Colloquium No.29, Budapest, 1-5 September 1975

* * *

In this short review I essayed to outline the first 75 years history of variable star research carried out at the Konkoly Observatory. Although the circumstances were not always favourable for research work, the accomplishment was impressive and has inspired, and may inspire the succeeding generations. The publications of staff members of the Konkoly Observatory on variable stars between 1901 and 1976 are given in the references section.

Acknowledgements The author is very grateful to Mr. Mihály Váradi for helping in the preparation of this paper. The financial support of OTKA grants T-043504, T-046207 and T-048961 is acknowledged.

References:

Almár I., 1959, Cepheid CY Cassiopeiae (in Russian), *Peremennye Zvezdy*, **12**, 437-439

Almár I., 1961, Perioden- und Lichtkurvenänderungen von AR Herculis, *Mitt. Sternwarte Budapest,* **4**, Nr. 51, 1-80

Almár I., 1968, Rotational velocity of RS (23) Sextantis, *Inf. Bull. Var. Stars,* **260**, 1-2

Almár I. & Illés Erzsébet, 1966, Photoelectric observations of Nova Her 1963, *Mitt. Sternwarte Budapest,* **5**, Nr. 60, 1-24

Balázs Júlia, 1935, Der photographische Lichtwechsel von AV Pegasi, *Astron. Nachr.*, **254**, 75-80

Balázs Júlia, 1936a, Der RR Lyrae-Veränderliche VZ Herculis, *Astron. Nachr.*, **258**, 305-310

Balázs Júlia, 1936b, WY Tau, *Beobachtungs-Zirkular der AN*, **18**, (Nr. 7) 14

Balázs Júlia, 1936c, WZ Cephei, *Beobachtungs-Zirkular der AN*, **19**, (Nr. 4) 7

Balázs Júlia, 1937a, Über den Lichtwechsel und die Periode von RR Leonis, *Astron. Nachr.*, **261**, 129-136

Balázs Júlia, 1937b, Der Veränderliche BH Pegasi, *Astron. Nachr.*, **262**, 437-441

Balázs Júlia, 1937c, Der Lichtwechsel von DH Pegasi, *Astron. Nachr.*, **262**, 441-444

Balázs Júlia, 1938, Der photographische Lichtwechsel von AA Aquilae, *Astron. Nachr.*, **265**, 69-74

Balázs Júlia, 1952a, Notes on BT Lyrae and on two new variables near M56, *Mitt. Sternwarte Budapest,* **3**, Nr. 30, 1-8

Balázs Júlia, 1952b, Bemerkungen über ST Draconis, *Mitt. Sternwarte Budapest,* **3**, Nr. 30, 8-9

Balázs Júlia, 1955, Über die sekundären Perioden von Y Leonis Minoris, *Mitt. Sternwarte Budapest,* **3**, Nr. 39, 6-9

Balázs Júlia, 1956, Discussion von 504 photographischen Beobachtungen von RV Arietis, *Mitt. Sternwarte Budapest,* **3**, Nr. 40, 8-17

Balázs Júlia, 1957, Sprunghafte und langsame Änderungen im Blaschko-Effekt von RW Draconis, *Mitt. Sternwarte Budapest,* **3**, Nr. 42, 99-101

Balázs Júlia, 1960, Zur Erklärung des Blaschko-Effekts, *Kleine Veröff. Bamberg*, **Nr. 27**, 26-27

Balázs Júlia, 1963, RR Lyrae stars, *Astron. Soc. of the Pacific Leaflet*, **No. 417**, 1-8

Balázs Júlia & Detre L., 1934, 391.1934 Aquarii, *Beobachtungs-Zirkular der AN*, **16**, (Nr. 38) 72

Balázs Júlia & Detre L., 1935, Der photographische Lichtwechsel von 391.1934 Aquarii, *Astron. Nachr.*, **256**, 87-92

Balázs Júlia & Detre L., 1938, Untersuchungen über die Perioden- und Lichtkurvenänderungen von kurzperiodischen δ Cephei-Sternen I. *Mitt. Sternwarte Budapest,* **1**, Nr. 5, 1-35

Balázs Júlia & Detre L., 1939, Untersuchungen über die Perioden- und Lichtkurvenänderungen von kurzperiodischen δ Cephei-Sternen. II. AR Herculis, *Mitt. Sternwarte Budapest,* **1**, Nr. 8, 1-49

Balázs Júlia & Detre L., 1940, Das photometrische Doppelsternsystem WY Tauri, *Mitt. Sternwarte Budapest,* **1**, Nr. 11, 1-10

Balázs Júlia & Detre L., 1941, Die sekundäre Periode von XZ Draconis, *Astron. Nachr.*, **271**, 231

Balázs Júlia & Detre L., 1943, Untersuchungen über die Perioden- und Lichtkurvenänderungen von kurzperiodischen δ Cephei-Sternen. IV. Die sekundären Helligkeitsschwankungen von RR Lyrae, *Mitt. Sternwarte Budapest,* **2**, Nr. 18, 1-35

Balázs Júlia & Detre L., 1949, Untersuchungen über die Perioden- und Lichtkurvenänderungen von kurzperiodischen δ Cephei-Sternen. V. RR Leonis, *Mitt. Sternwarte Budapest,* **2**, Nr. 21, 1-19

Balázs Júlia & Detre L., 1950, Untersuchungen über die Perioden- und Lichtkurvenänderungen von kurzperiodischen δ Cephei-Sternen. VI. RW Cancri, *Mitt. Sternwarte Budapest,* **2**, Nr. 23, 1-34

Balázs Júlia & Detre L., 1952, Untersuchungen über die Perioden- und Lichtkurvenäderungen von kurzperiodischen δ Cephei-Sternen. VII. Die Perioden von RW Draconis, *Mitt. Sternwarte Budapest,* **3**, Nr. 27, 1-60

Balázs Júlia & Detre L., 1954, Untersuchungen über die Perioden- und Lichtkurvenänderungen von kurzperiodischen δ Cephei-Sternen. VIII. SW Andromedae, *Mitt. Sternwarte Budapest,* **3**, Nr. 33, 1-46

Balázs Júlia & Detre L., 1957, Untersuchungen über die Perioden- und Lichtkurvenänderungen von kurzperiodischen δ Cephei-Sternen. IX. RV Ursae Maioris, *Mitt. Sternwarte Budapest,* **3**, Nr. 34, 1-37

Balázs Júlia & Detre L., 1961a, Photoelectric observations of VW Cep in 1950, 1952 and 1959, *Mitt. Sternwarte Budapest,* **4**, Nr. 50, 1-11

Balázs Júlia & Detre L., 1961b, Work on RR Lyrae variables at Budapest Observatory, *Acta Astronomica Sinica*, **9**, 77-82

Balázs Júlia & Detre L., 1962, Analyse des mehrfachperiodischen Lichtwechsels von RR Lyrae und RW Draconis, *Kleine Veröff. Remeis-Sternwarte Bamberg*, **Nr. 34**, 90-94

Balázs Júlia & Detre L., 1965, Period changes in variables and evolutionary paths in the Hertzsprung Russell-Diagram, *Kleine Veröff. Remeis-Sternwarte Bamberg*, **4**, (Nr. 40) 184-194

Barlai Katalin & Szeidl B., 1965, VZ Pegasi, *Mitt. Sternwarte Budapest,* **4**, Nr. 56, 1-9

Barlai Katalin, Szabados L., & Szeidl B., 1972, Photoelectric observations of AD Leonis, *Inf. Bull. Var. Stars,* **640**, 1

Batten A.H. & Szeidl B., 1972, The spectroscopic binary system HD 11860, *Publ. Dominion Astrophys. Obs.*, **14**, No. 5, 97-105

Detre L. (Dunst L.), 1931, RZ Cephei, *Beobachtungs-Zirkular der AN*, **13**, (Nr. 24) 42

Detre L. (Dunst L.), 1932a, Photometrische Beobachtung der Veränderlichen XY Cassiopeiae, *Astron. Nachr.*, **246**, 361-364
Detre L. (Dunst L.), 1932b, Bemerkungen über X Canum Venaticorum, *Astron. Nachr.*, **246**, 364-366
Detre L. (Dunst L.), 1932c, SV Cam, *Beobachtungs-Zirkular der AN*, **14**, (Nr. 34) 61
Detre L. (Dunst L.), 1933a, SZ Cassiopeiae, *Astron. Nachr.*, **247**, 309-312
Detre L. (Dunst L.), 1933b, Photometrische Lichtkurve und Systemkonstanten von SV Camelopardalis, *Astron. Nachr.*, **249**, 213-220
Detre L., 1934a, Die Lichtkurve von RU Piscium, *Astron. Nachr.*, **251**, 27-33
Detre L., 1934b, UU Herculis und UZ Aurigae, *Beobachtungs-Zirkular der AN*, **16**, (Nr. 18) 33
Detre L., 1934c, Der RR Lyrae-Veränderliche SW Andromedae, *Astron. Nachr.*, **252**, 327-336
Detre L., 1935a, Lichtwechsel von UZ Aurigae, *Astron. Nachr.*, **254**, 17-20
Detre L., 1935b, Über den RR Lyrae-Veränderlichen W Canum Venaticorum, *Astron. Nachr.*, **254**, 21-26
Detre L., 1935c, Der δ Cephei-Veränderliche YZ Aurigae, *Astron. Nachr.*, **257**, 361-364
Detre L., 1936a, XX Cygni, *Astron. Nachr.*, **258**, 329-336
Detre L., 1936b, Photometrische Beobachtungen von Veränderlichen, *Astron. Nachr.*, **259**, 305-310
Detre L., 1936c, RV (267.1934) Arietis, *Beobachtungs-Zirkular der AN*, **18**, (Nr. 1) 2
Detre L., 1936d, RV (267.1934) Arietis, *Beobachtungs-Zirkular der AN*, **18**, (Nr. 4) 8
Detre L., 1936e, RV (267.1934) Arietis, *Beobachtungs-Zirkular der AN*, **18**, (Nr. 38) 67
Detre L., 1937a, Neuer Veränderlicher 624.1936 Arietis, *Astron. Nachr.*, **261**, 9
Detre L., 1937b, Die Veränderlichen RV und 624.1936 Arietis, *Astron. Nachr.*, **262**, 81-90
Detre L., 1940, Das System WZ Cephei, *Mitt. Sternwarte Budapest,* **1**, Nr. 10, 1-11
Detre L., 1941, Über die sekundären Helligkeitsschwankungen von δ Scuti, *Astron. Nachr.*, **271**, 225-230
Detre L., 1942, Photometrie von Doppelsternkomponenten, *Astron. Nachr.*, **273**, 253-263
Detre L., 1943, Untersuchungen über die Perioden- und Lichtkurvenänderungen von kurzperiodischen δ Cephei-Sternen. III. Die Perioden von RR Lyrae, *Mitt. Sternwarte Budapest,* **2**, Nr. 17, 1-54
Detre L., 1954, Über den Blaschko-Effekt, *Die Sterne*, **30**, Heft 11/12, 214-215
Detre L., 1955, Izmenenye periodov korotkoperiodicheskyh Cefeid, *Trudy 4. Soveschanija po voprosam kozmogonii*, Izd. Akad. Nauk SSSR, Moskva, 389-399
Detre L., 1956a, The problem of RR Lyrae stars with several periods, *Vistas in Astronomy*, (ed. A. Beer) Pergamon Press, **2**, 1156-1165
Detre L., 1956b, Die sekundäre Periode von RV Arietis, *Mitt. Sternwarte Budapest,* **3**, Nr. 40, 1-7
Detre L., 1957, Resultate photoelektrischer Beobachtungen von RR Lyrae-Sternen, *Mitt. Sternwarte Budapest,* **3**, Nr. 42, 103-104
Detre L., 1960, Fotoelektrische Beobachtungen von RR Lyrae-Veränderlichen, *Kleine Veröff Remeis-Sternwarte Bamberg*, **Nr. 27**, 23-25
Detre L., 1962a, The Blashko effect in RR Lyrae variables, *IAU Transactions*, **XI.B**, (Proceedings) 293-296
Detre L., 1962b, Request for photoelectric observations of AC And, *Inf. Bull. Var. Stars,* **13**, 1
Detre L., 1965a, Die RR Lyrae Sterne, *Sterne und Weltraum*, **4**, 157-162

Detre L., 1965b, TV Bootis, ein RRc-Stern mit sekundärer Periode, *Astronomische Abhandlungen zum 70. Geburtstag von Prof. C. Hoffmeister*, Johann Ambrosius Barth Verlag, Leipzig, 62-64

Detre L., 1966a, Cosmogonia y estrellas variables, *Rev. Sc. Habana*, 30-37

Detre L., 1966b, Cyclic amplitude variations of RU Cam, *Inf. Bull. Var. Stars,* **152**, 3-4

Detre L., 1967, RR Lyrae Stjernerne, *Nordisk Astronomisk Tidskrift*, **1**, 7-19

Detre L., 1969a, A new decrease in the light variation amplitude of RU Camelopardalis, Editor's note, *Inf. Bull. Var. Stars,* **335**, 2

Detre L., 1969b, On the period changes of pulsars, *Inf. Bull. Var. Stars,* **380**, 1-2

Detre L., 1969c, Statistical and physical interpretation of non-periodic phenomena in variable stars, in *Non-Periodic Phenomena in Variable Stars*, IAU Coll. No. 4, (ed. L.Detre) Akadémiai Kiadó, 3-19

Detre L., 1970a, Variable Stars, *IAU Transactions*, **XIV.A**, (Reports) 259-285

Detre L., 1970b, Periodenänderungen bei Bedeckungs- und Pulsationsveränderlichen, *Ann. Univ.-Sternwarte Wien* **29**, (Nr. 2) 79-92

Detre L., 1973, RR Lyrae variables and dwarf cepheids, *IAU Transactions*, **XV.A**, (Reports) 333-335

Detre L., 1974, Supernova survey at the Konkoly Observatory, in *Supernovae and supernova Remnants*, (ed. C. B. Cosmovici), *Astrophys. and Space Sci. Library*, **45**, 51-53

Detre L. & Chang Y. C., 1960, Photoelectric observations of CY Aquarii and BE Monocerotis, *Acta Astronomica Sinica*, **8**, 50-59

Detre L. & Herczeg T., 1952, Photoelectric observations of the 1950 eclipse of Zeta Aurigae, *Mitt. Sternwarte Budapest,* **3**, Nr. 29, 1-3

Detre L. & Kanyó S., 1961, Four colour photometry of VW Cep during the international campaign in 1959, *Mitt. Sternwarte Budapest,* **4**, Nr. 49, 1-21

Detre L. & Lassovszky K., 1934a, Der Veränderliche UU Herculis in den Jahren 1932-33, *Astron. Nachr.*, **252**, 197-200

Detre L. & Lassovszky K., 1934b, Bemerkungen über TZ und UY Herculis, *Astron. Nachr.*, **252**, 201-202

Detre L. & Lassovszky K., 1939, Beobachtungen von veränderlichen Sternen, *Mitt. Sternwarte Budapest,* **1**, Nr. 9, 1-15

Detre L. & Szeidl B., 1967, Note on RU Camelopardalis, *Inf. Bull. Var. Stars,* **204**, 3

Detre L. & Szeidl B., 1973a, Development of a new 4 year cycle in the 41-day period of RR Lyrae, *Inf. Bull. Var. Stars,* **764**, 1-2

Detre L. & Szeidl B., 1973b, On the nature of the 41-day cycle of RR Lyrae, in: Variable Stars in *Globular Clusters and in Related Systems*, IAU Coll. No. 21 (ed. J. D. Fernie), *Astrophys. and Space Sci. Library*, **36**, 31-34

Dezső L., 1945, The short period Cepheid RU Piscium, *Mitt. Sternwarte Budapest,* **2**, Nr. 20, 1-13

Dezső L., 1949, Korotkoperiodicheskaja cefeida RU Piscium, *Peremennye Zvezdy*, **7**, 30-33

Fitch W. S. & Szeidl B., 1976, The three radial modes and evolutionary state of AC Andromedae, *Astrophys. Journal*, **203**, 616-624

Gefferth K. & Szeidl B., 1962, SZ Lyncis, *Inf. Bull. Var. Stars,* **7**, 1

Geyer E. H. & Szeidl B., 1965, Photometric study of the variable stars in Omega Centauri (NGC5139), in *The Position of Variable Stars in the Hertzsprung-Russell Diagram*, Proc. 3rd IAU Coll. on Variable Stars, *Kleine Veröff. Remeis-Sternw. Bamberg*, **4**, (Nr. 40) 63-65

Geyer E. H. & Szeidl B., 1970, The RR Lyrae gap in the colour-magnitude diagram of Omega Centauri (NGC 5139), *Astron. Astrophys.*, **4**, 40-52

Guman I., 1951, Das photometrische Doppelsternsystem CD Vulpeculae, *Mitt. Sternwarte Budapest,* **3**, Nr. 24, 1-13

Guman I., 1952, Beobachtungen von AI Andromedae und AV Vulpeculae, *Mitt. Sternwarte Budapest,* **3**, Nr. 31, 1-4

Guman I., 1955a, VZ Cancri, ein RR Lyrae-Stern mit sehr kurzer sekundärer Periode, *Mitt. Sternwarte Budapest,* **3**, Nr. 36, 1-16

Guman I., 1955b, Beobachtungen von AI und BE Andromedae, *Mitt. Sternwarte Budapest,* **3**, Nr. 39, 10-15

Harkányi B., 1901a, Photometrische Beobachtungen der Nova (3.1901) Persei, *Astron. Nachr.*, **155**, 155-156

Harkányi B., 1901b, Photometrische Beobachtungen der Nova (3.1901) Persei, *Astron. Nachr.*, **156**, 79-80

Harkányi B., 1903, Photometrische Beobachtungen der Nova (3.1901) Persei an der Sternwarte in Ó-Gyalla, *Mathematische und Naturwissenschaftliche Berichte aus Ungarn*, **19**, 31

Harkányi B., 1910, Darstellung der photometrischen und photographischen Grösse als Funktion der Temperatur der Sterne, *Astron. Nachr.*, **186**, 161-176

Herczeg T., 1956a, Photoelectric observations of the 1955-56 eclipse of Zeta Aurigae, *Mitt. Sternwarte Budapest,* **3**, Nr. 41, 18-22

Herczeg T., 1956b, A short note on 32 Cygni, *Mitt. Sternwarte Budapest,* **3**, Nr. 41, 23

Herczeg T., 1957a, Discussion of two visual binary systems, *Mitt. Sternwarte Budapest,* **3**, Nr. 35, 39-42

Herczeg T., 1957b, Notes on some eclipsing and visual binaries, *Mitt. Sternwarte Budapest,* **3**, Nr. 42, 39-44

Illés Erzsébet, 1960, BP Vulpeculae, *Astr. Tsirk.*, **210**, 21

Illés Erzsébet, 1963, AT Herculis, *Inf. Bull. Var. Stars,* **22**, 1

Illés Erzsébet, 1968, The light-surface of TU Cas, *Inf. Bull. Var. Stars,* **303**, 1-2

Illés Erzsébet & Almár I., 1963a, Ein Versuch zur Anwendung der Irwin'schen "standard light-time curves" bei einigen Bedeckungsveränderlichen, *Acta Astronomica*, **13**, 72-74

Illés Erzsébet & Almár I., 1963b, Einige Bemerkungen zur Anwendbarkeit der Lichtzeitbahn-Hypotese bei den Bedeckungsveränderlichen, *Acta Astronomica*, **13**, 75-78

Illés Erzsébet & Szabados L., 1976, Observational results of the beat period cepheid TU Cassiopeiae, in *Multiple Periodic Variable Stars*, Proc. IAU Coll. No. 29, Contributed Papers (Ed. W. S. Fitch) 165-170

Izsák I., 1952, Three new variable stars in the globular cluster M15, *Mitt. Sternwarte Budapest,* **3**, Nr. 28, 1-2

Izsák I., 1957, Untersuchungen über die Periodenänderungen der Veränderlichen im Kugelsternhaufen M15, *Mitt. Sternwarte Budapest,* **3**, Nr. 42, 63-79

Jankovics I., 1973, A new U Geminorum star in Cancer, *Inf. Bull. Var. Stars,* **840**, 1-2

Kanyó S., 1966, The secondary period of the RRab star Z Canum Venaticorum, *Inf. Bull. Var. Stars,* **146**, 1-2

Kanyó S., 1970, The secondary period of the RRab star SZ Hydrae, *Inf. Bull. Var. Stars,* **490**, 1-2

Kanyó S., 1972, The secondary period of RV Capricorni, *Inf. Bull. Var. Stars,* **737**, 1-2

Kanyó S., 1976a, UBV photometry of the multiple periodic RR Lyrae star RV Ursae Maioris, *Mitt. Sternwarte Budapest,* **7**, Nr. 69, 1-56

Kanyó S., 1976b, On the period-fluctuation of RR Lyrae stars with Blazhko-effect, in *Multiple Periodic Variable Stars*, Proc. IAU Coll. No.29, Contributed Papers (Ed. W. S. Fitch) 211-213

Kanyó S. & Szeidl B. 1974, Photoelectric observations of AN Serpentis, *Mitt. Sternwarte Budapest,* **5**, Nr. 64, 1-18

Lassovszky K., 1931a, 381.1931 And, *Beobachtungs-Zirkular der AN*, **13**, (Nr. 30) 51

Lassovszky K., 1931b, Beobachtung veränderlicher Sterne, *Astron. Nachr.*, **243**, 399-404

Lassovszky K., 1931c, Neuer Veränderlicher 381.1931, *Astron. Nachr.*, **243**, 404

Lassovszky K., 1932a, Der Veränderliche 381.1931 Andromedae, *Astron. Nachr.*, **245**, 349-356

Lassovszky K., 1932b, Der Veränderliche RW Cassiopeiae, *Astron. Nachr.*, **246**, 289-292

Lassovszky K., 1933a, Die Lichtkurve von SZ Cygni, *Astron. Nachr.*, **247**, 177-182

Lassovszky K., 1933b, TV Cygni, *Astron. Nachr.*, **247**, 182

Lassovszky K., 1933c, Der Veränderliche VY Cygni, *Astron. Nachr.*, **248**, 313-316

Lassovszky K., 1934, Der Bedeckungsveränderliche AB Persei, *Astron. Nachr.*, **252**, 221-230

Lassovszky K., 1935a, Der Veränderliche RR Lacertae, *Astron. Nachr.*, **254**, 25-30

Lassovszky K., 1935b, Der Bedeckungsveränderliche AT Pegasi, *Astron. Nachr.*, **256**, 167-172

Lassovszky K., 1936a, Der Bedeckungsveränderliche KR Cygni, *Astron. Nachr.*, **258**, 93-96

Lassovszky K., 1936b, Nova 605.1936 Lacertae, *Astron. Nachr.*, **259**, 343

Lassovszky K., 1936c, Beobachtungen von Nova CP Lac, *Astron. Nachr.*, **260**, 94

Lassovszky K., 1938, Der photometrische Doppelstern SV Tauri, *Mitt. Sternwarte Budapest,* **1**, Nr. 6, 1-26

Lovas M., 1952, Bemerkungen über ZZ Persei, *Mitt. Sternwarte Budapest,* **3**, Nr. 31, 4-5

Lovas M., 1965, Object Rosino-Zwicky near M88, *Inf. Bull. Var. Stars,* **99**, 1-2

Móra K. (Morawetz), 1930, Der Lichtwechsel des Veränderlichen R Scuti (1795-1927), *Math. Nat. Anzeiger d. Ung. Akad. d. Wiss.*, **47**, 403

Móra K., 1934, Der veränderliche Stern R Scuti, *Mitt. Sternwarte Budapest,* **1**, Nr. 3, 1-172

Oláh K., 1974, Note on the RRab star AT Andromedae, *Inf. Bull. Var. Stars,* **987**,

Ozsváth I., 1957, Über die Periodenänderungen der Veränderlichen im Kugelsternhaufen M3, *Mitt. Sternwarte Budapest,* **3**, Nr. 42, 81-84

Patkós L., 1975, Photoelectric minima of eclipsing variables, *Inf. Bull. Var. Stars,* **1065**, 1

Patkós L., 1976, Photoelectric minima of eclipsing variables, *Inf. Bull. Var. Stars,* **1200**, 1

Szabados L., 1974a, V445 is an eclipsing variable, *Inf. Bull. Var. Stars,* **867**, 1-2

Szabados L., 1974b, The peculiar variable star V361 Per, *Inf. Bull. Var. Stars,* **868**, 1-4

Szabados L., 1976a, The beat period of BQ Ser and BC Dra, in *Multiple Periodic Variable Stars*, Proc. IAU Coll. No. 29, Contributed Papers (Ed. W. S. Fitch) 159-164

Szabados L., 1976b, The period of the cepheid variable BD+56°2806, *Inf. Bull. Var. Stars,* **1107**, 1-2

Szabados L., Stobie R. S., & Pickup D. A., 1976, BC Draconis - an RR Lyrae variable, *Inf. Bull. Var. Stars,* **1197**, 1-3

Szeidl B., 1963, The secondary period of DL Herculis, *Inf. Bull. Var. Stars,* **36**, 1-2

Szeidl B., 1965, The RR Lyrae stars in Messier 3, *Mitt. Sternwarte Budapest,* **5**, Nr. 58, 1-265

Szeidl B., 1967, Secondary period of the RRab star AR Serpentis, *Inf. Bull. Var. Stars,* **220**, 1-2

Szeidl B., 1968a, The secondary period of the RRab star TT Cancri, *Inf. Bull. Var. Stars,* **278**, 1-2

Szeidl B., 1968b, Note on the RRab star AN Serpentis, *Inf. Bull. Var. Stars,* **291**, 1-2

Szeidl B., 1969a, Flares of AD Leonis, *Inf. Bull. Var. Stars,* **345**, 1-3

Szeidl B., 1969b, Note on RU Cam, *Inf. Bull. Var. Stars,* **385**, 1-2

Szeidl B., 1973, A study of some variable stars in Messier 3, *Mitt. Sternwarte Budapest,* **5**, Nr. 63, 1-33

Szeidl B., 1974, The secondary period of AE UMa, *Inf. Bull. Var. Stars,* **903**, 1-3

Szeidl B., 1975, Period changes of RR Lyrae stars in globular clusters, in *Variable Stars and Stellar Evolution*, Proc. IAU Symp. No. 67, Reidel Publ. Co., Dordrecht-Holland (eds.: V. E. Sherwood & L. Plaut) 545-552

Szeidl B., 1976, Multiple periodic RR Lyrae stars (Observational Review), in *Multiple Periodic Variable Stars*, Proc. IAU Coll. No. 29, *Astrophysics and Space Science Library*, **60**, Reidel Publ. Co., Dordrecht-Holland (ed.: W. S. Fitch) 133-151

Tass A., 1904a, Vorläufige Mitteilungen der Resultate photometrischer Beobachtungen langperiodischer Veränderlicher, *Astron. Nachr.*, **165**, 177-188

Tass A., 1904b, Photometrische Beobachtungen von S Sagittae and T Vulpeculae, *Kleinere Veröffentlichungen des Ó-Gyallaer Astrophysikalischen Observatoriums Stiftung v. Konkoly*, **Nr. 3**, 1-40

Tass A., 1905a, Neuer Veränderlicher 190.1904 Cassiopeiae, *Astron. Nachr.*, **167**, 109-110

Tass A., 1905b, Vorläufige Mitteilungen der Resultate photometrischer Beobachtungen veränderlicher Sterne, *Astron. Nachr.*, **168**, 197-208

Tass A., 1905c, Photometrische Beobachtungen des Veränderlichen 190.1904 Cassiopeiae, *Astron. Nachr.*, **168**, 207-210

Tass A., 1905d, Neuer Veränderlicher 63.1905 Geminorum, *Astron. Nachr.*, **168**, 321-324

Tass A., 1906, Vorläufige Mitteilungen der Resultate photometrischer Beobachtungen veränderlicher Sterne, *Astron. Nachr.*, **173**, 145-150

Tass A., 1908a, Vorläufige Mitteilungen der Resultate photometrischer Beobachtungen veränderlicher Sterne, *Astron. Nachr.*, **179**, 33-40

Tass A., 1908b, Photometrische Beobachtungen veränderlicher Sterne mit einem Keilphotometer, *Astron. Nachr.*, **179**, 341-356

Tass A., 1918, Nova Aquilae 3, *Astron. Nachr.*, **207**, 65

Tass A., 1925, Photometrische Beobachtungen veränderlicher Sterne, *Publ. Astrophysikalischen Observatoriums Stiftung v. Konkoly*, Budapest, **2**, (Nr. 2) 1-328

Tass A., & Terkán L., 1916, Photometrische Durchmusterung des südlichen Himmels, *Publ. des Ó-Gyallaer Astrophysikalischen Observatoriums Stiftung v. Konkoly*, **1**, (Nr. 1) 1-298

Terkán L., 1904, Die Temperaturbestimmung der Fixsterne mit dem Zöllner'schen Kolorimeter, *Kleinere Veröffentlichungen des Ó-Gyallaer Astrophysikalischen Observatoriums Stiftung v. Konkoly*, **Nr. 6**, 1-13

Terkán L., 1905, Photometrische Beobachtungen veränderlicher Sterne in Ó-Gyalla, *Astron. Nachr.*, **168**, 33-40

Terkán L., 1906a, Beitrag zur Berechnung der Bahnelemente von β Lyrae, *Astron. Nachr.*, **170**, 171-172

Terkán L., 1906b, Berechnung der Bahnelemente von β Lyrae, *Kleinere Veröffentlichungen des Ó-Gyallaer Astrophysikalischen Observatoriums Stiftung v. Konkoly*, **Nr. 10**, 1-31

Terkán L., 1910, Beiträge zur photographischen Photometrie, *Astron. Nachr.*, **186**, 113-122

Terkán L., 1926, Über die periodischen Temperaturveränderungen von β Lyrae, deren Verlauf nahe das Spiegelbild der Lichtkurve ist, *Astron. Nachr.*, **226**, 345-358

The Piszkéstető Mountain Station of the Konkoly Observatory

Béla A. Balázs

Department of Astronomy
Loránd Eötvös University
Budapest, Hungary

Overview

Under the directorship of *László Detre*, the Konkoly Observatory of the Hungarian Academy of Sciences has established a mountain station (on one of the highest points of Hungary) and has acquired three new telescopes. The building operations of the *Piszkéstető Mountain Station* (*Figs. 1-4*) started in 1958, their financial backing was provided by the Hungarian government. The completion of the main building took its turn in September 1960 and the dome of the Schmidt telescope was finished in 1961. The new telescope took up its duties in 1962. Detre was the originator and first leader of the Mountain Station. The realization of the project for itself was a great service to Hungarian science and it is really sorrowful that Detre could not live to see completion of this undertaking. The building up of the Station was finished in 1974 – with the installation of the 1 m RCC telescope – and since that time there has not been any significant astronomical building or instrumental investments in our country.

The 60/90 cm Schmidt telescope

The 120/180 cm Schmidt telescope of the Palomar Observatory was completed in 1948 (and for many years it was the largest Schmidt telescope in the world). One year later, the new wide-angle telescope starts the first Palomar Observatory Sky Survey, which maps the entire northern sky and a major share of the southern heavens as well (up to the 21st magnitude). The resulted Palomar Sky Survey Atlas is an indispensable tool of the astronomical investigations up to the present day.

This fact probably played a major role in the decision concerning the infrastructural facilities; consequently the first main acquisition was a 60/90 cm Schmidt telescope equipped with two (a 2° and a 5°) full aperture objective prisms (*Figs. 5-7*).

The installation of a 50 cm Cassegrain telescope was a logical extension of the instrumentation of the mountain station. The telescope arrived during the summer of 1966

and (as in the case of the Schmidt unit) it was assembled and examined by a team of Zeiss technicians in a new dome (*Figs. 8-9*). With the aid of a cooled UBV photoelectric photometer it became feasible to utilize the more favourable conditions of the mountain sky in the field of photoelectric photometry.

The 1 m Ritchey-Chrétien telescope

The last and at the same time largest building and instrumental investment at the mountain station was the installation of a 1 m RCC telescope (produced likewise by Carl Zeiss Jena). The guidance of the telescope and the data acquisition was solved by a CAMAC module and a small TPAi computer (KFKI products). The new facilities – including the 'home-made' photoelectric photometer – reassuringly matched the world-standard of that time and made possible the undertaking of more ambitious projects.

It is well known that Detre was fully aware of the importance of the observations. Perhaps observing was the only affair he took really seriously. But fate was not on his side: he could not live to see the completion of the truly remarkable 1 m RCC project. He died in 1974 when he was only at the age of 68. It is our honouring duty to worthily recall to mind the exceptional lifes work of László Detre, to keep his memory alive and continue his tireless efforts (*Figs. 10-13*).

The PPT version of the memorial lecture delivered is available at the author's home page: `http://astro.elte.hu/~bab/bb.html` .

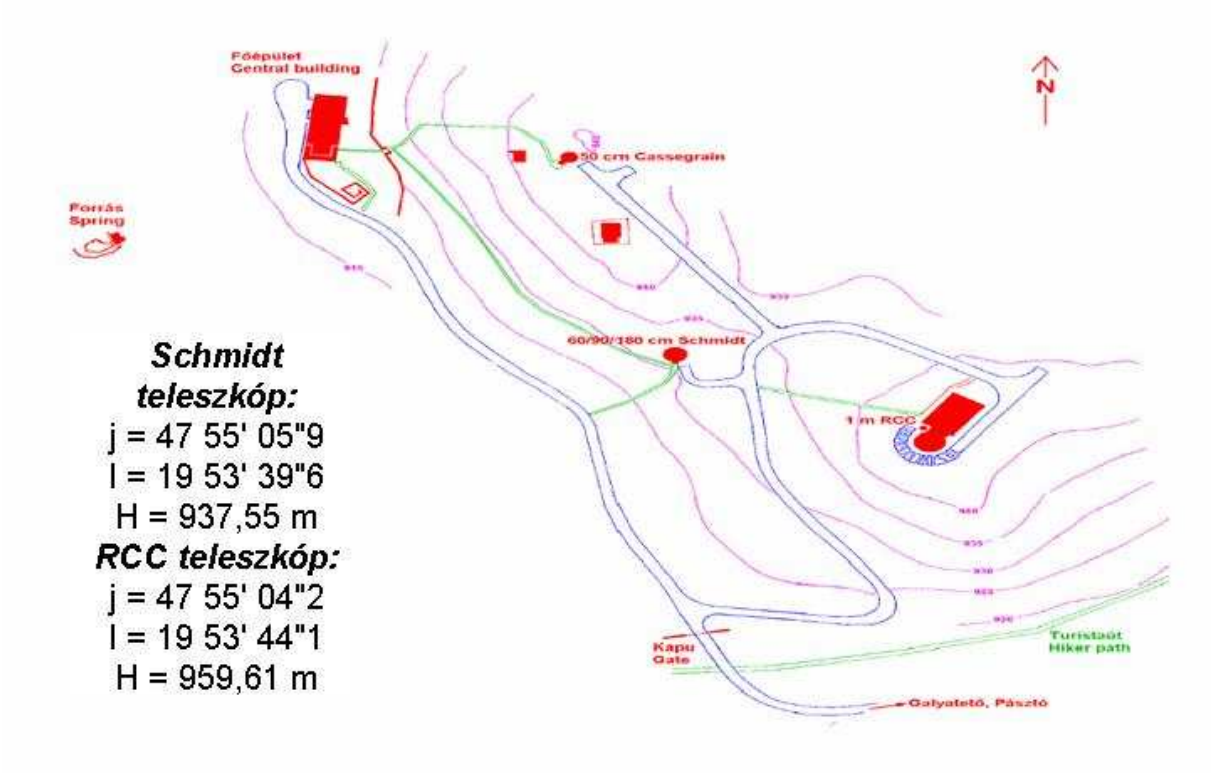

Figure 1: Sketch-map of the mountain station

Figure 2: Birds-eye view of the three domes of the mountain station

Figure 3: Aerial perspective of the main building

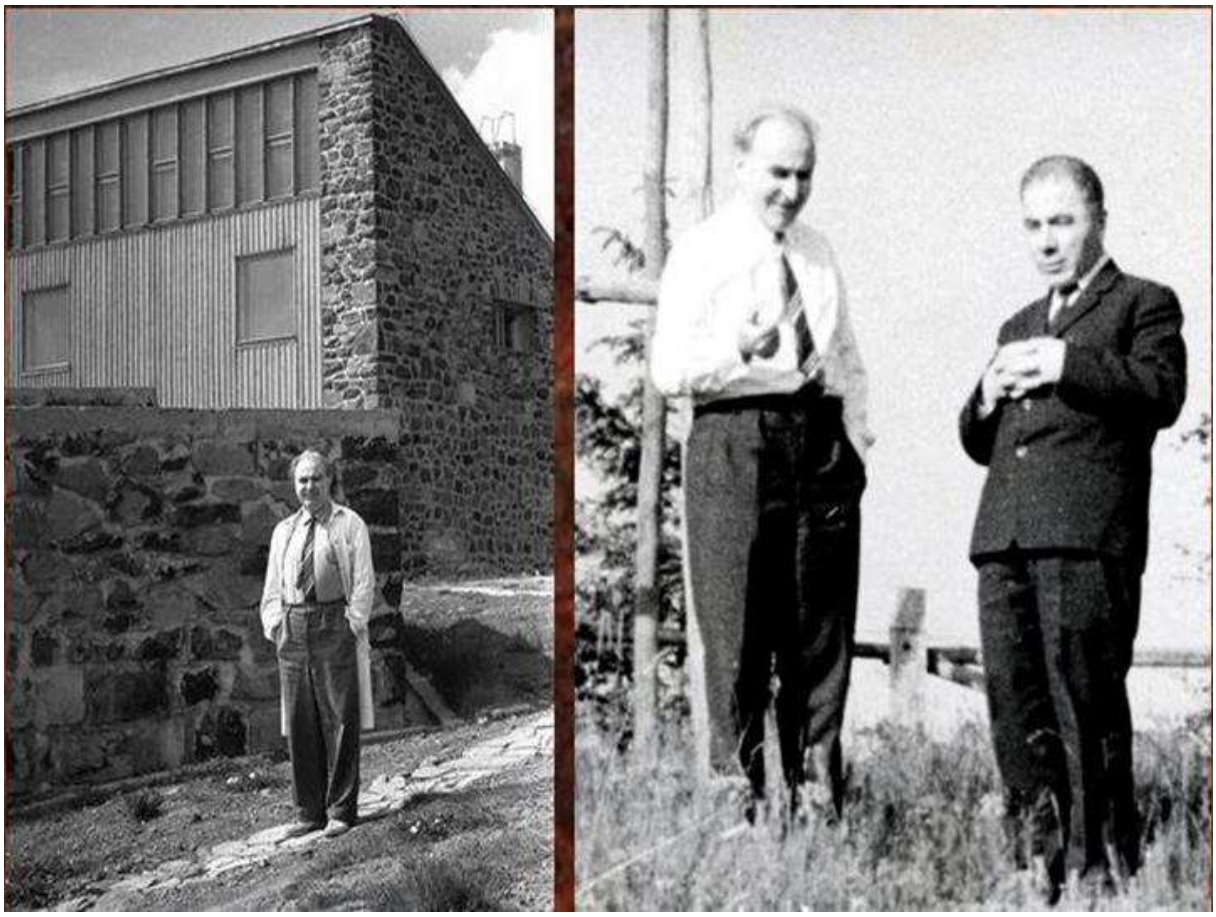

Figure 4: László Detre at the main building (*left*); László Detre and Viktor Amazaspovich Ambartsumian (president of the International Astronomical Union during 1961-1964) on the mountain station (*right*)

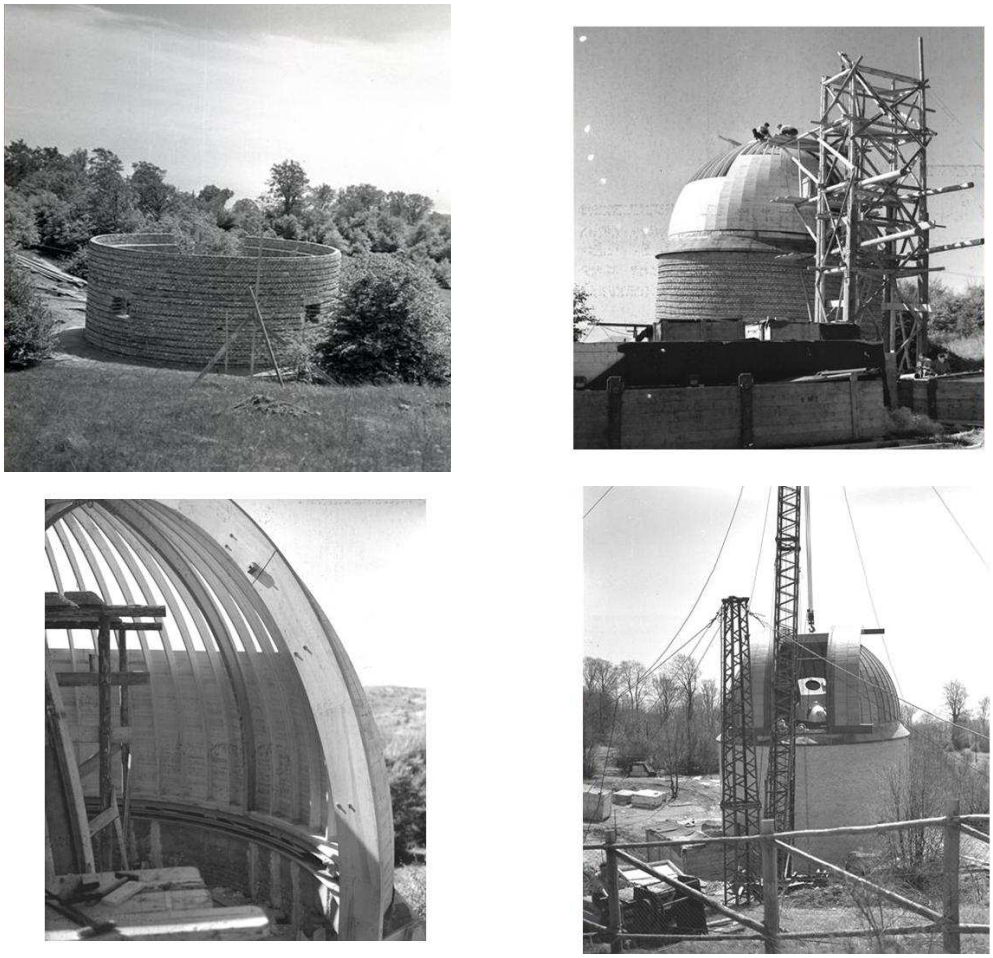

Figure 5: Four stages of the building process of the dome of the Schmidt telescope

Figure 6: László Detre (left), Viktor Ambartsumian (right), and the author in the Schmidt dome

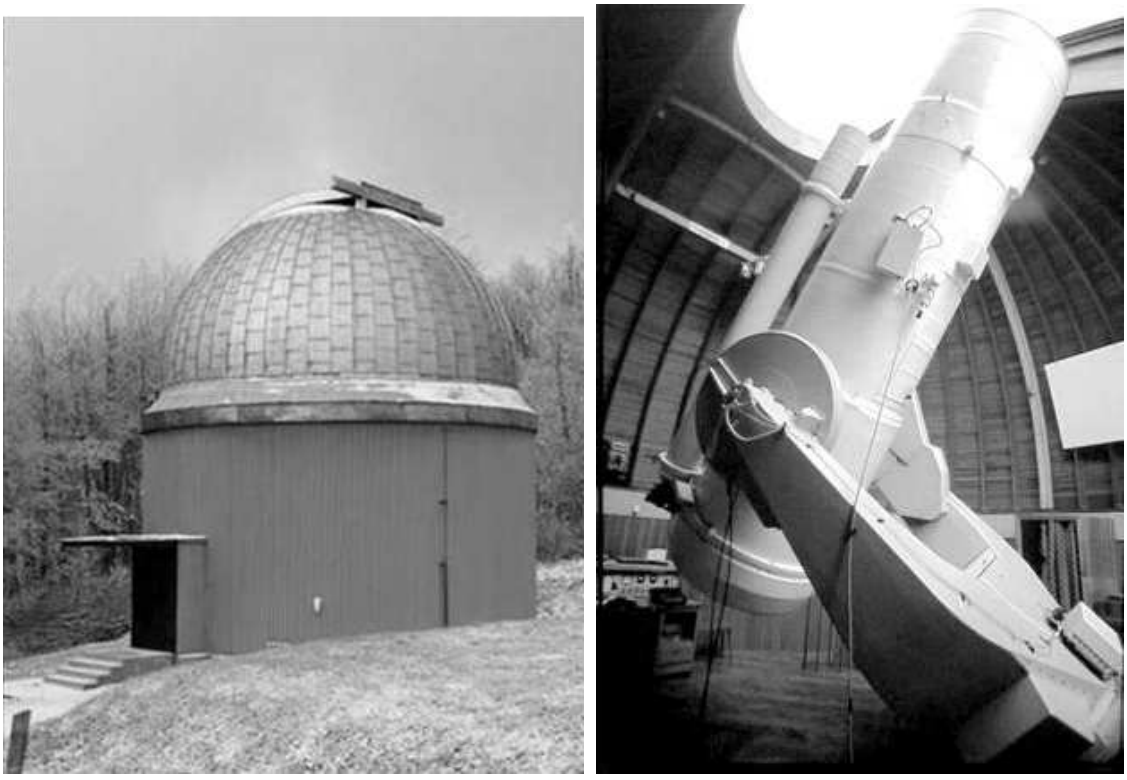

Figure 7: The Schmidt dome and the 60/90 cm Schmidt telescope. Main features: Manufacturer: Carl Zeiss Jena; Year of installation: 1962; Focal length: 1800 mm; Field: 5 degrees, 160×160 sq.mm; Optical instrumentation: 2° and 5° objective prism

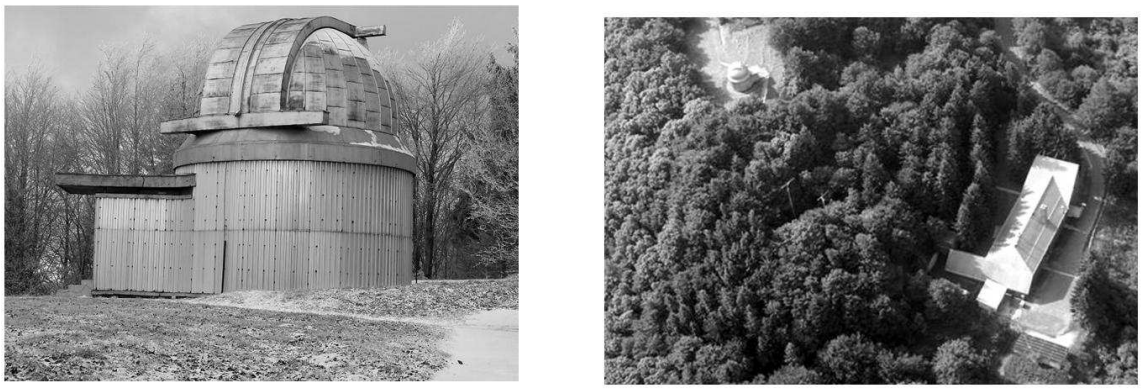

Figure 8: The dome of the 50 cm telescope and its aerial view (with the main building)

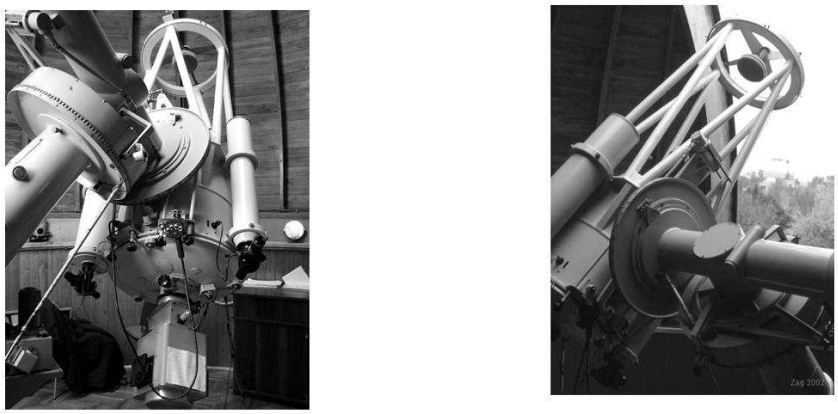

Figure 9: Two views of the 50cm Cassegrain telescope. Main features: Manufacturer: Carl Zeiss Jena; Year of installation: 1966; Focal length: 7500 mm

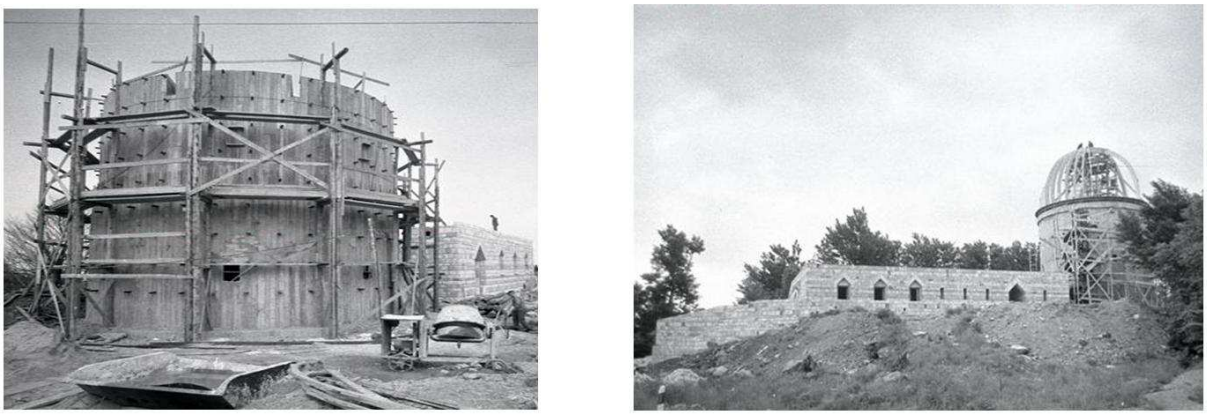

Figure 10: Two stages of the building process of the RCC facilities

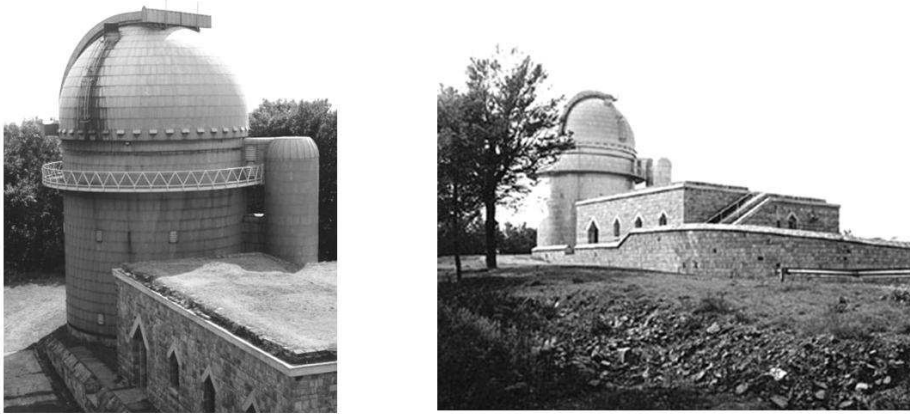

Figure 11: Two views of the RCC building

Figure 12: The 1 m RCC telescope. Main features: Manufacturer: Carl Zeiss Jena; Year of installation: 1974; Focal length: 13500 mm

Figure 13: Unveiling ceremony of the Detre memorial at the Mountain Station. From left to right: L. G. Balázs, J. Balázs (sculptor), N. Kroó (General Secretary of the HAS), and Villő Detre

László Detre and the Department of Astronomy of the Loránd Eötvös University

Bálint Érdi

Department of Astronomy
Loránd Eötvös University,
Budapest, Hungary

László Detre was appointed as professor and head of the Department of Astronomy of the Eötvös University from the 1st of August, 1964. Since he also was the director of the Astronomical Institute of the Hungarian Academy of Sciences, he served as a half time professor at the University. He was the leader of the Department of Astronomy until 1968 when, as a result of an agreement between the Academy and the University according to which a person cannot be a director of two institutes simultaneously, he resigned as head of department. He continued, however, giving lectures at the University as honorary professor until his death in 1974.

Before professor Detre the Department of Astronomy was led by István Földes, and Detre was followed as head by Béla Balázs.

The staff of the Department of Astronomy between 1964-1968 was

László Detre professor (in half time),
István Földes associate professor,
Béla Balázs associate professor (in half time),
Miklós Marik assistant professor.

Until 1967 the Department of Astronomy was in the main building of the Faculty of Natural Sciences at Múzeum Blvd. 6-8 on the first floor, where it had two rooms. Entering the department from the corridor there was a larger room which served as a seminar room and a library at the same time, and from here opened a smaller room for the staff, where in most of the cases only M. Marik could be met. Others came in just before their lectures.

In the early spring of 1967 the Department of Astronomy, together with other departments of the Faculty of Natural Sciences, moved to the building of the former Military Academy, the Ludovika, with the promise of being there just for a short transitory period, until the new campus of the Faculty would be built. This transitory period, however, lasted for more than three decades, and the author of this paper, who was a student of the department at the time of the movement, often thought that probably the department would still be in the Ludovika when he would retire.

In the building of the Ludovika the Department of Astronomy had a larger place and an astronomical research laboratory, supported both by the Academy and the University, could also be set up with the aim at reducing the large number of observations made by the Schmidt telescope of the Konkoly Observatory's Piszkéstető Mountain Station.

The regular astronomy education in the Eötvös University was initiated and organized by professor Detre. It began in the fall semester of the academic year 1965/1966. The Ministry of Education approved professor Detre's proposal according to which in each year four students, majoring either in physics, geophysics, or teaching of mathematics and physics, could also study astronomy from the third year as an additional major discipline, and after a successful state examination receive a university diploma in astronomy. Prior to this date astronomy could only be learned in special courses. The first diplomae in astronomy were issued in 1968.

While professor Detre was the head of the Department of Astronomy, among the students of the department were: Lajos Balázs, István Fejes, András Horváth, Péter Olaj, Koppány Thaly, József Abaffy, Szabolcs Barcza, István Jankovics.

Below is a (non-official) list of the students of astronomy with the year of the diploma whom professor Detre taught.

1968: Bálint Érdi, György Flórik, Lajos Galambos, László Varga;

1969: Barna Apagyi, Csaba Békássy, Sándor Nagy, Gyöngyi Rovó;

1970: Péter Horváth, Gábor Kilvády, Attila Matisz, Zoltán Nagy, Viktor Rónay;

1971: Lajos Márky-Zay, László Szabados, Gábor Szécsényi-Nagy, László Tihanyi;

1972: György Csaba, Mária Kun, László Patkós;

1973: József Csörgei, Pál Halász, János László Kókai, Anikó Paál;

1974: Lídia Gesztelyi, Attila Grandpierre, Katalin Oláh, Margit Paparó;

1975: Szaniszló Bérczi, Előd Both, Géza Kovács, Gábor Taracsák;

1976: András Bardócz, János Kelemen, Róbert Szabó, László Tóth, Márta Varga, Zsuzsanna Vizi.

Students who wanted majoring in astronomy from the third year, in the first two years had to take up an introductory course. In the following the schedule of astronomy courses is given. The numbers after the course names mean the number of hours per week, for example 2+1 means 2 hours lecture and 1 hour practice in a week. The lecturers' names are also given.

Figure 1: The main building of the Faculty of Natural Sciences on the Múzeum Boulvard, where the Department of Astronomy was until 1967.

Figure 2: The building of the Ludovika gave place for the Department of Astronomy from 1967 to 1998. Professor Detre held his lectures here in the period 1967-1974.

1st and 2nd years:
Introduction to astronomy. 2+1, B. Balázs, M. Marik.
1st semester: Astronomical objects of the Universe
2nd semester: Spherical astronomy
3rd semester: Elementary astrophysics
4th semester: Structure of the Galaxy
3rd year:
General astronomy. 2+1, L. Detre.
Introduction to celestial mechanics. 2+1, I. Földes.
Theoretical astrophysics. 2+0, M. Marik.
Practical astronomy. 0+1, B. Balázs.
Astronomical seminar. 0+2, L. Detre.
4th year:
General astronomy. 2+1, L. Detre.
Celestial mechanics. 2+1, I. Földes.
Theoretical astrophysics. 2+0, M. Marik.
Practical astronomy. 0+1, B. Balázs.
Astronomical seminar. 0+2, L. Detre.
5th year:
General astronomy. 2+1, L. Detre.
Celestial mechanics. 2+0, I. Földes.
Theoretical astrophysics. 2+0, M. Marik.
Practical astronomy. 0+1, B. Balázs.
Astronomical seminar. 0+2, L. Detre.
Seminar on the diploma work. 0+10, L. Detre.

The course of general astronomy was developed by professor Detre. It included fundamental astronomy, physics of the Sun and the stars, and stellar systems. Beside these fields he also reviewed the latest results of astronomy in his lectures and seminars.

In the lectures on theoretical astrophysics by M. Marik mainly the theoretical methods were treated in the fields of the physics of stellar atmospheres and the interstellar matter, and cosmic electrodynamics.

Celestial mechanics was taught by I. Földes, more known in astronomical circles by his widespread interest in music, languages, and arts. His lectures covered the two-body

problem, an introduction to the theory of perturbations, Delaunay's lunar theory, and somewhat surprisingly the theory of motion of artificial satellites.

Teaching of practical astronomy was the territory of B. Balázs. This included photographic and photoelectric photometry, techniques of astronomical instruments, and methods of evaluation of astronomical measurements. In the academic year 1967/1968, because of his research work in the USA, B. Balázs was substituted by Béla Szeidl who gave lectures on photoelectric photometry (fall semester) and on astronomical measuring technics (spring semester).

Professor Detre was internationally recognized for his variable star research. In his lectures, however, he covered all aspects of contemporary astrophysics not only the field of variable stars. He conveyed the most important recent results to his students and made them aware of the actual problems and main research directions. The years of the 1960's were especially rich in outstanding astronomical discoveries, several of them were later recognized by Nobel prize in physics. All these discoveries were discussed in detail in professor Detre's lectures. The main topics were the quasi stellar radio sources, the cosmic X-ray sources, the pulsars, the cosmic microwave background radiation, the beginning of infrared astronomy, and the observations of interstellar molecules. Throughout the years more and more information became available on these subjects, and he thoroughly followed the advance of all fields and was always up-to-date in the events, explanations and denials.

Interestingly, he lectured also on quite distant fields. He had several lectures on the phenomena of solar activity. In one year he gave a semester on supernova research. Years later, when I remember his lectures, the most interesting for me was that even he had given lectures on celestial mechanics. The difficult subject that I had heard from him as a student, later I recognized as the J_2 theory of the Earth's artificial satellites by the Poincaré–Zeipel method. This was undoubtedly due to his close relation to Imre G. Izsák, an internationally known expert of artificial satellite research at that time.

Professor Detre provided broad, comprehensive knowledge of astronomy and astrophysics to his students, many of whom became well known researchers of their fields playing leading roles in international bodies and organizations of astronomy.

László Detre had been a professor of the Eötvös University for ten years. His effect, however, has lasted longer than ten years, since the teaching of astronomy in the Department of Astronomy has been continued for decades, until very recently, on the bases established by him.

The University keeps memory of Professor Detre. A seminar room of the Department of Astronomy in the new university campus at Lágymányos has been named after him making Detre's name known and familiar for younger generations, and not only in astronomy. A bust of him has also been erected in the hall of the Faculty of Natural Sciences, among the busts of other great professors of the University.

Figure 3: The plaque of the Detre-room of the Astronomy Department in the new university campus at Lágymányos.

Figure 4: The bust of Professor Detre in the main hall of the Faculty of Natural Sciences at Lágymányos.

László Detre and German-Hungarian Relationships

Gudrun Wolfschmidt

Institute for History of Science
Hamburg University

Introduction: Konkoly and the Foundation of the Hungarian National Observatory

In the last quarter of the 19th century the Hungarian astronomy flourished and thanks to the activity of Nikolaus [Miklós] Konkoly Thege[1] (1842–1916) the German-Hungarian relationships in the field of astronomy could be activated.

Very clear is here the orientation of the periphery (Hungary) with respect to the center of development (Germany).[2] Astrophysics – with its topics: spectroscopy, photometry and photography – was born just before in Germany. Konkoly as an important scientist and organiser belonged to the few pioneers of astrophysics in the world. Already ten years after starting his astrophysical work he had an international reputation. Konkoly built up international contact through travelling, in order to get to know other astrophysicists and their observatories. There were especially good contacts to the Potsdam observatory. He had correspondence with astronomers everywhere in the world and scientists from abroad visited his observatory.

When Konkoly became director of the Hungarian National Institute for Meteorology and Terrestrial Magnetism in Budapest in 1890, he was so busy and had no time left for astronomical observations that he tried to get his observatory in O'Gyalla under state

[1]Kenessey, K. von: Nikolaus v. Konkoly Thege, der Astronom. In: Kleine Veröffentlichungen der dem kgl. ung. Ministerium für Ackerbau unterstehenden kgl. ung. Reichsanstalt für Meteorologie und Erdmagnetismus Budapest. Neue Reihe No. 14 (1942), p. 26. – Steiner, Lajos: [Biographie von Konkoly]. Budapest. – Marik, Miklós: Konkoly Thege Miklós (1842–1916). In: Csillagászati évkönyv (1992), p. 145–147. Bartha, Lajos: Konkoly Thege Miklós emlékezete. Budapest 1992. Vargha, Magda; Patkós, László; Tóth, Imre (eds.): The Role of Miklós Konkoly Thege in the History of Astronomy in Hungary. Proceedings of the International Meeting "120th Anniversary of Konkoly Observatory" in Budapest, 5–6. Sept. 1991. Konkoly Observatory of the Hungarian Academy of Sciences, Monographs No. 1, Budapest 1992.

[2]This article is based on an earlier publication: Wolfschmidt, Gudrun: Deutsch-ungarische Beziehungen in der Astronomie und Astrophysik. In: Fischer, Holger (ed.): Deutsch-ungarische Beziehungen in Naturwissenschaft und Technik nach dem Zweiten Weltkrieg. München: Oldenbourg (Südosteuropäische Arbeiten, 103) 1999, p. 337–373. This research was supported by Prof. Tibor Herczeg, Oklahoma, and in Budapest by Prof. Béla Szeidl and Magda Vargha, librarian of the Konkoly Observatory and Prof. Béla Balázs of the Eötvös University.

control. This initiative for institutionalisation of Hungarian astronomy with the help of the Astronomische Gesellschaft was successful. Already in the following year 1899 O'Gyalla became a national institute with the name Royal Hungarian Astrophysical Observatory – Radó von Kövesligethy (1862–1934) was vice-director from 1899 to 1904.[3]

László Detre and the Study of Hungarian Astronomers Abroad

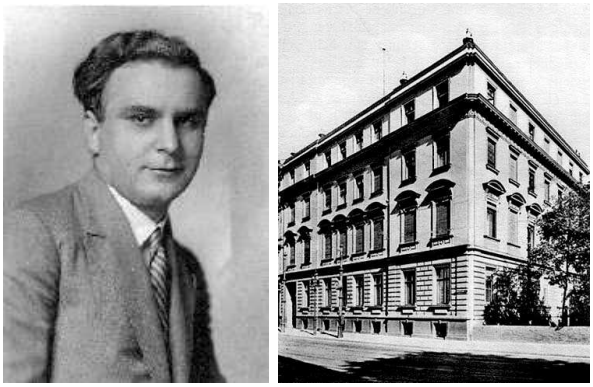

Figure 1: Left: László Detre (until 1933: László Dunst) (1906–1974). Right: Collegium Hungaricum in Berlin, founded in 1924

At the beginning of the 1920s, after WWI Hungary tried to get in closer connection to the cultural and scientific life in Europe: During the reign of the minister Kuno Graf Klebelsberg scientific and cultural institutes, the Collegia Hungarica, were opened in Vienna and Berlin in 1923/24. The Collegium in Berlin, Dorotheenstraße, under the director Professor Robert Gragger was in close cooperation with the Hungarian institute of Berlin university. The main task was the encouragement of talented young Hungarian scholars and artists. Living in Berlin, they should build up fruitful and long lasting contacts to Germany. Two decades very successful work was done until the building was destroyed in 1945.[4]

Like Konkoly in the 19th century also another director (since 1943) László Detre[5] [until 1933: László Dunst] (1906–1974) could get his scientific training in Germany, at the Collegium Hungaricum in Berlin, in 1927 to 1929 (*Fig. 1*).

After his dissertation he went to Kiel in 1929 and to Vienna in 1930.[6]

The whole staff in Budapest had got the training in Germany:

- Like Detre also his assistant Dr. Fr. Krbek studied in Berlin in 1927–29, then in Bonn in 1929–30 with Prof. Ernst Kohlschütter (1870–1942).
- The adjunct Dr. Károly Lassovszky got a grant for Babelsberg observatory in 1932 as a cooperator of Prof. Paul Guthnick (1879–1947).

[3]Study in Vienna from 1881 to 1884, 1882–87 observer in O'Gyalla, 1899–1904 vice-director of O'Gyalla Observatory, in 1904 full professor and in 1910 director of the Seismographical Observatory, who had closest contacts to the German Seismological Observatories. Cf. Oltay, Karl: Radó v. Kövesligethy. In: Gerlands Beiträge zur Geophysik 43, Leipzig 1935, Heft 4, p. 337–339.

[4]Information from the "Haus der Ungarischen Kultur", Alexanderplatz, 1973–1989, Cultural institute "Haus Ungarn" since 1990.

[5]Szeidl, Béla: László Detre. In: Mitteilungen der Astronomischen Gesellschaft 38 (1976), p. 7–9.

[6]Cf. VJS 65 (1930), p. 110.

- The assistant Károly Móra (1899–1938) could go to Leipzig observatory in 1932 – Prof. Josef Franz Hopmann (1890–1975) – and then in 1933 to Heidelberg, Hamburg-Bergedorf and Göttingen.
- Also Loránt Dezső (1914-2003), the later leader of the Hungarian Heliophysical Observatory,[7] went to a German speaking country. He visited Prof. Max Waldmeier (1912–2000) in Zürich in 1939.

The result of Detre's long stay in Germany was not only that he made a lot of friends but also his research method and scientific work was influenced very much.

> *„Die Sternwarte von Budapest, eingerichtet als nationale Institution, nach Verlusten des Ersten Weltkrieges auf dem Schwabenberg, später Szabadsághegy (= Freiheitsberg) umbenannt, hatte einen langsamen Start. Das wohl einzige, nennenswerte wissenschaftliche Programm lief in den 1930er Jahren. Dr. L. Detre und seine Mitarbeiter begannen mit einer systematischen Studie der Perioden- und Lichtkurvenänderungen von RR Lyrae Veränderlichen. Die konsequente Überwachung einiger "Schlüsselobjekte" fand bald internationale Anerkennung. Julia Balázs' und L. Detres erste Publikation einer längeren Serie behandelte das Verhalten des kurzperiodischen Delta Cephei-Sterns RW Draconis [vgl. AJB 40 (1938), Nr. 8496, p. 270], die zweite das Verhalten des Veränderlichen AR Herculis (aufgrund von nicht weniger als 3363 photographischen Beobachtungen in fünf Jahren) [vgl. AJB 41 (1939), Nr. 8482, p. 213]. Das Beobachtungsprogramm lief zunächst auf zwei kleineren Astrographen, nach dem Krieg wurde auch der 60cm-Spiegel verwendet, um RR Lyrae Variablen in mehreren Kugelsternhaufen zu untersuchen.*
> *Dr. Detre promovierte 1929 in Berlin und seine persönlichen Beziehungen zu deutschen Astronomen waren ausgedehnt. Obwohl es nicht bekannt ist, ob das RR Lyrae-Programm aus Diskussion mit deutschen Astronomen geboren oder gar von ihnen vorgeschlagen wurde* (ich persönlich halte dies nicht für wahrscheinlich), *durch Dr. Detres Person und seine ausgezeichneten Verbindungen hat die Forschung in Deutschland um 1925–30 bei der Geburt der Veränderlichenforschung (im weiteren Sinne der Astrophysik) in Ungarn sozusagen Pate gestanden."*[8]

German-Hungarian Cooperation from 1870 to 1945

If you look at the graphic of cooperation (*Fig. 2*), you will see a large activity in the 1880s – in the time of Konkoly. Besides contacts inside of Hungary there were cooperations with Bothkamp near Kiel, Potsdam, Göttingen, and Leipzig. Abroad one should mention Vienna, Prague, Zürich, and Italy. In the eastern foreign countries there was only one cooperation with Russia on the occasion of a lunar eclipse.

[7] The Heliophysical Observatory was in Budapest in the 1950s, then in Debrecen from 1958 on.

[8] Herczeg, Tibor: Deutsch-ungarische Beziehungen, Teil I: Vorgeschichte. Fax vom 26.8.1997. I am indebted to Professor Herczeg for giving me his report, and for proofreading my manuscript when we met in Gotha on 12 May 1998.

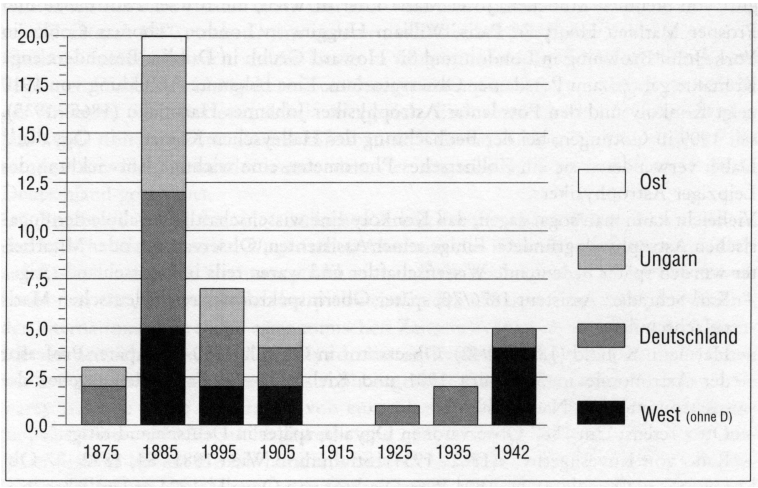

Figure 2: German-Hungarian cooperation from 1870 to 1945

- German-Hungarian Cooperation from 1870 to 1919

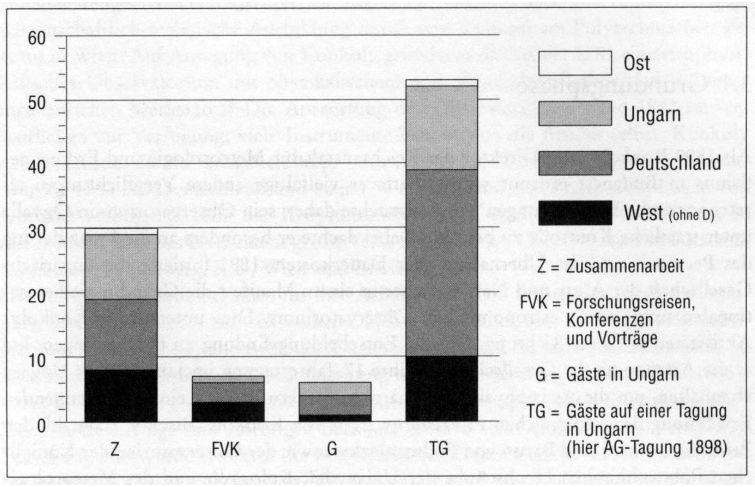

Figure 3: German-Hungarian cooperation from 1870 to 1899. Z: Cooperation, FKV: Scientific Travelling, Conferences and Lectures, G: Guests in Hungary, TG: Guests during a meeting in Hungary (here AG meeting 1898)

By analyzing the German-Hungarian contacts (cooperation, scientific travelling of Hungarians, guests from abroad in Hungary) from 1870 to 1899 (*Fig. 3*), one recognizes that Germany is in front compared to other western countries and there is only one example for a contact to eastern countries. During the meeting of the Astronomische Gesellschaft in 1898 in Budapest (cf. column TG) there were 53 astronomers: 29 Germans, 6 Austrians, 13 Hungarians and 5 more from Sweden, Russia, Denmark, and Italy. The executive council consisted of 4 Germans, one Austrian, one Swede, one Russian, and one Dutch in 1898.

It is obvious that the contacts decrease after the turn of the century (*Fig. 4*). But one has to consider that the annual reports given by Kövesligethy since 1900 are less detailed. And in addition there were no meetings in that time.

As honorary members of the Hungarian Academy of Sciences three Germans were

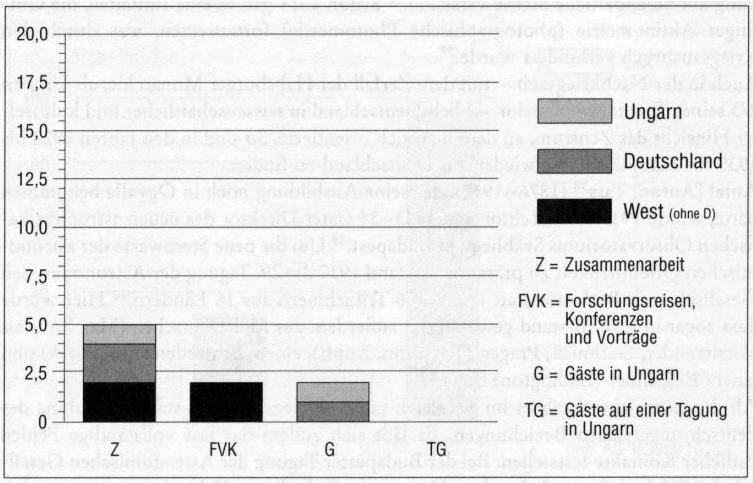

Figure 4: German-Hungarian cooperation from 1900 to 1919. The legend is explained in the caption to Figure 3.

elected until 1914: Arthur von Auwers (1838–1915), Berlin Academy of Sciences, in 1890, the director of Munich and Heidelberg observatories, Hugo von Seeliger (1849–1924), in 1899 and Max Wolf (1863–1932) in 1908 – in respect to their predicate to be president of the Astronomische Gesellschaft. These 3 astronomers from abroad in the Academy should be compared to 36 scholars from science (4 physicists, 6 chemists, and 7 mathematicians) and 60 scholars from the humanities.

- Development in the 1920s and 1930s

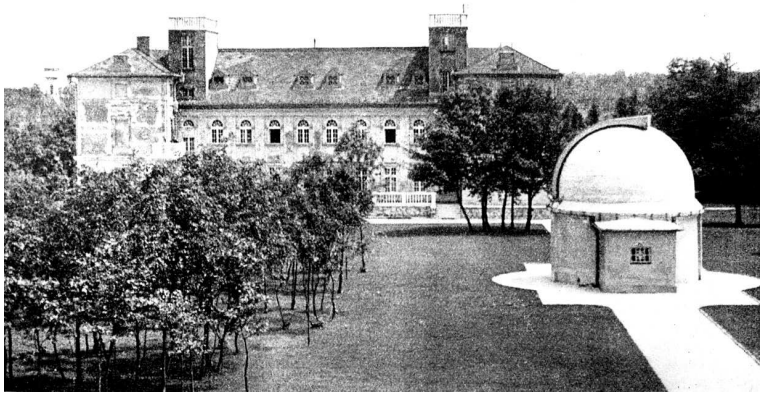

Figure 5: The Konkoly Observatory in Budapest, 1926

After WWI O'Gyalla was part of Czechoslovakia and was renamed to Stará Dala (today: Hurbanovo, Slovakia). Just in time – in 1921 – the instruments and the library of the observatory O'Gyalla could be transported to Budapest-Svábhegy. The building of the new National Observatory was finished in 1926 (*Fig. 5*).

The observatory in Budapest was named after its founder Konkoly.[9] The emphasis of the work was astrophysics, but in contrary to Konkoly's preference for spectroscopy since

[9]Kelényi, B. Ottó: A magyar csillagászat története. Über die Geschichte der ungarischen Astronomie. In: Astronomische Abhandlungen des Kgl.-Ung. Astrophysikalischen Observatoriums von Konkoly's

the turn of the century and especially in the 1920s, the main topic became photometry and variable stars.[10] Already in 1914 there was an initiative to continue the "Göttingen Aktinometrie" (photographic photometry), a project which was stopped by the outbreak of WWI.[11]

In the postwar period – with the collapse of the Habsburg monarchy, when Hungary lost two thirds of its territory – Germany continued to be in scientific and cultural respect the orientation point. Thus in the years 1920 to 1939 the main contacts are to be found with Germany (*Fig. 6*).

Anton [Antal] Tass[12] (1876–1937), who got his scientific training in O'Gyalla, became vice-director in 1913 and first director from 1923 to 1934.[13] In order to present the new observatory to the astronomical public in 1930 the 29th meeting of the Astronomische Gesellschaft took place in Budapest with 106 participants from 16 countries.[14] During this meeting Tass was elected as member of the executive council which consisted of 5 Germans (Max Wolf as president, Guthnick, Prager, Hopmann, Kopff), one Swede (Lundmark) and one English (Eddington).

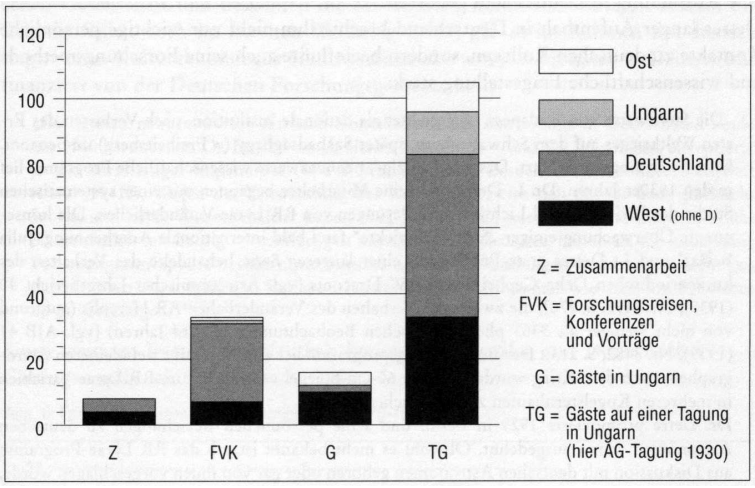

Figure 6: German-Hungarian cooperation from 1920 to 1945. The legend is explained in the caption to Figure 3.

Since the 1920s there was a prominent increase in the German-Hungarian relationships in comparison with the pre-war period. In addition one can recognize that contacts to eastern countries are practically totally missing. During the Budapest meeting (1930) (cf.

Stiftung in Budapest-Svábhegy Bd. 1 (1930), Nr. 2, p. 51–106 (in German). – Beckman, G.W.E.: Astronomie in Ungarn. In: Sterne und Weltraum 24 (1985), p. 439–443. – Herrmann, Dieter B.: Sternforscher und Sternfreunde in der VR Ungarn. In: Vorträge und Schriften der Archenhold-Sternwarte Berlin-Treptow Nr. 47 (1975), p. 1–16.

[10]In order to do photometry visual photometers were acquired in 1901–1903: a wedge photometer, a Zöllner photometer, a large astro photometer, all made by Toepfer in Potsdam, as well as a spectral photometer, made by Schmidt & Hänsch, Berlin, cf. VJS 36 (1901), p. 131, VJS 37 (1902), p. 143, VJS 38 (1903), p. 139.

[11]Cf. VJS 49 (1914), p. 186. An 8″, made by Heyde, Dresden, was used in combination with a Schwarzschild "Schraffierkassette" (like for the Göttingen Actinometry).

[12]Móra, K.: Anton Tass. In: VJS 73 (1938), p. 198–202.

[13]Tass was an assistant from 1899 and in 1902–13 observer in O'Gyalla, in 1913 vice-director of the O'Gyalla observatory.

[14]Bericht über die Versammlung der Astronomischen Gesellschaft zu Budapest 1930, August 8–12. In: VJS 65 (1930), p. 222–254, here p. 245.

column TG) there were 50 German participants, 13 Hungarians, 6 Austrians, and 27 other participants from western countries, here even from outside Europe: USA, Japan, and South Africa. Only 9 participants came from eastern countries: Soviet Union, Czechoslovakia, Poland, and Yugoslavia.

Even during WW II some cooperations with abroad existed: on one hand with Sweden where the "neutral bureau" was erected in Lund in order to keep up the exchange of important urgent astronomical information, but also on the other hand with Switzerland and the USA (Mt. Wilson Observatory) especially in the field of solar physics.

- ***Visits of meetings and research travels until 1945***

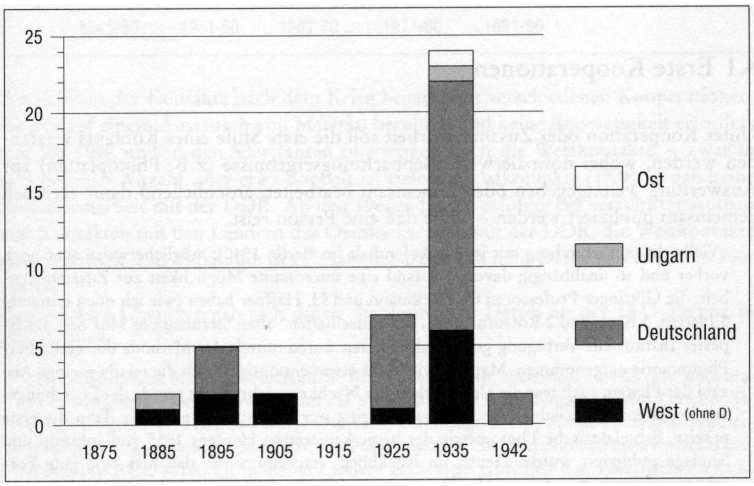

Figure 7: Research travels from 1870 to 1945

If one looks at the development of research travels, study visits and visits of meetings, one recognizes especially in the 1930s, in the period of Detre, a remarkable activity, especially visits in Germany, in the observatories Berlin-Babelsberg, Potsdam, Heidelberg, Göttingen, Hamburg, Bonn, Leipzig, and Munich and to the AG meeting in Danzig in 1939 (*Fig. 7*).

Travels to the western countries concern the meeting of the International Astronomical Union (IAU) in Stockholm, in addition visits in Vienna, Zürich, and Denmark. In the eastern countries only Kraków was visited in 1938.

László Detre and Júlia Balázs travelled in 1939 to Danzig to the meeting of the Astronomische Gesellschaft and visited the observatories Berlin-Babelsberg, Potsdam, and Leipzig.

Even during WWI (1940) there existed study visits of 5 month in Germany in the context of the German-Hungarian cultural agreement, financed by the Deutsche Forschungsgemeinschaft (DFG – German Research Organisation):

> *„Die letzten nennenswerten direkten Kontakte mit der Astronomie in Deutschland fanden um 1940 herum statt. Dr. Detre – noch nicht als Direktor – und Dr. Julia Balázs akzeptierten je ein kurzfristiges Stipendium (4–6–8 Monate?) zum Besuch der Münchner Sternwarte (1940 oder 1941?). Wegen der Entwicklung der Kriegslage erwies sich das als kein glücklicher Schritt und beide Wissenschaftler haben sich, Jahre später, wiederholt und mühsam – aber offensichtlich mit Erfolg – rechtfertigen müssen. (Wie behauptet, hatten sie die*

noch ruhige Forschungsatmosphäre des dortigen Instituts der von Befeindungen und Intrigen nicht ganz unbewährten Atmosphäre in Budapest (sowohl an der Universität wie auch am Schwabenberg) vorgezogen."[15]

A further research stay was given to Lassovszky and Detre in Göttingen in 1941.

Period of Isolation from 1945 to 1956/59

„Durch Detres Person haben ausgezeichnete Studien und konsequente Forschung viel von der besten deutschen Forschungstradition und Methoden auf dem "Schwabenberg" Wurzeln schlagen können."[16]

But the research stays, research travels, common meetings, and intense contacts to Germany and to abroad stopped completely after 1945.

- Scientific cooperation since 1945

Cooperation or team work should be understood as a first step of contacts; this could be the exchange of observing results – like photographic plates for reduction – or for discussion about the interpretation; finally the results can be published together – in this case there is no need that any person travels.

„Vielleicht in Verbindung mit jenem Aufenthalt [in Berlin 1940], möglicherweise aber noch vorher und so unabhängig davon, entstand eine interessante Möglichkeit zur Zusammenarbeit: die Göttinger Professoren O. Heckmann und H. Haffner haben (wie ich mich erinnere) 5 Platten, 3 Blau- und 2 Rotaufnahmen, des "rätselhaften" alten Sternhaufens M 67 dem Budapester Institut zur Verfügung gestellt; die Platten waren mittels der Methode der Halbfilter-Photometrie aufgenommen. Man war vielleicht etwas entmutigt durch die relativ geringe Anzahl der Platten, auch war die Unsicherheit der Nachkriegsjahre nicht gerade der Forschungsarbeit bestens förderlich – die Ausmessung ging nur schleppend voran, bis dann die erste präzise, lichtelektrische Photometrie des bemerkenswerten Haufens 1955 von Johnson und Sandage publiziert wurde. Heute, im Rückblick, erscheint wohl, daß hier eine gute Forschungsgelegenheit vertan wurde."[17]

The building up of contacts after the war started with different cooperations, which were only based on exchange of material; no travels were necessary. In the 1950s the contacts to the west dominated; it was only a small number but at least twice as much as the contacts to the east; there were no contacts to the GDR. Since the 1960s there existed a stronger contact to the countries of the Eastern European Bloc and also with the GDR; contacts with the west decreased. A maximum of cooperation with the east was reached in the 1970s (*Fig. 8*).

A further chance came up through Detre's participation, since 1943 director of the Konkoly Observatory, in the IAU meeting in Zürich in 1948:

[15]Herczeg, Tibor: Deutsch-ungarische Beziehungen, Teil I: Vorgeschichte. Fax vom 26.8.1997. Cf. VJS 76 (1941), p. 85.

[16]Herczeg, Tibor: Deutsch-ungarische Beziehungen, Teil I: Vorgeschichte. Fax vom 14.9.1997.

[17]Herczeg, Tibor: Deutsch-ungarische Beziehungen, Teil I: Vorgeschichte. Fax vom 28.8.1997. – Johnson, H. L., Sandage, A. R.: ApJ 121 (1955), p. 616. Cf. VJS 70 (1935), p. 144 (Photographs of M 67, made with Göttingen's astrograph by Móra with agreement of Heckmann and Kienle).

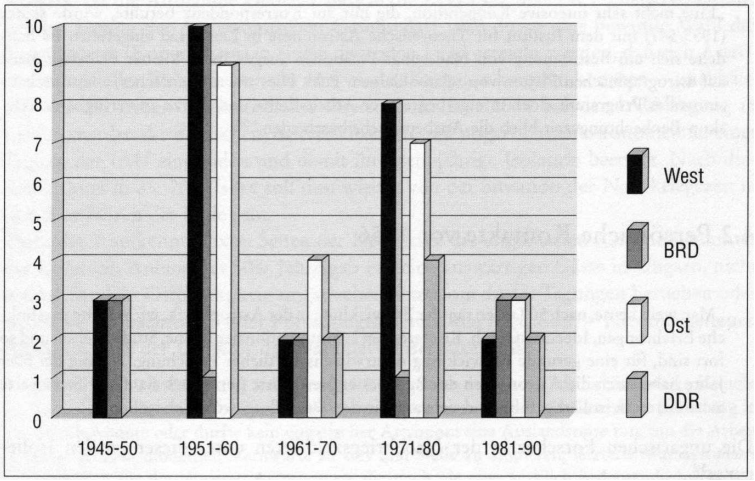

Figure 8: Cooperation from 1945 to 1990

„Diese Teilnahme brachte, als erfreuliche Konsequenz, wenn auch nicht eine direkte Kooperation, wenigstens eine Verbindung mit der amerikanischen Astronomie: Auf der Züricher Tagung übergab Prof. Harlow Shapley [Harvard, Cambridge/Mass.] für die astronomische Forschung in Ungarn (und – glaube ich – in Polen und der CSR) je eine Elektronenvervielfacherröhre Typ RCA 931A, die in diesen Ländern noch nicht erhältlich war. Die ersten Versuche am 60cm-Spiegel (die allerdings nur hellere Sterne bis zur 5. oder 6. Größenklasse erreichen konnten), verliefen 1949/50 mit der Unterstützung des Physikdozenten Péter Faragó; die erste kurze, aber erfolgreiche Messreihe bezog sich auf die August 1950-Bedeckung von Zeta Aurigae."[18]

In the beginning of the 1950s there existed a first cooperation with an Eastern partner:

„Eine nicht sehr intensive Kooperation, die nur auf Korrespondenz beruhte, wurde später (1953/54?) mit dem Institut für Theoretische Astronomie in Leningrad eingeführt. Es handelte sich um Bestimmung von Näherungs-Positionen ausgewählter kleiner Planeten, meist auf astrographischen Platten von relativ kleinem Feld. Dies war ein einfaches, aber durchaus sinnvolles Programm, doch infolge begrenzter Arbeitskräfte und Kürze an verfügbarer Teleskop-Beobachtungszeit blieb die Ausbeute sehr bescheiden."[19]

- *Personal Contacts before 1956*

„Man weiß heute, nach 50 Jahren rapider Entwicklung in der Astrophysik, wie wichtig persönliche Erfahrungen, Ideenaustausch, Konferenzen auf internationaler Ebene, Studienreisen und so fort sind, für eine gesunde Entwicklung naturwissenschaftlicher Forschung. Anfang der 50er Jahre haben sich die Astronomen der Budapester Sternwarte (jetzt auch Konkoly Sternwarte genannt) stark isoliert gefühlt und sie waren, in der Tat, außergewöhnlich isoliert."[20]

[18]Herczeg, Tibor: Deutsch-ungarische Beziehungen, Teil I: Vorgeschichte. Fax vom 31.8.1997. Cf. Mitteilungen der Konkoly Sternwarte Nr. 29. (1952).

[19]Herczeg, Tibor: Deutsch-ungarische Beziehungen, Teil I: Vorgeschichte. Fax vom 31.8.1997.

[20]Herczeg, Tibor: Deutsch-ungarische Beziehungen, Teil II: Isolation und erste Kontakte. Fax vom 2.9.1997.

The Hungarian scientists in the post-war time suffered from the large isolation:[21]

> *„In der ... [Nachkriegs-]Zeit sind wissenschaftliche Kontakte mit dem Ausland, insbesondere mit Deutschland, für fast zehn Jahre, praktisch auf Null gesunken. Man muß allerdings zwei wichtige Umstände beachten.*
> *1. Die Förderung der Bibliothek wurde aufrecht erhalten und die internationale Literatur stand uns immer prompt und ziemlich vollständig zur Verfügung.*
> *2. Ungarn wurde in der IAU [International Astronomical Union] zugelassen und Dr. Detre (der seit 1943 das Direktorat der Sternwarte innehatte) hatte an der Züricher IAU-Generalversammlung (1948) teilnehmen können."*[22]

The affiliation of Hungary in the International Astronomical Union (IAU) already in 1948 was very different from the development after WW I, when besides Germany among others Hungary was also excluded from international societies during the 1920s.[23] Not only personal contacts of the scientists with foreign colleagues were made difficult, but also the official contacts during meetings. Because the affiliation of Germany was not successful in 1922 and 1925, one succeeded by choosing a meeting place (Copenhagen) in a neutral country for the meeting of the Astronomische Gesellschaft (AG) in 1926, that astronomers from all over the world met again and made contacts – independent of the new international society. Not before 1928 during the IAU meeting in Leiden the 10 year long isolation of the German, Austrian, and Hungarian astronomers was finished because they were accepted as participants. After this additional information about the situation in the 1920s, we look again what happened in the 1950s.

Inspite of acceptance by the IAU the Hungarian astronomers suffered due to the isolation. In the beginning of the 1950s there were no external guests in Hungary, not even from the Eastern Bloc; no Hungarian astronomer was allowed to travel to a meeting or to travel for an observation or research stay abroad – with one rare exception only the director:

> *„Von 1945 bis 1955 [hatte] kein einziger Kollege aus dem Ausland die Sternwarte besucht und – abgesehen von Dr. Detres glücklicher Teilnahme an der IAU Generalversammlung in Zürich, konnte oder durfte kein ungarischer Astronom eine Auslandsreise tun, um die Arbeit einer großen, modernen Sternwarte an Ort und Stelle zu studieren; letzteres war besonders hinderlich für die jüngeren Astronomen, die noch nie eine wirklich bedeutende Institution gesehen hatten. Ich nehme an, ein ähnliches Problem bestand auch für die Astronomen der DDR – aber dort waren doch immerhin mehrere Universitäten und mehrere aktive Observatorien vorhanden (insbesondere [Berlin-]Babelsberg, [APO Potsdam], Sonneberg, auch Jena, später Tautenburg), die ein Maß von innerem Verkehr und Austausch hätten ermöglichen können.*
> *Kontakte mit der Astronomie in der DDR aufzunehmen erschien aussichtslos. Selbst Versuche, Kollegen in den Nachbarländern zu treffen, führte zu keinem Ergebnis. Detre versuchte, zum Beispiel, den rumänischen Astronomen Dr.*

[21] Contacts existed only in 1950 with the Astronomisches Recheninstitut in Berlin, further in 1952 with the Nautical Almanac in Washington, D.C., USA, and with Belgium, in 1953 with Leiden, Greenwich, and Mt. Wilson, USA (sunspots) as well as with Heidelberg in 1955.

[22] Herczeg, Tibor: Deutsch-ungarische Beziehungen, Teil I: Vorgeschichte. Fax vom 28.8.1997.

[23] Schröder-Gudehus, Brigitte: Deutsche Wissenschaft und internationale Zusammenarbeit 1914–1928. Ein Beitrag zum Studium kultureller Beziehungen in politischen Krisenzeiten. Genf 1966.

Armeanca (Cluj?) einzuladen – wie wir später erfuhren, hatte ihn die Einladung nie erreicht.
Wir fanden auf jeden Fall die Situation, täglich und jahraus-jahrein, zum selben kleinen Kreis von 4 bis 5 Kollegen zurückzukehren, sehr frustrierend und sogar hinderlich, was die Qualität der Forschung betrifft. Gewiß, wir lasen mit großem Interesse die Forschungsberichte und versuchten uns daran zu orientieren, aber ein Durchbruch in der herkömmlichen Arbeit war nicht zu erwarten.“[24]

The first meeting, which could be visited by many Hungarian astronomers, took place in Pulkovo Observatory near Leningrad, May 1954:

„Eine wesentliche Verbesserung der trostlos anmutenden Situation erfolgte jedoch im Jahr 1954, vielleicht Auswirkung der spürbaren (aber noch keineswegs einschneidenden) Änderungen im politischen System von Ost- und Mitteleuropa (“Tauwetter”). Im Mai 1954 erfolgte die Wiedereröffnung der im Krieg arg zerstörten, inzwischen neu aufgebauten Pulkowaer Sternwarte bei Leningrad. Aus diesem Anlaß hatte die Sowjetische Akademie der Wissenschaften eine viertägige Konferenz organisiert (20.–23.5.1954), mit unzähligen einheimischen Teilnehmern, aber auch mit großzügigen Einladungen aus dem Ausland. Eingeladen waren einige sehr bekannte, als “führend” geltende Astronomen aus dem Westen: die Professoren Oort [Holland], Danjon [Frankreich], Cowling [England], B. Lindblad [Schweden], Minnaert [Holland] unter anderen, Dr. Oosterhoff (Sekretär der IAU), Dirk Brower und D. Nassau aus den Vereinigten Staaten, weiterhin kleinere, 2- bis 9-köpfige Delegationen aus den sog. Volksdemokratien und 8 Astronomen aus China. Westdeutschland war leider nicht vertreten, die DDR mit drei Astronomen (J. Dick, C. Hoffmeister, O. Singer). Die Konferenz 1954 in Pulkowa war doch sehr wichtig sowohl für Ungarn als auch für die DDR.
Nach der Eröffnung gab es eine Möglichkeit, Leningrad und Moskau zu besichtigen und interessierte Teilnehmer hatten auch eine Einladung bekommen, die totale Sonnenfinsternis am 30. Juni 1954 vom Nordkaukasus aus, unweit von Pyatigorsk, mit ihren eigenen, mitgebrachten Instrumenten zu beobachten. So ergab sich für viele Gäste die Gelegenheit, fast zwei Monate in der Sowjetunion zu verbringen. Obwohl die erstaunlich zahlreiche ungarische Delegation (6 Astronomen, ein Mathematiker, ein Höhenstrahlungsphysiker und ein Beamter der Akademie) eigentlich kein eigenes Instrument vorweisen konnte, sind sie ebenfalls mitgefahren, dabei waren sie häufig zusammen mit der DDR, auch mit der tschechischen Delegation. Wichtige persönliche Kontakte wurden dabei angeknüpft, die zwei Jahre später eine nicht geringe Rolle spielten.
Dies war der Anfang der sich langsam normalisierenden internationalen Beziehungen.“[25]

After the Leningrad meeting they had the possibility to travel to the total solar eclipse, June 30, 1954, in North Kaukasus.

[24]Herczeg, Tibor: Deutsch-ungarische Beziehungen, Teil II: Isolation und erste Kontakte. Fax vom 2.9.1997.

[25]Herczeg, Tibor: Deutsch-ungarische Beziehungen, Teil II: Isolation und erste Kontakte. Fax vom 4.9.1997.

Two members of Konkoly Observatory, who were not present in Pulkovo, Júlia Balázs und I. Izsák, were allowed to visit in 1954 a Variable Star Conference in Moscow which lasted one week.

A real highlight was the travel of the director Detre to the meeting of the IAU in Dublin in 1955 and then a first travel to West Germany:

> *„. . . 1955 . . . wurde ein überaus wichtiger Kontakt mit der Forschung in Deutschland endlich wiederhergestellt: Detre und Julia Balázs haben an der Tagung der AG [Astronomischen Gesellschaft] in Hannover teilnehmen können.“*[26]

Since 1956 the important tradition of the Variable Star Colloquia of the IAU has been started. During the first colloquium there were not yet western participants, but four from eastern Germany (Ahnert, Güssow, Hoffmeister, and Schneller); the total number was 29 participants.[27] These IAU Colloquia took place later in Budapest (1968, 1975) and in Bamberg (1959, 1965, 1977, and 1983).[28]

- The events of the year 1956 – the Hungarian Revolution

Starting with a student demonstration in October 23, 1956, a revolution all over Hungary against the regime developed quickly. With the second Soviet intervention in November 4, 1956 a mass escape began over the border to Austria. As a whole, more than 189,000 people left the country; half of them went overseas (mainly USA and Canada), the other half stayed in Europe, 20,000 in UK and 14,000 in Germany.

> *„Eine wichtige und zunächst ganz unerwartete Nebenwirkung der Konferenz [in Budapest 1956] war, daß die angeknüpften persönlichen Beziehungen sich in den Plänen der bald flüchtig gewordenen Sternwartenmitglieder deutlich bemerkbar machten. Dieser Exodus hat die Sternwarte und die ungarische Astronomie tief beeinflußt, später praktisch gespalten. Ihre Geschichte ist hier kurz skizziert wie folgt:*
> *Zunächst schien in der Sternwarte eine neue Epoche begonnen zu haben: man plante verschiedene Kooperationen, besonders mit den DDR-Sternwarten aber auch mit Italien (Asiago). Diese Pläne wurden aber durch die rasch anrollenden Ereignisse des Oktoberaufstandes in den Schatten gestellt. Die Sternwarte hatte einen recht bescheidenen, aber aktiven Anteil an den Ereignissen und nach der fatalen Rückkehr der sowjetischen Truppen am 4. November 1956 tauchte sehr bald die Idee einer Flucht aus dem Lande auf. Furcht vor Retorsionen aber auch die damals anscheinend hoffnungslose Lage für zukünftige Forschung machten dies hauptsächlich zu einem Problem der jüngeren Leute.“*[29]

---

[26]Herczeg, Tibor: Deutsch-ungarische Beziehungen, Teil II: Isolation und erste Kontakte. Fax vom 4.9.1997. The subsequent meeting of the Astronomische Gesellschaft took place in Bamberg in 1957.

[27]Participants of the 1956 conference: (IAU): 9 Hungary, 4 GDR, 5 GFR, 1 UK, 2 Netherlands, 1 Italy, 1 Belgium, 3 Poland, 1 Czechoslovakia, 2 China, and 5 USSR. The lectures were published in the Mitteilungen series of the Konkoly Observatory: Nr. 42, Budapest 1957.

[28]The meeting in Bamberg in 1977 was my personal first meeting and I got to know among others Prof. Herczeg and the participants from Hungary.

[29]Herczeg, Tibor: Deutsch-ungarische Beziehungen, Teil III: Fluchtgeschichte. Fax vom 19.8.1997.

Figure 9: Left: Imre Izsák (1929–1965) – Right: Tibor Herczeg (* 1929)

Imre Izsák (1929–1965), a specialist for celestial mechanics (*Fig. 9*), was the first who left the country:[30]

> *„Der erste, der die chaotischen Zustände zu nützen wußte, war Imre Izsák. Sein Abgang war, sicherlich mit Dr. Detre's Hilfe, sehr "privat" organisiert. Er ging vermutlich sehr früh, vielleicht schon Anfang November (?): Wien, umgehend direkt nach Zürich, wo ihn Prof. M. Waldmeier offenbar sehr gerne empfangen hatte und ihm eine Forschungsstelle, hauptsächlich im Sonnenobservatorium Locarno-Monti geschaffen hat. Izsák beschäftigte sich mit den Bewegungen in Protuberanzen und publizierte darüber erfolgreich (in der "Zeitschrift für Astrophysik"). Sein eigentliches Interesse lag aber schon immer auf dem Gebiet der Himmelsmechanik, so hat er seine Stelle bei Prof. Waldmeier nach etwa zwei Jahren aufgegeben und ist in die Vereinigten Staaten übergesiedelt, zuerst nach Cincinnati, später nach der Harvard Sternwarte (oder Smithsonian Institution?). Er hat sehr bemerkenswerte Arbeit über die Bewegungen von Erdsatelliten geleistet."*[31]

Later four more members of the observatory fled, so that only half of the staff was left by the end of 1956.

> *„Der Weggang, besser gesagt die Flucht von weiteren drei oder vier jüngeren Mitgliedern der Sternwarte spielte sich unter wesentlich weniger Geheimhaltung ab, drei oder vier Wochen später. Auf jeden Fall wußte [der Direktor] Dr. Detre Bescheid und riet uns, zuerst nach Wien, in die Sternwarte zu gehen. Aus dieser Position wäre es möglich, wie es in der Tat möglich wurde, die neugewonnenen persönlichen Beziehungen zu deutschen Astronomen bestens zu nutzen. Zu dieser Gruppe gehörten die wissenschaftlichen Mitarbeiter T. Herczeg und I. Ozsváth, der "Aspirant" Karl Balogh und der Mechaniker István Vidéki. Die "Drehscheibe" des Unterfangens bildeten Balogh's Eltern, die nur 3 bis 4 km von der österreichischen Grenze, in dem früheren Grenzsperrgebiet wohnten. Durch diese Möglichkeit wurde die Flucht Anfang Dezember erfolgreich durchgeführt, so daß Herczeg, Ozsváth und Vidéki über die österreichische Grenze schlüpfen konnten und in 1 bis 2 Tagen Wien und*

[30] Fred Whipple has written an obituary. Cf. also Marik, Miklós: Csillagászattörténeti életrajzi lexikon A-Z. Budapest 1982. A gondolat tükre. Izsák Imre élete (1929–1965). Zalaegerszeg 1997.

[31] Herczeg, Tibor: Deutsch-ungarische Beziehungen, Teil III: Fluchtgeschichte. Fax vom 19.8.1997.

die Wiener Universitäts-Sternwarte erreicht haben. Die drei Ungarn aus der Sternwarte in Budapest wurden in der Wiener Sternwarte sehr freundlich, ja herzlich aufgenommen. (Balogh kehrte nach Budapest zurück, um seine Familie und Frau Ozsváth nachzuholen, fand aber dort eine wesentlich veränderte, schwierigere Situation vor und machte den "Sprung" nach Wien erst viel später – aber noch 1957 – möglich.)"[32]

Neither Herczeg, nor Ozsváth wanted to stay in Vienna, but tried to reach West Germany:[33]

„Herczeg und Ozsváth erhielten ziemlich gute Stipendien von der Rockefeller Stiftung und fingen an, mit westdeutschen Kollegen in Verbindung zu treten, da sie nicht unbedingt in Wien zu bleiben gedachten. Ozsváth kontaktierte zunächst Dr. Julius Dick (Potsdam? Babelsberg?), mit dem er auf der Konferenz in Budapest eine gute Beziehung angeknüpft hatte. Dr. Dick nahm Verbindung mit einer Anzahl westdeutscher Sternwartdirektoren auf, unter Verwendung von Dr. Kahrstedts [Direktor des Astronomischen Recheninstituts] Postadresse in West-Berlin. (Dies geschah Jahre bevor der Berliner Wall gebaut wurde.) Aus dieser Hilfsaktion resultierten zwei wertvolle Forschungsgelegenheiten für die Flüchtlinge, an zwei wichtigen astronomischen Instituten der Bundesrepublik.
Zuerst wurde Ozsváth eine Arbeitsmöglichkeit an der Hamburger Sternwarte in Bergedorf angeboten durch den Direktor Prof. O. Heckmann – schon im Februar 1957. Aus der ursprünglich bescheidenen Rechenarbeit am AG-Katalog wurde bald photographische Photometrie am großen Schmidt-Spiegel. Ozsváth promovierte 1959 an der Universität Hamburg mit einer photometrischen Studie des alten offenen Sternhaufens NGC 7789. Danach arbeitete er mit dem Theoretiker Dr. E. Schücking zusammen. Ihr wesentlicher Beitrag zur Kosmologie ("Finite rotating universe") wurde noch in Hamburg publiziert.
Herczeg wurde im April 1957 unter etwas ähnlichen Umständen ein Arbeitsplatz an der Bonner Universitäts-Sternwarte zuteil, durch dessen damaligen Direktor Prof. Friedrich Becker. Herczeg sollte auf der Außenstation in der Eifel, auf dem Observatorium Hoher List, seine in Budapest begonnene lichtelektrische Arbeit fortsetzen. Er promovierte 1959 an der Universität Bonn mit einer 3-Farben-Photometrie des Algol-(β Per) Systems. Er arbeitete an mehreren Bedeckungssystemen mit Dr. Hans Schmidt zusammen. Später (1962) siedelte er an die Hamburger Sternwarte über, als Observator, dann als Hauptobservator, und er habilitierte sich 1966 mit einem Thema in Planeten-Kosmogonie. Als Beobachter war er spektroskopisch tätig, mit Hilfe des 1 m-Spiegels."[34]

But there existed no possibility for both, to find a permanent position in Germany; finally they found a job in the USA:

„Bald danach (1962) gingen die beiden Forscher in die Vereinigten Staaten, Ozsváth zunächst nach Austin/Texas, dann nach Dallas, wo er bis heute als

[32]Herczeg, Tibor: Deutsch-ungarische Beziehungen, Teil III: Fluchtgeschichte. Fax vom 19.8.1997.
[33]There existed generous support by the Lions Club and by the Rockefeller Foundation, about 1000.-DM per month, later 250.-DM by the Ford Foundation.
[34]Herczeg, Tibor: Deutsch-ungarische Beziehungen, Teil III: Fluchtgeschichte. Fax vom 19.8.1997.

Professor der Mathematik an der University of Dallas (UTD) arbeitet.
Vidéki verließ auch bald Wien und wanderte nach Kanada aus. Wo Balogh verblieb ist unbekannt.
Herczeg akzeptierte 1970, endgültig 1971, eine Stelle als Professor of Physics and Astronomy an der University of Oklahoma in Norman/Oklahoma/USA. Es bestand für längere Zeit eine lebhafte, auch persönliche Verbindung zwischen dem kleinen Observatorium in Norman und der Bamberger Remeis-Sternwarte [Astronomisches Institut der Universität Erlangen-Nürnberg], gegründet auf verwandte Forschungsprojekte auf dem Gebiet der Veränderlichen Sterne, auch auf das Vorhandensein ausgedehnter Plattenarchive an beiden Instituten. Mehrere Mitglieder der Bamberger Sternwarte besuchten Norman, während Herczeg, aus Norman beurlaubt, vier Semester (1985–1987) in Bamberg bzw. an der Universität Erlangen verbracht hatte, als Vertreter für Prof. Jürgen Rahe (während seiner Beurlaubung zu NASA in Washington, D.C.).“[35]

How is the escape mentioned in Detre's annual report of the Konkoly Observatory?

„In den letzten Jahren wurde allmählich eine Gruppe junger Astronomen zusammengestellt, die große Hoffnungen erweckt hat, was die Zukunft der ungarischen Astronomie betrifft. Die Vorkommnisse des Oktober/November 1956 veranlaßten die meisten jungen Mitarbeiter, das Land zu verlassen. Sie haben Arbeit in verschiedenen internationalen Institutionen übernommen. Die stellarstatistische Gruppe hat folgende Leute verloren: die wissenschaftlichen Mitarbeiter Izsák Imre, Herczeg Tibor und Ozsváth István, den “Aspiranten” Balogh Károly, die Aushilfskraft Miklós János und auch den Mechaniker Vidéki István.“[36]

„Die zu Hause gebliebenen älteren Mitarbeiter haben den größten Teil ihrer Zeit dazu aufgewendet, die neuernannten Mitarbeiter einzuweisen. Weil uns die meisten jungen Forscher verlassen haben, war es nicht möglich, den internationalen Vereinbarungen nachzukommen, z. B. mit Izsák Imre waren die himmelsmechanischen Untersuchungen beendet, das Thema Doppelsterne von Herczeg wurde eingestellt. Zum Ausgleich konzentriert sich die Arbeit im Rahmen der IAU auf RR Lyrae.“[37]

- *The Development after 1956*

In *Fig. 10* the three years from 1957 to 1959 are analyzed. The contacts to the Eastern bloc countries and to the GDR increased considerably, the contacts to the West and to the German Federal Republic were only possible in a restricted way.

[35]Herczeg, Tibor: Deutsch-ungarische Beziehungen, Teil III: Fluchtgeschichte. Fax vom 19.8.1997. Also me – as a student of the Remeis Observatory in Bamberg – visited Professor Herczeg in Oklahoma in December 1978 and made reduction of variable stars on photographic plates.

[36]Detre, L.: Jahresbericht für Jan. 1956 bis Sept. 1957. In: Évi jelentések 1940–1960, p. 92.

[37]Detre, L.: Jahresbericht für 1957. In: Évi jelentések 1940–1960, p. 98.

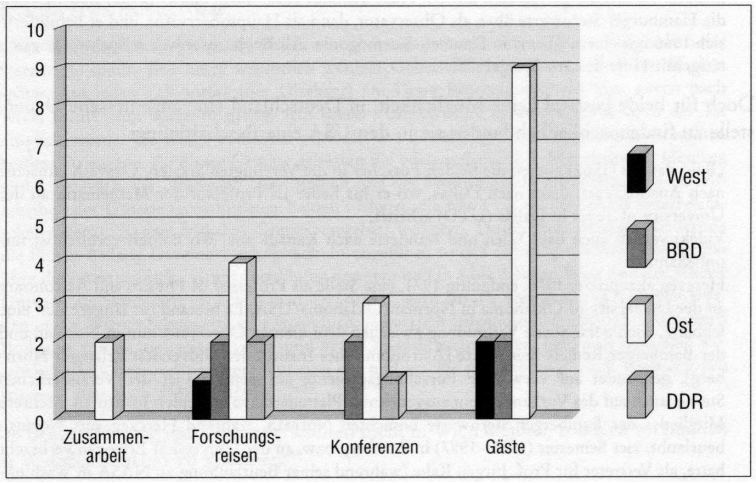

Figure 10: Cooperation, research travels, conferences, and guests after 1956

Scientific Cooperation from 1960 to 1990

- *The Development in the 1960s*

A large variety of sources was available for analyzing the development from the 1950s to the 1980s.[38]

After a certain transition time of a few years a positive development came up with the motto "Who is not against us, is for us". The rules were interpreted in a more liberal way; practically everybody was at least one time abroad, in the Western countries.[39] Especially in the field of science, where a strong interdependence from the modern development is obvious, there were only a few problems with travels from the 1960s on (*Figs. 11-12*). For travels to West Germany it was easier to get a permission, but for travels to the USA it was easier to get a grant (a financial support).

[38]1. Archive material in the Konkoly Observatory – offered by the librarian Magda Vargha:
– Annual reports of the Konkoly Observatory by Detre, from 1940 to 1973 (two volumes – typewritten with handwritten supplements)
– Annual reports of Debrecen by Dezső, from 1962 to 1982
– Guest book of the Konkoly Observatory
2. Handwritten supplements of Prof. Tibor Herczeg, transmitted by fax in Aug./Sept. 1997
3. Printed annual reports in Csillagászati évkönyv from 1959 to 1987, especially since 1974, written by Dr. Béla Szeidl, successor of L. Detre. – Printed annual reports in the Almanach MTA (1967–1980, 1985, 1991), in the Academy (1975–1980), in Meteor 1991–1997. – Printed annual reports of the University Budapest (ELTE) in Csillagászati évkönyv 1970–1992, written by Miklós Marik, later by Béla Balázs
4. Interview (Aug. 1997) with director Béla Szeidl, Konkoly Observatory, and Prof. Béla Balázs, Eötvös University, Budapest
5. Papers and documents of the Humboldt-Stiftung concerning I. Jankovics, director of the Gothard-Observatory in Szombathely, department of Budapest University
6. Annual reports of observatories in Western Germany, published in the Mitteilungen der Astronomischen Gesellschaft and discussions with German and Austrian astronomers.
7. Compilation of a data base with over 900 entries. The translation of the Hungarian material was done with the help of Andreas Korpas and typed in the data base by Celia von Lindern.

[39]Reported by Béla Balázs, in Aug. 1997. He spent one year (1961/62) in Hamburg and in 1964 again four months.

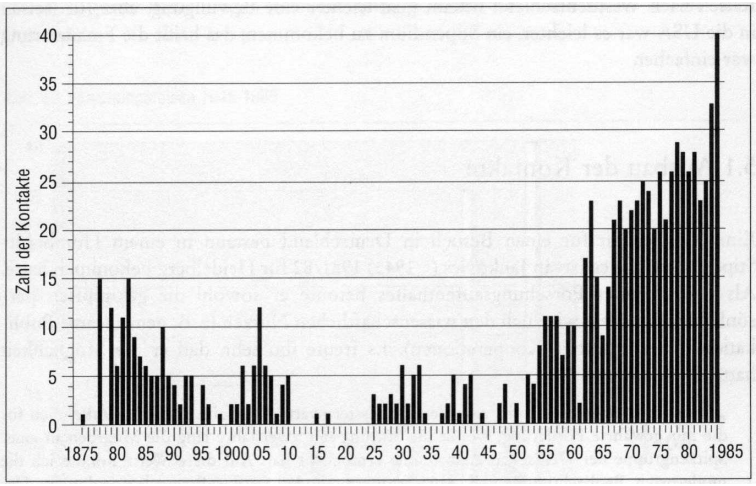

Figure 11: German-Hungarian relationships from 1874 to 1985

- Extension of the Contacts in the 1970/80s

One possibility for a visit in Germany was to get a Humboldt-Stipendium; this was given to István Jankovics (* 1943) in 1981/82 for Heidelberg. As a success of his research travel he emphasized the new personal contacts as well as the scientific profit (e. g. common publications and cooperations in the future). He reported: I was very glad, that I had the possibility,

> *„die schöpferische Atmosphäre an der Landessternwarte zu erfahren. Ich bedanke mich für die mir gewährte Förderung, womit die Stiftung mir zwei Jahre lang die Mitarbeit in einer Spitzengruppe der Deutschen Astronomie ermöglicht hat. Auf diese Weise konnte ich die modernsten Beobachtungs- und Auswertungsmethoden in der Praxis kennenlernen. Das führte dazu, daß mich mit den Kollegen nun nicht nur berufliche, sondern auch sehr gute persönliche Kontakte verbinden. ... Auch nach meiner Heimkehr bestehen gemeinsame Forschungsinteressen. Wir planen die langfristige spektroskopische und photoelektrische Überwachung junger Veränderlicher Sterne der Orion-Population. ... Für dieses Projekt ist eine Bildwandlerkamera geplant. Mit Heidelberger Kollegen werden gegenwärtig detaillierte Konstruktionspläne ausgearbeitet.“*[40]

The Budapest University (Béla Balázs) started official relationships to Jena University (Pfau, Zimmermann); already in the middle of the 1960s it became partner university.

In the 1970s and 1980s mainly the Soviet Union and the GDR were predominant for the studies and research travels. Thus Jankovics got a further grant in 1986/87 for Potsdam, GDR. Since 1992 he has been director in Szombathely, where he further on kept good relationships to Heidelberg – a tradition which has started already in the time of the Gothard brothers.

In the 1960s until the 1980s a permanent increase of the Eastern travels (maximum around 1980) is obvious; examples are visits, common projects for cooperation, travels for studying or astronomical observations. Already in the 1950s there existed more contacts in this field with the East and the GDR than with the West. Since the 1970s the travels to the German Federal Republic preponderated in comparison with travels to the GDR.

[40] Jankovics, István: Bericht an die Humboldt-Stiftung vom 26.11.1983.

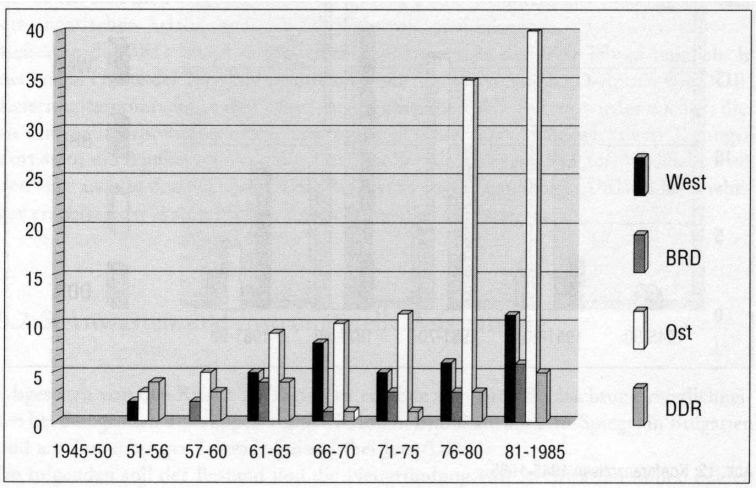

Figure 12: Research travels from 1945 to 1990

Regarding the travels one can recognise that the Hungarians preferred contacts with the GFR to the GDR.

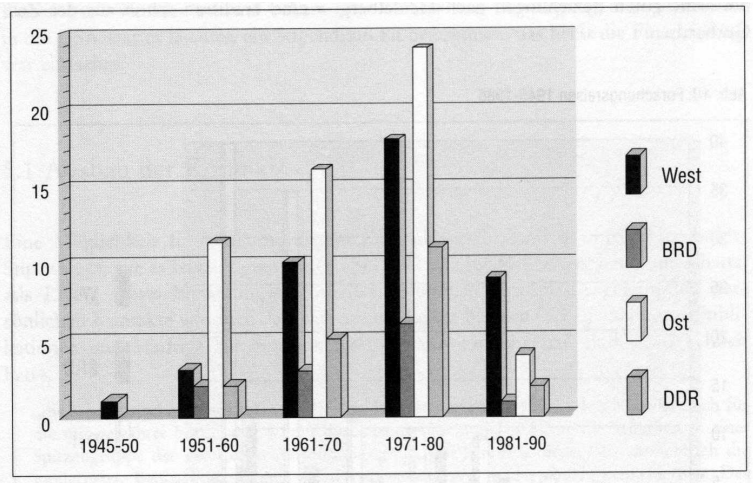

Figure 13: Guests in Hungary, 1945–1990

The guests from the Eastern Bloc increase from the 1950s until the 1970s; in the 1970s there is a maximum of guests from the GDR (three times more from the GFR) (*Fig. 13*). The interest of the Western side concerning visits in Hungary was relatively small in comparison to the East.

Detre as director of the Konkoly Observatory kept the contacts to the Western and Eastern astronomers, but also the international relationships. In September 1968 a meeting of the Commission 27 of the International Astronomical Union (IAU) took place in Budapest; there were 66 lectures and 93 participants: 7 GFR, 3 Austrian, 40 further participants from the West, 9 Hungarians, 9 GDR, and 26 from the East.[41] Detre was vice-president in 1964–67, in 1967–70 President of the Commission 27 of the IAU and founder and the first editor of the IBVS (Information Bulletin on Variable Stars).

[41]The lectures were published: Detre, L. (ed.): Non-periodic Phenomena in Variable Stars. Budapest 1969.

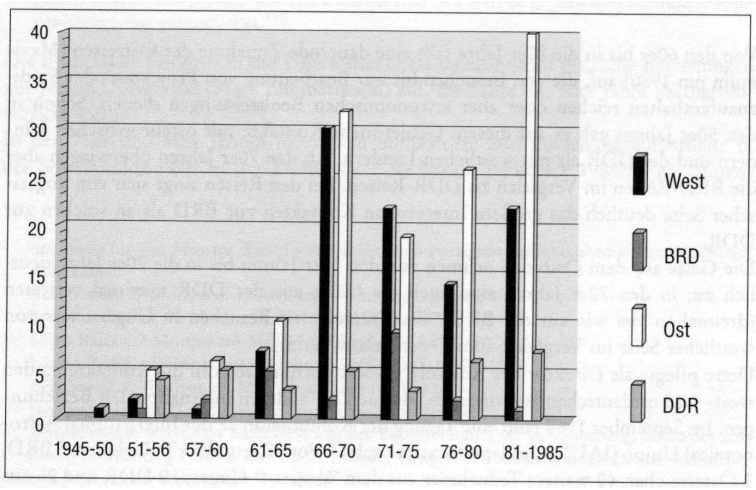

Figure 14: Conference travels, 1945–1990

In the 1950s the travels to the East predominated. In the middle of the 1960s there was a large increase of conference and lecture travels to the east, but also to the West. In the 1970s regular annual colloquia were introduced, where astronomers from the Eastern Bloc could meat each other, especially the Hungarian astronomers could meet the GDR astronomers (*Fig. 14*).

Travels to the German Federal Republic were possible in a larger amount not before the 1960s. In the first half of the 1970s twice more GFR-travels were undertaken as compared with the GDR-travels. In the 1980s the GFR-travels decrease; this is difficult to understand and to interpret, perhaps there are fewer important meetings in this time in the West; at least the Bamberg Colloquia on Variable Stars stopped in 1983.

Hungarian Members in the Astronomische Gesellschaft

Although the Astronomische Gesellschaft, founded in 1863, had its place of business and legal seat in Germany, but it represented with an amount of foreigners of 60% of the members the international astronomical society until the 1930s. The amount of Hungarians was from 1913 to 1935 around 2-3%, for example in 1913 there were 13 Hungarians in comparison to 421 members in the Astronomische Gesellschaft, in 1930 there were 16 Hungarians out of 509 members.

In the time after WW II the Astronomische Gesellschaft had lost its reputation as an international society, it included then mainly the German linguistic area; for example there were three Hungarians in 1962 (Detre (until 1974), Herczeg, and Ozsváth) out of 322 members (cf. six from Czechoslovakia, one Rumanian, and one Yugoslav) or in 1978 five Hungarians (Balázs B., Herczeg, Ozsváth, Pauliny-Tóth, Szeidl) out of 433 members, finally in 1996 six Hungarians (Balázs Béla, Herczeg, Jankovics, Kelemen János, Pauliny-Tóth, Szeidl) out of 793 members.

Language in the Publications

In Konkoly's time the German language was without concurrence the language of science. The publication series Mitteilungen der Konkoly-Sternwarte was published from

the 1920s until around 1950 overwhelmingly in German.

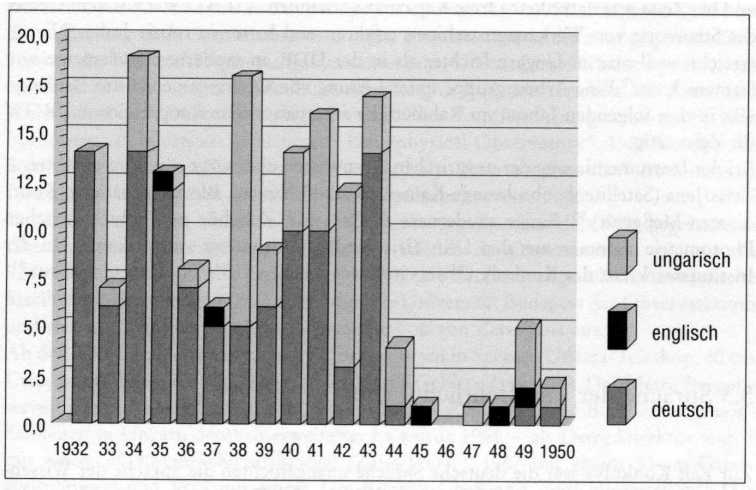

Figure 15: Language of the publications from 1932 to 1950

Regarding the histogram in *Fig. 15*, one can recognize, that until 1950 mainly German was used, practically no English; Hungarian was used especially in the case of popular astronomical journals.[42]

In the 1950s a discussion started, whether German is the suitable language for the publications further on.

> *„Die Publikation [über die Bedeckung von Zeta Aurigae] war die erste englischsprachige aus Budapest und auch der Titel der Reihe wurde zu "Contributions" geändert, allerdings als zweiten Titel "Mitteilungen" beibehaltend."*[43]

Since the middle of the 1960s one recognizes a strong increase of the English and thus a decrease of the German publications; a certain part of publications in Russian can also be found besides some Hungarian publications (*Fig. 16*).

Looking at the publications of Budapest University from 1978 to 1986, one recognizes English as the prominent language, but here no Russian is present (*Fig. 17*).

In analyzing the language used in meetings or for guest lectures (taken from the title of the lecture in the programme or in the annual report), one recognizes, that German played still an important role, but English increased in its significance. Only in the 1970s Russian was used several times; but it is not clear, whether the lecture was presented in Russian or it was translated (*Fig. 18*).

[42]In 1924 the astronomical society "Stella" was founded by Antal Tass and József Wodetzky, "Almanach" appeared in 1924, the journal "Stella" in 1926 (it existed only until 1931 due to the unfavourable economic development). In 1933 the astronomical society "Stella" was changed into a section of the "Kgl. Ungarische Naturwissenschaftliche Gesellschaft" (Royal Hungarian Scientific Society). The Stella Almanach was merged with the yearbook of the "Naturwissenschaftliche Gesellschaft". Cf. VJS 70 (1935), p. 145–146.

[43]Herczeg, Tibor: Deutsch-ungarische Beziehungen, Teil I: Vorgeschichte. Fax vom 31.8.1997. Cf. Mitteilungen der Konkoly Sternwarte Nr. 29 (1952).

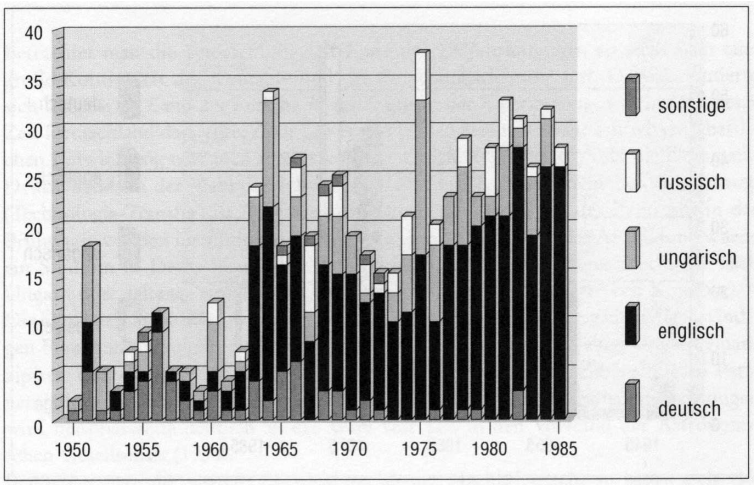

Figure 16: Language of the publications from 1950 to 1985

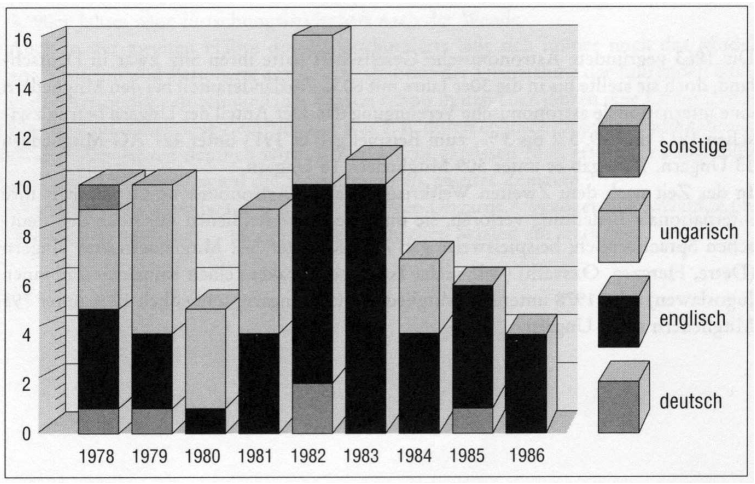

Figure 17: Language of the publications from 1978 to 1986, University Budapest

Observatories and Instrumental Equipment

- Provenience of the Instruments from 1870 to 1945

A compilation of the instruments used by Konkoly in his observatory O'Gyalla is given in *Fig. 19.* Around 66% came from German makers and 17% from abroad, half of them from England.[44] If you look in detail at the provenience of the instruments, one can recognize that in the beginnings of the 1870s – due to Konkoly's travels abroad – the English instruments have overweight in comparison to the German instruments. In the last two decades of the 19th century the amount of German instruments increases similarly

[44]Today many of them are in the Technical Museum of Budapest. Cf. Wolfschmidt, Gudrun: Astronomical Instruments of the Era Konkoly in Respect to their Significance to Astrophysics. In: Vargha, Magda; Patkós, László; Tóth, Imre (eds.): The Role of Miklós Konkoly Thege in the History of Astronomy in Hungary. Proceedings of the International Meeting "120th Anniversary of Konkoly Observatory" in Budapest, 5.–6. Sept. 1991. Konkoly Observatory of the Hungarian Academy of Sciences, Monographs No. 1, Budapest 1992, p. 69–82. – Bartha, Lajos: Astrophysical Instruments in Hungary, 1871–1911. In: Journal for History of Astronomy 25 (1994), No. 2, p. 77–91.

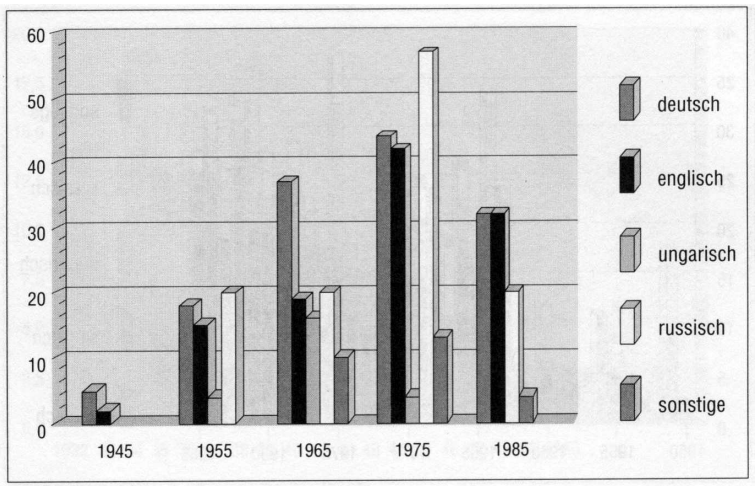

Figure 18: Comparison of the used languages during meetings from 1945 to 1985

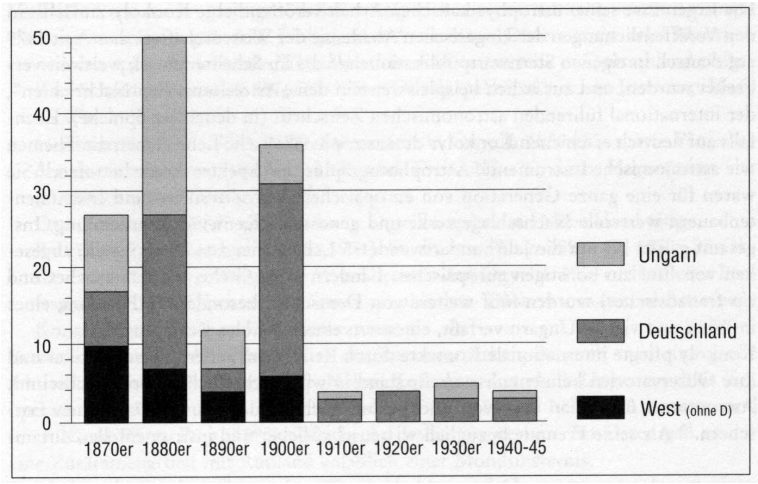

Figure 19: Origin of the instruments, 1870–1945

to the percentage of instruments, made in Hungary or especially in the workshops of the observatory. In 1900 the origin of the instruments is mainly Germany; from 1910 on there are no instruments from abroad any more.

- Observatories since 1945 in Eastern-Western Comparison

In the following the existing and newly founded observatories in the German states and in Hungary should be compared. In Germany there were 16 observatories around 1900 and this number did not change until 1945.

After WW II there existed eight observatories in West Germany (Bamberg, Bonn, Freiburg, Göttingen, Hamburg-Bergedorf, Heidelberg Landessternwarte, Kiel, München) and four in East Germany (APO Potsdam, Potsdam-Babelsberg, Jena, Sonneberg). In the GFR 14 institutes/institutions for astronomical research were founded,[45] but only one

[45]Astronomisches Rechen-Institut (ARI) Heidelberg, Institut für Theoretische Astrophysik Heidelberg, Astronomisches Institut der Universität Tübingen, Lehr- und Forschungsbereich Theoretische Astrophysik der Universität Tübingen, Institut für Astronomie und Astrophysik der TU Berlin, MPI für Astrophysik München-Garching, MPI für Extraterrestrische Physik München-Garching, MPI für Astronomie

new institute in the GDR.[46]

In 1945 Hungary had the Konkoly Observatory as a national observatory and a chair for astronomy at Budapest University.[47]

In 1958 the institute in Debrecen was founded as a solar observatory (Dezső director). In 1982 this Heliophysical Observatory and the Konkoly Observatory were unified as the Astronomical Institute of the Hungarian Academy of Sciences.

- Instrumental Equipment since 1960

In the 1960s Szombathely, followed from Gothard's Observatory in Herény (founded in 1881), was used again as an observatory. In Szombathely an observing station was erected for tracking soviet satellites already in the 1960s. In 1977/78 the university of Budapest took over the observatory and bought a 60-cm-reflector from Carl Zeiss Jena.

Since the 1960s smaller observatories have been built in Szeged (Odessa-Telescope, 40 cm Cassegrain) and in Baja (1966).

The Piszkéstető Mountain Station (in the Mátra mountains) of the Konkoly Observatory is especially important, because it enlarged the possibilities of observation for Hungary considerably.

- As a first instrument in 1961 – when Detre was the acting director – a 60 cm Schmidt-telescope, correction plate 90 cm, was acquired from Zeiss of Jena.[48]
- In 1966 a 50 cm Cassegrain-reflector was delivered.
- In 1974 the observatory was provided with a 1 m Ritchey-Chrétien-Coudé.[49]

The 1 m telescope (1974) was made – according to an information from Hans G. Beck – in cooperation with the Hungarian firm VILATI, Institute for Electroautomatics, in Budapest.[50] In the following time VILATI built computer guiding devices for further nine 1 m telescopes, for the two 2 m telescopes for Bulgaria (Rozhen) and Ukraine (Kiev, Terskol), and for the horizontal solar research equipment. Also for the 2 m telescope in Ondřejov near Prague a VILATI guiding system was added during a modernisation.[51]

Heidelberg, MPI für Radioastronomie Bonn, Observatorium Hoher List (Bonn), Astronomisches Institut der Universität Münster, Astronomisches Institut der Universität Würzburg, 1. Physikalisches Institut der Universität Köln, Astronomisches Institut der Universität Bochum

[46]Tautenburg Observatory.

[47]Department of Astronomy at Péter Pázmány University in Budapest; since 1950 Eötvös Loránd Tudományegyetem (ELTE), headed by: Radó von Kövesligethy (1897–1933), Károly Móra (1933–1934), József Wodetzky (1934–1941), Károly Lassovszky (1942–1949, he had to change to "Amerikanistik" due to political reasons), István Földes (1949-1964), László Detre (1964–1968, at the same time director of the Konkoly Observatory), Béla Balázs (1968–1990), Marik Miklós (1990–1998), and Bálint Érdi (1998–). Cf. VJS 70 (1935), p. 138 and Csillagászati évkönyv (1970), p. 94–100.

[48]According to an information from Hans G. Beck (May 12, 1998), former head of the department astronomy of Zeiss in Jena, four such Schmidt-telescopes (technical dates: 600 mm, correction plate 900 mm, focal length 1800 mm) were made in the end of the 1950s and delivered apart from Budapest also to Jena, Torún [Thorn], and Beijing.

[49]According to an information from Hans G. Beck in Jena (May 12, 1998) the 1 m telescope with an English mounting EM 1 saw first light in 1974 thanks to Béla Balázs who was very active in getting this telescope for the observatory.

[50]Zeiss had made in advance two nearly identical telescopes and delivered to India (Nainital and Kavalur). For the telescope for Hungary already a digital guiding was introduced, while the telescopes for India had still analogue guiding.

[51]It was necessary to improve the electrical guiding system of the telescope and Zeiss had no free

Looking at the equipment of the Hungarian observatories, Zeiss of Jena – like you would expect – is dominating: Satellite observing cameras, Schmidt cameras, blink comparator, coordinate measuring machine.[52] Some more modern instruments and auxiliary equipment for photoelectric photometry were ordered in the USA (iris diaphragm photometer made by Askania). In the workshop of the Konkoly Observatory UBV photoelectric photometers were built.[53]

Observing possibilities for Hungarian astronomers existed also with the large telescopes on Crimea, in Byurakan, with the 2 m reflector in Bulgaria, and with the Schmidt reflector of Tautenburg Observatory near Jena, GDR.

Conclusion

At the end of the 19th century Hungary as a country at the periphery used as an orientation always a country in the center of scientific development – this was at that time Germany. The predominance of Germany in choosing the emphasis of fields of research is very easy to recognize and also in choosing the instrumental equipment (transfer of technology).

But the contacts had not only one direction; Hungary emancipated itself in scientific respect since the 1920s and developed in the direction to a scientifically equivalent partner by delivering important contributions. The appreciation of the Hungarian achievements is obvious in electing Tass in the managing committee of the Astronomische Gesellschaft in 1930.

Looking at the further development after WW II, where László Detre had an important influence, one can distinguish four periods:

from 1945 to 1956/59 – period of isolation

in the 1960s – starting of contacts

from the 1970s to the 1980s – extension of contacts

in the 1990s – new research landscape.

Also in the second half of the 20th century one can apply the model of center and periphery. With the taking over of the leading role in astronomy of the USA or in general the Western English speaking countries Hungary started already in the 1960s to use this development as an orientation. This is obvious already in the 1950s e. g. by starting to use the English language in the publications. But up to a certain point there was inevitably also an orientation towards the Soviet Union as a second center of scientific development. Apart from this orientation the relationships of Hungary were always – in respect to amount, continuity and intensity – the strongest with both German states.

---

capacity at that time. VILATI had a lot of experience in the field of guiding of machine tools and had reached a relatively high standard. The reason was that it was easier in Hungary than in the GDR to get modern chips from Siemens. A team under leadership of the engineer Ottó Bánhegyi was active in the following years in the framework of international cooperation in the RGW for Zeiss.

[52]For the importance and development of the Zeiss works see e. g. Stolz, R., Wittig, J. (eds.): Carl Zeiss und Ernst Abbe – Leben, Wirken und Bedeutung. Jena: Universitätsverlag 1993. Dorschner, Johann: Astronomie in Thüringen. Skizzen aus acht Jahrhunderten. Mit besonderer Berücksichtigung der DDR-Zeit und der neuen astronomischen Forschungslandschaft im Freistaat Thüringen. Jenzig-Verlag 1998.

[53]A UBV photometer was built: in 1972 for the 50 cm reflector and in 1974 for the 1 m reflector in the Piszkéstető Mountain Station; in 1986 a new UBVRI photometer with photon counting device.

Figure 20: László Detre and Júlia Balázs

Astronomische Geräte von Carl Zeiss Jena in Ungarn

Hans G. Beck

Jena

Sehr geehrte Damen und Herren des Festkolloquiums zu Ehren von Herrn Professor László Detre!

Leider ist es mir aus gesundheitlichen Gründen nicht möglich, selbst einen Beitrag über die Beziehungen zwischen den ungarischen Astronomen und der Astro-Abteilung von Carl Zeiss Jena hier vorzutragen. Ich bedanke mich bei Herrn Professor Lajos Balázs für die Einladung und wäre gern nach über 30 Jahren wieder nach Budapest gekommen.

Die Beziehungen begannen bereits vor der Gründung der Abteilung durch freundschaftliche Kontakte und Lieferungen für das Privatobservatorium von Miklos von Konkoly-Thege in O´Gyalla. Pauly war ein Zeitgenosse Konkolys, beide waren etwa gleich alt. Als promovierter Chemiker leitete Pauly eine große Zuckerfabrik bei Mühlberg/Elbe mit bedeutendem Erfolg, insbesondere durch die Entwicklung neuer Technologien und Ausrüstungen für die Verarbeitung von Zuckerrüben. Pauly interessierte sich aber schon von Jugend an für die Astronomie und hatte nun finanzielle Mittel, sich intensiver mit dieser Wissenschaft zu beschäftigen. So baute er sich eine eigene Sternwarte auf, wobei ihn Konkoly unterstützte. Es gab zwischen beiden eine Art Seelenverwandtschaft, aus eigenen Kräften sich die Mittel für Forschung und Entwicklung zu schaffen.

Das besondere Interesse Paulys galt der Astro-Optik und er schuf eine leistungsfähige Optikwerkstatt mit einem großen Kundenkreis. Um 1890 lieferte er ein 6-Zoll-Objektivprisma und zwei 8-Zoll-Objektive nach O´Gyalla und nach Herény.

Große Aufmerksamkeit erregte Paulys Apochromat aus neuen Schott-Gläsern, den Professor Max Wolf von der Heidelberger Sternwarte auf dem Königstuhl als einen wesentlichen Fortschritt auf dem Gebiete der Fernrohroptik rühmte. Damit war eine Innovation entstanden, die die Grundlage für den Aufbau einer Werkstatt für astronomische Optik bei Carl Zeiss Jena bilden konnte.

Über dieses neue Objektiv und die neue Abteilung für astronomische Objektive berichtete Max Pauly auf der Tagung der Astronomischen Gesellschaft in Budapest im Jahre 1898, die von Konkoly organisiert worden war. An dieser Tagung nahm auch der Observator der Jenaer Sternwarte Otto Knopf teil, der von Ernst Abbe, dem führenden Wissenschaftler des aufstrebenden Weltunternehmens der Feinmechanik und Optik in Jena, mit den Geschäften der Astronomischen Lehre und Forschung betraut worden war.

Zu den Teilnehmern der Tagung der Astronomischen Gesellschaft in Jena im Jahre 1906 gehörte auch Konkoly, der sich von den Fortschritten in Jena überzeugen konnte. Aus der Werkstatt für astronomische Optik war eine Abteilung geworden, die bereits

astronomische Groß geräte wie das 720-mm-Spiegelteleskop für Heidelberg und das 400-mm-Spiegel-teleskop für Innsbruck hergestellt hatte.

Solche Groß geräte zählten nicht zur Planung Konkolys, aber er erwarb die neue Zeiss´schen Wechselvorrichtung mit der bekannten Ringschwalbe für seine Teleskope, um beim Austausch von Nebengeräten die Beobachtungstätigkeit zu rationalisieren.

Mit der Übertragung der Konkoly´schen Sternwarte an den Staat im Jahre 1899 war deren Existenz für die Zukunft gesichert und wie wir mit Befriedigung feststellen können, selbst nach dem Untergang der K.u.K. Monarchie.

Die neue Sternwarte in Budapest erhielt 1928 ein großes Doppel-Teleskop mit einer Montierung von Heyde/Dresden mit einem 600-mm-Spiegelteleskop und einem 300-mm-Refraktor von Carl Zeiss Jena, das heute noch in modifizierter Form als automatisiertes Teleskop im aktiven Dienst steht. Auch zwei Kuppeln, verschiedene kleinere Teleskope und Auswertegeräte gehörten zu den Geräten von Carl Zeiss Jena.

Das Hauptarbeitsgebiet der Sternwarte blieb die von Konkoly intensiv betriebene Beobachtung veränderlicher Sterne, auf dem man auch mit kleineren Teleskopen, wie sie in Budapest vorhanden waren, erfolgreich tätig sein. In Deutschland gab dafür Cuno Hoffmeister in Sonneberg ein Beispiel. Nach Abschluß seines Studiums in Berlin im Jahre 1929 begann László Detre seine Forschungsarbeiten in der Konkoly-Sternwarte mit großem persönlichen Einsatz bei der Beobachtungsarbeit. Ähnlich wie bei Cuno Hoffmeister in Sonneberg wurde jede klare Minute zum Beobachten genutzt und eine große Zahl photographischer Himmelsaufnahmen gewonnen und ausgewertet.

Als László Detre 1943 Direktor der Konkoly-Sternwarte wurde, war überhaupt nicht daran zu denken, daß die ungarische Astronomie durch neue, leistungsfähigere Teleskope und Ausrüstungen die von Konkoly geschaffenen Grundlagen der Astrophysikalischen Forschungen weiter ausbauen könnte.

Es ist bemerkenswert, daß – ähnlich wie nach dem Ersten Weltkrieg – viele zerstörte Sternwarten wieder aufgebaut wurden und darüber hinaus neue Forschungsgeräte installiert wurden. Damit hatte auch die Astroabteilung von Carl Zeiss Jena eine Chance, im Rahmen des Wiederaufbaus des Zeisswerkes die Tradition der Astroabteilung fortzusetzen und sogar ein höheres Leistungsniveau anzustreben.

An vorderer Stelle standen die Schmidtspiegelteleskope und in Jena folgte dem 2-m-Universal-Spiegelteleskop mit dem größten Schmidtspiegelsystem der Welt, das Große Schmidtteleskop für die Sternwarte Hamburg-Bergedorf.

Die ersten Gespräche um eine Modernisierung und Vergrößerung der Ausrüstung der Sternwarte fanden 1956 anläßlich der Konferenz über Veränderliche Sterne statt. Es ging um ein Schmidtspiegelteleskop, das den in der Veränderlichforschung eingesetzten Astrographen überlegen war.

Es trat dann der günstige Fall ein, daß mehrere Sternwarten an einem Spiegelteleskop-Typ interessiert waren, der für die Ausbildung von Studenten in gleicher Weise wie für die Forschung geeignet war. Mit dem Teleskop, so war die Konzeption von Zeiss, sollte, ähnlich wie bei dem 2-m-Spiegelteleskop, das 1960 in Tautenburg in Betrieb genommen worden war, neben dem Schmidtsystem auch noch eine Cassegrainvariante Einzeluntersuchungen astronomischer Objekte ermöglichen.

An diesem Schmidtspiegelteleskop waren die Sternwarten Jena, Budapest, Poznan und Peking interessiert und so kam es zu einer intensiven Zusammenarbeit zwischen den Jenaer und den Budapester Astronomen. 1962 wurde das Schmidtspiegelteleskop 600/900/1800 auf der neuen Bergstation Piszkéstető in dem Mátra-Gebirge in Betrieb genommen. Ihm folgte 1966 ein 500-mm-Cassegrain-Teleskop.

In dieser Zeit waren in Jena die neuen 2-m-Spiegelteleskope für Schemacha (Aserbeidshan) und Ondrejov (CSSR) im Bau und zwei 1-m-Teleskope mit Ritchey-Chrétien-Spiegelsystemen für die indischen Sternwarten in Kavalur und Nainital in Entwicklung.

Dieser Teleskoptyp war für die Konkoly-Sternwarte ein optimaler Kompromiß zwischen Leistungsfähigkeit und Kostenaufwand verglichen mit einem 2-m-Teleskop. Zeiss hatte Vorteile mit einer weiteren Fertigung für Sternwarten in aller Welt. Durch die niedrigen Polhöhen der indischen Sternwarten war eine sogenannte Englische Montierung vorteilhaft, bei der die Stundenachse von zwei Pfeilern getragen wird. Für die Fertigung dieses Typs konnte eine Standardkonstruktion verwendet werden, die für den Kunden und den Lieferanten ökonomische Vorteile bot.

Damals entwickelte sich ein Umbruch in der Antriebs- und Steuertechnik der Teleskope, aber auch der gesamten Gerätetechnik des Zeiss-Fertigungsprogramms.

Die Astroabteilung von Carl Zeiss Jena stand vor einem Dilemma. Die bisherige Elektrotechnik war nicht mehr zukunftsträchtig, es gab aber keinen Partner mit entsprechenden Erfahrungen in der DDR für eine moderne Lösung.

Bei der Beratung dieser Problematik in Budapest ergab sich der Glücksfall, daß in der Budapester Firma VILATI ein potentieller Partner mit Erfahrungen auf dem Gebiet der Steuerung von Werkzeugmaschinen existierte, der zudem noch Zugriff auf moderne westliche Bauelemente der Elektronik hatte. Dank der Bemühungen von Prof. Béla Balázs und einer glücklichen Konstellation der kommerziellen Beziehungen zwischen Ungarn und der DDR im Rahmen der Gegenseitigen Wirtschaftshilfe konnte das Problem gelöst werden.

Die Zusammenarbeit mit den Spezialisten der Firma VILATI unter Leitung von Diplomingenieur Otto Bánhegyi war hervorragend und es gab keine Schwierigkeiten bei der Übertragung der Steuerung einer Werkzeugmaschine auf ein Teleskop.

Von besonderem Vorteil war, daß die erste neue Teleskopsteuerung in Ungarn zur Anwendung kam und die Betreuung des Teleskops gesichert war.

Das Teleskop wurde 1974 in Betrieb genommen.

Was zunächst nur als eine Lösung für das ungarische Teleskop angesehen wurde, entwickelte sich für Carl Zeiss Jena und die Firma VILATI zu einer Erfolgsgeschichte. Von dem 1-m-Teleskop-Typ wurden bis 1990 weitere 10 Geräte vor allem in den astroklimatisch günstigen Gebieten Mittelasiens in Betrieb genommen.

Inzwischen war auch die Digitaltechnik produktionsreif geworden und so konnte Carl Zeiss Jena dank der guten Zusammenarbeit mit der Firma VILATI auch auf diesem Gebiet mithalten und die Beobachtungsarbeit rationalisieren. Die mit dem 1-m-Teleskop gewonnenen Erfahrungen konnten auf die neuen 2-m-Ritchey-Chrétien-Teleskope für die Observatorien Roshen/Bulgarien und Terskol/Kaukasus übertragen werden.

Wie Sie sehen können, verdankt die Astroabteilung von Carl Zeiss Jena wesentliche Impulse ihrer Entwicklung der ausgezeichneten Zusammenarbeit mit bedeutenden ungarischen Astronomen und Institutionen. Es ist erfreulich festzustellen, daß Professor László Detre zur richtigen Zeit diese Impulse auslösen konnte. Persönlich freue ich mich, daß ich in meiner Funktion als wissenschaftlicher Leiter der Abteilung für Astronomische Geräte bei Carl Zeiss Jena diesen Aufbau fördern konnte. Ich hatte als Praktikant an der Sternwarte Sonneberg meine Lehrzeit als Astronom mit der Beobachtung von Veränderlichen Sternen begonnen ebenso wie mein engster Mitarbeiter Alfred Jensch, der dann Chefkonstrukteur der Astroabteilung wurde.

Ich wünsche der ungarischen Astronomie weiterhin eine gute Entwicklung und viele Erfolge.

Photographic observation of globular clusters in the Konkoly Observatory

Katalin Barlai

Konkoly Observatory of the Hungarian Academy of Sciences
P.O. Box 67, H-1525 Budapest, Hungary

In the last years of the XIXth century Solon I. Bailey made photographic observations at Arequipa, Peru, at the observational station of the Harvard Observatory. He obtained long series of photographs on M3, M5, and ω Cen clusters and discovered hundreds of RR Lyrae variables on them.

About four decades later (1938) W. Christian Martin found increased periods based on new plates taken of ω Cen. This result made further research promising. They brought up the idea to grasp stellar evolution through period changes.

In Budapest the photographic observations of globular clusters span almost 30 years (1937–1966) (*Fig. 1*). These observations have been initiated by L. Detre. In the beginning he took the considerable part of plates at the Newtonian focus of the Observatory's 24" telescope. Later the program was continued by the staff members of the observatory. Júlia Balázs-Detre, Tibor Herczeg, György Kulin, Miklós Lovas, Béla Szeidl, and the author participated in the observations.

The globulars M3, M5, M15, M56, and M92 have been photographed systematically. The contribution by G. Kulin and M. Lovas has been extremely high to this plate collection. Apart from a few Kodak products and Agfa Astro special plates, the majority of the plates used were Guilleminot Superfulgur. With a few exception, exposition times extended 10-20 minutes. In course of these three decades hundreds of plates have been obtained on the clusters mentioned above.

In order to study the period changes, mean light curves and O−C diagrams have been constructed. Studies of this type have been published on about 60 RR Lyrae variables in M3 by István Ozsváth (1957) and 21 variables in M15 by Imre Izsák (1957). Further studies based on Budapest plates of M3 concerning 112 measurable variables were carried out and published (Szeidl, 1965) (*Fig. 2*). Later data on 54 RR Lyrae stars in the cluster M15 were published by the author (Barlai, 1989) (*Fig. 3*).

It is worth mentioning that the brightness of overwhelming majority of the RR Lyrae variables in M5 have been measured or estimated by M. Lovas. This database is to be analysed.

In 1975 a new 1-meter RCC telescope was installed at our Piszkéstető mountain station. Since then the photographic observations have continued there until the beginning of the 1990s. Several hundreds of plates have been obtained on M3, M5, and M15 globular

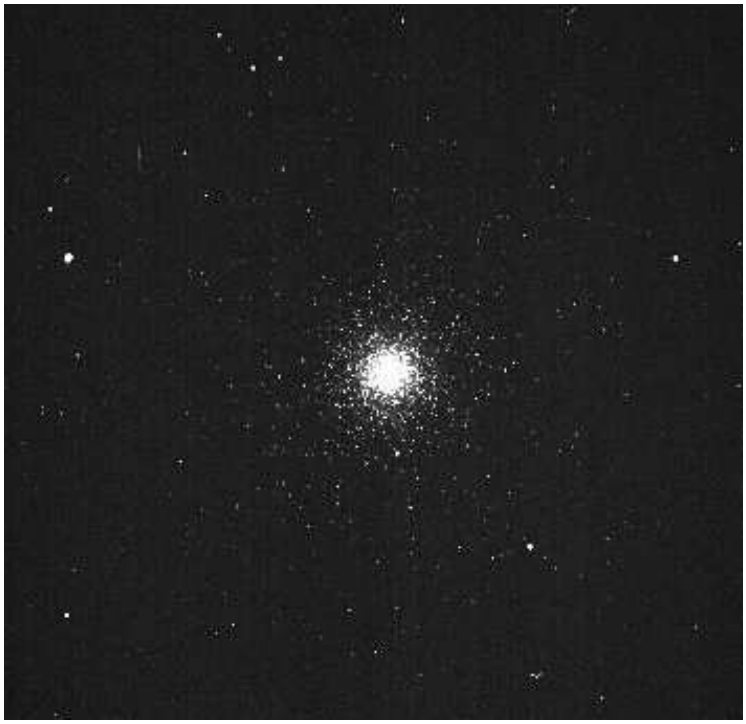

Figure 1: A "historic" photograph from the year 1950.

clusters. Due to the better resolution, further details can be revealed on the variables closer to the dense central region or the ones having close companions on the plates taken in Budapest with the Newtonian telescope. Analysis of their data means a task for the future.

Although the study of period changes did not fulfill the original expectations to show immediately the direction of cluster evolution still they and the numerous brightness data obtained gave us a deeper insight into the nature of RR Lyrae stars.

The new CCD technique made further photographic observation of globular clusters obsolete (*Fig. 4*). This "old" plate material, however, means a base for new approaches to these fascinating objects.

References:

Barlai K., 1989, *Mitt. Sternw. Ungar. Akad. Wiss.*, No. 92
Izsák I., 1957, *Mitt. Sternw. Ungar. Akad. Wiss.*, No. 42, 63
Ozsváth I., 1957, *Mitt. Sternw. Ungar. Akad. Wiss.*, No. 42, 81
Szeidl B., 1965, *Mitt. Sternw. Ungar. Akad. Wiss.*, No. 58

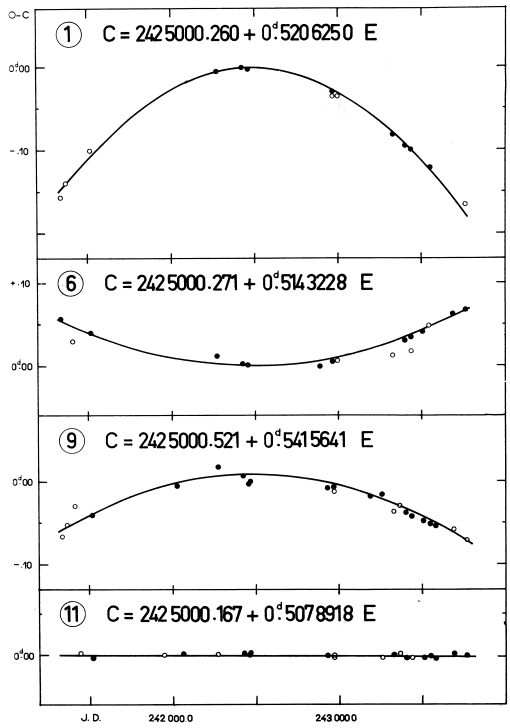

Figure 2: O−C diagrams of some RR Lyrae variables in M3. Increasing and decreasing periods can be seen and a constant period, as well (Szeidl 1965).

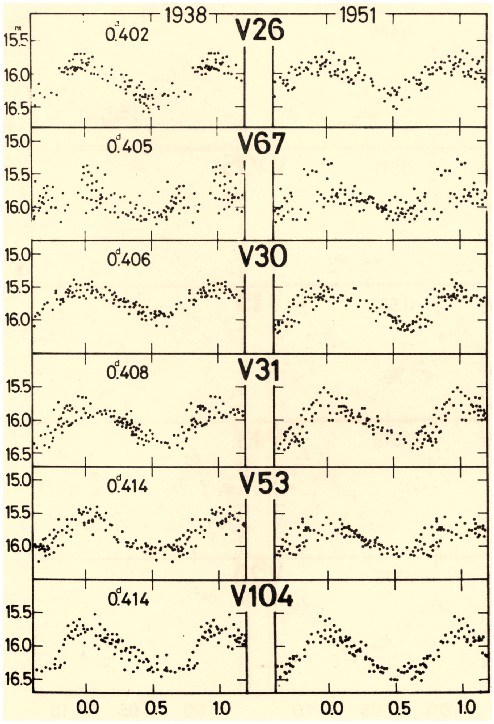

Figure 3: Some mean light curves of RR Lyrae stars in the globular cluster M15. Except V104 the other stars are of double mode nature or show suspect of Blazhko effect (Barlai 1989).

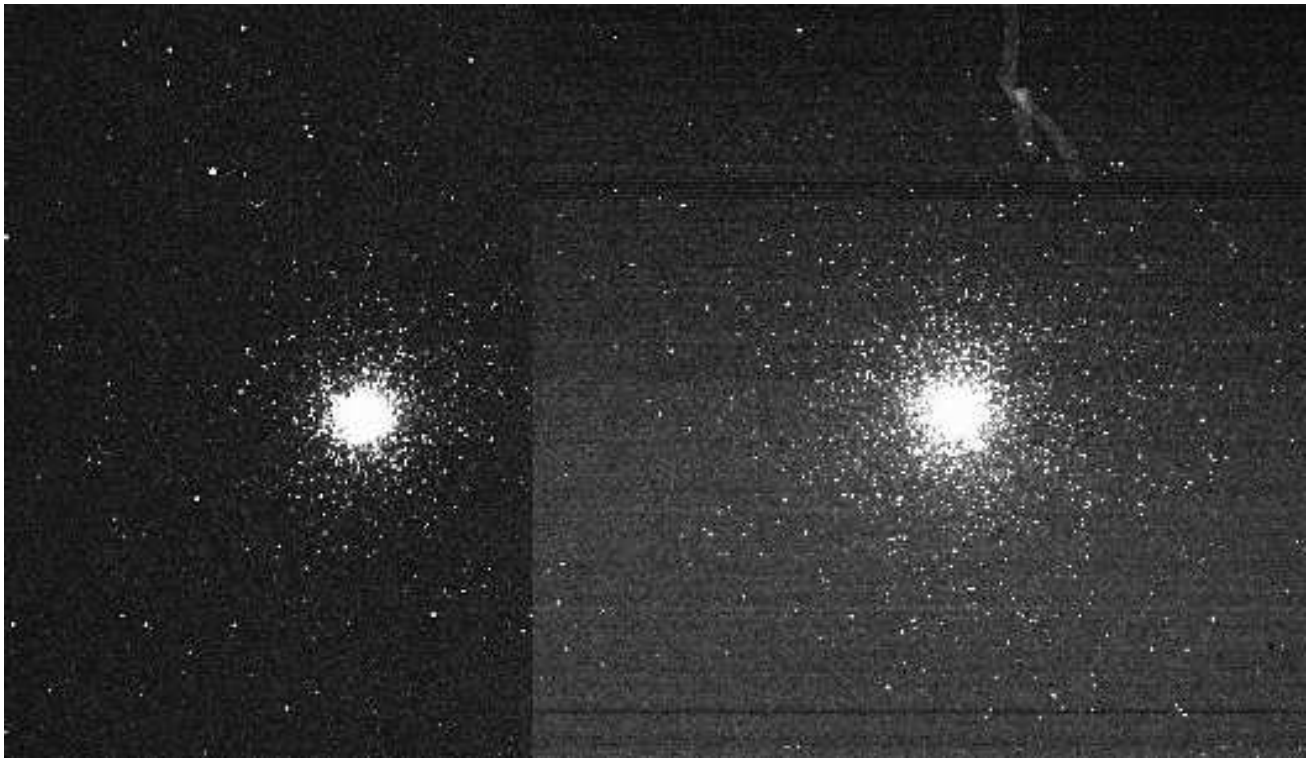

Figure 4: Image of M15 on the plates taken with the Newtonian telescope and with the RCC telescope, respectively. Casting a glance on the two photographs they clearly show the improvement in the resolution.

Conventional and new directions in studying Cepheids

László Szabados

Konkoly Observatory of the Hungarian Academy of Sciences
P.O. Box 67, H-1525 Budapest, Hungary

In the first part of this paper, traditional methods of studying Cepheids are summarized, mentioning Detre's contribution to this field. Then the new directions of Cepheid related research are reviewed with an emphasis on the problems concerning the period-luminosity relationship.

Introduction

Cepheids are supergiant stars that perform radial pulsation when they cross the classical instability strip in the Hertzsprung-Russell diagram during their post-main sequence evolution. It is the outer layers of Cepheids which oscillate, and the pulsation is maintained by the opacity changes in the partially ionised zones of neutral hydrogen and singly ionised helium capable for transforming heat into mechanical energy via the κ-mechanism (κ is the conventional sign of the opacity).

The mostly monoperiodic Cepheids may seem to be boring targets with respect to the multiperiodic radial and/or non-radial pulsating stars of different types but, in fact, Cepheids are neither perfectly regular, nor homogeneous. Subtle deviations from regularity and homogeneity result in important astronomical consequences. No wonder, Cepheids have remained in the forefront of the variable star studies in spite of the fact that a number of astrophysically important new types of variable stars emerged in the last decades. Due to variety and richness of the relevant studies, selected results are only mentioned in this review.

Traditional studies and Detre's contribution

The Cepheid pulsation is a free oscillation of the star whose frequency corresponds to the eigenfrequency of the stellar plasma sphere. The value of the frequency and its

reciprocal, the pulsation period, is governed by the structure of the star, especially by the average density. This dependence gives rise to the well known period-luminosity relationship that exists for various types of pulsating stars. The period-luminosity (P-L) relationship was discovered a century ago by studying Cepheids in the Magellanic Clouds, and since that time this relationship has been instrumental in establishing the extragalactic distance scale.

By the time of mid-20th century, it became obvious that Cepheids are found in at least two varieties: the classical Cepheids belonging to Population I, and the older Type II Cepheids which are less luminous at a given pulsation period. In what follows, the term Cepheid covers classical Cepheids only.

The simplest observational study of Cepheids (and any other periodic variable stars) is to obtain photometric data from which the light curve can be constructed and long-term stability of both the light curve and the pulsation period can be investigated. László Detre also observed Cepheids – at the beginning of his career the Cepheids and the RR Lyrae type variables were not even strictly separated: the RR Lyrae type stars used to be referred to as short period Cepheids. Detre published three papers on classical Cepheids based on his visual photometric data. The targets of these studies were XY Cas (Dunst, 1932), SZ Cas (Dunst, 1933), and YZ Aur (Detre, 1935).

Two decades later, when the first photoelectric photometer was installed at the Konkoly Observatory, Detre included some bright Cepheids (FF Aql, SU Cyg, T Vul, and U Vul) in the observational programme. These photoelectric data were only published after Detre's death (Szabados, 1977, 1980).

Long-term changes in the pulsation period can be studied with the help of the O−C method. In the case of Cepheids, the amount and sign of the period variations can serve as an observational check of stellar evolutionary models. During the Cepheid stage of stellar evolution, the supergiant star crosses the instability strip in either direction. A monotonously increasing pulsation period reflects redward crossing of the instability strip, while the blueward transition results in continuously decreasing period. In reality, period fluctuations are often superimposed on the period changes of evolutionary origin. The erratic changes in the pulsation period reflect the physical conditions in the upper layers of Cepheids because this radial pulsation is an atmospheric phenomenon. Detre pioneered the study of period changes of regularly pulsating variable stars. His paper involving O−C diagrams for a number of Cepheids was published in 1970.

Role of Cepheids in astronomy

Importance of Cepheids in astronomy is twofold. In astrophysics they are *test objects for stellar evolution theory* (as mentioned above) and models of stellar structure. In extragalactic astronomy and cosmology, Cepheids are considered as *primary distance indicators* and the cosmic distance scale is chiefly based on Cepheids. They serve as standard candles because a close correlation exists between the pulsation period and stellar luminosity. The most recent review on the *period-luminosity relationship* is written by Sandage & Tammann (2006).

In addition to the P-L relationship, Cepheids obey a number of other relationships owing to regularity of their pulsation and some well-known physical principles (e.g. Stefan-Boltzmann law). Close relationships are valid between the period and the spectrum, the period and the radius, the period and the age of the Cepheid, etc.

Studies of Cepheids have been motivated mostly by the intention of improving any of these relationships either observationally or by theoretical calculations. Nevertheless, existence of period variations is already a hint that one cannot expect perfect regularity in the pulsation of Cepheids. Knowledge of the means how the individual Cepheids deviate from the regular behaviour and the physical explanation of these deviations is essential for the precise calibration of various Cepheid-related relationships, as well as from the point of view of astrophysics.

Recent developments

In spite of the fact that a number of methods suitable for extragalactic distance determination were devised in the last decades, the role of Cepheids as primary distance calibrators has not lessened. The interest in studying Cepheids has been facilitated by the rapid progress in both observational and theoretical astrophysics, especially by the following facts: availability of imaging detectors in the near infrared, existence of massive photometries (with the primary aim at detecting microlensing events), and the enormous increase in computing power.

The advantages of *observing Cepheids in infrared* are as follows:
- The photometric amplitude at near IR wavelengths is smaller than in the optical spectral region, therefore the mean brightness can be determined reliably from a few observations obtained at random phases. (In the optical band, at least 15-20 observational points are necessary for covering the light curve.) Thus projects aimed at determining extragalactic distances based on the P-L relationship of Cepheids are more feasible in the near IR.
- Infrared magnitudes are less affected by interstellar absorption. Thus the P-L relationship has a smaller scatter around the ridge line fit in the near IR photometric bands.
- The finite width of the P-L relationship at a given period is partly due to the temperature sensitivity of the pulsation period because the P-L relation is, in fact, period-luminosity-colour (P-L-C) relationship. At longer wavelengths, the monochromatic flux becomes less sensitive to temperature, thus the width of the P-L relation is reduced in the IR bands.
- Many Cepheids belong to binary systems whose secondary star is usually a less massive blue or yellow star on or near the main sequence. The photometric contribution from the companion is negligible in the near IR.
- The effects of metallicity are much reduced in the infrared as compared with the optical spectral region where metallic absorption lines dominate. Therefore, the Baade-Wesselink method of radius determination can be reliably applied in the near IR.

The main benefit from the *massive photometries*, especially MACHO, OGLE, and EROS, on Cepheid research is the availability of large body of homogeneous photometric data on Cepheids in both Magellanic Clouds. Using these databases, the period dependent behaviour of Cepheids can be studied much more precisely than before. In addition, many new Cepheids were discovered in both satellite galaxies including dozens of double-mode Cepheids (Alcock et al., 1995; Udalski et al., 1999a; Soszyński et al., 2000) and Cepheids which are members in eclipsing binary systems (Udalski et al., 1999c; Alcock et al., 2002). The Magellanic double-mode Cepheids outnumber their Galactic counterparts. Their simultaneously excited two modes can be either the fundamental mode and the first overtone, or the first and second overtones. Surprisingly, single-mode Cepheids pulsating in the second overtone have been also found in the Small Magellanic Cloud (Udalski et al., 1999b). Such stars are not known in our Galaxy, possibly because the mode identification

for the Milky Way Cepheids is very difficult and uncertain.

The increasing number of large telescopes and very sophisticated auxiliary equipments facilitate the discovery of Cepheids in remote galaxies as well as deeper studies of individual Galactic Cepheids. In September 2006 Cepheids were *known in 76 galaxies.* Over 5000 Cepheids have been detected beyond the Magellanic Clouds, and about 400 such variables are known in various galaxies of the Virgo Cluster. The number of the known classical Cepheids in our Galaxy only amounts to about 6 per cent of the total known Cepheid sample.

The high precision photometric and deep spectroscopic studies of Galactic Cepheids facilitated a reliable determination of physical properties and surface chemical composition of a large number of these variables. With a spectacular progress in the last decade, *abundance determination* based on high resolution spectra has been already performed for more than 150 Cepheids (Kovtyukh et al., 2005 and references therein). The classical Baade-Wesselink method of *radius determination* has been replaced by the infrared surface brightness method (Welch, 1994). The estimated precision of radius determination of Cepheids was about 7 per cent several years ago (Gieren et al., 1999).

The long-lasting discrepancy between *Cepheid masses* derived by various methods was already resolved in early 1990es by using modified opacity values characteristic of stellar interior (Rogers & Iglesias, 1992; Seaton et al., 1994). Nevertheless, the agreement is not satisfactory yet. Now, the masses derived from stellar pulsation are smaller by about 10-20 per cent than the mass values deduced from evolutionary models. This problem can be resolved either by more appropriate stellar models or assuming a significant mass loss in pre-Cepheid evolutionary phases (Bono et al., 2006).

Quite recently, important observational results were achieved on the circumstellar environment of Cepheids: extended envelopes have been found around the brightest Cepheids from near-IR interferometric observations (Kervella et al., 2006; Mérand et al., 2006) testifying that *mass loss* occurred in the recent past.

The ample and precise observational data on Cepheids can be used even for studies of *star formation history* in particular stellar regions. The period distribution coupled with the period-age relationship is indicative of star formation in the recent past. For example, the period distribution of Cepheids in the Large Magellanic Cloud shows that star formation propagated along the bar of our largest satellite galaxy with a velocity of 100 $\mathrm{km\,s^{-1}}$ from SE to NW during the last hundred million years (Alcock et al., 1999).

Similarly, Cepheids are instrumental in following spatial motion of the point of intersection of two spiral arms in M31. The interaction point could be followed from the age, i.e. the period distribution of Cepheids (Magnier et al., 1997). The location of intersection now coincides with the superassociation NGC 206.

Moreover, some characteristics of star formation history in our own galaxy can be investigated, as well. The distribution of metallicity and its gradient as a function of galactocentric radius is an important feature determined from Cepheid studies (Kovtyukh et al., 2005).

In addition to investigations based on large numbers of Cepheids, *studies of individual Cepheid variables* have also resulted in spectacular results. There are quite a few Cepheids that exhibit peculiar behaviour. Polaris (α UMi), the brightest Cepheid, showed a secularly decreasing pulsation amplitude throughout most of the 20th century, but instead of ceasing pulsation, now it oscillates with an extremely small amplitude (Turner et al., 2005 and references therein). Strangely enough, the locus of Polaris in the H-R diagram is in the middle of the instability strip, so this Cepheid is not about leaving the instability

region (Evans et al., 2002). Another example for secularly declining pulsation amplitude may be the case of Y Oph (Fernie et al., 1995). An even more strangely behaving Cepheid is V19 in M33 (Macri et al., 2001). The tremendous decrease in its pulsation amplitude was accompanied with increasing mean brightness during the 20th century.

In addition to these secular changes, important *periodic phenomena* also appear among Cepheids. V473 Lyrae, a very short period classical Cepheid (with a pulsation period of 1.491 days), cyclically varies its amplitude by a factor of about 15. The modulation period is as long as 1200 days (Burki et al., 1986 and references therein). The physical cause of this unprecedented behaviour has not been clarified yet.

Another type of independent periodicity is due to the orbital motion, if the Cepheid is a member in a binary system. The frequency of occurrence of *binaries among Cepheids* is as large as incidence of binarity among common stars in the solar neighbourhood, i.e. *exceeds 50 per cent* (Szabados, 2003). Such a high percentage was not foreseen earlier. Cepheids belonging to binary systems are key objects for determining the physical properties of Cepheid variables, including stellar luminosity which facilitates reliable calibration of the zero-point of the P-L relationship (e.g. Evans, 1992). Especially valuable are in this respect the eclipsing systems involving a Cepheid component, because the inclination of the orbital plane follows from the eclipsing nature, and knowledge of the inclination removes uncertainty in the mass determination. Unfortunately, such pairs have not been found in our Galaxy but three *eclipsing binary systems with Cepheid primaries* have been revealed in the LMC (Alcock et al., 2002; Udalski et al., 1999b).

The *pairs consisting of two Cepheid variables* are extremely interesting objects from the viewpoint of stellar evolution. In addition to the archetype, CE Cas, Alcock et al. (1995) revealed three such pairs in the LMC, while Udalski et al. (1999a) detected one pair in the SMC. Though the two components cannot be separated, it is clear from the period ratio of the two excited oscillations that the observed variations cannot be explained with double-mode pulsation of a solitary Cepheid in any of these cases.

In the *beat Cepheids*, the two excited oscillations are not independent of each other: they correspond to low order radial modes of stellar pulsation. Though a number of faint Galactic double-mode Cepheids have been discovered in the last decade, the number of such variables is only slightly over twenty, i.e. much less than their known counterparts discovered from the data collected during the photometries of either Magellanic Cloud. Quite recently, double-mode Cepheids were discovered in M33 (Beaulieu et al., 2006) among the huge sample of the photometric survey performed by Hartman et al. (2006). The survey covering the whole area of this more remote galaxy resulted in identifying about 2000 Cepheids in M33 (Hartman et al., 2006). There has been a spectacular *progress in modelling* double-mode pulsation in Cepheids, too. While purely radiative models have failed to reproduce simultaneous double-mode periodicity of Cepheids for decades, when taking into account turbulent convection in the hydrodynamic calculations, Kolláth et al. (2002) succeeded in obtaining a stable beat Cepheid behaviour.

Another major result among the Cepheid related theoretical investigations is the confirmation of existence of strange Cepheids. Stars performing surface mode pulsation were predicted by Buchler et al. (1997), and the first representatives of such short period, ultralow amplitude variables were discovered from the MACHO photometry of the LMC by Buchler et al. (2005). Discovery of non-radial oscillations as well as triple-mode pulsation in classical Cepheids were also announced based on the OGLE LMC data (Moskalik et al., 2004).

Problem of universality of the P-L relationship

There are quite a few effects that place the individual Cepheids scattered around the ridge line P-L(-C) relationship, thus resulting in a finite width of this plot. The most important effects being:
- interstellar reddening and absorption;
- presence of a companion star;
- mass loss;
- magnetic field;
- mode of pulsation;
- nonlinearity of the relation;
- differences in the chemical composition.

The amount and effects of interstellar absorption has been widely discussed and thoroughly studied in the Cepheid related literature. For Galactic Cepheids, the reddening correction and the intrinsic colour index is determined individually. In the case of extragalactic Cepheids, however, this is not a viable procedure, and, instead, the practically reddening-free Wesenheit function, W, is used (see Madore, 1976):

$W = \langle V \rangle - R(\langle B \rangle - \langle V \rangle)$

where R is the ratio of total-to-selective absorption. The assumption that R is constant throughout any galaxy is only a rough approximation. For extragalactic Cepheids, the absorption consists of two parts: internal absorption in the galaxy hosting the Cepheid and foreground absorption produced by interstellar matter along the given line of sight in our Galaxy. The effect of this latter component can be readily determined by multicolour photometry (Freedman & Madore, 1990 and references therein).

The photometric effect of possible companion stars (either physical or optical companions) is usually not taken into account. Neglect of binarity may lead to a systematic error in determining the luminosity of Cepheids useful for the calibration of the P-L relationship (Szabados, 1997), while line-of sight companions in crowded stellar fields of remote galaxies falsify the distance modulus derived for the given system.

Studies on the mass loss can gather a new impetus by recent discoveries of envelopes around bright Cepheids (Kervella et al., 2006; Mérand et al., 2006).

Existence of magnetic field and its effect on luminosity of Cepheids is a topic of worthy of closer attention from both theoretical and observational points of view.

The pulsation mode of extragalactic Cepheids can be determined relatively simply because stars oscillating in different modes are situated along distinct P-L relationships. In the case of Galactic Cepheids, however, the determination of the pulsation mode is not easy. There are contradictory propositions on the pulsation mode of some well studied bright Cepheids. Difficulties in the mode identification may also cause that no singly periodic Cepheid pulsating in the second overtone is known in our Galaxy, while a plenty of such stars have been found in the SMC (Udalski et al., 1999b).

Quite recently, it turned out that the P-L relationship of the LMC is nonlinear, showing a break at the pulsation period of about ten days (Sandage et al., 2004; Ngeow & Kanbur, 2006 and references therein). This effect is caused by nonlinearity of the period-colour relation and has its physical origin in the interaction of the hydrogen ionization front with the Cepheid photosphere. This interaction changes with the phase of pulsation and metallicity producing the observed changes in the Cepheid P-C and P-L relationships. Note that nonlinearity is characteristic of the relationships of the metal poor LMC, while the corresponding relations valid for the Milky Way galaxy are linear.

The role of *metallicity* in modifying the relationships valid for Cepheids is the key issue in the recent Cepheid related literature. The very precisely measurable period ratio of double-mode Cepheids clearly depends on the abundance of the heavy elements as shown by the comparison of Galactic beat Cepheids and their siblings in the Large Magellanic Cloud (Alcock et al., 1999). The [Fe/H] values of Galactic beat Cepheids determined individually from high resolution spectra also confirm existence of metallicity dependence of the period ratio (Sziládi et al., 2006). Moreover, Klagyivik & Szabados (2006) pointed out that some phenomenological properties of Cepheids, e.g. ratio of amplitudes of photometric and radial velocity variations also depend on the heavy element abundance, Z.

Nevertheless, the most important problem in this respect is the dependence of the zero point and the slope of the P-L relationship on metallicity. The era of contradictory results has not been over yet. A numerical parameter, γ, describing this metallicity dependence has been introduced by Sakai et al. (2004): $\gamma = \delta(m-M)/\delta \log Z$ where $\delta(m-M) = (m-M)_Z - (m-M)_0$ is the difference of distance modulus corrected for the effect of metallicity and the uncorrected value, and $\delta \log Z = (\log Z)_{LMC} - (\log Z)_{\rm extragal}$. The most recent studies (Sakai et al., 2004) resulted in $\gamma = -0.24 \pm 0.05$ mag/dex. It is worthy to mention that Freedman et al. (2001) used practically the same value of the γ in the final paper on the HST Key Project on the Hubble constant. However, theoretical models calculated by Romaniello et al. (2005), taking into account the variable He content, are not compatible with these observational findings.

In order to determine a reliable value of the distance modulus of the galaxy, at least the average metallicity of the host galaxy has to be known, in any case. Caputo et al.'s (2004) new method is a promising development in this respect. They pointed out that the luminosity difference between the RR Lyrae type variables and the more massive pulsators with the same period is a function of metallicity. The more massive, short period pulsators involved in this method are the so called *anomalous Cepheids*. According to the new paradigm, however, the anomalous Cepheids are classical Cepheids with extremely low metal content (Caputo et al., 2004; Marconi et al., 2004).

Knowledge of metallicity of Cepheids is, therefore, especially important for the precise calibration of the P-L relationship, i.e. to fix the bottom rung of the cosmic distance ladder.

Acknowledgements Cepheid related studies at the Konkoly Observatory are partly supported by the Hungarian OTKA grant T046207.

References:

Alcock C., Allsman R. A., Axelrod T. S., et al. (The MACHO Collaboration), 1995, *AJ*, **109**, 1653

Alcock C., Allsman R. A., Alves D. R., et al. (The MACHO Collaboration), 1999, *AJ*, **117**, 920

Alcock C., Allsman R. A., Alves D. R., et al. (The MACHO Collaboration), 2002, *ApJ*, **573**, 338

Beaulieu J.-P., Buchler J.-R., Marquette J.-B., et al., 2006, *ApJ*, (accepted), astro-ph/0610749

Bono G., Caputo F., & Castellani V., 2006, *MemSAIt*, **77**, 207

Buchler J. R., Wood R. R., Keller S., & Soszyński I., 2005, *ApJ*, **631**, L151

Buchler J. R., Yecko P. A., & Kolláth Z., 1997, *A&A*, **326**, 669
Burki G., Schmidt E. G., Arellano Ferro A., et al., 1986, *A&A*, **168**, 139
Caputo F., Castellani V., Degl'Innocenti S., Fiorentino G., & Marconi M., 2004, *A&A*, **424**, 927
Dunst L., 1932, *Astr. Nachr.*, **246**, 361
Dunst L., 1933, *Astr. Nachr.*, **247**, 309
Detre L., 1935, *Astr. Nachr.*, **257**, 361
Detre L., 1970, *Ann. Univ-Sternw. Wien*, **29**, No. 2, 79
Evans N. R., 1992, *ApJ*, **389**, 657
Evans N. R., Sasselov D. D., & Short C. I., 2002, *ApJ*, **567**, 1121
Fernie J. D., Khosnevissan M. H., & Seager S., 1995, *AJ*, **110**, 1326
Freedman W. L. & Madore B. F., 1990, *ApJ*, **365**, 186
Freedman W. L., Madore B. F., Gibson B. K. et al., 2001, *ApJ*, **553**, 47
Gieren W. P., Moffett T. J., & Barnes T. G. III, 1999, *ApJ*, **512**, 553
Hartman J. D., Bersier D., Stanek K. Z., et al., 2006, *MNRAS*, **371**, 1405
Kervella P., Mérand A., Perrin G., Coudé du Foresto V., 2006, *A&A*, **448**, 623
Klagyivik P. & Szabados L., 2006, *Publ. Astron. Dept. of Eötvös Univ.*, Budapest, **17**, 121
Kolláth Z., Buchler J. R., Szabó R., & Csubry Z., 2002, *A&A*, **385**, 932
Kovtyukh V. V., Wallerstein G., & Andrievsky S. M., 2005, *PASP*, **117**, 1173
Macri L. M., Sasselov D. D., & Stanek K. Z., 2001, *ApJ*, **550**, L159
Madore B. F., 1976, *RGO Bull.*, No182, 153
Magnier E. A., Prins S., & Augusteijn T., 1997, *A&A*, **326**, 442
Marconi M., Fiorentino G., & Caputo F., 2004, *A&A*, **417**, 1101
Mérand A., Kervella P., Coudé du Foresto V., et al., 2006, *A&A*, **453**, 155
Moskalik P., Kołaczkowski Z., & Mizerski T., 2004, in Proc. IAU Coll. 193, *Variable Stars in the Local Group*, eds. D. W. Kurtz & K. R. Pollard, ASPC 310 (San Francisco: ASP), 498
Ngeow C. & Kanbur S. M. 2006, *ApJ*, **650**, 180
Rogers F. J. & Iglesias C. A., 1992, *ApJS*, **79**, 507
Romaniello M., Primas F., Mottini M., Groenewegen M., Bono G., & François P., 2005, *A&A*, **429**, L37
Sakai S., Ferrarese L., Kennicutt R. C. Jr., & Saha A., 2004, *ApJ*, **608**, 42
Sandage A. & Tammann G. A., 2006, *ARA&A*, **44**, 93
Sandage A., Tammann G. A., & Reindl B., 2004, *A&A*, **424**, 43
Seaton M. J., Yan Y., Mihalas D., & Pradhan A. K., 1994, *MNRAS*, **266**, 805
Soszyński I., Udalski A., Szymański M., et al., 2000, *AcA*, **50**, 451
Szabados L., 1977, *Mitt. Sternw. ung. Akad. Wiss.*, Budapest, No. 70.
Szabados L., 1980, *Commun. Konkoly Obs. Hung. Acad. Sci.*, Budapest, No. 76.
Szabados L., 1997, in Proc. Conf. *HIPPARCOS Venice'97*, ed. B. Battrick, ESA SP-402, 657
Szabados L., 2003, *IBVS*, No. 5394
Sziládi K., Vinkó J., Poretti E., et al., 2006, in preparation
Turner D. G., Savoy J., Derrah J., et al., 2005, *PASP*, **117**, 207
Udalski A., Soszyński I., Szymański M., et al., 1999a, *AcA*, **49**, 1
Udalski A., Soszyński I., Szymański M., et al., 1999b, *AcA*, **49**, 45
Udalski A., Soszyński I., Szymański M., et al., 1999c, *AcA*, **49**, 223
Welch D. L., 1994, *AJ*, **108**, 1421

Stellar activity and the Konkoly Observatory: the beginnings

Katalin Oláh

Konkoly Observatory of the Hungarian Academy of Sciences
P.O. Box 67, H-1525 Budapest, Hungary
olah@konkoly.hu

The early observational facts on stellar activity are discussed with special emphasis on L. Detre's interest in those results.

Introduction

The discovery of starspots has a long history. Curiously, the establishment of the class of active stars is strongly connected with Detre's Institute. The real discovery of starspots (on AR Lac) happened just in the middle of the XXth century by Kron (1947) and soon after on two other objects. But this discovery was forgotten for more than a decade. In 1965 Chugainov (1966) made a series of observations on HDE 234677 (BY Dra) and explained the resulting light curve by starspots. That paper was published in the *Information Bulletin on Variable Stars*, which has been edited by the Konkoly Observatory from the beginnings. At that time the editor was L. Detre. Observing flare stars became popular: during 1971 *Information Bulletin on Variable Stars* published about 100 issues, and 25% of those dealt with flare stars and related objects. In 1971 the *General Catalogue of Variable Stars* announced a new class of variables, the so-called BY Dra-type stars. The final step of establishing the class of active stars is connected with an IAU Colloquium held in Budapest in 1975, which will be mentioned in the Epilogue. The interested reader may find a thorough review about the discovery of starspots in Hall's (1994) excellent work. L. Detre has been interested in this new type of variables, as in every other novelties. In what follows, a few examples of this interest is presented.

Starspots and flares

In late 1960s and early 1970s, flare stars were increasingly observed. Beside flares, rotational modulations were revealed in several cases. Some stars, like BY Dra showed

flares as well as rotational modulation. *Fig. 1* shows a light curve of HDE 234677 observed in 1966 by Krzeminski (1968), which appeared in a conference proceedings on the light variation of dM and dMe stars. At that time the star did not have a variable star designation, but slightly later aroused L. Detre's attention: he marked the name of the variable in the book. This variable was later observed with the 60-cm telescope in Budapest, and in 5 colours ($UBVR_CI_C$) with the 1-m telescope at Piszkéstető mountain station, which is also plotted in *Fig. 1.*

Photoelectric monitoring of flare stars were carried out as well in the late 1960s. Among the targets were BY Dra itself and also AD Leo. A huge flare observed in the latter object by Szeidl (1969) is shown in *Fig. 2.* These measurements clearly show, that L. Detre was interested in this new type of variable stars. At that time, in lack of clear definition, one could not call them a *new class* of variables.

Long-term variations: cycles

From the time of the discovery of starspots it was obvious to relate these features with those observed on the Sun for already centuries. Flares were thought to be huge eruptions on stellar surfaces, just like those detected on the Sun. The search for solar analogues on stars continued and Wilson (1968) initiated a long-term study for searching cycles of solar-type stars through measuring CaII H&K activity, which is continuing to date. But before this, already in 1966, L. Detre published a note of just once sentence, calling the attention on the possible presence of a spot cycle on BY Dra, as shown in *Fig. 3* (upper and middle panels). This small remark was surely among the first ones (if not exactly the first) suggesting cycles on other stars than the Sun.

In the lower part of *Fig. 3* the continuation of the long-term light variability of BY Dra is plotted. Clearly, cycles are present in the overall brightness of this system with quasiperiods of decades, about 14 and 3 years (see Oláh et al. 2000 for the details).

University classes

The author had the pleasure to attend L. Detre's classes of astronomy. Those lectures usually dealt with the newest results in variable star astronomy, which were found very useful even long after the graduation. Another topic of his lectures was solar physics, which is strongly connected with the active star research. *Figures 4* and *5* are examples of L. Detre's handwritten notes for the university lectures on the solar cycle and on the differential rotation.

Epilogue

L. Detre passed away on 1974 autumn. At that time the organization of the IAU Colloquium No. 29, *Multiple Periodic Variable Stars* which he initiated, was underway. His successor, B. Szeidl took over the conference organization, and among others, he invited Douglas S. Hall to give a review on *The RS CVn Binaries and Binaries with Similar Properties.* This talk and its published version became of fundamental importance in studying active stars: it determined the class of active stars and its subsystems, which is used (with later modifications) to date. The paper has more than 400 citations during the last 30 years by the ADS.

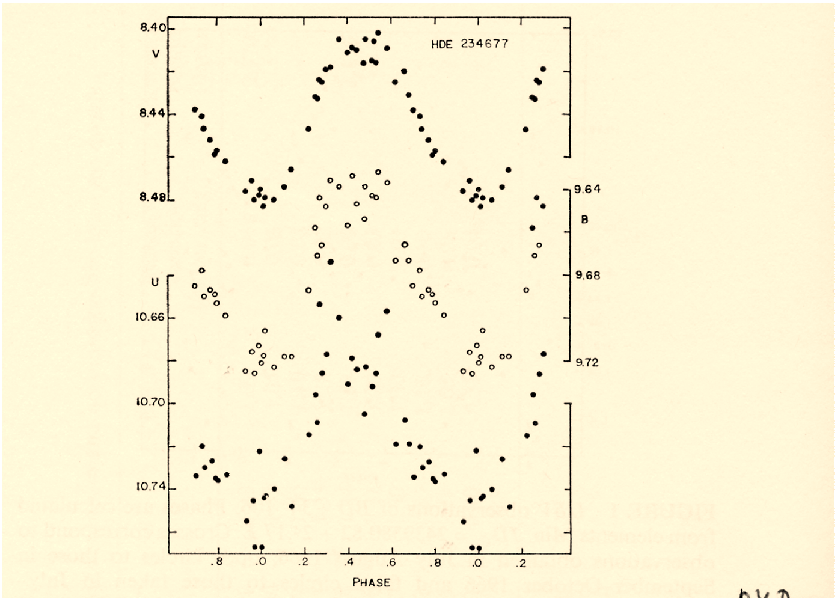

FIGURE 2 *UBV* observations of HDE 234677 in 1966. Phases are calculated from elements Min. $JD_{\odot} = 2439033.48 + 3^{d}.836\,E$.

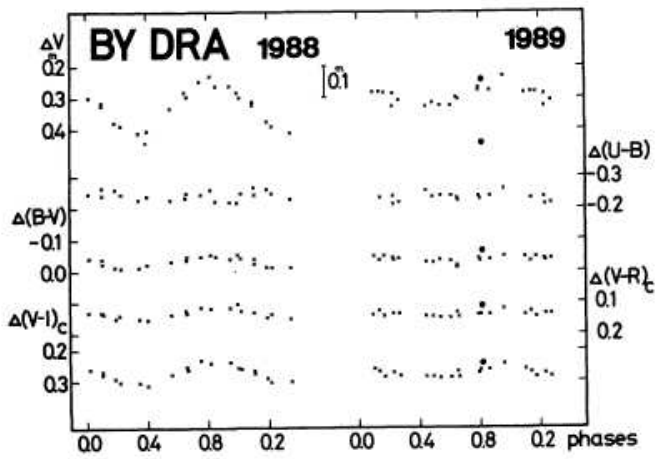

Figure 1: Top: An early light curve of HDE 234677 by Krzeminski (1968) from 1966. The star at that time did not have variable star designation. In the right corner L. Detre's handwriting is seen marking the name BY Dra of the variable. Bottom: Five colour observations of BY Dra with the 1 m telescope (see Pettersen et al. 1992).

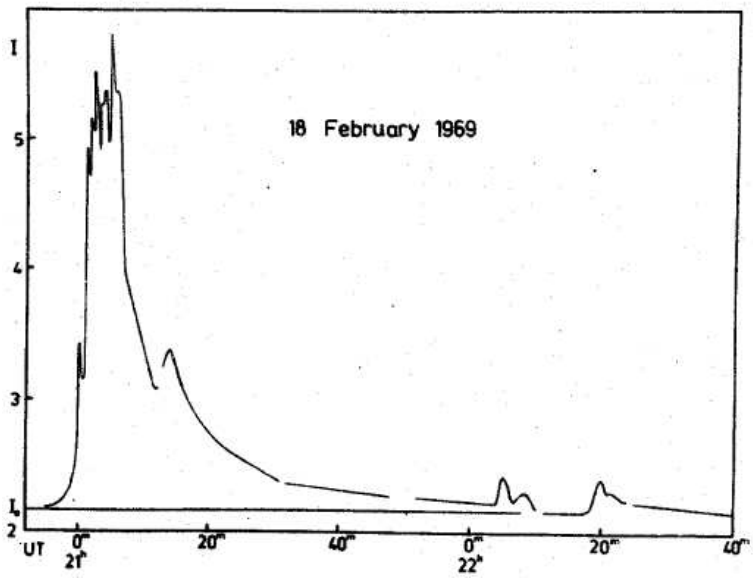

Figure 2: A flare of AD Leo observed by the 60-cm telescope of the Konkoly Observatory (Szeidl 1969).

Thus, the beginnings of stellar activity research is strongly connected with the Konkoly Observatory. It started with the rediscovery of starspots by Chugainov (1966) published in the *Information Bulletin on Variable Stars*, continued with publishing many observations there, and finished with Hall's (1976) historical talk. L. Detre played an active role in all of these.

Thirty years have passed already, and during all these years stellar activity research has been continuously developing. Simultaneously with the delivery of Hall's (1976) talk studying active stars began at the Konkoly Observatory as well, and the author of this paper, who talked about spotted stars with L. Detre as a student, finally got this subject as a lifetime project from B. Szeidl. It was a unique possibility to take part in a research field from its very beginning. At present, mapping stellar surfaces is a routine task. *Figure 6* shows the surface of an active giant star derived from spectral line profile analysis (Doppler imaging) and the modelled brightness variation from photometric measurements made in four colours by Oláh et al. (2002).

Acknowledgements Support from the Hungarian Research Grants OTKA T-043504 and T-048961 is acknowledged.

References:

Chugainov P.F., 1966, *IBVS*, **No. 122**
Chugainov P.F., 1971, *IBVS*, **No. 520**
Detre L., 1971, *IBVS*, **No. 520**
Hall D.S., 1976, in *Multiple Periodic Variable Stars*, IAU Coll. No. 29, ed. W. S. Fitch, Budapest, Akadémiai Kiadó, p. 287
Hall D.S., 1994, *IAPPP Comm.*, **No. 54**, 1
Kron G.E., 1947, *PASP*, **59**, 261
Krzeminski W., 1968, in *Light Variability of dMe and dM stars*, Gordon and Breach Science Publishers, ed. S. S. Kumar, p. 56

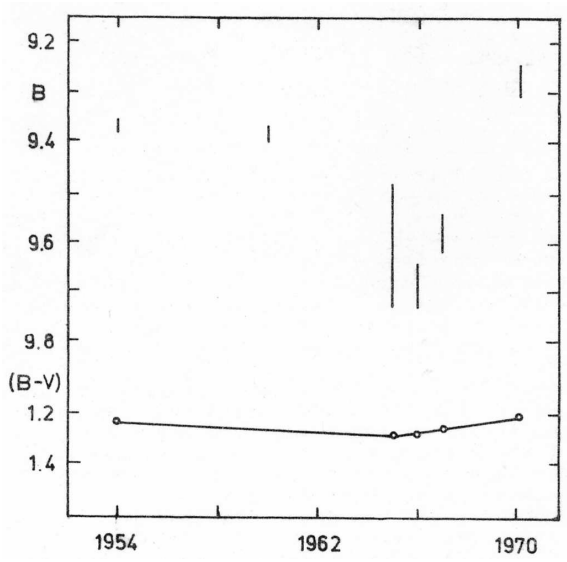

Editor's note:

The continuous observation of Chugainov's stars would be extremely important because diagrams like that on the opposite page may reveal the existence of cycles similar to the solar cycle in these stars.

L. DETRE

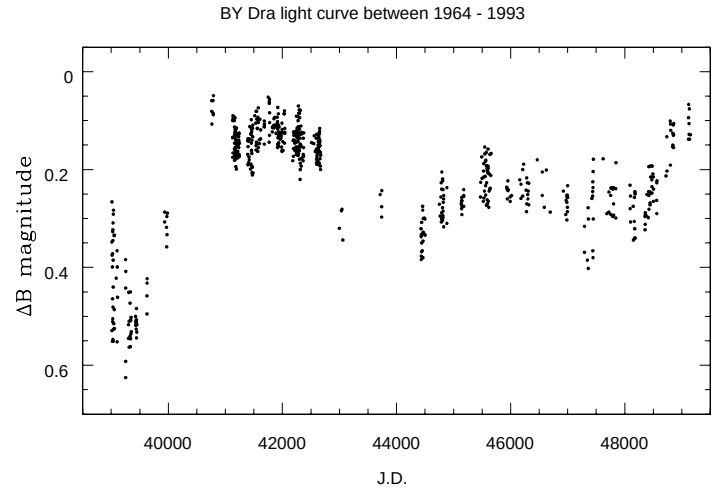

Figure 3: Top: Long-term brightness change of BY Dra by Chugainov (1971), and L. Detre's editorial note, commenting the figure. Bottom: the brightness change of BY Dra during almost 30 years, from the literature.

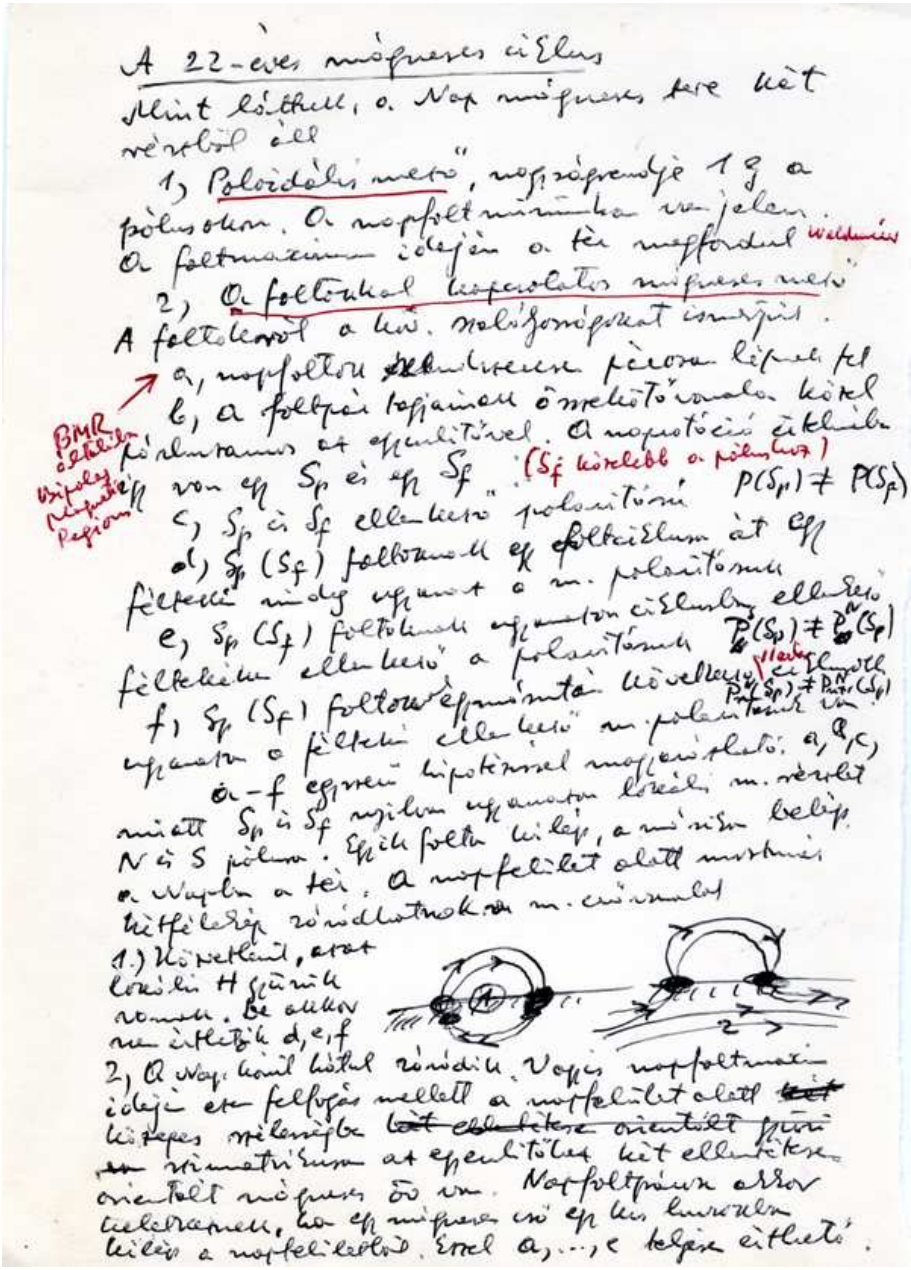

Figure 4: Excerpt from L. Detre's handwritten notes preparing the university classes, about the solar cycle (in Hungarian).

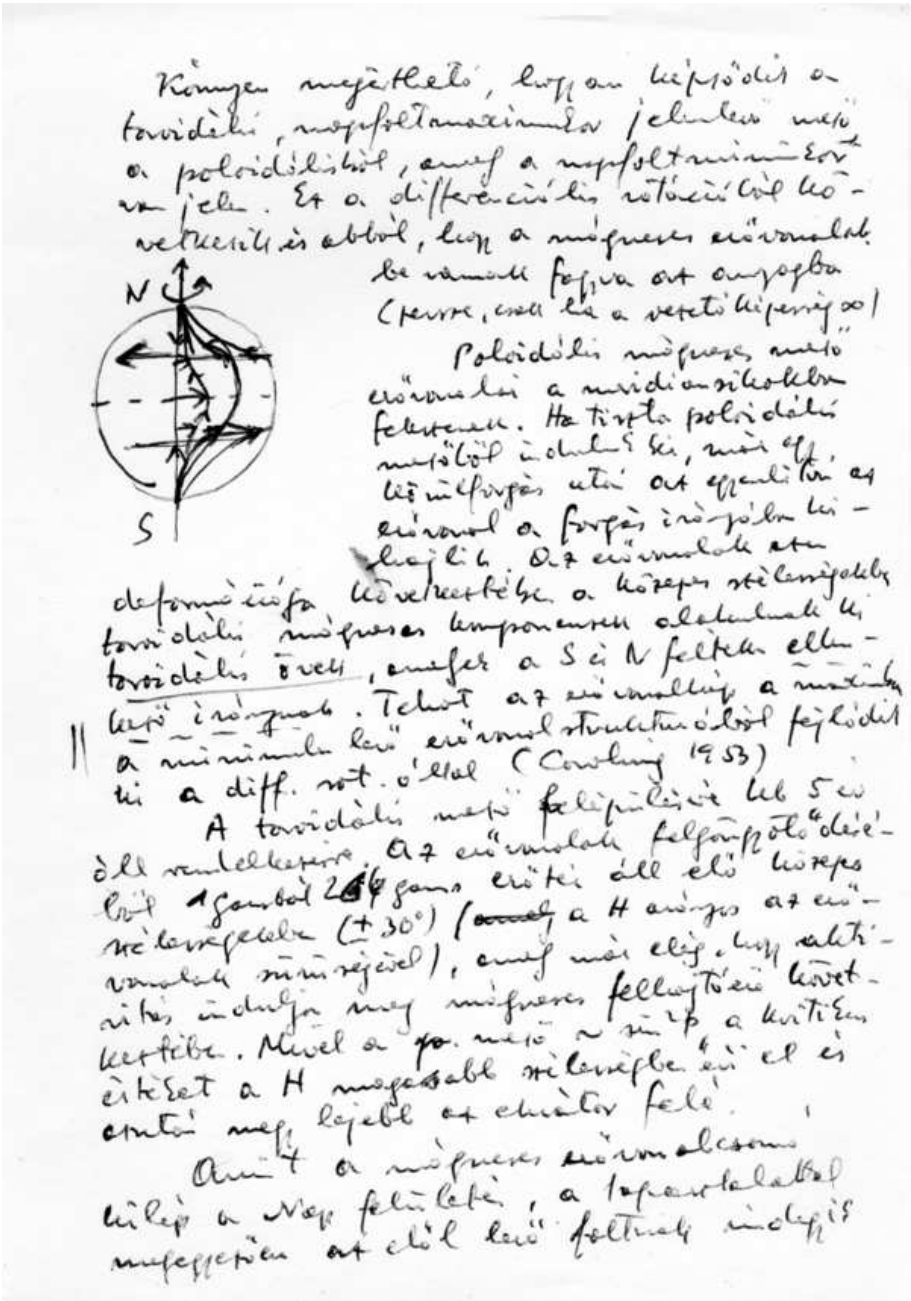

Figure 5: Same as *Fig. 4*, about the poloidal and toroidal magnetic fields, and the differential rotation of the Sun (in Hungarian).

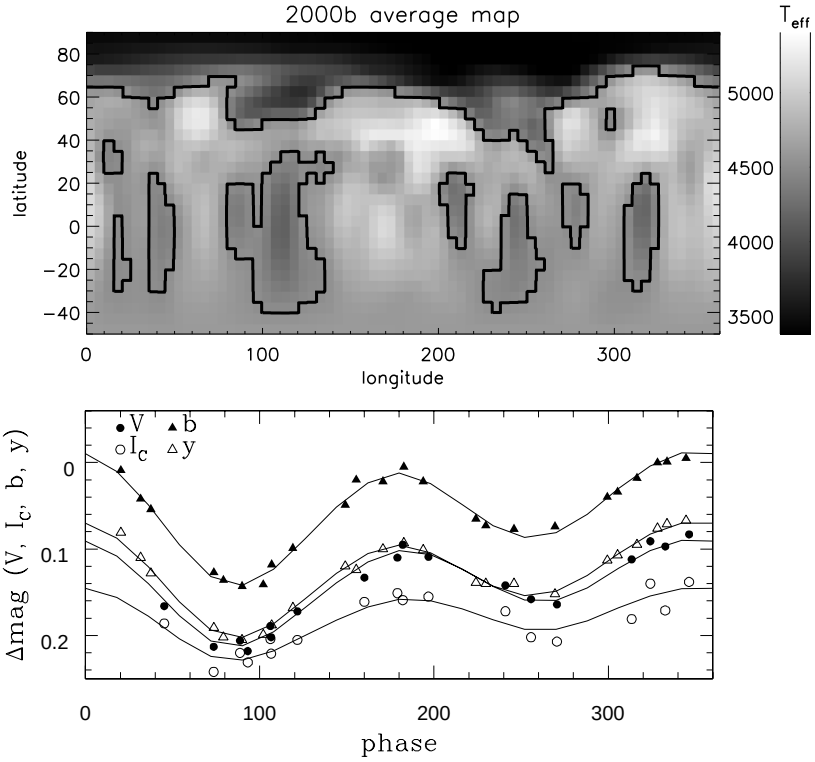

Figure 6: An example for the recent possibilities for modelling stellar surface structure: a surface temperature distribution map (Doppler image) of UZ Lib from high resolution spectra, and modelled light curves in 4 colours, for the same time interval (Oláh et al. 2002).

Oláh K., Strassmeier K. G., & Weber M., 2002, *A&A*, **389**, 202
Oláh K., Kolláth Z., & Strassmeier K. G., 2000, *A&A*, **356**, 643
Pettersen B. R., Oláh K., & Sandmann W. H., 1992, *A&AS*, **96**, 497
Szeidl B., 1969, *IBVS*, **No. 345**
Wilson O.J., 1968, *ApJ*, **153**, 221

Spectroscopic studies of star forming regions

Mária Kun

Konkoly Observatory of the Hungarian Academy of Sciences
P.O. Box 67, H-1525 Budapest, Hungary

This paper reviews the results of studies of star forming regions, carried out at the Konkoly Observatory in the last two decades. The studies involved distance determination of star-forming dark clouds, search for candidate pre-main sequence stars, and determination of the masses and ages of the candidates by spectroscopic follow-up observations. The results expanded the list of the well-studied star forming regions in our galactic environment. Data obtained by this manner may be useful in addressing several open questions related to galactic star forming processes.

Introduction

The first instrument of the Piszkéstető Observatory, the 60/90/180 cm Schmidt telescope with two objective prisms has been a precious part of Detre's legacy. We inherited with this instrument a challenge to probe new paths of research, inspired by the attributes of the Schmidt telescope, and use techniques apparently very different from those of variable star researches, our most important scientific heritage.

The telescope with its field of view of 5 degrees was suitable for performing homogeneous, moderate-accuracy photographic photometry and low-dispersion slitless spectroscopy of large number of stars simultaneously. Traditional topics for Schmidt telescopes equipped with objective prisms included studying the space distribution of the stars and the light-absorbing diffuse matter in our galactic neighbourhood. Detre's early paper (Dunst, 1929) testifies that this subject was close to his scientific interest at the beginning of his career. Searching for objects of peculiar spectra in objective prism plates is another suitable project for this instrument. This kind of study has to be followed by slit spectroscopy of the selected objects, in order to establish their real nature. Galactic star forming regions, extending over large volumes of space and containing large amount of interstellar gas and dust, as well as young stellar objects of emission spectra are suitable targets for both kinds of Schmidt surveys. During the past two decades several star forming regions were discovered and studied using the Schmidt telescope with the 5-degree

objective prism. The studies included distance determination and identifying optically visible pre-main sequence stars. The follow-up spectroscopic studies of the candidate pre-main sequence stars have been performed with larger telescopes available thanks to the OPTICON project. In this paper I introduce some star forming regions whose basic properties have been determined using the Schmidt telescope at Piszkéstető.

Star forming regions

- Open issues of star formation

Several important properties of the star forming processes can be understood only by comprehensive, large-scale, multi-wavelength studies of star forming regions. For instance, complete mapping and detailed photometric and spectroscopic studies of the young stellar population are required for establishing the stellar initial mass function, the age distribution of young stars, and studying the time scale of star formation. Both the star forming cloud and the stars born in it have to be mapped in order to study the efficiency of the star forming process and its propagation within the cloud.

Another group of open questions cannot be answered by detailed studies of a single nearby star forming region, but requires comparison of several regions. Which properties of molecular clouds influence the time scale and efficiency of star formation, the clustered and isolated modes, and the mass spectrum of the newborn stars? How does the early evolution of the stars depend on the environment of the star formation? Is star formation a fast and dynamic process governed by supersonic turbulence or rather a slow, quasistatic process controlled by static magnetic fields? To answer these questions, the stellar content of several star forming regions has to be assessed, and then the mass and age distributions of young stellar objects over the whole area of the star forming region, as well as the spectral energy distribution, characterizing the circumstellar environments of the young stars have to be determined.

- Scope of our researches

In the 1980's the development of the millimetre-wave radio astronomy led to the discovery of a large population of molecular clouds outside the galactic plane ($|b| > 10^{\circ}$). Part of them are smaller and more transparent than their galactic plane siblings. The discovery of the new molecular clouds aroused new problems: How far are the newly discovered molecular clouds from us? Do they form low-mass stars? Objective prism observations of the molecular cloud regions and follow-up spectroscopy provide the most suitable means of finding the answers to the questions.

We selected for studies molecular clouds which have already been mapped in ^{12}CO or/and ^{13}CO. Some of the target clouds also have shown evidence of low-mass star formation, e.g. embedded *IRAS* sources are associated with them. These clouds certainly contain a less conspicuous population of young pre-main sequence stars. The goal of our studies is to derive some basic properties of the selected star forming regions: to determine their distances, to assess the number of pre-main sequence stars, as well as to estimate their mass and age distributions. The first steps of the studies were based on objective prism observations using the 60/90/180 cm Schmidt telescope of the Konkoly

Observatory. Follow-up observations of the candidate pre-main-sequence stars have been carried out with various optical telescopes.

Methods

- *Distance determination*

In determining distances to nearby molecular clouds their interactions with the light of embedded or background stars can be utilized. While distances of normal stars can be determined from their apparent and absolute magnitudes (spectral types and colours), no properties of dark clouds indicate how far they are located from us. This is especially true for nearby clouds, whose galactic orbital velocities are close to the solar value. Neither the young, embedded stars are good distance indicators, because their luminosities strongly decrease during the pre-main sequence evolution. Extinction of starlight by the dust content of the cloud, interstellar absorption lines in the spectra of background stars, and embedded stars illuminating reflection nebulae can be used for distance determination. Distance is a basic data, which is important for determining the size and mass of the cloud, and the absolute luminosities of young stars.

In order to determine the distances of the selected clouds we examined the cumulative distribution of the field star distance moduli along the line of sight to the clouds. If $y = V - M_{\rm V}$ is the distance modulus of the stars, and $N(y)$ denotes the number of stars whose distance modulus is smaller than y (i.e. brighter than $V = M_{\rm V} + y$), then the distance modulus for distances smaller than that of the obscuring cloud can be written as $y = V - M_V = 5 \log r - 5$, whereas behind the cloud it is $y = 5 \log r - 5 + A_V$, where A_V is the visual extinction caused by the cloud. Thus the presence of a cloud along the line of sight shows up as a distortion in the shape of the $logN(y)$ *vs.* y curve (*Wolf diagram*), and its distance modulus can directly be read from the diagram.

The absolute magnitudes of stars were estimated from their objective prism spectral types. The spectra were obtained with the Schmidt telescope of the Konkoly Observatory equipped with a UV-transmitting objective prism having a refracting angle of 5° and a dispersion of 580 Å/mm at Hγ. The field of view of the telescope was 19.5 square degrees. Absolute magnitudes of stars belonging to different spectral classes were taken from Allen (1973) and Cox (1999). For calculating the apparent distance moduli $V - M_{\rm V}$ of the stars the V magnitudes listed in the *Guide Star Catalog* were used.

In this manner the distances of the dark clouds L 694 (Kawamura et al., 2001), L 1228, L 1235, L 1241, L 1251, L 1261 (Kun, 1998), L 1333 (Obayashi et al., 1998), and L 1340 (Kun et al., 1994) were determined. During this work spectral types of some 5000 stars have been determined visually, on objective prism plates.

An example for the Wolf diagram, showing the distribution of stellar distance moduli in the region of L1333, is shown in *Fig. 1.* The number of stars is normalized to one square degree. Filled circles connected by solid line show the cumulative distribution of distance moduli determined for a field of 19 square degrees centered on the cloud, and the dashed line is the reference curve displaying the same distribution without extinction at the galactic latitude of the cloud, +15°. The error of this kind of distance determination can be estimated as $\pm$ 10 percent, from the accuracy of spectral classification and the GSC magnitudes, as well as from the number of stars involved in the curves (Obayashi et al., 1998).

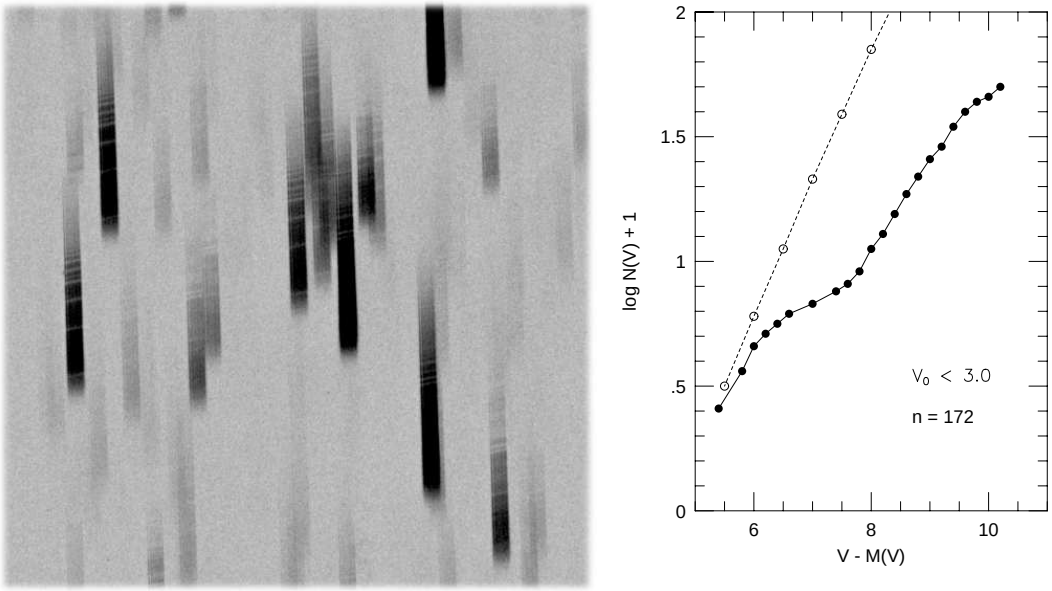

Figure 1: *Left*: Part of a blue-sensitive (emulsion type IIaO) objective prism plate obtained with the Schmidt telescope through the 5-degree prism. *Right*: Plot of $logN(V)$ vs. $V - M_V$ for the stars with $M_V < 3.0$. *N(V)* is the number of stars with apparent magnitudes brighter than V within 1 deg^2. The dashed line indicates the absorption-free reference curve.

- Search for candidate pre-main sequence stars

I have been searching for pre-main sequence star candidates using objective prism spectra taken with the Schmidt telescope through a red filter. The dispersion of the objective prism is about 2000 Å/mm at Hα. *Fig. 2* shows an example of a plate taken through a red (Schott RG 1) filter. *Fig. 3* shows examples of the objective prism spectra of various Hα emission objects obtained with the Photometrics CCD camera installed on the Schmidt telescope. The wavelength scale of the very low dispersion spectra was established in possession of the geometric and optical properties of the prism and camera, and using the atmospheric A-band at 7600 Å as reference wavelength. The quality of such a low dispersion slitless spectrum highly depends on the atmospheric conditions. This method is suitable for finding classical T Tauri stars, displaying strong Hα emission (EW(Hα) $\geq$10 Å). In addition to the objective prism spectra, infrared point sources of the *IRAS* Point Source Catalog and Faint Source Catalog were used to find further pre-main sequence stars born in the selected clouds.

- Spectroscopic follow-up observations

The real nature of the selected stars has to be established by medium-resolution spectroscopic follow-up observations. We performed spectroscopic observations of a few regions studied earlier with the objective prism using different telescopes and instruments: the *Intermediate Dispersion Spectrograph* on Isaac Newton Telescope, La Palma, *CAFOS* on the 2.2 m telescope of Calar Alto Observatory, as well as *ALFOSC* on the Nordic Optical Telescope. The spectra were used for determining the spectral types of the stars and

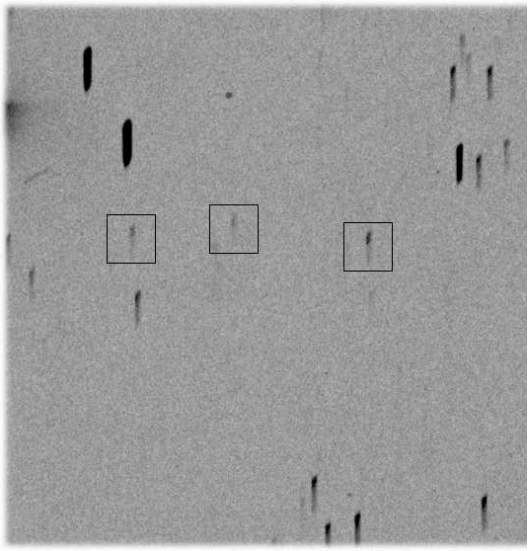

Figure 2: Objective prism image of the northern core of the dark cloud Lynds 1251. Part of a plate taken on Kodak 098-02 emulsion and through an RG1 filter with an exposure time 60 min. The images of three Hα emission stars are framed.

for establishing their pre-main sequence nature. Criteria for classification are described in Kirkpatrick et al. (1991), Preibisch et al. (2001), and Martín & Kun (1996). Several candidate pre-main sequence stars proved to be field stars without Hα emission. Nevertheless, a number of classical T Tauri stars were found in molecular clouds where no pre-main sequence stars had been identified earlier.

Results

- Low-mass star formation in small molecular clouds

Star forming molecular clouds tend to be parts of giant molecular complexes. The small translucent clouds found at high galactic latitudes usually are not associated with prominent signposts of star formation, such as far-infrared point sources. Our objective prism search for pre-main sequence stars at high galactic latitudes in most cases had negative results: spectroscopic follow-up observations have not confirmed the pre-main sequence nature of the candidate stars picked up from the photographic plates (Martín & Kun, 1996). The following sections show a few exceptions.

— The Lynds 134 complex

The members of this complex are the small dark clouds L 134, L 169, L 183, L 1780, located at a distance of 110 pc from us (Franco, 1989). No star formation was found earlier in the L 134 complex. The first star formation signpost in this region was the very low mass, young T Tauri star (spectral type: M 5.5IV) found during our survey (Martín & Kun, 1996) at an angular distance of 5 arcmin (0.16 pc) from the dense core L 183*i* (Laureijs et al., 1995). The radial velocities of the cloud and the star are close to each other, suggesting that the star was born in the cloud a few million years ago. The pre-protostellar condensations revealed recently in the same cloud by far-infrared and submm observations (Lehtinen et al., 2003) indicate ongoing star formation in L 183.

We found a binary system of very low mass, weak-line T Tauri stars (spectral types: M4V and M5IV) in the same region, to the west from the cometary cloud L 1780. The

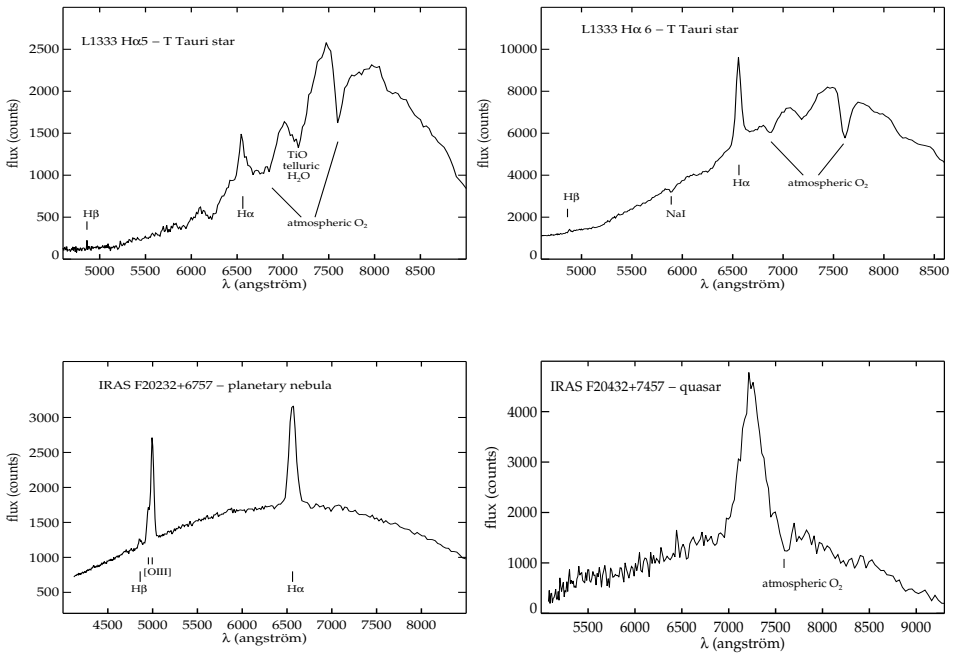

Figure 3: Objective prism spectra of various objects shown up as Hα emission stars. Position of the Hα line and the *A*-band of the atmospheric oxygen are indicated.

morphology of the region suggests that both the cometary shape of L 1780 and the formation of the low-mass stars were triggered by stellar winds form the Sco-Cen association (see Tóth et al., 2003).

— *IC 2118*

IC 2118 is an extended reflection nebulosity at high galactic latitude ($27^\circ < b < 33^\circ$), illuminated by β Orionis. It is situated at a distance of 210 pc from the Sun, and at some ten degrees to the west from the Orion star forming region. The bright nebula is associated by several small molecular clouds (Kun et al., 2001), among others MBM 21 and 22 (Magnani et al., 1995). Two young stellar object (YSO)-like *IRAS* sources, *IRAS* 04591−0856 and *IRAS* 05050−0614 are indicative of ongoing low-mass star formation in this region. Follow-up spectroscopic studies of our Hα emission stars selected as pre-main sequence star candidates, performed with the *ALFOSC* spectrograph on Nordic Optical Telescope, resulted in the discovery of five classical T Tauri stars (cTTS) projected on the molecular clouds (Kun et al., 2004). Their distribution is shown in the left panel of *Fig. 4*, overlaid on the *IRAS* 100μm image of the region. The spectra and the JHK photometric data of the 2MASS All Sky Survey (Cutri et al., 2003) made it possible to determine the effective temperature $T_{\rm eff}$ and luminosities $L/L_\odot$ of the young stars. The spectra of the T Tauri stars of IC 2118 are shown in the right panel of *Fig. 4*, and their positions in Hertzsprung–Russell diagram can be seen in *Fig. 5*.

The molecular clouds associated with IC 2118 are among the smallest known star form-

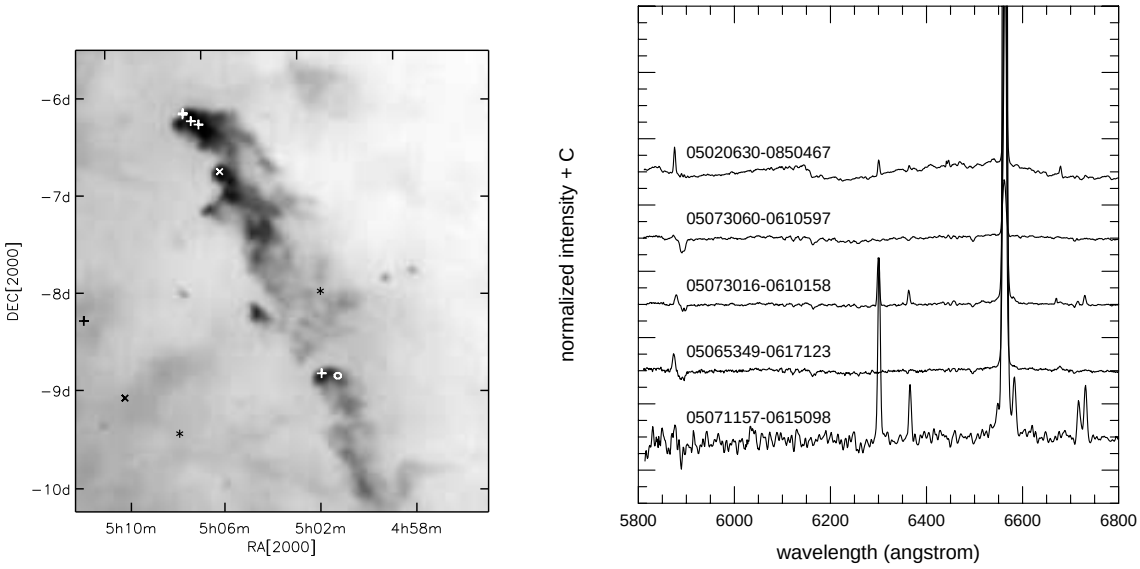

Figure 4: *Left*: Distribution of classical T Tauri stars on the 100μm IRAS map of IC 2118. *Right*: Optical spectra of classical T Tauri stars in IC 2118 over the wavelength region 5800–6800 Å.

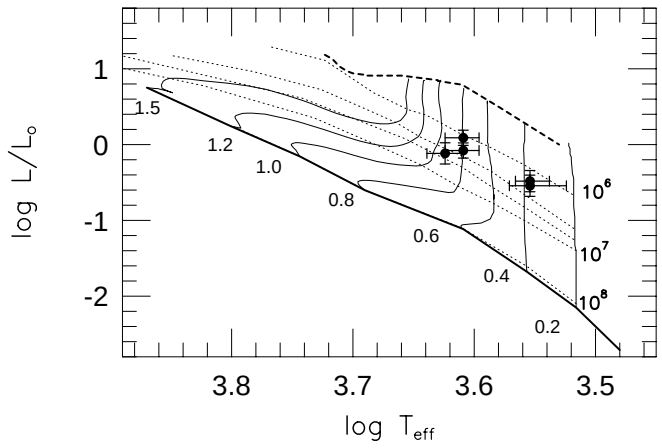

Figure 5: Location of the IC 2118 pre-main-sequence stars in the Hertzsprung–Russell diagram, together with the pre-main-sequence evolutionary tracks and isochrones published by (Palla & Stahler, 1999).

ing clouds. They probably lie near the surface of the *Orion–Eridanus Bubble*, being blown by the stellar winds and supernova explosions of the massive stars of Orion OB1 during the past ten million years. Given the large line-of-sight distance between the clouds and Orion OB1, star formation in this region propagates not only from the east to the west, but also towards us. The ages of the pre-main sequence stars found in the clouds are compatible with the assumption that star formation has been triggered by the superbubble. The complicated geometry and wind history of the OB association (Brown et al., 1995) hinders any detailed speculation on the exact position and age of the sources of trigger. Recently observations by the Spitzer Space Telescope revealed several very low mass young stars in these clouds.

- L 1333

L 1333 is a small dark cloud in Cassiopeia. The basic properties of the cloud and its environment were studied by Obayashi et al. (1998) within the framework of the collaboration between the Konkoly Observatory and the Radio Astronomy Laboratory of Nagoya University. We obtained a distance of 180 ± 30 pc for the cloud. ^{13}CO and C^{18}O observations revealed that the dark cloud is a part of a filamentary molecular complex, consisting of small dense clumps separated by some 6 pc from each other along a narrow line. The total mass of the complex, determined from the molecular observations, is about $720\,M_\odot$. Star formation is indicated by the protostellar-like *IRAS* source *IRAS* 02086+7600. Our objective prism and subsequent spectroscopic studies of L 1333 (Kun et al., 2006) revealed four classical T Tauri stars in the region of L 1333, associated with the *IRAS* sources F02084+7605, 02103+7621, and 02368+7453. One of the *IRAS* sources, *IRAS* 02103+7621 (OKS Hα 6 in Obayashi et al., 1998) proved to be a visual binary, whose both components are cTTS, separated by about 1.8 arcsec (corresponding to ~ 320 AU at 180 pc).

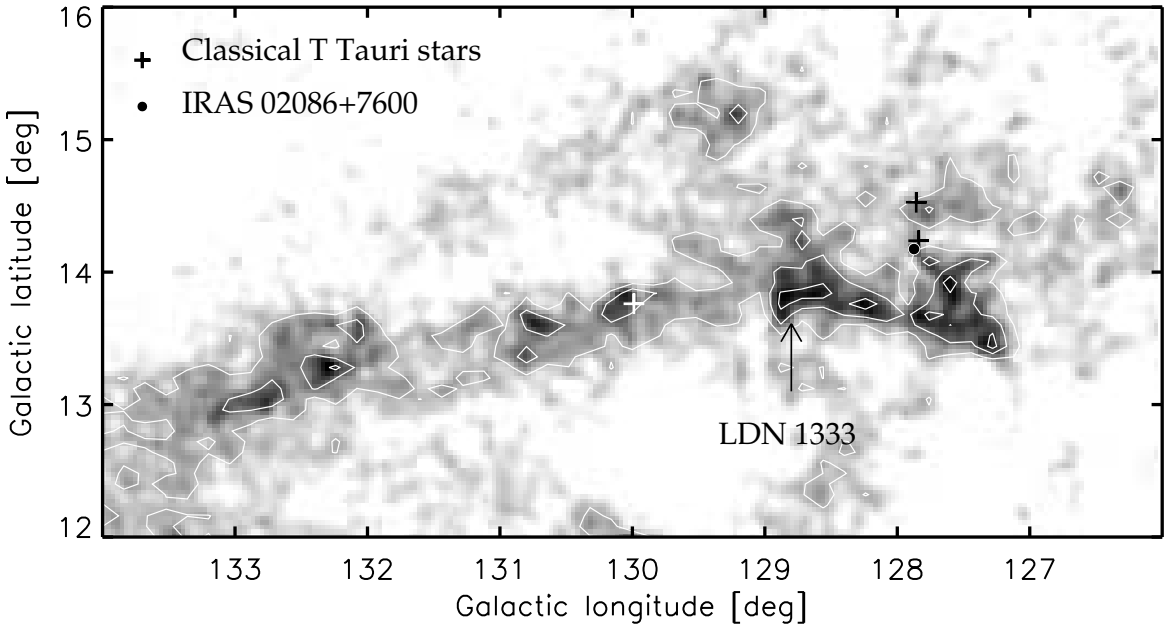

Figure 6: Distribution of the visual extinction and the young stars in the region of L 1333.

The positions of the young stars mark two star-forming clumps along the filamentary cloud complex. Compared to other nearby star forming regions these star forming clumps are very small, similar to those found at high galactic latitudes ($24\,M_\odot$ and $15\,M_\odot$, respectively; Obayashi et al., 1998). The filamentary morphology of the cloud complex resembles the L 1495–B 211–B 213–B 216 system in Taurus, but the separation of dense clumps along the filament is larger, and the star formation efficiency is smaller in L 1333 than in Taurus. *Fig. 6* shows the distribution of the visual extinction in the region containing L 1333 (Dobashi et al., 2005). The position of the dark cloud and the young stellar objects are marked. *Fig. 7* shows the optical spectra of the young stars, obtained with the Nordic Optical Telescope, as well as their positions in the $\log T_{\rm eff}$ vs. $\log L$ diagram.

Like in IC 2118, the star forming cores of L 1333 are significantly smaller than those of other well known nearby star forming regions (e.g. Taurus, Ophiuchus, Chamaeleon, Lupus). Interestingly, the young stars are located on the high galactic latitude side of the

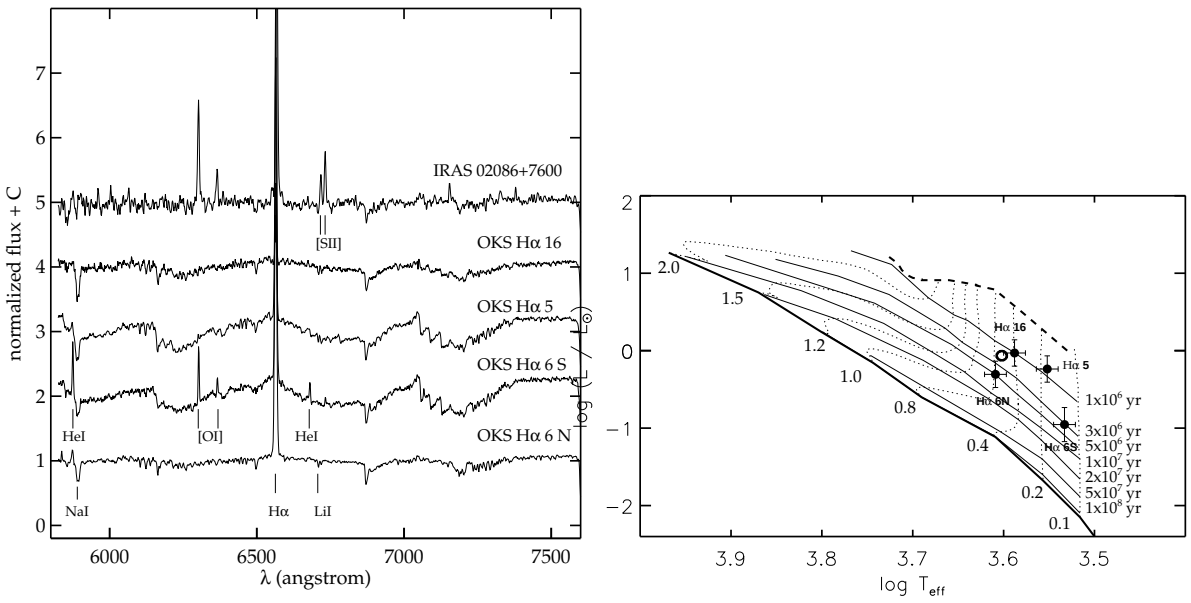

Figure 7: *Left*: Optical spectra of the young stellar objects in Lynds 1333. *Right*: Location of the same stars in the HRD, together with the pre-main-sequence evolutionary tracks and isochrones published by Palla & Stahler (1999).

cloud, so that the oldest member of the group lies farthest from the cloud. Star formation in such small clumps is thought to be assisted by an external trigger. The observed morphology of the L 1333 region suggests that the source of the trigger lies probably at the higher galactic latitudes (Kun et al., 2006).

- *The Cepheus flare giant molecular complex*

The interstellar matter in the Cepheus at $100^\circ < l < 120^\circ$ and $b > 10^\circ$ is distributed over large spatial and velocity range (see e.g. Heiles, 1967; Lebrun, 1986; Yonekura et al., 1999). Molecular gas has been observed in the radial velocity interval $-15\,\mathrm{km\,s^{-1}} < v_{LSR} < +5\,\mathrm{km\,s^{-1}}$ (Grenier et al., 1989; Yonekura et al., 1999). The nearby giant molecular complex of the Cepheus flare is comparable in mass with the Taurus, Ophiuchus, and Chamaeleon complexes.

I determined the distances of the absorbing clouds using optical star counts (Kun, 1998), and found three absorbing layers, located at 200, 300 and 450 pc from the Sun, and equally at $z \approx 90\,\mathrm{pc}$ from the galactic plane. Farther away, at 600–800 pc from us, the outer regions of the associations Cep OB2 and Cep OB3 are projected on the southern part of the Cepheus flare. Our study of A-type stars of the region having far-infrared excess confirmed this space distribution of the clouds (Kun, Vinkó, & Szabados, 2000). This morphology suggests that the clouds are part of a larger interstellar structure parallel to the galactic plane. Recently, Olano, Meschin, & Niemela (2006) have shown that the interstellar matter in the Cepheus flare is distributed over the surface of an expanding shell. The presence of the shell can account for the different distances of the dark clouds of the region.

I detected more than a hundred candidate pre-main-sequence stars over an area of some 200 square degrees, covered by the clouds. Their distribution suggests that the three cloud complexes differ from each other in star forming activity. No high-mass

star formation can be observed in the Cepheus flare region. Low-mass YSOs can be found in the component at 200 pc (L 1228) and in the 300 pc component (NGC 7023, L 1235, L 1251). The most distant component of the region can be found at the southern boundary of the complex. We searched for intermediate-mass pre-main sequence stars among the A and B type stars of the region exhibiting infrared excess, and identified a new Herbig Ae star, BD +68°1118 (Kun, Vinkó, & Szabados, 2000). This star, together with a neighbouring HAe star HD 203024, is projected on a relatively transparent region of the cloud complex close to the star forming globule L 1177 (CB 230).

Spectroscopic follow-up observations of the candidate pre-main sequence stars were carried out using the 2.2 m telescope of Calar Alto Observatory. BVR_CI_C photometric observations of the same stars are in progress. The first results are published by Eredics & Kun (2003).

- L 1340: A region of intermediate-mass star formation

It is well known that high mass stars are born as members of dense clusters in giant molecular clouds, whereas small, cold cores give birth to one or a few solar type stars. The transition from isolated to clustered mode of star formation occurs smoothly in molecular clouds forming intermediate mass stars.

Lynds 1340 is a molecular cloud in Cassiopeia, near (l,b)=(130,11), and associated with the reflection nebula DG 9 (Dorschner & Gürtler, 1966) illuminated by B and A-type stars. The small nebulosities RNO 7, 8, and 9 (Cohen, 1980), associated with the cloud, are probably signposts of recent star formation. We studied the structure and young stellar objects of Lynds 1340 in order to find how this birthplace of Herbig Ae/Be stars fits into the sequence of star forming environments.

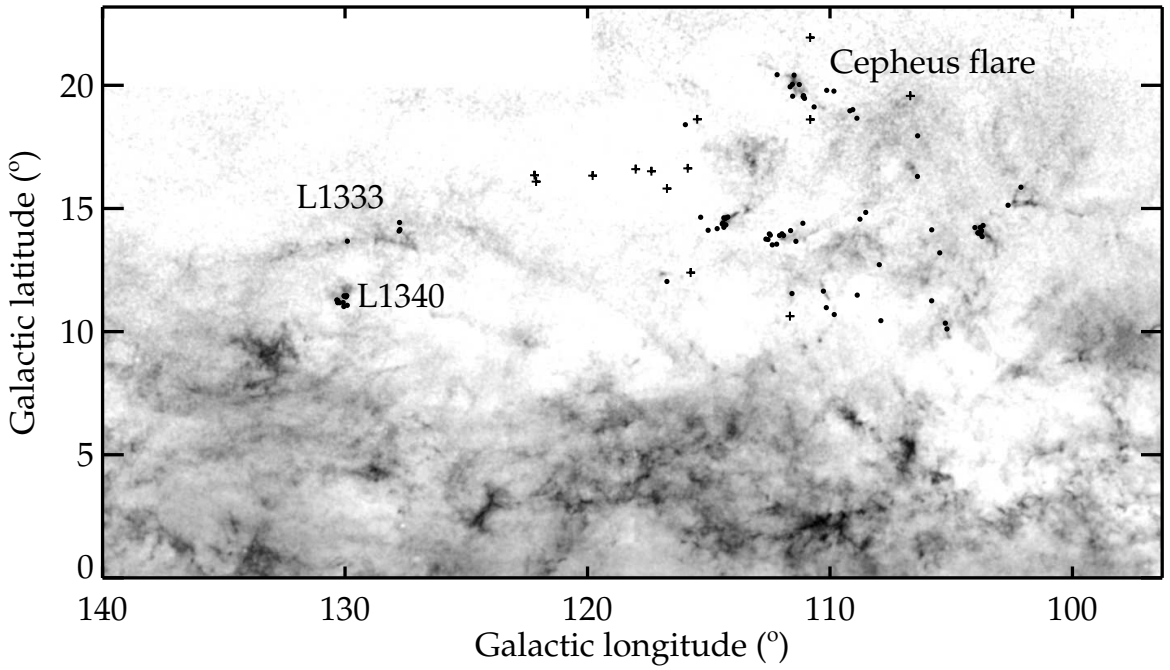

Figure 8: Distribution of the visual extinction and the young stars in the Cepheus–Cassiopeia region.

The basic properties of the cloud are studied within the framework of the collaboration between the Konkoly Observatory and the Radio Astronomy Laboratory of Nagoya University (Kun et al., 1994). ^{13}CO and C^{18}O maps of the cloud, obtained with the 4-m radio telescope of Nagoya University, distance determination, and a list of the candidate young stellar objects have been presented. The distribution of ^{13}CO has revealed three clumps within the cloud, each associated with a number of *IRAS* point sources and Hα emission stars. The total mass of the molecular cloud is some 1300 $M_\odot$. Follow-up spectroscopic, as well as optical and infrared photometric observations of L 1340 revealed that a star as massive as some 6 $M_\odot$ has been born in the cloud. This Herbig Be star is a member of the embedded cluster RNO 7, consisting of some 25 stars. Follow-up radio observations in the 1.3 cm inversion lines of the ammonia molecule have shown that several dense cores, future sites of star formation are embedded in L 1340 (Kun et al., 2003). Our results inspired several further studies of this interesting star forming region. For instance, Nanda Kumar et al. (2002) and Magakian et al. (2003) discovered several Herbig–Haro objects powered by the young stars embedded in the cloud. Submillimeter observations by O'Linger et al. (2006) revealed protostellar objects at very early stages of star formation.

The surface distribution of the young stellar objects in the Cepheus–Cassiopeia region at latitudes $b > +10^\circ$, discovered with the Schmidt telescope, is displayed in *Fig. 8* on the large-scale extinction map of the region (Dobashi et al., 1995).

Future prospects

The newly discovered nearby star forming regions are good targets for more sensitive observations, aimed at revealing the whole stellar populations born in them. Their comparison with the few well-known nearby star forming regions (Orion, Taurus, Chamaeleon, Lupus) may shed light on hidden laws of star forming processes. Further spectroscopic and photometric studies of the pre-main-sequence stars discovered will allow us to study some environmental effects of early stellar evolution.

Acknowledgements The researches presented in this paper have been supported by the OTKA grants T 022946, T 034584, and T 049082.

References:

Allen C. W., 1973, *Astrophysical Quantities*, Athlone Press, London
Brown A.G.A., Hartmann D., & Burton W., 1995, *A&A*, **300**, 903
Cohen M., 1980, *AJ*, **85**, 29
Cox A. N. (editor), 1999, *Allen's Astrophysical Quantities, Fourth Edition*, Springer
Cutri R. M., Skrutskie M. F., van Dyk S., et al., 2003, VizieR On-line Data Catalog: II/246
Dobashi K., Uehara H., Kandori R., Sakurai T., Kaiden M., Umemoto T., & Sato F., 2005, *PASJ*, **57**, S1
Dorschner J. & Gürtler J., 1966, *AN*, **289**, 57
Dunst L., 1929, *Mitt Sternw. ung. Akad. Wiss.*, Budapest, No. 1
Eredics M. & Kun M., 2003, in *The interaction of stars with their environments II*, eds. Cs. Kiss et al., Comm. Konkoly Obs., Budapest, No. 103, p. 27
Franco G. A. P., 1989, *A&A*, **223**, 313

Grenier I. A., Lebrun F., Arnaud M., et al., 1989, *ApJ*, **347**, 231
Hartmann D. & Burton W. B., 1997, *Atlas of Galactic Neutral Hydrogen*, Cambridge Univ. Press
Heiles C., 1967, *ApJS*, **15**, 97
Kawamura A., Kun M., Onishi T., Vavrek R., Domsa I., Mizuno A., & Fukui Y., 2001, *PASJ*, **53**, 1097
Kirkpatrick J. D., Henry T. J., & McCarthy D. W., 1991, *ApJS*, **77**, 417
Klessen R. S., Heitsch F., & Mac Low M.-M., 2000, *ApJ*, **535**, 887
Kun M., 1998, *ApJS*, **115**, 59
Kun M. & Prusti T., 1993, *A&A*, **272**, 235
Kun M., Obayashi A., Sato F., Yonekura Y., Fukui Y., Balázs L. G., Ábrahám P., Szabados L., & Kelemen J., 1994, *A&A*, **292**, 249
Kun M., Vinkó J., & Szabados L., 2000, *MNRAS*, **319**, 777
Kun M., Aoyama H., Yoshikawa N., Kawamura A., Yonekura Y., Onishi T., & Fukui Y., 2001, *PASJ*, **53**, 1063
Kun M., Wouterloot J. G. A., & Tóth L. V., 2003, *A&A*, **398**, 169
Kun M., Prusti T., Nikolić S., Johansson L. E. B., & Walton N. A., 2004, *A&A*, **418**, 89
Kun M., Nikolić S., Johansson L. E. B., Balog, Z., & Gáspár A., 2006, *MNRAS*, **371**, 732
Laureijs R. J., Fukui Y., Helou G., Mizuno A., Imaoka K., & Clark F. O., 1995, *ApJS*, **101**, 87
Lebrun F., 1986, *ApJ*, **306**, 16
Lehtinen K., Mattila K., Lemke D., Juvela M., Prusti T., & Laureijs R., 2003, *A&A*, **398**, 571
Magakian T. Yu., Movsessian T. A., & Nikogossian E. H., 2003, *Astrophysics*, **46**, 1
Magnani L., Blitz L., & Mundy L., 1985, *ApJ*, **295**, 402
Martín E. L. & Kun M., 1996, *A&AS*, **116**, 467
Nanda Kumar, M. S., Anandarao B. G., & Yu K. C., 2002, *AJ*, **123**, 2583
Obayashi A., Kun M., Sato F., Yonekura Y., & Fukui Y., 1998, *AJ*, **115**, 274
Olano C.A., Meschin P.I., & Niemela V. S., 2006, *MNRAS*, **369**, 867
O'Linger J., Moriarty-Schieven G. H., & Wolf-Chase G. A., 2006, submitted
Palla F. & Stahler S. W., 1999, *ApJ*, **525**, 772
Preibisch T., Guenther E., & Zinnecker H., 2001, *AJ*, **121**, 1040
Tóth L. V., Hotzel S., Krause O., Lemke D., Kiss Cs., & Moór A., 2003, in *The interaction of stars with their environments II*, eds. Cs. Kiss et al., Comm. Konkoly Obs., Budapest, No. 103, p. 45
Yonekura Y., Dobashi K., Mizuno A., et al., 1997, *ApJS*, **110**, 21

Flare star investigation – two decades of cooperative observational study in Budapest and Byurakan

István Jankovics

Gothard Astrophysical Observatory
Loránd Eötvös University
Szombathely

In 1969, when I got acquainted with the questions of flare phenomena, the investigation of these eruptive stars was over on the early stages of research. The first known flare star, DH Carinae, was discovered by E. Hertzsprung in 1924. Hertzsprung took plates for finding variable stars in the region of Carina and a flare of 1.8 magnitude was observed. Hertzsprung (1924) wrote in his note: "After the outburst, which took place on the third plate, the star lost about a magnitude in brightness in the course of about 1.3 hours." This observation had been forgotten and only after the discovery of the UV Ceti was it brought to the center of attention. It is interesting that Hertzsprung tried to consider a mechanism which could explain the phenomenon: "A rough estimate indicates that a fall into the star of a body like a small planet would yield sufficient energy for an outburst as observed..."

In the following 15 years a whole range of authors reported on accidentally observed flare events. For example, in the Orion nebula several stars showing similar changes of brightness have also been discovered. Among the numerous reports on extremely sudden increase in the brightness of some stars Wachmann's (1939) article was the first note on a flare event observed spectroscopically.

The star is now designated as V371 Ori. The lines of Balmer series were seen during the flare and the first small part of the trailed spectrogram was very intense followed with an abrupt drop in the spectroscopic continuum during the last part of the spectra (Wachmann, 1939).

Many of the flare stars were discovered during observations aimed at finding high proper motion stars. So the existing early data on the accidentally discovered flare stars are of a heterogeneous origin. The first observed flare stars were large proper motions objects in the vicinity of the Sun. They are low luminosity dwarf stars with spectral types of M0 or later and they have emission lines mainly of H and CaII during the normal state. The similarity of the observed features led van Maanen (1945) first to the idea that these stars may belong to the same class.

The field of flare star research really took off with the discovery of flares on Luyten 7268. The star had been known for its high proper motion and on 7 December 1948, E.F. Carpenter in Tucson made a multiple exposure plate for parallax purposes (see

Luyten, 1949). There are five consecutive exposures on the plate, each exposure took 4 minutes, while the total observation lasted about 20 minutes. The rapid increase in brightness of about two magnitudes, followed by a decrease of the same amount and all this happened in a 20 minute interval. From this moment it was clear that a new and until then unknown form of the brightness variation had happened and a new type of variable stars had been discovered. Today, the star is known as UV Ceti, the prototype of the flare stars. I have to mention, that three months earlier, even in September, Joy & Humason (1949) recorded the spectrum of UV Ceti during an eruptive change of brightness.

Also, as a class, the flare stars have spectral types of late M through late K, corresponding to the effective temperatures between about 2500 to 4000 K. They often have detectable emission lines of hydrogen and calcium in their spectra, indicating chromospheric activity. They have masses between 0.1 and 0.6 solar masses. Variability in the flare stars is characterized by rapid, irregular, large amplitude increases in stellar brightness, followed by a much slower decay (from minutes to hours) back to a quiescent level. Before the abrupt changes, a smooth light enhancement occurs in the continuum brightness. After this the really flare up takes only several seconds. The first part of the decay is also steep but slower than the brightening, which is followed by a longer lasting, quasi exponential part. The strongest variations occur in the blue and in the UV range: a flare may cause a one magnitude change in the V band, but more magnitudes in the U band. And during the flare event the star makes a loop on the colour-colour diagram. From the spectroscopic point of view, flares are typically accompanied by brightening of the emission line spectra of the star, particularly of the Balmer series of hydrogen, and the appearance of ionized helium lines as well. Flares have also been observed in the radio and X-ray regions of the spectrum, though they are not necessarily coincident with optical flares.

In 1945 Alfred Joy published a pioneering paper that initiated the study of emission-line stars associated with nebulosity. Ambartsumian (1947) showed that the bright-line variables are concentrated in certain regions where the star density is ten to one hundred times larger than in the neighbouring stellar fields. From this evident clustering of these objects Ambartsumian concluded that these stars had a definite genetic relationship and perhaps a common origin. Ambartsumian called these regions T-associations.

In 1953 Haro and Morgan reported on three rapid variables discovered in the Orion nebula. In rapid succession flare stars were found in other stellar aggregates and clusters of different ages – for example in NGC 2264, Pleiades, Coma, Praesepe, and Hyades clusters.

These flare stars in stellar aggregates radically changed the earlier picture based on the UV Ceti variables in the solar vicinity. Flares have been observed not only in Me dwarfs but also in stars of spectral type as early as K0, or earlier, and the absolute luminosities of these stars during quiescence correspond to cool subgiants as well as to dwarfs.

The *great flare hunting* started at the end of the 1960s. It was begun by Haro and his collaborators in Tonantzintla, and followed at Asiago – by Rosino –, in Byurakan – by a whole group of observers –, and in Budapest. The most intense observing campaign took place at the Byurakan observatory.

The Byurakan Astrophysical Observatory was founded in 1946 on Victor Ambartsumian's initiative. He became the first director of the observatory, and the main direction of astrophysical investigations – observational and theoretical aspects of stellar evolution – was determined by him. The scientific results came just after the foundation of the Byurakan Observatory. New type stellar systems, the stellar associations were discovered.

It was proved that stars are formed by groups. During 15 years intense observing campaign (until 1980) with wide-angle telescopes at the observatories Tonantzintla, Asiago, Byurakan, and Budapest for about 4000 hours of effective time of photographic observations nearly one thousand flare stars were discovered in several stellar aggregates of different ages. My contribution to this observational study was the comparative analysis of Pleiades and Praesepe clusters with about 400 hours effective exposure time, between 1971 and 1980. Photographic methods are usually unsuitable for photometric and colorimetric investigations of rapid variables. Nevertheless, a great number of flare events had been observed by this method. On the one hand, the multi-exposure plates taken with wide-field cameras are excellent means to discover that a change of brightness has taken place but it is not possible to determine the real amplitude of the flare event nor the correct light curve. On the other hand, the data obtained by the photographic method can be used excellently *for statistical investigations.*

Ambartsumian (1969) published the results of first statistical study based on the data of the first 60 Pleiades flare stars published by Haro. Suppose that the sequence of flares of any flare star is of the type of Poissonian stationary process with some mean frequency of occurrence, ν. Then it can be shown that the expected value, n_k of the number of stars that have flared k times during the total duration of observations, follows the relation:

$$n_k = \frac{n_{k+1}^2}{2n_{k+2}}$$

According to the definition, n_0 is the expectation of the number of flare stars that have not flared during the whole time of observation. In fact, it is the number of stars that are not yet discovered. Therefore adding this n_0 to the sum $n_1 + n_2 + ...$ of all stars observed in flares (this is the number of discovered flare stars), we can obtain the total number, N of flare stars in the given stellar aggregate:

$$N = \sum_0^\infty n_k$$

References:

Ambartsumian V. A., 1947, *Commun. of Armenian Academy of Sciences*

Ambartsumian V. A., 1969, in *Stars, Nebulae, Galaxies* [in Russian], Izd Akad. Nauk Arm. SSR, p. 283

Haro G. & Morgan W. W., 1953, *ApJ*, **118**, 16

Hertzsprung E., 1924, *BAN*, **2**, 87

Joy A. H., 1945, *ApJ*, **102**, 168

Joy A. H. & Humason M. L., 1949, *PASP*, **61**, 133

Luyten W. J., 1949, *ApJ*, **109**, 532

van Maanen A., 1945, *PASP*, **57**, 216

Wachmann A. A., 1939, *BZ*, **21**, 25

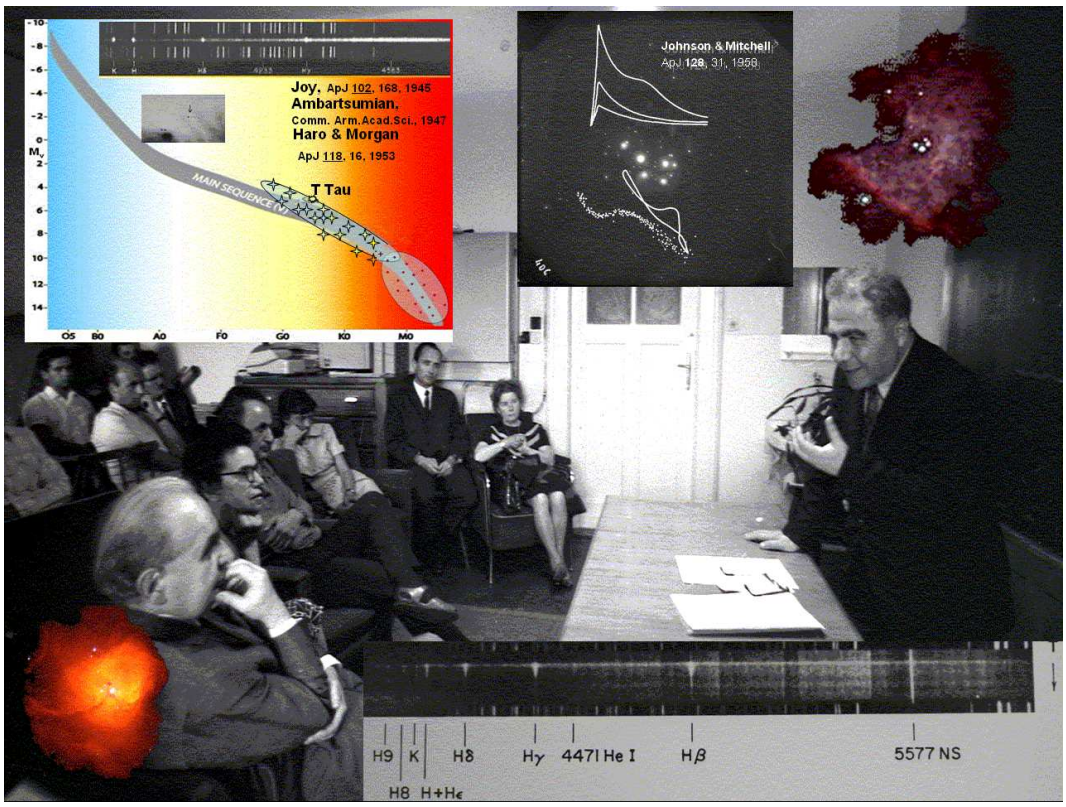

Figure 1: Ambartsumian's lecture for the staff of the Konkoly Observatory in 1969.

Active binary stars

László Patkós

Konkoly Observatory
H-1525 Budapest XII, P.O. Box 67, Hungary

The study of active binary stars at the Konkoly Observatory started in the early 1970's. The director of the observatory *László Detre* and my chief *Béla Szeidl* proposed me to deal with binary stars. At that time it was possible to get one week observational time at the Piszkéstető Mountain Station each month. This possibility could be best used for stars with assumed characteristic light-curve changes on time scales of months. For variable star research we had the 50 cm Cassegrain telescope equipped with the photoelectric photometer designed and built by *Géza Virághalmy*. I prepared a list of eclipsing binaries with possible period and light-curve changes. This list contained more than a hundred items. In one week observational time – according to the given weather conditions – about three clear nights were expected. This means, that to get a complete light curve, the ideal orbital period of the target binary had to be near 0.5 days. For the optimal use of the one week per month observational possibility the whole year over, stars with high declination were preferred. Further point of view was that the target star should not be too bright, nor too faint for the given telescope-photometer combination.

The binary system SV Camelopardalis was on top of my list with nearly 10 mag brightness, 0.6 day orbital period, 82° declination and with suspected irregular period and light-curve changes on month's time scales. SV Camelopardalis is one of the closest systems of the short period group of RS CVn binaries. Basic data of the system are: $P_{\rm orb} = P_{\rm rot} = 0.5930$ day, $a = 4R_\odot$, $i = 89.6°$, $r_2/r_1 = 0.64$, $r_1 = 1.3R_\odot$, $T_1 = 5750$K, $T_2 = 4500$K, $d = 74$ pc.

SV Cam proved to be a good choice. The system has been monitored at the Konkoly Observatory for more than 30 years, and the system did show interesting features like migration waves, optical flare events, moving dark and bright spots on the stellar surfaces. According to our measurements, the presence of a third component is also possible in the system.

The migrating distortion wave

Due to the close monitoring of the system it turned out that the reported "irregular light-curve changes" were not irregular. It turned out that there exists a distortion wave, rapidly moving with advancing phase. Former studies could not find this, as the observations were not frequent enough, and because the distortion wave was not always present in the system.

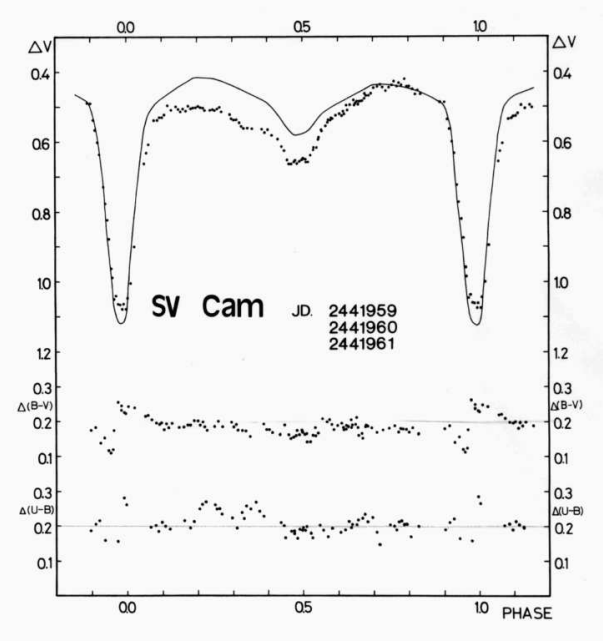

Figure 1: Light curve of SV Cam. The solid curve represents the unspotted reference curve, the points represent the observed brightness of the system. The measured points are below the reference curve, because large dark spots on the surface dim the brightness of the star. The centrum of the distortion wave is before phase 0.5.

The distortion wave is caused by dark spots on the surface of the brighter component of the binary star. In a close binary system – like SV Cam – the stellar rotation is synchronized to the orbital period. But differential rotation is also present. As there exists a co-rotational latitude, the forming distortion wave will move according to or against phase, depending on whether the spots are at higher or lower latitude than the co-rotational latitude. In the case represented in *Figs. 1* and *2* the distortion wave moved with growing orbital phase. This means, that the centrum of the spots which caused the wave was below the co-rotational latitude, consequently, the spots that caused the distortion were near the equator.

The amplitude of the observed waves sometimes exceeded 0.1 mag. (According to my observations migration waves in the system SV Cam do not always move as fast as in this example, and in the same direction either.)

Flare events in the optical range

Monitoring the system SV Cam – for the first time – optical flare events were measured in an RS CVn system. Optical flare events are very rare in RS CVn systems. Another example is the one observed by Zeilik et al. (1983) in the system XY UMa, which also belongs to the short period group of RS CVn systems.

I observed another optical flare event in the system SV Cam, but the three most pronounced events were observed in a single night at J.D. 2444582 during the whole – more than 30 years long – observational period (*Fig. 3*). This means, that the system was in an extraordinary enhanced activity phase around J.D. 2444582. The observed flare curves seem to be less asymmetric than usual, although the first one (near phase 0.6) was obviously the superposition of several different flares.

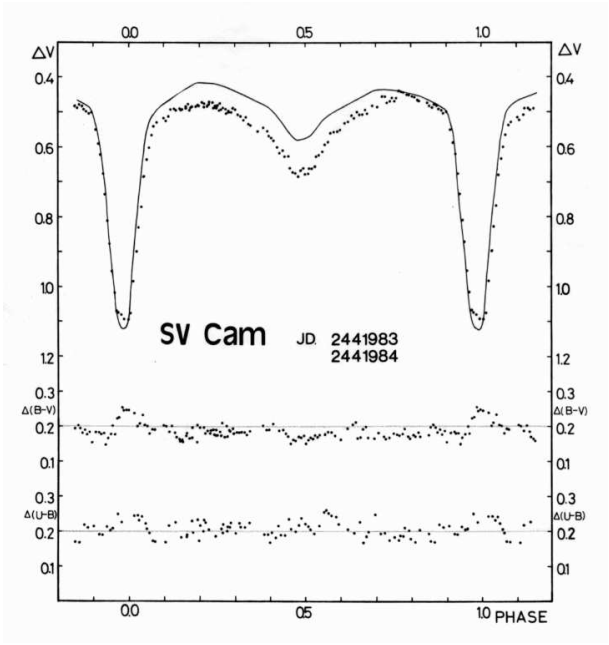

Figure 2: Just 3 weeks later, the centrum of the distortion wave is already near phase 0.5

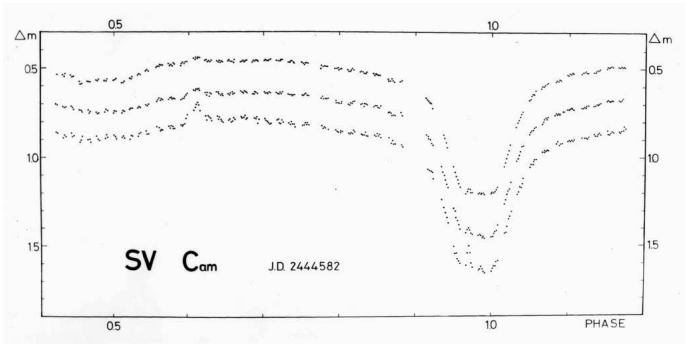

Figure 3: Three flare events on a single night (J.D. 2444582). The three (shifted) light curves are in V, B, and U band respectively. One (complex) flare was near the phase 0.6, the second and the third one at the bottom of primary minimum. The amplitudes were the largest in U and the smallest in V.

Bight spots on the primary component

As the migrating distortion wave was caused by dark spots on the stellar surface, all the observational points had to be below the reference curve which represents the totally unspotted case.

At J.D. 2442405 there were no spots on the stellar surface, measured light curve data fitted the reference curve. At J.D. 2442432 (one month later) the measured points still fitted the reference curve, but after another month points in the phase interval 0.2-0.7 were significantly higher. This means that the system suffered an exceptional brightening. This peculiar brightening was confirmed by the light curve observed five days later (at J.D. 2442466, *Fig. 4*).

After another two months (at J.D. 2442523) some residual brightening was still visible near the phase 0.5. The spot that might caused the brightening significantly diminished. In the light curve obtained four months later (at J.D. 2442634) we can see the start of a

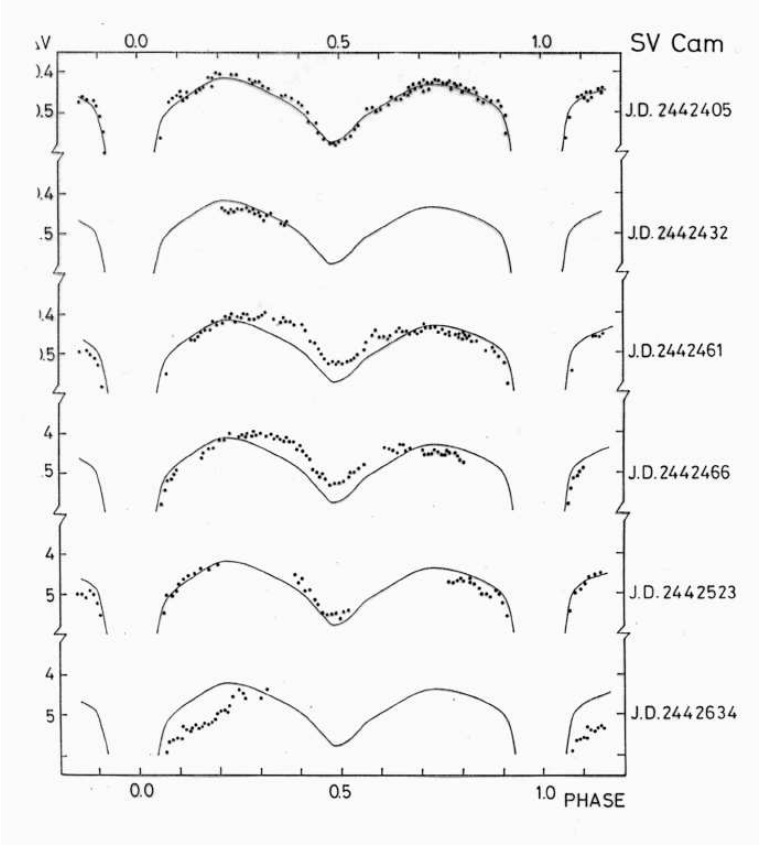

Figure 4: Parts of the light curves between J.D. 2442405-J.D. 2442634. (Points at or near the primary minimum are not plotted).

new distortion wave.

We analyzed the unusual brightening of SV Cam. A temporarily existing bright spot was supposed which appeared on the primary star of the binary system. A location near the stellar equator and the spot radius were derived. According to the analysis, the temperature difference between the spot and its surroundings was up to 110 K.

The existence of the spot might be related to an observed change of the orbital period. The suspected period change is depicted in *Fig. 5.*

Assuming that the observed phenomena were caused by an episodic mass transfer from the secondary to the primary component – the direction of the period change (period increase) is adequate. However, according to our own (Patkós & Hempelmann 1994) and other (e.g. Özeren et al., 2001; Albayrak et al., 2001; Kjurkchieva et al., 2002) investigations the Roche lobe of the secondary component of SV Cam was not completely filled.

Since 1973 the appearance of the bright hot spot on SV Cam around J.D. 2442461 was a particular event. But there are some other indications that bright spots do exist on the surface of the primary component. My observations indicate another (significantly less bright) spot (*Fig 6.*) at around J.D. 2441963-J.D. 2442019.

During the primary minima of SV Cam, the smaller, darker secondary component is moving in front of the larger and brighter primary. In that case a small part of the primary surface dominates the system's brightness. In contrast to this reduced brightness relatively smaller spots can be noticed. This was the case in the interval J.D. 2441963-2441984. At J.D. 2441963 a bright spot appeared near the edge of the visible part of the

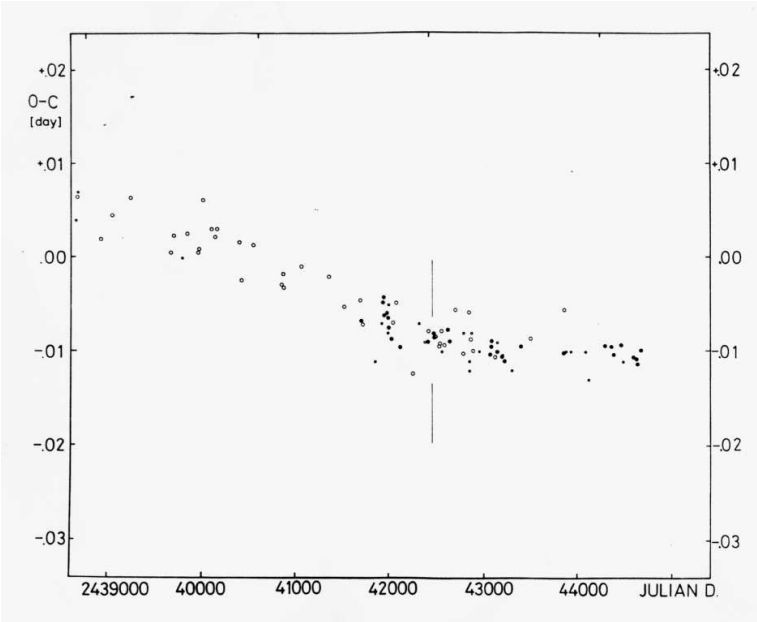

Figure 5: Part of the O−C diagram of the system SV Cam. Moment of the peculiar brightening is denoted by a vertical line. This seems to coincide with a break in the O−C curve. Black dots are minima measured by Patkós, open circles are minima from the literature.

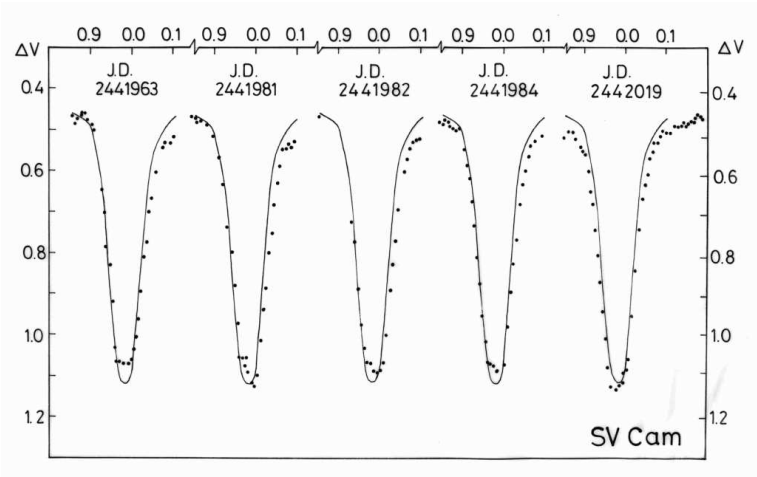

Figure 6: Primary minima of the SV Cam light curves between J.D. 2441963-J.D. 2442019. Solid lines represent the reference curve. At the bottom of the observed curves the measured points were higher than the reference curve at J.D. 2441963. At J.D. 2441981, 2441982, and 2441963 there was a significant step at the bottom. At J.D. 2442019 the points were again at the normal low level.

primary surface. This spot was present during the whole transit. The bottom of the primary minimum was therefore a bit brighter. Some days later (J.D. 2441981, 2441982, 2441984) the spot moved towards the central meridian. As result there was an abrupt step at the bottom of the primary minima when the dark secondary disk eclipsed the spot. Some days later the small bright spot moved further towards the central meridian and the bottom brightness of the system slid back to its original level.

In conclusion, bright spots do exist on the surface of the primary component of SV Cam, but they are not always bright enough to measure them against the whole stellar disk.

Activity minimum in the system SV Cam

The typical light curve of SV Cam is the one with the migrating distortion wave. It is a normal eclipsing light curve, but the measured points – in some phase interval – are below the usual brightness level because of the dark spots somewhere on the stellar surface. With the help of different spot solution methods (e.g. Wilson-Devinney code) it is possible to determine the parameters of the dark spots on the stellar surface. Then subtracting the effects of the dark spots we can get the unspotted eclipsing light curve suitable for the determination of the system parameters.

In the case of SV Cam – due to the data from the 33 years long monitoring – it was possible to choose a light curve (*Fig. 7*) which was almost completely free of maculation. (Stellar activity was at minimum or at least near to minimum). With the help of this light curve we could determine system parameters with a sufficient precision.

Photospheric-coronal connections in SV Cam

An important question in RS CVn studies is whether photospherically observed spots correlate with observed phenomena at other layers of the stellar atmosphere. To study spatial connections to other atmospheric layers we needed additional spectroscopic (Doppler imaging) and X-ray observations. As a result we could establish clear spatial correlations between the photosphere and corona.

We organized simultaneous X-ray, spectroscopic and optical observations of SV Cam. An international team was formed to establish spatial connections between photosphere and corona. Members of the group were A. Hempelmann (Astrophysikalisches Institut Potsdam, Germany), A.P. Hatzes (McDonald Observatory, The University of Texas at Austin, U.S.A.), M. Kürster (Max-Planck-Institut für Extraterrestrische Physik, Garching, Germany), and L. Patkós (Konkoly Observatory of the Hungarian Academy of Sciences, Hungary).

We observed SV Cam photometrically between J.D. 2449254-J.D. 2449257 with the 50 cm telescope at Piszkéstető Mountain station of Konkoly Observatory. A second complete light curve was observed with the same instrument at J.D. 2449310-J.D. 2449311 (*Fig. 8*).

We observed SV Cam with the ROSAT PSPC in the X-ray spectral region 0.1-2.4 keV. The total exposure time, 35.5 ksec, between J.D. 2449225-J.D. 2449229 was split into eleven half-hour exposures and seven exposures lasting only a few minutes. The main part of these observations covered 3.5 consecutive binary orbits of SV Cam. The spectroscopic observations were carried out at Sandiford Cassegrain Echelle spectrograph of the 2.1 m telescope of McDonald Observatory. Because of some technical difficulties,

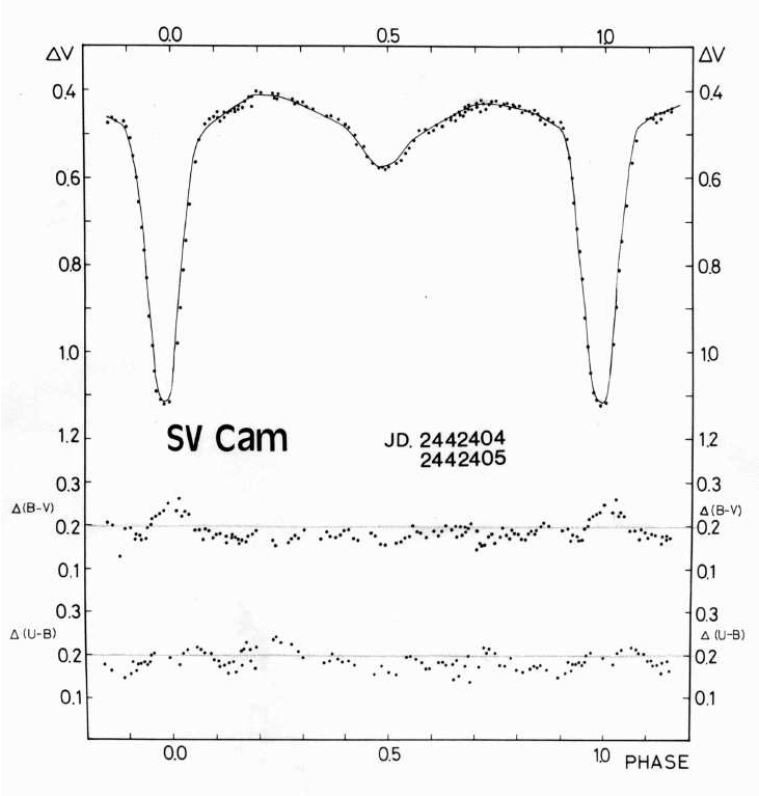

Figure 7: Light curve of SV Cam at J.D. 2442404-2442405. Measured brightness points nearly fit the unspotted reference curve.

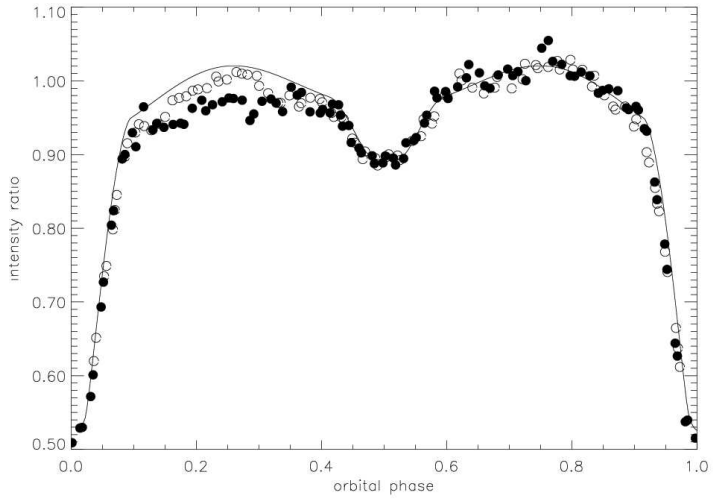

Figure 8: Photoelectrically observed light curves of SV Cam at J.D. 2449254-J.D. 2449257 and at J.D. 2449310-J.D. 2449311.

our spectroscopic observations (J.D. 2449288-J.D. 2449357) were delayed in comparison to the X-ray and optical observations. We obtained 13 spectra well distributed in phase. Exposure times were limited to 20 min to minimize phase smearing.

In the optical light curve it was obvious that there was a significant deviation from the unspotted light curve. This deviation was more pronounced in the J.D. 2449254-J.D. 2449257 light curve than the one obtained two months later at J.D. 2449310-J.D. 2449311. We assumed photospheric spots only on the surface of the primary star, because the possible contribution of spots over the secondary star was too small to account significantly to the light curve changes.

According to our analysis in the case of the first light curve there was a round dark spot with a radius of $27° \pm 12°$ at latitude $50° \pm 20°$ and longitude $78° \pm 2°$. In the light curve at J.D. 2449310-2449311 the maculation effect was much smaller. In that case we could not do detailed spot model analysis. We could determine the latitude of this smaller spot to be around 37°.

To produce the X-ray light curve we binned photon counts into time intervals of maximum 200 sec. To reduce scatter we binned the observational points in phase intervals of about 0.02.

We modeled the X-ray light curve with two coronal emission regions over the primary star. The X-ray spectrum of SV Cam could be explained by two different temperatures of $T_1 = 3 \times 10^6$ K and $T_2 = 1.5 \times 10^7$ K.

As SV Cam is a single lined binary, the mutual blending of the absorption systems originating from the second component is therefore no problem. But because of the high rotational velocity neighboring lines can blend each other significantly. We had to use only lines which seemed to be blend-free. Our analysis was based on four absorption lines: CaI 610.28 nm, CaI 612.20 nm, Fe I 640.00 nm, and CaI 643.91 nm.

We obtained independent Doppler images of the four lines (*Fig. 9*). The maps we got were not identical, but were very alike, and they agreed well with the map obtained analyzing the photometric data (*Fig. 10*).

Notice that the photometric spot analysis and the Doppler imaging are two completely different methods based on different data. It is very important that even in the case of a nearly 90° inclination the two methods yielded the same result.

According to the average picture, we got a spot distribution which was dominated by a strong circular spot at around latitude 60° and longitude 75°. There seemed to exist also an appendage to this spot with a longitude similar to the one we got from the J.D. 2449310-2449311 optical light curve. This also coincides with the position of one of the derived coronal X-ray emission regions. One possible explanation could be that the spot observed at J.D. 2449254-2449257 might have vanished by J.D. 2449310 or drifted to a new position. As the spectroscopic observations were done later (between J.D. 2449288 and J.D. 2449357) – a new strong spot might have emerged at the original position.

This kind of rapid spot evolution seems to be the regular behavior of SV Cam (Patkós, 1982; Zeilik et al., 1988). Note that we cannot distinguish between spots on the "upper" and "lower" hemispheres. The spots might be on either or both hemispheres. It could be that the above mentioned spot and its appendage were not connected, they might be at different hemispheres, and therefore physically not related.

A third active region was also derived from the spectroscopic observations. It seemed to be near the equator at around latitude 270°. It had a lower contrast in our Doppler image map. Despite this, it had a position near the second coronal X-ray source which we derived from the ROSAT light curve. This indicates a complete magnetically active region

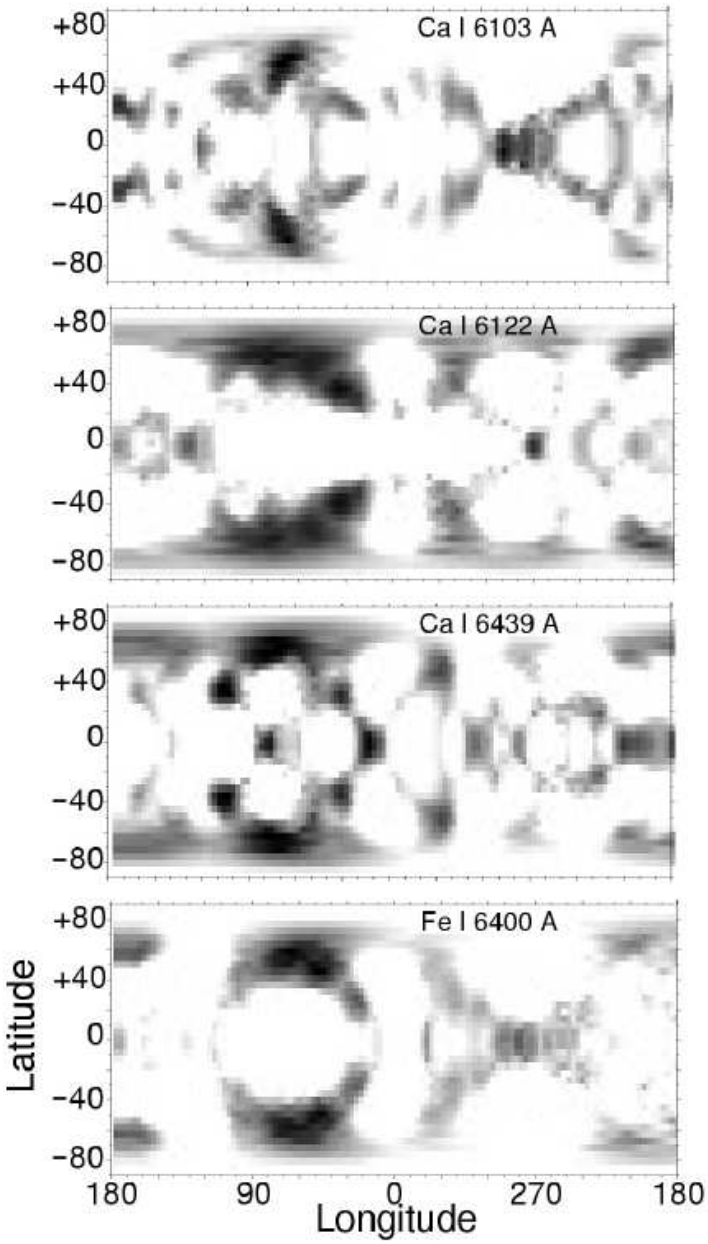

Figure 9: Four Doppler imaging results of SV Cam. Stellar longitude vs. latitude of the primary component.

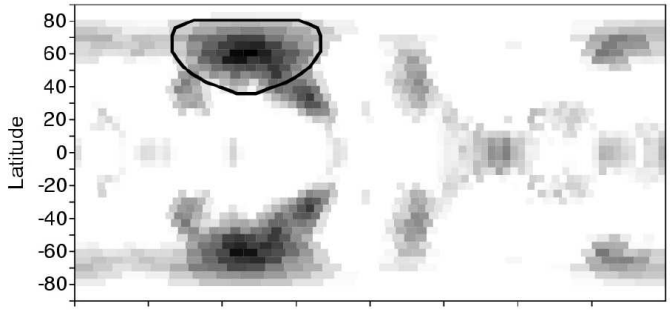

Figure 10: Averaged Doppler imaging result and the result of the independent photometric spot solution (solid circle).

at this position. Reality of this spot is further strengthened by the fact, that surface spots have been frequently observed at the same position (see e.g. Zeilik et al., 1988).

The large wavelength coverage of the Sandiford Echelle Spectrograph made it possible to acquire data simultaneously in Hα. These spectral profiles were examined to see if any rotational modulation – which may be an indication of a surface plage – could be detected. There was a strong distortion (pseudo-emission bump) in the red wing of the line at the phase of 0.004 that might be due to the secondary. The secondary star with an estimated spectral type of K4 is considerably cooler than the primary and when it transits it appears as a dark spot against the primary's surface. It thus produces a pseudo-emission distortion in the spectral line profile in the same manner as a cool surface spot.

The X-ray light curve could be explained with a model of two localized coronal sources in the binary system. One source was located closer to the primary star (most probably 0.8 $R_\odot$ above its surface), the other source was in the middle between the two stellar components. It remained unsolved whether this source has its origin in magnetism of either component or whether it results from an interaction of the two stellar magnetospheres.

On the primary star we found two photospheric active regions. The first active region has been exhibited by Doppler tomography to be of complex nature. Its main structure is a large spot of almost circular shape. This spot was also found from optical light curve analysis. The optical light curve was completely explained with this spot alone. However, the Doppler image showed an additional feature in this active region: an appendage to the circular spot. The whole region looks similar to a spot group on the Sun although one has to keep in mind that there is latitude ambiguity with respect to the equator, so that the circular spot may be in the one hemisphere while the appendage might be in the other hemisphere.

The presence of this appendage (a second spot inside a common active region) produces a noticeable change in the light curve and this would have been detected by the photometric measurements. There are, two explanations to solve this contradiction. The first but less likely possibility is that it was an artifact in the Doppler image resulting from observational errors and noise. However, this feature is evident in all four spectral lines analyzed. Hence, we felt its existence was real. The other possibility was the assumption of a temporary development of an active region. The spectrograms were obtained one month later than the light curve. Such rapid changes of spottedness might not be abnormal in case of SV Cam as some of the figures by Patkós (1982) demonstrate.

Finding of spots exclusively on the primary star does not imply inactivity nor absence of spots on the secondary star. Normally they cannot be seen in broad-band light curves, nor in the absorption lines outside the primary eclipse because of a too little contribution of the secondary star to the total light output. However, this may not be the case during primary eclipse when all the photospheric lines in the primary show absorption features that are believed to come from the secondary star. However, no such absorption feature is seen in the Hα profile, which should be present if the secondary were an inactive K4 star. The implication is that at primary eclipse the light from the secondary (at the wavelength of Hα) is predominantly continuum or possibly even in emission.

Further evidence of such activity was seen at secondary eclipse. The Hα line strength of the primary increased at this phase. This was expected because outside eclipse light from the secondary filled in the absorption lines of the primary making them shallower. However, the increase in Hα line strength was a factor of 1.6 larger than that expected from the continuum (near 656.3 nm) from the secondary for its spectral type. Again the conclusion is that the secondary is chromospherically active.

The Hα variations showed rotational modulation with a maximum near phase 0.8 and minimum near phase 0.3. It is not known whether the origin of this variation – if it were real – originated with surface features on the primary or secondary stars. If the chromospheric plages which might be responsible for this variation were located on the primary, then they might be associated with the large photospheric spot found by Doppler imaging and photometry. If the secondary star produced this variation, then the stellar surface region below one X-ray source was the more active one. In each case, the conclusion is that the strong spot on the primary star, the enhanced chromospheric activity of the secondary star and an intermediate coronal X-ray source were correlated with each other physically.

The light from the secondary could have strong influence on the Hα line strength and this complicates interpretations of the Hα variations.

References:

Albayrak, B., Demircan, O., Djurašević, G., Erkapić, S., & Ak, H., 2001, *A&A*, **376**, 158
Kjurkchieva, D. P., Marchev, D. V., & Zola, S., 2002, *A&A*, **386**, 548
Ottmann, R., Schmitt, J. H. M. M., & Kürster, M., 1993, *ApJ*, **413**, 710
Özeren, F. F., Gunn, A. G., Doyle, J. G., & Jevremović, D., 2001, *A&A*, **366**, 202
Patkós, L., 1982, *Comm. Konkoly Obs.*, Budapest, No. 80
Patkós, L. & Hempelmann, A., 1994, *A&A*, **292**, 119
Zeilik, M., Elston, R., Henson, G., & Smith, P., 1983, in *Activity in Red-Dwarf Stars*, IAU Colloquium No. 71. eds. P. B. Byrne & M. Rodono (Reidel: Dordrecht), 411
Zeilik, M., De Blasi, C., Rhodes, M., & Budding, E., 1988, *ApJ*, **332**, 293

Fundamental parameters of pulsating stars from atmospheric models

Szabolcs Barcza

Konkoly Observatory of the Hungarian Academy of Sciences
P.O. Box 67, H-1525 Budapest, Hungary

A purely photometric method is reviewed to determine distance, mass, equilibrium temperature, and luminosity of pulsating stars by using model atmospheres and hydrodynamics. T Sex is given as an example: on the basis of Kurucz atmospheric models and $UBVRI$ (in both Johnson and Kron-Cousins systems) data, variation of angular diameter, effective temperature, and surface gravity is derived as a function of phase, mass $\mathcal{M} = (0.76 \pm 0.09)\mathcal{M}_{\odot}$, distance $d = 530 \pm 67$ pc, $R_{\max} = 2.99R_{\odot}$, $R_{\min} = 2.87R_{\odot}$, magnitude averaged visual absolute brightness $\langle M_V^{\rm mag} \rangle = 1.17 \pm 0.26$ mag are found. During a pulsation cycle four standstills of the atmosphere are pointed out indicating the occurrence of two shocks in the atmosphere. The derived equilibrium temperature $T_{\rm eq} = 7781$ K and luminosity $(28.3 \pm 8.8)L_{\odot}$ locate T Sex on the blue edge of the instability strip in a theoretical Hertzsprung-Russell diagram. The differences of the physical parameters from this study and Liu & Janes (1990) are discussed.

Introduction

Except for supergiants and cool stars with effective temperature $T_{\rm e} < 4000$K a large grid of model atmospheres is available in the literature (Kurucz, 1997 for the latest versions). The conversion of theoretical fluxes to observational magnitude and colour indices has been solved (e.g. for Johnson and Kron-Cousins photometries, Castelli, 1999) opening the way to a determination of the atmospheric parameters effective temperature, $T_{\rm e}$, and surface gravity if broad band photometry is available for the target star.

The stellar angular diameter can be derived in the following manner from atmospheric models. Monochromatic flux $\mathcal{F}_{\lambda}(0)$ of the models at optical depth $\tau = 0$ is given in tabular form for a large grid of $T_{\rm e}$, g, metallicity $[M]$, etc., furthermore, by integrating $\mathcal{F}_{\lambda}(0)$ for a number of photometric systems the fluxes $\mathcal{F}_X(0)$ were computed in physical

units erg s^{-1} cm^{-2} as well, and the corrections from interstellar absorption, reddening were included (Kurucz, 1997). X represents the photometric band, e.g. V in the Johnson system. On the other hand, observed physical fluxes, $\mathcal{I}_X$, of stars in band X can be derived by using the absolute flux calibration of Vega (Tüg et al., 1977). If the interstellar extinction is A_X magnitude, the half angular diameter of a spherical (i.e. non-distorted) star can be derived from the simple formula

$$\vartheta = R/d = [10^{A_X/2.5}\mathcal{I}_X/\mathcal{F}_X]^{1/2} \tag{1}$$

where d is the distance to the star, R is the radius of $\tau = 0$ (Barcza, 2003).

For giant, main sequence, or white dwarf stars the stellar atmosphere is a thin layer in comparison with R. The gravitational acceleration

$$g(r) = -G\frac{\mathcal{M}}{r^2} = \varrho^{-1}(r)\nabla p(r) \tag{2}$$

is practically constant in the atmosphere, i.e. at $r \approx R$, where $\varrho(r)$, $p(r)$, $\mathcal{M}$, G are density, pressure, mass, and the Newtonian gravitational constant, respectively. The surface gravity, $g(R)$, is an important parameter of the static atmospheric models given conventionally as $\log|g|$ and it can be used to weigh a star if the stellar radius, R, is known. Relation (2) was applied for a number of non-variable stars enhancing our knowledge on stellar masses: e.g. for white dwarfs purely from $\log|g(R)|$ of model atmospheres and R $\mathcal{M}_{\rm wd} = 0.480 \pm 0.014$ average mass was derived (McMahan, 1989) for a sample of 53 stars while other methods gave somewhat larger mass, $\mathcal{M}_{\rm wd} = 0.58 \pm 0.10$ for 64 stars (Koester et al., 1979).

Problems, dependence of g, ϑ, $\mathcal{M}$ on $E(B-V), [M]$ were discussed in numerous papers, e.g. Kinman & Castelli (2002), Decin et al. (2003). Accuracy of the data from broad band photometry is inferior to that from fine analysis of spectra or interferometry, respectively, and $\mathcal{M}$ can be determined much better from binary orbits. However, if the more accurate methods are not available, the photometric determination of g, ϑ, and $\mathcal{M}$ must be appreciated.

Implementation for $UBV(RI)_{\rm C}$ photometry

The main parameters of atmospheric models are $T_{\rm e}$, g, $[M]$, and in addition to them the interstellar reddening, extinction (e.g. $E(B-V)$, A_X) must be known. From observational point of view colour indices, $C_i, (i = 1, 2, ...)$ are the input parameters and the inverse problem of ordering a model to them must be solved. In optimal cases the typical errors of interpolation are 0.1 in $\log|g|$ while a few hundredth in $\mathcal{F}_X$, respectively, however, the successful solution depends on the shape of the functions $T_{\rm e}(C_1, ...)$ and $\log|g(C_1, ...)|$. The final step is that theoretical $\mathcal{F}_X(C_1, ...)$ belonging to the selected model must be compared with $\mathcal{I}_X$ from observed magnitudes according to (1).

From inspecting the Kurucz tables some general rules can be inferred, we mention a few of them. For main sequence or giant stars UBV photometry must be preferred if $7000 < T_{\rm e} < 10^4$ K while for cooler stars $BVI_{\rm C}$ gives reliable results as well. Below $T_{\rm e} = 9000$ K the dependence of $\log|g|$ on $U-B$ becomes more pronounced, $U-B$ itself is sensitive to $[M]$ because of the appearance of metallic lines in ultraviolet. In favourable cases $T_{\rm e}$ and g can be determined from a two colour diagram if $[M]$, $E(B-V)$ were already known while the procedure is more uncertain if $[M]$ and $E(B-V)$ must be estimated from colour indices as well, in this case more than two colour indices are necessary.

Table 1: Half angular diameter of some stars from intensity interferometry ($\vartheta_{\rm HB}$) and V, $B-V$, $U-B$ of Kurucz models (ϑ), the units are 10^{-9}. The mass was calculated from the *Hipparcos* parallax π (ESA, 1997) and using $R = 3.086 \times 10^{13}\vartheta/\pi$ in (2).

HR	V	$B-V$	$U-B$	$\vartheta_{\rm HB}$	ϑ	π	$\mathcal{M}_\odot$
2421	1.93	0.00	0.04	$3.37 \pm .21$	3.55	0.031	1.51
2491[1]	−1.46	0.00	−0.05	$14.28 \pm .39$	14.31	0.379	3.47
2943[2]	0.38	0.42	0.02	$13.47 \pm .42$	11.80	0.286	1.7
3685	1.68	0.00	0.03	$3.85 \pm .17$	3.89	0.029	4.07
4534	2.14	0.09	0.07	$3.22 \pm .24$	3.33	0.090	1.70
6556	2.08	0.15	0.10	$3.95 \pm .31$	3.79	0.070	2.24
7001	0.03	0.00	−0.01	$7.85 \pm .11$	7.97	0.129	2.47
7557[3]	0.77	0.22	0.09	$7.22 \pm .34$	7.65	0.194	1.18
8728	1.16	0.09	0.08	$5.09 \pm .34$	5.29	0.130	1.55

1: The uncertainty of the mass values is indicated by $3.47_\odot$ for Sirius (HR 2491) in contrast with $2.143_\odot$ from binary orbit (Gatewood & Gatewood, 1978). This severe discrepancy is caused by the steep function $\log|g(U-B, B-V)|$ if $T_{\rm e} > 9800$K: small shifts $U-B = -0.05 \rightarrow -0.04$ or $B-V = 0.00 \rightarrow -0.01$ would result in $\log|g| = 4.52 \rightarrow 4.3$ i.e. $3.47_\odot \rightarrow 2.4_\odot$ with unchanged ϑ.

2: In the effective temperature range of Procyon (HR 2943) ($T_{\rm e} \approx 6600$ K) the dependence $\Delta\log|g|/\Delta[M] \approx 1.5$ is strong, $[M] = 0.4$ must be taken to reproduce the mass $\mathcal{M} = 1.75$ from binary orbit solution, in spite of the solar atmospheric composition (Drake & Laming, 1995). The change $B-V = 0.42 \rightarrow 0.43$ could lead to $\vartheta \approx \vartheta_{\rm HB}$.

3: The difference of ϑ and $\vartheta_{\rm HB}$ exceeds the error for Altair (HR 7557). Its rotational oblateness (Belle et al., 2001) may be responsible because both ϑ and $\vartheta_{\rm HB}$ assume spherical symmetry of the visible disc of the star. From $R/d = (ab)^{1/2} = (7.85 \pm 0.27) \times 10^{-9}$ a better agreement could be obtained where a, b are the visible minor and major axes, respectively.

To demonstrate reliability of the method, some date are given in Table 1: ϑ was derived from observed V, $B-V$, $U-B$ (Hoffleit, 1982) by using $\mathcal{F}_V(U-B, B-V)$ of the Kurucz models while for comparison the value $\vartheta_{\rm HB}$ is given from intensity interferometry corrected for limb darkening (Hanbury Brown et al., 1974). Using the *Hipparcos* parallaxes (ESA, 1997) $R = 3.086 \times 10^{13}\vartheta/\pi$ km was calculated and the mass was obtained by (2) from $\log|g(U-B, B-V)|$. It can be noted that the weakest sampling of the spectrum is provided by $(U-B, B-V)$ since the wavelength interval $\approx 360 - 540$ nm is covered in this case. Of course an inclusion of other colour indices could improve the values of $\vartheta, \log|g|$.

For pulsating stars with periods exceeding 0.1 day the characteristic time of changes of the main atmospheric parameters $T_{\rm e}, g_{\rm e}, \mathcal{F}_X$ is long in comparison with the formation of radiative (and convective) equilibrium, therefore, the static atmospheric models account satisfactorily for the changes of $g_{\rm e}$ and ϑ as a function of pulsation phase φ (Buonaura et al., 1985). The subscript in $g_{\rm e}(= -\varrho(r)\nabla p(r) > 0)$ indicates that this is an effective outward acceleration produced by the pressure gradient in the atmosphere. On appropriately selected two colour diagrams the loop of a variable star gives $\log g_{\rm e}(\varphi), T_{\rm e}(\varphi), \mathcal{F}_X(\varphi)$ etc. of the models while photometric observations can be reduced to $\mathcal{I}_X(\varphi)$ giving finally $\vartheta(\varphi)$ by (1).

- Mass and distance from $\vartheta(\varphi)$, $g_{\rm e}(\varphi)$ by using the radial momentum balance in the pulsation

If $\vartheta(\varphi_j), j = 1, 2, ..., N$ points are available in a sufficient number to numerical differentiation of $\vartheta(\varphi)$ the angular acceleration can be converted to $\ddot{R}(t) = \ddot{\vartheta}(t)d$, $t = \varphi P$, where P is the period in seconds. Numerical experience showed that $N \approx 500$ or more points gave reliable $\ddot{R}(\varphi)$ if they were distributed uniformly in $0 \leq \varphi \leq 1$.

Now the main innovation is that $\ddot{R}(\varphi_j)$, $g_{\rm e}(\varphi_j), j = 1, 2, ...$ are introduced in the radial component of the Euler equation of hydrodynamics and we exploit that the atmosphere must be in standstill at least twice in a pulsation cycle. At these phases $\varphi_i (i = 1, 2)$ the radial component of the non-linear term vanishes: the non-radial motions are expected to contribute negligibly to the momentum balance in radial direction, therefore, $(\mathbf{v}, \nabla)\mathbf{v} \propto \dot{R} \approx 0$ and we have the equations:

$$\ddot{\vartheta}(\varphi_i)d = -\frac{G\mathcal{M}}{[\vartheta(\varphi_i)d]^2} + g_{\rm e}(\varphi_i), \quad i = 1, 2. \tag{3}$$

The fundamental stellar parameters: distance and mass

$$d = \frac{g_{\rm e}(\varphi_1) + \ddot{R}_a(\varphi_1) - [g_{\rm e}(\varphi_2) + \ddot{R}_a(\varphi_2)][\vartheta(\varphi_2)/\vartheta(\varphi_1)]^2}{\ddot{\vartheta}_0(\varphi_1) - \ddot{\vartheta}_0(\varphi_2)[\vartheta(\varphi_2)/\vartheta(\varphi_1)]^2}, \tag{4}$$

$$\mathcal{M} = [g_{\rm e}(\varphi) - \ddot{\vartheta}(\varphi)d]\vartheta^2(\varphi)d^2/G \tag{5}$$

(Barcza, 2003) follow from (3) by elementary operations. The apparent accelerations $\ddot{R}_a$ can be neglected if the characteristic spatial extension of the atmosphere – i.e. the size of the interval $0 \leq \tau_{\rm Rosseland} \leq 1$ varies slightly during the whole pulsation cycle. If there are more than two standstills, then $i \geq 3$ in (3). Eventual different values of $\mathcal{M}, d$ from $i = 1, 3$, $i = 2, 3$ etc. can indicate e.g. non-radial pulsation because radial pulsation was assumed throughout the procedure outlined here.

The fundamental stellar parameters equilibrium luminosity and temperature (Carney et al., 1992) are obtained from $\vartheta(\varphi), T_{\rm e}(\varphi), d$ by

$$L_{\rm eq} = 4\pi\sigma\langle\vartheta^2(\varphi)d^2T_{\rm e}^4(\varphi)\rangle, \tag{6}$$

$$T_{\rm eq} = \{L_{\rm eq}/4\pi\sigma[\langle\vartheta(\varphi)\rangle d]^2\}^{1/4} = \langle\vartheta^2(\varphi)T_{\rm e}^4(\varphi)\rangle^{1/4}\langle\vartheta(\varphi)\rangle^{-1/2} \tag{7}$$

where σ is the Stefan-Boltzmann constant, $T_{\rm eq}$ differs slightly from the average effective temperature $\langle T_e(\varphi)\rangle$. $L_{\rm eq}, T_{\rm eq}$ allow to locate a variable star in theoretical Hertzsprung-Russell diagram: of course on the basis of [colours – $T_{\rm e}, \mathcal{F}_X$] calibration of the used atmospheric models.

— Comparison with the Baade-Wesselink method

The determination of $\vartheta(\varphi)$ is common in both methods. The difference lies in its further use.

In the BW method the radius change is derived from integrating the radial velocity curve and it is equated with ϑd. The kinematic equation

$$\vartheta(\varphi)d = R_0 + \delta R = R_0 + \int_{\varphi_0}^{\varphi P} p_{\rm p}(t)[v_\gamma - v_{\rm radial}(t)]{\rm d}t \tag{8}$$

must be solved for d where $p_{\rm p}$ is the projection factor of converting radial to pulsation velocity and v_γ is the barycentric velocity of the star. Physical input comes from the time-dependent projection factor. A much more serious uncertainty of kinematic nature is imported in this procedure by the error Δv_γ. If $\Delta v_\gamma \ll \overline{|v_\gamma - v_{\rm radial}(t)|}$ a negligible error is propagated into δR, however, it is problematic to achieve this desired accuracy because the observed radial velocities are an integral of the radial component of true, non-uniform motions in the atmosphere contaminated by apparent velocity changes from varying opacity during phases of different compression. The difficulties from the uncertain value of v_γ could be circumvented by differentiating $p_{\rm p}(t)v_{\rm radial}(t)$ and substituting it for $\ddot{\vartheta}d$ in (3). However, because of low number, large scatter of the observed radial velocities, and eventual time dependence of $p_{\rm p}(t)$ this principally correct use of (3) cannot result in $d, \mathcal{M}$ of acceptably small error.

By using $\vartheta, \ddot{\vartheta}, g_{\rm e}$ in (3) radial velocity observations and their problematic conversion to radius changes are not necessary at all at the price of differentiating $\vartheta(\varphi)$ twice plus more physical input: $g_{\rm e}(\varphi)$ and the assumption of radial momentum balance must be used. Finally d and $\mathcal{M}$ are obtained by solving algebraic equations. The method was described in detail and applied for the $\rm RR_{ab}$ star SU Dra by Barcza (2003). We mention two remarkable details from this study. (i) At minimum radius, i.e. at maximum compression in the atmosphere, $g_{\rm e} = 50.1\,{\rm ms}^{-2} \gg G\mathcal{M}/R^2 \approx 8\,{\rm ms}^{-2}$ reduces (3) to $d < g_{\rm e}/\ddot{\vartheta}$ giving $d < 718$pc. This upper value is very close to $d = 647$pc from the solution of (3) for three observed standstills. From them the unequivocal $d, \mathcal{M}$ show that a non-radial mode, if there is any, is negligible in comparison with the radial oscillation of SU Dra. (ii) During a time interval t the small uncertainty $\Delta v_\gamma \approx +5.9{\rm kms}^{-1} \approx 0.04 v_\gamma$ (Liu & Janes, 1990 vs. Oke et al., 1962) leads to a phase dependent error $\Delta R = p_{\rm p}\Delta v_\gamma t \leq 3.43 \times 10^5{\rm km}\,(\approx (R_{\rm max} - R_{\rm min})/2!)$ which has a considerable effect on d. If the method by Liu & Janes (1990) is followed to solve the kinematic equation, the increment of d is 1.26 from $\Delta v_\gamma = 5.9\ {\rm km\,s}^{-1}$. This results in correction $\langle M_V^{\rm mag}\rangle = 0.78 \rightarrow 0.28$ for the magnitude average absolute magnitude. (Roughly this is the difference between the short and long extragalactic distance scales – Gratton, 1998. The distance 815 pc corresponding to the long distance scale is ruled out by $d < 718$pc.)

Application to T Sex

Now we apply the method for the RRc variable T Sex. Good quality photoelectric observational material was collected from the literature, the sources are given in Table 2.

- Period, $O-C$, average light and colour curves

The periods given by TS58, PP64, EE73, BM88, LJ89 indicated period changes of $O(10^{-6})$. To clarify it string length minimization (SLM) was applied, since good conversion of the observations to average light curve and colour-colour loops is crucial to determine $\vartheta(\varphi), g_{\rm e}(\varphi)$. (The adaptation of SLM to pulsating stars was described by Barcza (2002), the notation of this paper will be used here. The essence of SLM is that first the segments $k = 1, 2, ...$ of the observed V magnitudes are projected onto the phase axis $\varphi, 0 \leq \varphi \leq 1$ by the saw tooth function which is perturbed by a term $\delta_k \equiv (O-C)_k \ll P_0$ accounting for the phase shift of segment k and next the neighbouring points are con-

Table 2: $V, UBV, BVRI, UBV(RI)_C$ data of T Sex used for constructing average light and colour curves, k is the serial number of the segment, n_k is the number of V points in the segment, δ_k, E_k are the phase shift and epoch in (9)

k	HJD − 2400000	n_k		δ_k	E_k	Source
1	34311.8675 − .9315	31	V	−0.0160	6	TS58
2	34350.8051 − .9402	66	V	−0.0247	126	TS58
3	34363.7245 − .8531	64	V	−0.0300	166	TS58
4	34508.5948 − .6598	10	V	−0.0766	612	TS58
5	35190.7392 − .8208	2	UBV	0.0593	2712	TS58
6	35191.6423 − .8871	72	UBV	0.0586	2715	TS58
7	35195.6440 − .9000	106	UBV	0.0470	2727	TS58
8	35513.7227 − .9620	40	UBV	−0.0286	3707	TS58
9	35514.6815 − .9477	60	UBV	−0.0275	3710	TS58
10	35516.6802 − .9387	73	UBV	−0.0272	3716	TS58
11	38017.9584 − 8.0870	43	UBV	0.0322	11417	PP64
12	38035.8141 − .9985	55	UBV	0.0280	11472	PP64
13	38038.8007 − .8928	28	UBV	0.0227	11481	PP64
14	40678.6990 − .7931	10	V	0.0778	19610	EE73
15	40680.6390 − .7382	8	V	0.0757	19616	EE73
16	41013.7358 − .7565	4	V	−0.0127	20641	EE73
17	43525.792 − 56.694	11	V	0.0588	28418	E94
18	45387.7850 − .9212	76	$BVRI$	0.0010	34109	BM88
19	45388.6578 − .7634	69	$BVRI$	0.0026	34112	BM88
20	45389.6382 − .8760	113	$BVRI$	0.0029	34115	BM88
21	45393.7134 − .8596	98	$BVRI$	0.0000	34127	BM88
22	45400.6689 − .7235	45	$BVRI$	−0.0021	34149	BM88
23	46845.6886 − .7489	6	$UBV(RI)_C$	0.0540	38598	LJ89
24	46846.8005 − .8859	7	$UBV(RI)_C$	0.0429	38601	LJ89
25	46847.6521	1	$UBV(RI)_C$	0.0480	38604	LJ89
26	46848.6547 − .9614	25	$UBV(RI)_C$	0.0432	38607	LJ89
27	47197.7625 − 8.0035	16	$UBV(RI)_C$	−0.0301	39682	LJ89
28	47226.6368 − .9153	3	VR_C	−0.0258	39771	LJ89
29	47488.8955 − .9059	7	$BVRI$	−0.0881	40578	BM92

nected by straight strings. Finally the normalized sum νl of the string lengths is minimized numerically as a function of period P_0 and phase shifts $\delta_1, ...$)

The V file contains 1149 observations in 29 segments, SLM gave for the maxima

$$\mathrm{HJD}_{\max} = 2434310.035 + P_0 E_k + \delta_k \tag{9}$$

with $P_0 = 0.3247796 \pm 0.0000032$ and the values δ_k in Table 2. The summed string length was $\nu l_0(P_0, \delta = \mathbf{0}) = 0.330$ with standard deviation SD $= 0.069$ magnitude, the folded light curve belonging to it is plotted in *Fig. 1a*. Applying the values δ_k of Table 2 reduced $\nu l(P_0, \delta)$ to 0.062 with $\mathrm{SD}(P_0, \delta) = 0.012$ mag, dots of *Fig. 1b* are a plot of the folded light curve, its SD $= 0.012$ does not exceed the expected random error of a V point, it is lower than the claimed amplitude 0.028, 0.015 mag for the second and third periods of T Sex (Hobart et al., 1991). Thus, the conclusion must be drawn that between HJD 2434311-2447488 the light curve of T Sex can perfectly be reproduced if the light curve segments in *Fig. 1a* are shifted to the $\mathrm{HJD}_{\max}$ given by (9). The colour indices were shifted by δ_k of the segment, *Figs. 1c-f* are their plots. The line in *Figs. 1b-f* was obtained by fitting high order (≤ 9) polynomials to the points. These drawn light and colour curves were used to construct colour-colour loops and to interpolate the physical parameters of the Kurucz models.

Two remarks on the homogenization of the colour curves. (1) In $U-B$ of segments 5,6,7 a zero point correction +0.08 was applied while for 8,9,10 it was +0.05 in order to bring the TS58 observations in coincidence with those of PP64 and LJ89. (2) The Johnson $V-R, V-I$ colours of BM88 and BM92 were converted to $V-R_{\mathrm{C}}, V-I_{\mathrm{C}}$ by Taylor's (1986) empirical formulae.

- *The physical parameters*

The colour-colour loops $(U-B, B-V), (U-B, V-R_{\mathrm{C}}), (U-B, V-I_{\mathrm{C}}), (B-V, V-I_{\mathrm{C}})$ could be used to interpolate $T_{\mathrm{e}}(\varphi)$, $\log g_{\mathrm{e}}(\varphi)$, $\mathcal{F}_V(\varphi)$, $\mathcal{F}_{R_{\mathrm{C}}}(\varphi)$, $\mathrm{BC}(\varphi)$. Using a midpoint formula the half angular velocity $\dot{\vartheta}$ and acceleration $\ddot{\vartheta}$ were determined from $\vartheta(\varphi)$. *Fig. 2* is a plot of the results for $E(B-V) = 0.095, [M] = -1.2$. From the different loops the scatter of $\log g_{\mathrm{e}}$ was the largest: $\pm 0.11, \pm 0.03$ at $\varphi = 0.3, 0.9$, respectively, the scatter in $\mathcal{F}_V, \mathcal{F}_{R_{\mathrm{C}}}, T_{\mathrm{e}}$ was ≤ 0.02. Therefore, $\log g_{\mathrm{e}}, \dot{\vartheta}, T_{\mathrm{e}}$ were averaged at each φ from the four loops. The scatters result in an error of ≈ 0.15 for the derived mass and distance if one pair of standstills is used.

- *Distance, mass, equilibrium luminosity and effective temperature*

The standstills of the atmosphere were found at $\varphi \approx 0.31, 0.56, 0.65, 0.90$ by searching for zero average angular velocity $\overline{\dot{\vartheta}(\varphi)} \approx 0$. $\ddot{\vartheta}, \log g_{\mathrm{e}}$ were averaged here in an interval $\Delta\varphi \approx 0.02$ (i.e. ≈ 10 min). Table 3 reports the results for some values of $E(B-V) = 0.095, [M] = -1.2, -1.0$.

The characteristic size of the atmosphere is $\approx 10^4$ km, $\ddot{R}_a \ll g_{\mathrm{e}}$, therefore, $\ddot{R}_a$ can be neglected.

$\langle T_{\mathrm{e}}(\varphi) \rangle, T_{\mathrm{eq}}$ and from pairs of standstills AD,BD,CD the average d, $\mathcal{M}$, R, L_{eq} are given in Table 4 to some values of $E(B-V)$. The estimated errors from the averaging are in accordance with that of the interpolation of $\log g_{\mathrm{e}}$, the other quantities propagate negligible errors in (4),(5).

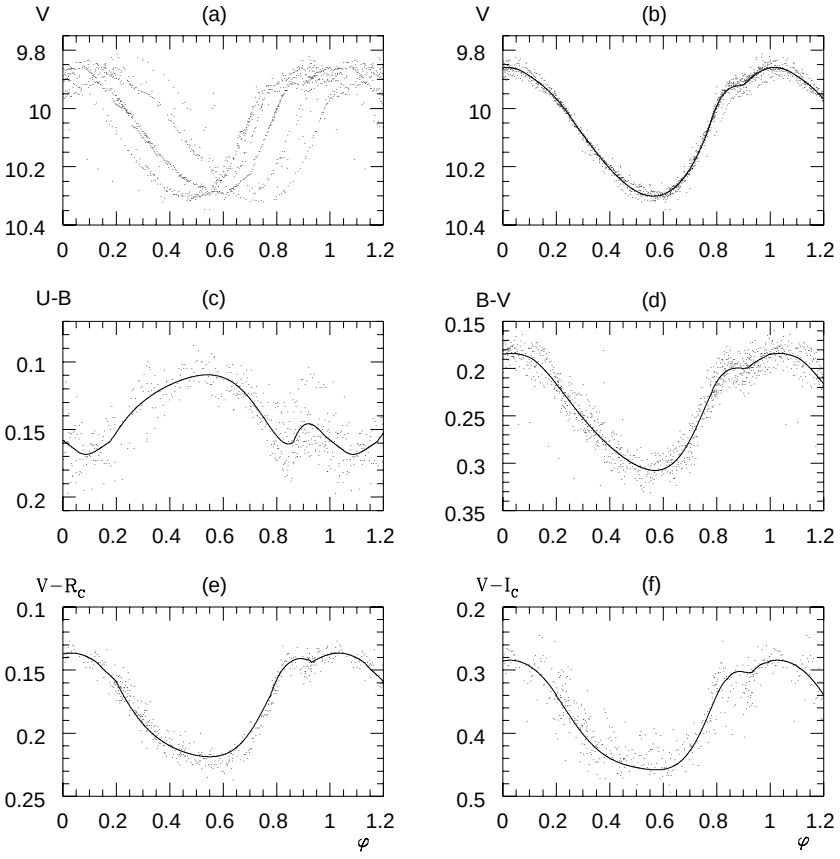

Figure 1: Panel (a): 1149 V observations folded by $P_0 = 0.3247796$ days, $\delta = \mathbf{0}$. Panels (b)-(f): dots: $V, U-B, B-V, V-R_{\rm C}, V-I_{\rm C}$ observations folded with the values δ_k given in Table 1. Lines: High order polynomial fitting curves.

Table 3: Average ϑ, $\ddot{\vartheta}$, $\log g_{\rm e}$ at $\varphi = 0.31,\ 0.56,\ 0.65,\ 0.90$ for $E(B-V) = 0.095, [M] = -1.2, -1.0$. The units are: radian, radian s^{-2}, $\mathrm{cm\,s}^{-2}$.

	φ	$\vartheta \times 10^{10}$	$\ddot{\vartheta} \times 10^{18}$	$\log g_{\rm e}$
$[M] = -1.20$				
A	0.31	1.273	$-0.334 \pm .013$	$3.38 \pm .11$
B	0.56	1.242	$0.189 \pm .012$	$3.37 \pm .10$
C	0.65	1.247	$-0.257 \pm .020$	$3.36 \pm .07$
D	0.90	1.222	$1.56 \pm .02$	$3.71 \pm .03$
$[M] = -1.00$				
A′	0.31	1.264	$-0.331 \pm .013$	$3.45 \pm .10$
D′	0.90	1.217	$1.58 \pm .02$	$3.74 \pm .03$

Table 4: Average physical quantities from the pairs of standstills AD,BD,CD assuming $M = -1.20$ and different reddenings. The units are: K, K, pc, solar mass, radius, and luminosity. Our final choice is $E(B-V) = 0.095$.

$E(B-V)$	$\langle T_e \rangle$	T_{eq}	d	$\mathcal{M}$	$\langle R \rangle$	L_{eq}
0.08	7607	7625	452 ± 73	$0.37 \pm .06$	2.54	19.6 ± 6.9
0.09	7712	7728	514 ± 84	$0.55 \pm .08$	2.86	26.5 ± 9.4
0.095	**7765**	**7781**	$\mathbf{530 \pm 67}$	$\mathbf{0.76 \pm .09}$	**2.93**	$\mathbf{28.3 \pm 8.8}$
0.10	7816	7834	558 ± 65	$1.06 \pm .16$	3.07	31.9 ± 6.9
0.105	7871	7886	892 ± 130	$3.04 \pm .44$	4.89	84 ± 26

Discussion

- Dependence of the physical quantities on reddening

The strong dependence of $T_e(\varphi), \log g_e(\varphi)$ and the derived $d, \mathcal{M}$ on $E(B-V)$ is a surprising result of this study while the value of $[M]$ is of secondary importance. $E(B-V) = 0.05 \pm 0.02$ by Liu & Janes (1990) gives very small $d, \mathcal{M}$ which cannot be reconciled with our present day theoretical knowledge on RR Lyrae or other type of pulsating stars. Reddening $E(B-V) = 0.07$ and 0.09 were suggested by Hobart et al. (1991) and Hemenway (1975), respectively, our finding is that $E(B-V) = 0.09 - 0.1$ is the only possible choice.

- Effective temperature, surface gravity

$T_e(\varphi), \log g_e(\varphi)$ of the present study are significantly higher by some 650 K and ≈ 0.4 than those of Liu & Janes (1990). Since essentially the same Kurucz tables were used we attribute the difference to the different philosophy of the interpolation procedure:

> Liu & Janes (1990) determined $g_e(\varphi) = 0.6\mathcal{M}_\odot G/R^2(\varphi)$ from kinematics with assuming the canonical mass $0.6\mathcal{M}_\odot$ of RR Lyrae stars. Next, one arbitrarily chosen colour index, $V-K$ was taken as sole source of $T_e(\varphi)$ belonging to $\log g_e(\varphi)$ from the kinematics and $T_e(\varphi)$ from the other colour indices were neglected leading to their very low $\langle T_e \rangle = 7137$ K. To check this procedure their $T_e(B-V), T_e(V-R_C), T_e(V-I_C), T_e(V-K)$ tables were all used for $\log g_e = 3, 3.5$: according to our opinion no reason can be found to reject any T_e since the difference was ≤ 250 K with no systematically decreasing trend when going more and more to the infrared indices. Therefore, averaging could have been more appropriate. Theoretical colour indices differing systematically from the observed ones by $0.02 - 0.04$ mag correspond to their lower $\log g_e(\varphi)$ values.
>
> In the present study two colour diagrams were used to determine a pair of $T_e(\varphi)$, $\log g_e(\varphi)$ simultaneously taking into account the dependence of $T_e(\varphi)$ on $\log g_e(\varphi)$ automatically and the small differences (≤ 250 K in T_e, ≤ 0.11 in $\log g_e$) from the four colour-colour loops justified averaging. This is a self-consistent procedure trusting on the Kurucz models exclusively. By using four colour-colour loops, different parts of the whole spectrum $\mathcal{F}_\lambda(0)$ were sampled in the λ interval $360 - 1000$ nm.

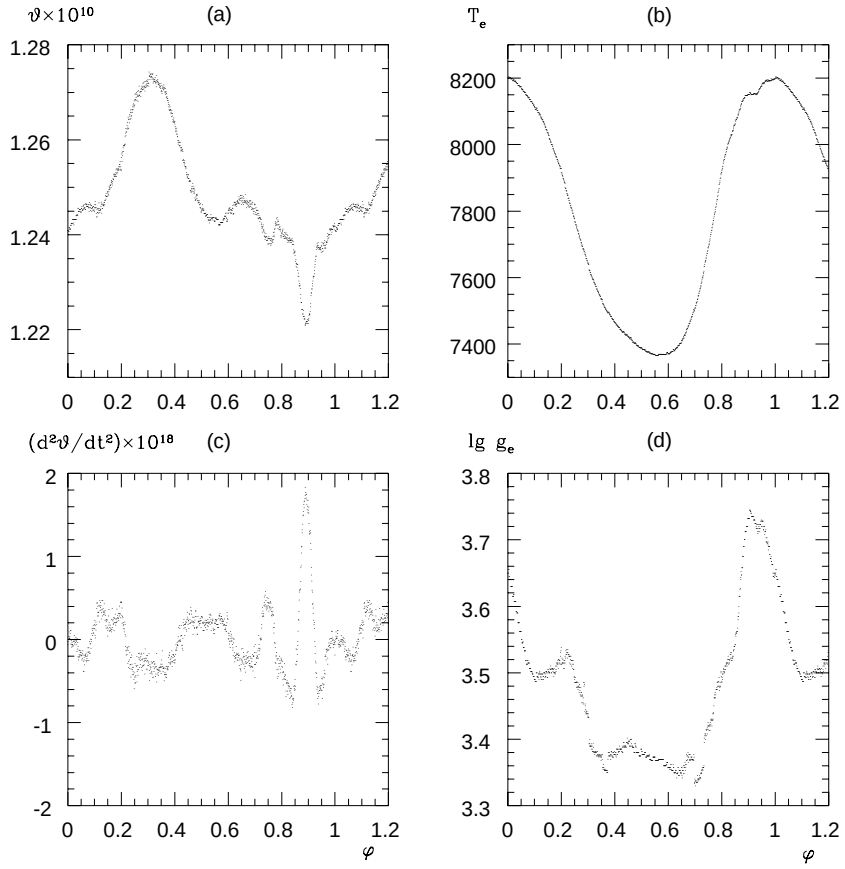

Figure 2: The average variable parameters of T Sex for $E(B-V)=0.095, [M]=-1.2$ from the loops $(U-B, B-V), (U-B, V-R_{\rm C}), (U-B, V-I_{\rm C}), (B-V, V-I_{\rm C})$. The outlier points of panels (a,c,d) at $\varphi \approx 0.36, 0.72-0.76$ are artifacts of interpolation, they were not smoothed out to show the effect of eventual uncertainties in the interpolation.

- Position in a theoretical HRD, absolute brightness

The values of the fundamental parameters $\log T_{\rm eq}=3.891$, $\log L_{\rm eq}=1.452$, $\mathcal{M}=0.76_{\odot}$ for $E(B-V)=0.095$ place T Sex just to the blue edge of the instability strip given by Tuggle & Iben (1972) and Lee et al. (1990). This position is expected for an $\rm RR_c$ variable and it was our main argument to accept the large reddening. With distance $d=530$ pc we get $R(\varphi=0.31)=2.99R_{\odot}, R(\varphi=0.91)=2.87R_{\odot}$, and magnitude averaged visual absolute brightness $\langle M_V^{\rm mag}\rangle = 1.17\pm0.26\,$mag. These values come purely from atmospheric models which are trustable to a few percent level and verify figures from stellar structure calculations. The values $d=578.5$ pc and $\langle M_V^{\rm mag}\rangle = 1.06\pm0.38$ of Hobart et al. (1991) agree with the present results within the quoted errors. The physical parameters of Liu & Janes (1990), ($0.47\mathcal{M}_{\odot}$, $d=667$ pc, $\langle T_{\rm e}\rangle = 7137$ K, $\langle R\rangle = 4.05R_{\odot}$, $\langle M_V\rangle = 0.76\pm0.27$ mag $\langle \log g_{\rm e}\rangle = 2.98$) are unreliable.

Figs. 3a-c are plots of the variable acceleration, velocity, radius in absolute units for a pulsation cycle if $d=530$ pc. The sharp undulation of the curves in $0.72<\varphi<0.78$ is not real, it originates from the interpolation artifact indicated in the caption to *Fig. 2.*

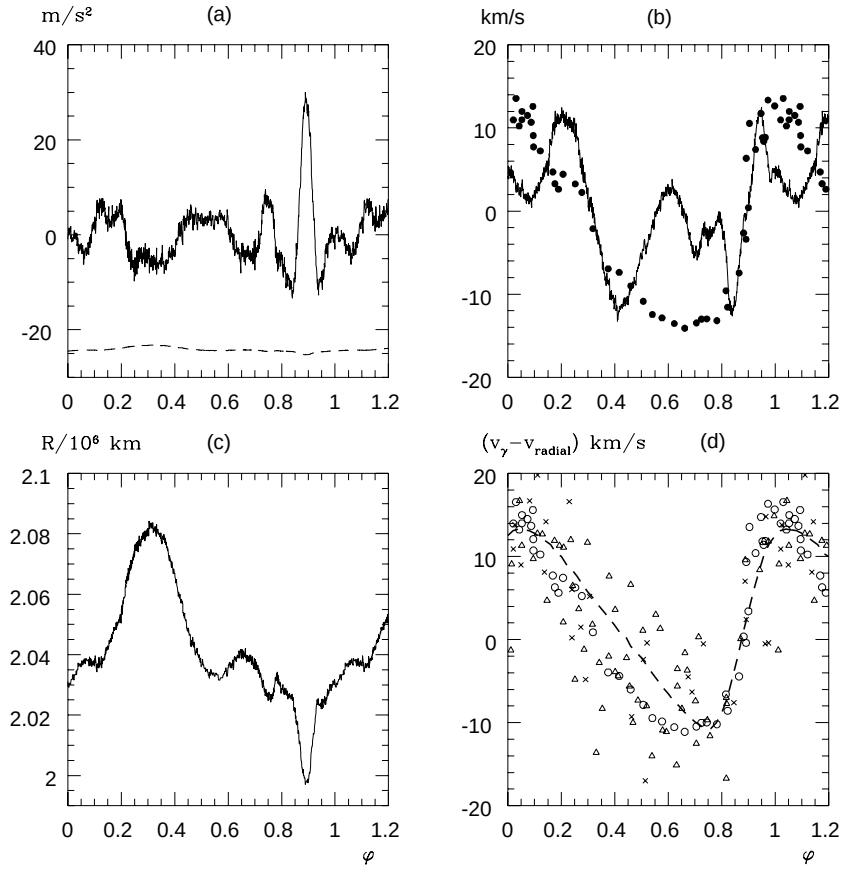

Figure 3: Panel (a): line: $g_e(\varphi)$, dashed: $-0.76\mathcal{M}_\odot G/R^2(\varphi)$. Panel (b): $\dot{R}(\varphi)$, filled circles: $25 - v_{\rm radial}(\varphi)$ from Liu & Janes (1989). Panel (c): $R(\varphi)$. Panel (d): circles: $28 - v_{\rm radial}(\varphi)$ from Liu & Janes (1989), triangles: $38 - v_{\rm radial}(\varphi)$ from Barnes et al. (1988), crosses: $38 - v_{\rm radial}(\varphi)$ from Tifft & Smith (1958), dashed line: mean of $38 - v_{\rm radial}(\varphi)$ from Barnes et al. (1988). The outlier points of panels (a)-(c) at $0.72 < \varphi < 0.78$ are artifacts of interpolation, they were not smoothed out to show the effect of eventual uncertainties in the interpolation.

- *Open problems*

There is a systematic difference in the $v_{\rm radial}(\varphi)$ curves of Barnes et al. (1988), Tifft & Smith (1958), and Liu & Janes (1989): $v_\gamma = 38$, and 28.0 ± 1.4 km s^{-1}, respectively, which exceed the expected observational errors. On the basis of *Fig. 3b* $v_\gamma = 25$ km s^{-1} seems even more probable. The amplitudes $28, 24, 24$ km s^{-1} of TS58, BM88, LJ89 do not differ significantly. *Fig. 3d* shows that subtracting $v_{\rm radial}(\varphi)$ from the different barycentric velocities does not bring the different observations to full coincidence. The stability of the light and colour curves is, however, obvious from *Fig. 1*, therefore, secular change of the shape of $v_{\rm radial}(\varphi)$ seems to be improbable. A variable v_γ i.e. duplicity cannot be excluded in spite of the large scatter of $v_{\rm radial}(\varphi)$ of TS58, BM88, furthermore, the scatter of δ_k is some 3 hours. This is significantly higher than the imaginable error of a δ_k value and for its explanation barycentric motion i.e. light-time effect can even be considered.

On speculation level the extreme sensitivity of the BW method on Δv_γ may be guessed

as the main source of the discrepant d of Liu & Janes (1989) which was propagated into their $\mathcal{M}$, $\langle R\rangle$, $\langle M_V\rangle$. Since the radial amplitude of T Sex is only some $\delta R = 80000$ km for a BW analysis v_γ ought to be known by an accuracy $\mathrm{O}(100)\mathrm{m\,s^{-2}}$ which was obviously not reached, another factor is their low $T_\mathrm{e}(\varphi)$. (Their quoted error $\Delta v_\gamma = \pm 1.4$ $\mathrm{km\,s^{-1}}$ leads to an error $\approx \pm 18000$ km in δR resulting in an error $\Delta d/d \approx 0.21$.)

The product $p_\mathrm{p}[v_\gamma - v_\mathrm{radial}(\varphi)]$ is the comparable quantity with $\dot{R}$ plotted in *Fig. 3b*. The spectral lines originate from $0 < \tau_\mathrm{Rosseland} < 0.4$, therefore, we expect $p_\mathrm{p}|v_\gamma - v_\mathrm{radial}(\varphi)| < |\dot{R}(\varphi)|$. It is satisfied if $p_\mathrm{p}(t) \approx 1$, however, the large scatter of the radial velocities gives weak basis for this very small value. Remarkable is that the most accurate radial velocities i.e. those of Liu & Janes (1989) show small humps at the extreme values of $\dot{R}$ at $\varphi \approx 0.2, 0.4, 0.6$ and $\dot{R}_\mathrm{max} - \dot{R}_\mathrm{min}$ agrees better with the extreme values of $v_\gamma - v_\mathrm{radial}$ if $v_\gamma = 25$ $\mathrm{km\,s^{-1}}$.

The rather loose correlation of $\dot{R}$ and $25 - v_\mathrm{radial}(\varphi)$ is similar to that found in SU Dra (Barcza, 2003) and it raises a serious question concerning the basic equation (8) of the BW method. A qualitative explanation can be guessed from gas dynamics and the technique of measuring radial velocity.

> $\dot{\vartheta}(\varphi), \dot{R}(\varphi)$ reflect the motion of $\tau = 0$ while the spectral lines originate from the surroundings of $\tau_{\lambda_\mathrm{line}} \approx 0.3$. Non-negligible velocity gradient is definitely present in an RR Lyrae atmosphere (e.g. Oke et al., 1962) and the limb darkening integrates the non-uniform motion of the layers $0 < \tau < 0.5$ into a single value $v_\mathrm{radial}(\varphi)$. (Dynamical atmospheric models are not available to treat quantitatively the conversion of the pulsation velocity to $v_\mathrm{radial}(\varphi)$.)
>
> CORAVEL technique is itself accurate for stars of non-variable spectra while applying it for a variable spectrum may result in systematic errors which are not easy to survey. The coarse agreement of $v_\mathrm{radial}(\varphi)$ from spectroscopy and CORAVEL is obvious in *Fig. 3d*, however, the large scatter indicates that some caution is appropriate, especially, since fine details of $\vartheta(\varphi)$, $v_\mathrm{radial}(\varphi)$ play some role in a BW analysis.

Conclusions

The purely photometrically derived fundamental parameters of T Sex (see Table 4) have been found from ATLAS atmospheric models of Kurucz (1997) and their calibration to stellar photometric systems (Castelli, 1999). They have been found to be in consensus with our knowledge on stellar models and pulsation theory of asymptotic giant branch stars. In addition to bridging over these remote branches of astrophysics some details have been revealed on RR Lyrae type pulsation: at the RRc variable T Sex fine structure, definite footprint of two shocks have been found in the variable stellar radius $R(\varphi)$ (i.e. in the distance of zero optical depth from the stellar centre). In a previous study of SU Dra similar details were found concerning the fine structure of the atmospheric pulsation: there is at least one pair of temporal, intermediate, minor standstills of the pulsating atmosphere between maximum and minimum extension. This seems to be a common feature of RRab and RRc stars at phase ≈ 0.55, it was not considered (or it was smoothed out) in the previous BW studies, presumably because it is a sub-oscillation in the upper stellar atmosphere which is scarcely reflected in the radial velocities. (The radial velocities give information on the motion of the deeper layers.) To derive the fundamental parameters

the less accurate radial velocity observations and their problematic conversion to radius changes had not to be used at all, however, an indication of eventual variable barycentric velocity of T Sex has arisen.

Acknowledgements This research has made use of SIMBAD database operated at CDS, Strasbourg, France and ADS of NASA. The author is grateful to J. M. Benkő for comments on the text.

References:

Barcza S., 2002, *A&A*, **384**, 460
Barcza S., 2003, *A&A*, **403**, 683
Barnes T. G. III, Moffett T. J., Hawley S. L., Slovak M. H., & Frueh, M. L., 1988, *ApJS*, **67**, 403 (BM88)
Barnes T. G. III, Moffett T. J., & Frueh M. L., 1992, *PASP*, **104**, 514 (BM 92)
Belle van G. T., Ciardi D. R., Thompson R. R., Akeson R. L., & Lada E. A., 2001, *ApJ*, **559**, 1155
Buonaura B., Caccin B., Onnembo, A, Russo G., & Sollazzo C., 1985, *Mem. Soc. Astron. Ital.*, **56**, 153
Carney B. W., Strom J., & Jones R. V., 1992, *ApJ*, **386**, 663
Castelli F., 1999, *A&A*, **346**, 564
Decin L., Vandenbussche B., Waelkens K., Eriksson C., Gustafsson B., Plez B., & Sauval A. J., 2003, *A&A*, **400**, 695
Drake J. & Laming M., 1995, *The Observatory*, **115**, 118
Eggen O. J., 1994, *AJ*, **107**, 1834 (E94)
Epstein I. & Epstein A. E. A., 1973, *AJ*, **78**, 83 (EE73)
ESA, 1997, *The Hipparcos Catalogue*, ESA SP-1200
Gatewood G. D. & Gatewood C. V., 1978, *ApJ*, **225**, 191
Gratton R. G., 1998, *MNRAS*, **296**, 739
Hanbury Brown R., Davis J., & Allen L. R., 1974, *MNRAS*, **167**, 121
Hemenway M. K., 1975, *AJ*, **80**, 199
Hobart M. A., Peña J. H., & Peniche R., 1991, *Rev. Mexicana Astr. Ap.*, **22**, 275
Hoffleit D., 1982, *The Bright Star Catalogue*, Yale Univ. Obs.
Kinman T. & Castelli F., 2002, *A&A*, **391**, 1039
Koester D., Schulz H., & Weidemann V., 1979, *A&A*, **76**, 262
Kurucz R. L., 1997, `http://cfaku5.cfa.harvard.edu`
Lee Y.-W., Demarque P., & Zinn R., 1990, *ApJ*, **350**, 155
Liu T. & Janes K. A., 1989, *ApJS*, **69**, 593 (LJ89)
Liu T. & Janes K. A., 1990, *ApJ*, **354**, 273
McMahan R. K., 1989, *ApJ*, **336**, 409
Oke J. B., Giver L. P., & Searle L., 1962, *ApJ*, **136**, 393
Preston G. W. & Paczyński B., 1964, *ApJ*, **140**, 181 (PP64)
Taylor B. J., 1986, *ApJS*, **60**, 577
Tifft W. G. & Smith H. J., 1958, *ApJ*, **127**, 591 (TS58)
Tuggle R. S. & Iben I. Jr, 1972, *ApJ*, **178**, 455
Tüg H., White N. M., & Lockwood G. W., 1977, *A&A*, **61**, 679

Formation of the Supercluster-Void Network

Jaan Einasto

Tartu Observatory
61602 Tõravere, Estonia

A review of the study of superclusters based on the 2dFGRS and SDSS is given. Real superclusters are compared with models using simulated galaxies of the Millennium Run. We show that the fraction of very luminous superclusters in real samples is about five times larger than in simulated samples. Superclusters are generated by large-scale density perturbations which evolve very slowly. The absence of very luminous superclusters in simulations can be explained either by non-proper treatment of large-scale perturbations, or by some yet unknown processes in the very early Universe.

Introduction

Superclusters are the most extensive density enhancements in the Universe of common origin. Investigation of large systems of galaxies was pioneered by the study of the *Local Supercluster* by de Vaucouleurs (1953) and by Abell (1961) and using rich clusters of galaxies by Abell (1958) and Abell et al. (1989). Superclusters consist of galaxy systems of different richness: single galaxies, galaxy groups and clusters, aligned in chains (Jõeveer, Einasto, & Tago, 1978; Gregory & Thompson, 1978; Zeldovich, Einasto, & Shandarin 1982).

New deep galaxy surveys, such as the Las Campanas Galaxy Redshift Survey, the 2 degree Field Galaxy Redshift Survey (2dFGRS, Colless et al., 2001, 2003), and the Sloan Digital Sky Survey (SDSS, Adelman-McCarthy et al. 2006) cover large areas in the sky and are almost complete up to fairly faint apparent magnitudes. Thus these surveys are convenient to detect superclusters using both galaxy and cluster data. This possibility has been used by Basilakos (2003), Basilakos et al. (2001), Erdogdu et al. (2004), Porter & Raychaudhury (2005), and Einasto et al. (2003a, 2003b, 2005, 2006a).

The goal of the present review is to analyse properties of superclusters based on the 2dF Galaxy Redshift Survey and the Sloan Digital Sky Survey Data Release 4 by Einasto et al. (2006a, 2006b, 2006c), and to compare properties of real superclusters with theoretical models. 2dFGRS and SDSS supercluster catalogues have been compiled using group

catalogues of 2dFGRS and SDSS DR4 surveys, found by Tago et al. (2006a, 2006b). For comparison we use the superclusters found for the Millennium Run mock galaxy catalogue by Croton et al. (2006), that itself is based on the Millennium Simulation of the evolution of the Universe by Springel et al. (2005).

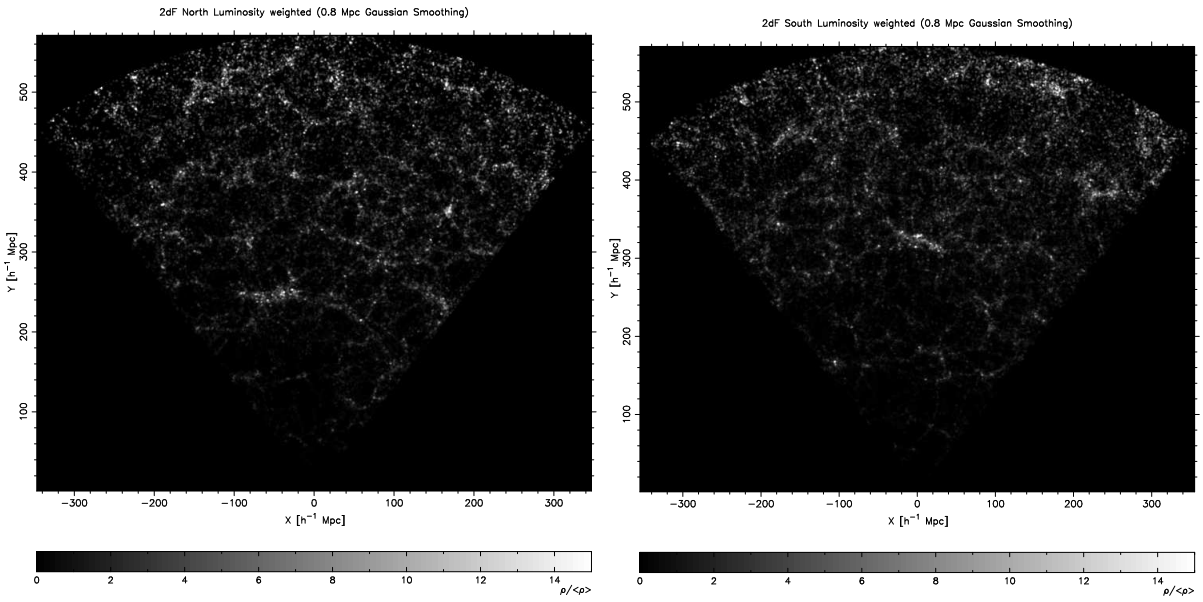

Figure 1: The high-resolution 2-dimensional density fields of the Northern and Southern parts of the 2dF redshift survey are shown in the left and right panels, respectively. The samples are conical, i.e. their thickness increases with distance, thus at large distances from the observer we see many more systems of galaxies. The richest supercluster in the Northern region is SCL126 in the list by Einasto et al. (1997), also called the Sloan Great Wall by Vogeley et al. (2004); the richest Southern supercluster is SCL9 by Einasto et al. (1997), or the Sculptor Supercluster.

Superclusters in the 2dF and Sloan surveys and in the Millennium simulation

Both real and model superclusters were found using the luminosity density fields calculated using Epanechnikov smoothing with a radius of 8 h^{-1} Mpc. Superclusters were defined as connected non-percolating systems with densities above a certain threshold density. These density fields were normalized to identical mean levels, and all regions above a threshold density 6 (in units of the mean density) were considered as superclusters. The density fields were calculated for a grid step of 1 h^{-1} Mpc, which allows to investigate the detailed spatial structure of superclusters. The 2dFGRS superclusters were found separately for the Northern and Southern regions of the 2dF Survey, and SDSS superclusters – for the high-declination region of the SDSS DR4 Survey in the Northern hemisphere. The 2dF Northern and Southern regions together contain 544 superclusters, the SDSS Northern survey has 911 superclusters. The comparison model samples have 1733 and 1068 superclusters (the full model sample and the simulated 2dF sample, respectively).

In *Figs. 1* and *2* we show high-resolution density fields on the 2dFGRS and SDSS surveys. All wedges are about 10 degrees thick, thus near to the observer they are thin. These figures show the cosmic web – a continuous network of galaxy systems of various

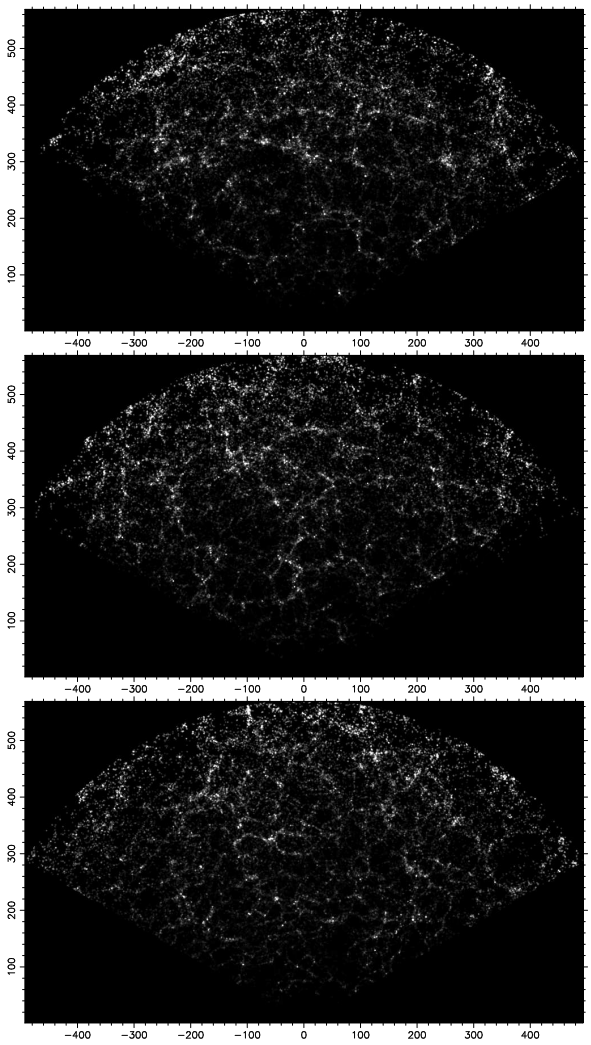

Figure 2: The high-resolution 2-dimensional density field of the SDSS DR4 Northern high-declination region. The wedges are drawn in rectangular coordinates based on the SDSS survey coordinates η and λ, and have a thickness of 9.33 degrees in λ; the panels from bottom to top correspond to increasing λ values. Note the presence of rich superclusters in all wedges.

luminosity densities, and voids between them. All luminous regions seen in these figures are superclusters. We see that they have very different richness, some are very small and resemble the Local Supercluster around the Virgo cluster, some are large and very rich.

For all superclusters their geometric and physical properties were found. Among the geometrical properties are the position (RA, DEC, and distance), the size, and the offset of the geometrical center from the dynamical one, defined as the center of the main (most luminous) cluster. The physical properties are the mean and maximum luminosity densities, the total luminosity and the luminosity of the main cluster and of the main galaxy (the brightest galaxy of the main cluster).

Comparison of properties of model superclusters with properties of real superclusters shows that they are very similar. Superclusters consist of several chains (filaments) of galaxies, groups, and clusters. These chains have various length, thus superclusters are asymmetrical in shape. The degree of asymmetry is higher in rich superclusters. Rich superclusters are also denser and contain luminous knots – high-density nuclei.

Rich superclusters in real data and models

One important property of superclusters is different in real and model samples – the supercluster richness. To characterise the richness we used two independent characteristics: the total luminosity and the number of rich clusters, i.e. the multiplicity.

The multiplicity was derived from the number of high-density knots of the density field. We call these knots DF-clusters. The spatial density of DF-clusters is about twice that of Abell clusters in the same volume, thus the expected number of DF-clusters in superclusters is about twice the number of Abell clusters. Both functions were determined separately for the 2dFGRS and SDSS superclusters, and for the total observational sample.

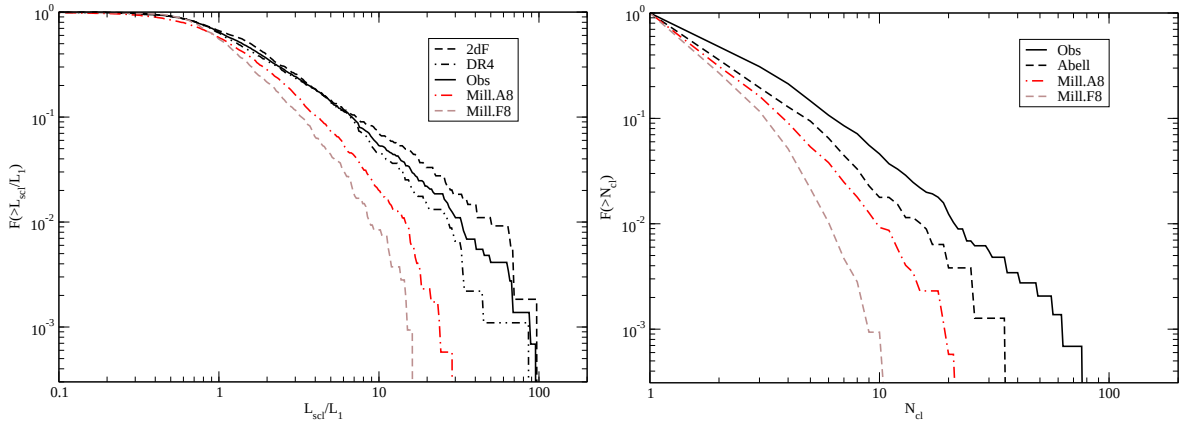

Figure 3: Comparison of relative luminosity functions and multiplicity functions of observational and model supercluster samples (in left and right panels, respectively). The spatial density of superclusters is expressed in terms of the total number of superclusters in a sample to avoid small differences due to different mean supercluster number densities in different samples. In the left panel we show the relative luminosity functions separately for the observational samples SDSS DR4, 2dF, and for the combined sample Obs, in the right panel we use the combined observational sample Obs, and the Abell supercluster sample (here the multiplicity is defined by the number of Abell clusters, and isolated Abell clusters are considered as richness class 1 superclusters). Mill.A8 and Mill.F8 denote the full and simulated 2dF Millennium supercluster samples, respectively.

The total luminosity was calculated by summing the luminosities of galaxies and clusters of galaxies inside the density contour, which defines the boundary of the supercluster. In our case the threshold density was chosen to be 6 (in units of the mean density). In calculating total luminosities we used weights for galaxies which take into account the galaxies outside the observational luminosity window of a survey. To avoid complications due to the use of different color systems and mean luminosities, we used *relative* luminosities, normalized by the mean luminosity of poor superclusters, i.e. the superclusters that contain only one DF-cluster.

For model samples we calculated these functions for two cases. One sample uses all model galaxies and can be considered as the "true" model sample. The second model sample simulates the 2dF sample, where an "observer" was put into one corner of the sample, and only these galaxies were included, which satisfy the same selection criteria as used in the real 2dF sample.

The luminosity and multiplicity functions of real and model samples are compared in *Fig. 3*. We see that both functions show much more rich superclusters for real samples

than for model samples. This difference is the major cosmological result of the analysis of our supercluster survey. The presence of very rich superclusters in our vicinity is well known; good examples are the Shapley Supercluster and the Horologium-Reticulum Supercluster (see Fleenor et al., 2005; Proust et al., 2006; Nichol et al., 2006; Ragone et al., 2006, and references therein). But until recently the number of such extremely massive superclusters was too small to make definite conclusions about their abundance.

When comparing models with observations we have to use the simulated 2dF sample, which is formed using the same selection criteria as used for the observational sample. The most luminous simulated superclusters of this sample have a relative luminosity of about 15 in terms of the mean luminosity of richness class 1 superclusters, whereas the most luminous superclusters of real samples have a relative luminosity about 100, i.e. they are about 6 times more luminous. The richest model superclusters have a multiplicity of 10, whereas the multiplicity of the richest real superclusters is over 70. The number of Abell clusters in the richest Abell supercluster is 34 (Einasto et al., 2001).

Figures 1 and *2* show that very luminous superclusters are located in *all subsamples* (the Northern and Southern regions of the 2dFGRS, and in subregions of the SDSS DR4 sample, if divided into 3 wedges of equal width). These subsamples have characteristic volumes of about 10 million cubic h^{-1} Mpc, whereas model samples of 10 times larger volume have no extremely rich superclusters.

Formation of the supercluster-void network

To check these results we used a number of independent numerical simulations, carried out for simulation boxes of size of 500 h^{-1} Mpc and 768 h^{-1} Mpc, using 512^3 Dark Matter particles. We found DM-halos in simulations, and used them to calculate the smoothed density field as for real and Millennium Simulation. For all simulations we then found simulated superclusters as previously, and found the distribution of dense knots (simulated rich clusters). These calculations confirmed our previous result: the number of dense knots in simulated superclusters is much smaller than in real superclusters.

This striking conflict between model and reality needs explanation. In order to understand the formation of rich superclusters we used wavelet analysis to investigate the role of density waves of different scales. The á trous wavelet technique we used allows to divide the density field into components of various wavelength bands, so that the field is restored by summing all components. The wavelet analysis was carried out both for real and model samples.

Our results show that in all cases superclusters form only in regions where *large density waves combine in similar local phases to generate high density peaks.* Very rich superclusters are objects where density waves of all large scales (up to a wavelength $\sim 250\ h^{-1}$ Mpc) have similar phases. The smaller is the maximum wavelength of such phase synchronization, the lower is the richness of superclusters. Similarly, large voids are caused by large-scale density perturbations of wavelength $\sim 100\ h^{-1}$ Mpc, here large-wavelength modes combine *in similar local phases to generate under-densities.*

Superclusters of galaxies are formed by density perturbations of large scales. These perturbations evolve very slowly. As shown by Kofman & Shandarin (1988), the present structure on large scales is built-in already in the initial field of linear gravitational potential fluctuations. Actually they are remnants of the very early evolution and stem from the inflationary stage of the Universe (see Kofman et al., 1987). The distribution of

luminosities of superclusters allows us to probe processes acting at these very early phases of the evolution of the Universe.

There are two possible explanations for the large difference between the distribution of luminosities of real and simulated samples. One possibility is that in present simulations the role of very large density perturbations, responsible for the formation of these very luminous superclusters, is underestimated. The other feasible explanation of the differences between models and reality may be the presence of some unknown processes in the very early Universe which give rise to the formation of extremely luminous and massive superclusters.

Conclusions

1. Geometric properties of superclusters are well explained by current models.
2. There are much more very rich superclusters than models predict.
3. Large perturbations evolve very slowly and represent the fluctuation field at the epoch of inflation.
4. The difference between observations and models can be explained in two ways:
   large-scale perturbations are not incorporated in the models, i.e. models need improvement;
   there occurred presently unknown processes during inflation.

The present review is based on talks held in Budapest on April 20, 2006 in Detre Centenary, in Uppsala University on April 27, 2006, and in Aspen Workshop on Cosmic Voids on June 6, 2006. I thank my collaborators Maret Einasto, Enn Saar, Erik Tago, and Volker Müller for permission to use results of our common work in this review. We are pleased to thank the 2dFGRS and SDSS Teams for the publicly available data releases. The present study was supported by Estonian Science Foundation grants No. 4695, 5347, and 6104, and Estonian Ministry for Education and Science support by grant TO 0060058S98. I thank Astrophysikalisches Institut Potsdam (using DFG-grant 436 EST 17/2/05) and Uppsala University for hospitality where part of this study was performed. 2dFGRS supercluster catalogues are available at `http://www.aai.ee/~maret/2dfscl.html`, Sloan DR4 supercluster catalogues at `http://www.aai.ee/~maret/SDSSDR4scl.html`.

References:

Abell G., 1958, *ApJS*, **3**, 211
Abell G., 1961, *AJ*, **66**, 607
Abell G., Corwin H., & Olowin R., 1989, *ApJS*, **70**, 1
Adelman-McCarthy J. K., Agüeros M. A., Allam S. S., et al., 2006, *ApJS*, **162**, 38
Basilakos S., 2003, *MNRAS*, **344**, 602
Basilakos S., Plionis M., & Rowan-Robinson, M., 2001, *MNRAS*, **323**, 47
Colless M. M., Dalton G. B., Maddox S.J., et al., 2001, *MNRAS*, **328**, 1039
Colless M. M., Peterson B. A., Jackson C.A., et al., 2003, (astro-ph/0306581)
Croton D. J., Springel V., White S. D. M., et al., 2006, *MNRAS*, **365**, 11
de Vaucouleurs G., 1953, *AJ*, **58**, 30

Einasto J., Einasto M., Hütsi G., et al., 2003a, *A&A*, **410**, 425
Einasto J., Einasto M., Saar E., et al., 2006b, *A&A*, (accepted, Paper II, astro-ph/0604539)
Einasto J., Einasto M., Saar E., et al., 2006c, *A&A*, **459**, L1
Einasto J., Einasto M., Tago E., et al., 2006a, *A&A*, (submitted, Paper I, astro-ph/0603764)
Einasto J., Hütsi G., Einasto M., et al., 2003b, *A&A*, **405**, 425
Einasto J., Tago E., Einasto M., et al., 2005, *A&A*, **439**, 45
Einasto M., Einasto J., Tago E., Müller V., & Andernach H., 2001, *AJ*, **122**, 2222
Einasto M., Tago E., Jaaniste J., Einasto J., & Andernach H., 1997, *A&A Suppl.*, **123**, 119
Erdogdu P., Lahav O., Zaroubi S., et al., 2004, *MNRAS*, **352**, 939
Fleenor M. C., Rose J.A., Christiansen W. A., et al., 2005, *AJ*, **130**, 957
Gregory S. A. & Thompson L.A., 1978, *ApJ*, **222**, 784
Jõeveer M., Einasto J. & Tago E., 1978, *MNRAS*, **185**, 357
Kofman L. A., Linde A.D., & Einasto J., 1987, *Nature*, **326**, 48
Kofman L. A. & Shandarin S. F., 1988, *Nature*, **334**, 129
Nichol R. C., Sheth R. K., Suto Y., et al., 2006, *MNRAS*, **368**, 1507
Porter S. C. & Raychaudhury S., 2005, *MNRAS*, **364**, 1387
Proust D., Quintana H., Carrasco E. R., et al., 2006, *A&A*, **447**, 133
Ragone C. J., Muriel H., Proust D., et al., 2006, *A&A*, **445**, 819
Springel V., White S. D. M., Jenkins A., et al., 2005, *Nature*, **435**, 629
Tago E., Einasto J., Saar E., et al., 2006a, *AN*, **327**, 365
Tago E., Einasto J., Saar E., Einasto M., 2006b, (in preparation)
Vogeley M. S., Hoyle F., Rojas R. R., et al., 2004, in *Outskirts of Galaxy Clusters*, Proc. IAU Coll. 195, ed. A. Diaferio, CUP, p. 5
Zeldovich Ya. B., Einasto J., & Shandarin S. F., 1982, *Nature*, **300**, 407